

NASA Technical Memorandum 101599

AVSCOM

Technical Memorandum 89-B-002

**INFLOW MEASUREMENTS MADE WITH A LASER VELOCIMETER ON A HELICOPTER
MODEL IN FORWARD FLIGHT**

Volume VII: RECTANGULAR PLANFORM BLADES AT AN ADVANCE RATIO OF 0.40

Danny R. Hoad, Susan L. Althoff, and Joe W. Elliott
 Aerostructures Directorate
 USAARTA - AVSCOM
 Langley Research Center
 Hampton, Virginia

Richard H. Sailey
 Planning Research Corporation
 Aerospace Technologies Division
 Hampton, Virginia

April 1989

(NASA-TM-101599) INFLOW
 MEASUREMENTS MADE WITH A LASER
 VELOCIMETER ON A HELICOPTER MODEL
 IN FORWARD FLIGHT. VOLUME 7:
 RECTANGULAR PLANFORM BLADES AT AN
 ADVANCE RATIO OF 0.40 (Diskette
 Supplement) (NASA) 388 p

N93-24538

Unclassified

G3/02 0159783

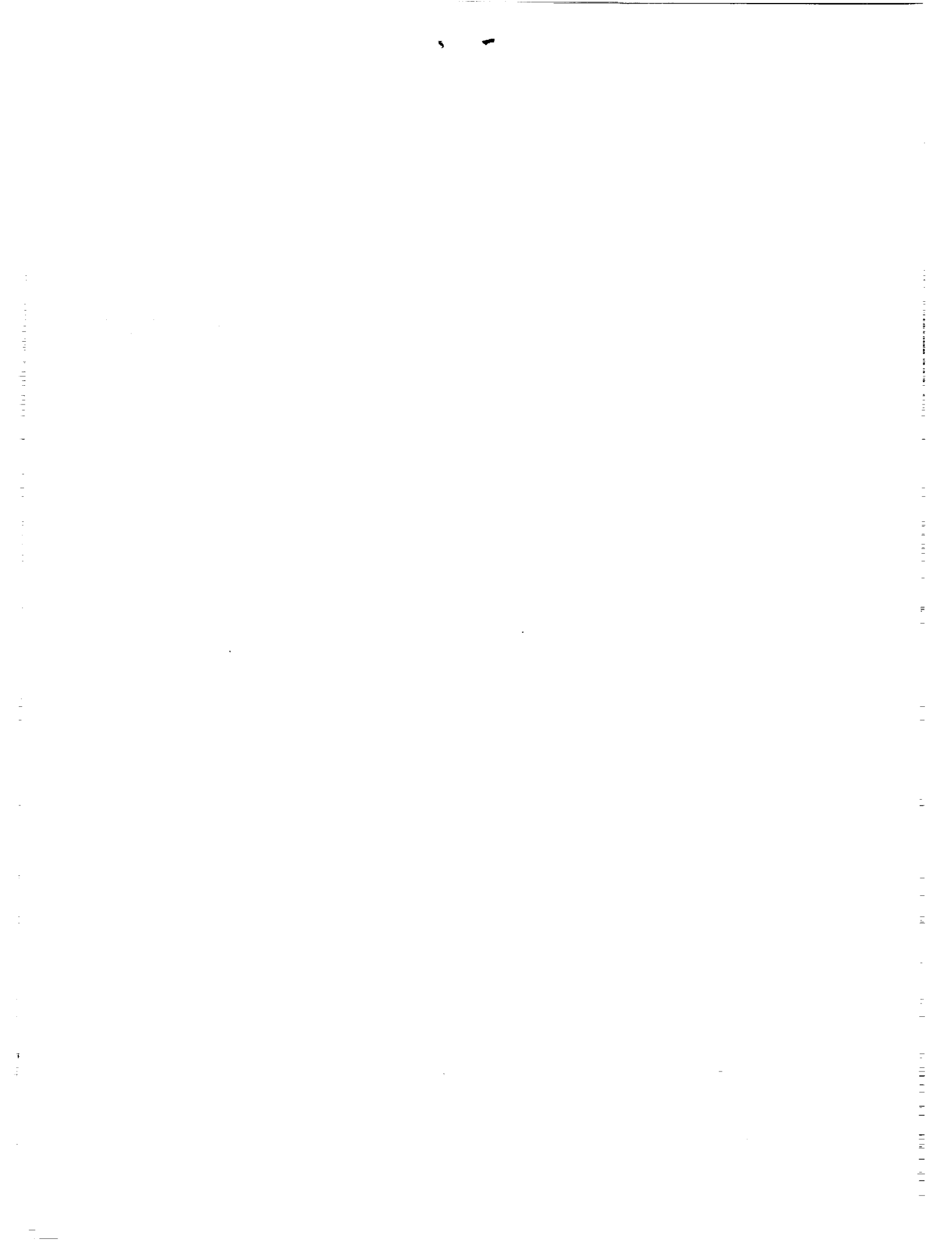


National Aeronautics and
 Space Administration

Langley Research Center
 Hampton, Virginia 23665-5225



US ARMY
 AVIATION
 SYSTEMS COMMAND
 AVIATION R&T ACTIVITY



SUMMARY

An experimental investigation was conducted in the 14- by 22-Foot Subsonic Tunnel at the NASA Langley Research Center to measure the inflow into a scale model helicopter rotor in forward flight ($\mu = 0.40$). The measurements were made with a two-component Laser Velocimeter (LV) one chord above the plane formed by the path of the rotor tips (tip-path-plane). A conditional sampling technique was used to determine the position of the rotor at the time that each velocity measurement was made so that the azimuthal fluctuations in velocity could be determined. Measurements were made at a total of 178 separate locations in order to clearly define the inflow character. The mean and standard deviation of the induced inflow velocities and the azimuthally dependent induced inflow velocities are included on a 5.25 flexible disk in the pocket on the inside of the rear cover of this report. These data are presented herein without analysis.

INTRODUCTION

One of the problems confronting the helicopter industry is the lack of detailed information about the velocity fluctuations around and through rotating blades. This information is needed for two reasons: to ensure a more complete understanding of the flow field environment associated with a thrusting rotor and to provide data for the validation of rapidly emerging computational codes. One explanation for the lack of available data is the absence, until recent years, of a suitable device for making such measurements. Making measurements of the velocity around a system of rotating blades requires an accurate, nonintrusive measurement capability that presents a minimum risk to the systems involved. The LV, which uses high energy light beams to measure velocities, is ideally suited to this task.

The LV has been successfully used to measure specific areas and localized phenomena within the rotor disk (references 1 through 3). In addition, the hotwire anemometer and pressure probe, both having directional measuring limitations, have been used in similar programs (references 4 and 5). This comprehensive program has been conducted to measure the flow into a representative rotor system as a function of azimuth using a two-component (stream-wise and vertical direction) LV system.

NOTATION

A	rotor disc area, (πR^2), ft ²
A ₀	Constant term in Fourier series of blade feathering (collective) at r/R = 0.75, deg
A ₁	Coefficient of cosine term in Fourier series of blade feathering, deg
b	Number of blades
B ₁	Coefficient of sine term in Fourier series of blade feathering, deg
C _Q	Rotor torque coefficient, Q/(\rho A(12R)V _{tip} ²), nondimensional
C _D	Rotor drag coefficient, D/(\rho A V _{tip} ²), nondimensional
C _T	Rotor thrust coefficient, T/(\rho A V _{tip} ²), nondimensional
D	Rotor drag, lbf (positive to the rear)
q	Dynamic pressure, lb/ft ²
Q	Rotor torque, in-lbf
r	Local radius of the rotor system, ft
R	Rotor radius, ft
T	Thrust produced by the rotor, lbf
U _∞	Tunnel freestream velocity, ft/sec, (positive downstream)
U	Freestream component of velocity, ft/sec, (positive downstream)
u _i	Induced component of velocity parallel to the tip path plane (positive downstream), ft/sec
v	Vertical component of velocity, ft/sec, (positive up)
v _i	Induced component of velocity normal to the tip path plane, ft/sec (positive up)
V _{tip}	Rotor blade hover-tip velocity, ft/sec, (ΩR)

GREEK

α	Angle between rotor disk and freestream velocity (positive nose up), deg
λ	Inflow Ratio normal to tip path plane (positive up), $(U_{\infty} \sin \alpha + v_i)/V_{tip}$
λ_i	Induced Inflow Ratio normal to tip path plane (positive up), v_i/V_{tip}
μ_{∞}	Rotor advance ratio, $U_{\infty} \cos \alpha/V_{tip}$
μ	Inflow Ratio parallel to tip path plane (positive downstream), $(U_{\infty} \cos \alpha + u_i)/V_{tip}$
μ_i	Induced Inflow Ratio parallel to tip path plane (positive downstream), u_i/V_{tip}
Ω	Rotor rotational speed, radians/sec
ψ	Rotor azimuth measured from downstream position, positive counterclockwise, as viewed from above, deg
ρ	Air density, slug/ft ³
θ	Blade pitch angle at a specific azimuth (positive nose up), deg, $\theta = A_0 - A_1 \cos \psi - B_1 \sin \psi$
\overline{xx}	Mean value

EXPERIMENTAL APPARATUS

The experimental apparatus used in this investigation included the NASA Langley Research Center 14- by 22-Foot Subsonic Tunnel, the 2-Meter Rotor Test System (2MRTS), and a two-component Laser Velocimeter system.

The 14- by 22-Foot Subsonic Tunnel is an atmospheric, closed-circuit wind tunnel of conventional design with enhancements for the testing of powered and high-lift configurations (reference 6). The tunnel is shown in figure 1. When the tunnel is operated in the open configuration, the walls and ceiling of the test section are lifted out of the flow leaving only a solid floor and a flow collector. In this configuration, the tunnel can be driven to about 170 knots. This investigation was conducted with the tunnel in the open configuration to allow complete optical access to the rotor flow field.

The 2MRTS is a general purpose rotorcraft model testing system which was mounted on a strut in the forward part of the test section (see figure 2). The system consists of a 29-horsepower electric drive motor and 90° speed-reducing transmission, a blade pitch remote control system, and two six-component strain gage balances used for measuring forces and moments on the rotor system and the generic fuselage shell (ROBIN). The four-bladed rotor hub is fully articulated with viscous dampers for lead-lag motion and coincident flap and lag hinges. A more detailed description of the 2MRTS and the ROBIN fuselage can be found in reference 7. The characteristics of the rotor blades used during this investigation can be found in table 1. No attempt was made to dynamically scale the rotor blades; rather, they were very rigid to minimize blade aeroelastic response uncertainties.

The LV system used in this investigation was designed to measure the instantaneous components of velocity in the longitudinal (freestream) and vertical directions and is described in reference 8. The system is comprised of four subsystems: optics, traverse, data acquisition, and seeding. The optics subsystem, which is shown in figure 3, operates in backscatter mode and at high power (4 watts in all lines) in order to accommodate the long focal lengths needed to scan the wide test section. The transmitting and receiving optics packages are augmented by a zoom lens system consisting of a 3-inch clear aperture negative lens and a 12-inch clear aperture positive lens. Bragg cells in each of the optical paths provide a directional measurement capability. The velocity measurements are made at a point in space where the four beams cross, called the sample volume. The length of the sample volume (transverse to the flow direction) increases as the sample volume is moved away from the optics assembly. The sample volume length, over the 10- to 20-foot focal length of the system, is less than 1 cm and has a nearly constant diameter of 0.2 mm.

The traverse subsystem provides five degrees of freedom in positioning the sample volume and is controlled by the same computer that is used for data acquisition. Translation of the sample volume in the horizontal and vertical direction is accomplished by displacing the entire optics platform. Translation along the lateral axis is accomplished by displacing the negative lens located in the zoom lens assembly, thus refocusing the sample volume along the axis of optical transmission. The other two degrees of freedom, pan and tilt, are implemented by rotating the final mirror about its vertical and horizontal axes in order to change the direction of optical transmission. The total range of the traversing system is 7 feet vertically, 6 feet streamwise, 16.5 feet laterally, and 10° in both pan and tilt. Measurements can be made outside of this envelope by re-positioning the optics platform, which is mounted on wheels to facilitate such relocations. For this study the traversing system was positioned to the left of the test section when looking downstream as shown in figure 2.

The data acquisition subsystem is shown schematically in figure 4 and interfaces with the optical signal processing equipment to receive two channels of raw LV data and up to five channels of auxiliary data. In this investigation, two auxiliary channels were used for the acquisition of data relative to blade position (one each for the U and V components). The system converts the raw LV data to engineering units and determines the statistical characteristics of the acquired data so that the test results can be evaluated during the acquisition process. The raw data and up to 64 parameters from the tunnel static data acquisition system are written to magnetic tape for later analysis. The final function performed by the data system is to control the five degree-of-freedom scan system.

The seeding subsystem, shown schematically in figure 5 and in the photo in figure 6, is a solid particle, liquid dispensing system (reference 9). Polystyrene latex microspheres are suspended in a mixture containing, by volume, 50 percent water and 50 percent ethyl alcohol. The advantages of the polystyrene particles are their low density, high reflectivity, and precise particle size. The particles used in this investigation were 1.7 microns in diameter with a standard deviation of 0.0239 microns. The particle mixture is pumped to an array of nozzles where compressed air is used to atomize the mixture. These nozzles are mounted on a frame that can be moved about the settling chamber of the tunnel using the remote positioning system recently installed (figure 6). The low vapor pressure of water/alcohol mixture allows it to evaporate as it travels the 85 feet from the settling chamber to the test section. This process provides isolated single particles in the flow field whose velocities are measured as they pass through the sample volume. The local fluid velocity is inferred from the seed particle velocity.

ERROR ANALYSIS

The overall LV system error is obtained by summing the error of all of the components that contribute to an error in the velocity measurement. The error sources are summarized in the table below and are defined in references 10 and 11. The resulting total bias error of -0.806 to 1.820 percent is obtained by adding the percents contributed by each error source. The total random error of 1.120 percent is obtained by taking the square root of the sum of the squared percents of the random sources. Taking the square root of the sum of the squares of the random and bias errors gives a total system error of 1.38 percent to 2.14 percent.

Error Source	Bias Error	Random Error
Cross Beam Angle Measurement	± 0.813	N/A
Diverging Fringes	A	A
Time Jitter	N/A	N/A
Clock Synchronization	0.507	± 0.507
Quantization	A	$\pm .999$
Velocity Bias	B	B
Bragg Bias	B	B
Velocity Gradient	B	B
Particle Lag	± 0.50	B
Total Error	-0.806 to 1.820	1.120

A Not Measured

B Negligible

N/A Not Applicable

TEST PROCEDURES

In all cases measurements were made at azimuthal increments of 30° from $\psi = 0$, at 3.0 inches (approximately 1 chord) above the plane formed by the tips of the blades. Measurements were made from a radial location of $r/R = 0.2$ to $r/R = 1.10$, with the majority of the measurement locations concentrated toward the outboard portion of the disk. Figure 7 shows the measurement locations superimposed on the rotor disk. During the test, the rotor tip path plane angle-of attack was set at -6.8° relative to the freestream by zeroing the blade flapping relative to the shaft and setting the shaft angle to -6.8° . The operating hover-tip speed for the test was held at 624 ft/sec (2113 rpm), the nominal tunnel speed was 250 ft/sec ($\mu_\infty = 0.40$), and the nominal rotor thrust coefficient was 0.0064. Table 2 lists the nominal test conditions and selected parameters. The LV data acquisition process consisted of placing the sample volume at the measurement location and acquiring data for a period of 1 minute or until 4096 velocity measurements were made in either the longitudinal or the vertical component. During this process, conditional sampling techniques were used to permanently associate each measured velocity with the location of the rotor blades at the time when the measurement was made. At the conclusion of the process, the measurement location was changed and the acquisition process was repeated.

DATA REDUCTION

Independent velocity measurements in the freestream and vertical direction were made at each measurement location. At the same instant in time that a velocity measurement was made, the location of the blades was recorded for that velocity component. The maximum time required to acquire this data was 1 minute (2113 rotor revolutions for this test) and the minimum was approximately 10 seconds. These data, collected over many revolutions, were sorted into 128 equally spaced azimuth segments (2.81° wide) that are representative of blade position. Careful measurements indicated that the lead-lag motion was well within this azimuth resolution (2.81°); therefore, no corrections to blade position were made due to lead-lag. The velocity value assigned to each interval at a measurement location is the arithmetic mean of all the measurements that were taken in the respective 2.81° wide azimuthal range. The results of this sorting process provide the azimuthally dependent velocity data. The "mean velocity" value refers to the velocity calculated from the arithmetic mean of all the measurements made at a single measurement location.

EXPERIMENTAL RESULTS

Table 3 lists the measurement locations, the mean and standard deviation of the two components of induced inflow ratio, and the number of measurements in each of the measured components (U and V). In figure 8 the mean longitudinal induced component of inflow ratio, μ_i , with a band of \pm one standard deviation is plotted vs. blade radius for each radial scan. The standard deviation represents the fluctuation in velocity at a given measurement location. It is not an indication of the error in the mean measurements. The size of the symbols used for plotting the mean velocity values is an approximation of the calculated error in the measurements. Figure 9 presents in the same format the mean normal induced component of inflow ratio, λ_i . The same data without the \pm one standard deviation is presented in a contour plot format in figures 10 and 11 in order to show more clearly the interactions over the whole disk (viewed from above). Azimuth dependent data are presented in figures 12-189. The format for these include the induced inflow ratio vs azimuth at the top of the figure, the number of measurements that were used in determining the inflow ratio value for each azimuth segment in the center, and a

conditionally sampled amplitude spectrum (order ratio analysis) of the azimuthal variation at the bottom of the figure. The figure numbers for the azimuthal and radial measurement locations are indicated:

r/R	.20	.40	.50	.60	.70	.74	.78	.82	.86	.90	.94	.98	1.02	1.04	1.10
Ψ															
0	12	13	14	15	16	17	18	19	20	21	22	23	24	25	26
30	27	28	29	30	31	32	33	34	35	36	37	38	39	40	41
60	42	43	44	45	46	47	48	49	50	51	52	53	54	55	56
90	57	58	59	60	61	62	63	64	65	66	67	68	69	70	71
120	72	73	74	75	76	77	78	79	80	81	82	83	84	85	86
150	87	88	89	90	91	92	93	94	95	96	97	98	99	100	101
180	102	103	104	105	106	107	108	109	110	111	112	113	114		
210	115	116	117	118	119	120	121	122	123	124	125	126	127	128	129
240	130	131	132	133	134	135	136	137	138	139	140	141	142	143	144
270	145	146	147	148	149	150	151	152	153	154	155	156	157	158	159
300	160	161	162	163	164	165	166	167	168	169	170	171	172	173	174
330	175	176	177	178	179	180	181	182	183	184	185	186	187	188	189

The mean and standard deviation of the induced inflow ratios (table 3) and the azimuthally dependent induced inflow ratios (figures 12 through 189) are included on a 5.25 flexible disk in the pocket on the inside of the rear cover of this report. The details of the data format and the file structure are located in the file "README.DOC". The disk format is 360 byte double-sided, written using the Microsoft Corporation MS-DOS operating system.

CONCLUDING REMARKS

The Laser Velocimeter provides an effective system for making measurements in the dynamic environment associated with rotor blades. It has been used on numerous occasions to measure the localized flow phenomena encountered in such flows. This investigation demonstrates the use of a matured LV system to map the flow into a representative rotor in forward flight by making velocity measurements at 178 locations above the rotor disk. These measurements provide both the mean and azimuthally dependent velocity values, and they provide a detailed look at the nature of this flow. The mean and standard deviation of the induced inflow velocities and the azimuthally dependent induced inflow velocities are included on a 5.25 flexible disk in the pocket on the inside of the rear cover of this report.

REFERENCES

1. Landgrebe, A. J.; and Johnson, B. V.: Measurement of Model Helicopter Rotor Flow Velocities with a Laser Doppler Velocimeter. American Helicopter Society Journal, Vol 19, July 1974, p. 39-43.
2. Biggers, J. C.; and Orloff, K. L.: Laser Velocimeter Measurements of the Helicopter Rotor-Induced Flowfield. American Helicopter Society, Annual National V/STOL Forum, 30th, Washington, D.C. May 7-9, 1974.
3. Owen F. K.; and Taubert M. E.: Measurement and Prediction of Model-Rotor Flowfields. AIAA, 18th Fluid Dynamics, Plasmadynamics and Laser Conference, Cincinnati, Ohio, July 16-18, 1985.
4. Tangler, J. L.; Wohlfeld, R. M.; and Miley, S. J.: An Experimental Investigation of Vortex Stability, Tip Shapes, Compressibility and Noise for Hovering Models. NASA CR-2305, September 1973.
5. Junker, B.: Investigations of Blade-vortices in the Rotor Downwash. Twelfth European Rotorcraft Forum, Garmish-Partenkirchen, Federal Republic of Germany, September 22-25, 1986.
6. Applin, Z. T.: Flow Improvements in the Circuit of the Langley 4- by 7-Meter Tunnel. NASA TM 85662, December 1983.
7. Phelps, A. E. III; and Berry, J. D.: Description of the U.S. Army 2-Meter Rotor Test System. NASA TM 87762, AVSCOM TM 86-B-4, January 1987.
8. Sellers, W. L.; and Elliott, J. W.: Applications of a Laser Velocimeter in the Langley 4- by 7-Meter Tunnel. Proceedings of the Workshop on Flow Visualization and Laser Velocimetry for Wind Tunnels, NASA CP 2243, March 1982, pp. 283-293.
9. Elliott, J. W.; and Nichols, C. E.: Seeding Systems for Use with a Laser Velocimeter in Large Scale Wind Tunnels. Proceedings of the Workshop on Wind Tunnel Seeding Systems for Laser Velocimeters, NASA CP 2393, March 1985, pp. 93-103.
10. Young, W. H.; Meyers, J. F.; and Hepner, T. E.: Laser Velocimeter Systems Analysis to a Flow Survey above a Stalled Wing. NASA TN D-8408, August 1977.
11. Dring, R. P.: Sizing Criteria for Laser Anemometry Particles. Journal of Fluids Engineering, Vol. 104, March 1982, p. 15-17.

TABLE 1 - 2MRTS ROTOR AND BLADE CHARACTERSTICS

HUB TYPE	FULLY ARTICULATED
Number of blades	4
Airfoil section	NACA 0012
Hinge offset, in, r/R	2.00, .06
Root cutout, in, r/R	8.25, .24
Pitch-flap coupling angle, deg	0.0
Twist linear, deg	-8.0
Radius, R, in	33.88
Airfoil chord, C, in	2.6
Rotor solidity, bc/ π R	0.0977
Blade stiffness	
Flapwise lb-in ²	11500
Torsional lb-in ²	25500
Blade weight, grams	259.3
Lead/lag damping in-lb/deg/sec	182.4

TABLE 2 - NOMINAL ROTOR CONTROL AND PERFORMANCE PARAMETERS

C_T	0.0064
C_Q	0.00063
C_D	0.00
α , deg	-6.8°
Coning, deg	1.8
A_0 , deg	9.4
A_1 , deg	-0.5
B_1 , deg	8.2
μ_∞	0.40
U_∞ , ft/sec	250.5
V_{tip} , ft/sec	624.0
Lag angle (mean), degrees	1.4

TABLE 3 - INFLOW VELOCITY SUMMARY

Ψ	r/R	μ_i			λ_i		
		Mean	Standard deviation	# of Measurements	Mean	Standard deviation	# of Measurements
0	0.20	0.0143	0.0158	2144	-0.0008	0.0213	3253
0	0.40	0.0088	0.0130	1884	-0.0221	0.0138	3375
0	0.50	0.0039	0.0130	2155	-0.0241	0.0117	3213
0	0.60	0.0036	0.0127	2204	-0.0257	0.0101	3107
0	0.70	0.0007	0.0132	2198	-0.0267	0.0105	2807
0	0.74	0.0015	0.0134	2172	-0.0269	0.0105	3018
0	0.78	-0.0010	0.0124	2176	-0.0284	0.0116	2885
0	0.82	0.0001	0.0126	2079	-0.0292	0.0115	3080
0	0.86	-0.0016	0.0120	2099	-0.0287	0.0110	3031
0	0.90	-0.0021	0.0119	2120	-0.0302	0.0112	3031
0	0.94	-0.0040	0.0118	2062	-0.0308	0.0109	3111
0	0.98	-0.0074	0.0113	1900	-0.0310	0.0107	3152
0	1.02	-0.0093	0.0128	1910	-0.0317	0.0101	3197
0	1.04	-0.0104	0.0128	1984	-0.0321	0.0098	3232
0	1.10	-0.0122	0.0130	2066	-0.0309	0.0092	3258
30	0.20	0.0116	0.0145	1779	-0.0004	0.0128	3611
30	0.40	0.0051	0.0119	968	-0.0110	0.0095	1935
30	0.50	0.0060	0.0118	1702	-0.0193	0.0100	2918
30	0.60	0.0059	0.0119	1138	-0.0219	0.0104	2774
30	0.70	0.0042	0.0121	1288	-0.0237	0.0089	3112
30	0.74	0.0031	0.0117	1373	-0.0249	0.0088	3196
30	0.78	0.0057	0.0115	1392	-0.0270	0.0091	3371
30	0.82	0.0048	0.0110	1543	-0.0247	0.0082	2770
30	0.86	0.0006	0.0109	989	-0.0254	0.0093	1717
30	0.90	0.0017	0.0108	2025	-0.0244	0.0077	3271
30	0.94	-0.0012	0.0105	1975	-0.0242	0.0076	3141
30	0.98	-0.0032	0.0103	1689	-0.0250	0.0075	2856
30	1.02	-0.0028	0.0108	1569	-0.0242	0.0069	3303
30	1.04	-0.0030	0.0106	1472	-0.0236	0.0067	3331
30	1.10	-0.0078	0.0116	1794	-0.0207	0.0063	3356
60	0.20	0.0070	0.0133	1561	0.0019	0.0081	3674
60	0.40	0.0081	0.0134	1274	-0.0179	0.0080	3721
60	0.50	0.0098	0.0116	1592	-0.0191	0.0084	3136
60	0.60	0.0055	0.0117	1908	-0.0145	0.0083	2483
60	0.70	0.0055	0.0119	1816	-0.0120	0.0080	3350
60	0.74	0.0059	0.0117	2002	-0.0093	0.0073	3181
60	0.78	0.0022	0.0115	1915	-0.0065	0.0072	3155
60	0.82	0.0018	0.0115	1879	-0.0059	0.0068	3253
60	0.86	0.0003	0.0117	1534	-0.0057	0.0069	3375
60	0.90	-0.0001	0.0119	1645	-0.0031	0.0064	3326
60	0.94	0.0009	0.0114	1375	-0.0008	0.0058	3342
60	0.98	-0.0026	0.0112	1610	0.0019	0.0055	3510
60	1.02	-0.0034	0.0113	1621	0.0058	0.0045	3515
60	1.04	-0.0033	0.0121	1527	0.0078	0.0041	3544
60	1.10	-0.0039	0.0118	1622	0.0112	0.0038	3411

TABLE 3 - CONTINUED

Ψ	r/R	μ_i			λ_i		
		Mean	Standard deviation	# of Measurements	Mean	Standard deviation	# of Measurements
90	0.20	-0.0030	0.0134	1339	0.0046	0.0055	1297
90	0.40	0.0108	0.0129	2171	-0.0125	0.0078	3583
90	0.50	0.0071	0.0131	2936	-0.0102	0.0082	3369
90	0.60	0.0063	0.0143	2850	-0.0046	0.0082	2451
90	0.70	0.0026	0.0134	2898	0.0001	0.0084	2885
90	0.74	0.0014	0.0132	2890	0.0010	0.0089	3762
90	0.78	0.0012	0.0133	3060	0.0039	0.0084	3360
90	0.82	0.0007	0.0132	3066	0.0060	0.0085	3781
90	0.86	-0.0008	0.0128	2686	0.0080	0.0081	3868
90	0.90	-0.0068	0.0139	2475	0.0097	0.0043	3374
90	0.94	-0.0060	0.0144	2531	0.0103	0.0044	3415
90	0.98	-0.0061	0.0140	2368	0.0098	0.0044	3430
90	1.02	-0.0041	0.0137	1737	0.0085	0.0042	3466
90	1.04	-0.0045	0.0136	2075	0.0077	0.0042	3434
90	1.10	-0.0063	0.0132	2073	0.0061	0.0036	3537
120	0.20	-0.0062	0.0110	1820	0.0094	0.0087	3071
120	0.40	0.0051	0.0126	2060	-0.0052	0.0094	3103
120	0.50	0.0039	0.0119	2283	-0.0022	0.0077	2824
120	0.60	0.0035	0.0120	2553	0.0001	0.0076	3389
120	0.70	-0.0003	0.0115	2011	0.0030	0.0071	2353
120	0.74	-0.0033	0.0114	1711	0.0037	0.0066	2012
120	0.78	-0.0063	0.0116	1869	0.0057	0.0060	2641
120	0.82	-0.0046	0.0109	2834	0.0066	0.0061	2767
120	0.86	-0.0101	0.0108	1507	0.0060	0.0059	1535
120	0.90	-0.0093	0.0107	2174	0.0063	0.0057	2715
120	0.94	-0.0104	0.0102	2234	0.0060	0.0055	2539
120	0.98	-0.0110	0.0105	2351	0.0055	0.0054	2742
120	1.02	-0.0085	0.0108	2436	0.0038	0.0050	3026
120	1.04	-0.0125	0.0107	2519	0.0033	0.0050	3058
120	1.10	-0.0108	0.0108	2737	0.0026	0.0049	3043
150	0.20	-0.0145	0.0100	2287	0.0119	0.0084	3192
150	0.40	-0.0056	0.0097	2510	0.0017	0.0076	3247
150	0.50	-0.0068	0.0103	2394	0.0020	0.0085	3362
150	0.60	-0.0042	0.0097	2007	0.0027	0.0102	3520
150	0.70	-0.0048	0.0098	2320	0.0042	0.0100	3339
150	0.74	-0.0056	0.0107	2768	0.0044	0.0107	3482
150	0.78	-0.0071	0.0110	2196	0.0044	0.0107	3352
150	0.82	-0.0060	0.0110	2515	0.0048	0.0091	3189
150	0.86	-0.0074	0.0114	2749	0.0047	0.0087	2501
150	0.90	-0.0084	0.0112	2772	0.0044	0.0079	2620
150	0.94	-0.0086	0.0116	2777	0.0047	0.0069	2764
150	0.98	-0.0100	0.0112	2703	0.0044	0.0063	2996
150	1.02	-0.0100	0.0115	2758	0.0038	0.0059	2814
150	1.04	-0.0108	0.0113	2765	0.0038	0.0057	2937
150	1.10	-0.0122	0.0113	2758	0.0026	0.0055	2770

TABLE 3 - CONTINUED

Ψ	r/R		μ_i			λ_i		
			Mean	Standard deviation	# of Measurements	Mean	Standard deviation	# of Measurements
180	0.20		-0.0158	0.0095	2373	0.0144	0.0075	3267
180	0.40		-0.0125	0.0104	2492	0.0093	0.0082	3278
180	0.50		-0.0125	0.0108	2767	0.0093	0.0104	2834
180	0.60		-0.0134	0.0107	2753	0.0094	0.0114	2819
180	0.70		-0.0154	0.0105	2752	0.0094	0.0105	2908
180	0.74		-0.0160	0.0104	2083	0.0094	0.0112	3084
180	0.78		-0.0157	0.0105	2191	0.0088	0.0104	3100
180	0.82		-0.0169	0.0108	2440	0.0092	0.0095	3032
180	0.86		-0.0170	0.0105	2708	0.0082	0.0089	3055
180	0.90		-0.0172	0.0105	2585	0.0082	0.0079	3011
180	0.94		-0.0180	0.0100	2304	0.0086	0.0079	3122
180	0.98		-0.0197	0.0101	2016	0.0083	0.0077	3187
180	1.02		-0.0200	0.0097	1836	0.0082	0.0069	3204
210	0.20		-0.0173	0.0105	2573	0.0185	0.0069	3613
210	0.40		-0.0095	0.0125	2852	0.0066	0.0106	3603
210	0.50		-0.0087	0.0130	2916	0.0049	0.0124	3585
210	0.60		-0.0097	0.0125	2344	0.0020	0.0077	2204
210	0.70		-0.0115	0.0128	2388	0.0020	0.0079	2352
210	0.74		-0.0085	0.0119	2455	0.0024	0.0080	2541
210	0.78		-0.0097	0.0118	2531	0.0029	0.0078	2599
210	0.82		-0.0110	0.0112	2333	0.0037	0.0086	2899
210	0.86		-0.0078	0.0113	2544	0.0025	0.0074	2656
210	0.90		-0.0089	0.0111	2582	0.0025	0.0069	2697
210	0.94		-0.0117	0.0107	2586	0.0035	0.0070	2896
210	0.98		-0.0115	0.0105	2662	0.0028	0.0069	2853
210	1.02		-0.0145	0.0100	2675	0.0030	0.0067	2988
210	1.04		-0.0122	0.0097	2477	0.0030	0.0065	3007
210	1.10		-0.0142	0.0093	2071	0.0026	0.0066	3100
240	0.20		-0.0097	0.0113	3040	0.0156	0.0070	3078
240	0.40		-0.0075	0.0132	2934	0.0028	0.0105	2979
240	0.50		-0.0031	0.0127	2674	-0.0017	0.0103	2595
240	0.60		-0.0055	0.0135	2666	-0.0013	0.0111	3224
240	0.70		-0.0056	0.0133	2844	-0.0011	0.0116	3125
240	0.74		-0.0057	0.0133	1982	-0.0020	0.0116	3252
240	0.78		-0.0081	0.0129	2605	-0.0007	0.0098	2019
240	0.82		-0.0069	0.0125	2560	-0.0010	0.0114	2926
240	0.86		-0.0067	0.0123	2756	-0.0006	0.0104	2971
240	0.90		-0.0053	0.0120	2696	0.0006	0.0089	2951
240	0.94		-0.0060	0.0115	2760	0.0015	0.0073	2670
240	0.98		-0.0089	0.0115	2722	0.0022	0.0073	2974
240	1.02		-0.0079	0.0113	1921	0.0027	0.0070	2591
240	1.04		-0.0094	0.0111	2784	0.0025	0.0067	2951
240	1.10		-0.0068	0.0110	1860	0.0016	0.0069	2152

TABLE 3 - CONCLUDED

Ψ	r/R	μ_i	Mean	Standard deviation	# of Measurements	λ_i	Mean	Standard deviation	# of Measurements
270	0.20	-0.0043	0.0110	2769	0.0117	0.0071	2357		
270	0.40	-0.0024	0.0116	2688	0.0016	0.0090	3009		
270	0.50	-0.0021	0.0116	2727	-0.0006	0.0093	3006		
270	0.60	-0.0028	0.0119	2700	-0.0015	0.0090	2999		
270	0.70	-0.0048	0.0117	2863	-0.0029	0.0090	2412		
270	0.74	-0.0032	0.0118	2795	-0.0030	0.0091	2877		
270	0.78	-0.0040	0.0118	2753	-0.0029	0.0092	3175		
270	0.82	-0.0023	0.0113	2574	-0.0027	0.0091	3069		
270	0.86	-0.0016	0.0111	2693	-0.0020	0.0074	2350		
270	0.90	-0.0024	0.0111	2780	-0.0015	0.0069	2872		
270	0.94	-0.0024	0.0110	2658	-0.0006	0.0063	3007		
270	0.98	-0.0032	0.0113	2642	0.0009	0.0058	2912		
270	1.02	-0.0053	0.0109	2458	0.0027	0.0052	3052		
270	1.04	-0.0032	0.0119	2454	0.0026	0.0053	3033		
270	1.10	-0.0030	0.0121	2605	0.0029	0.0055	3098		
300	0.20	0.0049	0.0124	2655	0.0105	0.0073	2573		
300	0.40	0.0023	0.0129	2564	0.0043	0.0089	2110		
300	0.50	0.0009	0.0137	2554	0.0017	0.0084	2123		
300	0.60	0.0010	0.0131	2481	-0.0024	0.0075	2438		
300	0.70	-0.0001	0.0123	2515	-0.0035	0.0074	2102		
300	0.74	-0.0010	0.0124	2531	-0.0050	0.0082	2251		
300	0.78	-0.0016	0.0115	2556	-0.0066	0.0084	2291		
300	0.82	-0.0024	0.0119	2579	-0.0072	0.0079	1925		
300	0.86	0.0017	0.0117	2550	-0.0072	0.0082	2312		
300	0.90	-0.0005	0.0115	2509	-0.0082	0.0080	1837		
300	0.94	0.0003	0.0113	2530	-0.0089	0.0091	2561		
300	0.98	-0.0021	0.0116	2467	-0.0090	0.0089	2327		
300	1.02	-0.0024	0.0116	2427	-0.0078	0.0089	2300		
300	1.04	-0.0025	0.0126	2429	-0.0062	0.0080	2334		
300	1.10	-0.0043	0.0133	2358	-0.0031	0.0075	2291		
330	0.20	0.0097	0.0132	2694	0.0103	0.0085	2383		
330	0.40	0.0072	0.0134	2495	0.0011	0.0067	1985		
330	0.50	0.0085	0.0147	2517	0.0007	0.0075	2084		
330	0.60	0.0094	0.0158	2485	-0.0019	0.0072	2396		
330	0.70	0.0096	0.0160	2376	-0.0038	0.0065	2425		
330	0.74	0.0078	0.0158	2376	-0.0045	0.0072	2385		
330	0.78	0.0043	0.0145	2606	-0.0041	0.0064	2406		
330	0.82	0.0040	0.0145	2635	-0.0046	0.0066	2323		
330	0.86	0.0074	0.0152	1996	-0.0068	0.0089	2425		
330	0.90	0.0064	0.0146	2100	-0.0082	0.0089	2490		
330	0.94	0.0032	0.0144	2562	-0.0099	0.0096	2496		
330	0.98	0.0070	0.0168	2125	-0.0108	0.0111	2466		
330	1.02	0.0046	0.0155	1763	-0.0114	0.0102	2333		
330	1.04	0.0037	0.0138	2062	-0.0121	0.0104	2375		
330	1.10	-0.0012	0.0144	2084	-0.0120	0.0096	2427		



Figure 1. Aerial view of 14- by 22- Foot Subsonic Tunnel.

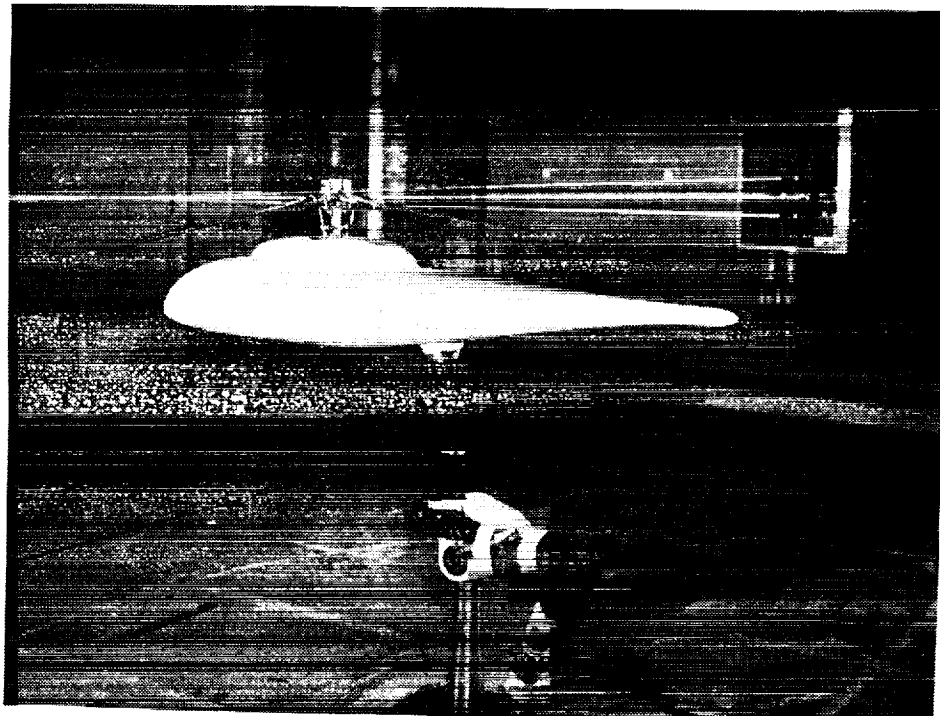


Figure 2. 2 MRTS mounted in forward bay of the test section.

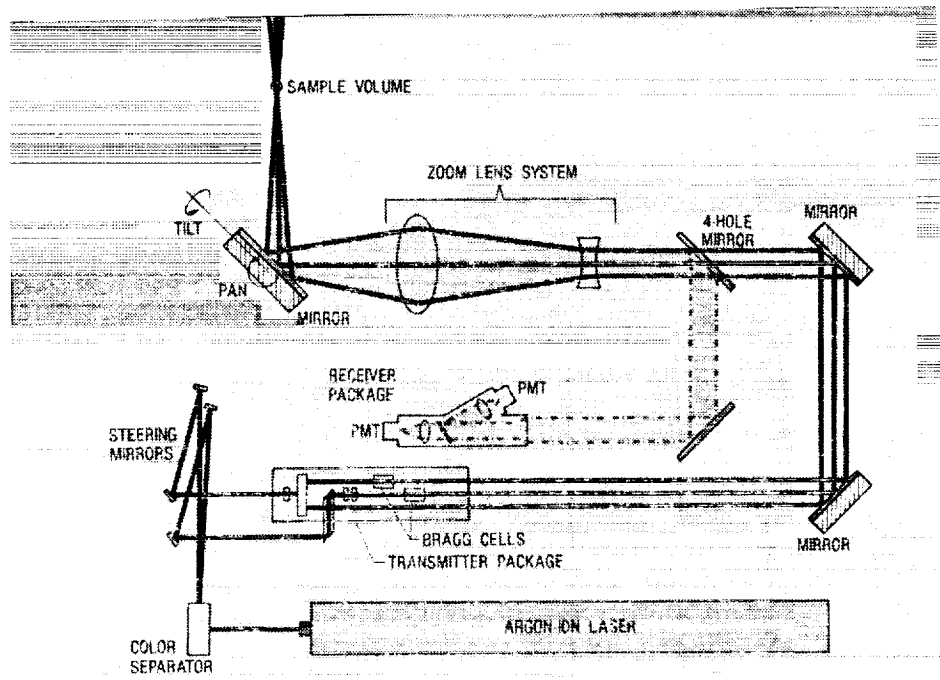


Figure 3. Schematic of Laser Velocimeter optics subsystem.

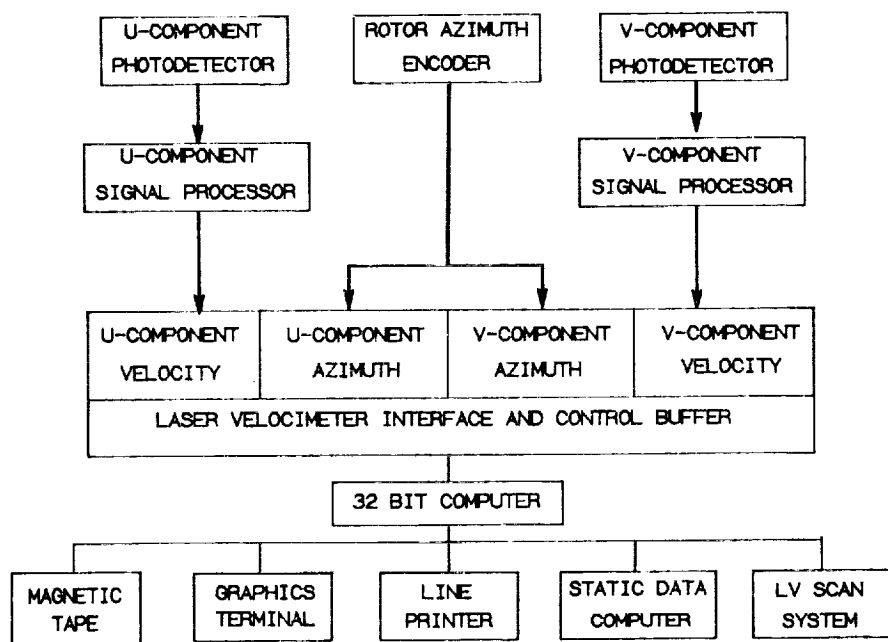


Figure 4. Schematic of data acquisition and control subsystem.

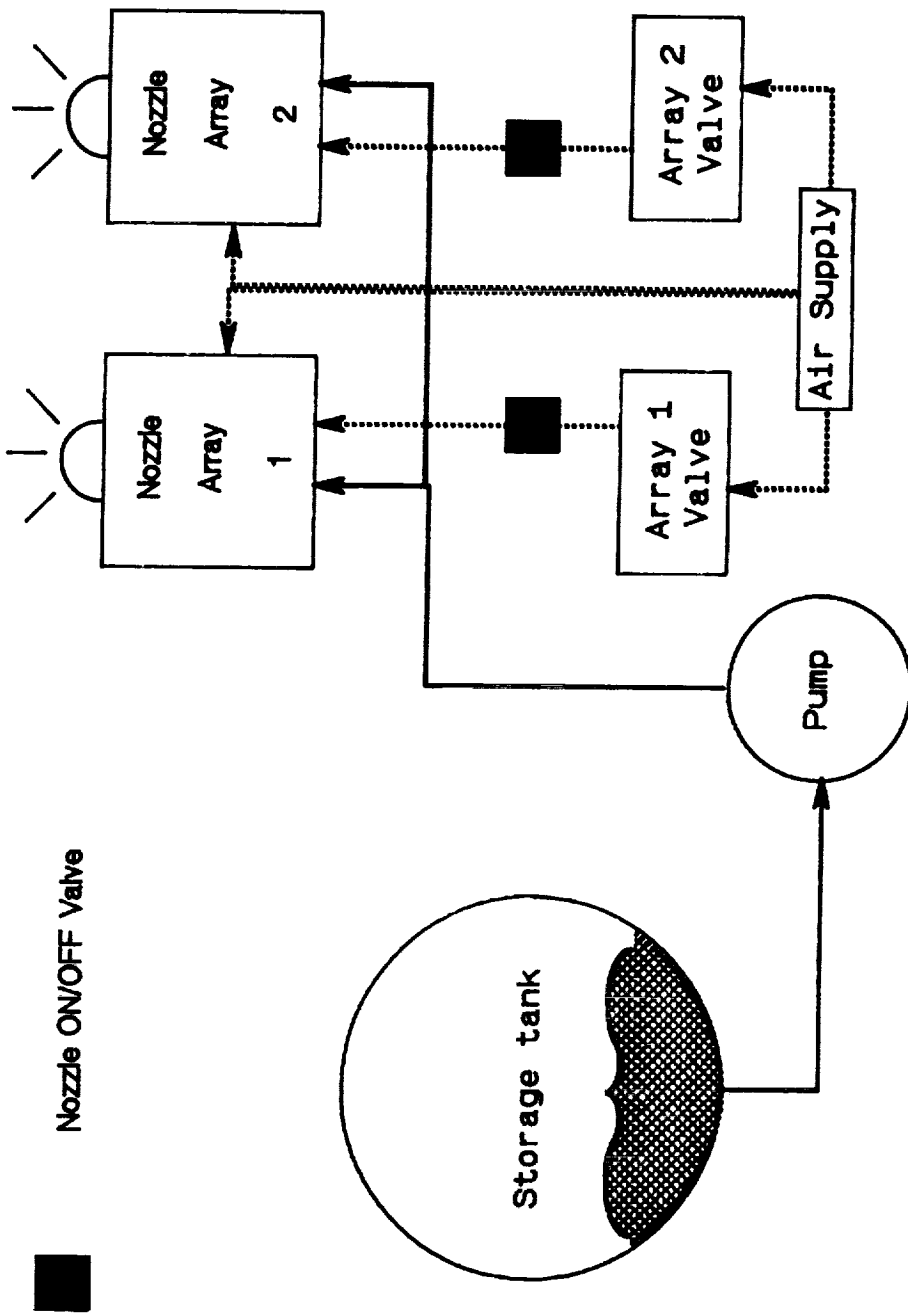


Figure 5. Schematic of seeding system.

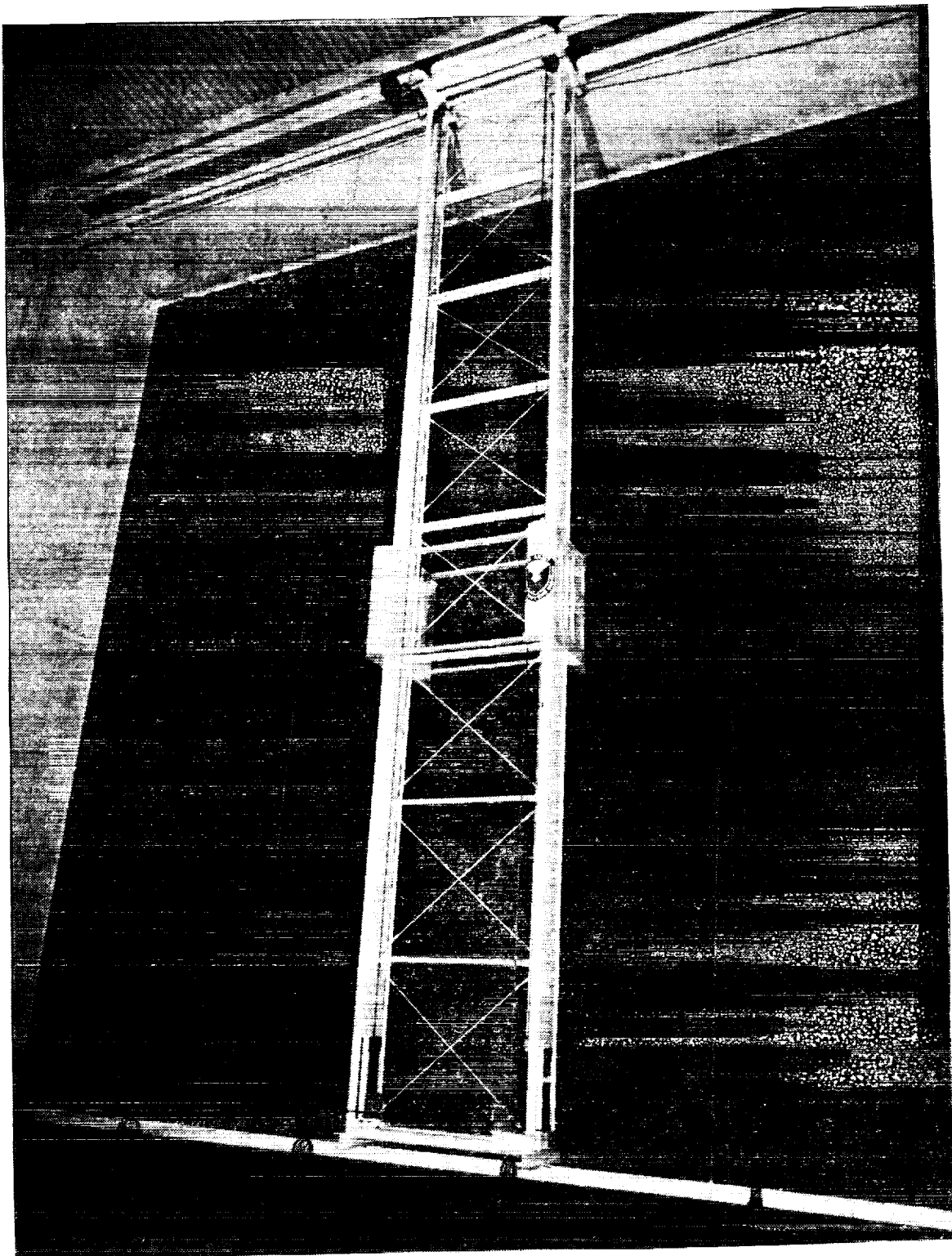


Figure 6. Photograph of remote control positioner for seeding system.

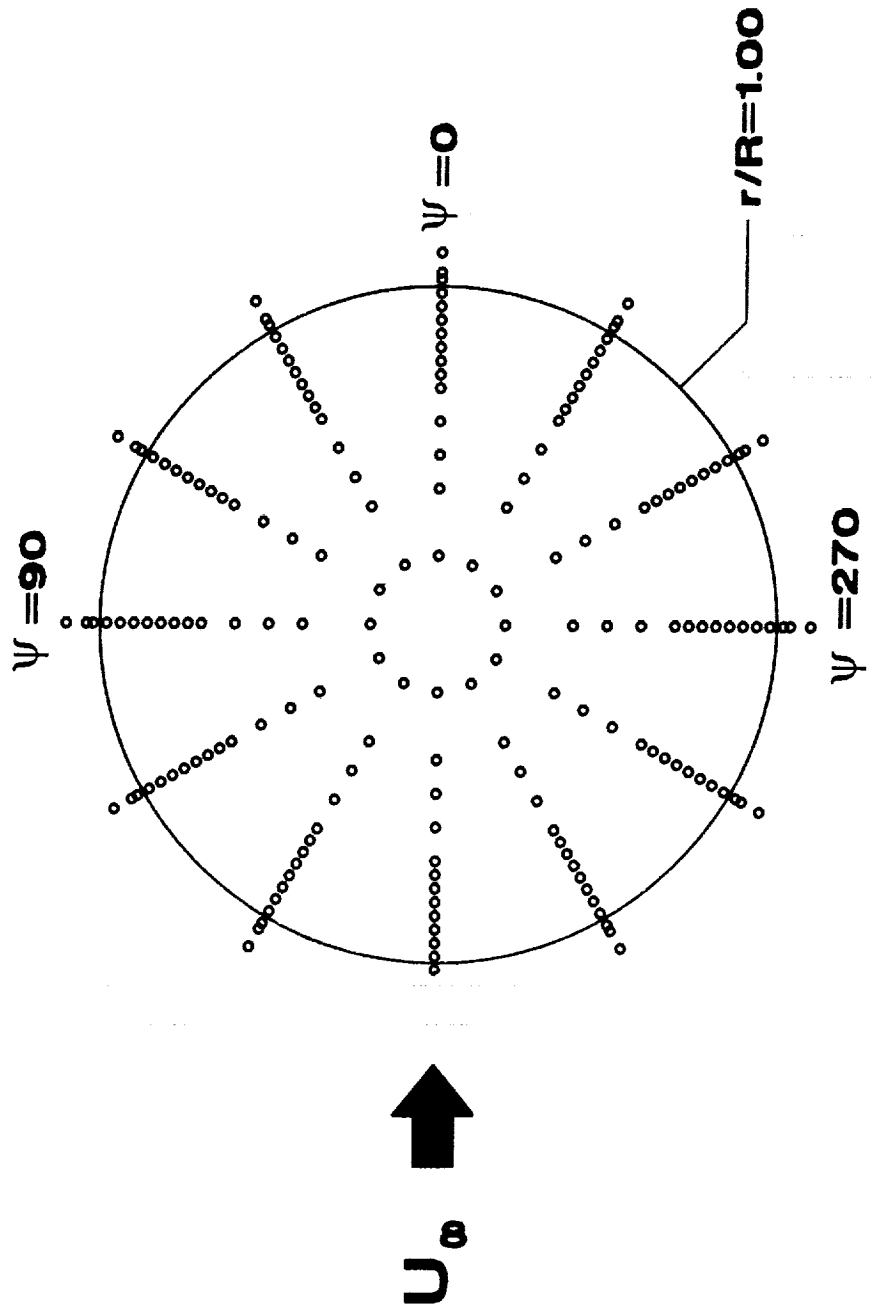


Figure 7. Locations of velocity measurements, 3.0 inches above rotor tip path plane.

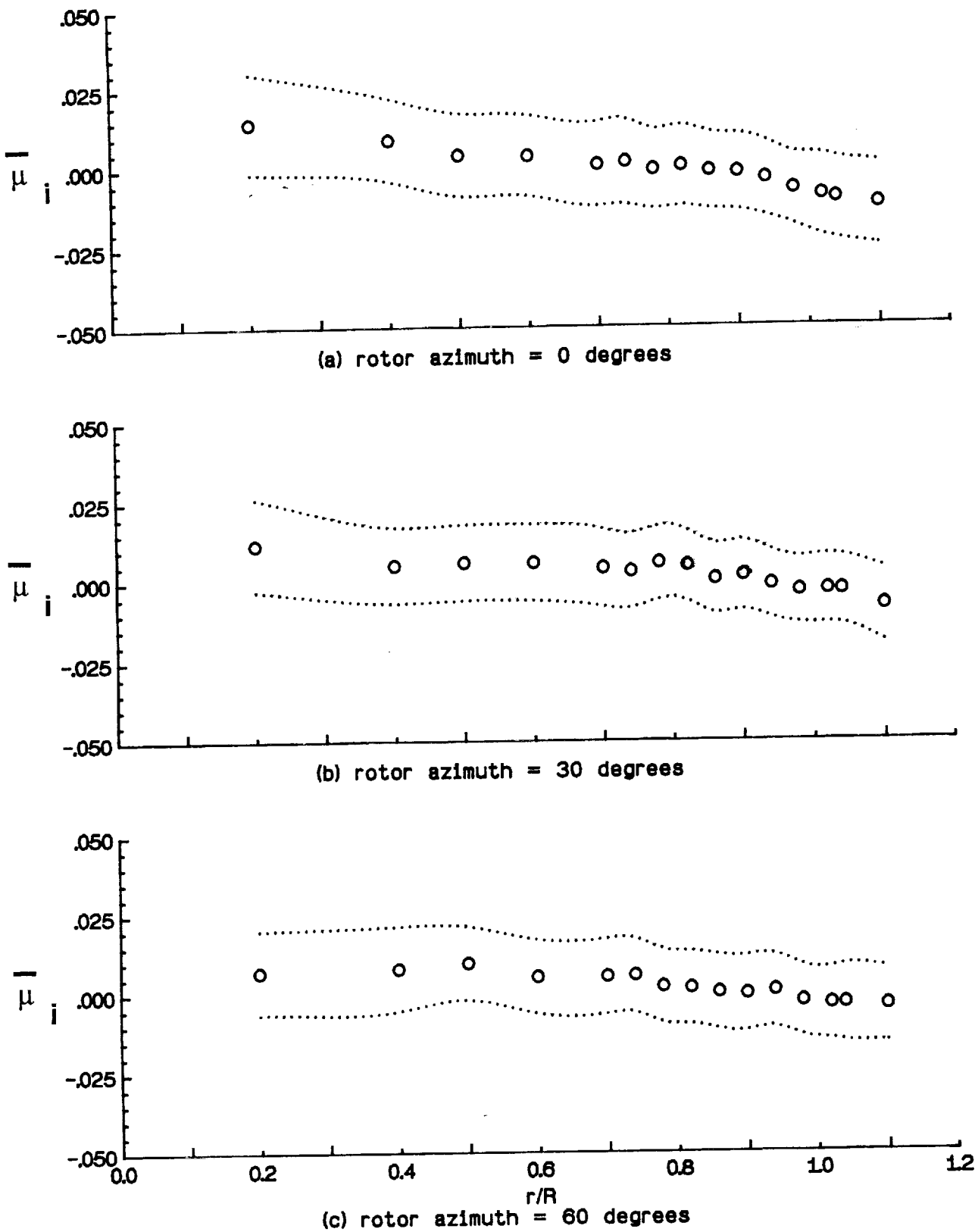


Figure 8. Radial distribution of mean induced inflow ratio $\bar{\mu}_i$.

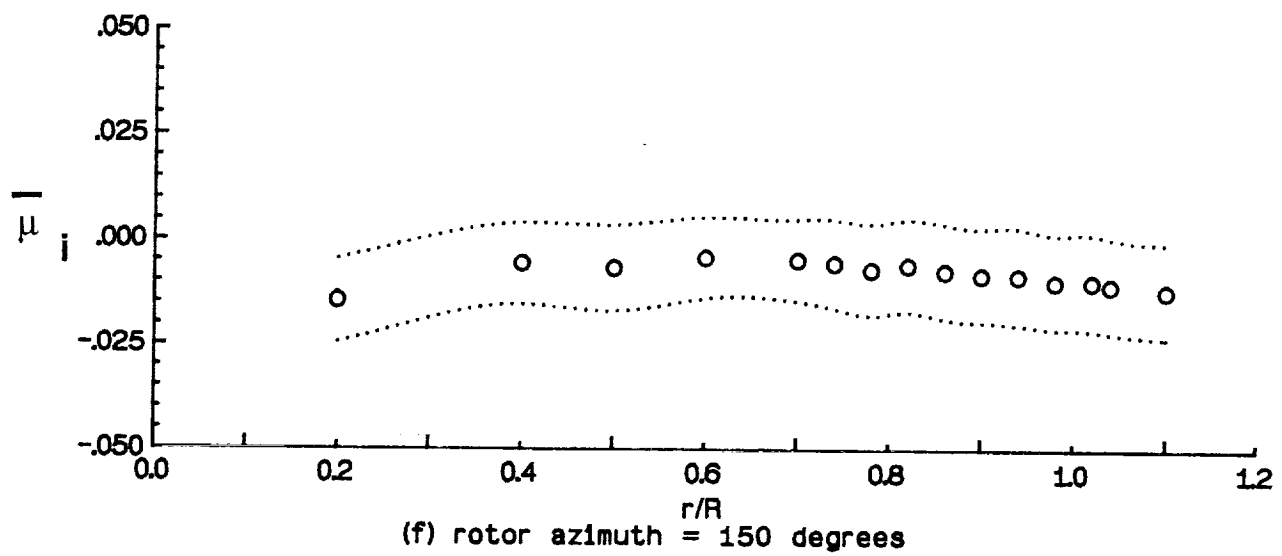
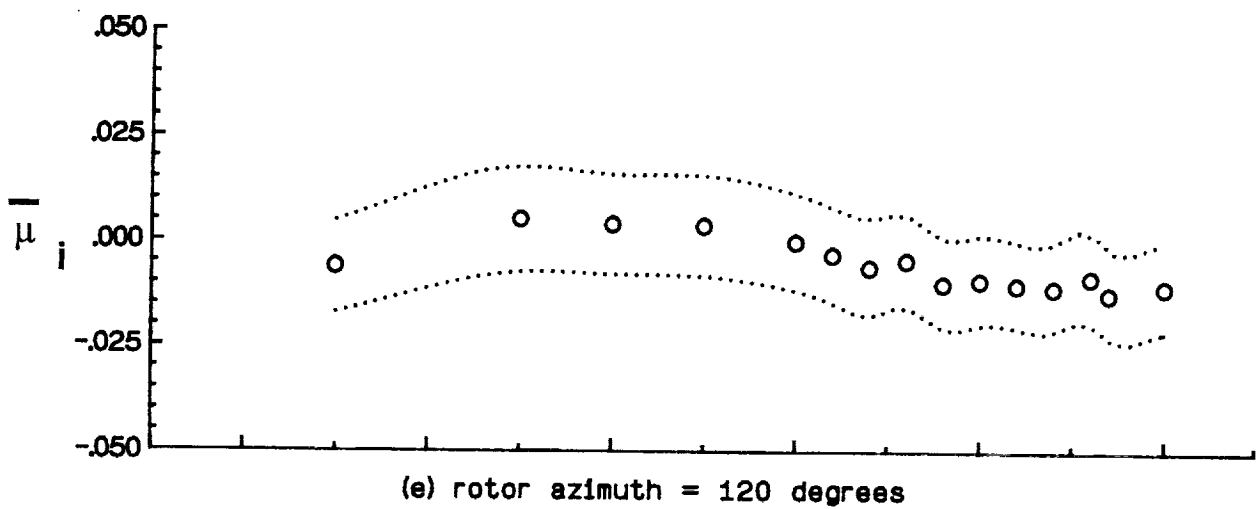
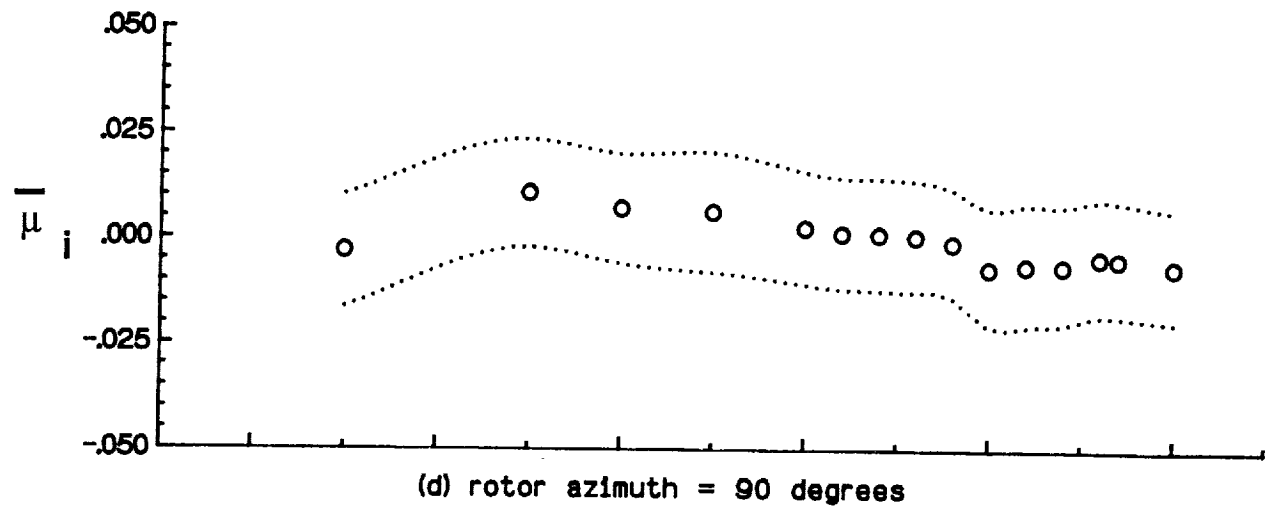
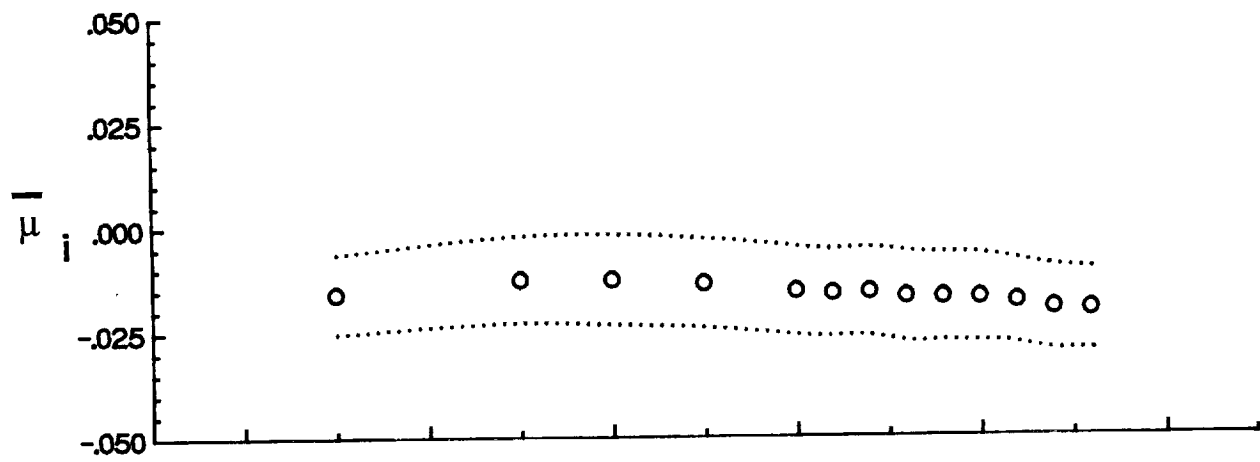
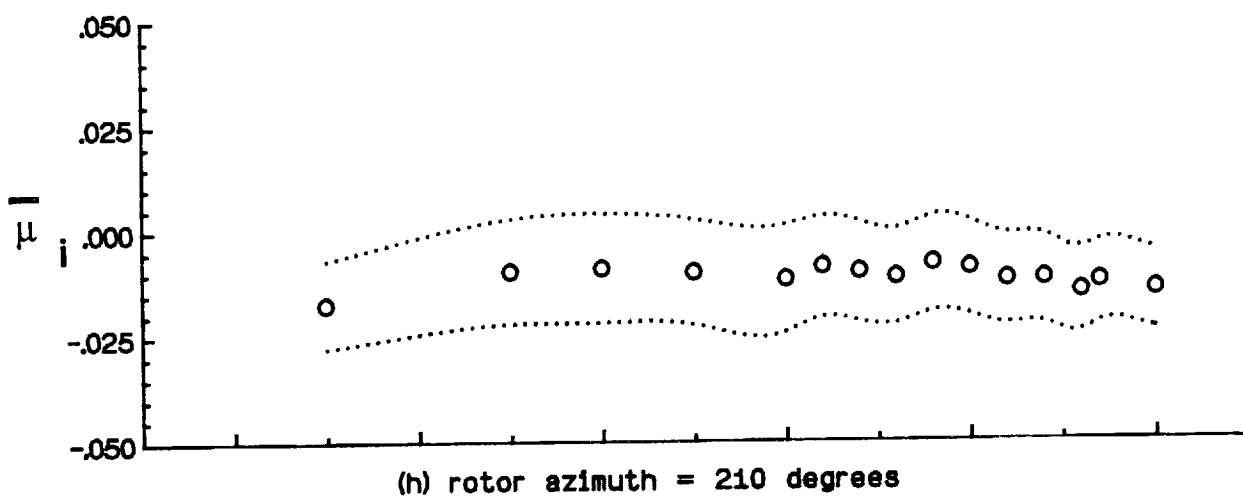


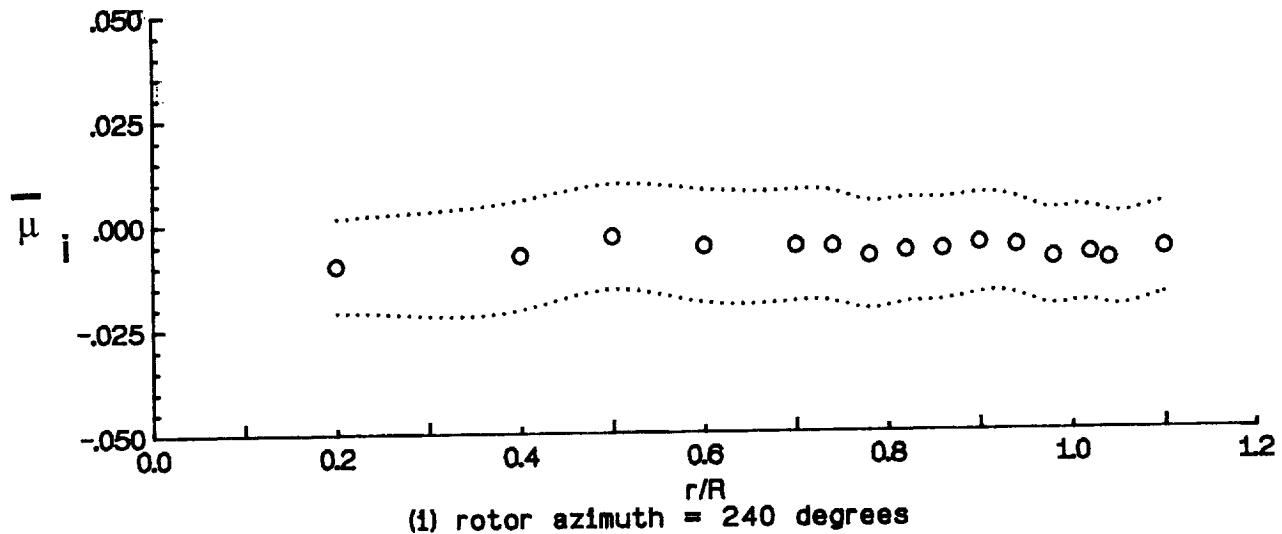
Figure 8. Continued.



(g) rotor azimuth = 180 degrees



(h) rotor azimuth = 210 degrees



(i) rotor azimuth = 240 degrees

Figure 8. Continued.

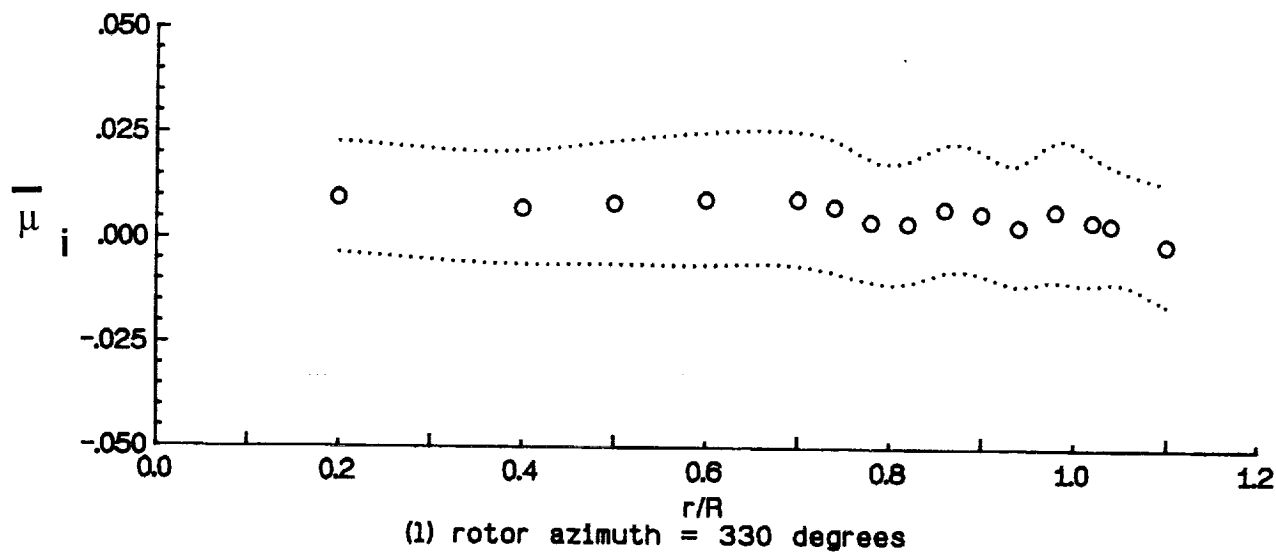
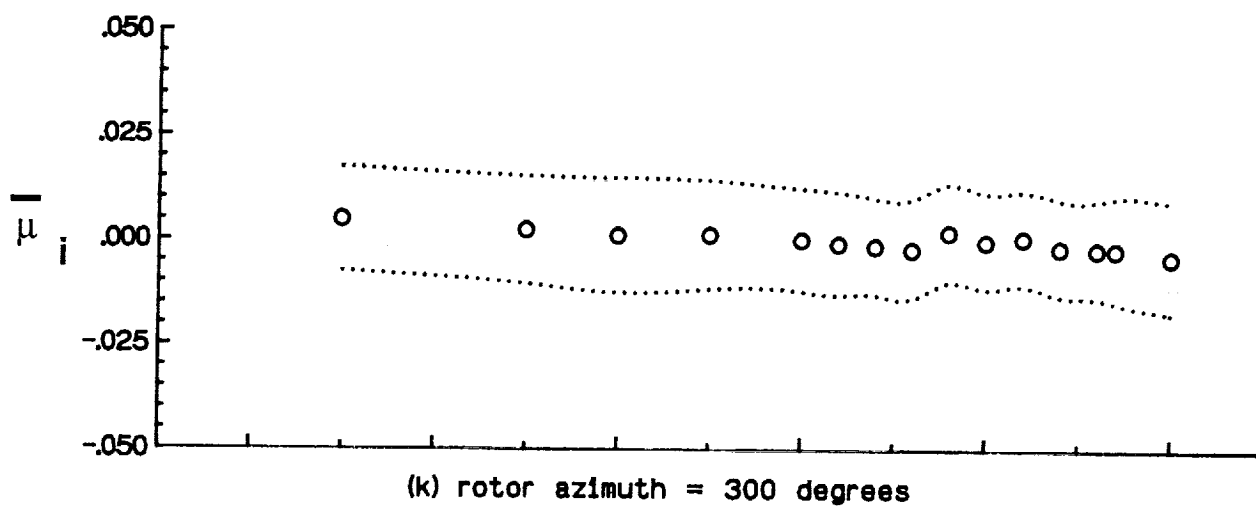
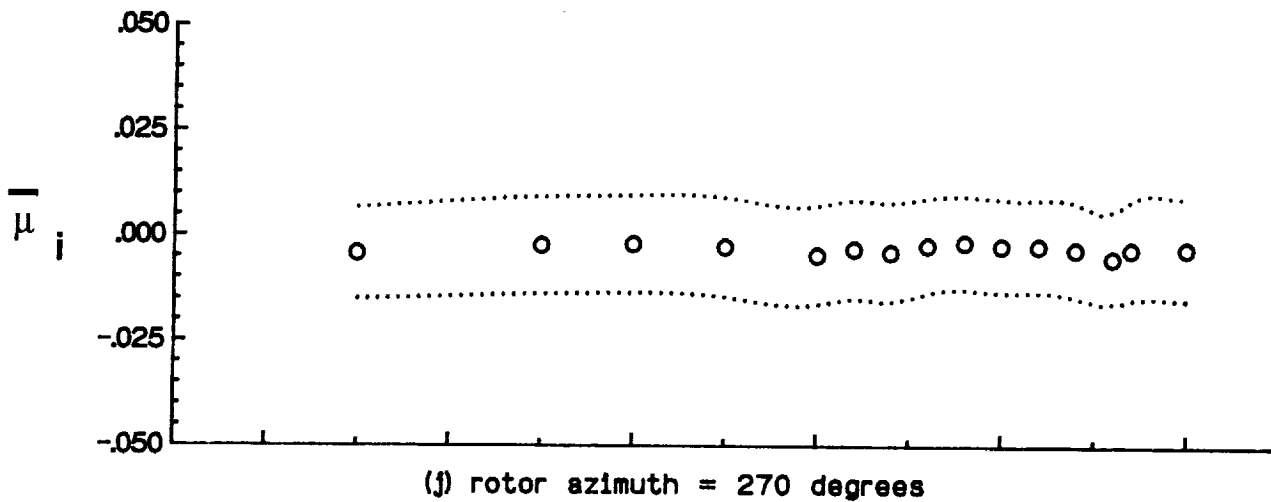


Figure 8. Concluded.

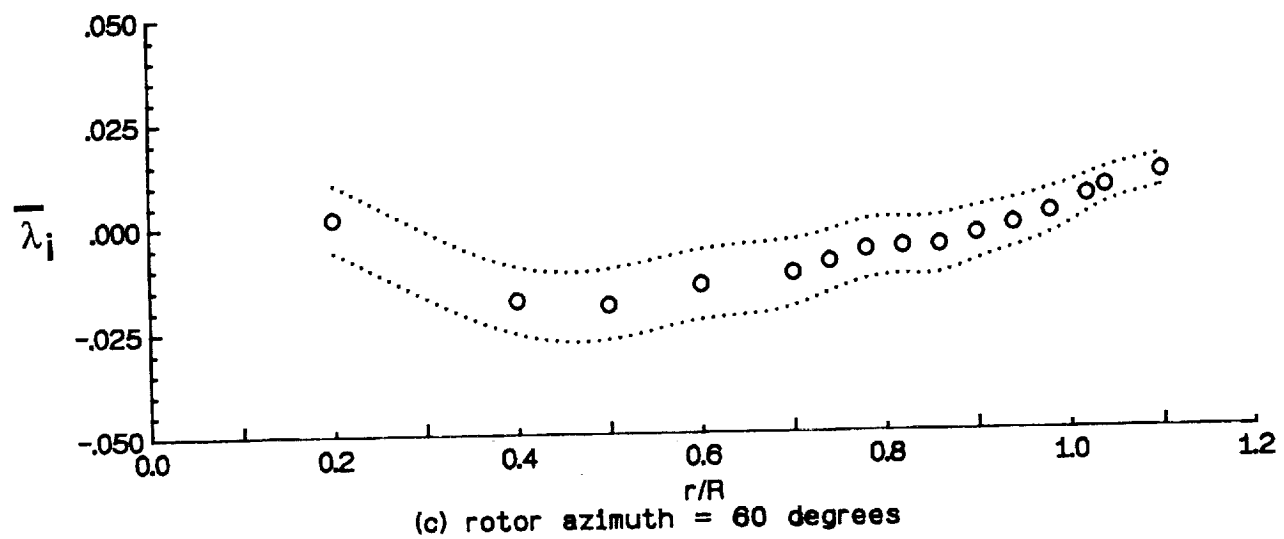
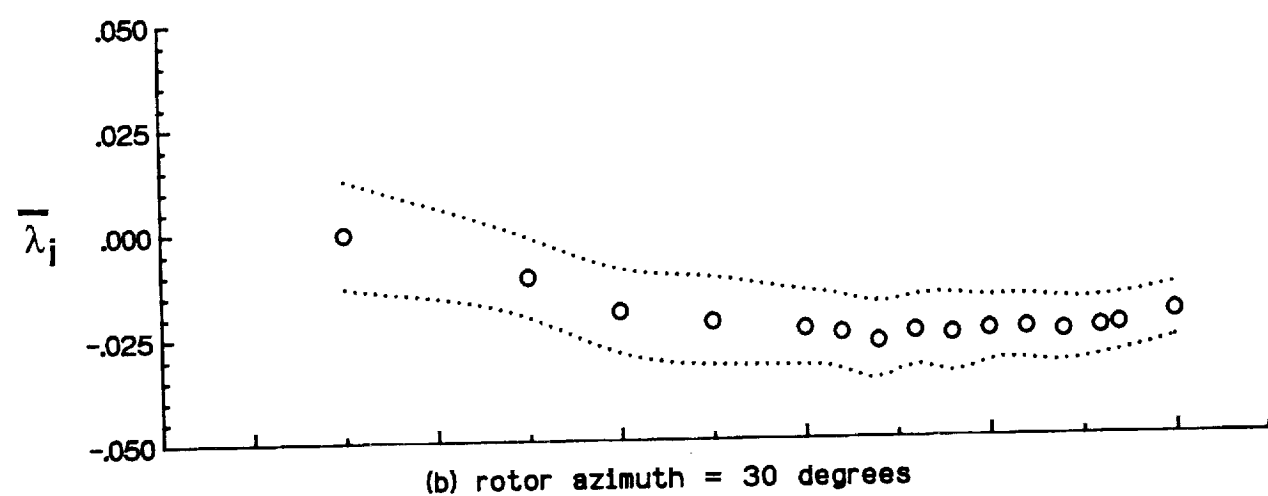
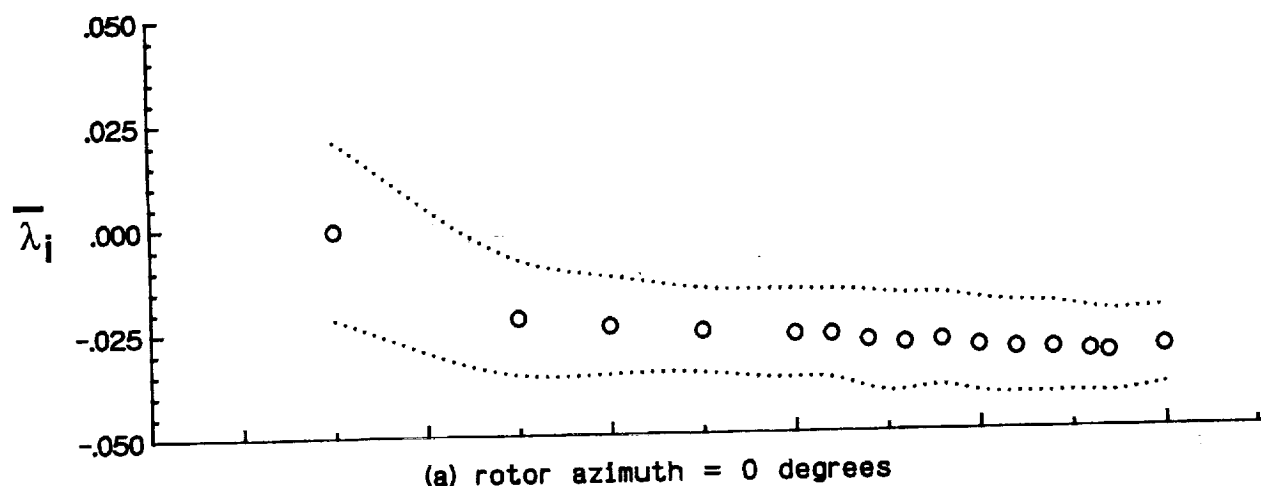


Figure 9. Radial distribution of mean induced inflow ratio - $\bar{\lambda}_i$.

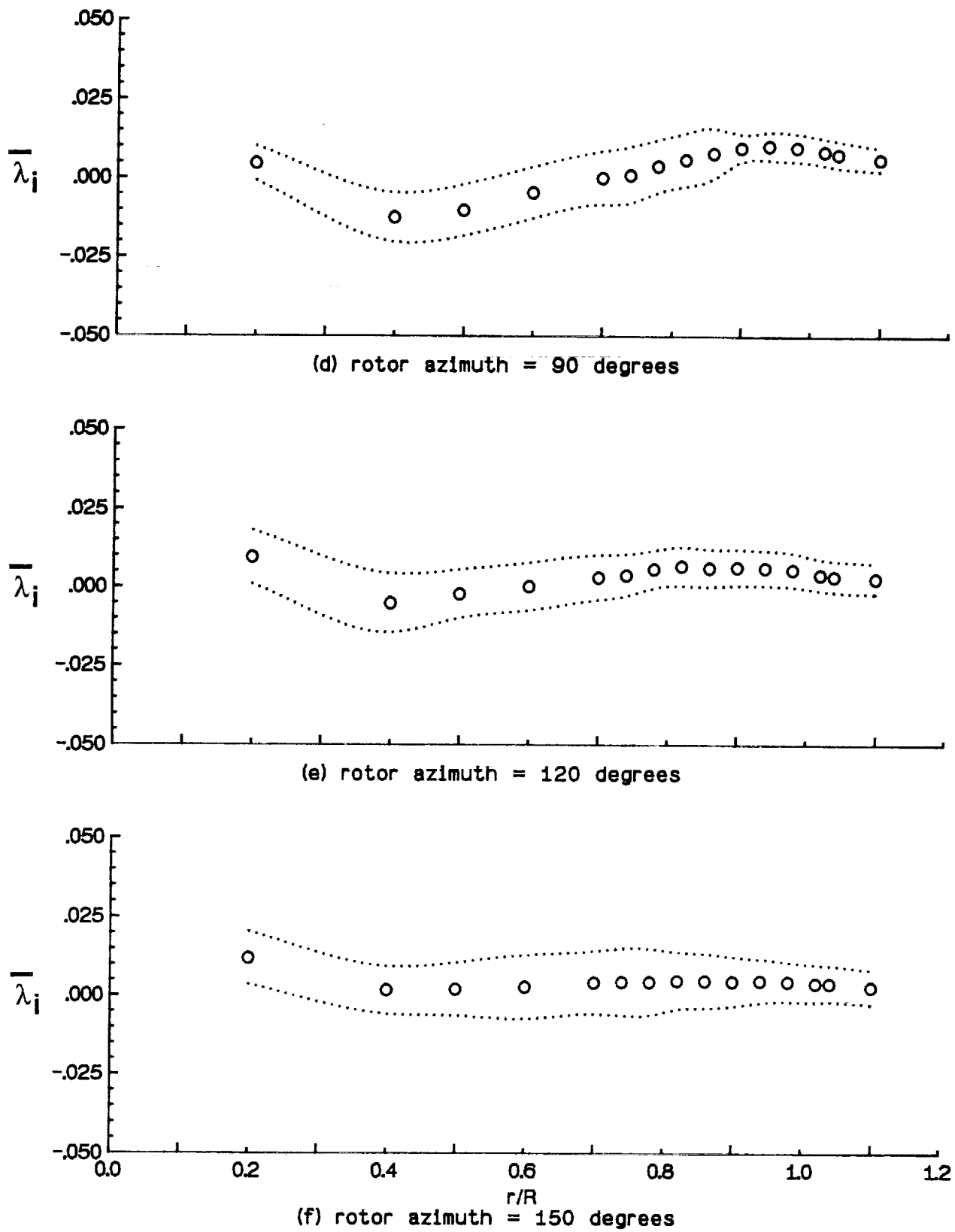
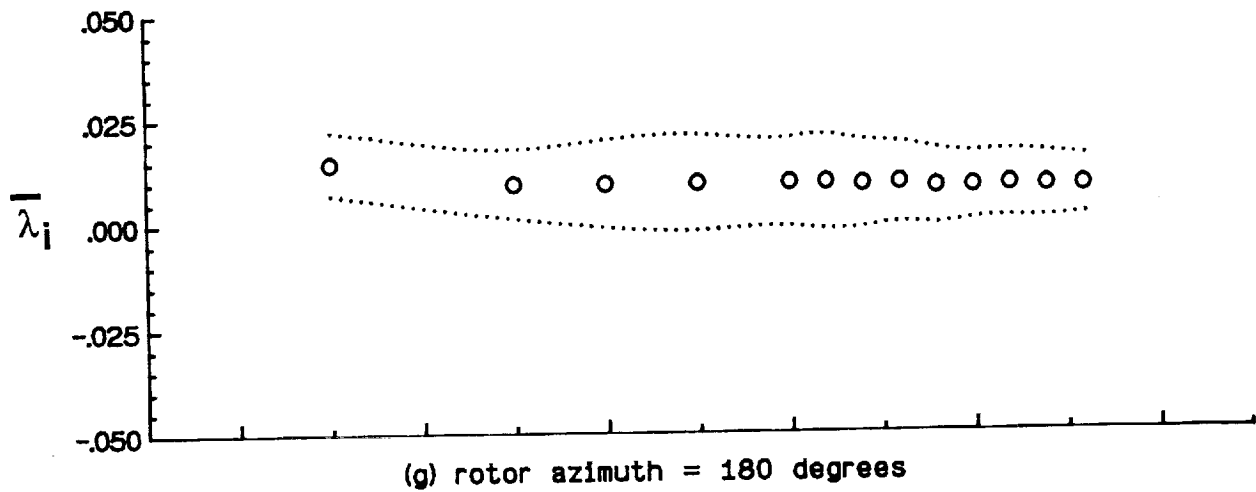
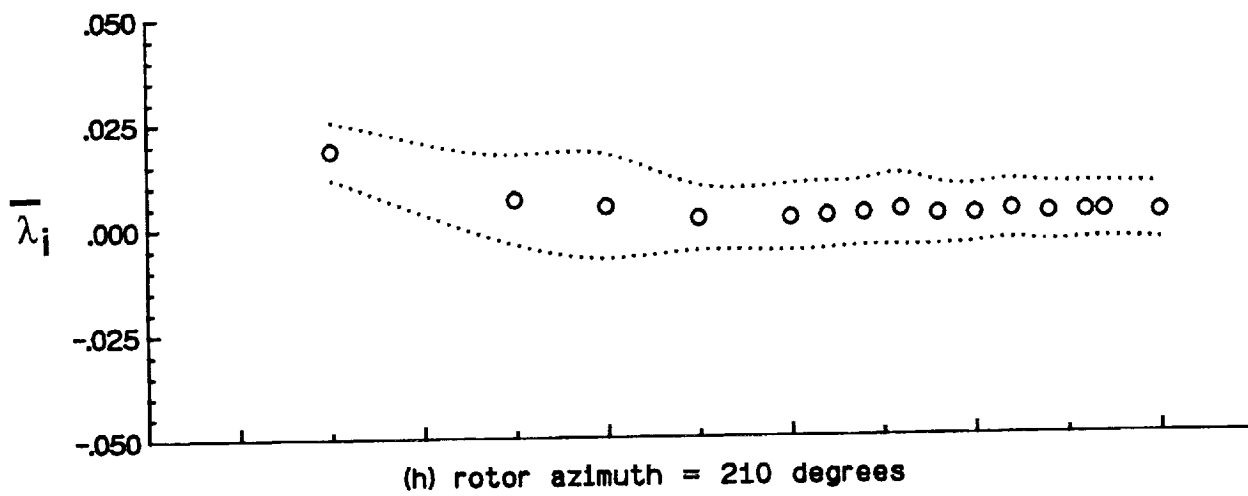


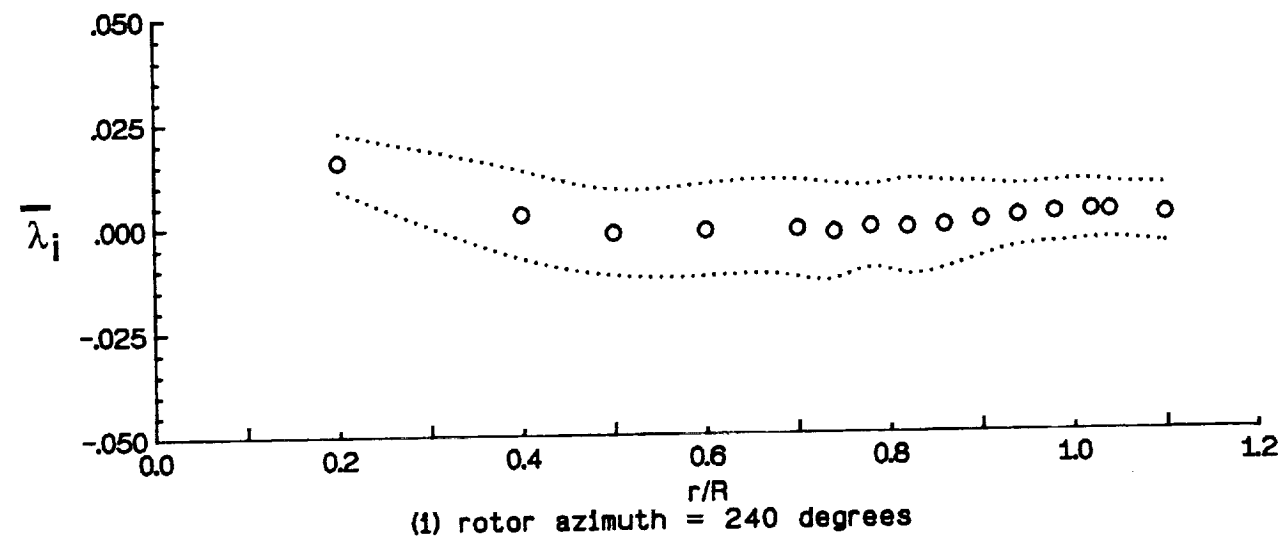
Figure 9. Continued.



(g) rotor azimuth = 180 degrees



(h) rotor azimuth = 210 degrees



(i) rotor azimuth = 240 degrees

Figure 9. Continued.

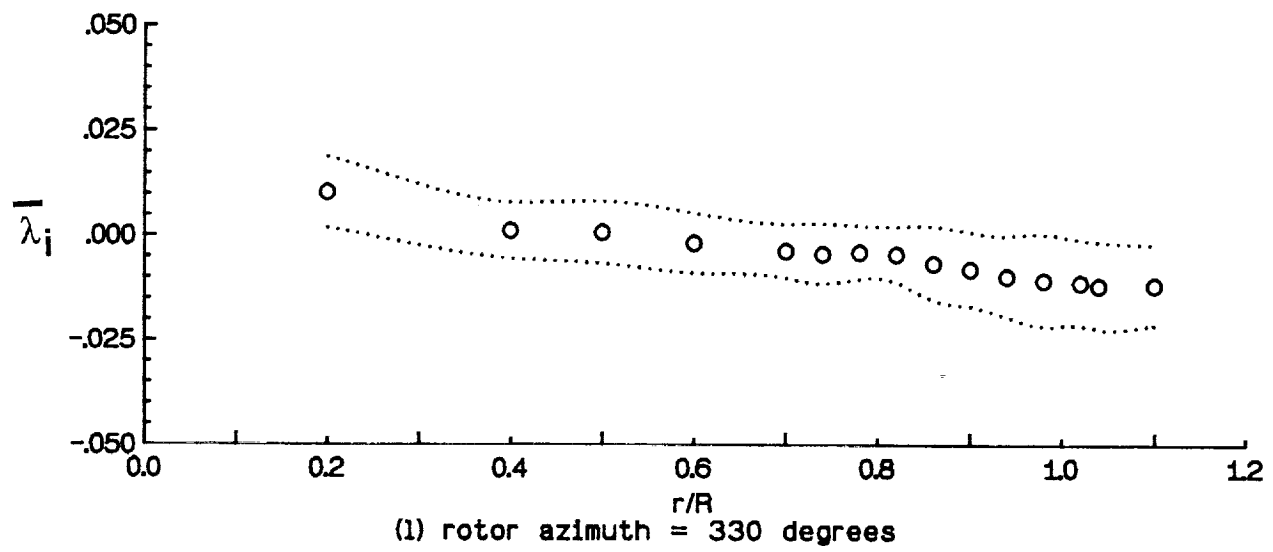
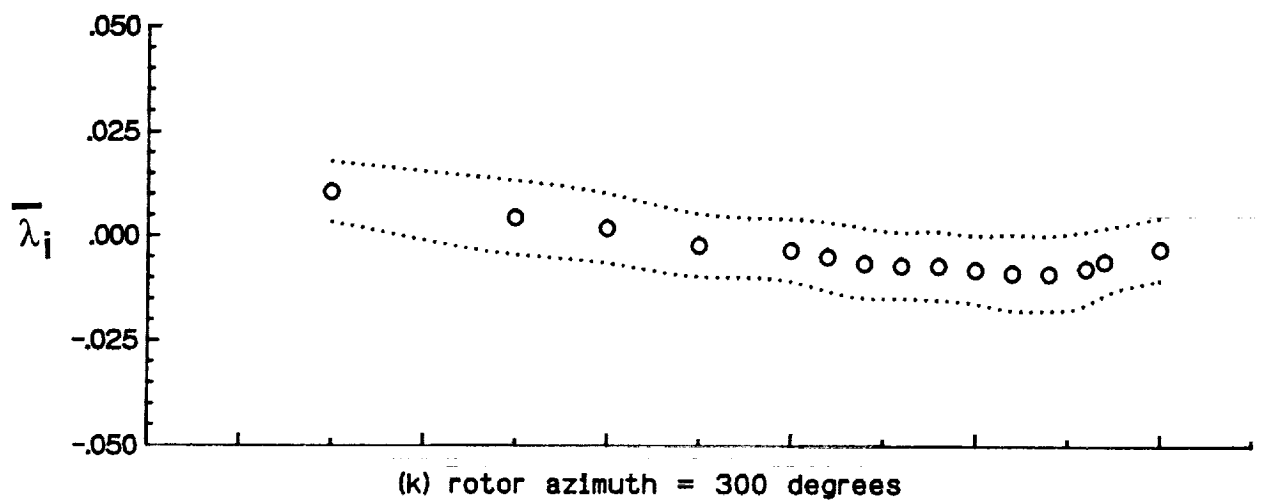
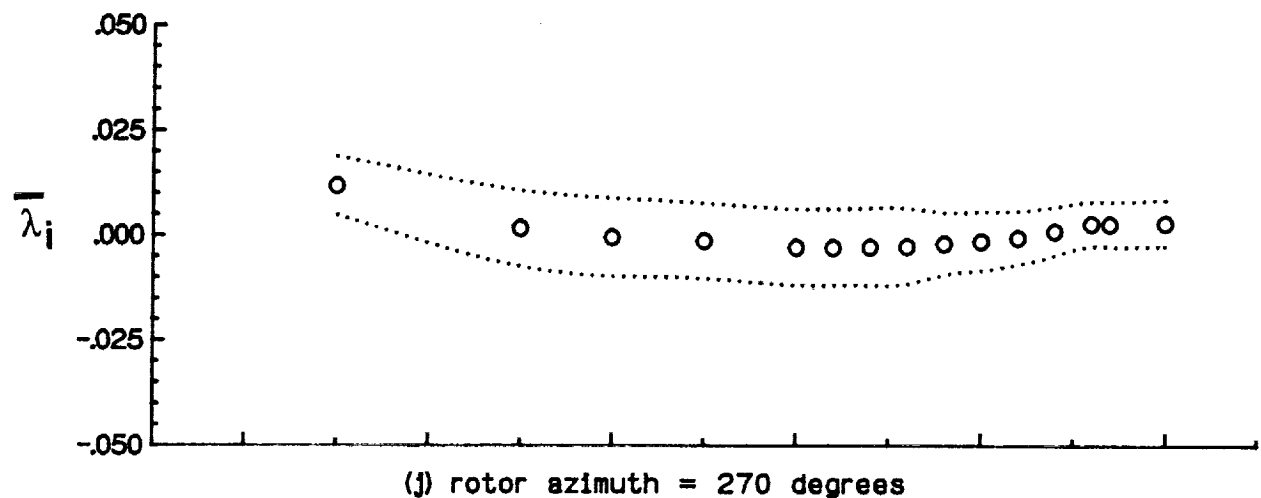


Figure 9. Concluded.



$$\int_{\mathbb{R}^d} \psi(t) \left| \int_0^t \nabla u(s) ds \right|^2 dx \leq C \int_0^t \| \nabla u(s) \|_{L^2(\mathbb{R}^d)}^2 ds.$$

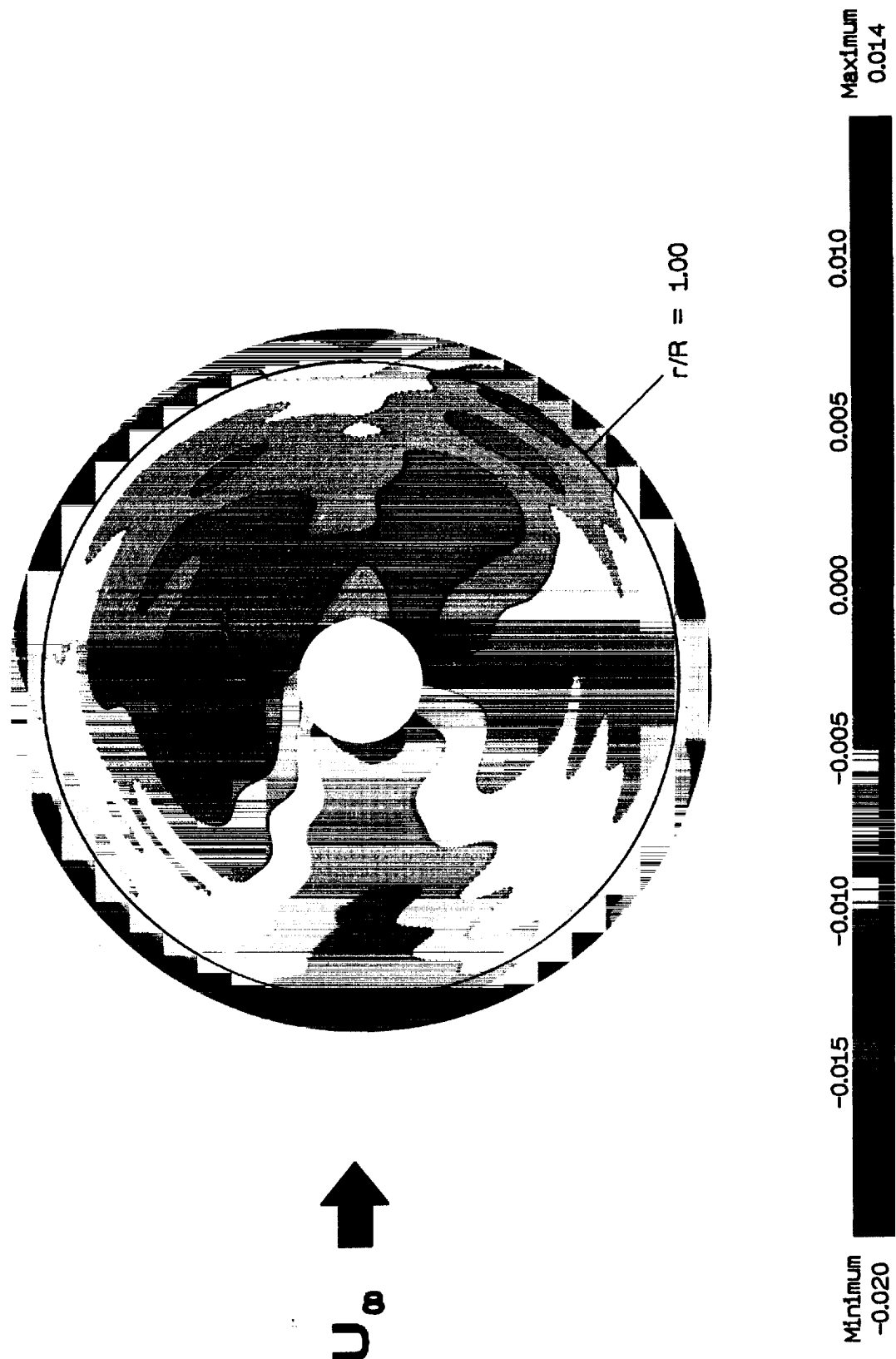


Figure 10. Contour plot of mean induced inflow ratio \bar{U}_i^8 .



Figure 11. Contour plot of mean induced inflow ratio $\bar{\lambda}_i$.

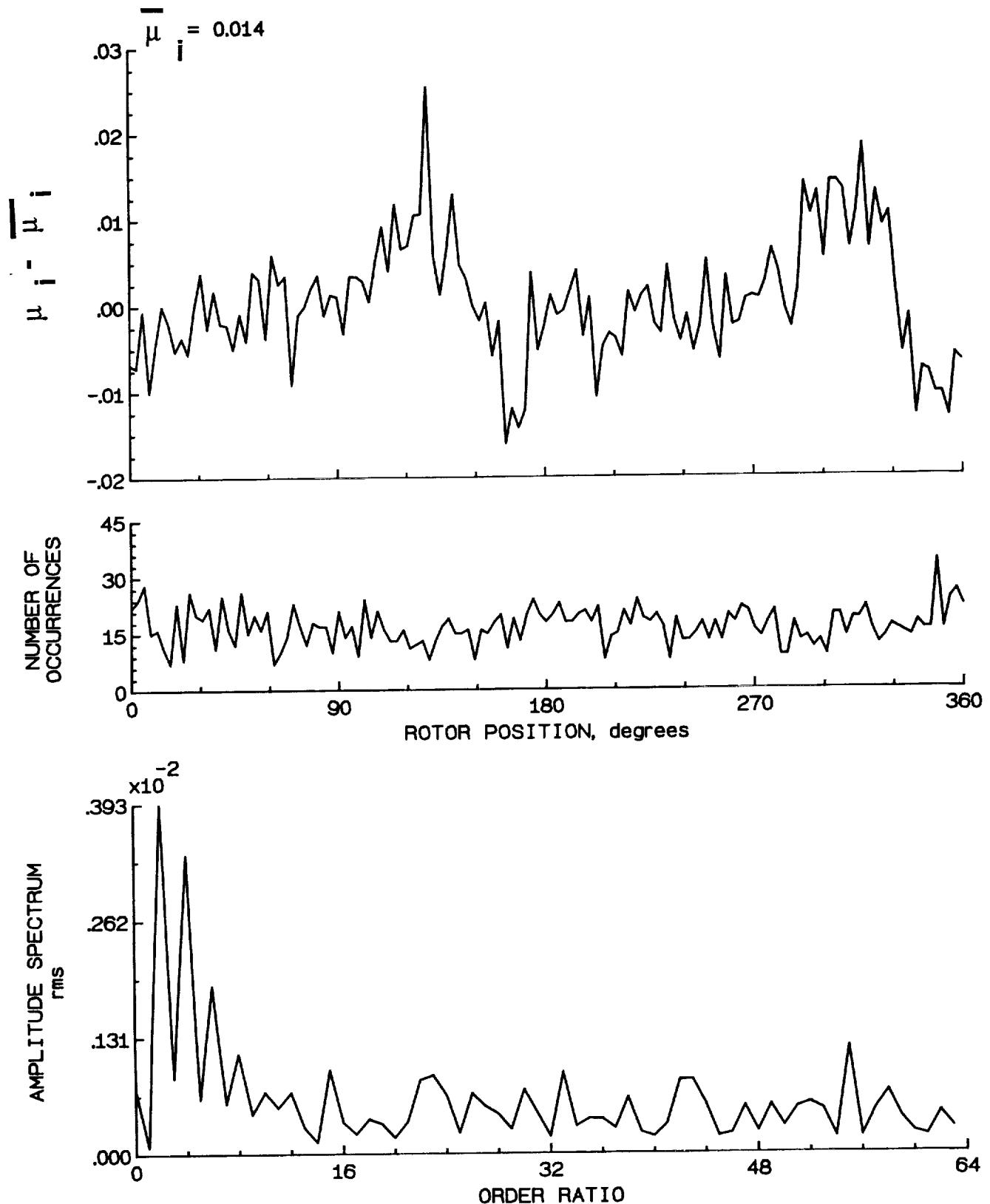


Figure 12.- Induced inflow velocity measured at 0 degrees and r/R of 0.20.

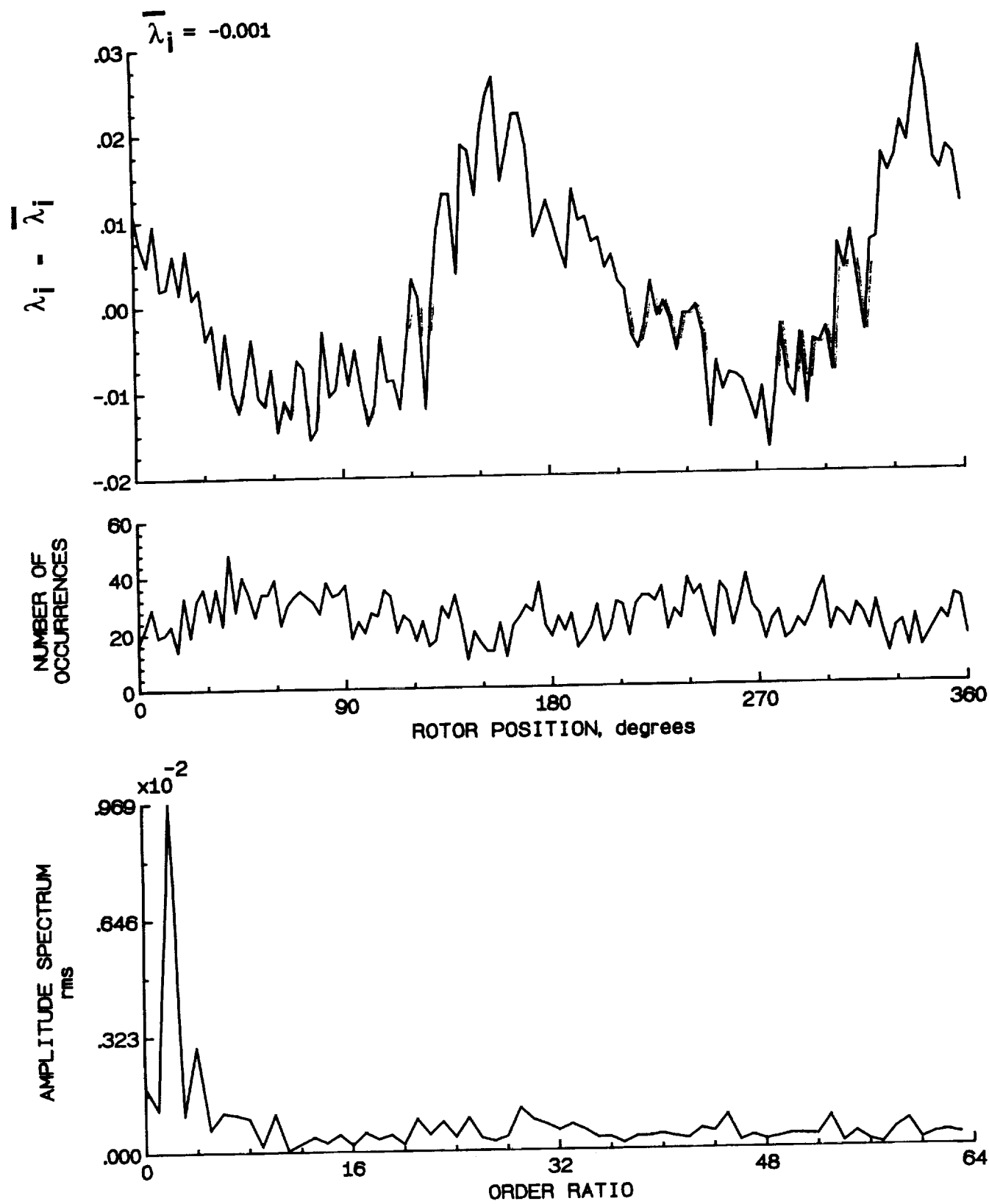


Figure 12.- Concluded.

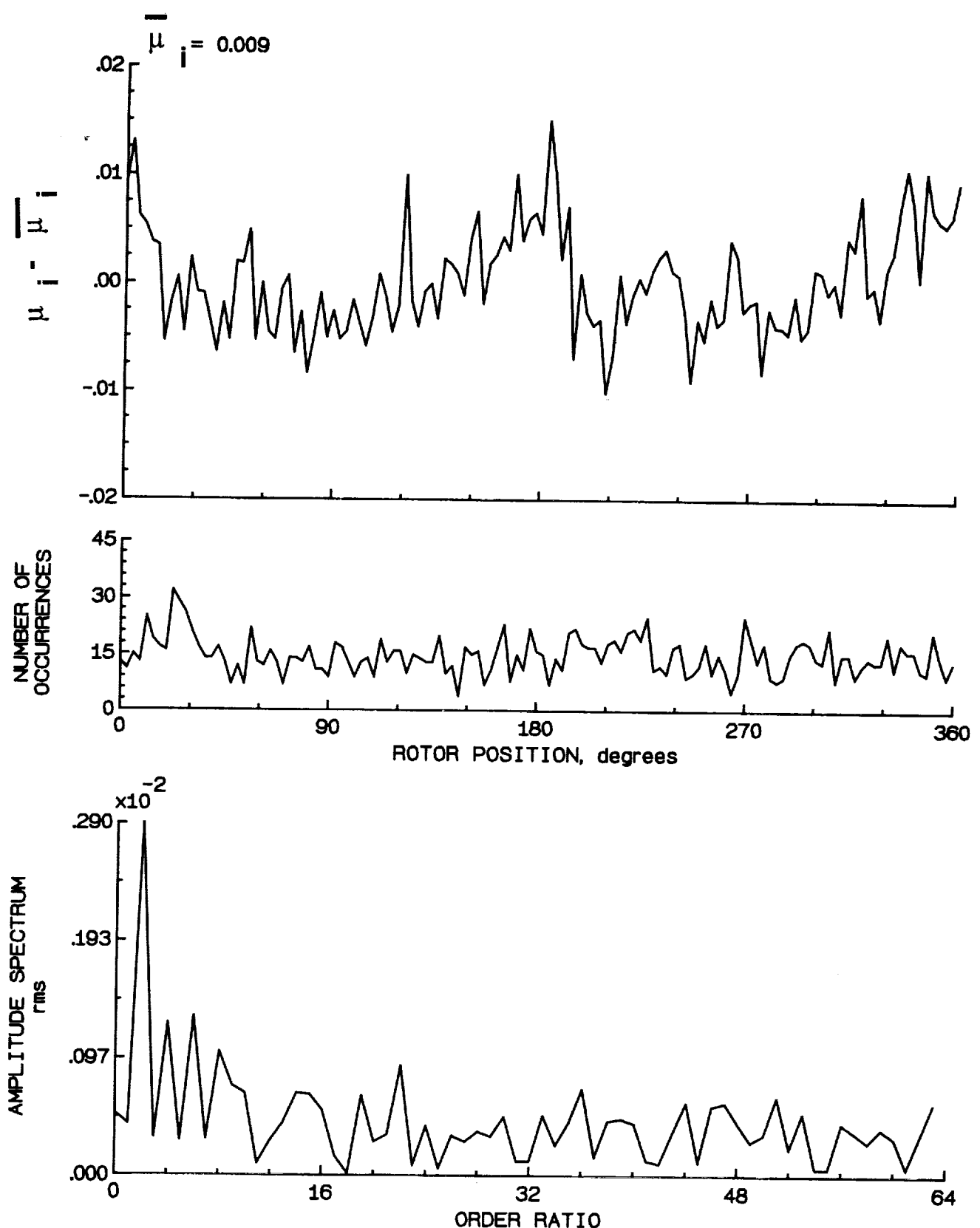


Figure 13.- Induced inflow velocity measured at 0 degrees and r/R of 0.40.

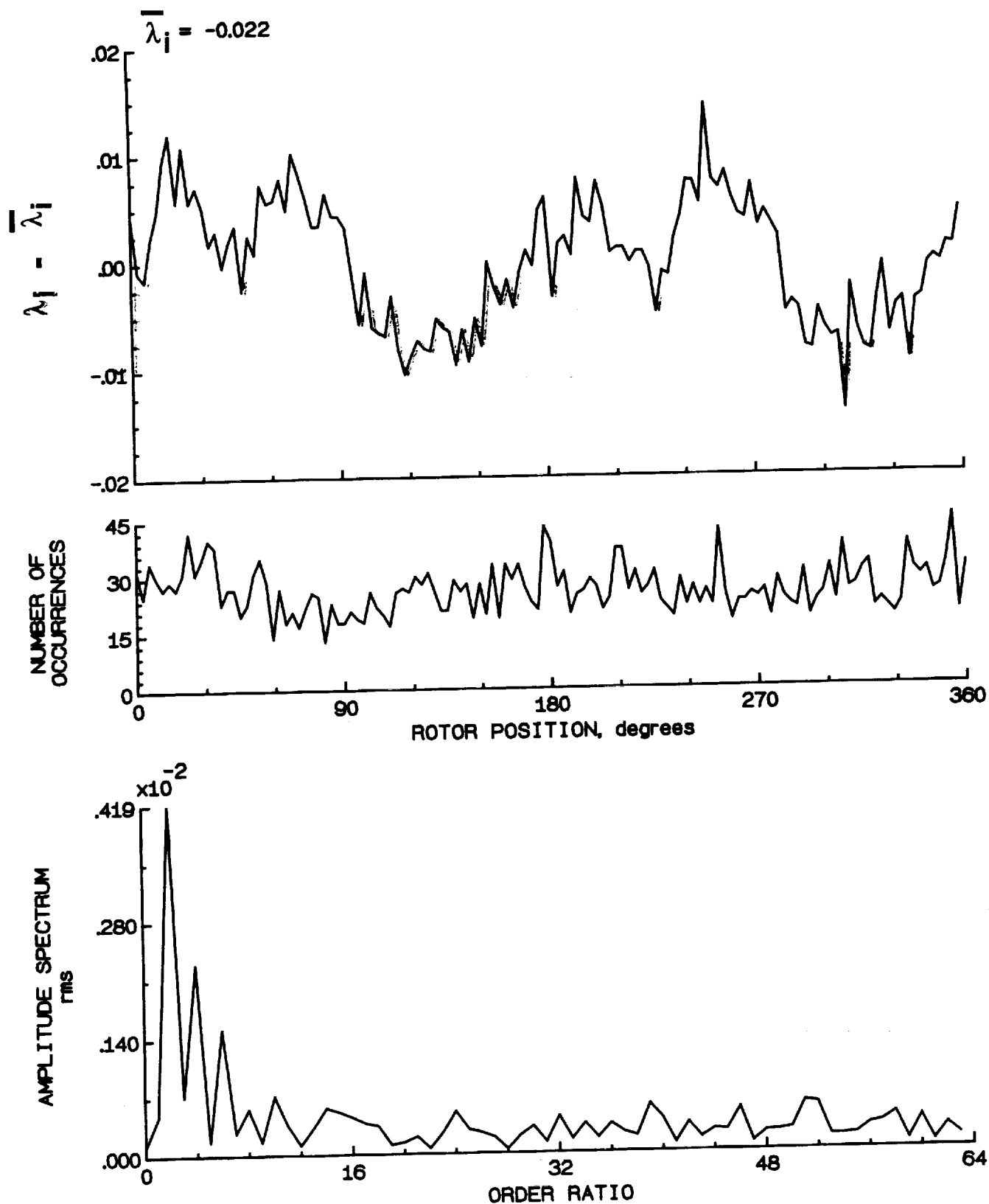


Figure 13.- Concluded.

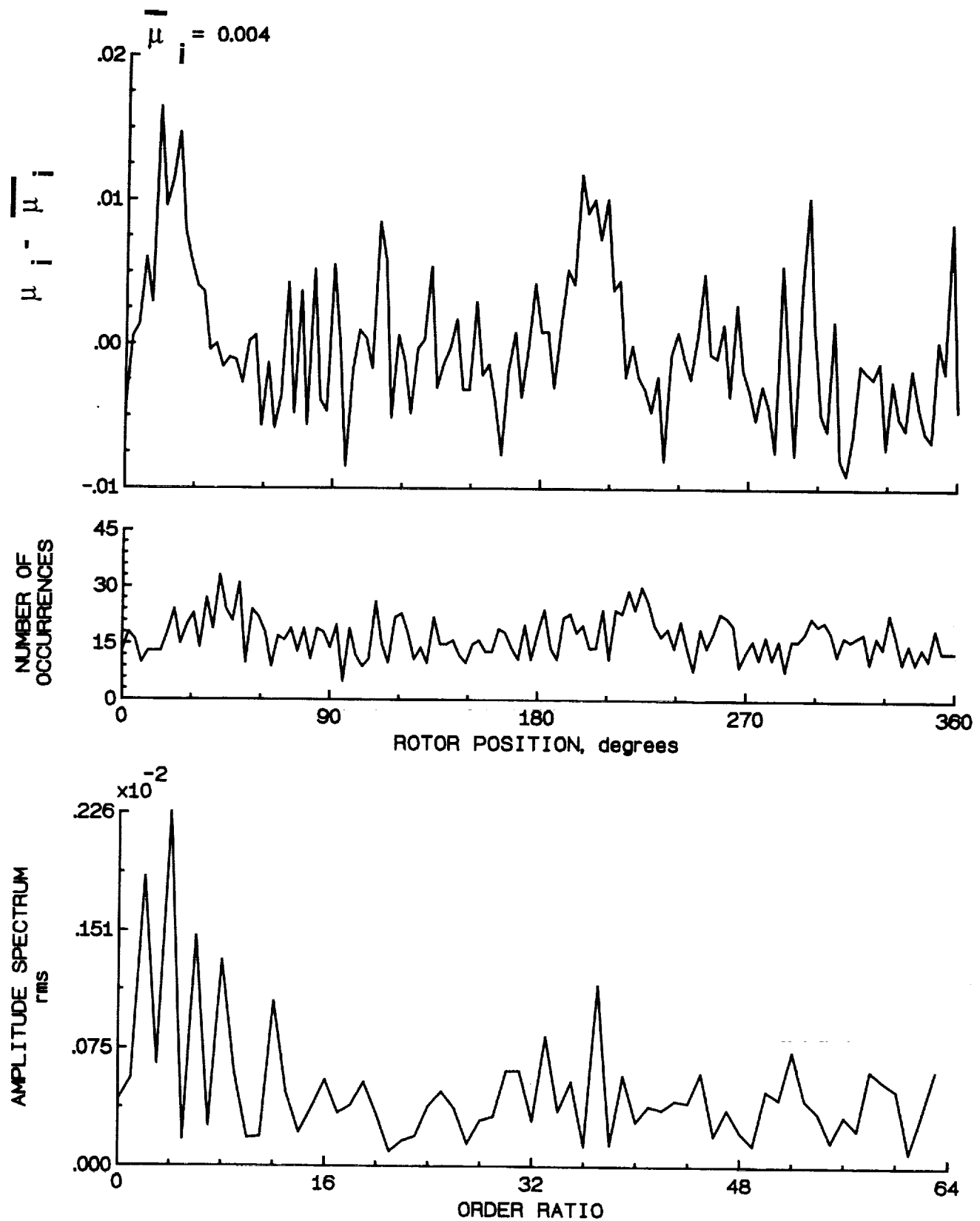


Figure 14.- Induced inflow velocity measured at 0 degrees and r/R of 0.50.

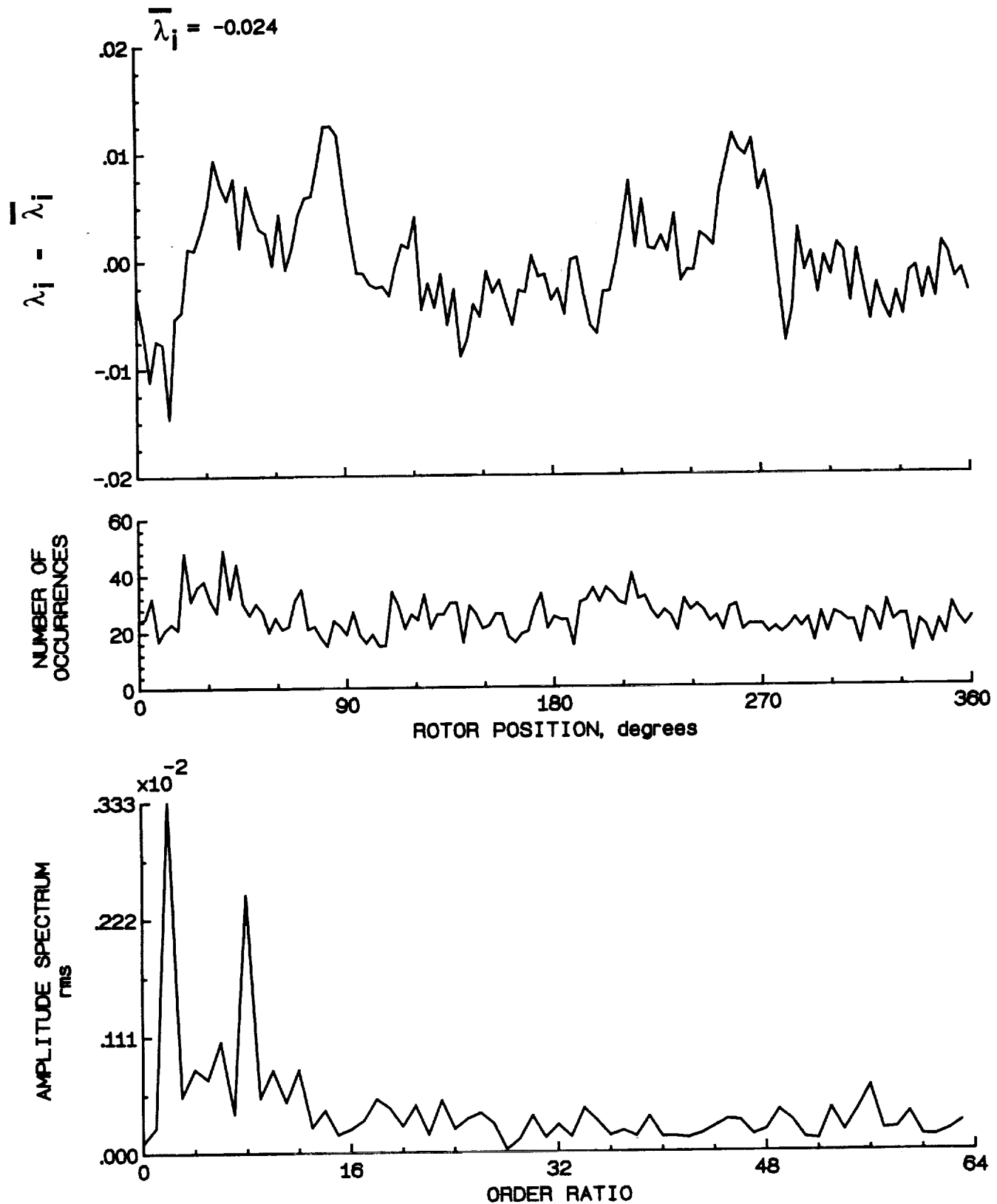


Figure 14.- Concluded.

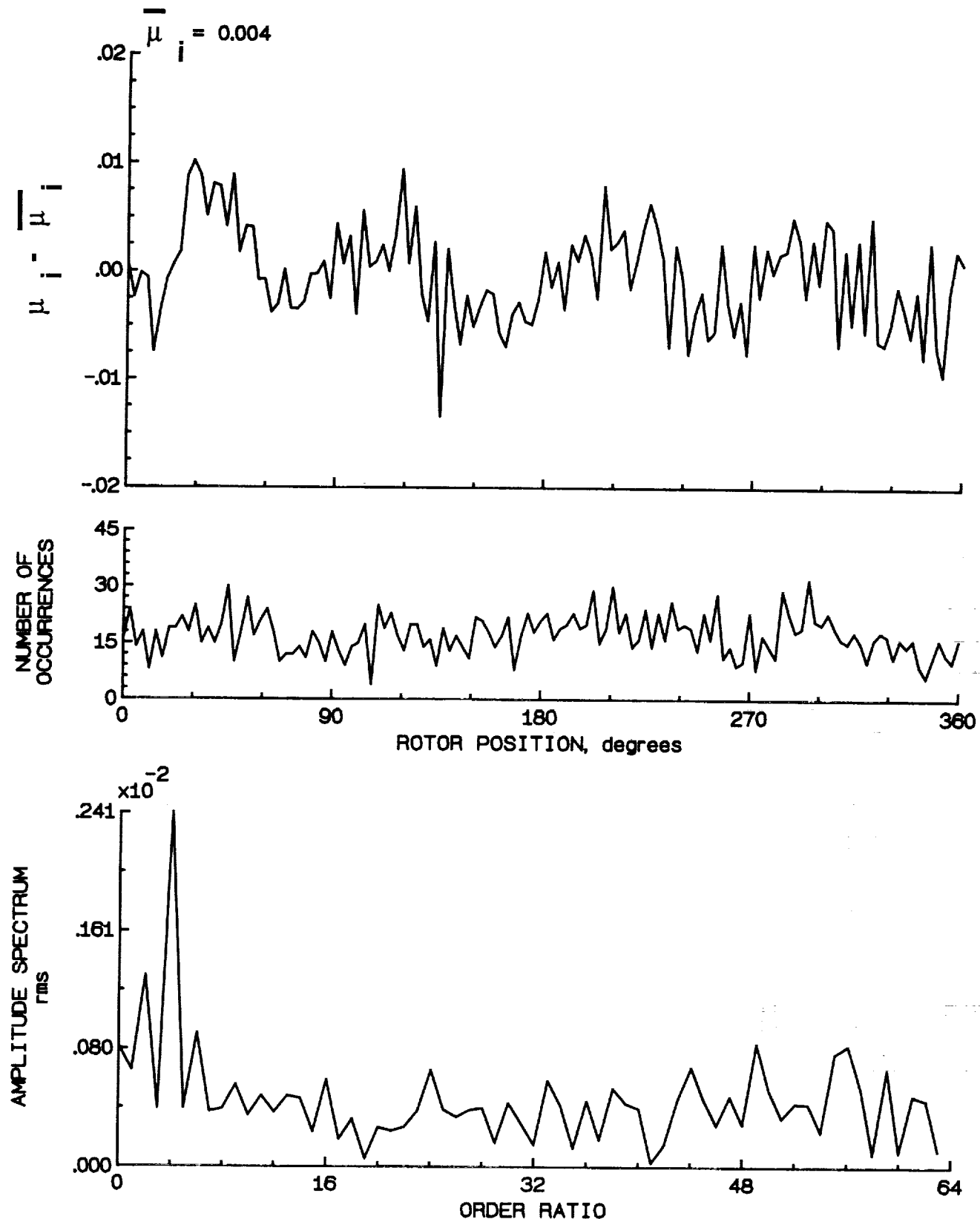


Figure 15.- Induced inflow velocity measured at 0 degrees and r/R of 0.60.

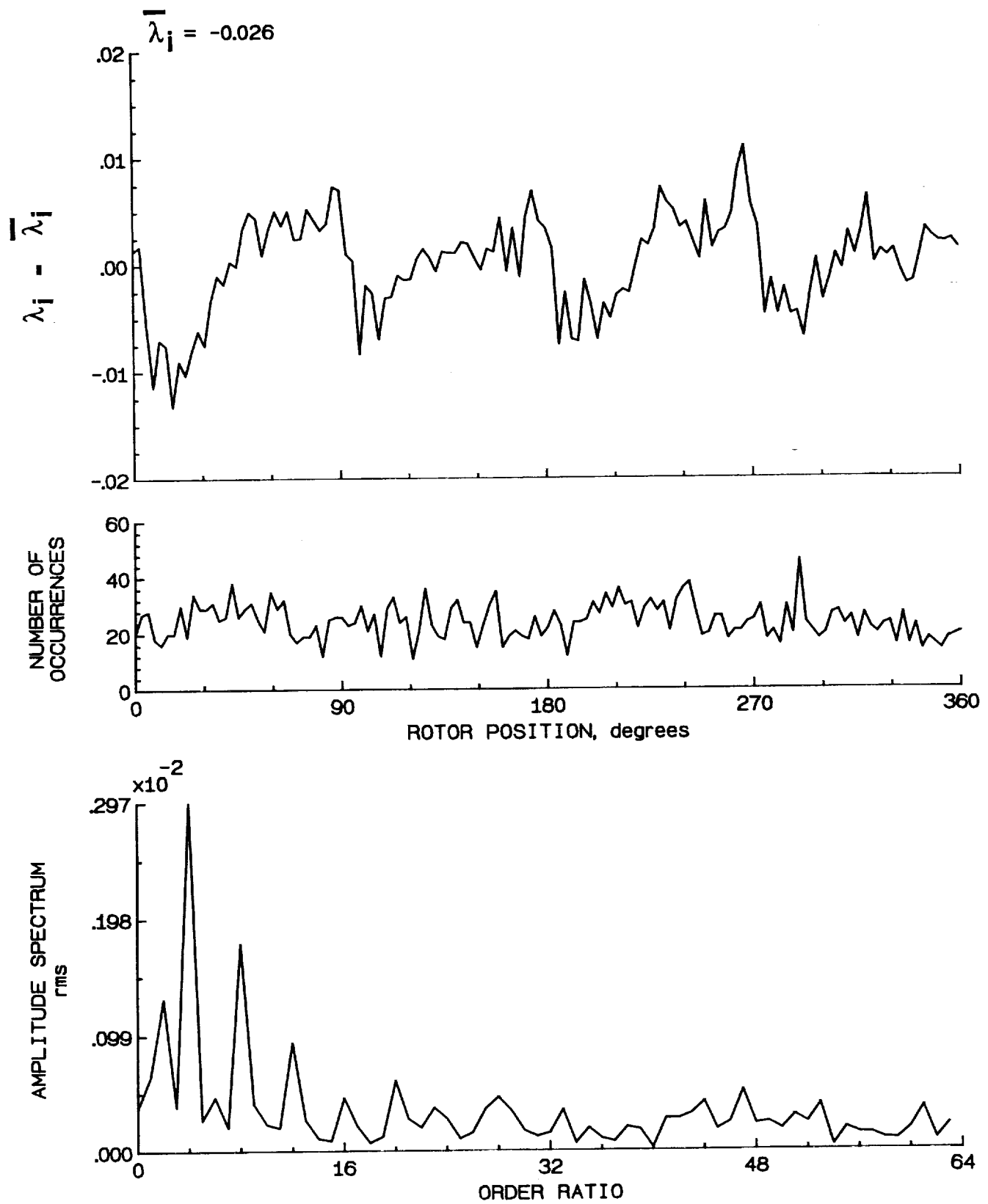


Figure 15.- Concluded.

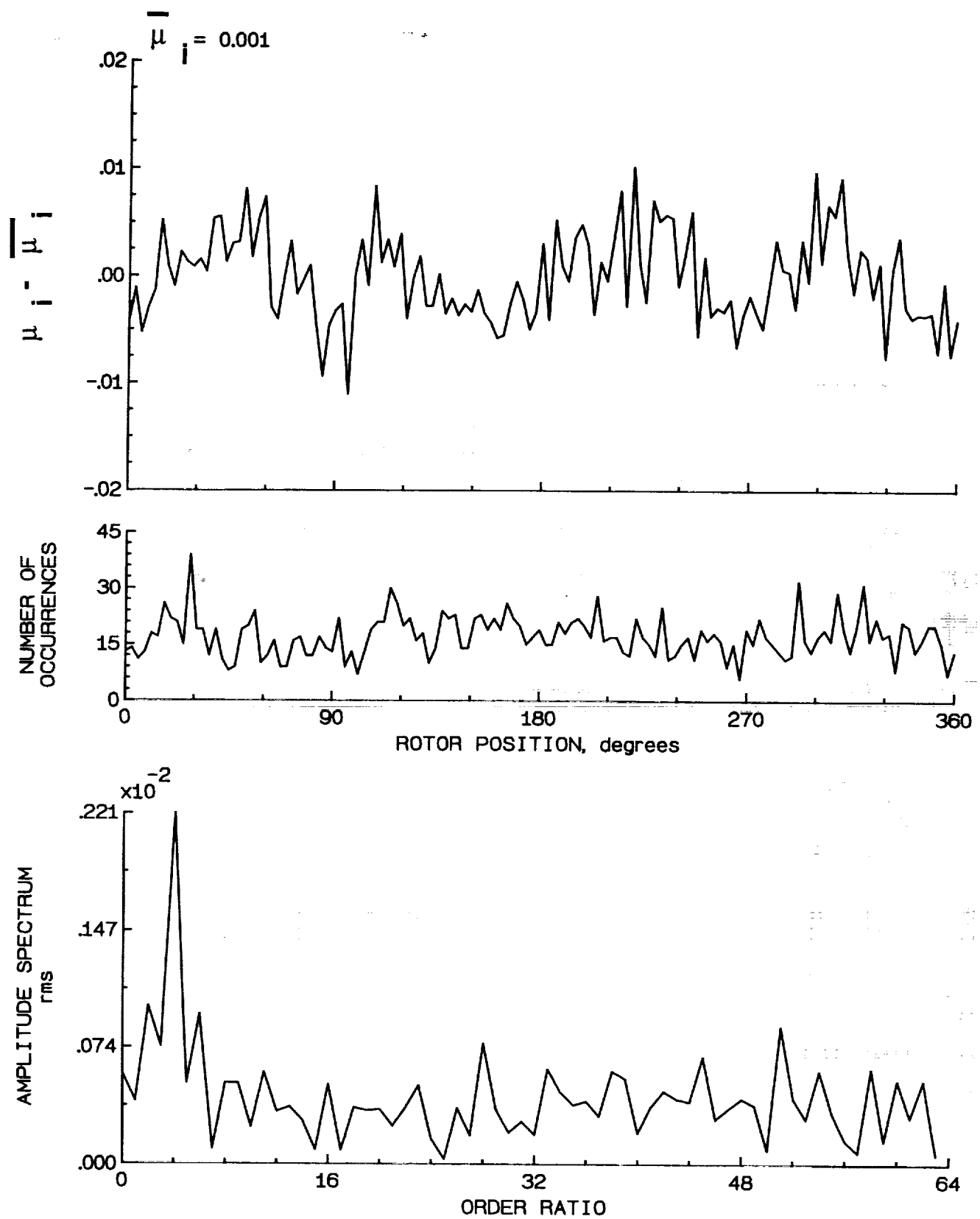


Figure 16.- Induced inflow velocity measured at 0 degrees and r/R of 0.70.

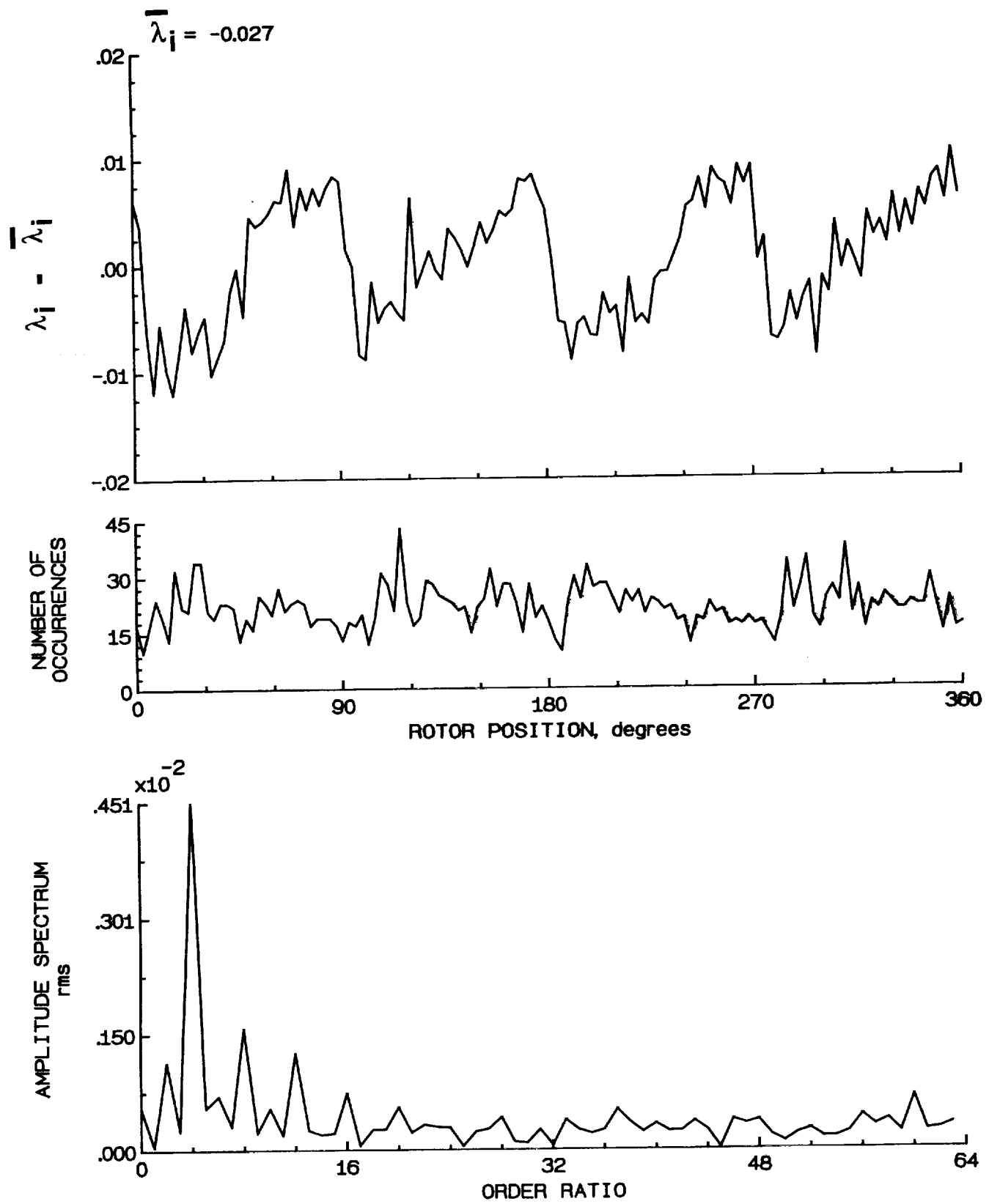


Figure 16.- Concluded.

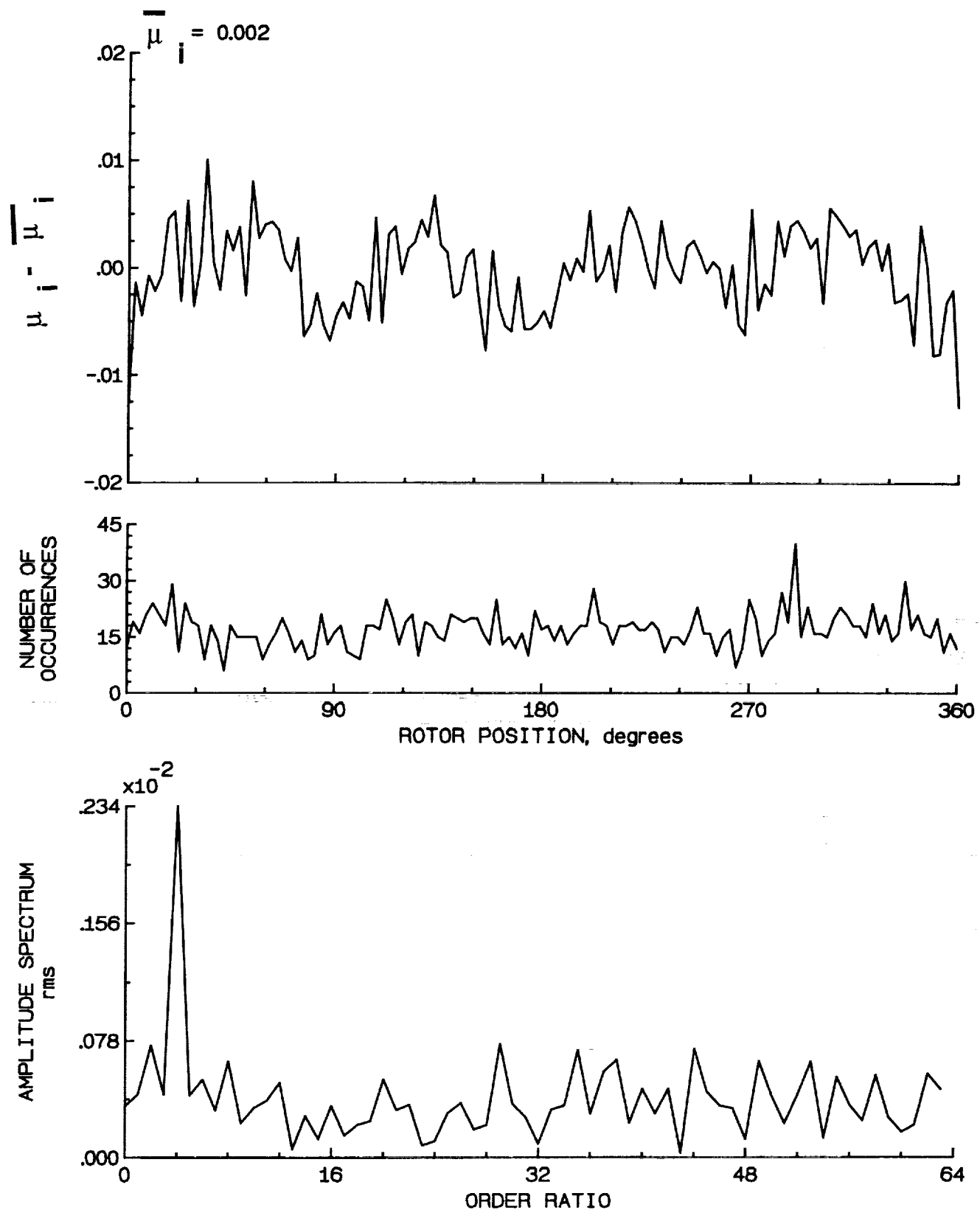


Figure 17.- Induced inflow velocity measured at 0 degrees and r/R of 0.74.

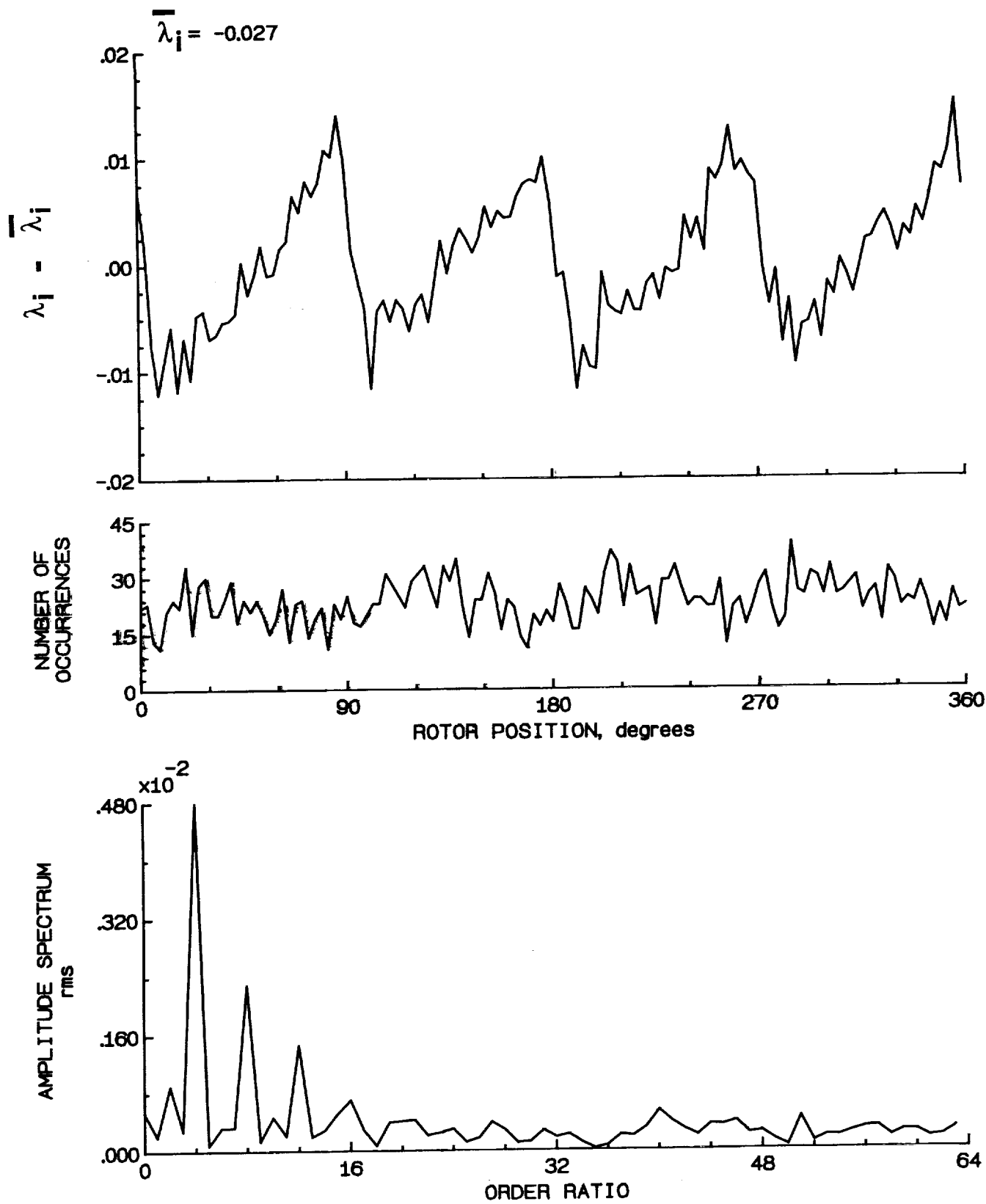


Figure 17.- Concluded.

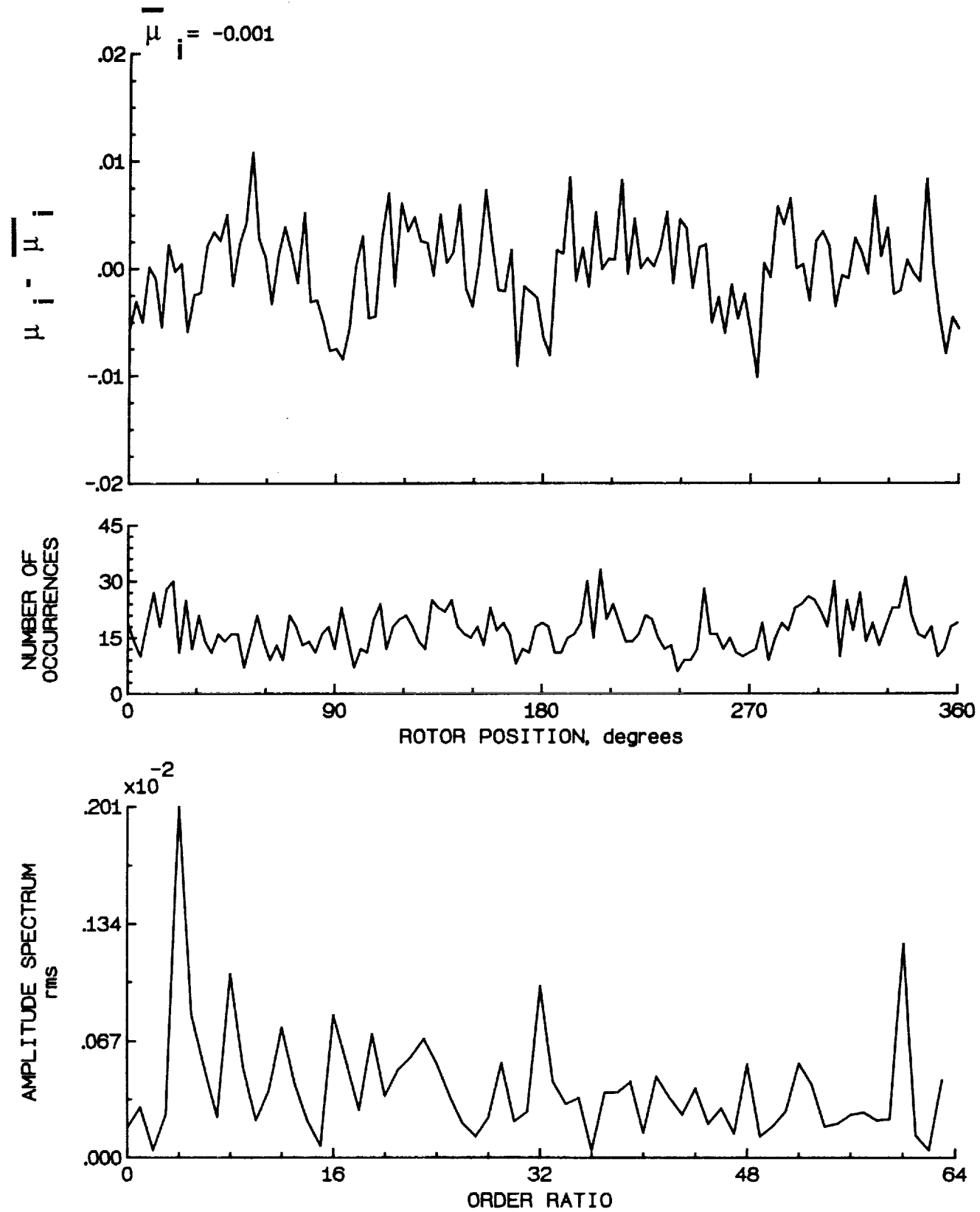


Figure 18.- Induced inflow velocity measured at 0 degrees and r/R of 0.78.

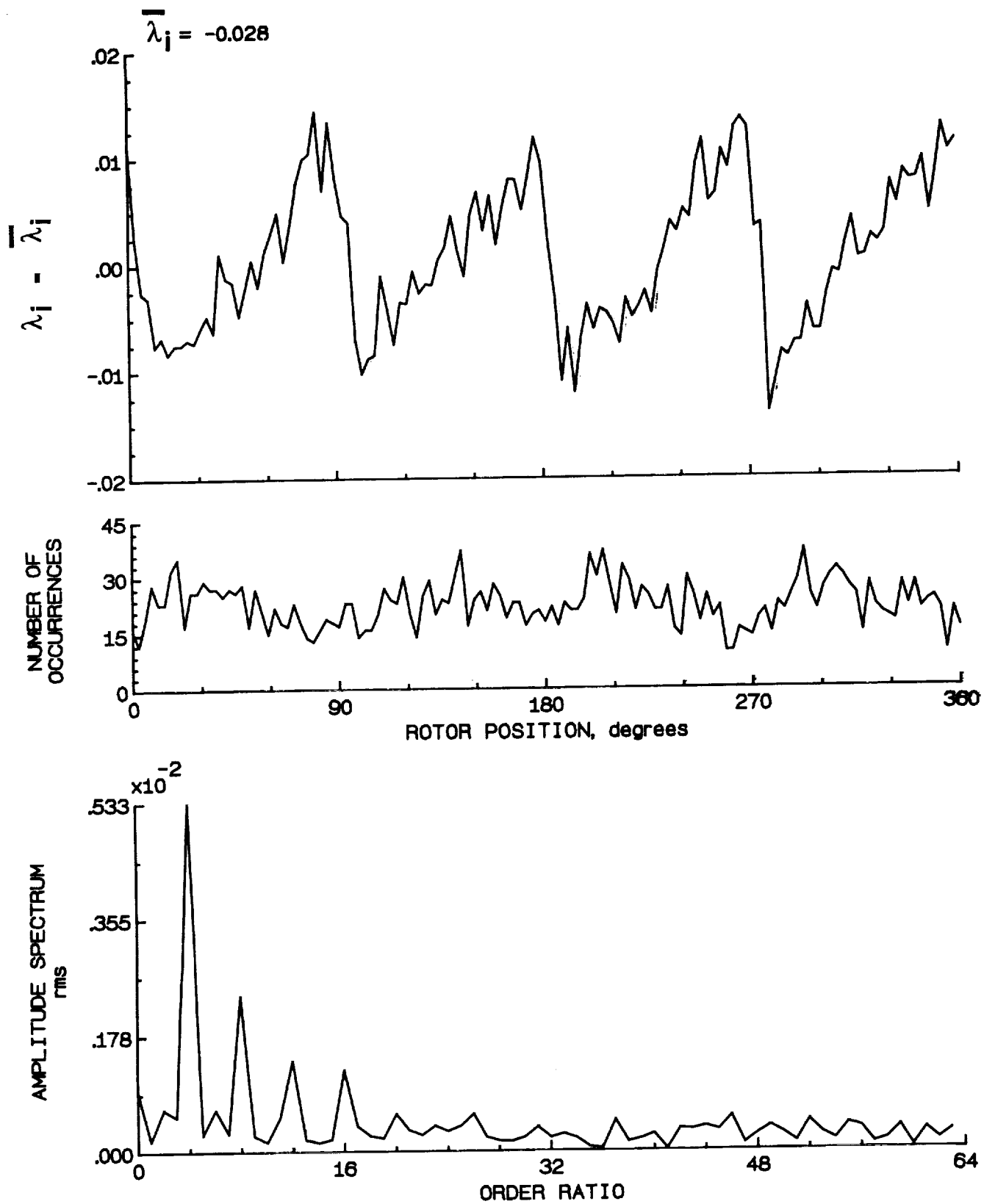


Figure 18.- Concluded.

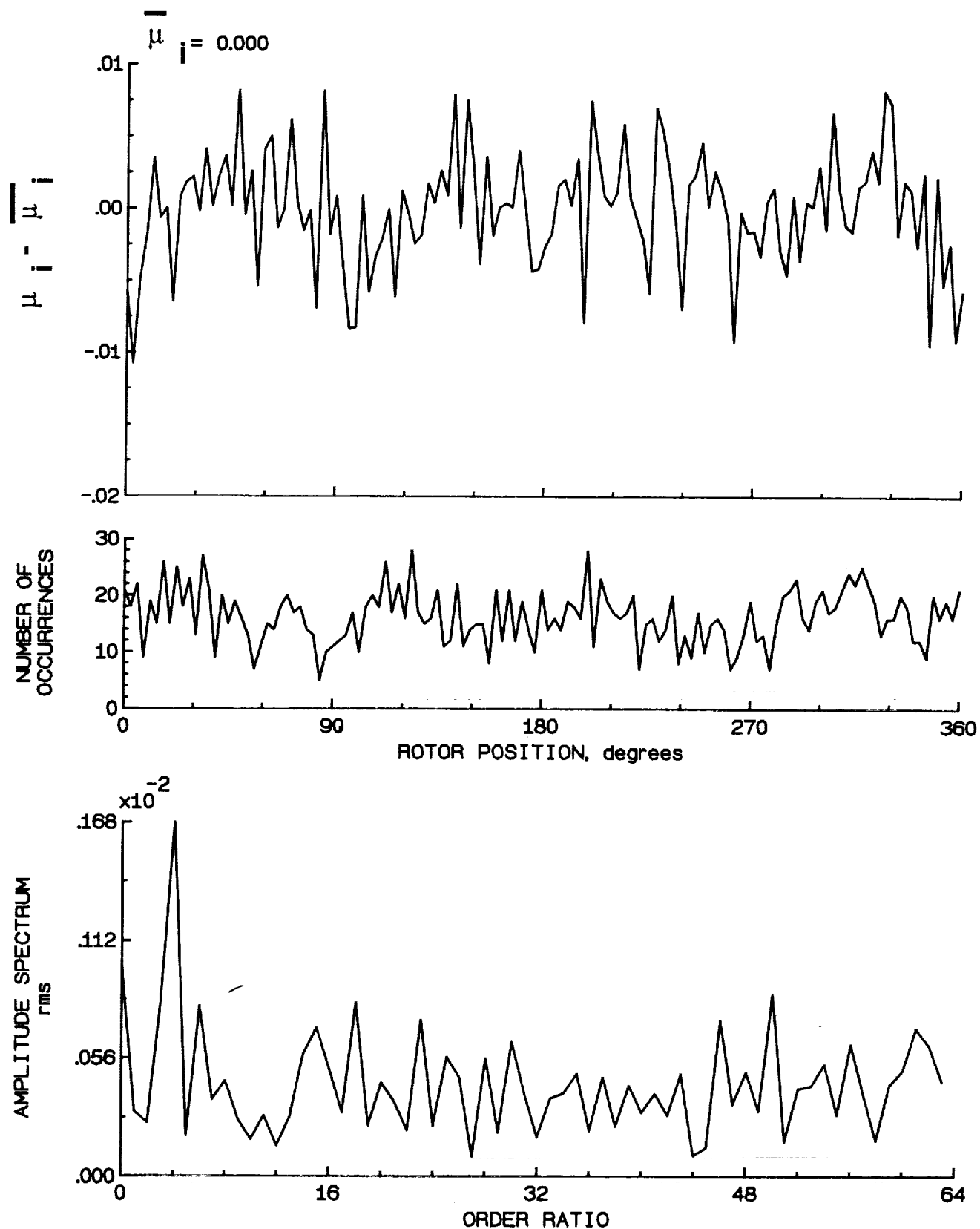


Figure 19.- Induced inflow velocity measured at 0 degrees and r/R of 0.82.

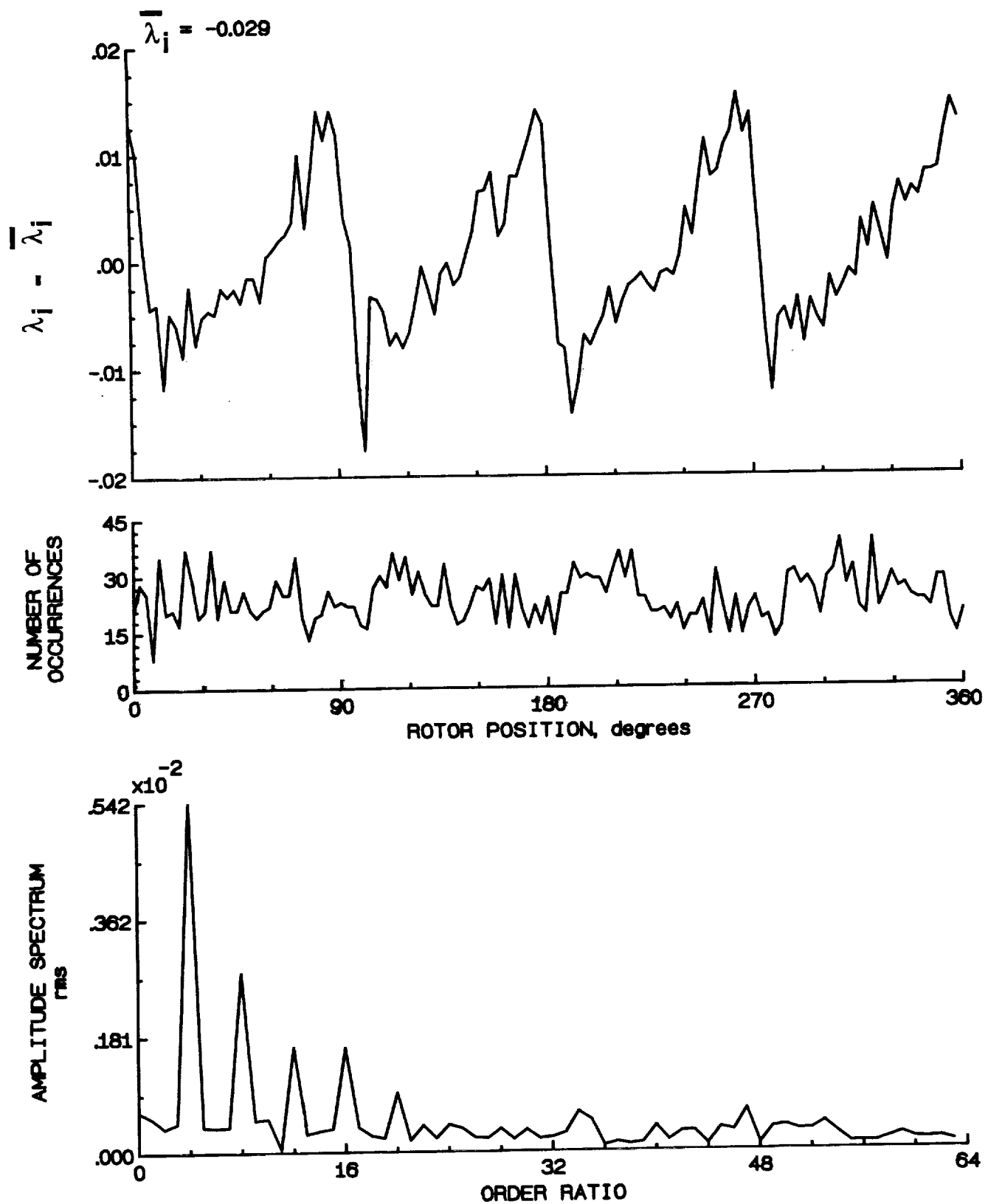


Figure 19.- Concluded.

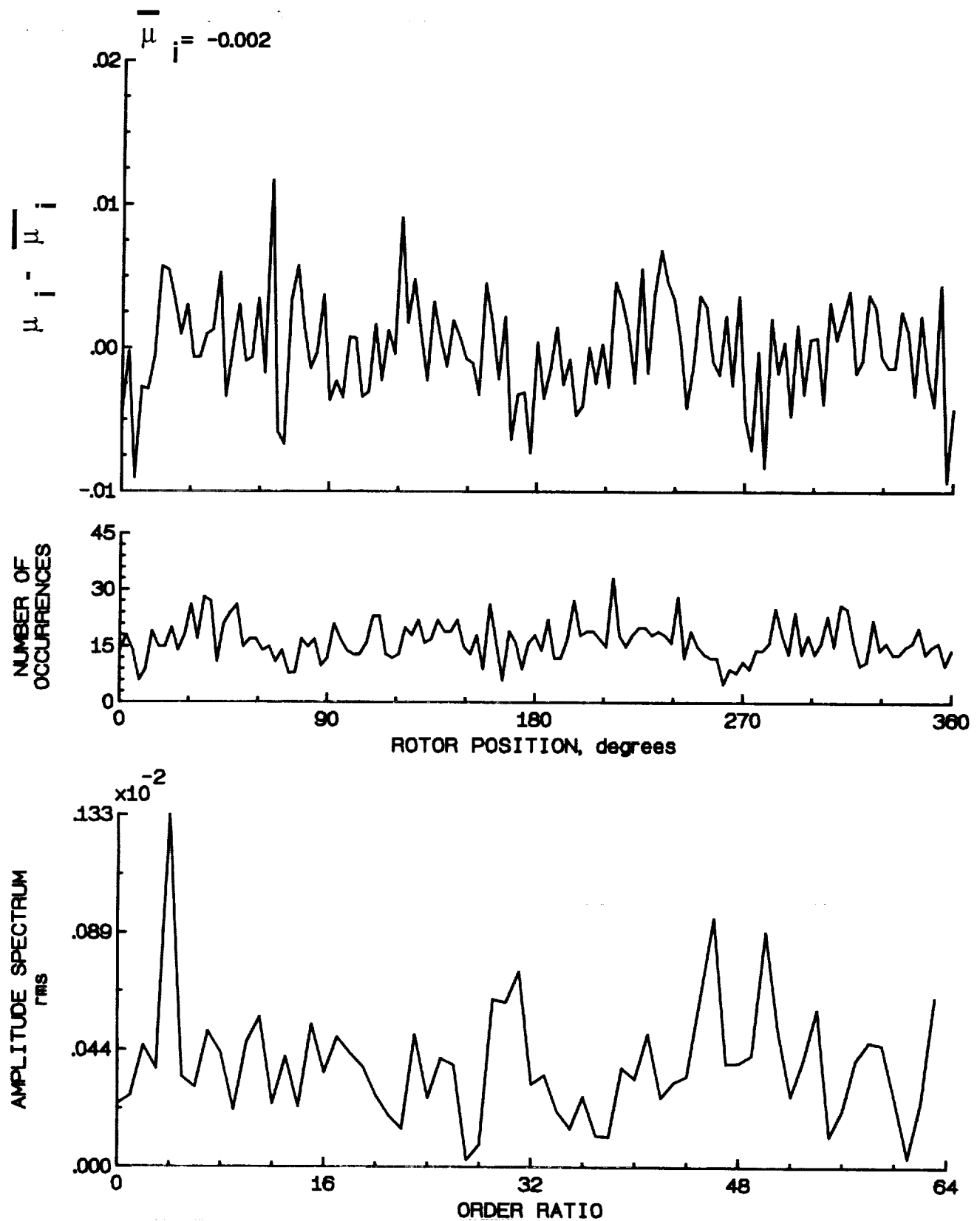


Figure 20.- Induced inflow velocity measured at 0 degrees and r/R of 0.86.

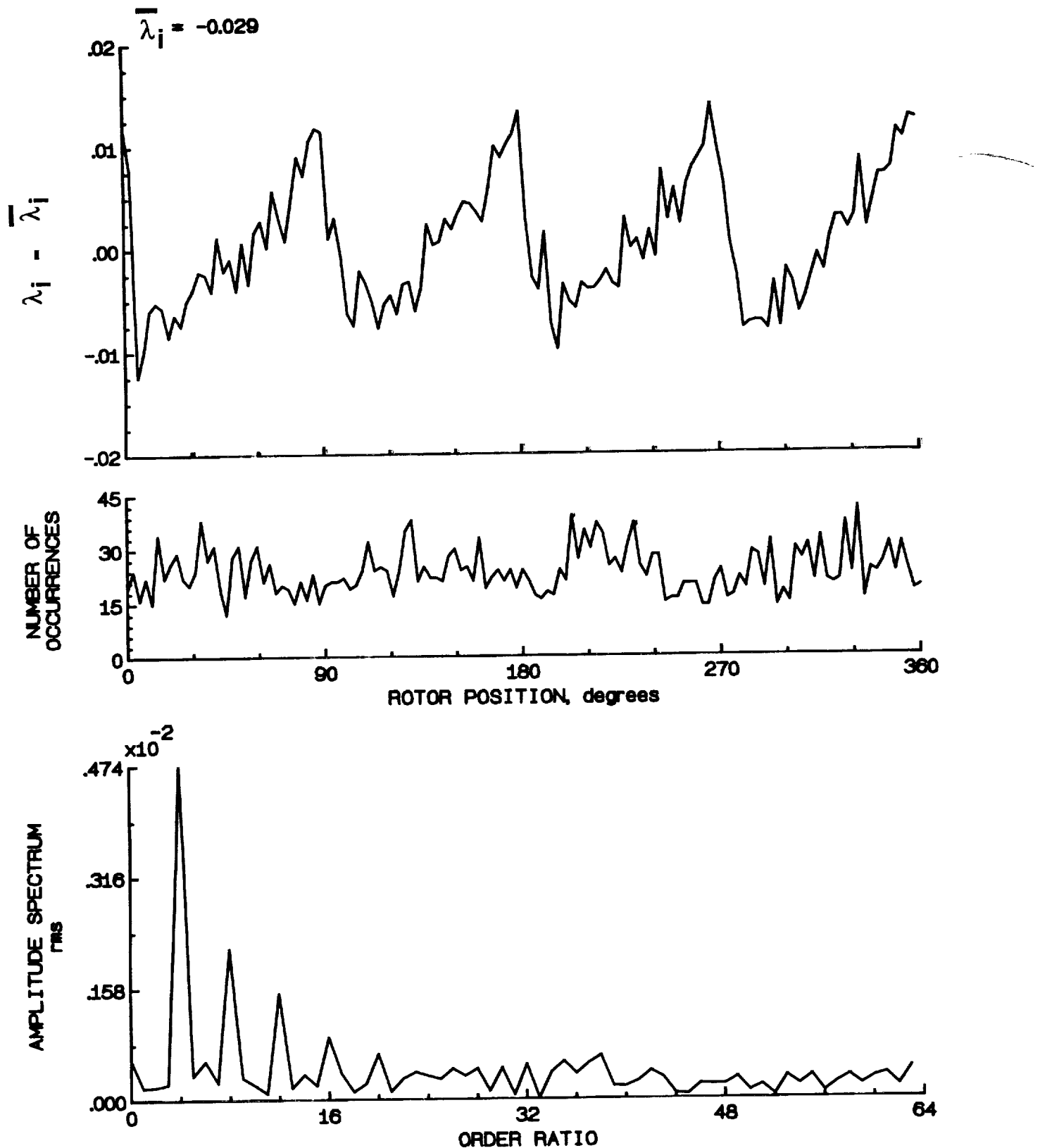


Figure 20.- Concluded.

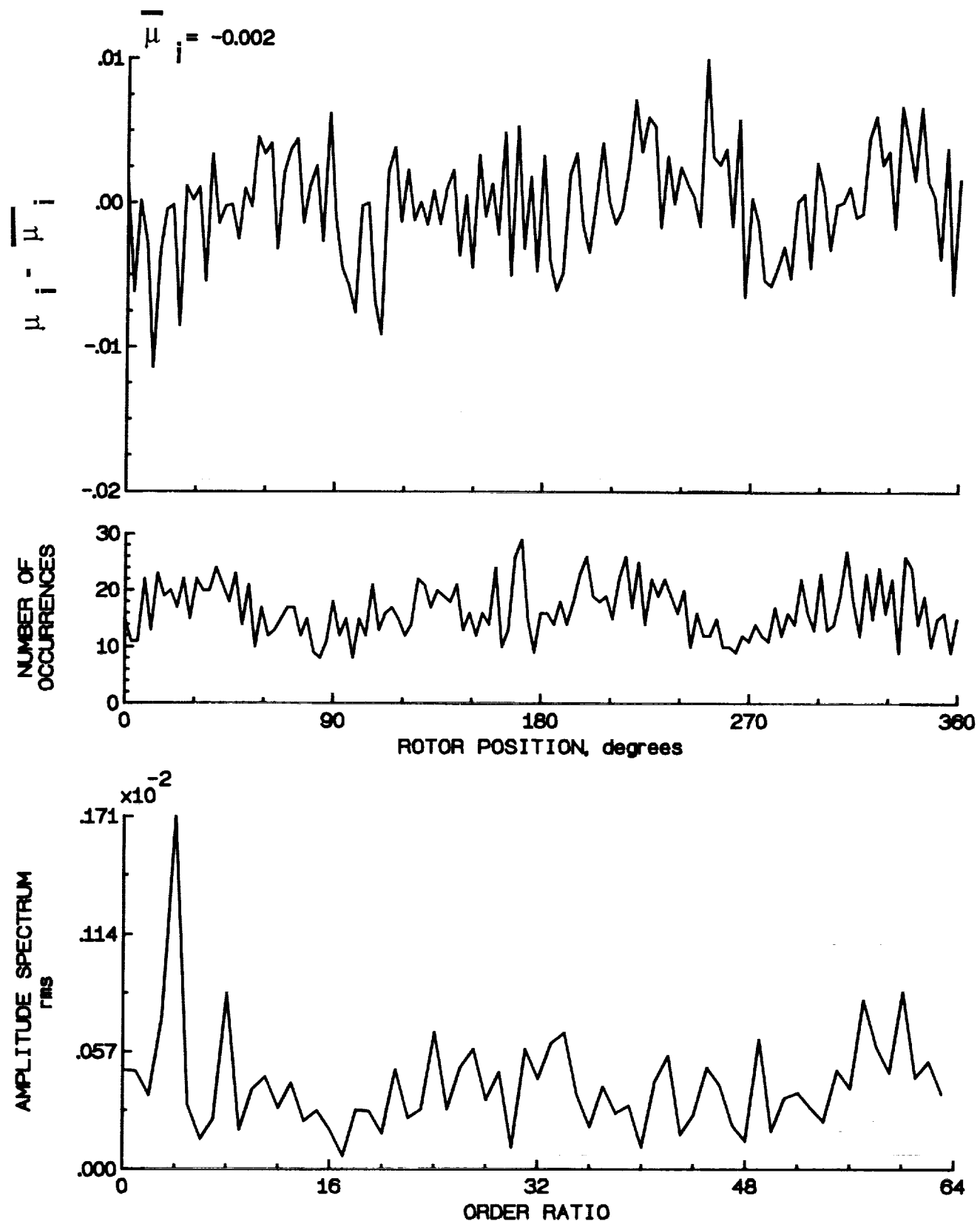


Figure 21.- Induced inflow velocity measured at 0 degrees and r/R of 0.90.

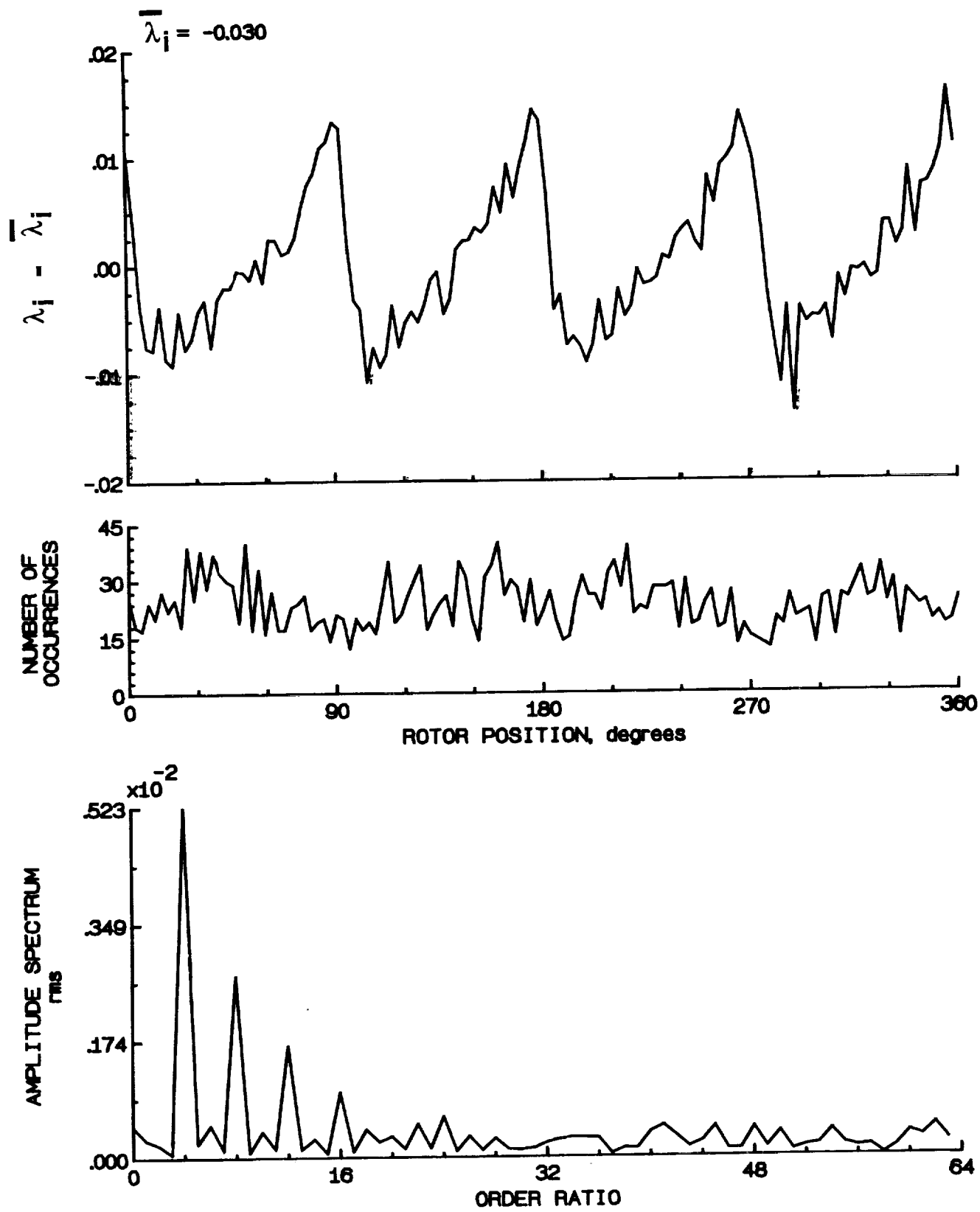


Figure 21.- Concluded.

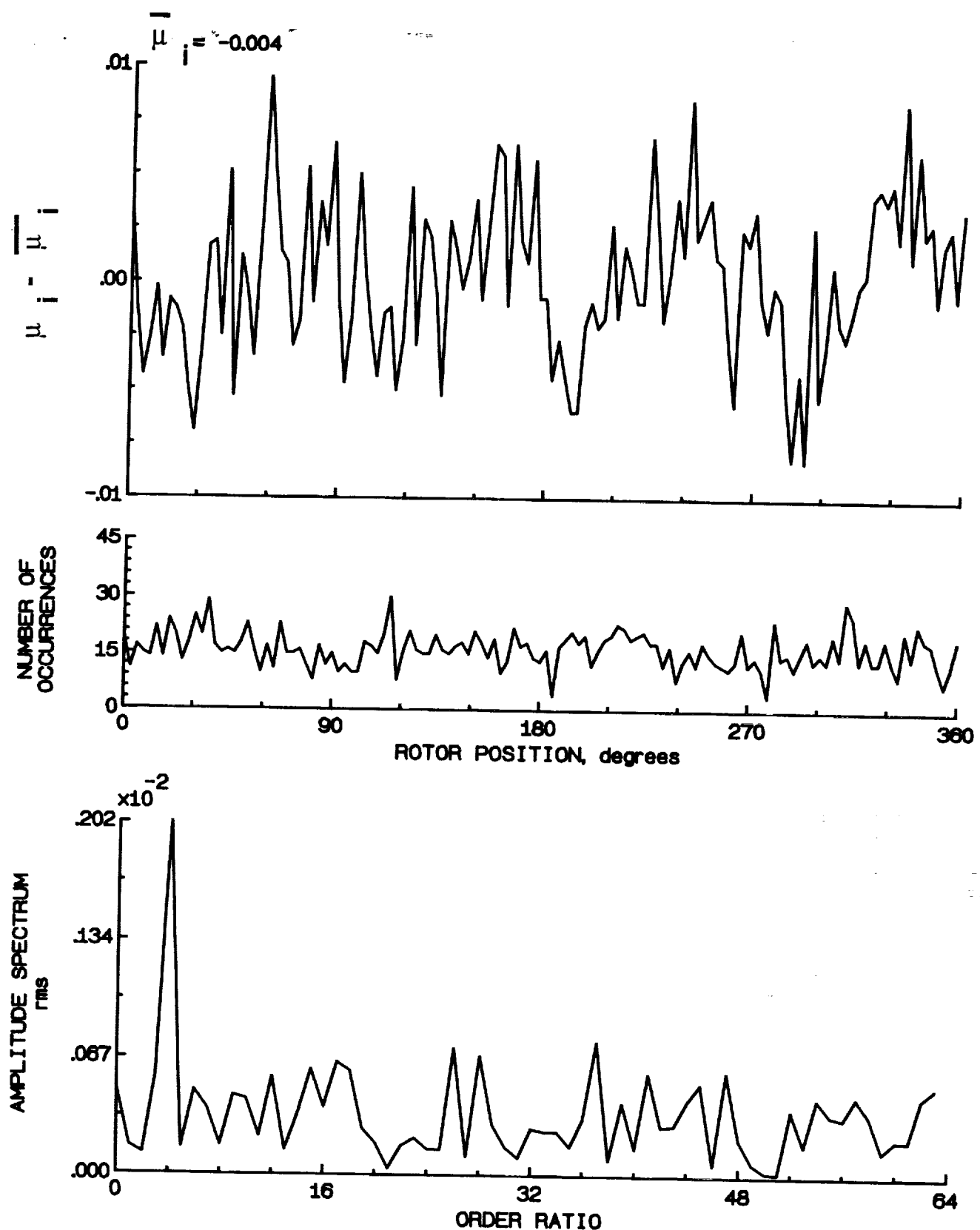


Figure 22.- Induced inflow velocity measured at 0 degrees and r/R of 0.94.

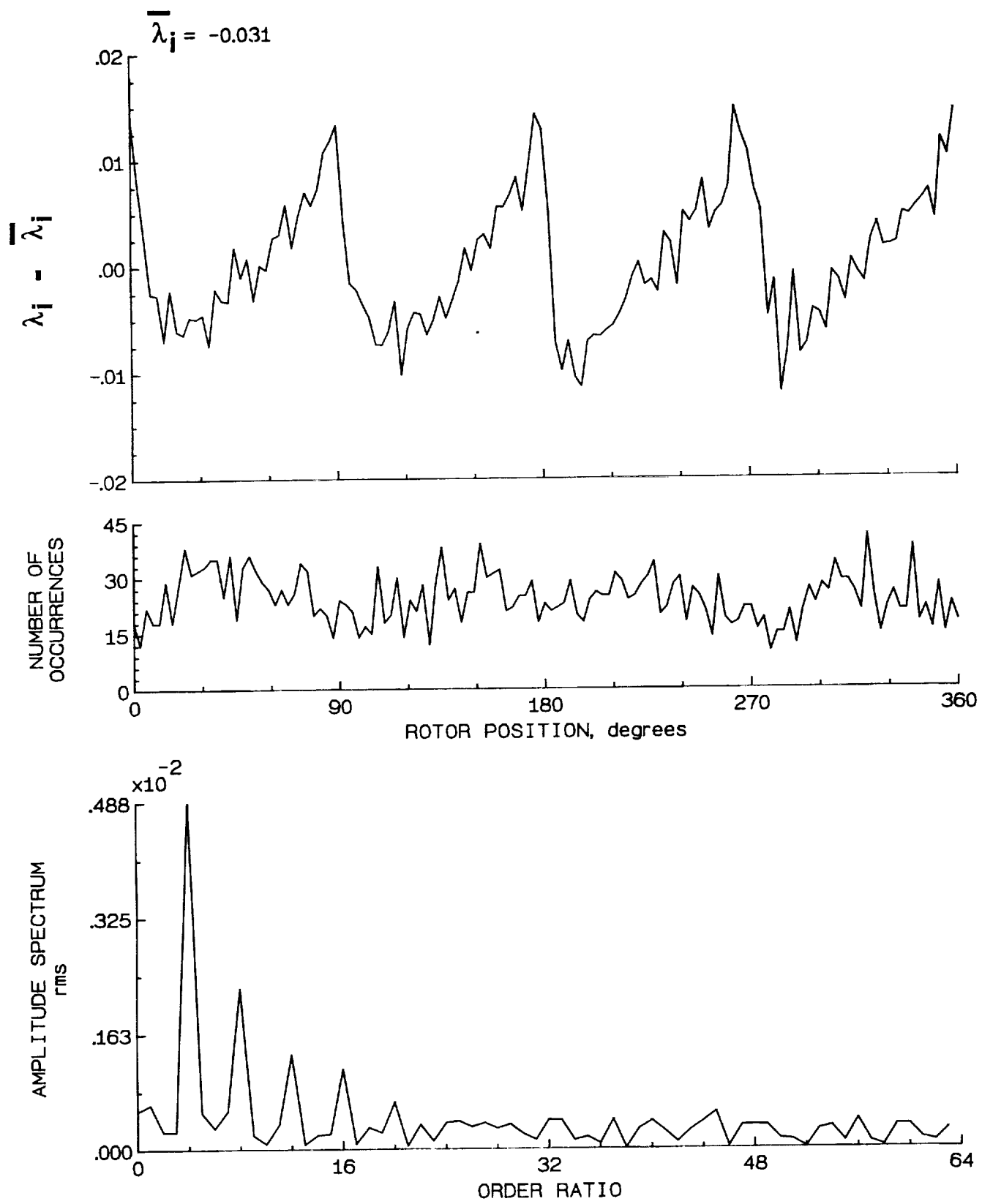


Figure 22.- Concluded.

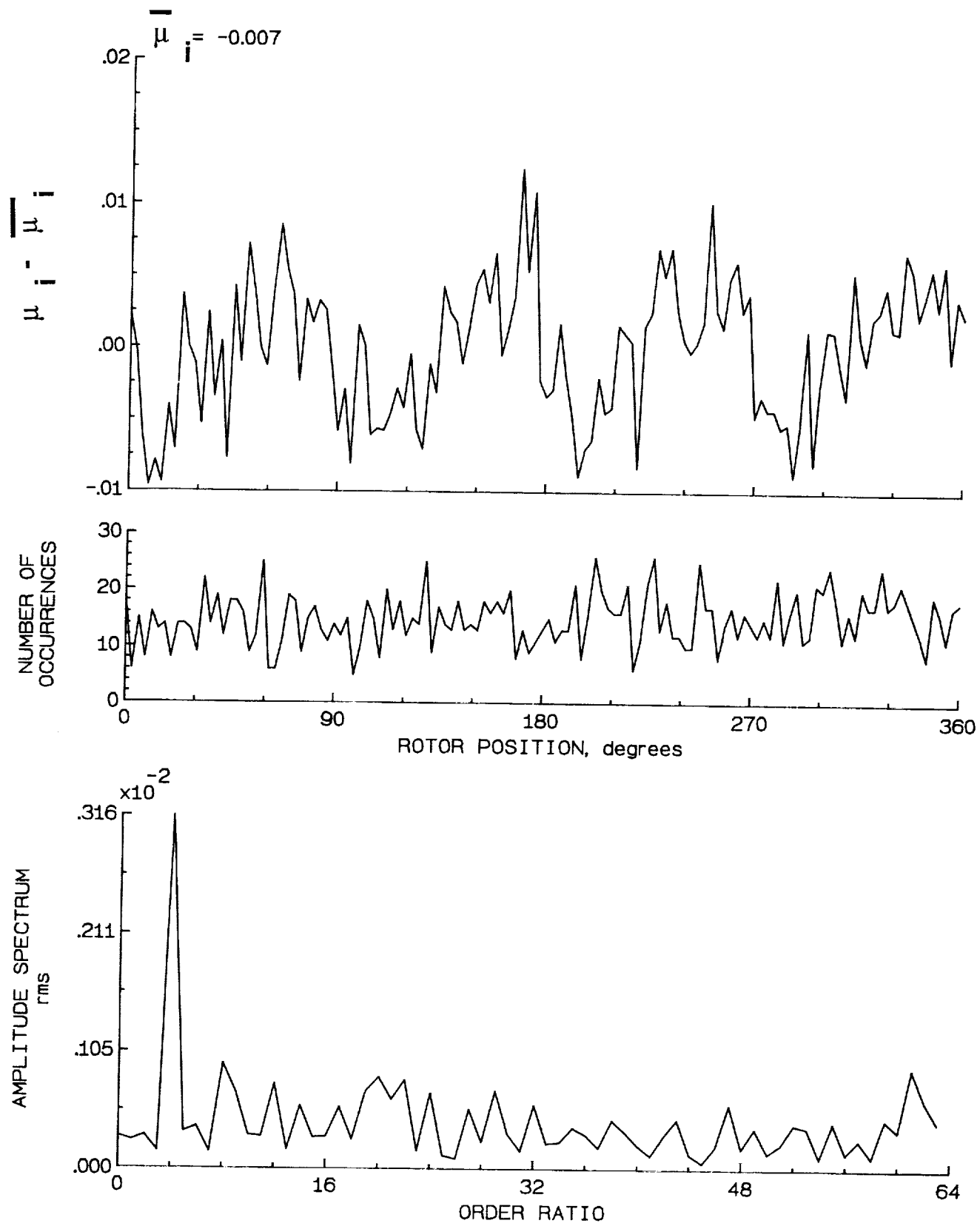


Figure 23.- Induced inflow velocity measured at 0 degrees and r/R of 0.98.

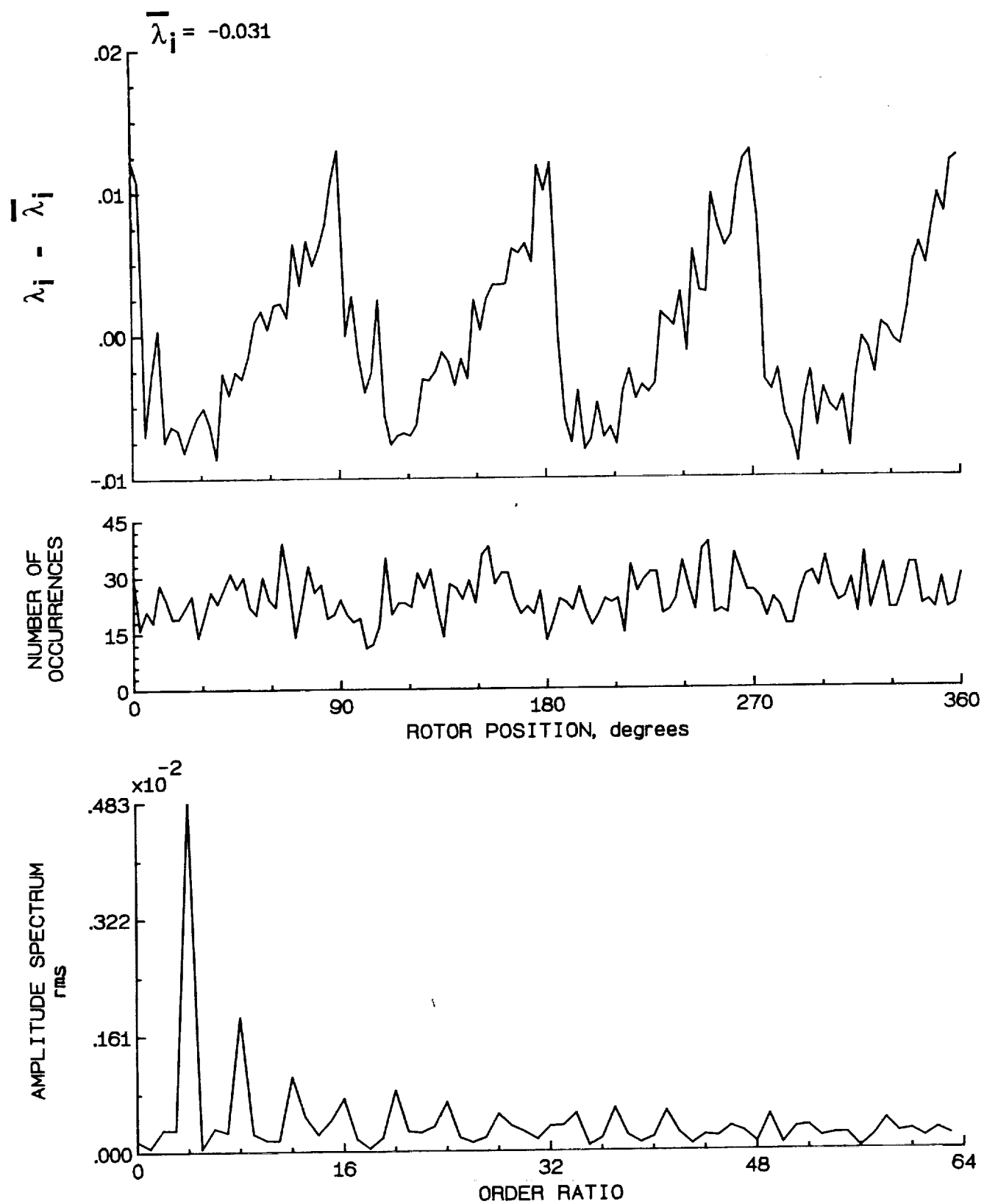


Figure 23.- Concluded.

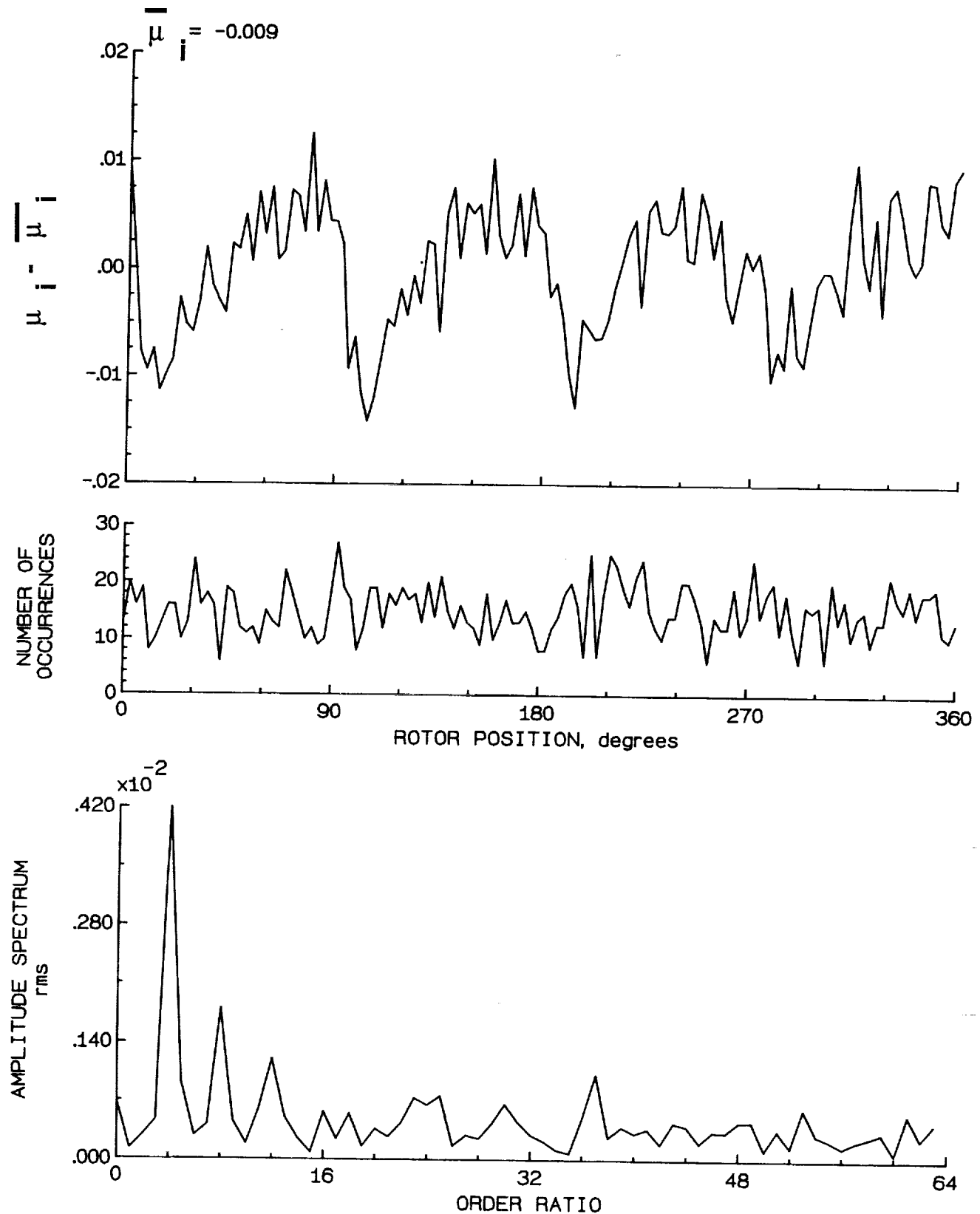


Figure 24.- Induced inflow velocity measured at 0 degrees and r/R of 1.02.

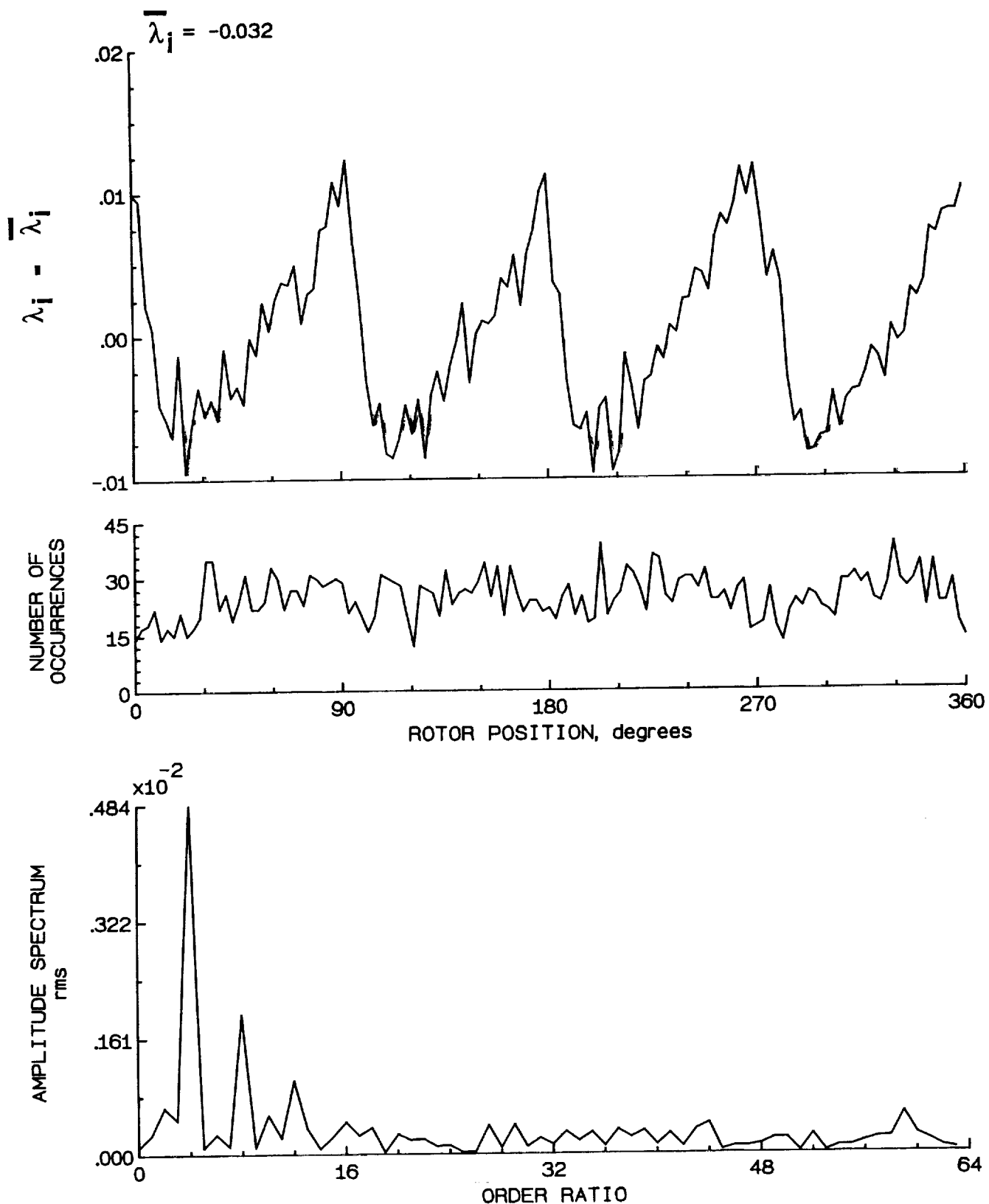


Figure 24.- Concluded.

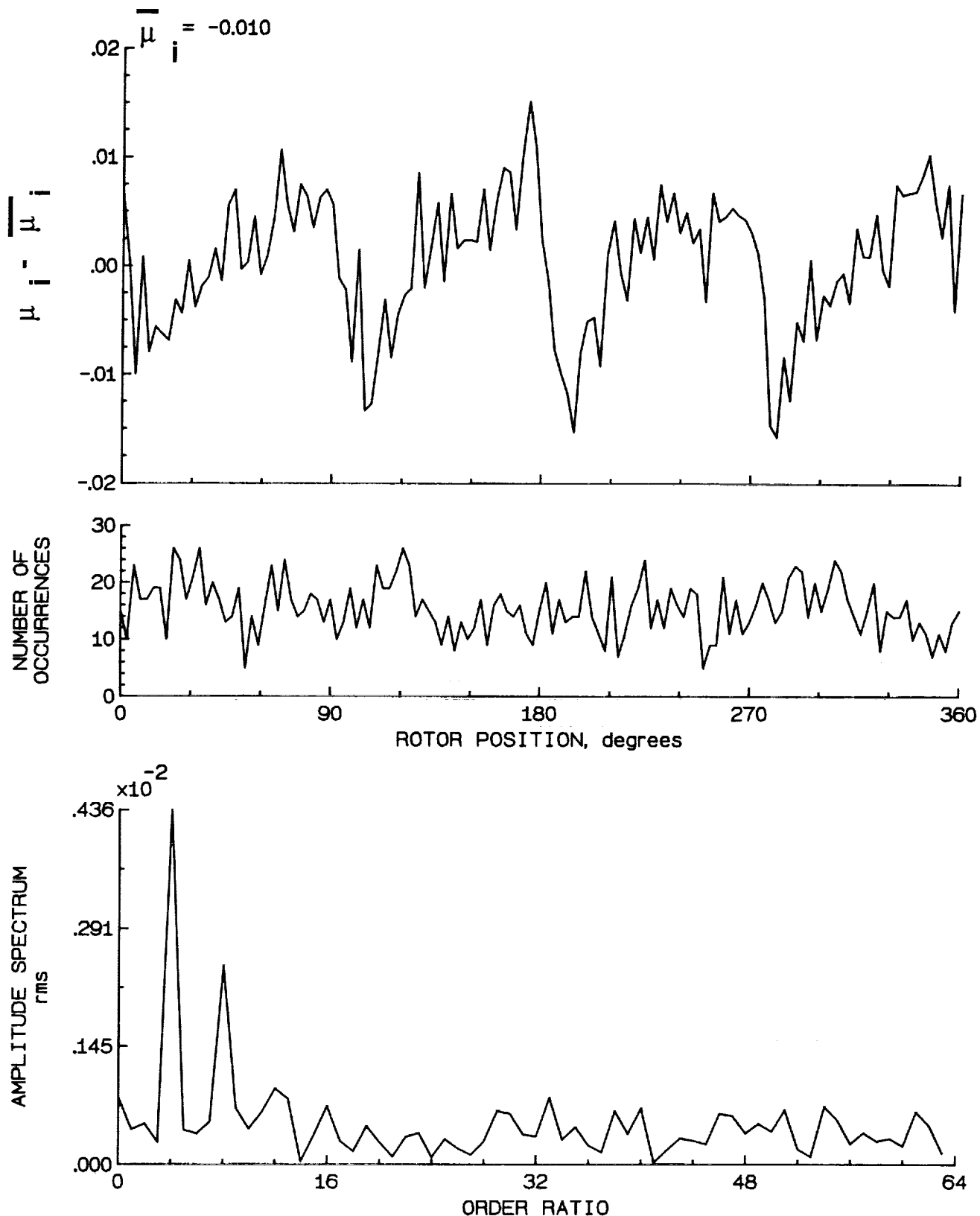


Figure 25.- Induced inflow velocity measured at 0 degrees and r/R of 1.04.

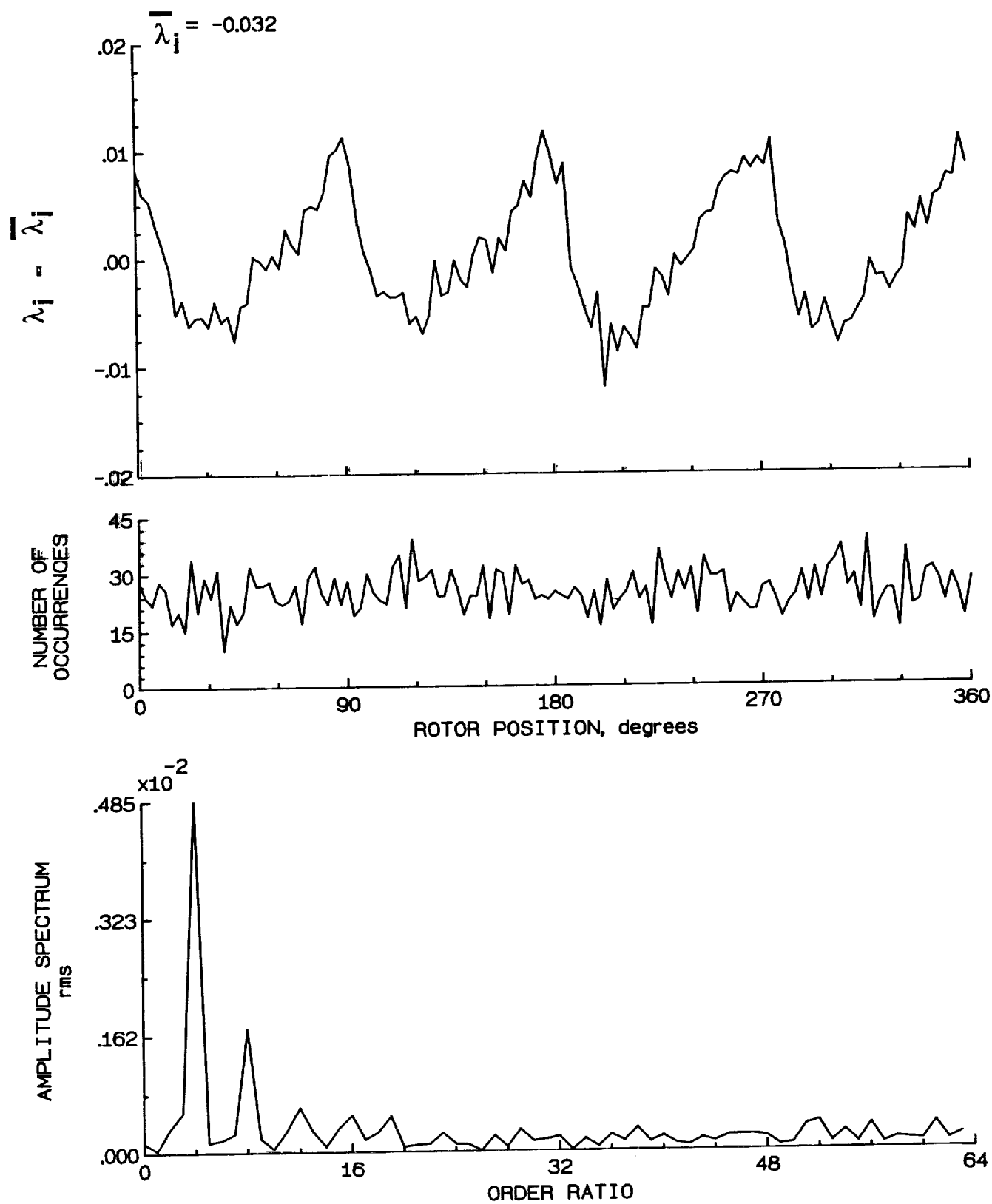


Figure 25.- Concluded.

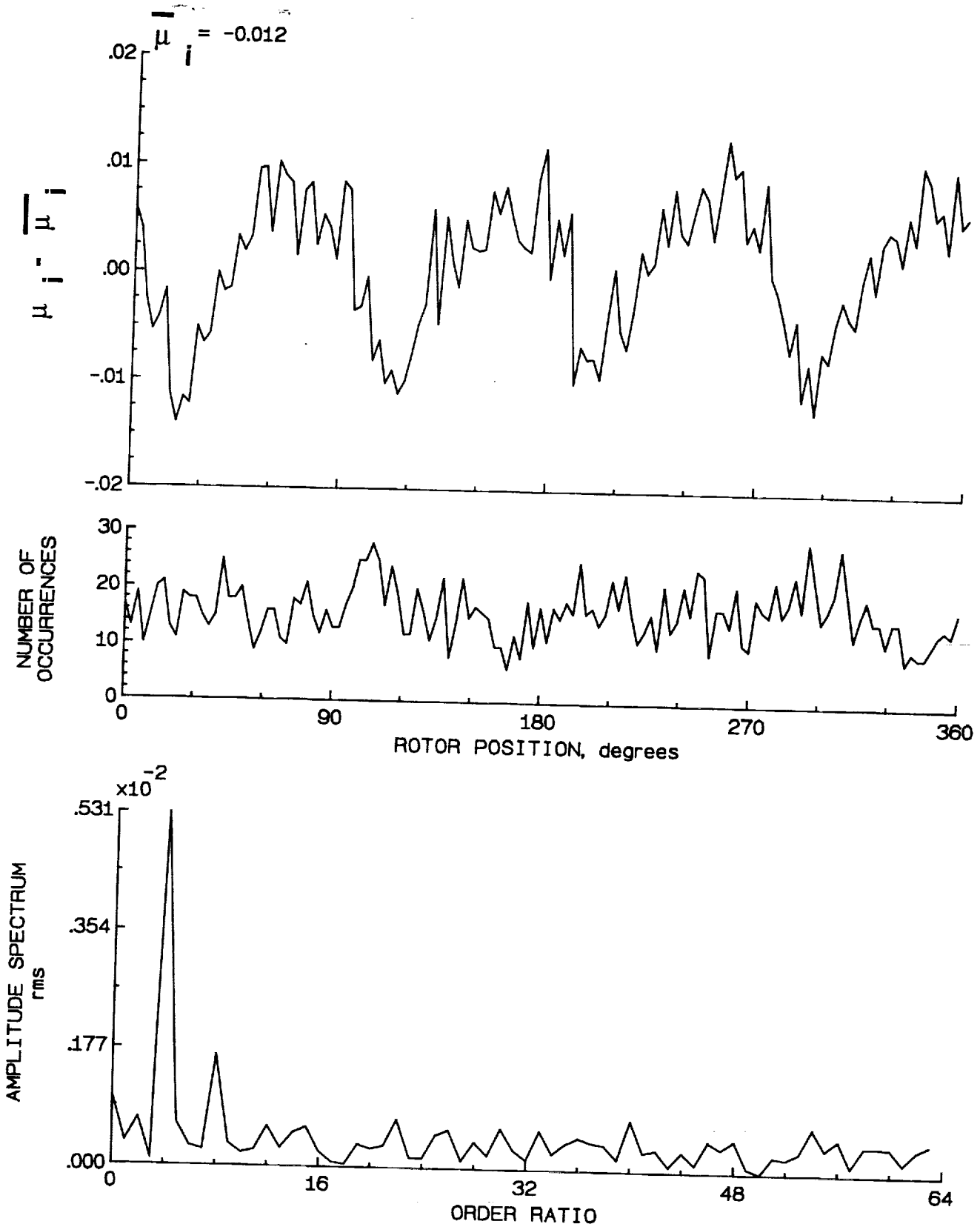


Figure 26.- Induced inflow velocity measured at 0 degrees and r/R of 1.10.

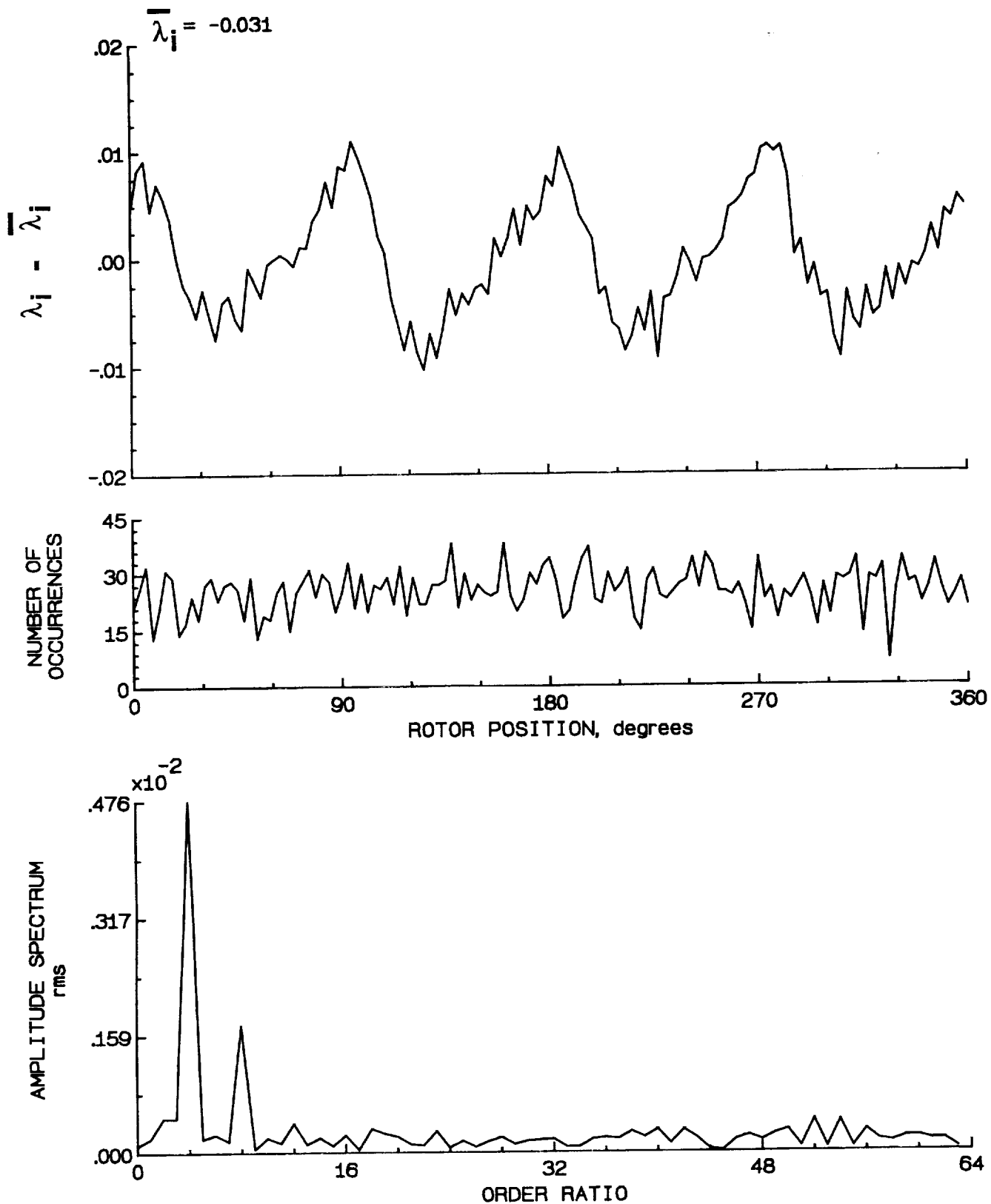


Figure 26.- Concluded.

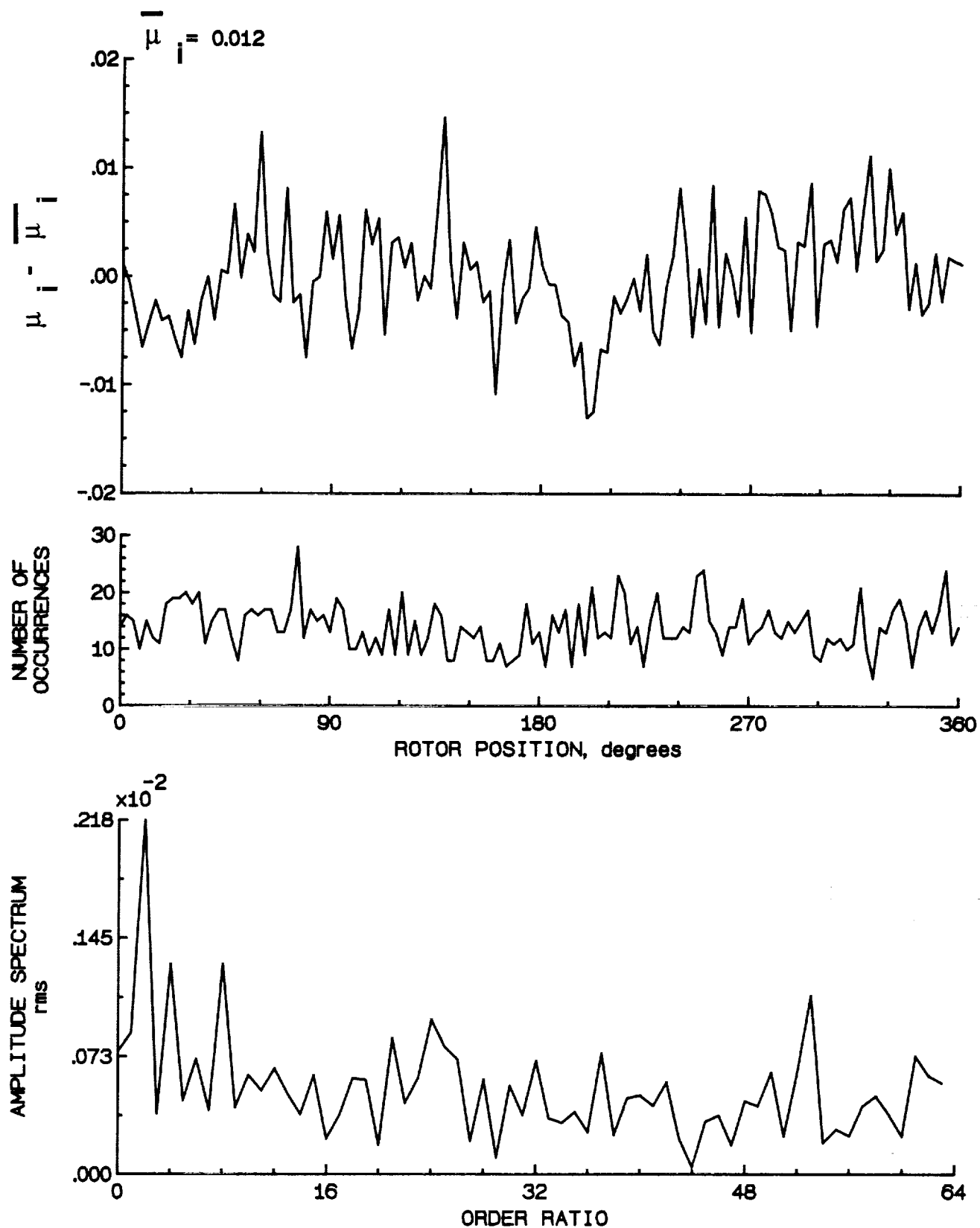


Figure 27.- Induced inflow velocity measured at 30 degrees and r/R of 0.20.

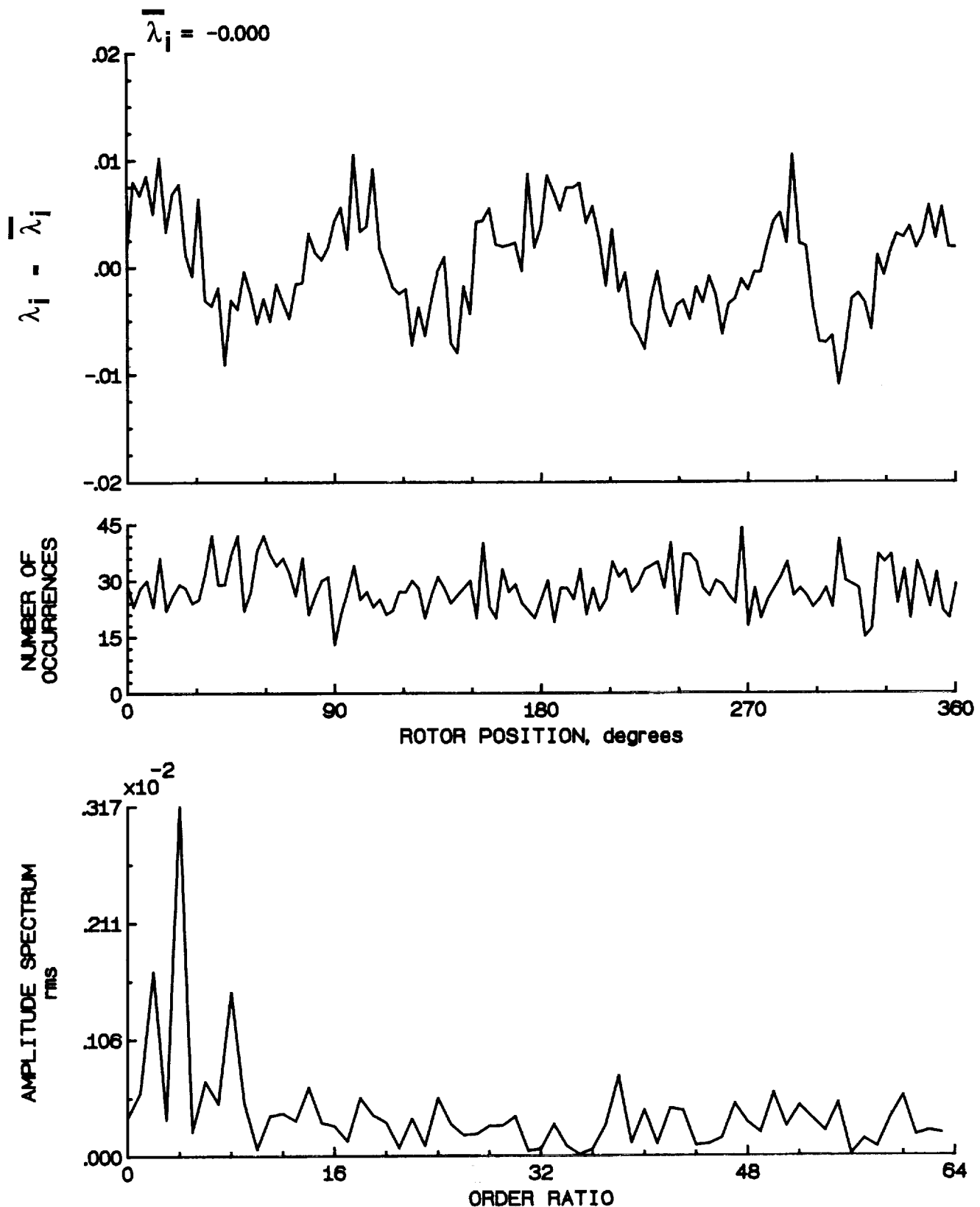


Figure 27.- Concluded.

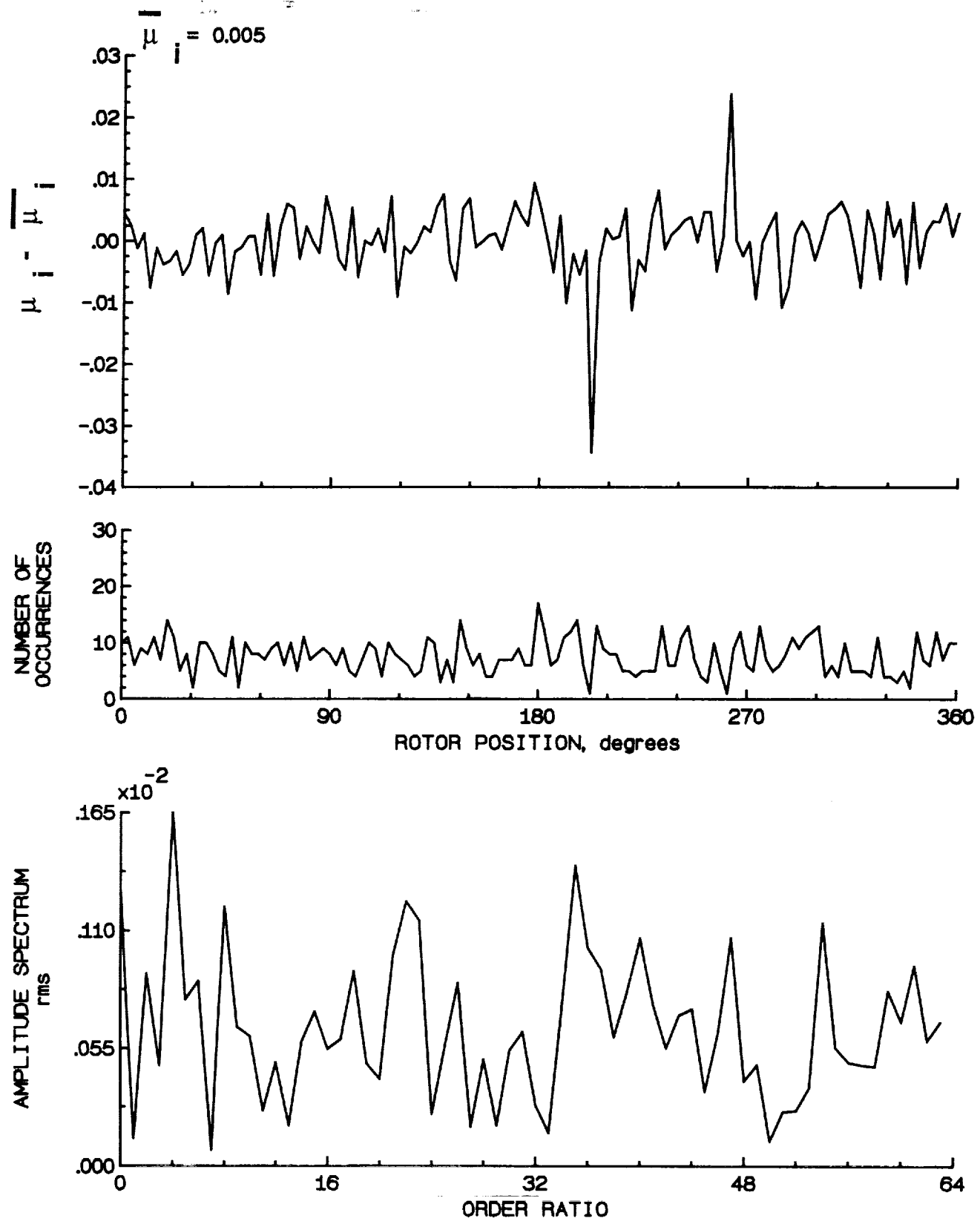


Figure 28.- Induced inflow velocity measured at 30 degrees and r/R of 0.40.

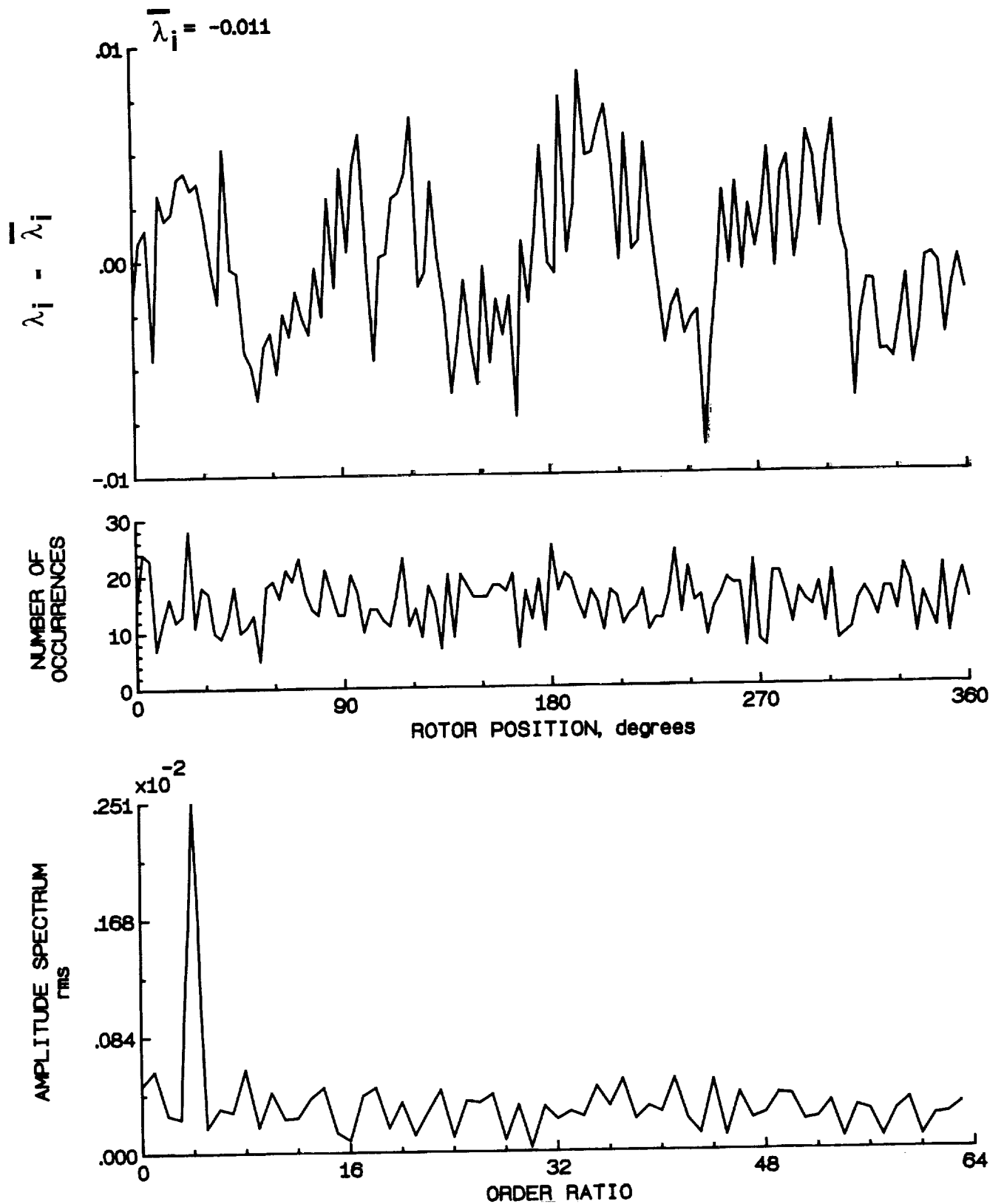


Figure 28.- Concluded.

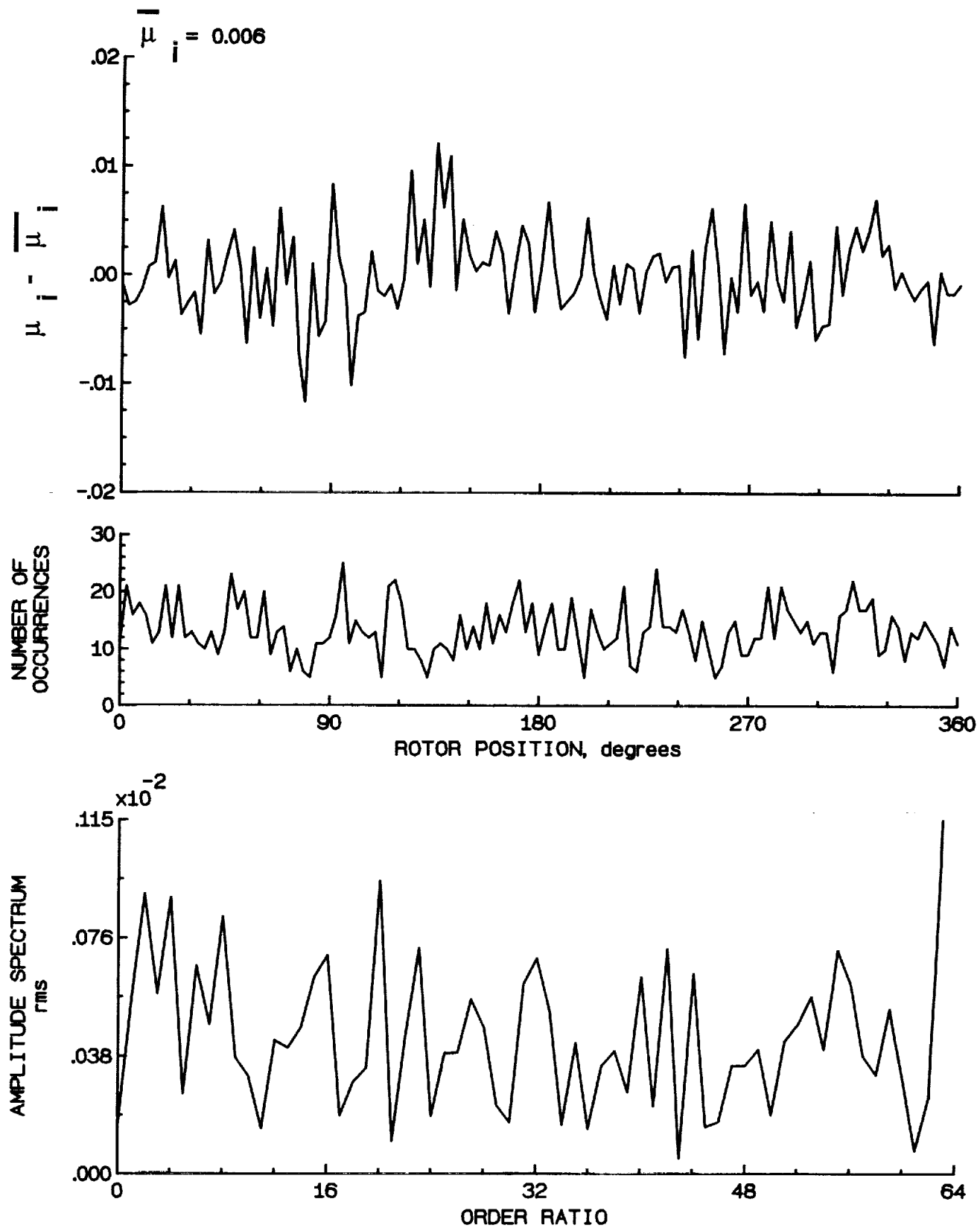


Figure 29.- Induced inflow velocity measured at 30 degrees and r/R of 0.50.

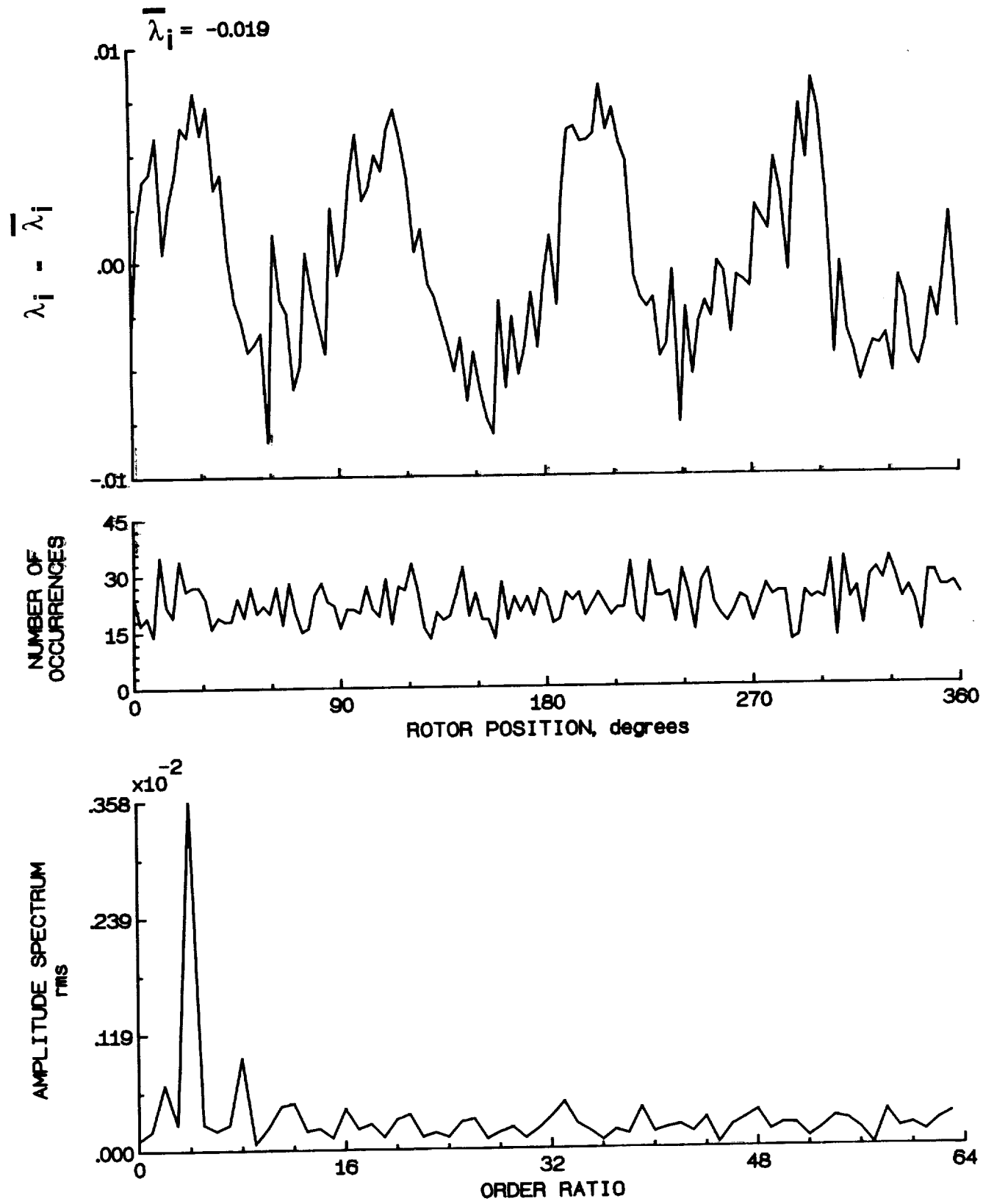


Figure 29.- Concluded.

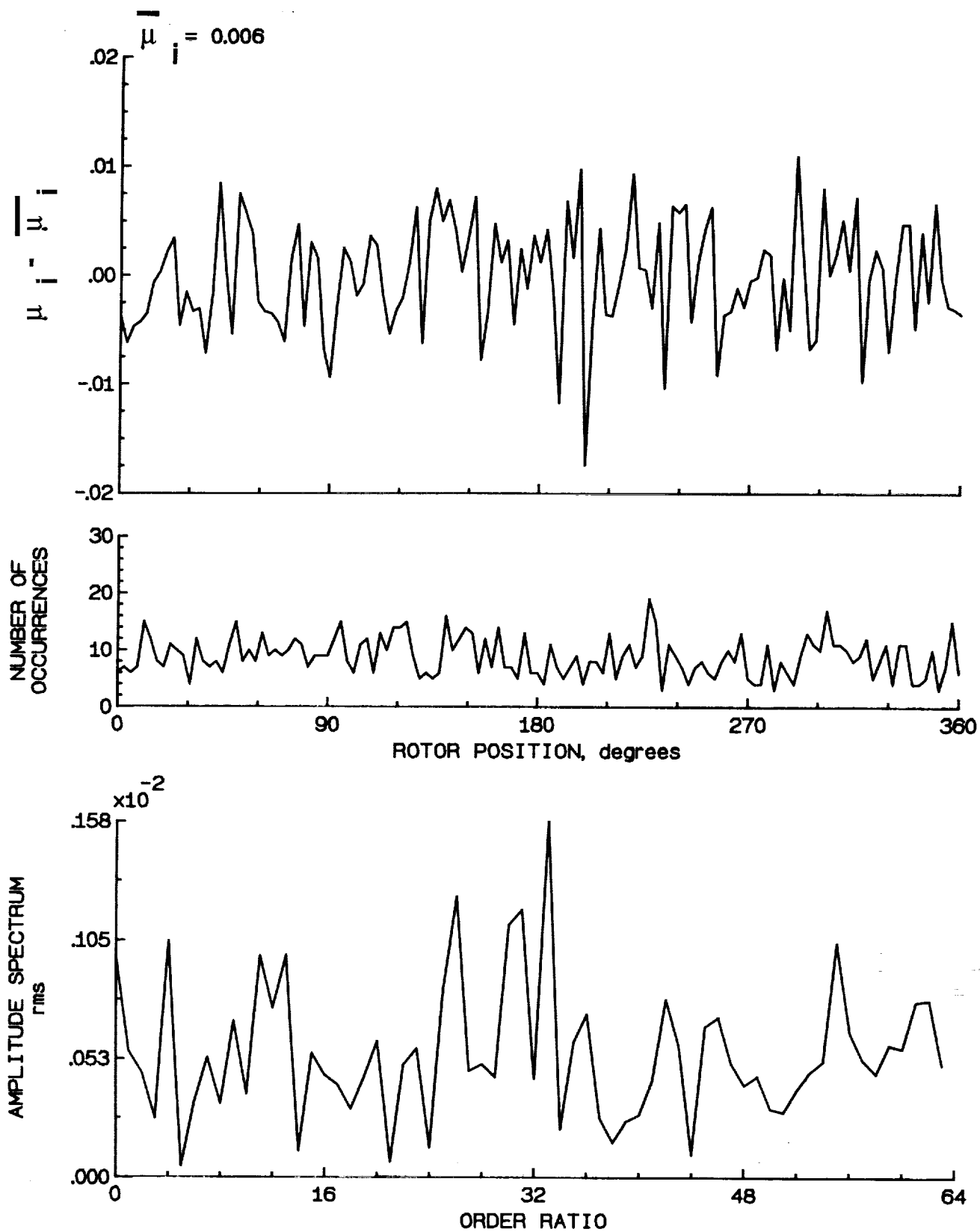


Figure 30.- Induced inflow velocity measured at 30 degrees and r/R of 0.60.

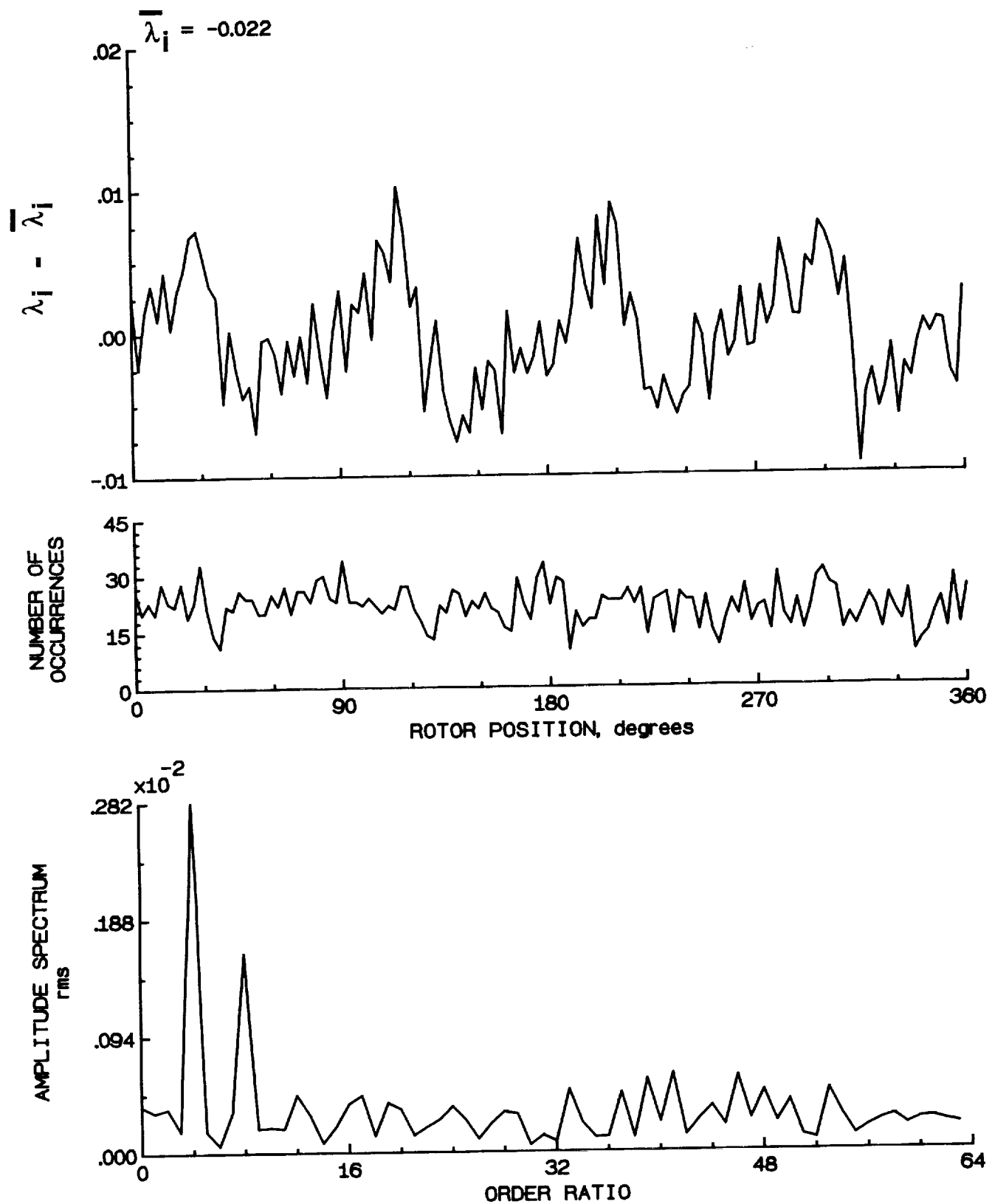


Figure 30.- Concluded.

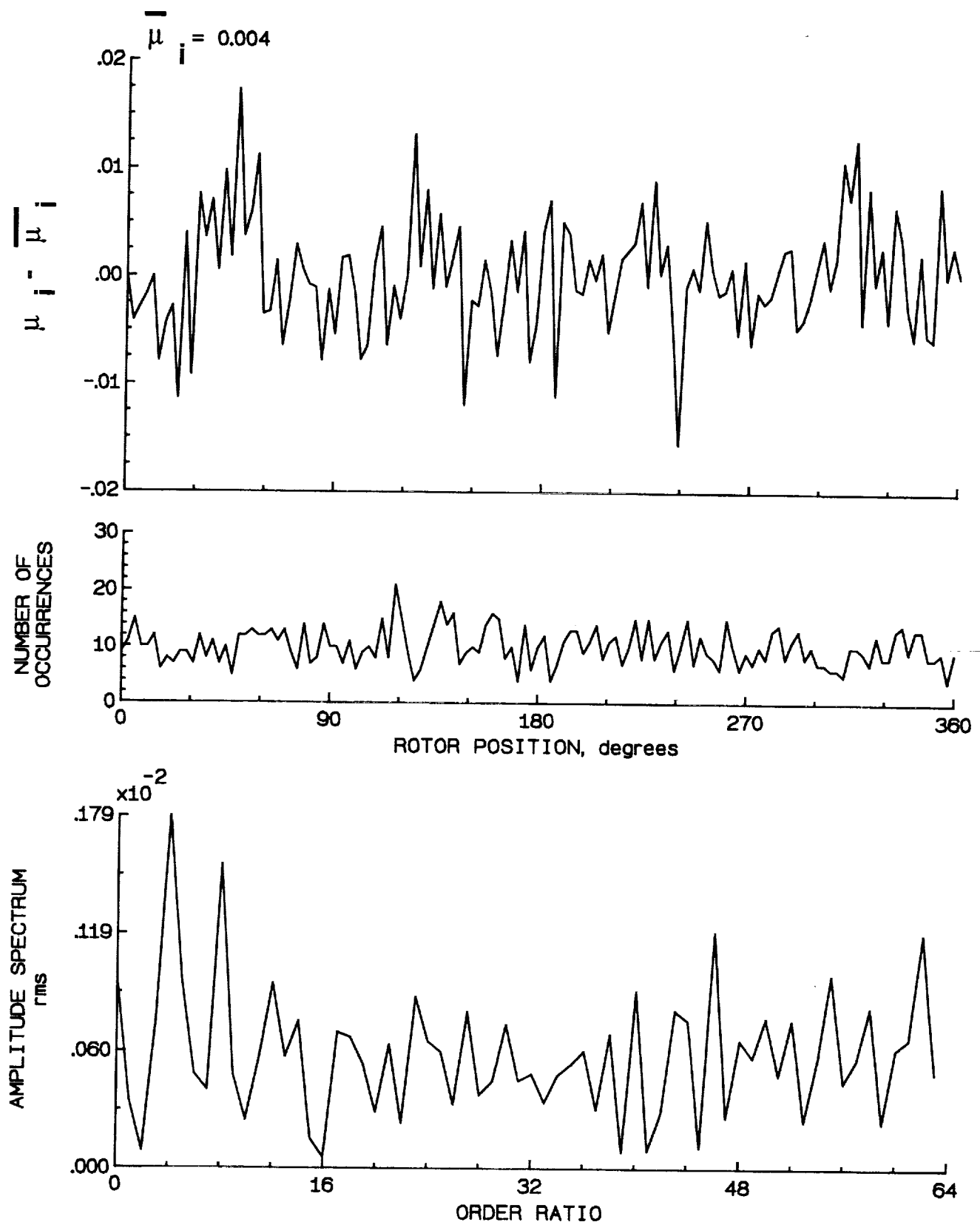


Figure 31.- Induced inflow velocity measured at 30 degrees and r/R of 0.70.

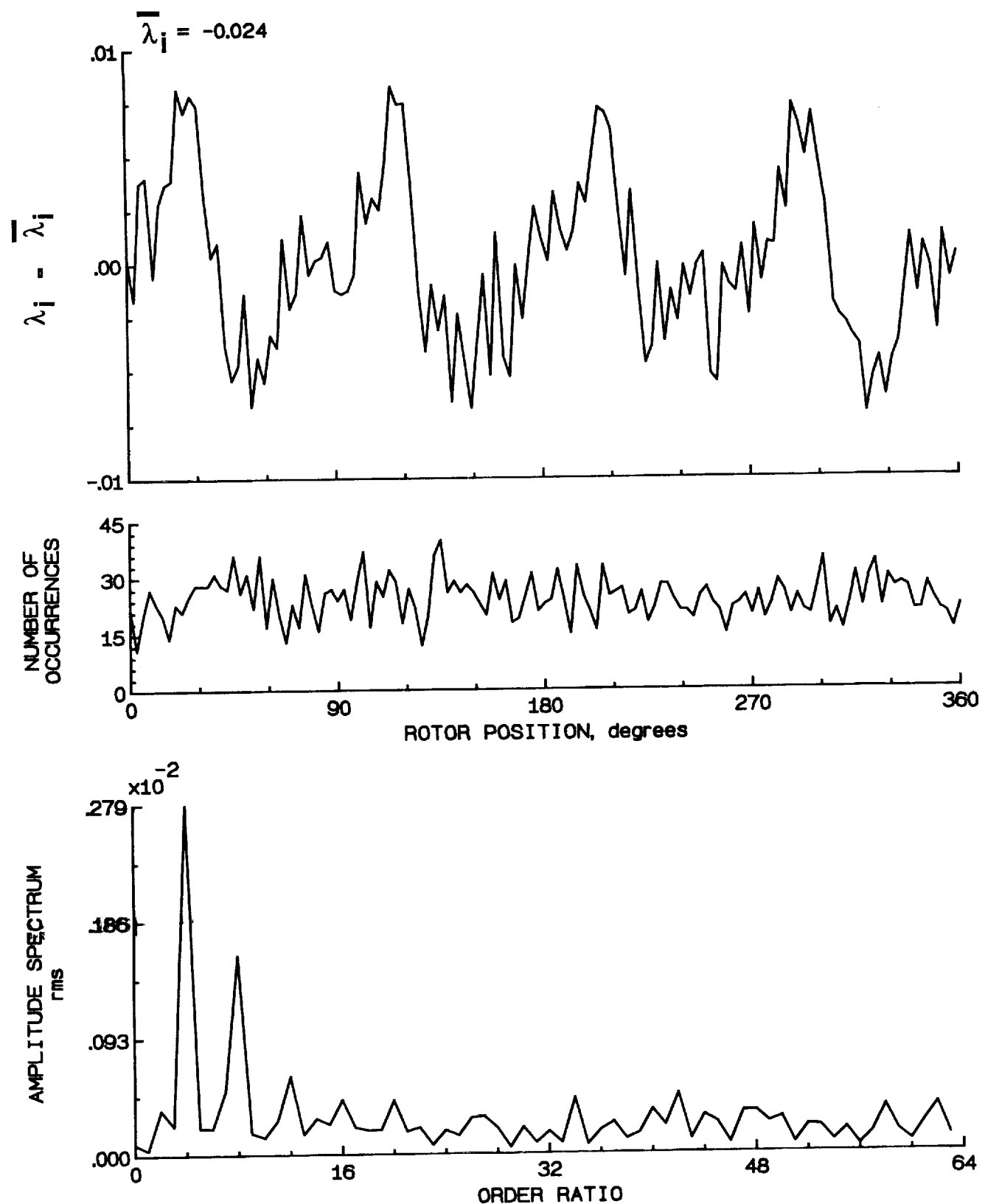


Figure 31.- Concluded.

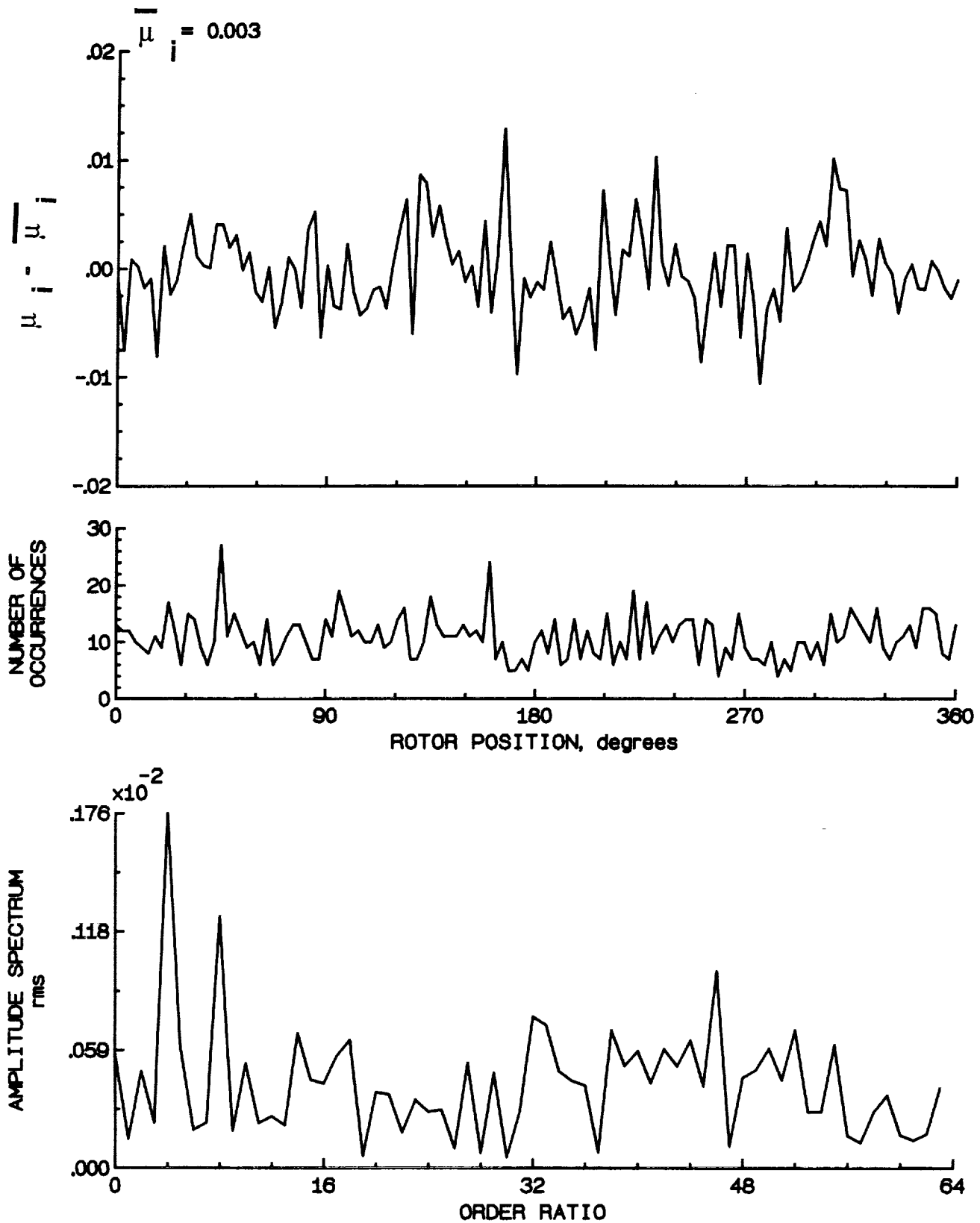


Figure 32.- Induced inflow velocity measured at 30 degrees and r/R of 0.74.

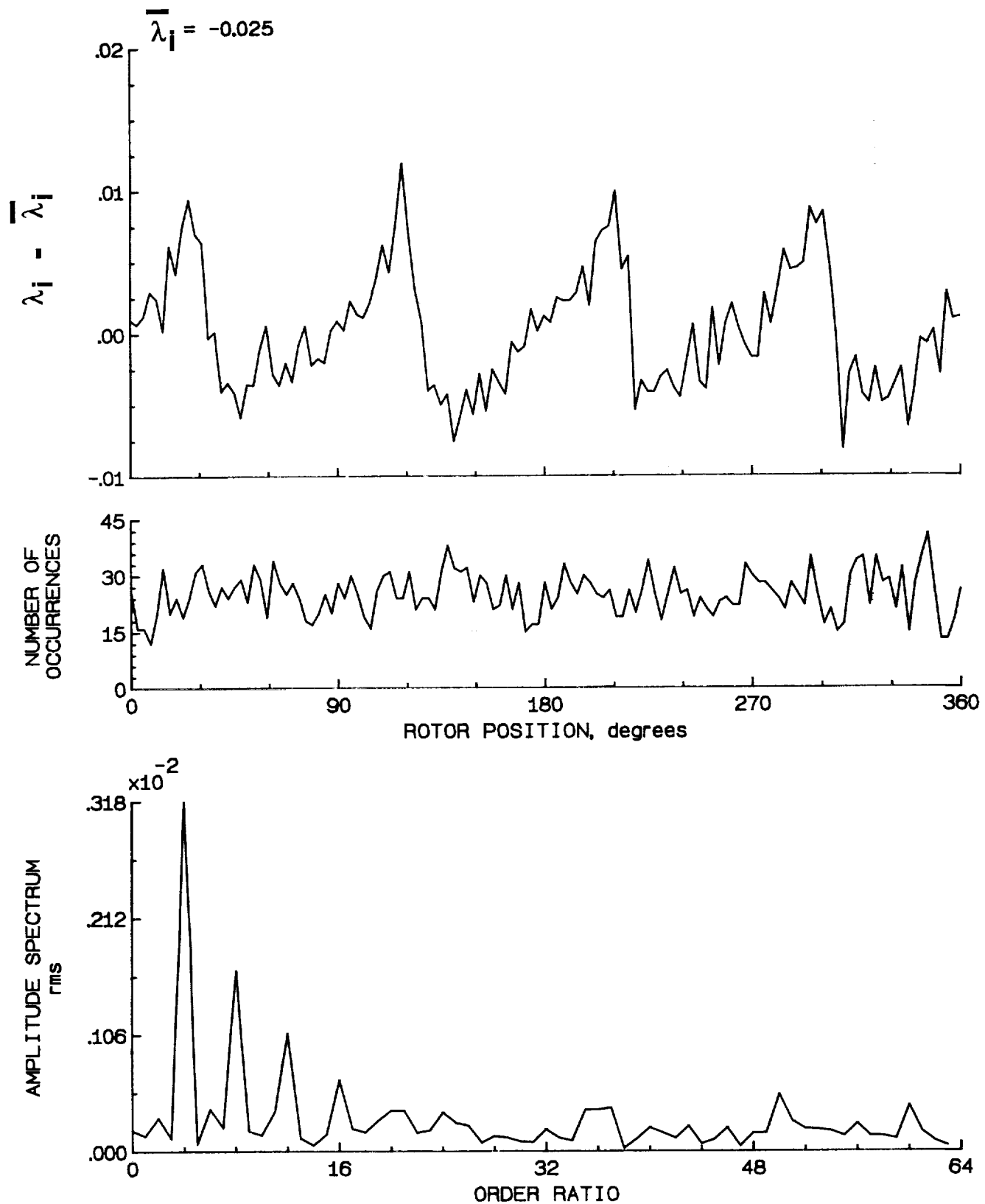


Figure 32.- Concluded.

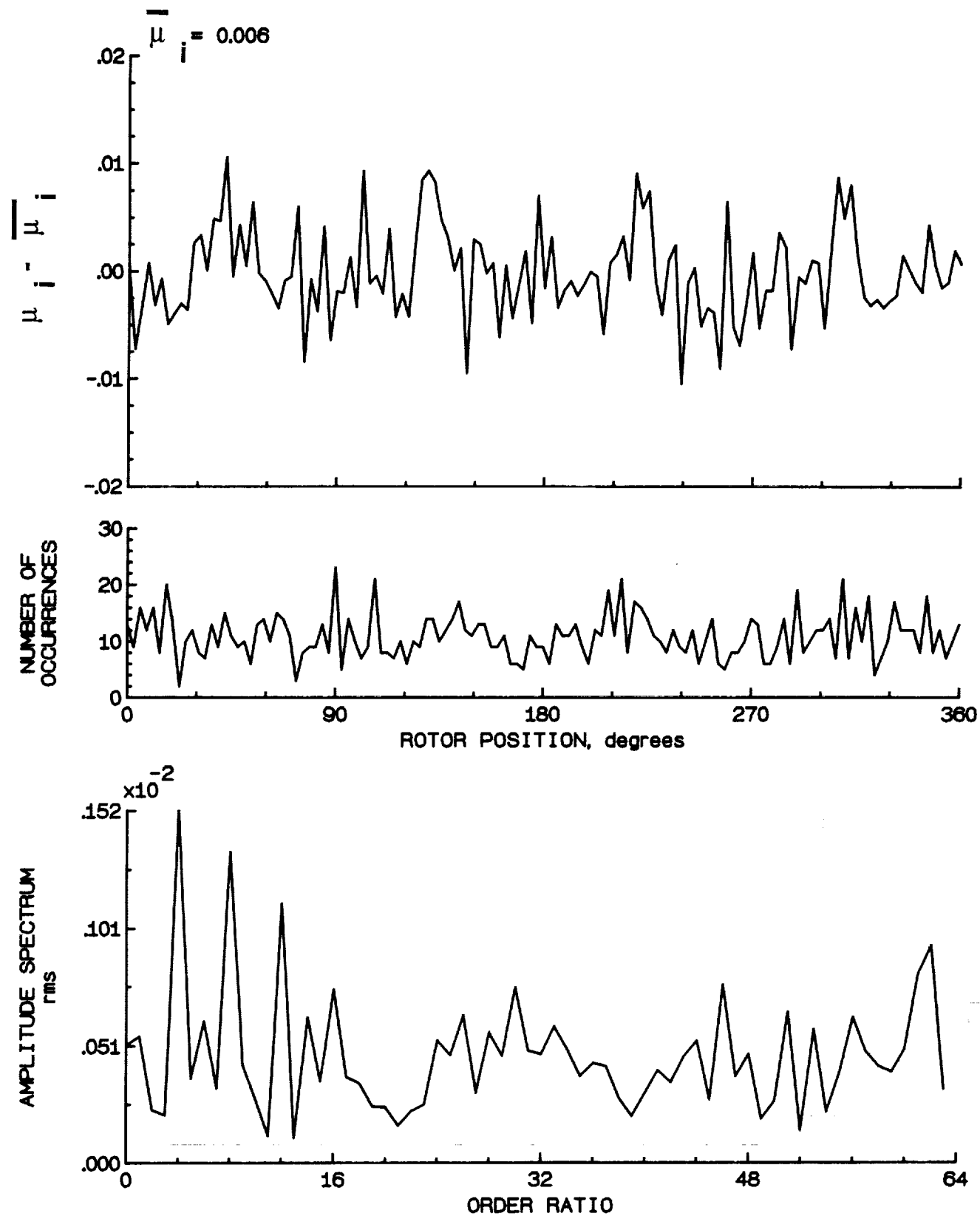


Figure 33.- Induced inflow velocity measured at 30 degrees and r/R of 0.78.

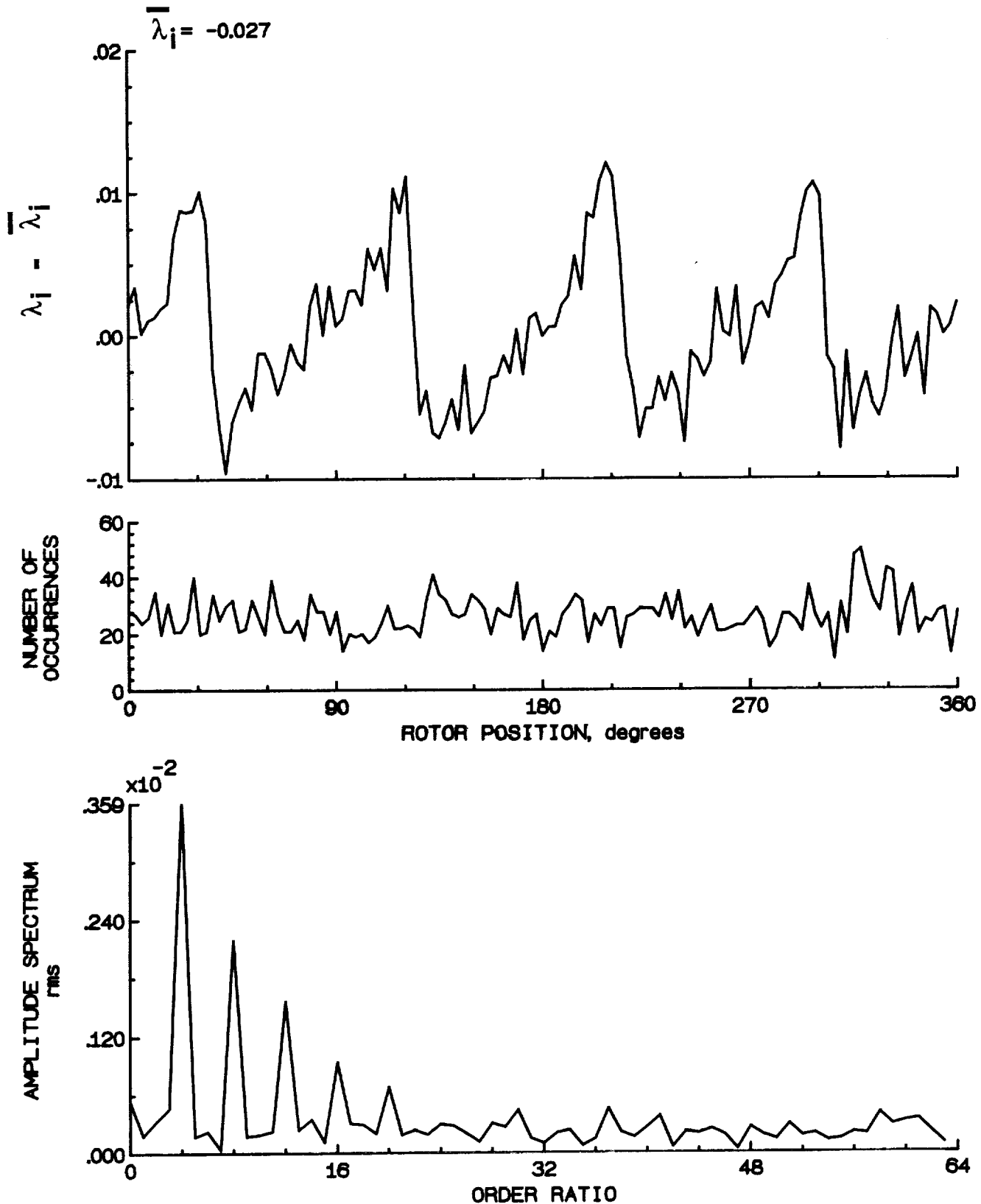


Figure 33.- Concluded.

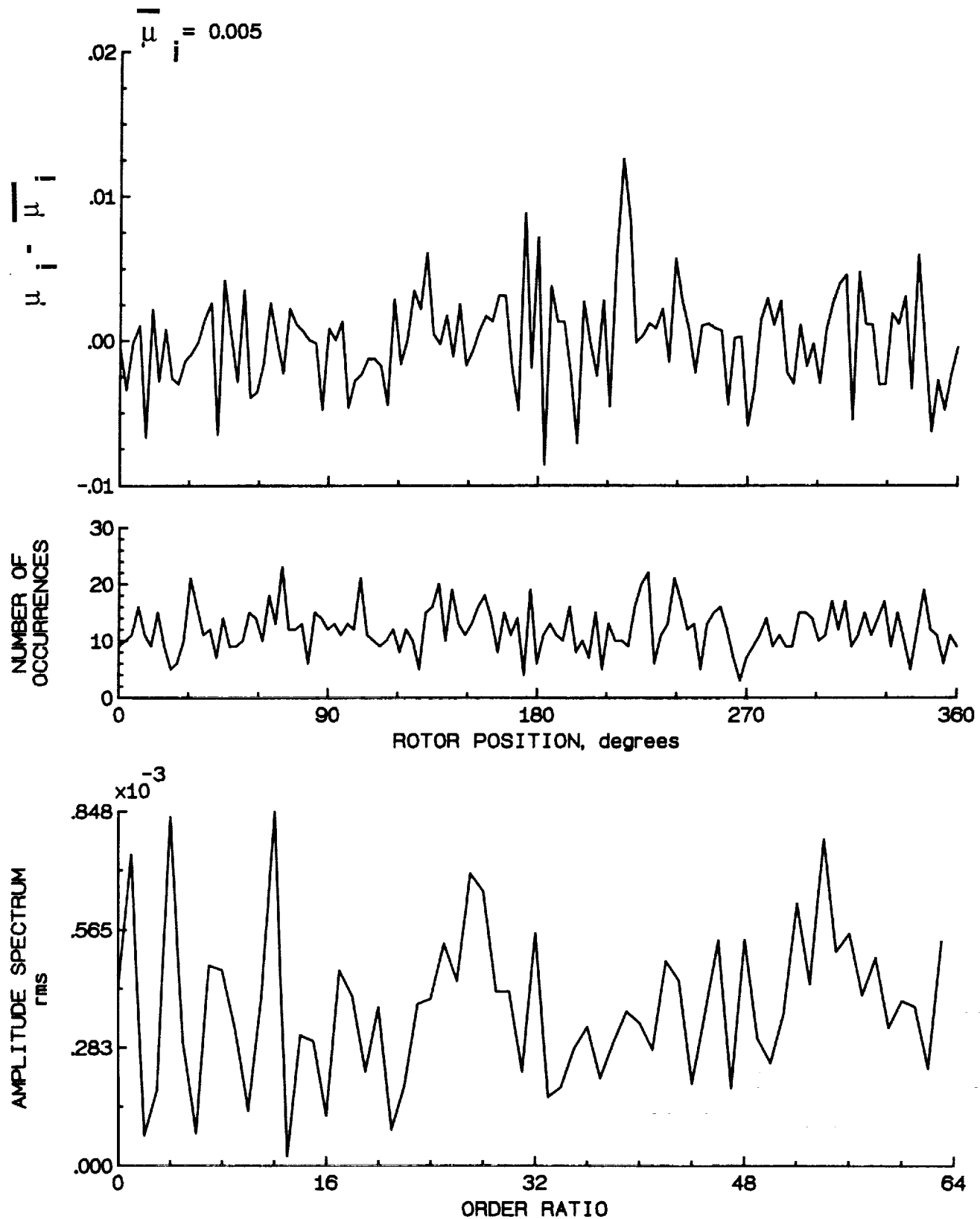


Figure 34.- Induced inflow velocity measured at 30 degrees and r/R of 0.82.

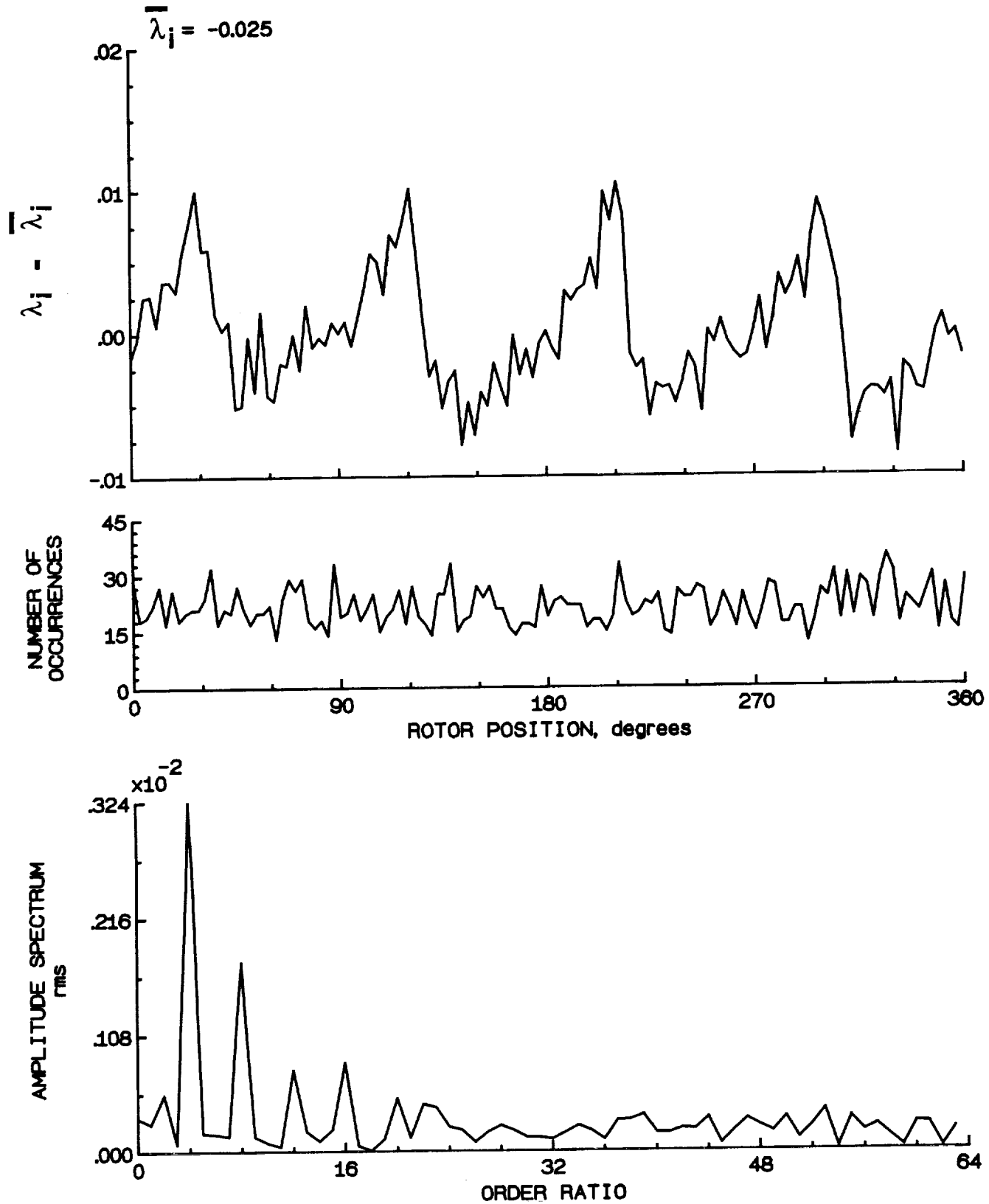


Figure 34.- Concluded.

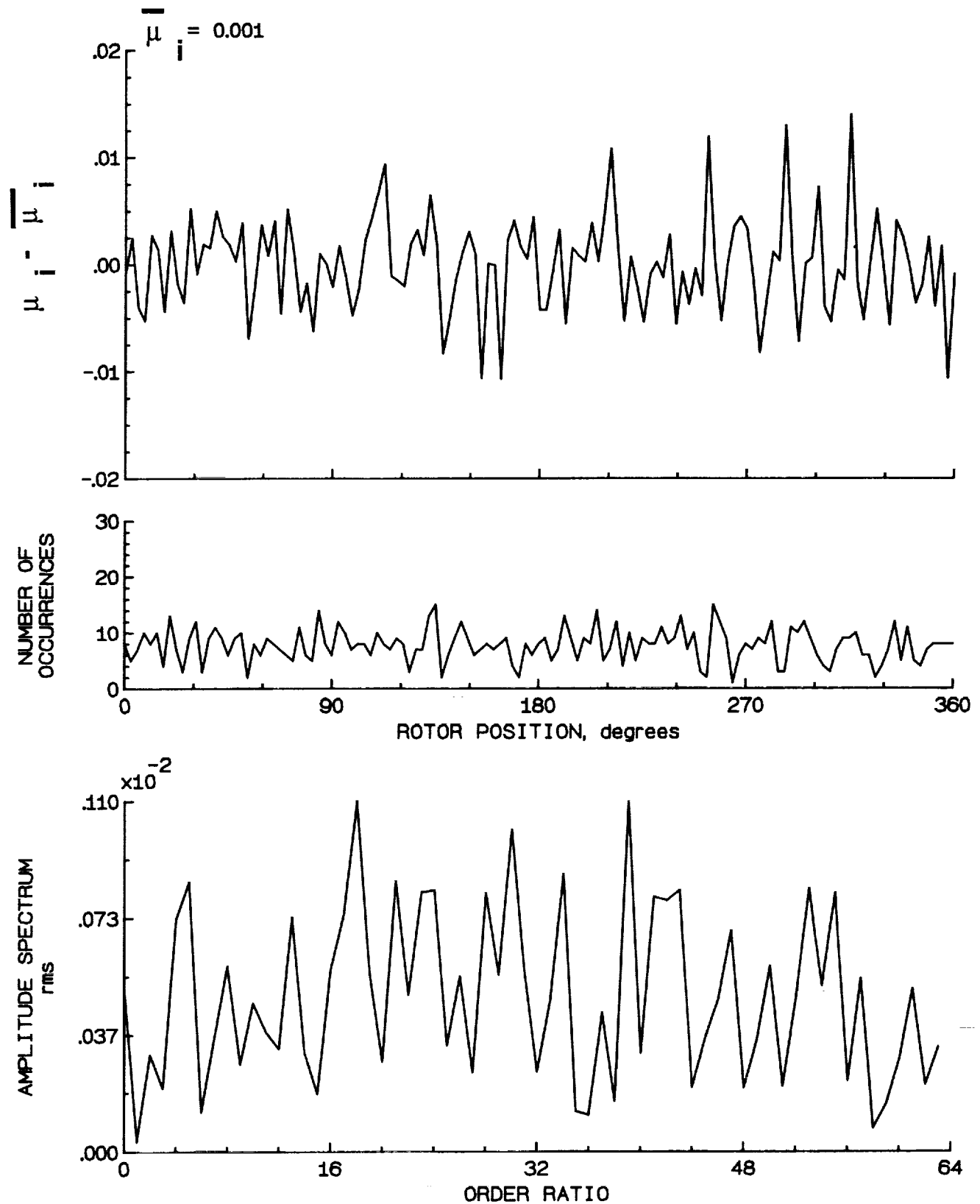


Figure 35.- Induced inflow velocity measured at 30 degrees and r/R of 0.86.

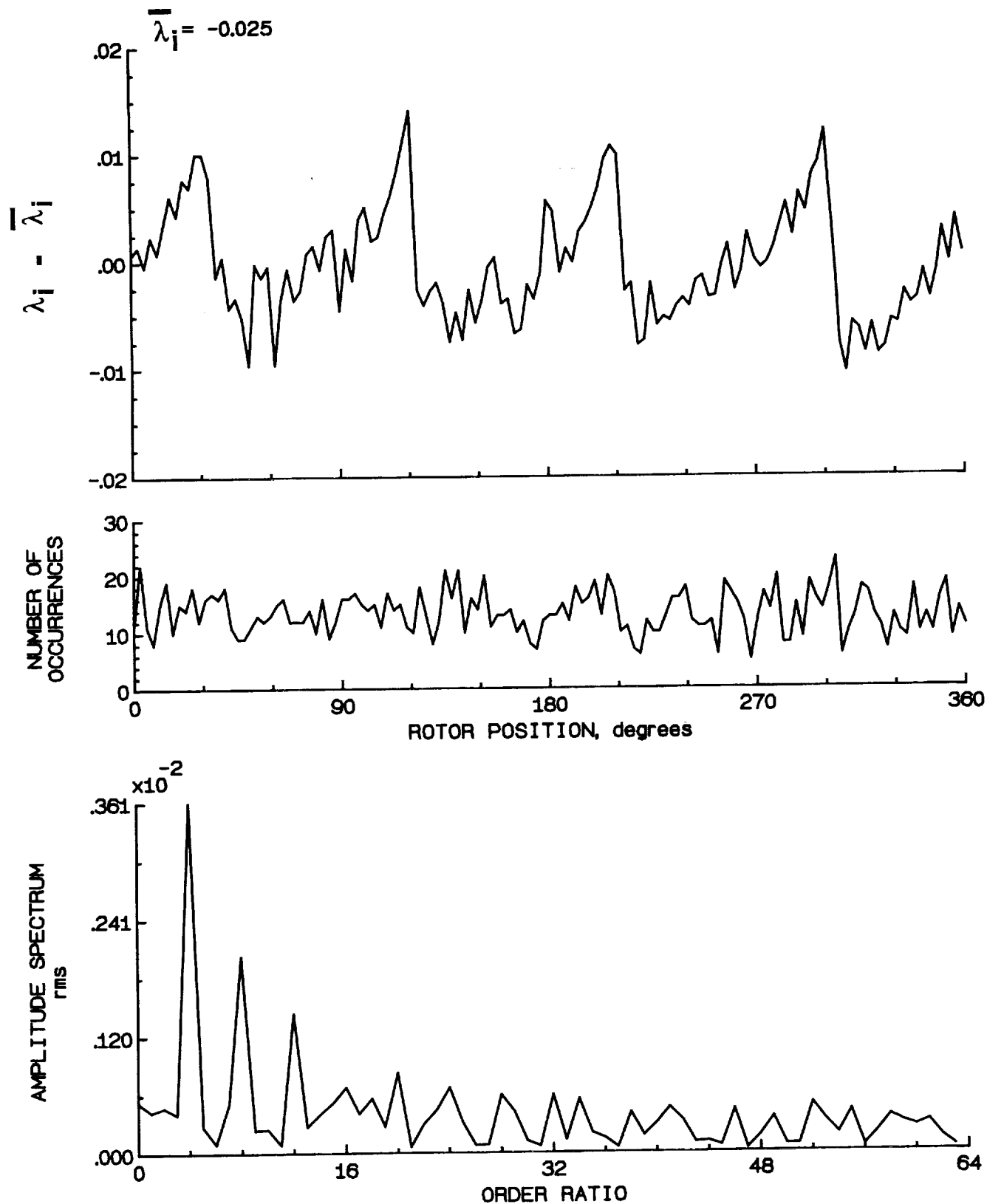


Figure 35.- Concluded.

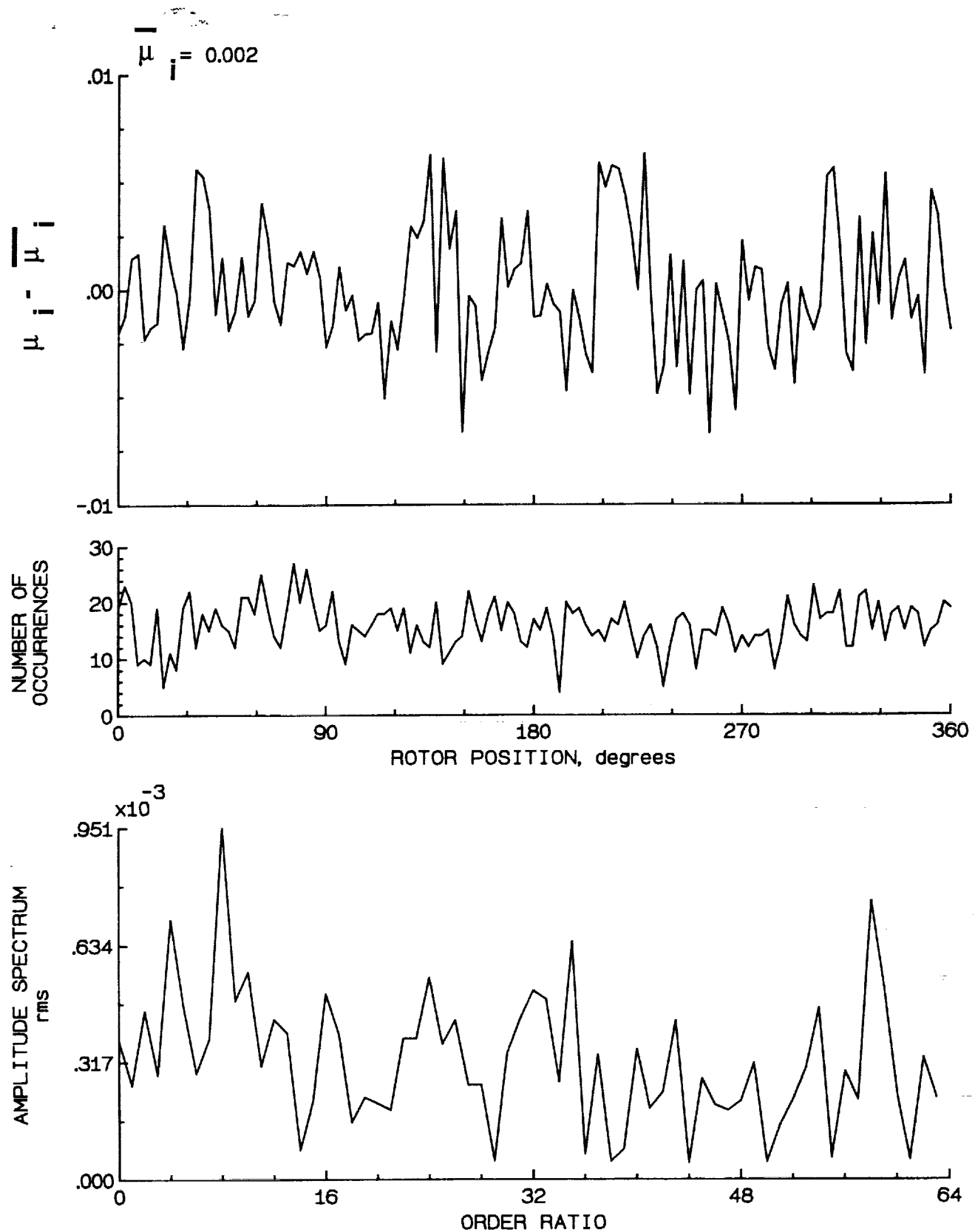


Figure 36.- Induced inflow velocity measured at 30 degrees and r/R of 0.90.

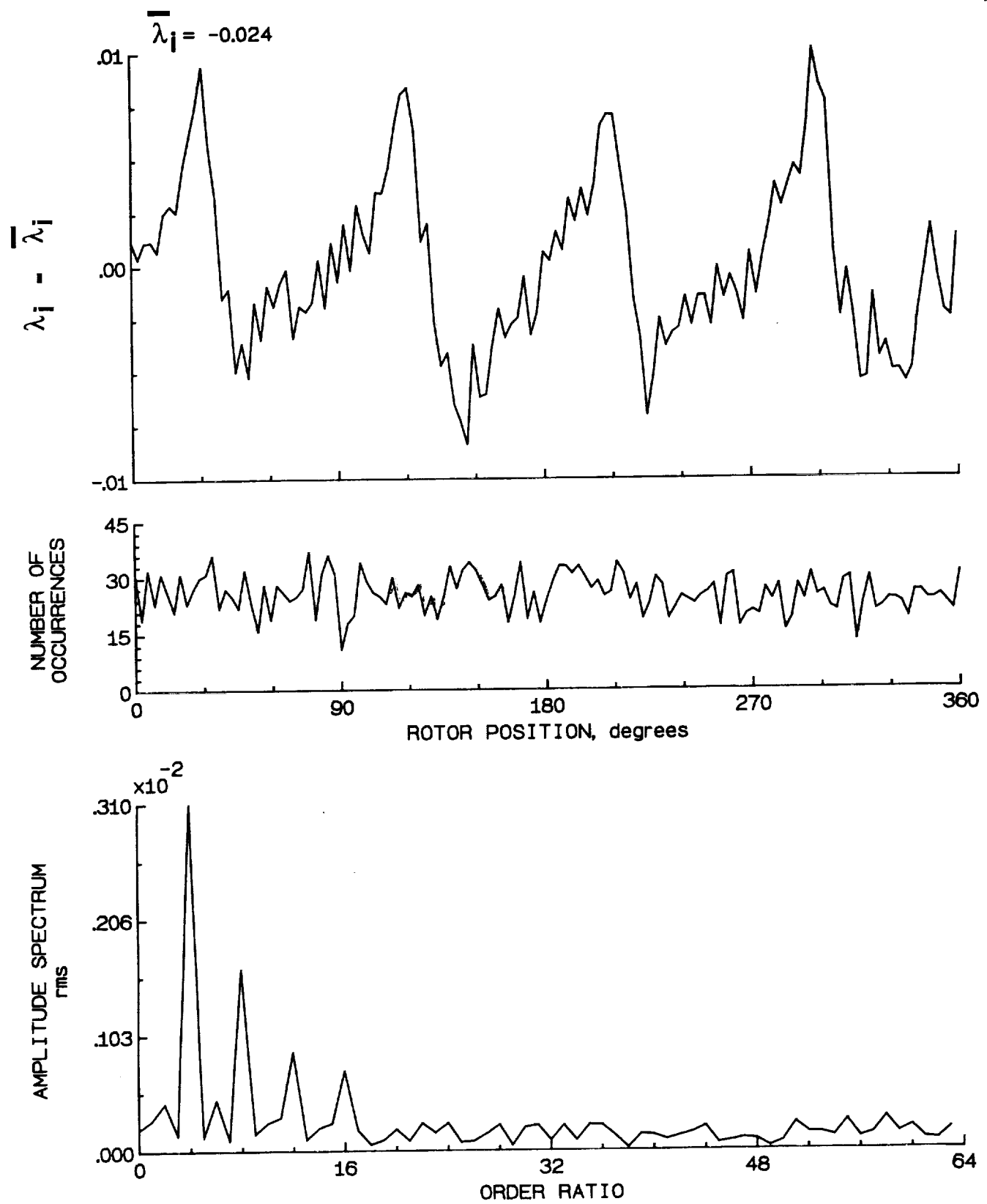


Figure 36.- Concluded.

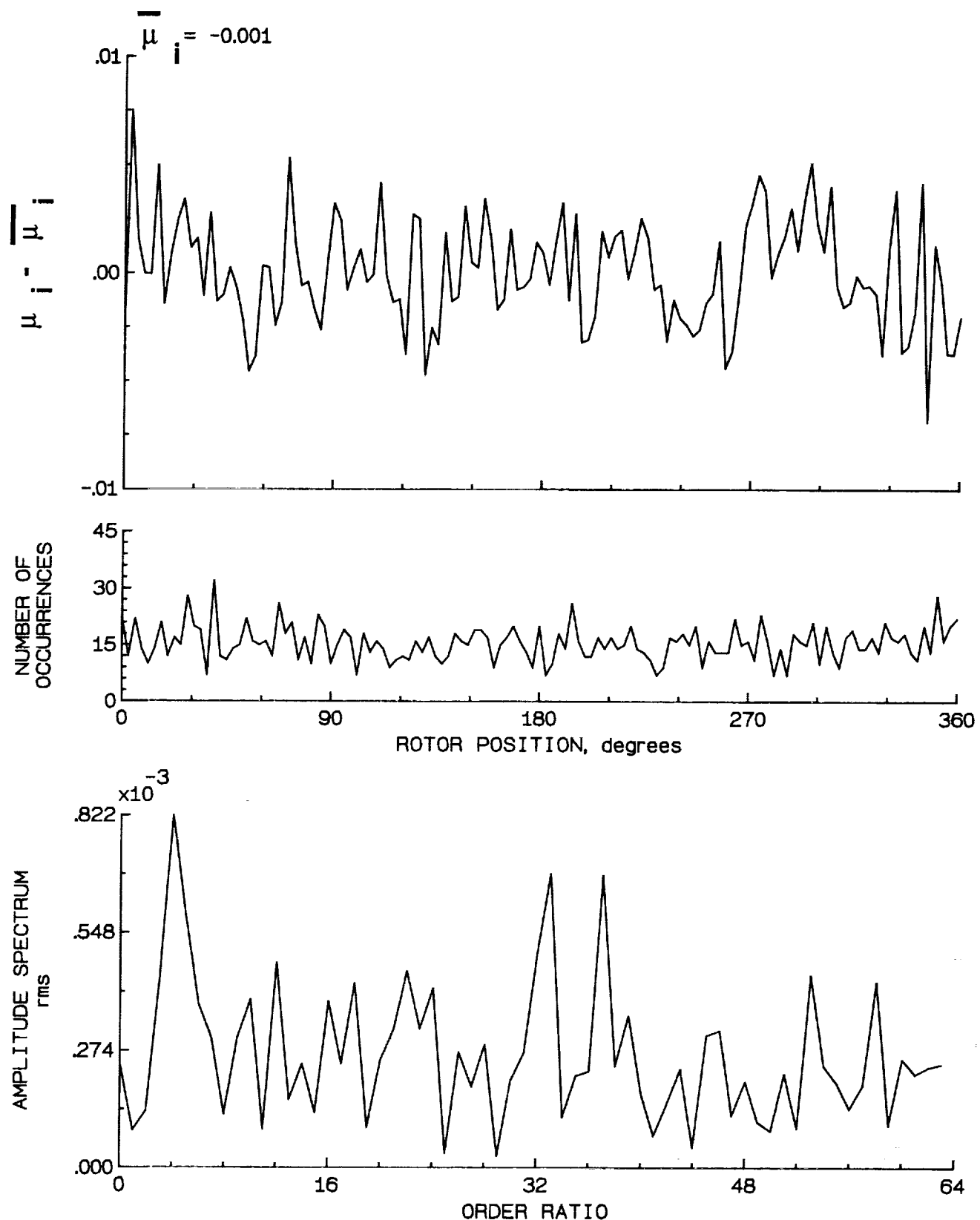


Figure 37.- Induced inflow velocity measured at 30 degrees and r/R of 0.94.

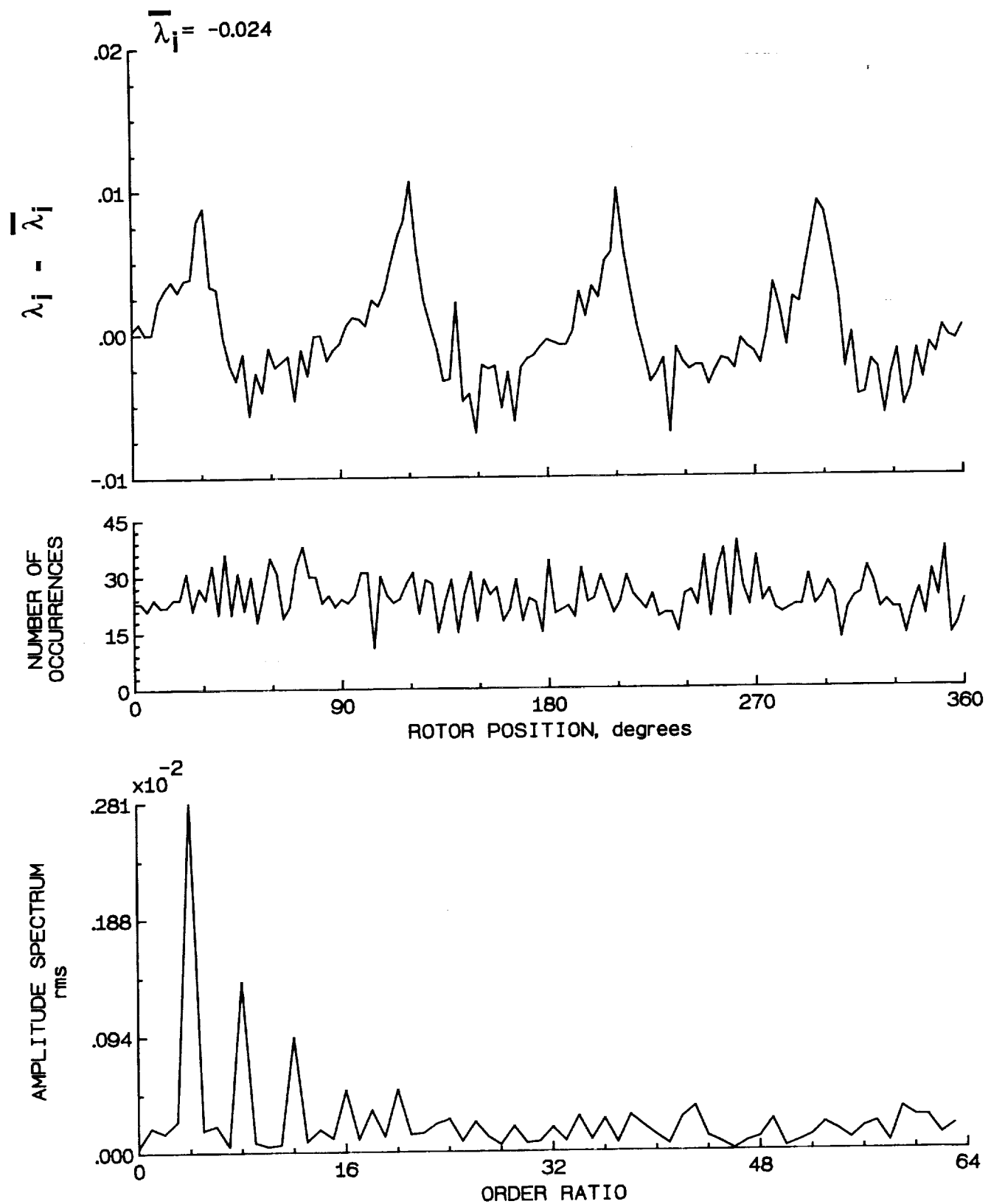


Figure 37.- Concluded.

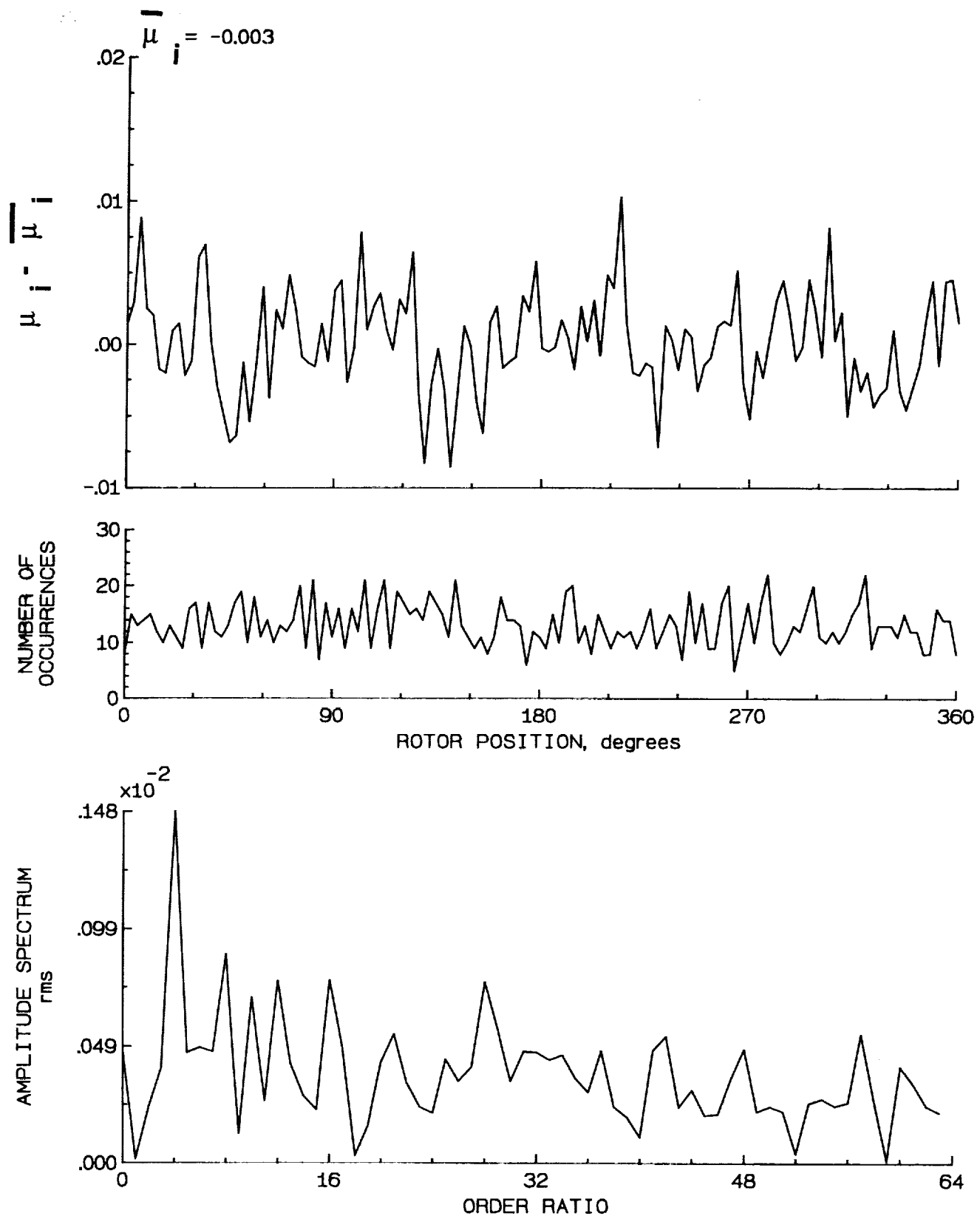


Figure 38.- Induced inflow velocity measured at 30 degrees and r/R of 0.98.

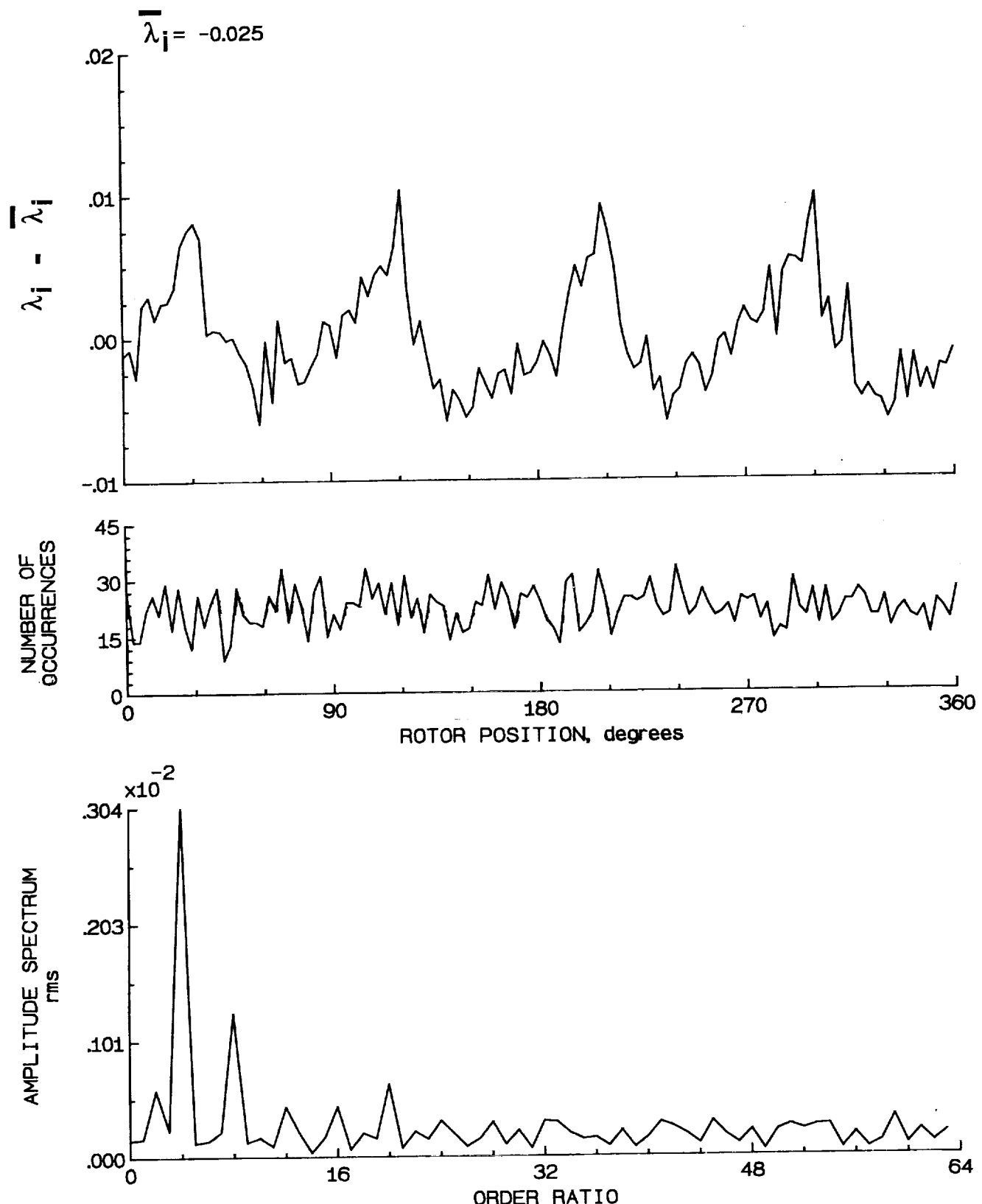


Figure 38.- Concluded.

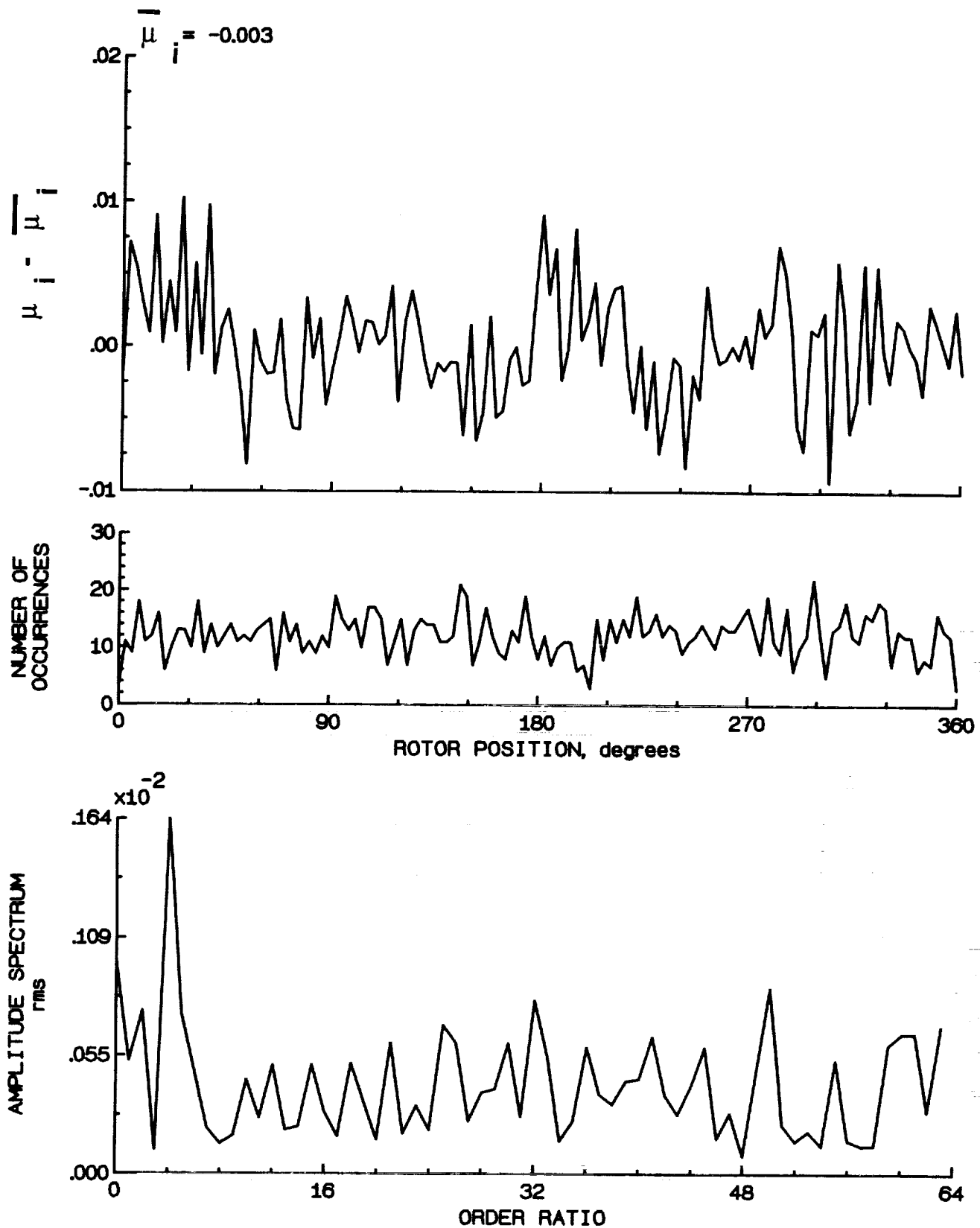


Figure 39.- Induced inflow velocity measured at 30 degrees and r/R of 1.02.

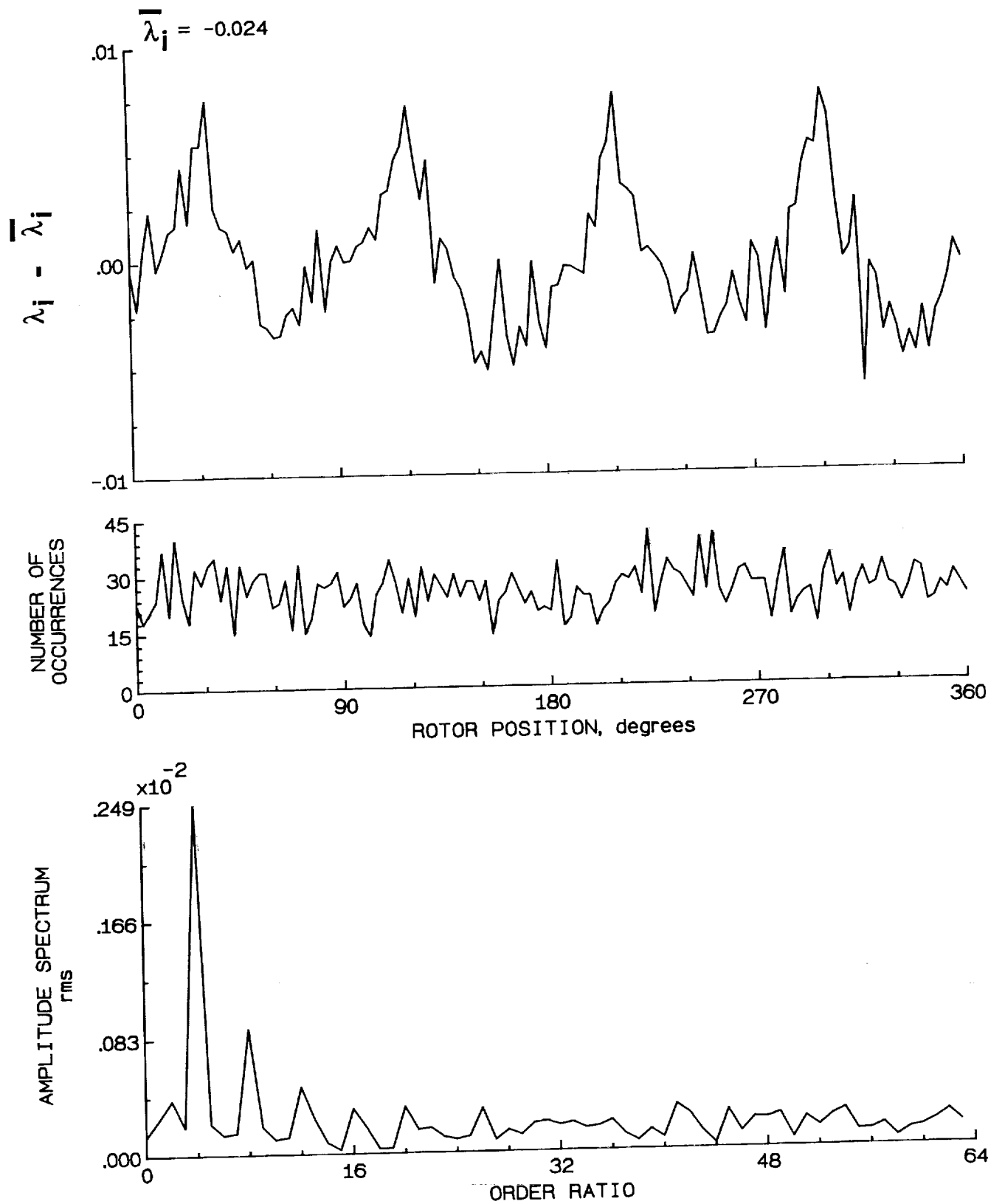


Figure 39.- Concluded.

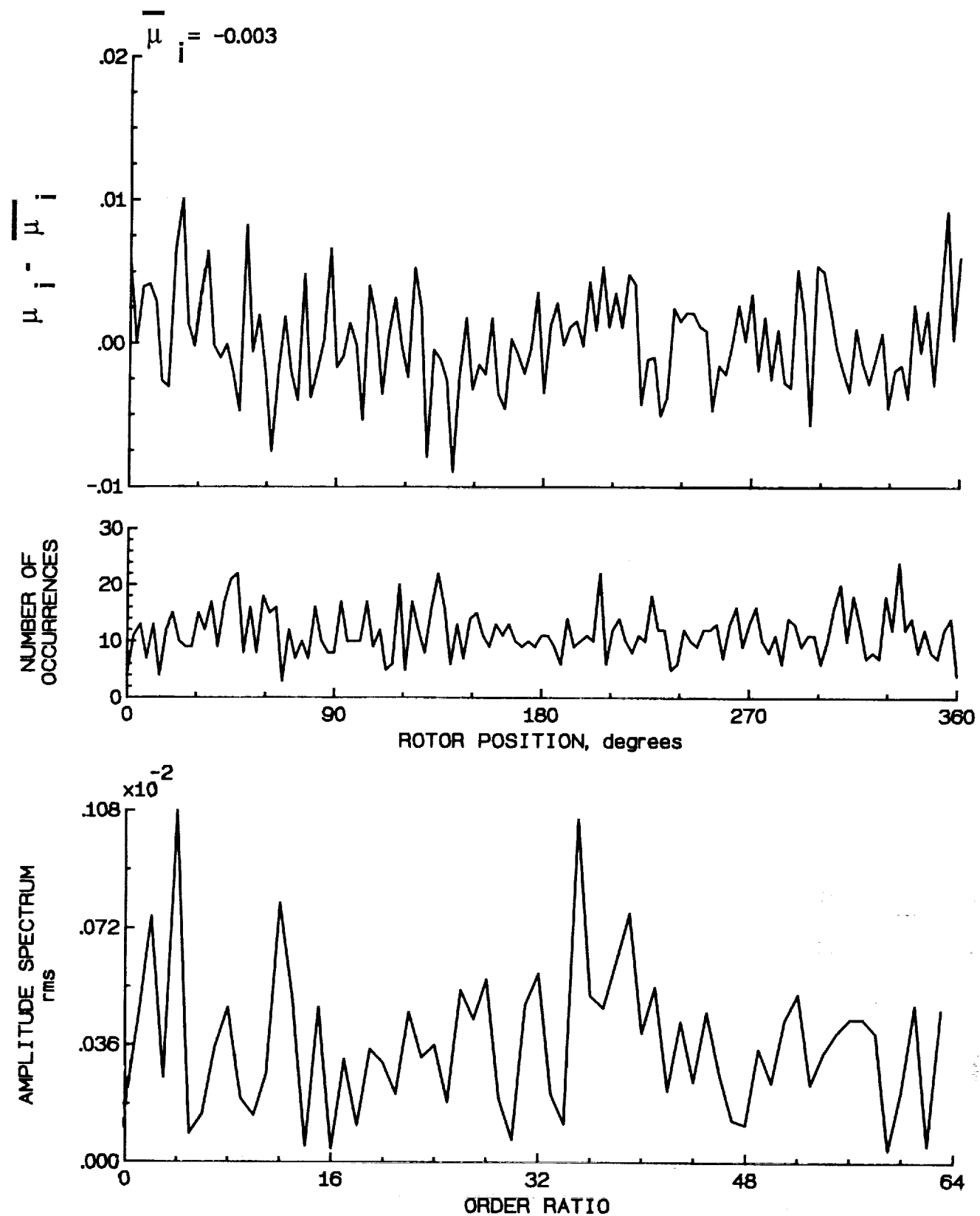


Figure 40.- Induced inflow velocity measured at 30 degrees and r/R of 1.04.

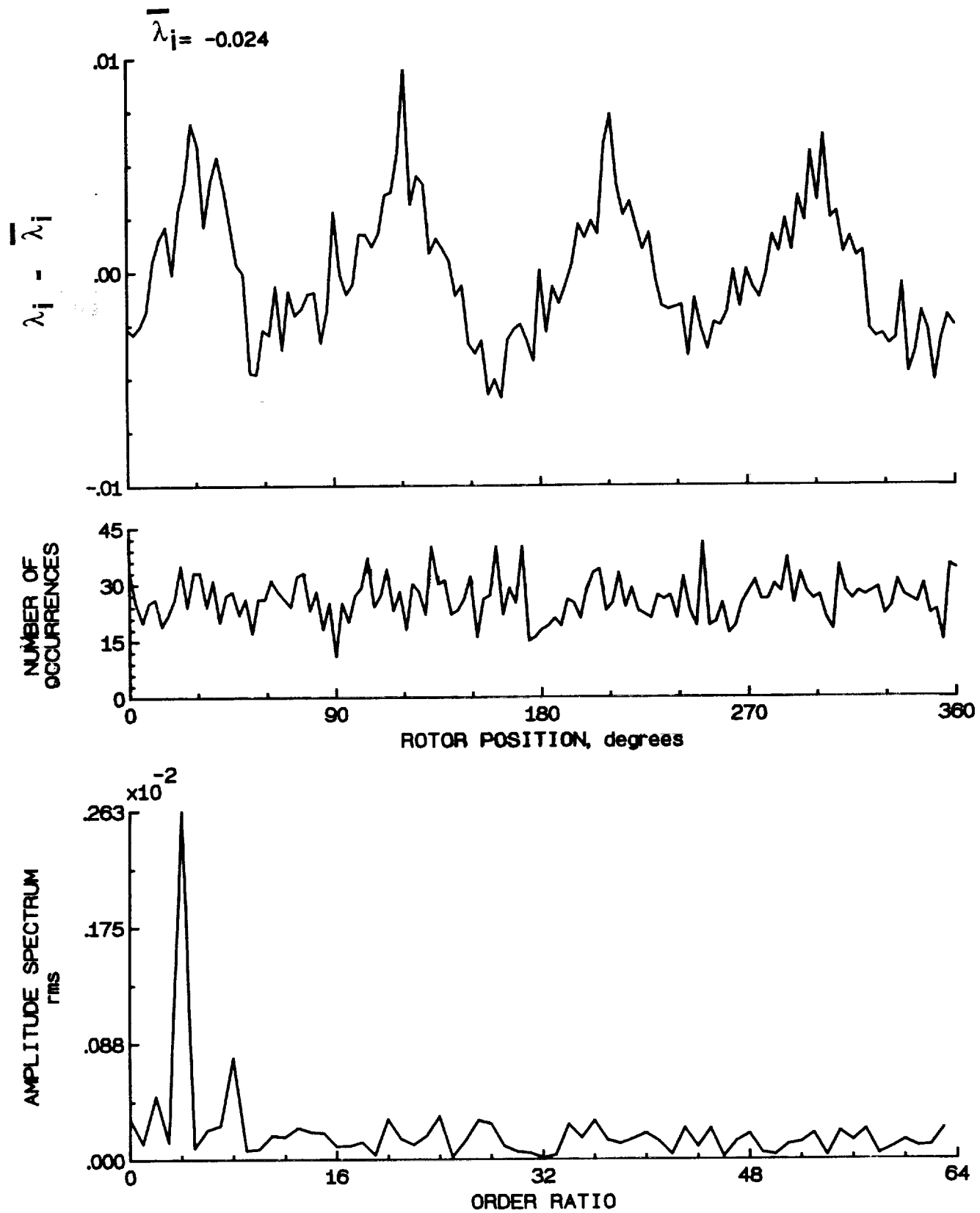


Figure 40.- Concluded.

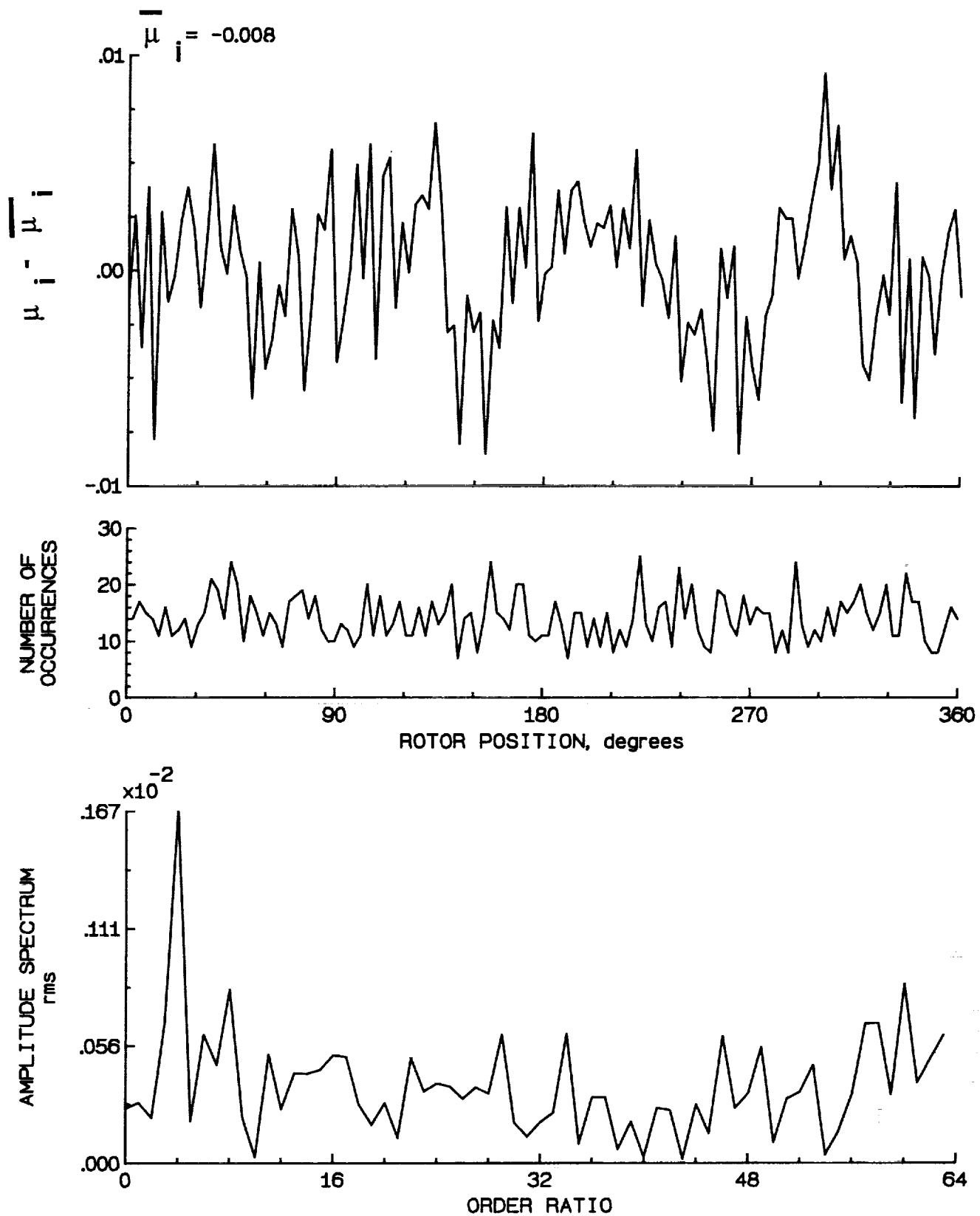


Figure 41.- Induced inflow velocity measured at 30 degrees and r/R of 1.10.

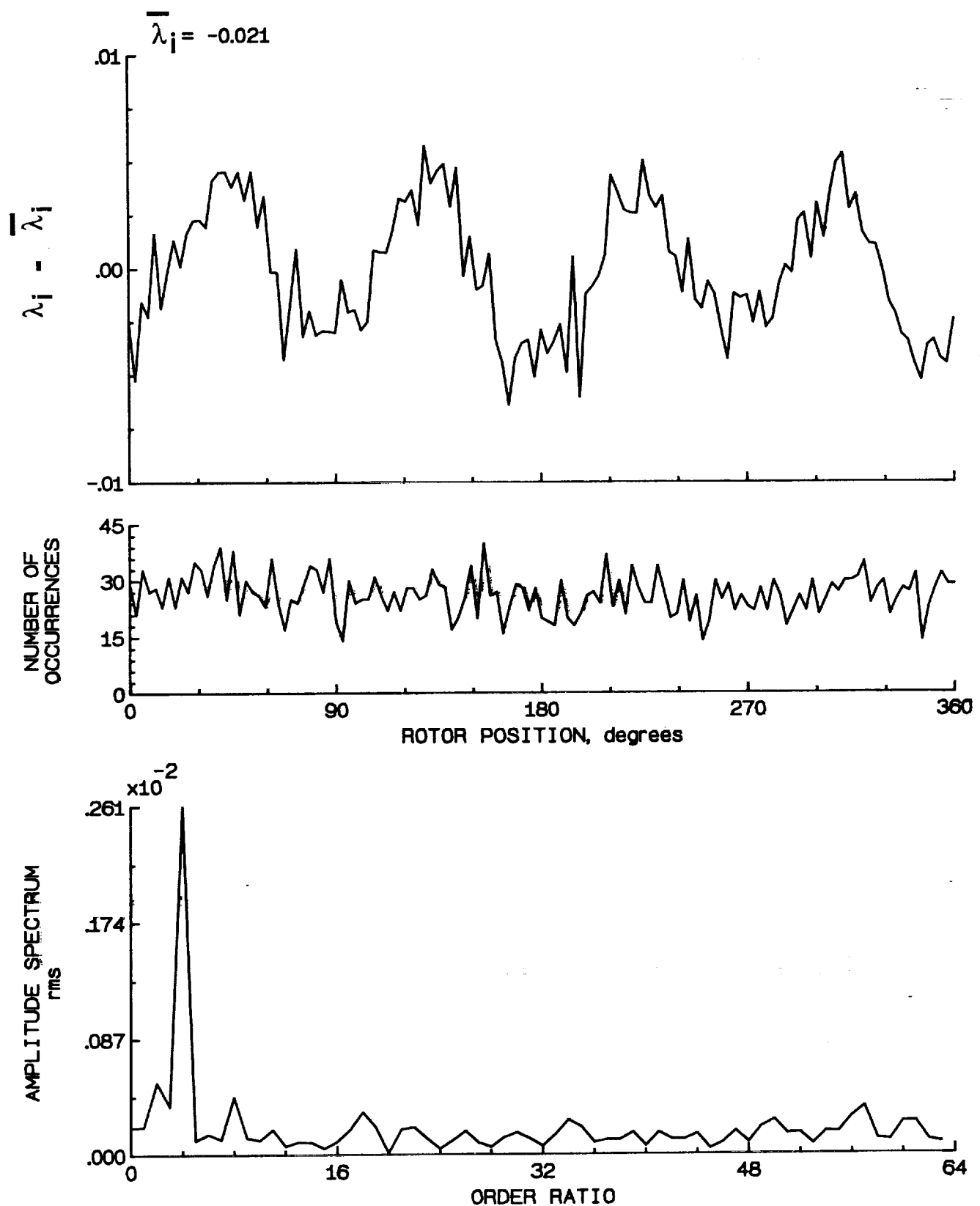


Figure 41.- Concluded.

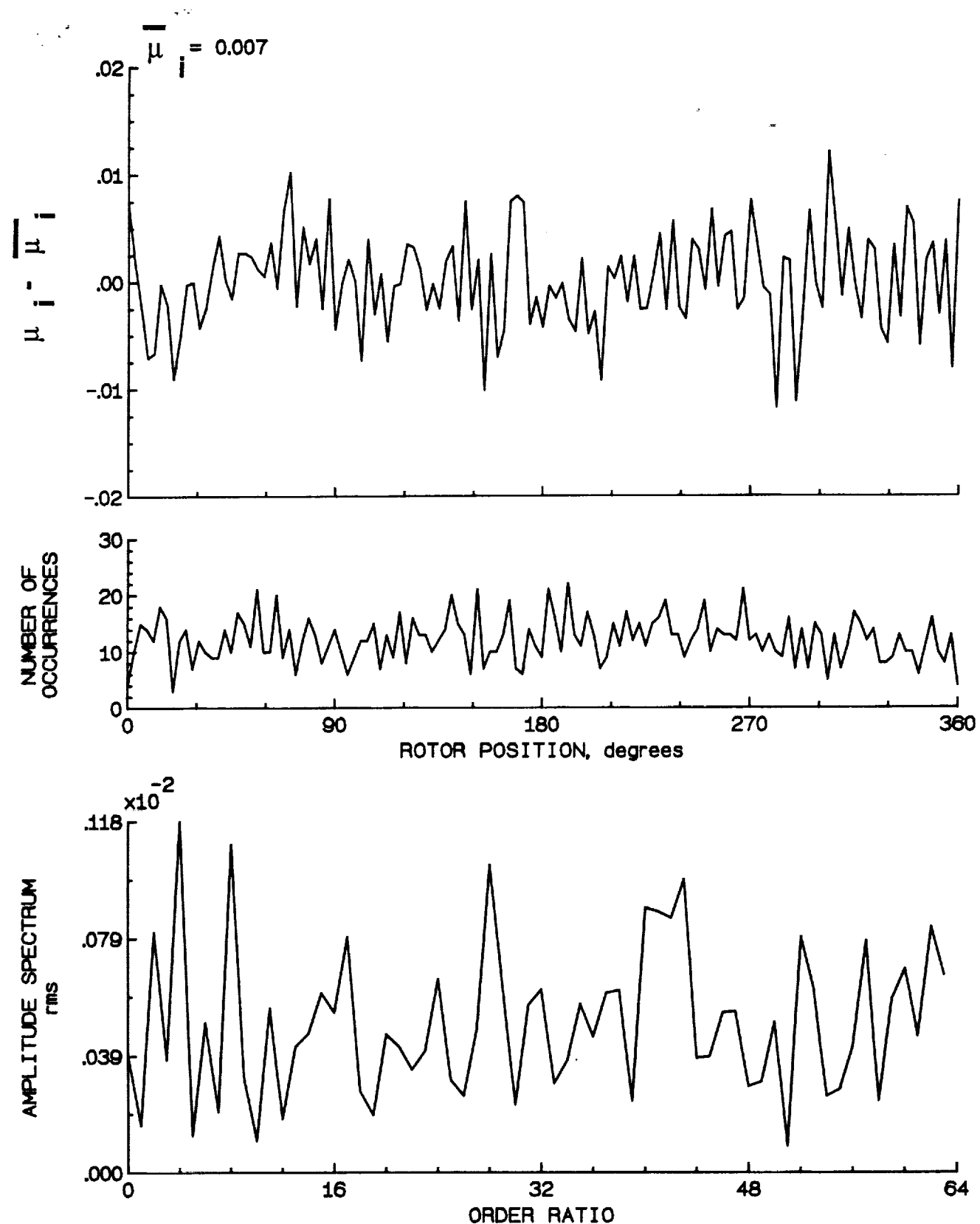


Figure 42.- Induced inflow velocity measured at 60 degrees and r/R of 0.20.

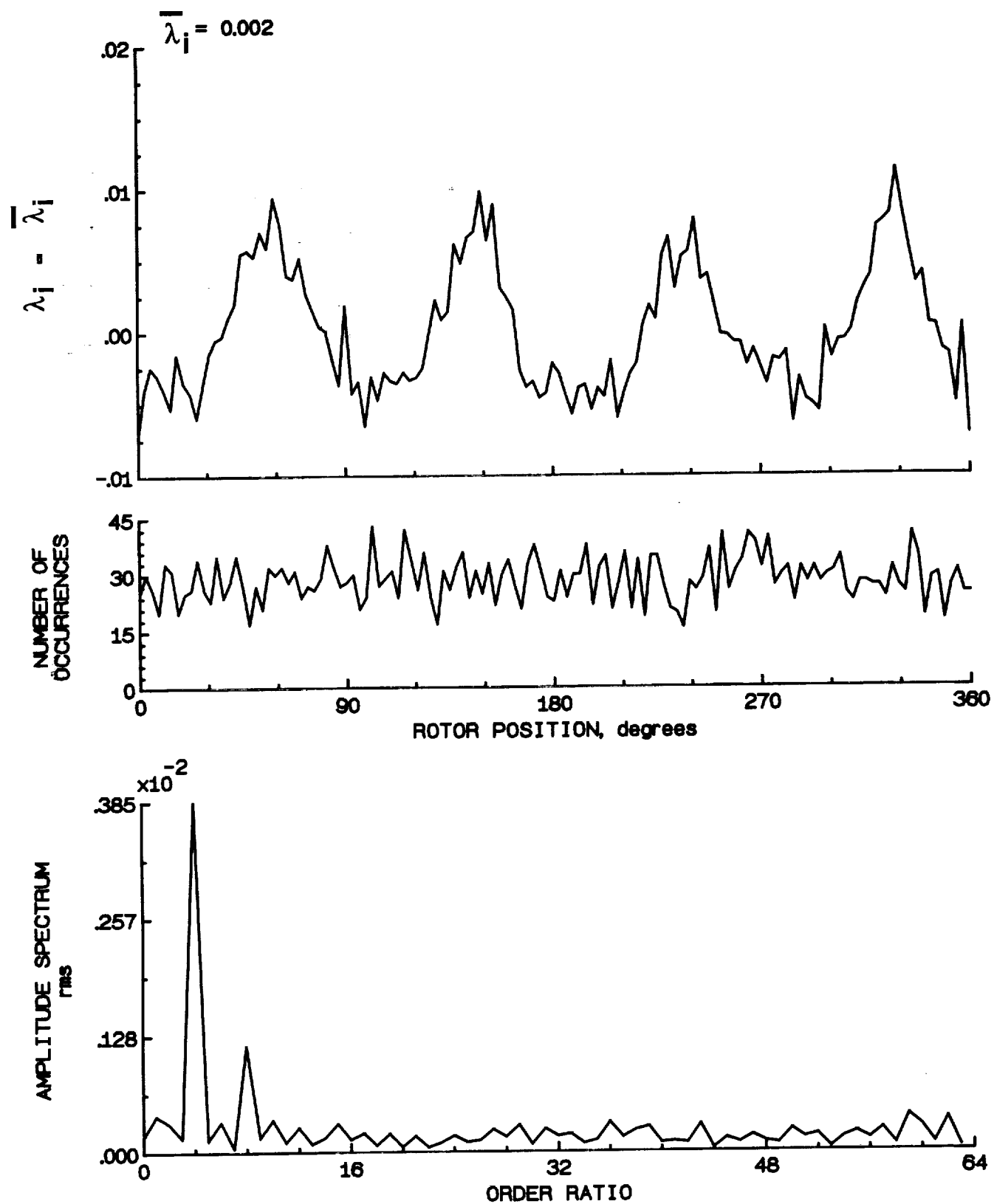


Figure 42.- Concluded.

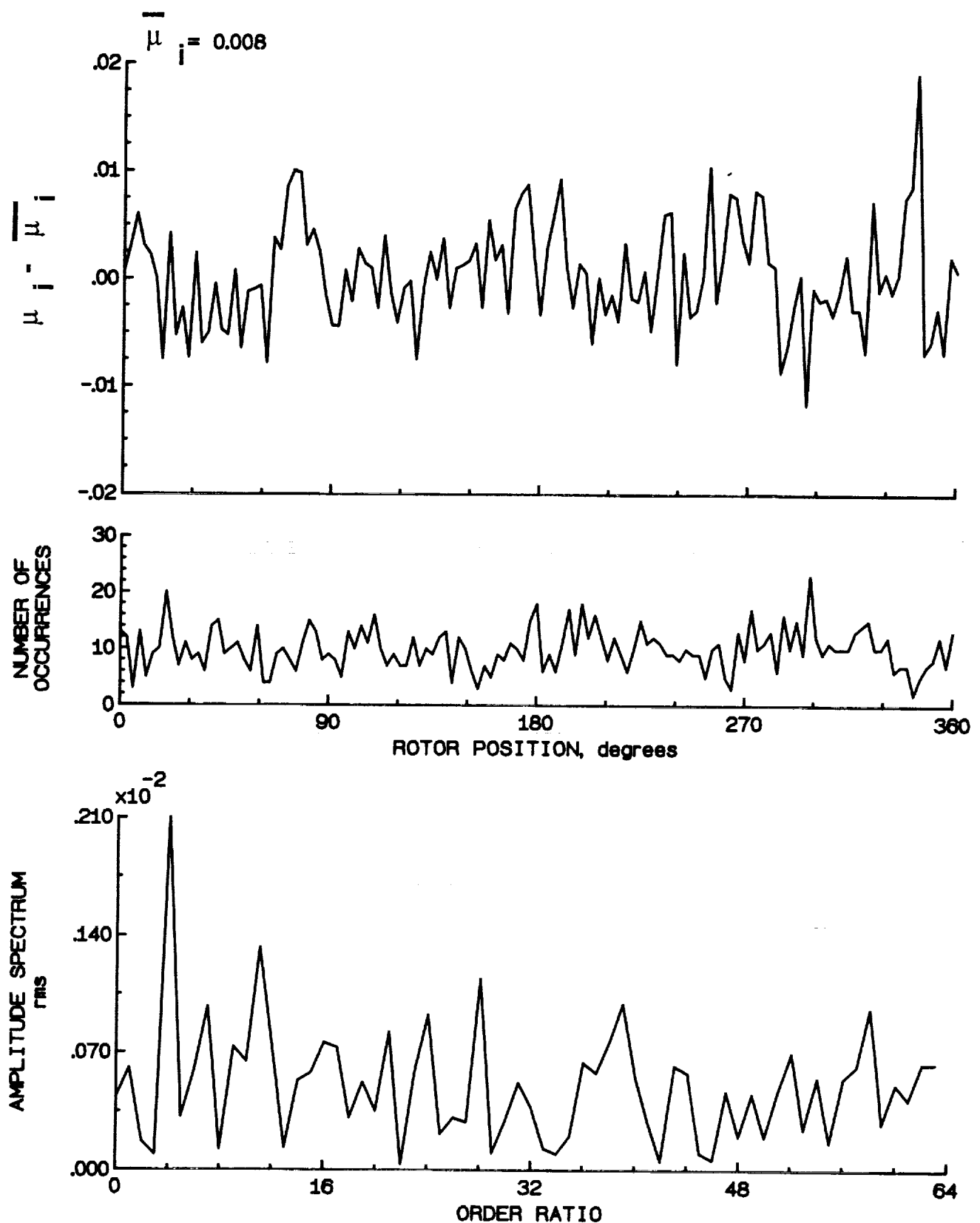


Figure 43.- Induced inflow velocity measured at 60 degrees and r/R of 0.40.

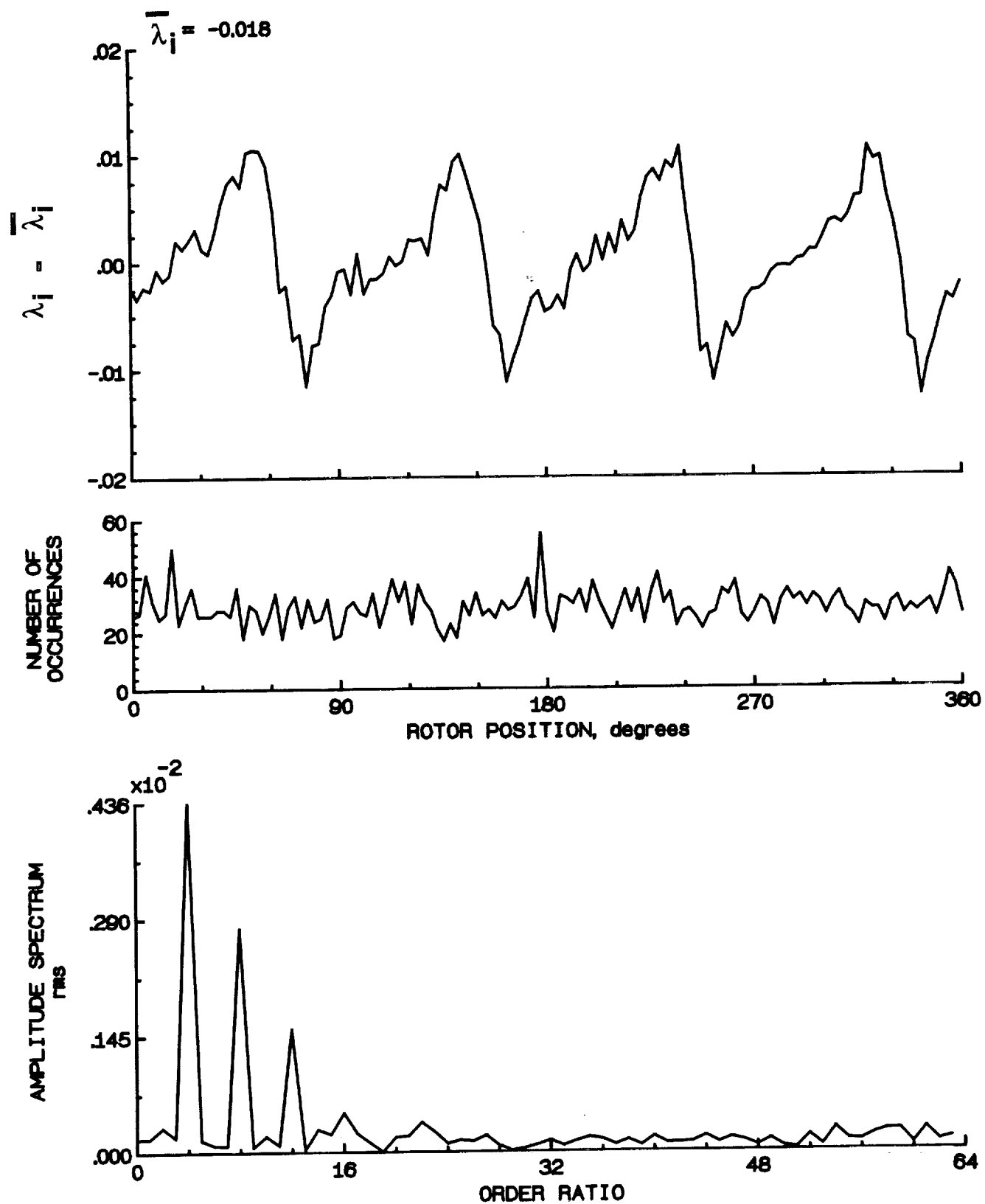


Figure 43.- Concluded.

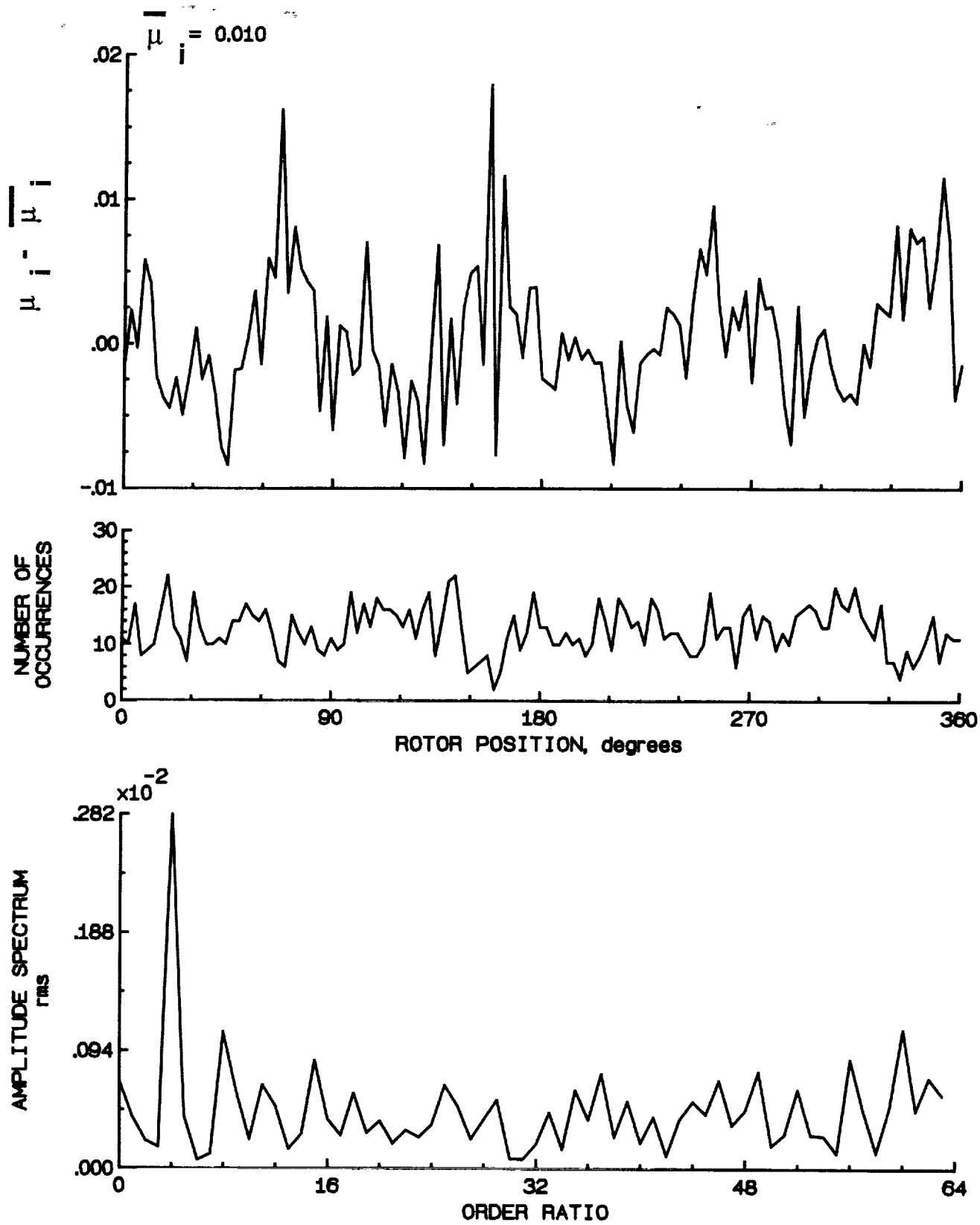


Figure 44.- Induced inflow velocity measured at 60 degrees and r/R of 0.50.

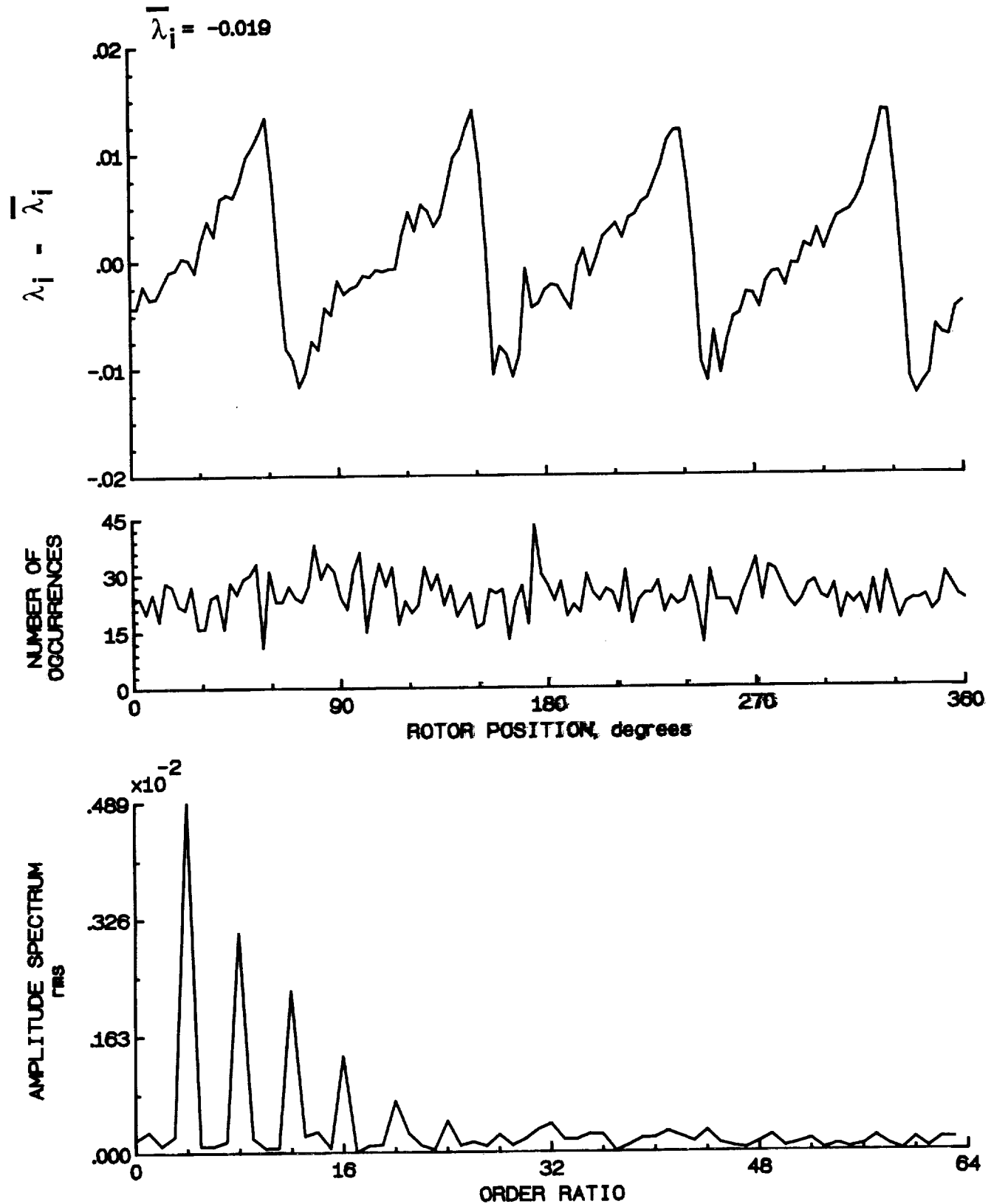


Figure 44.- Concluded.

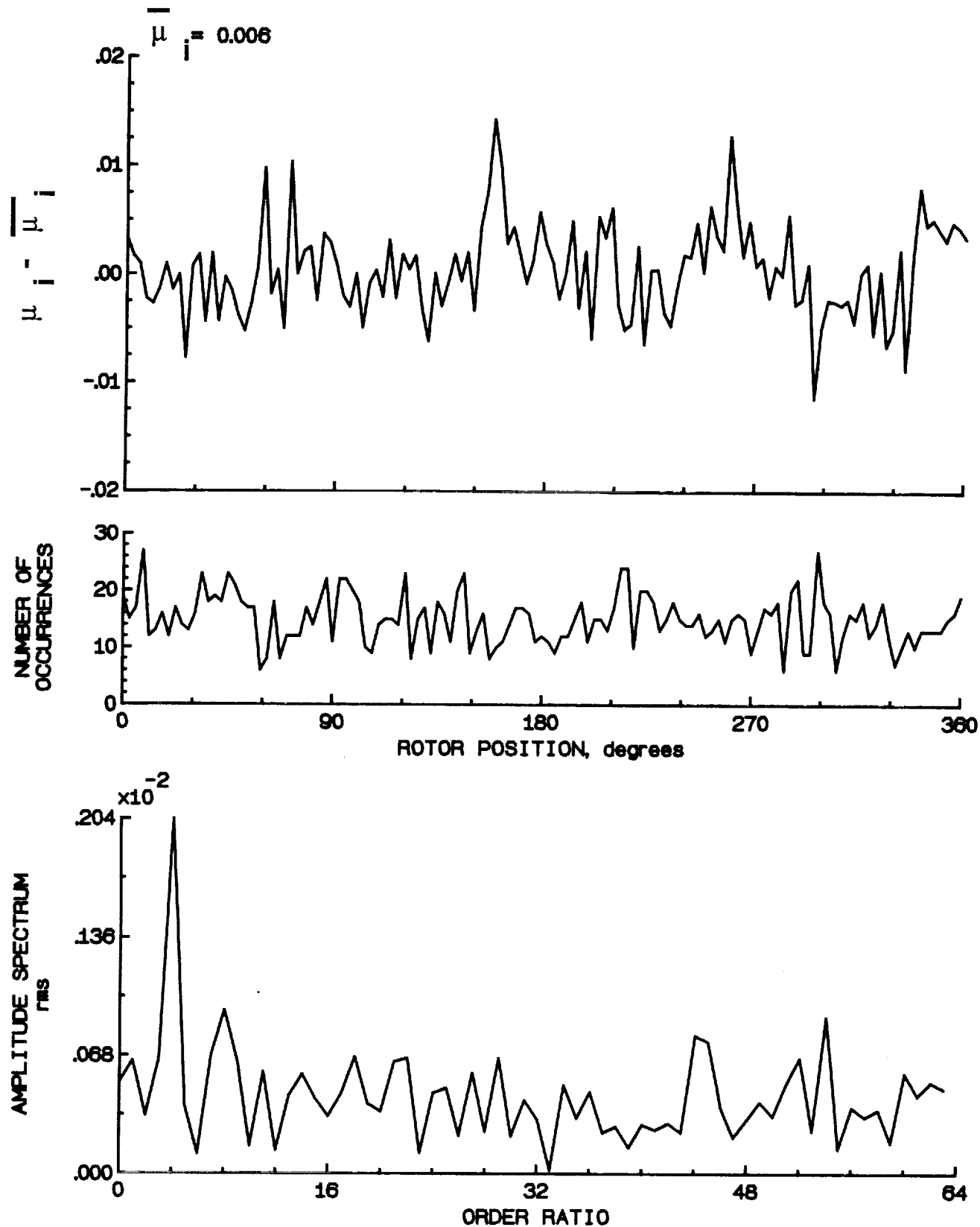


Figure 45.- Induced inflow velocity measured at 60 degrees and r/R of 0.60.

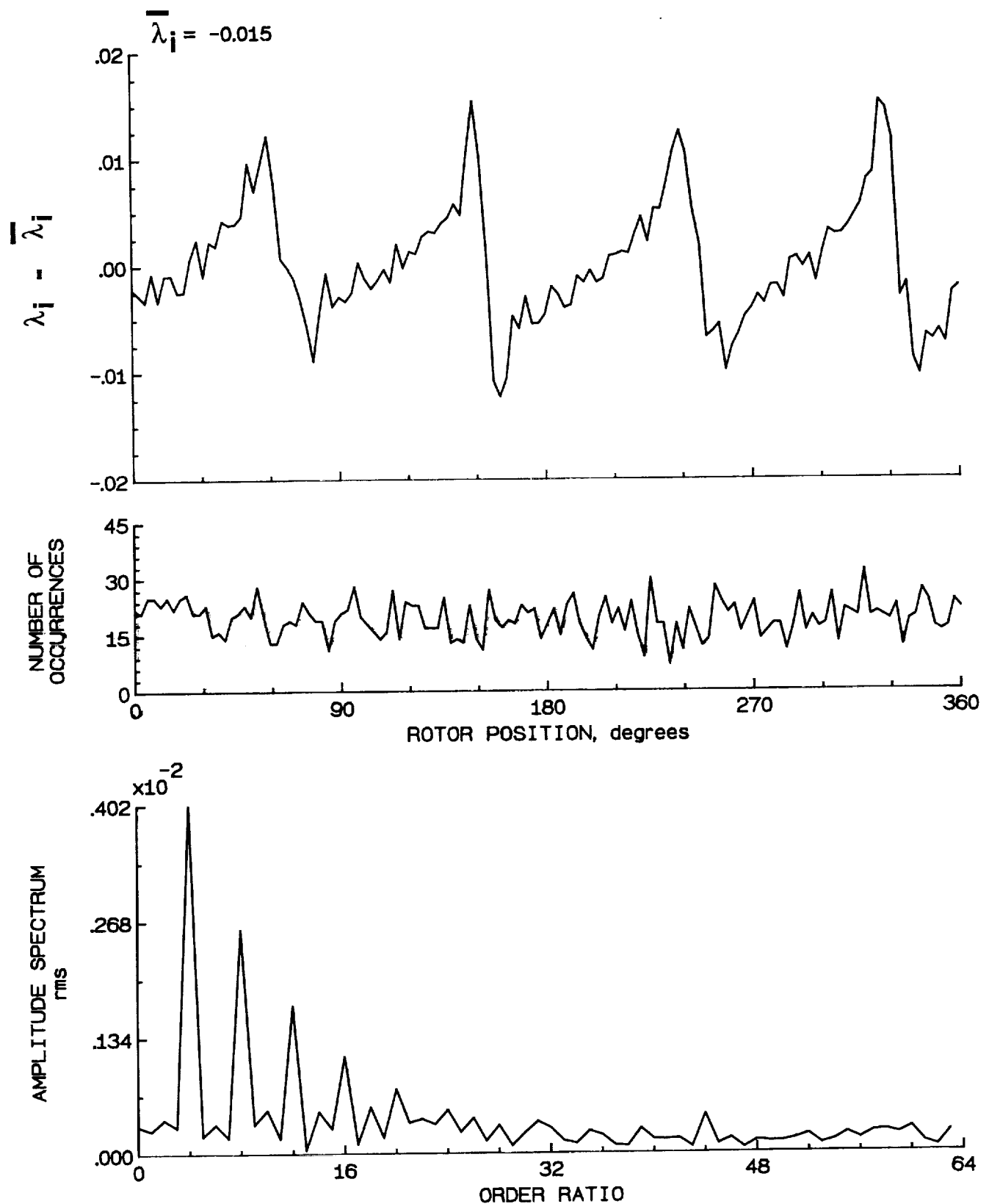


Figure 45.- Concluded.

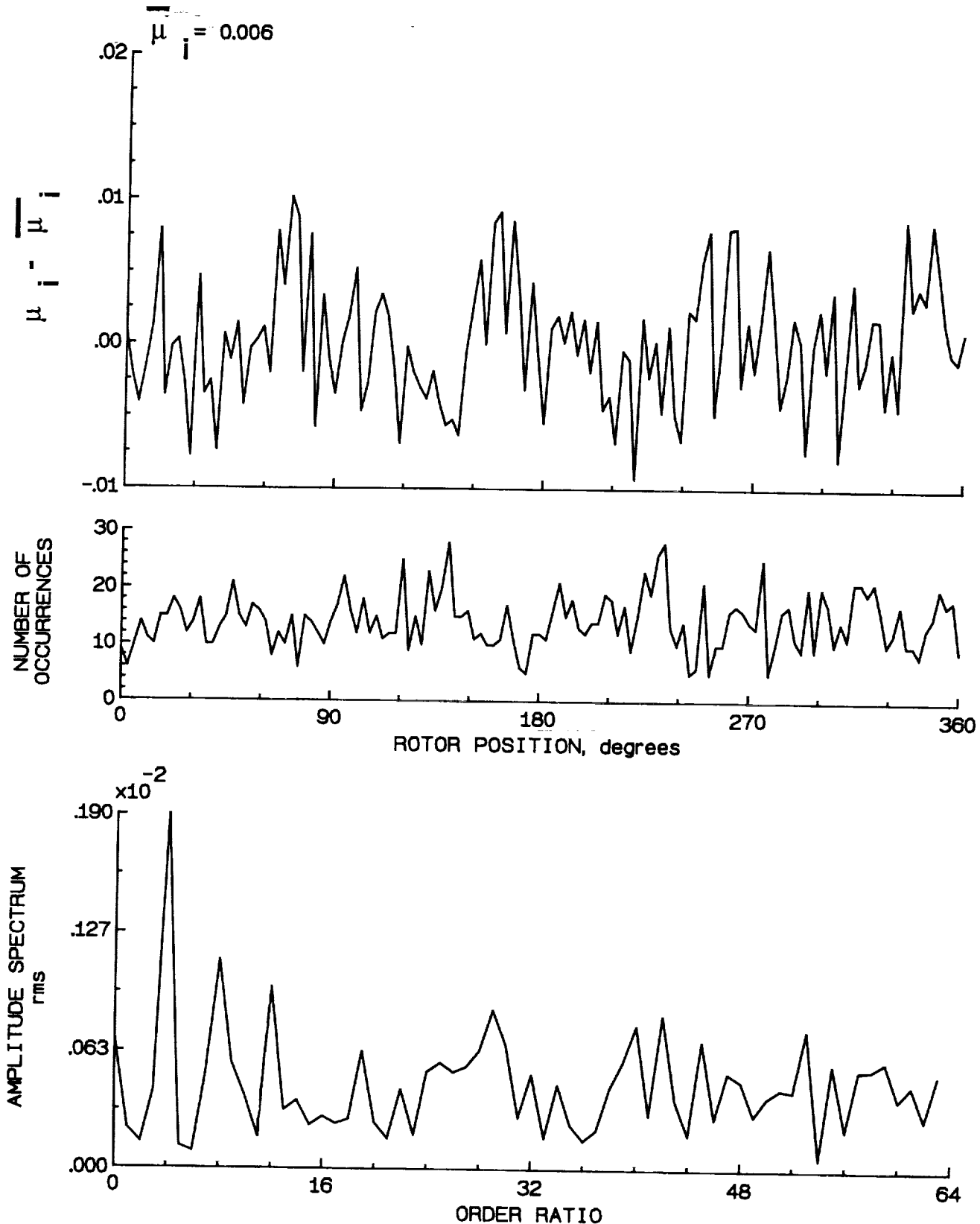


Figure 46.- Induced inflow velocity measured at 60 degrees and r/R of 0.70.

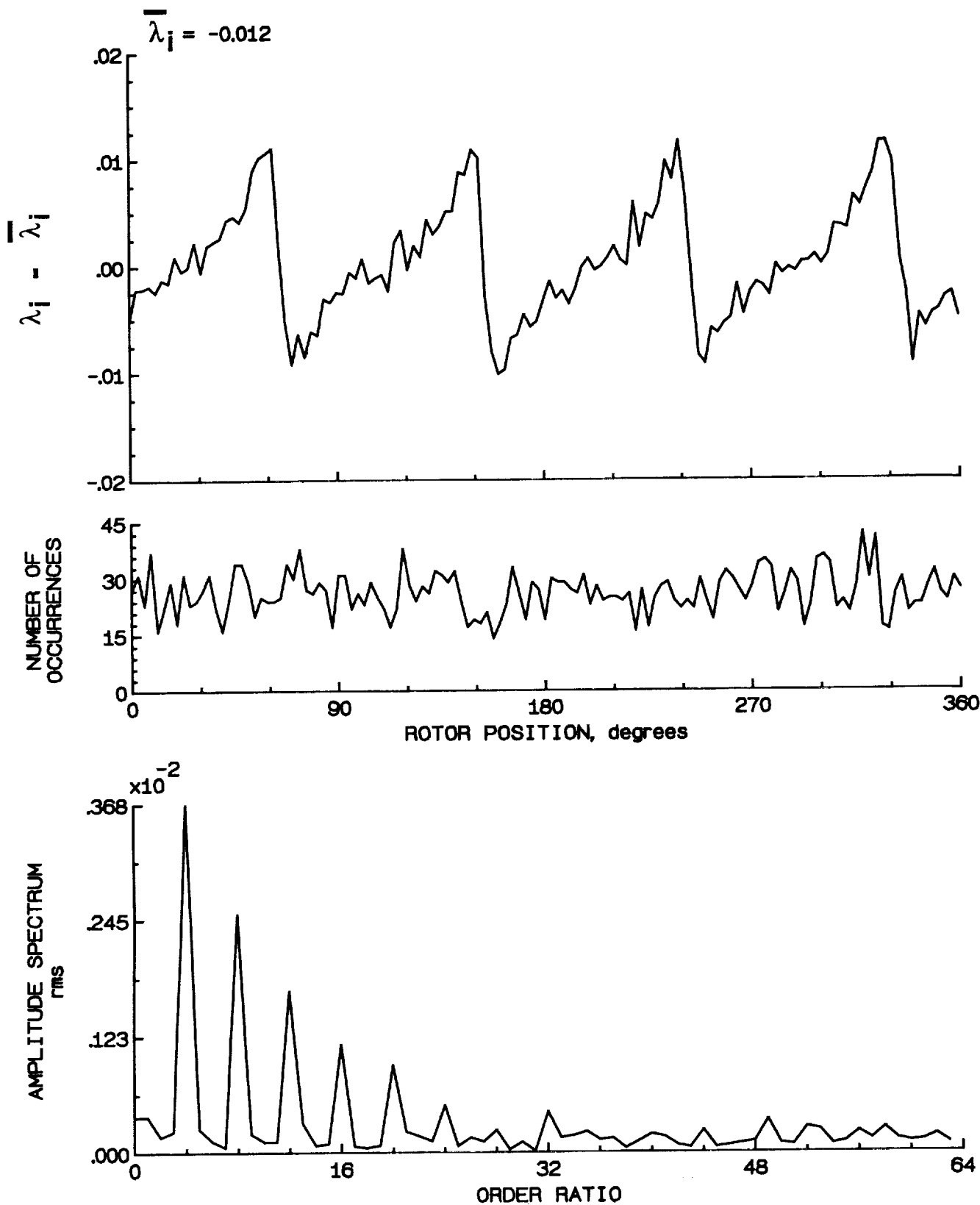


Figure 46.- Concluded.

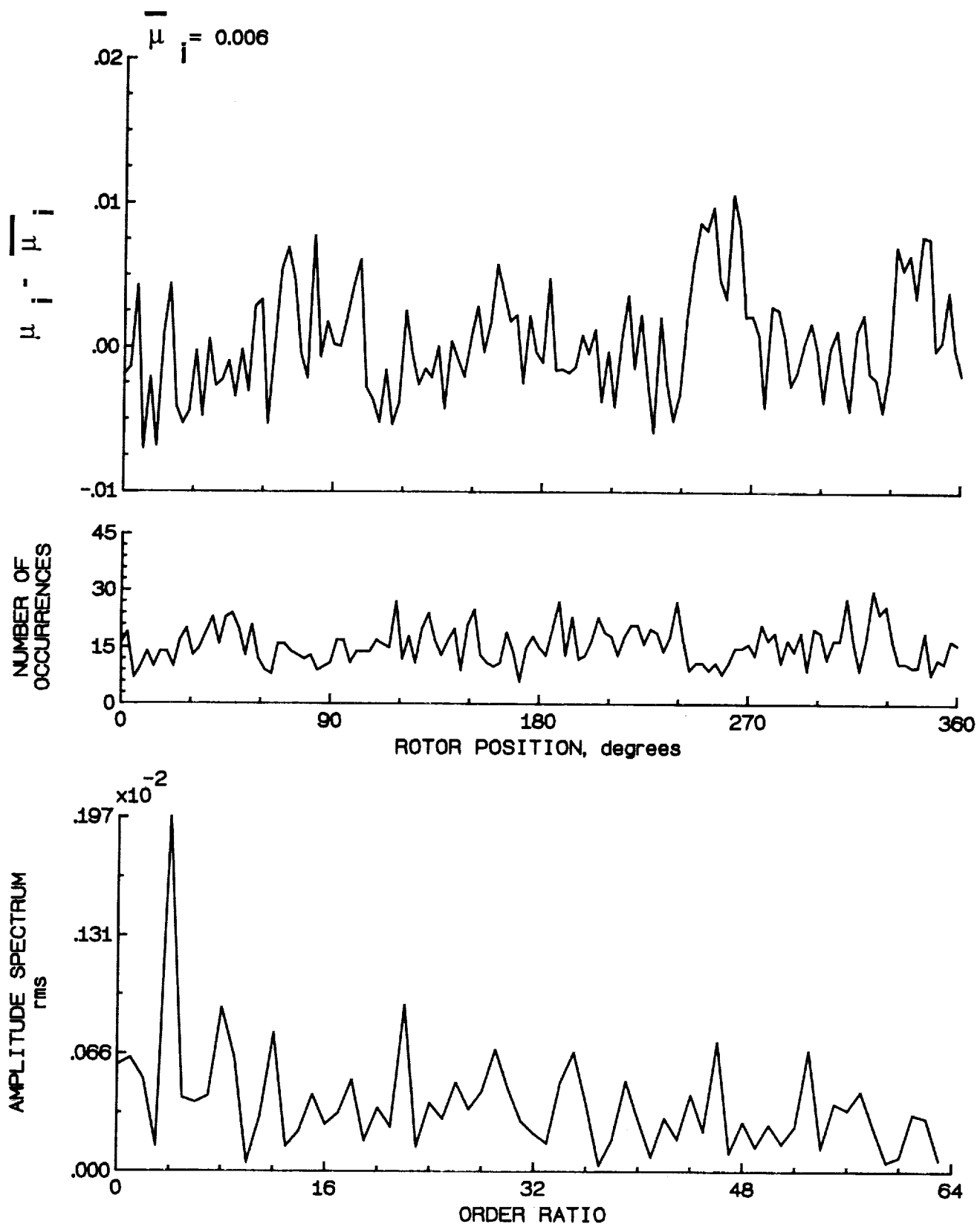


Figure 47.- Induced inflow velocity measured at 60 degrees and r/R of 0.74.

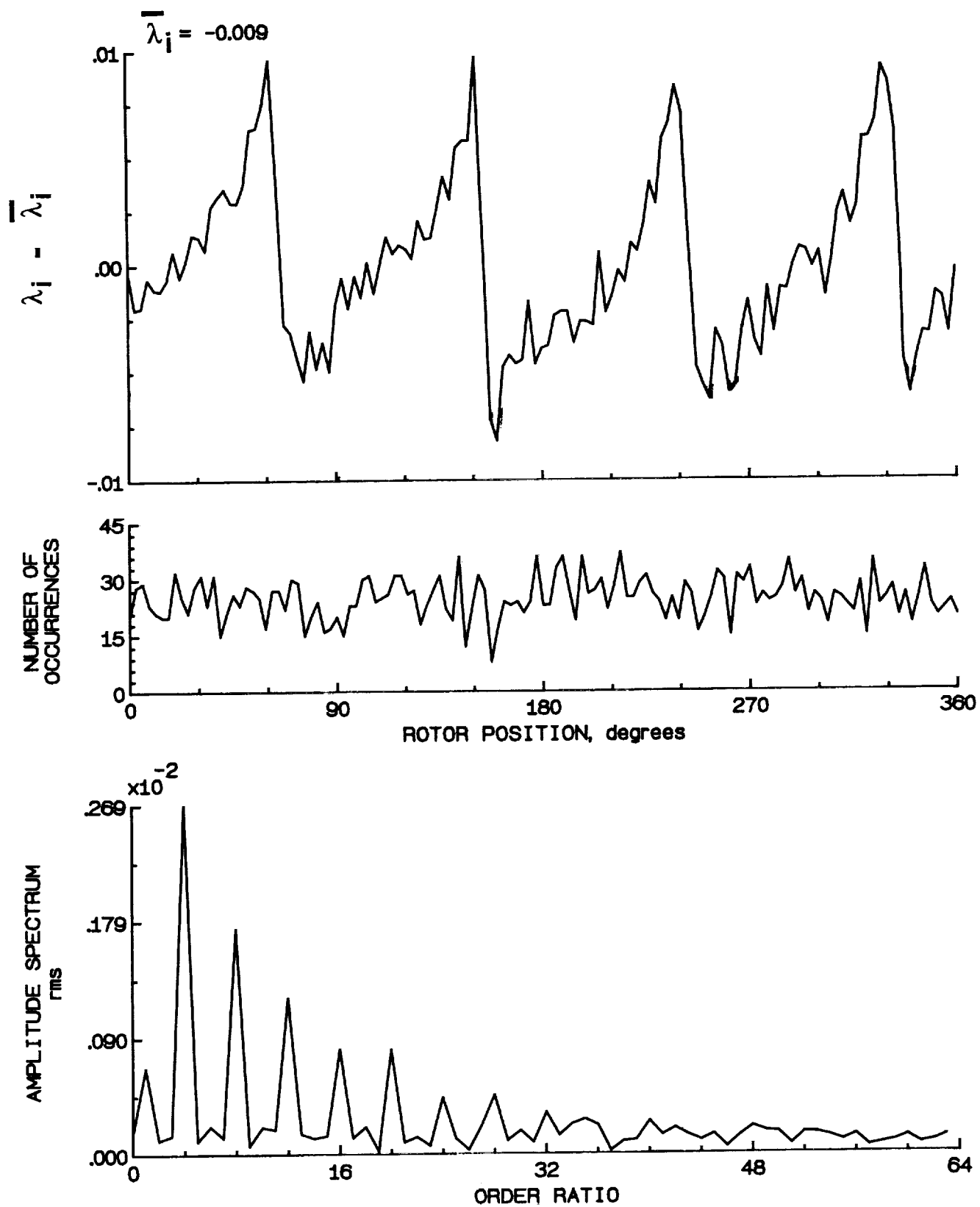


Figure 47.- Concluded.

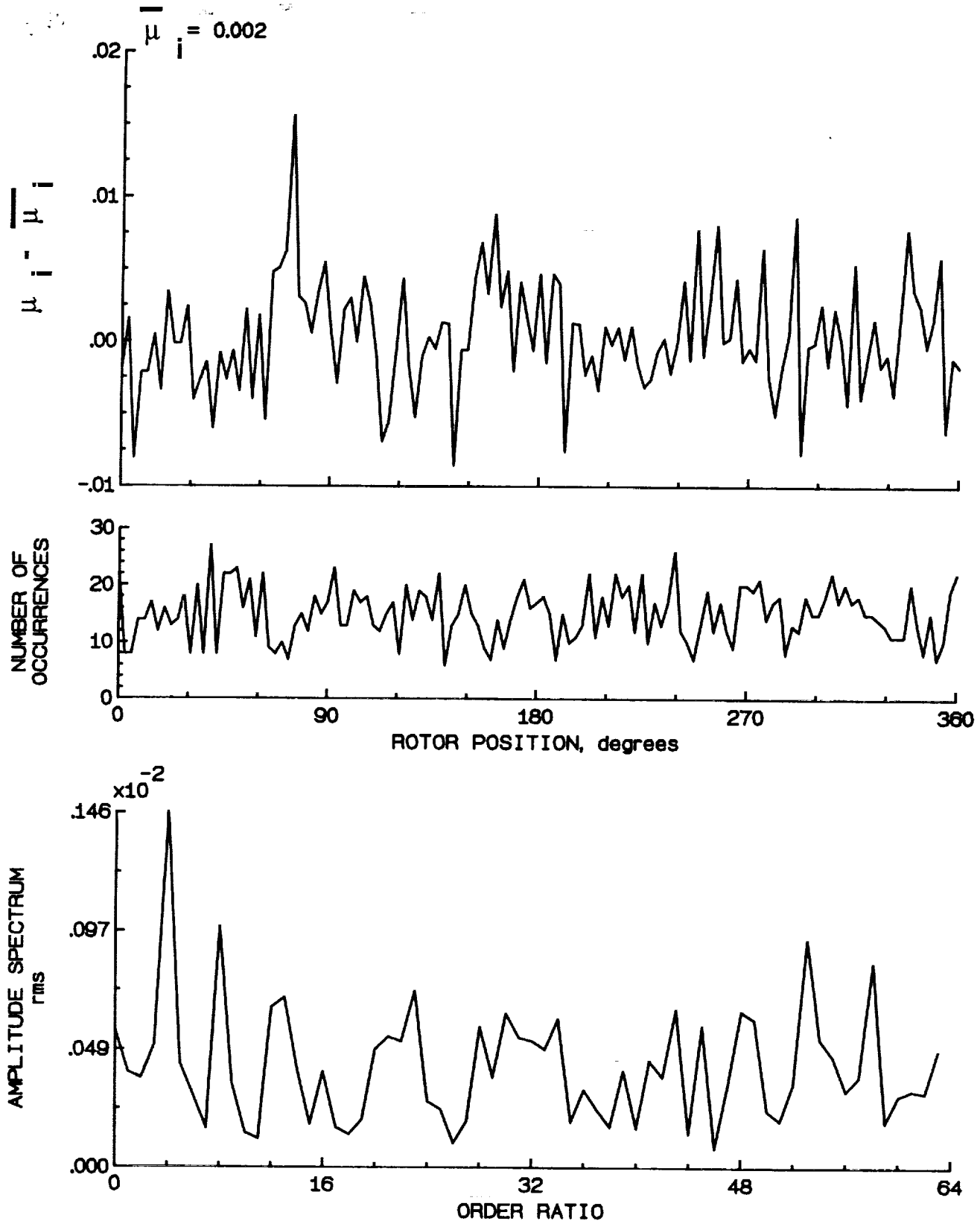


Figure 48.- Induced inflow velocity measured at 60 degrees and r/R of 0.78.

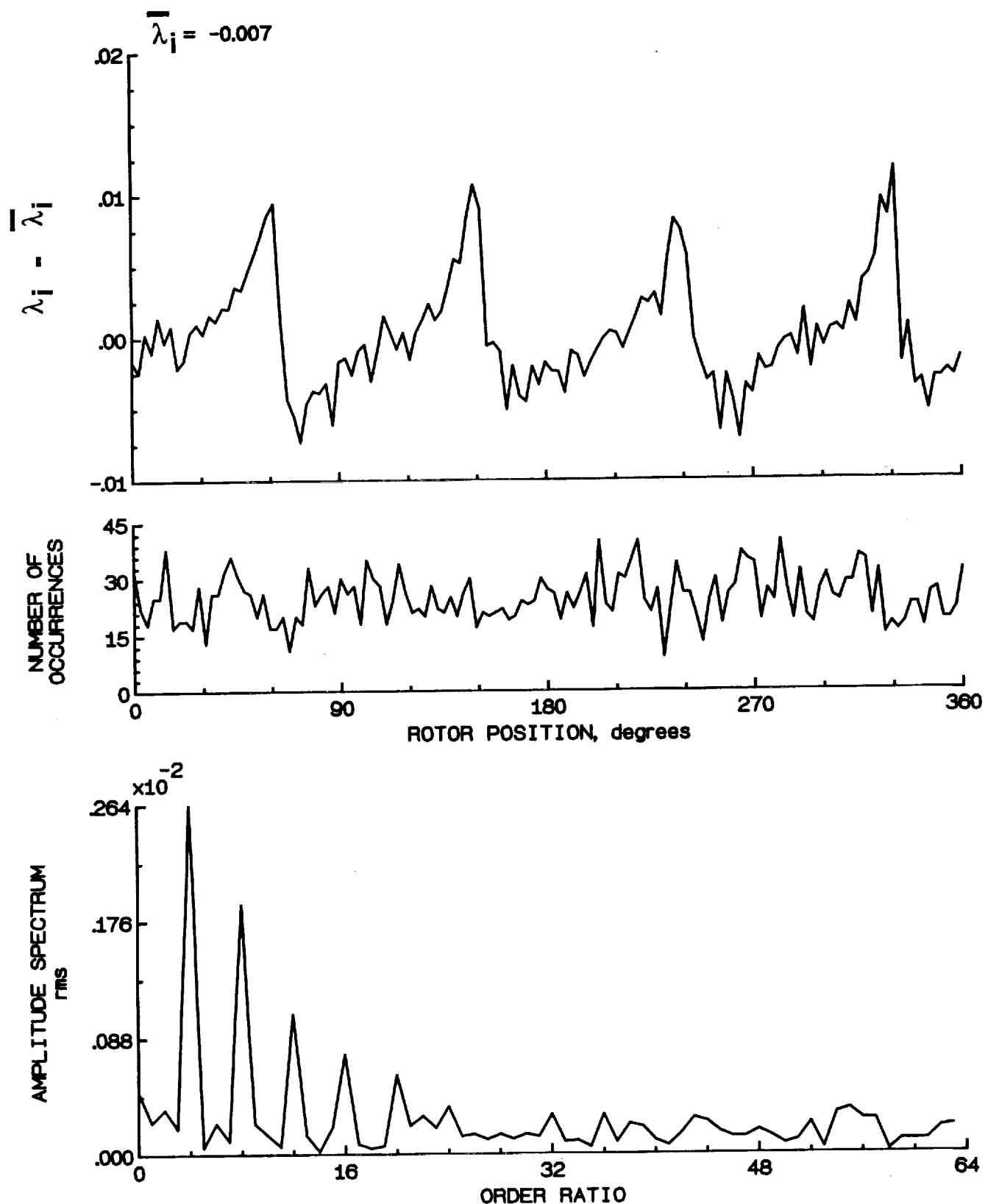


Figure 48.- Concluded.

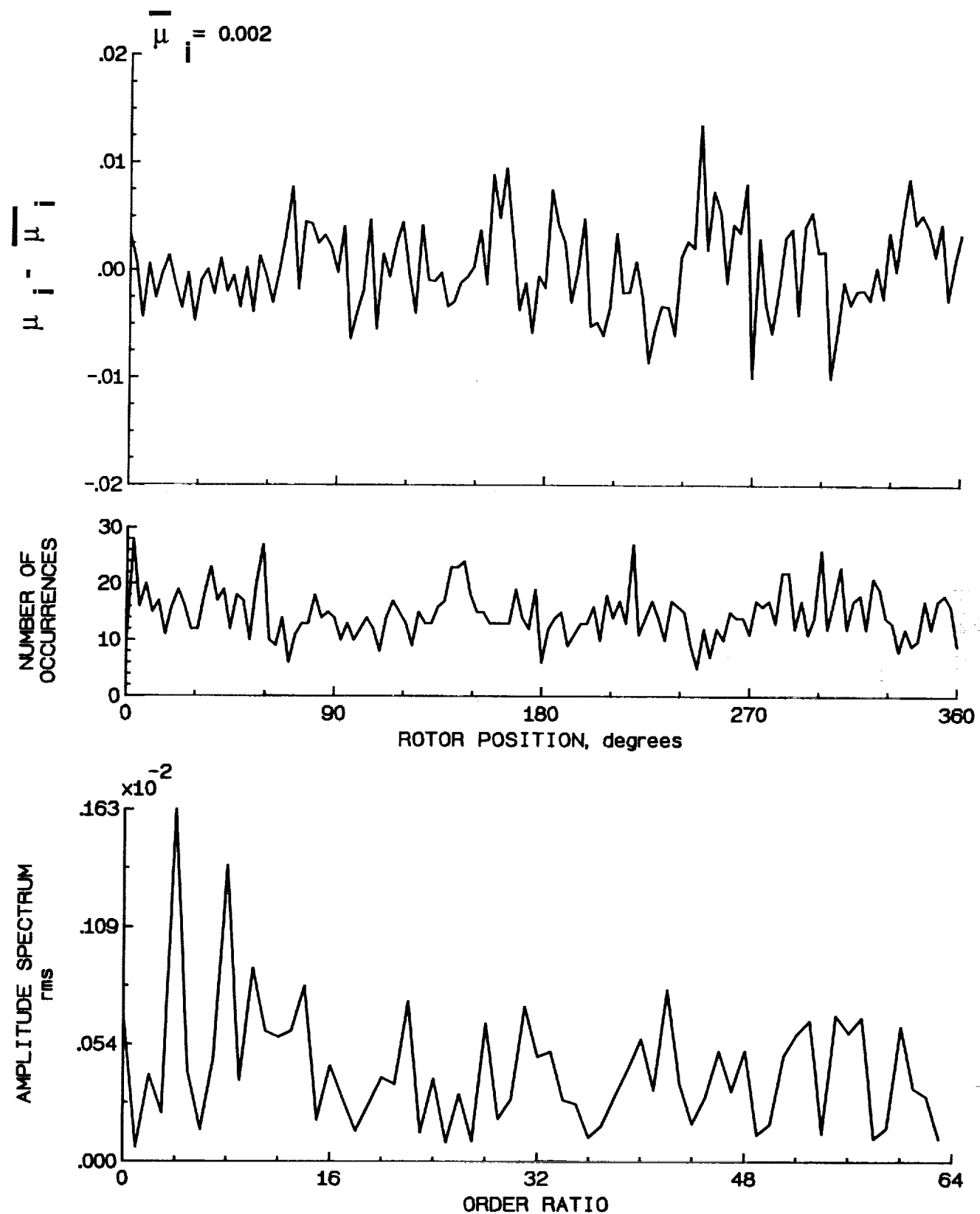


Figure 49.- Induced inflow velocity measured at 60 degrees and r/R of 0.82.

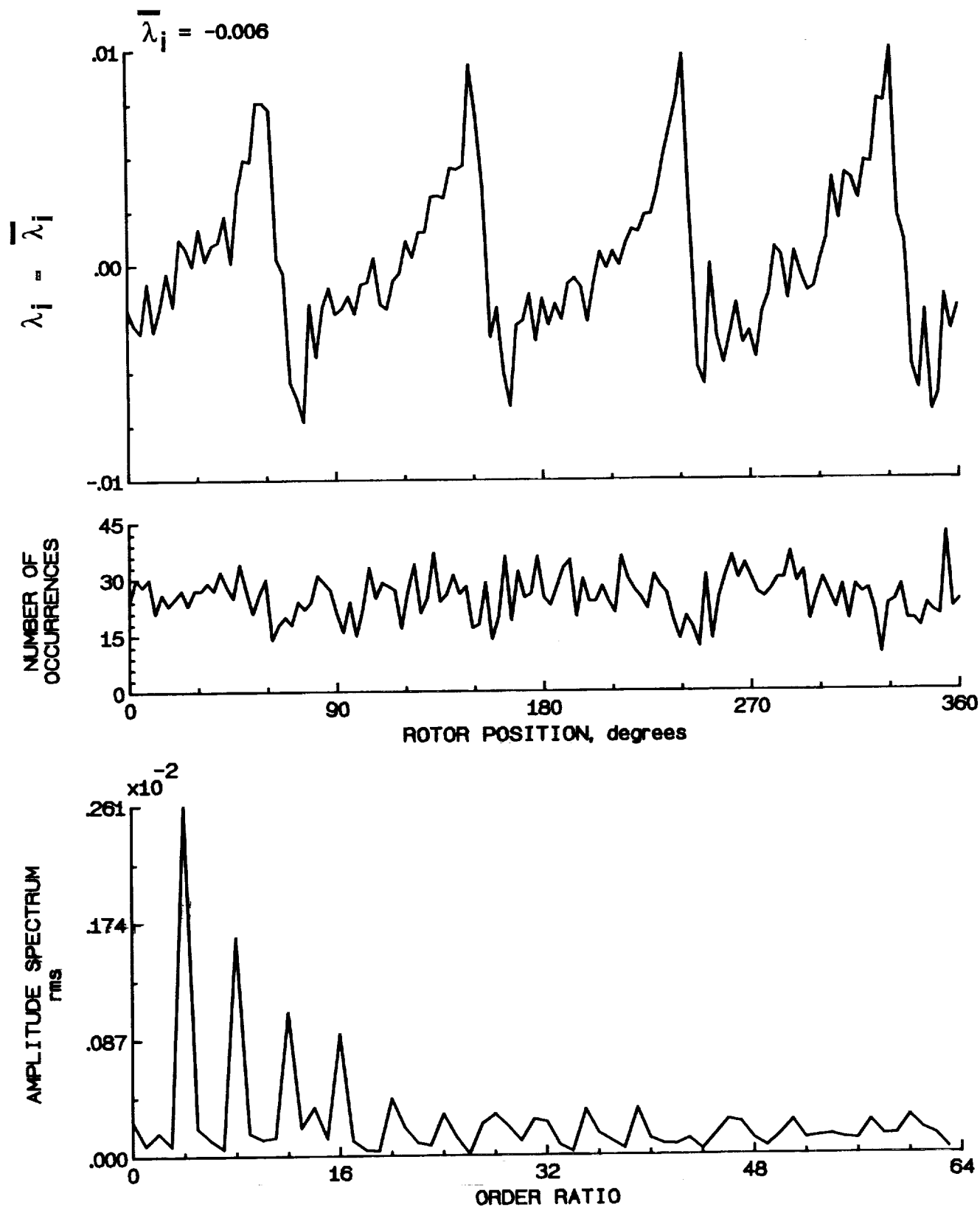


Figure 49.- Concluded.

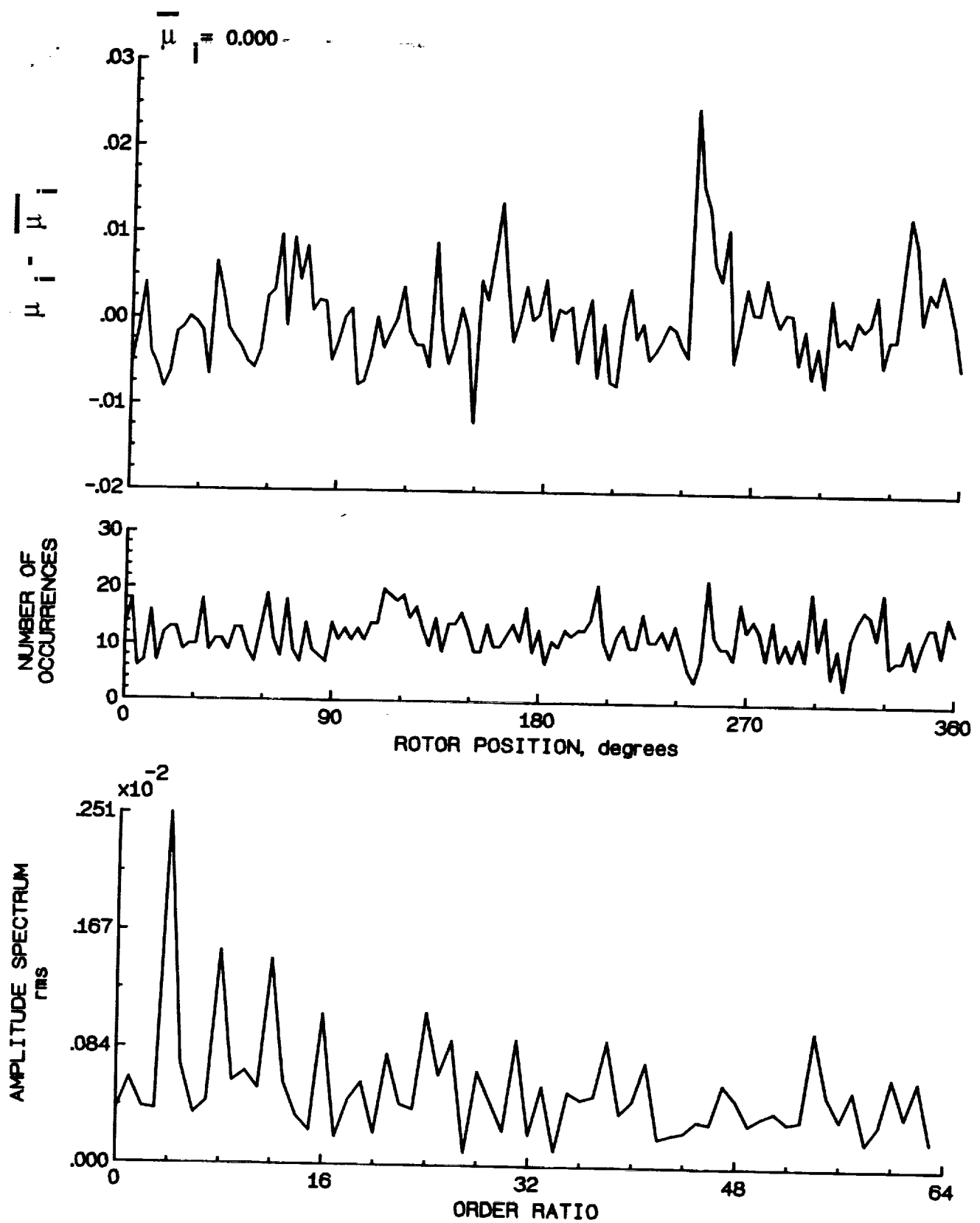


Figure 50.- Induced inflow velocity measured at 60 degrees and r/R of 0.86.

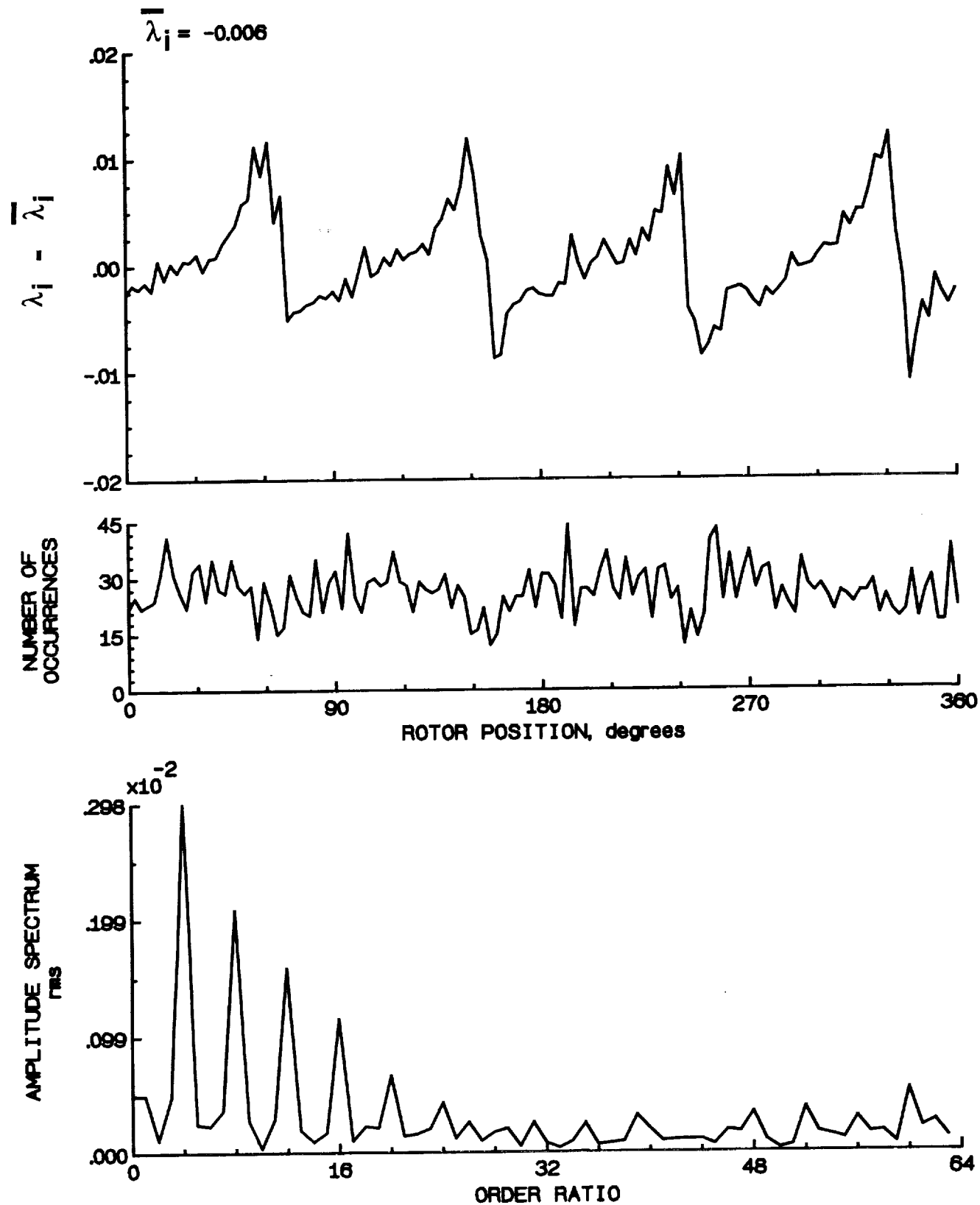


Figure 50.- Concluded.

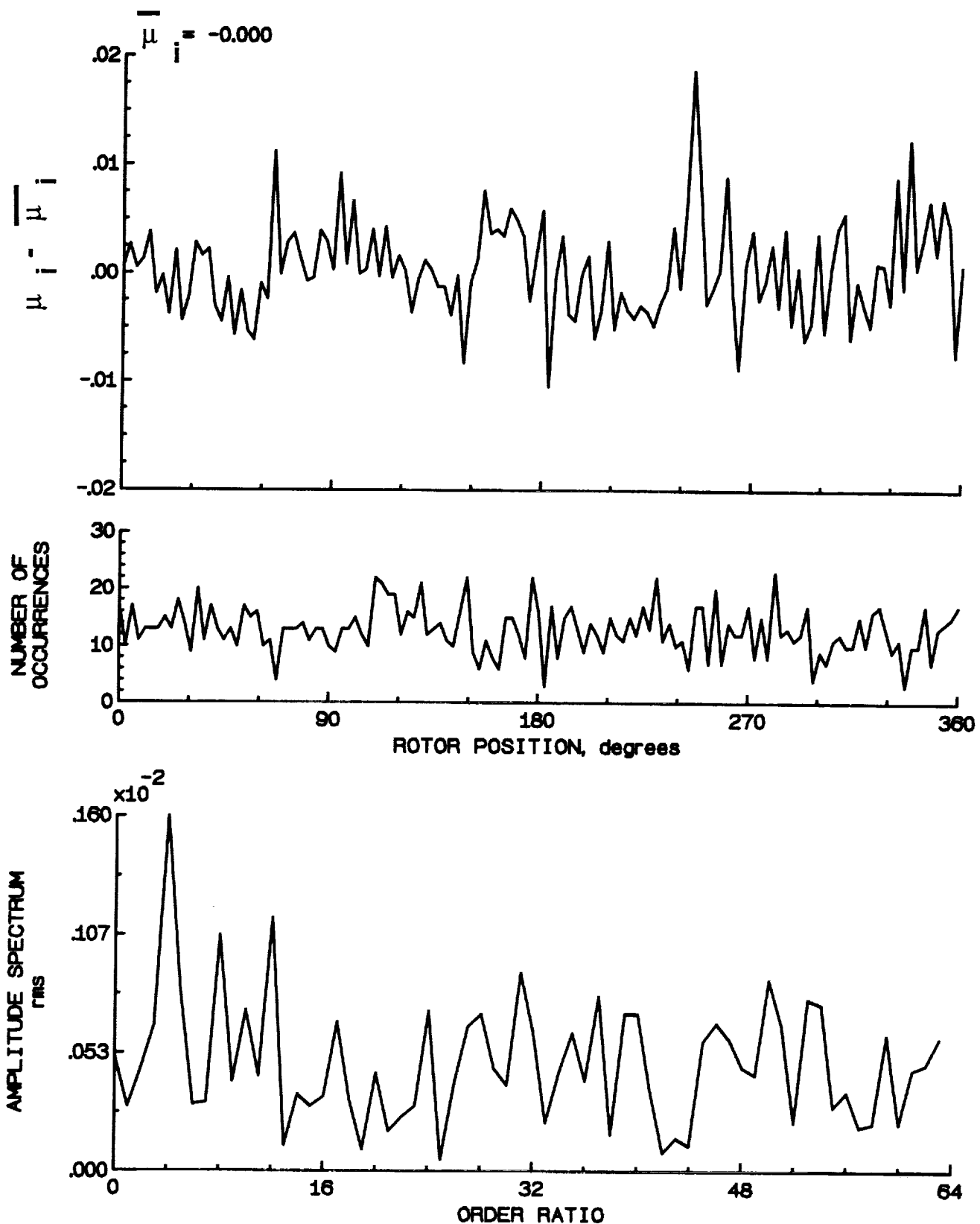


Figure 51.- Induced inflow velocity measured at 60 degrees and r/R of 0.90.

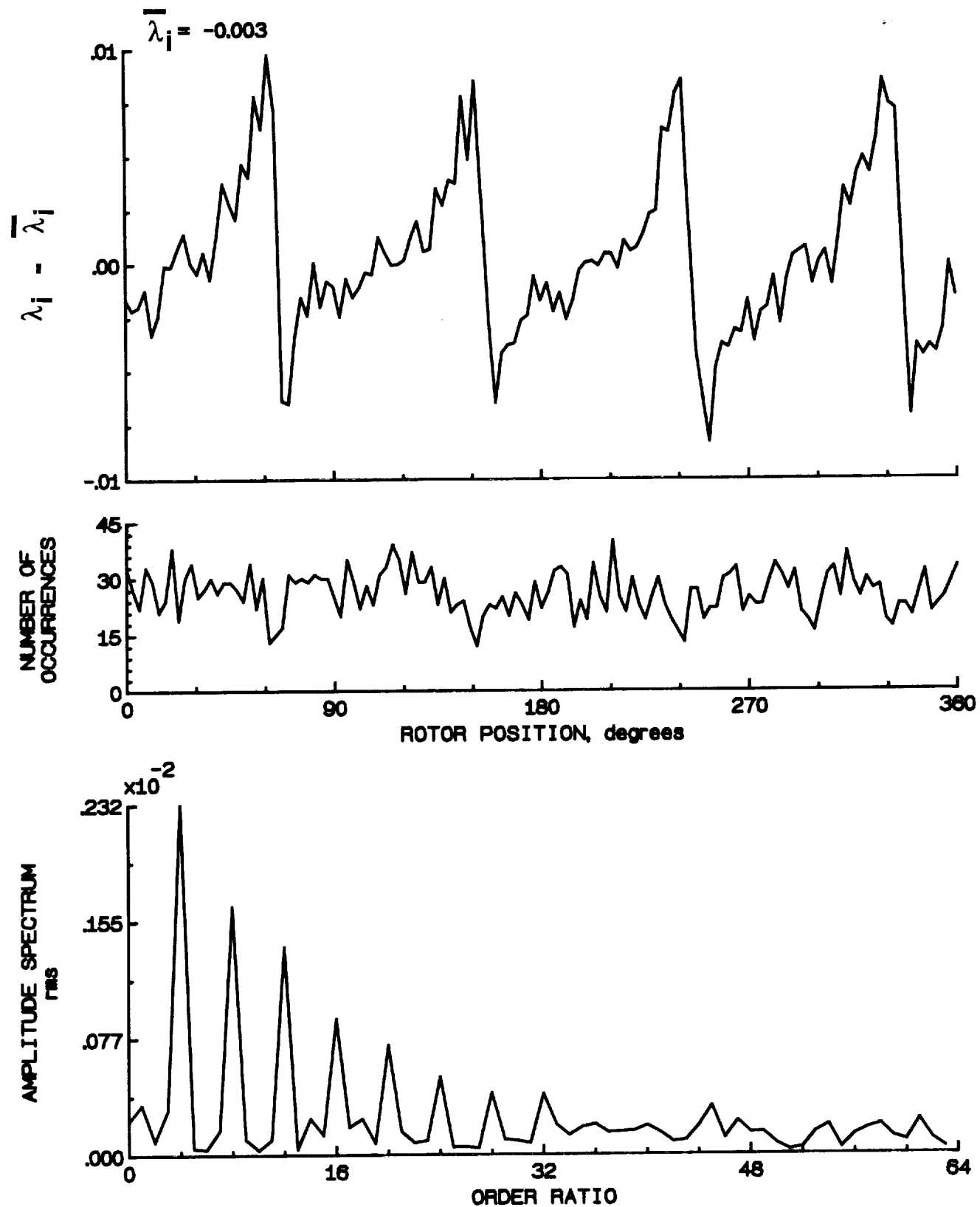


Figure 51.- Concluded.

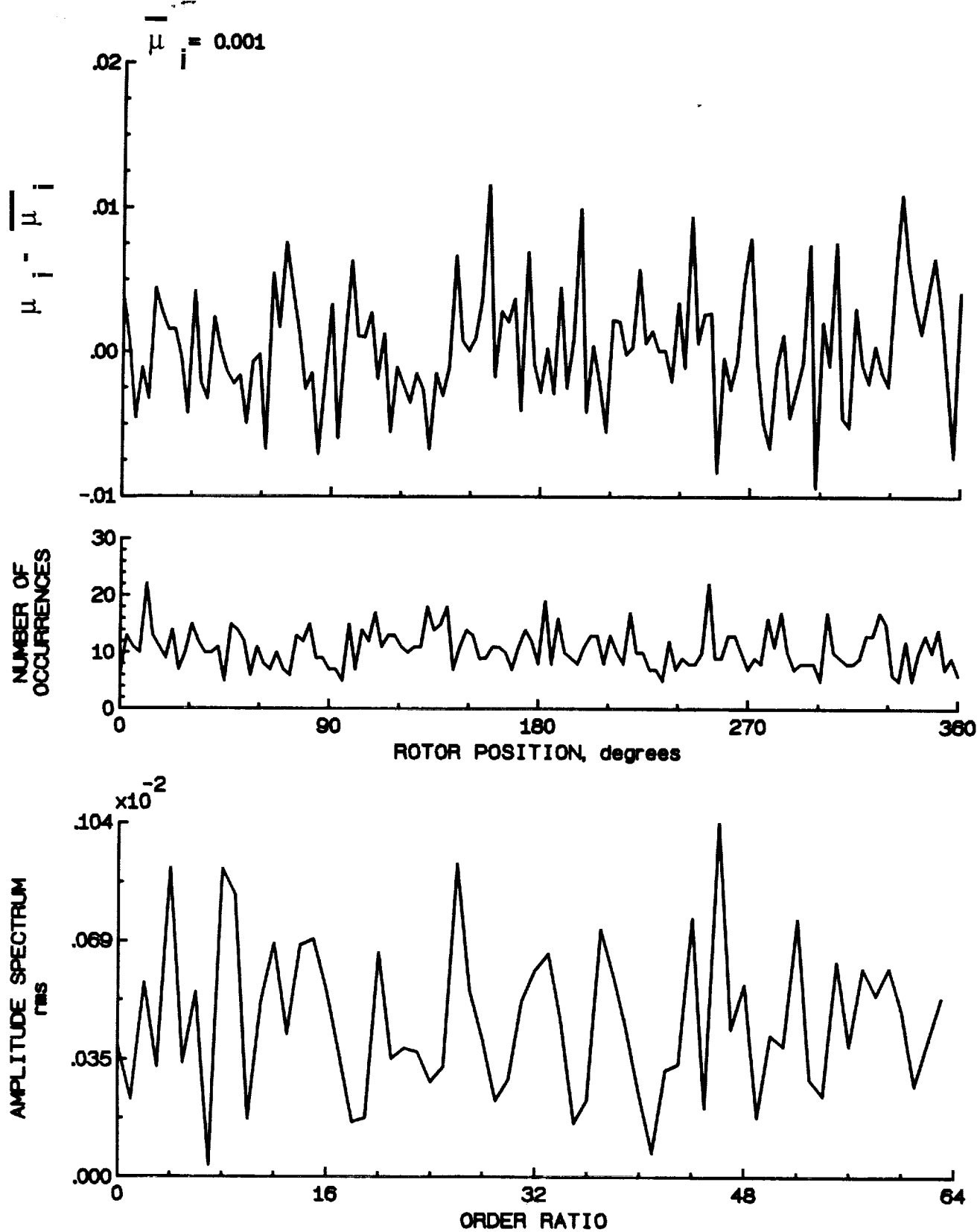


Figure 52.- Induced inflow velocity measured at 80 degrees and r/R of 0.94.

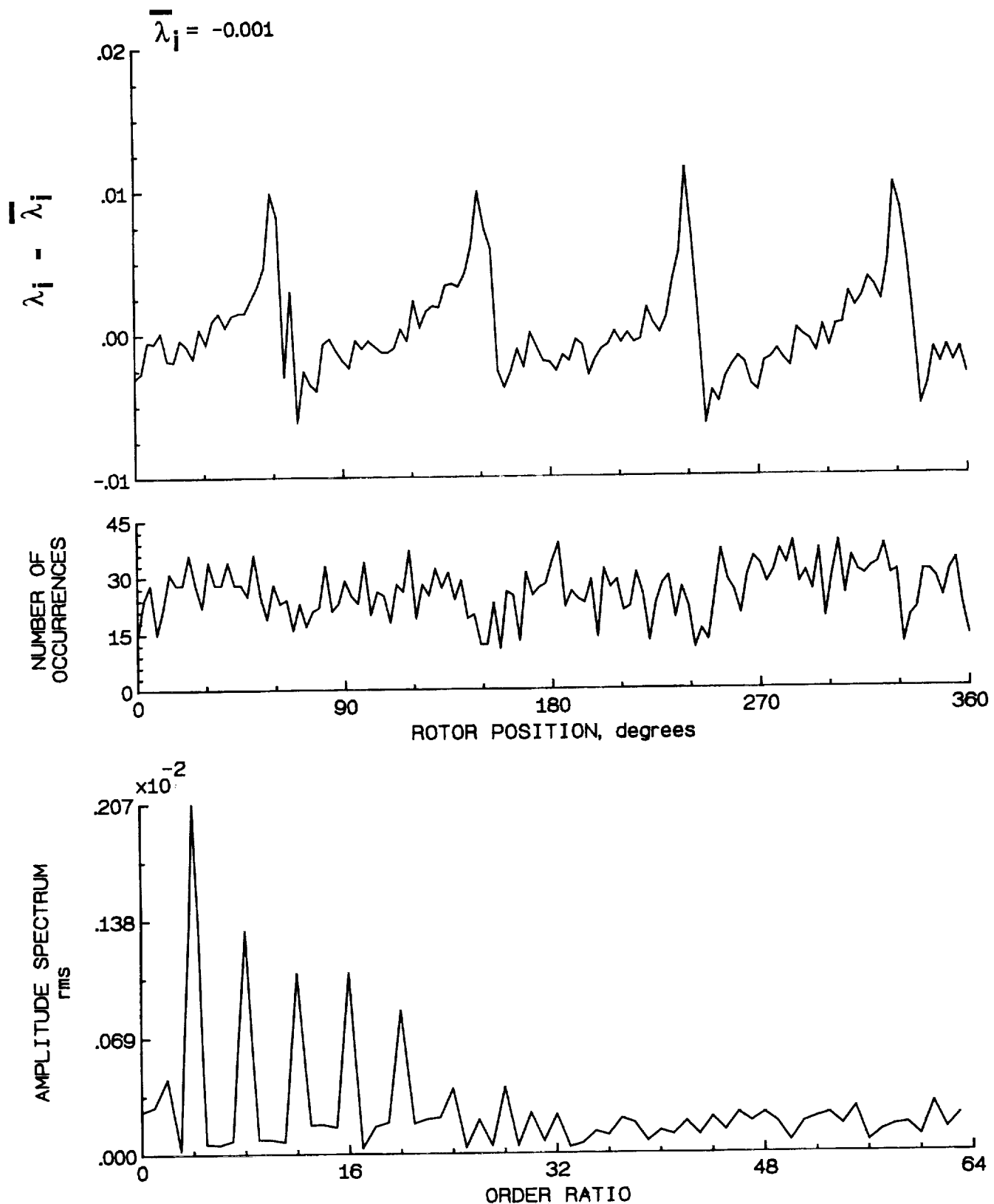


Figure 52.- Concluded.

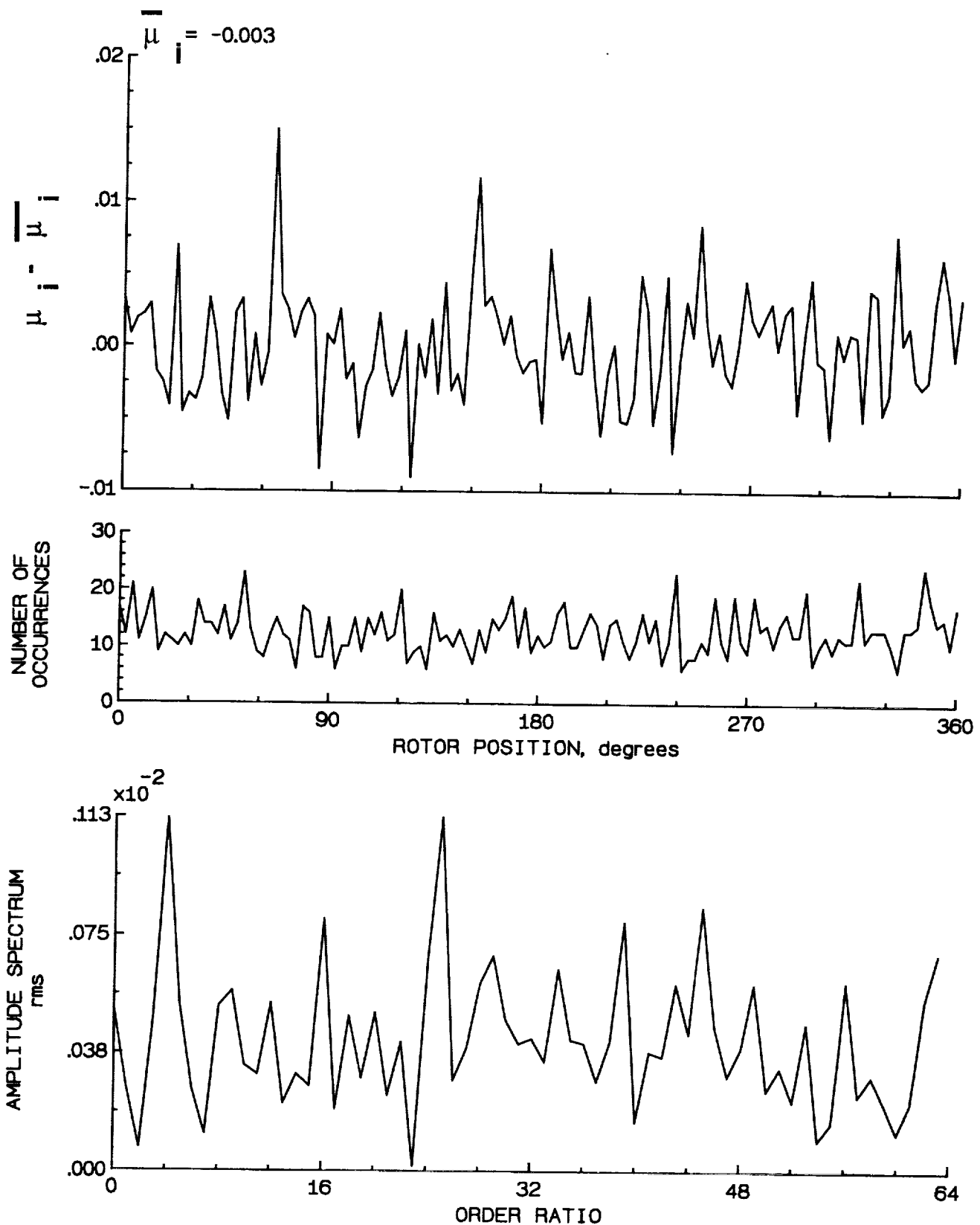


Figure 53.- Induced inflow velocity measured at 60 degrees and r/R of 0.98.

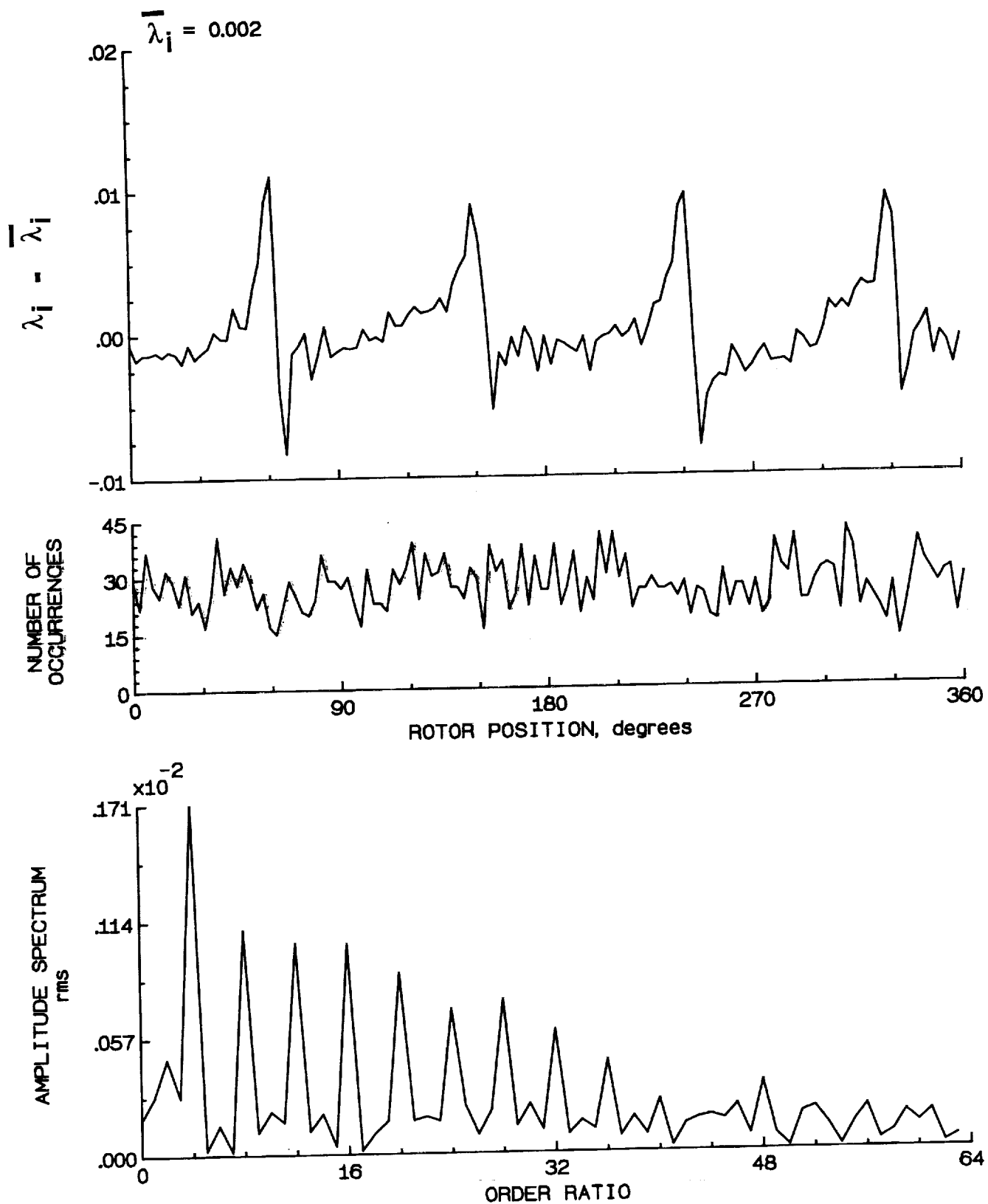


Figure 53.- Concluded.

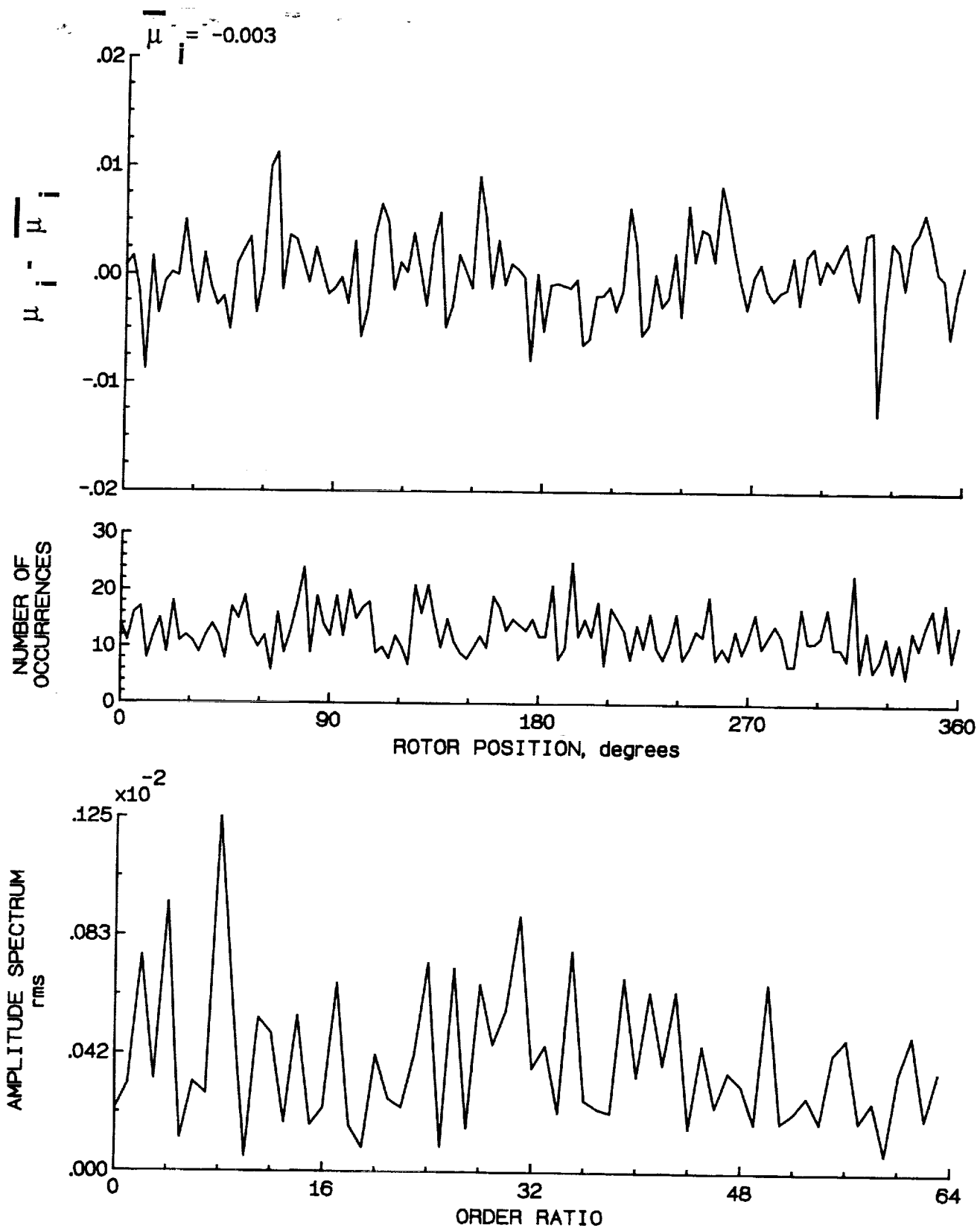


Figure 54.- Induced inflow velocity measured at 60 degrees and r/R of 1.02.

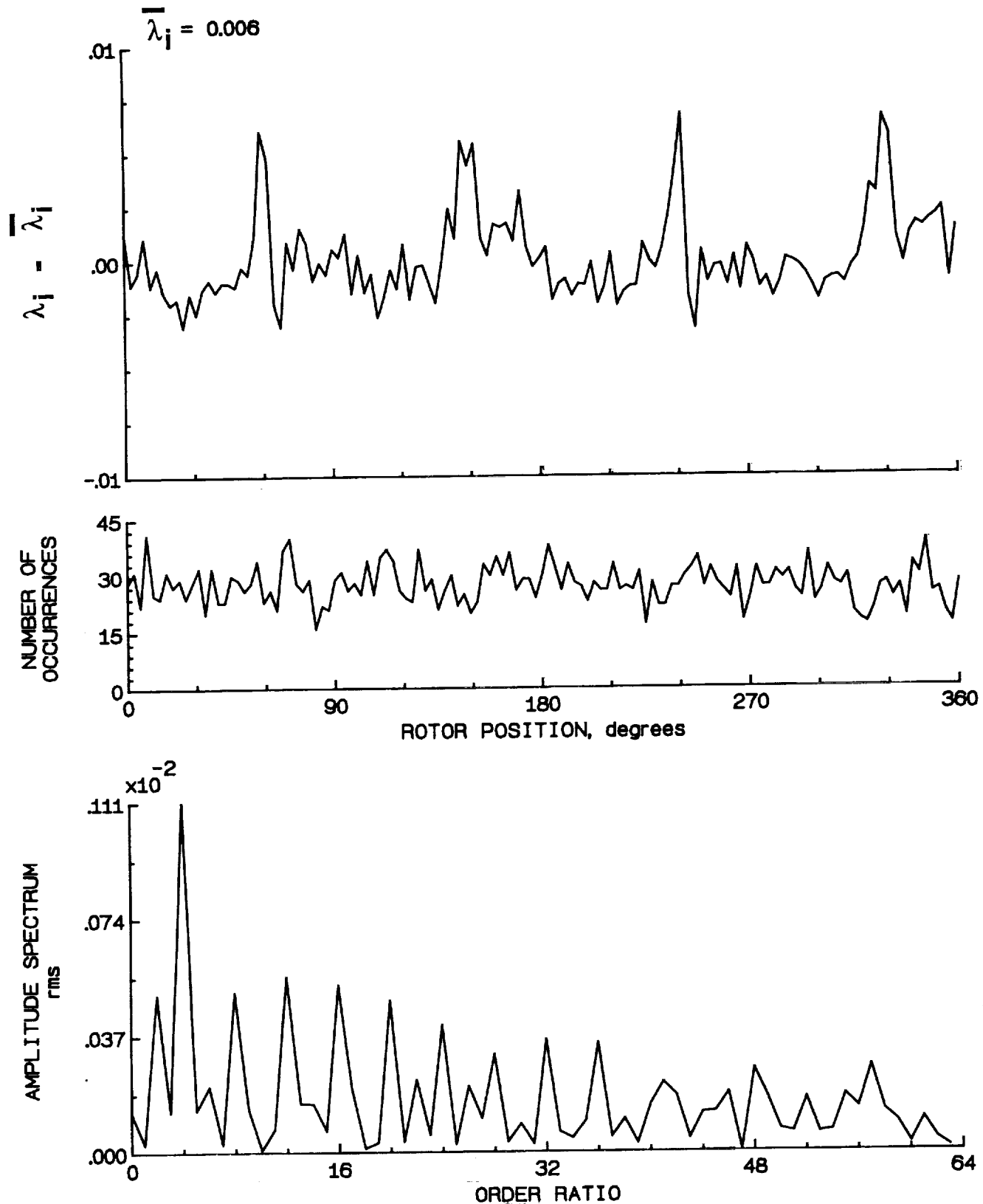


Figure 54.- Concluded.

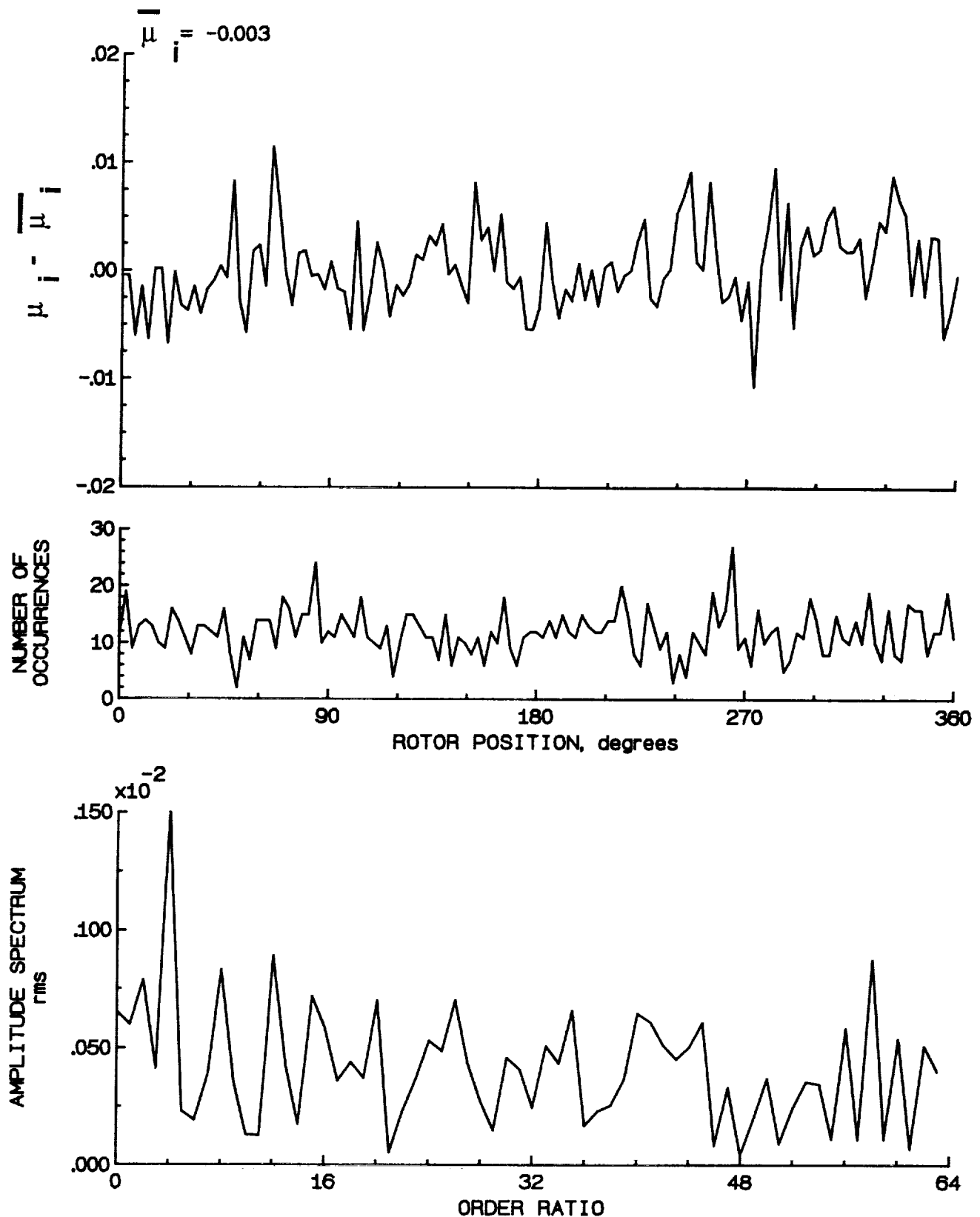


Figure 55.- Induced inflow velocity measured at 60 degrees and r/R of 1.04.

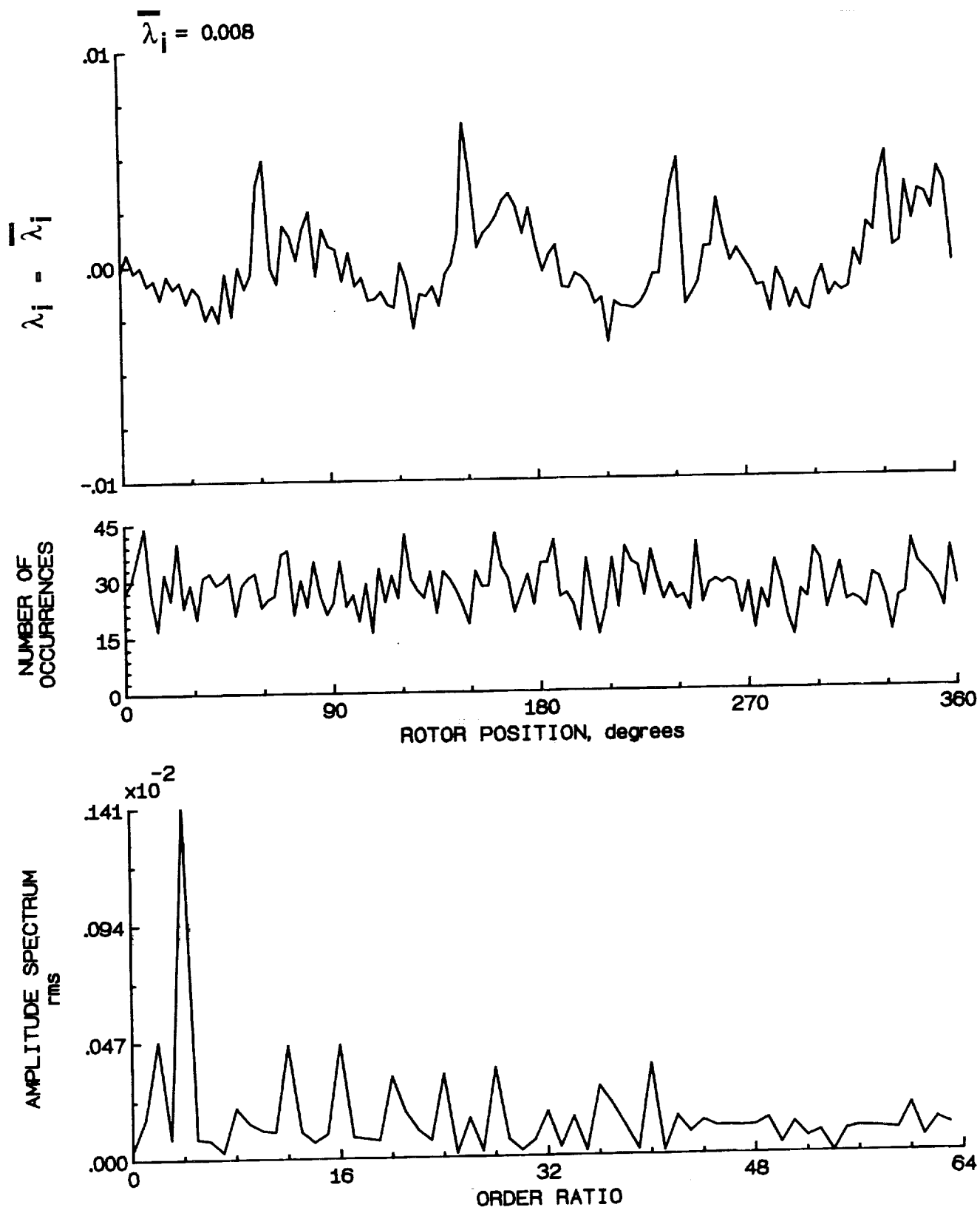


Figure 55.- Concluded.

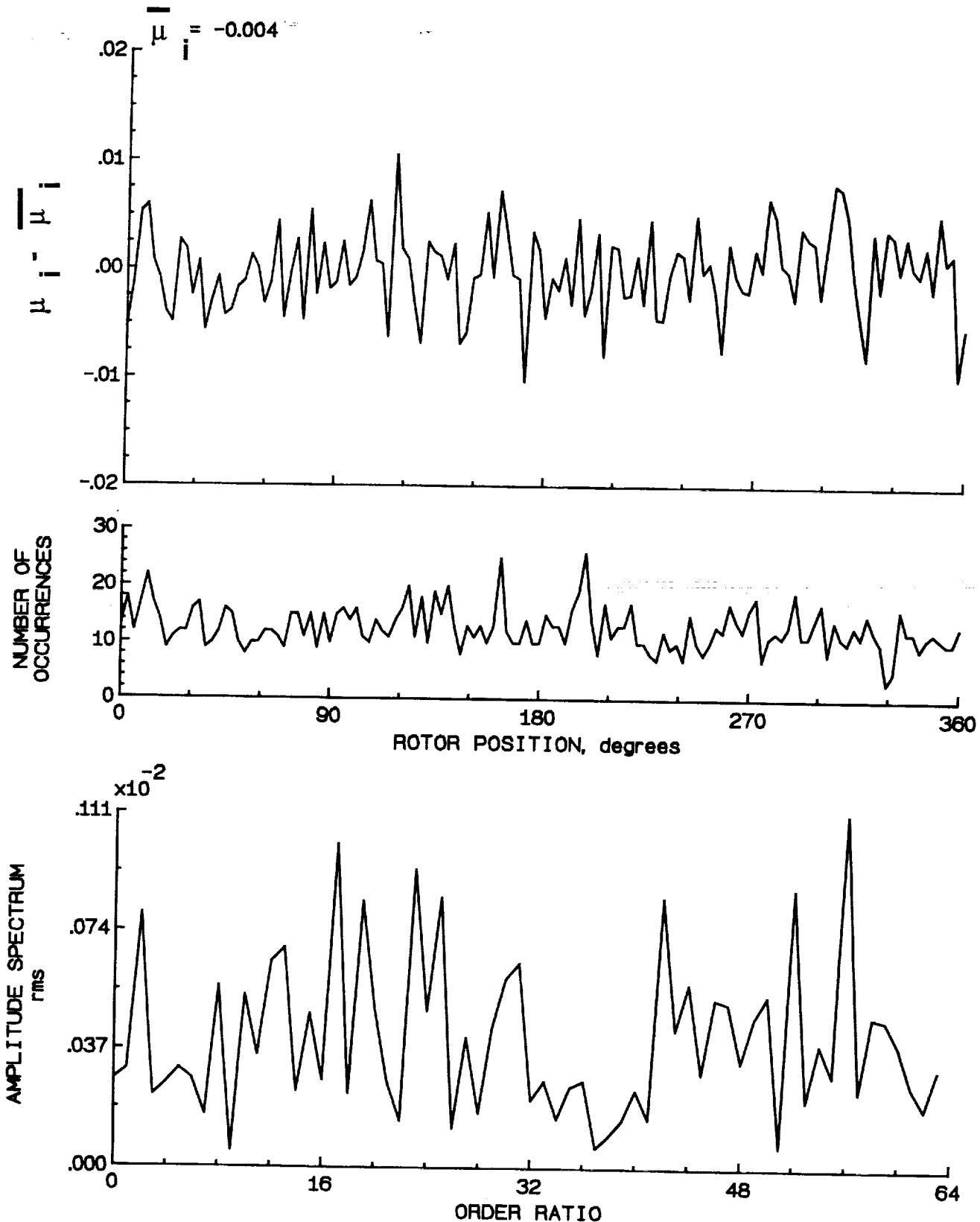


Figure 56.- Induced inflow velocity measured at 60 degrees and r/R of 1.10.

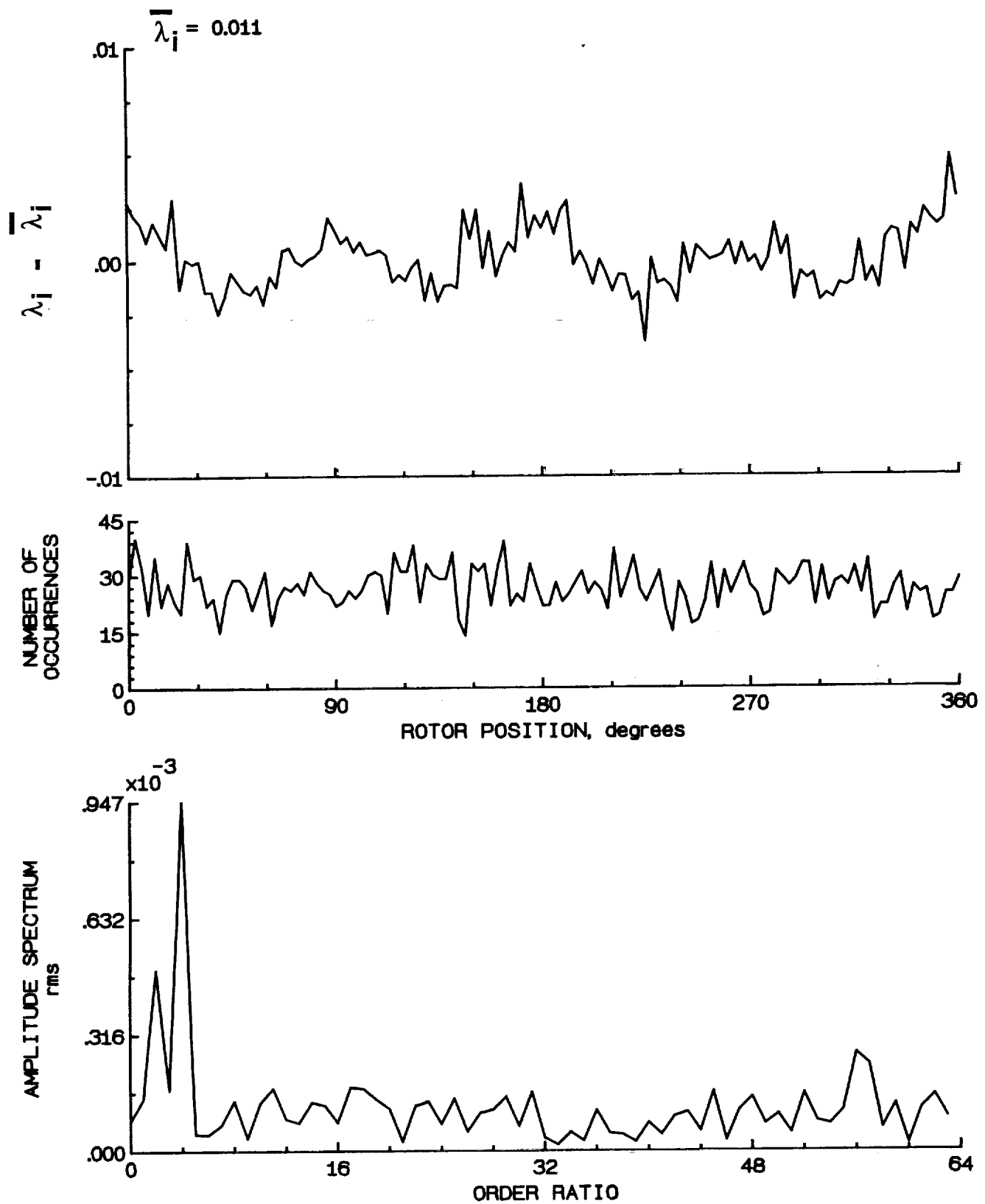


Figure 56.- Concluded.

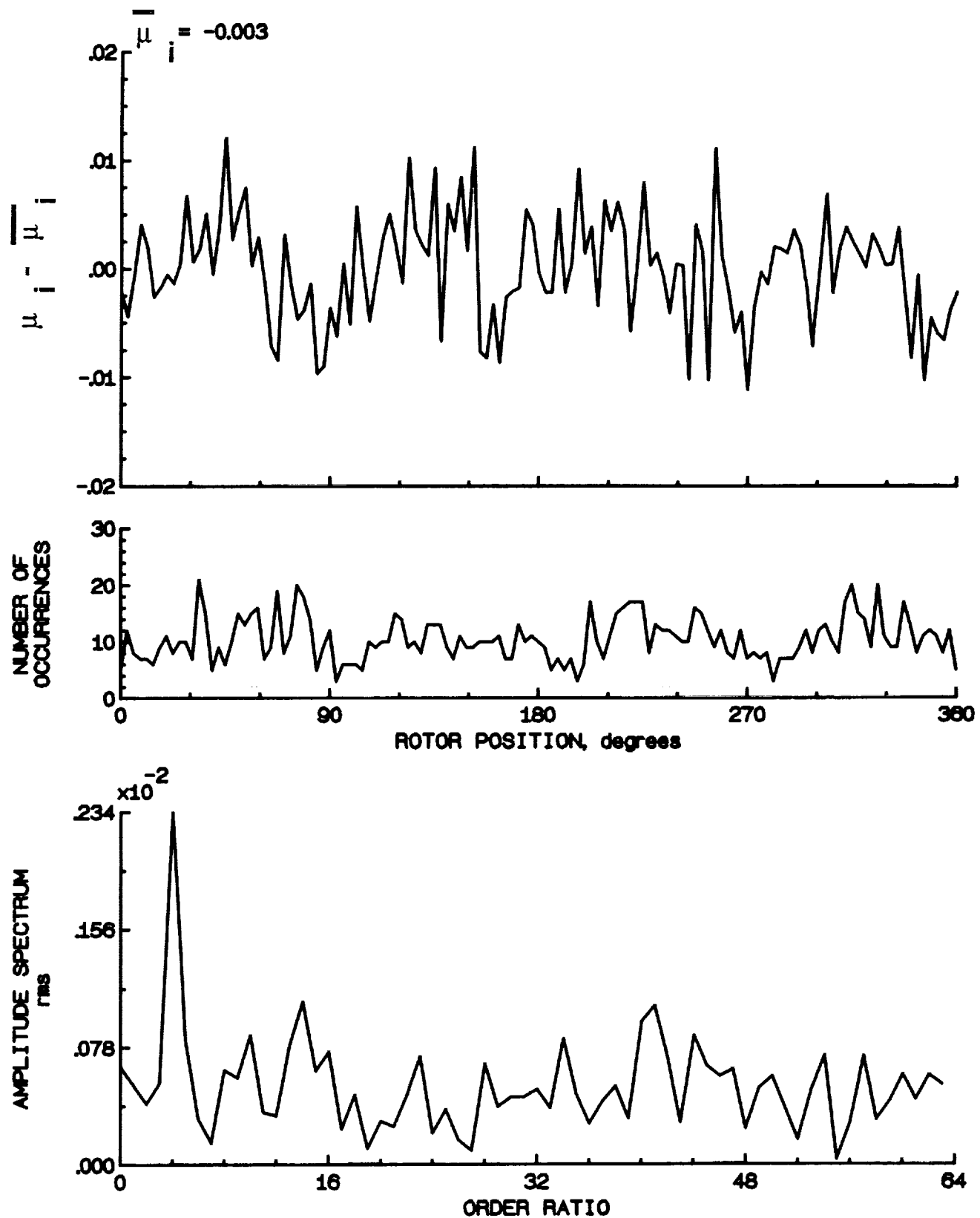


Figure 57.- Induced inflow velocity measured at 90 degrees and r/R of 0.20.

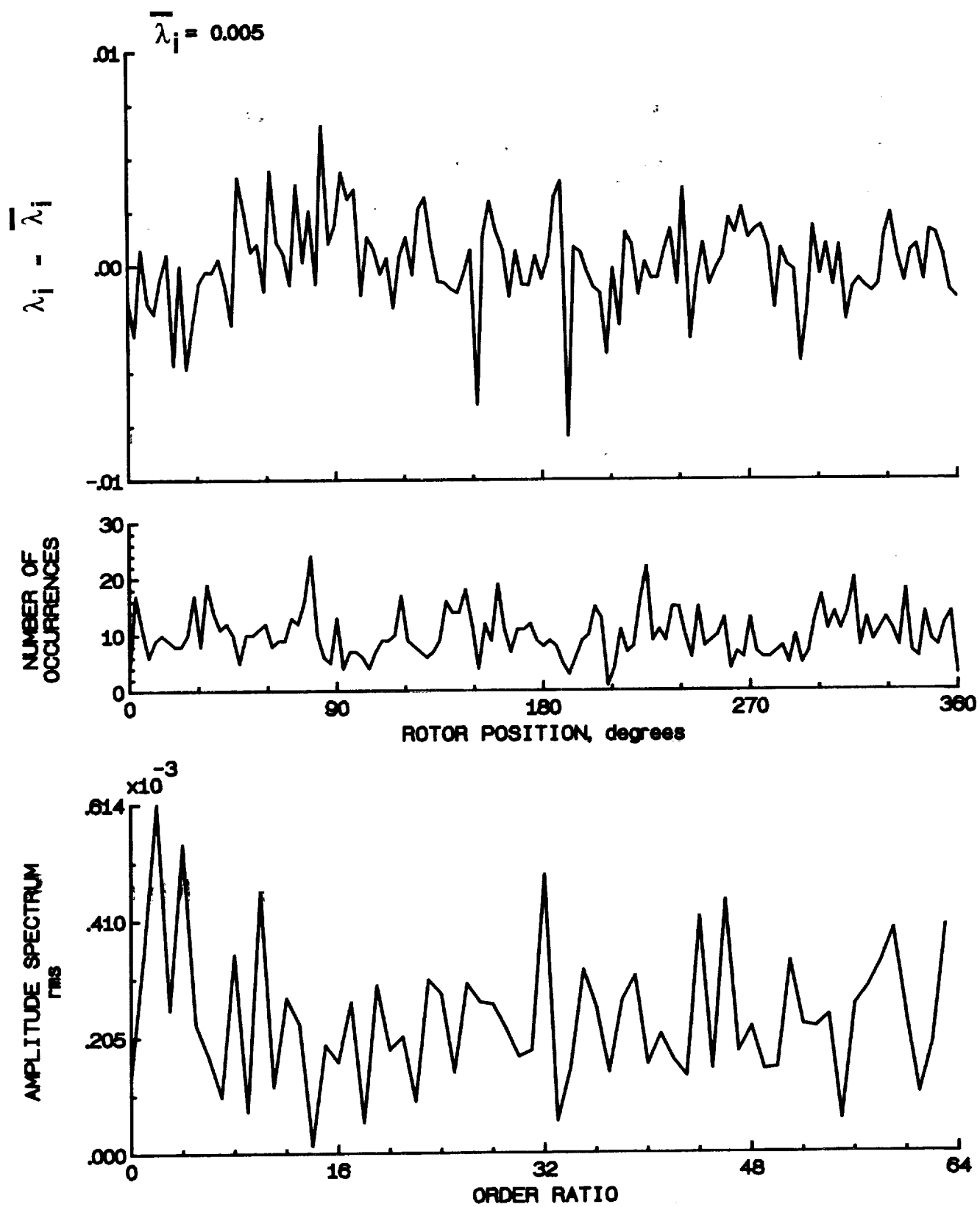


Figure 57.- Concluded.

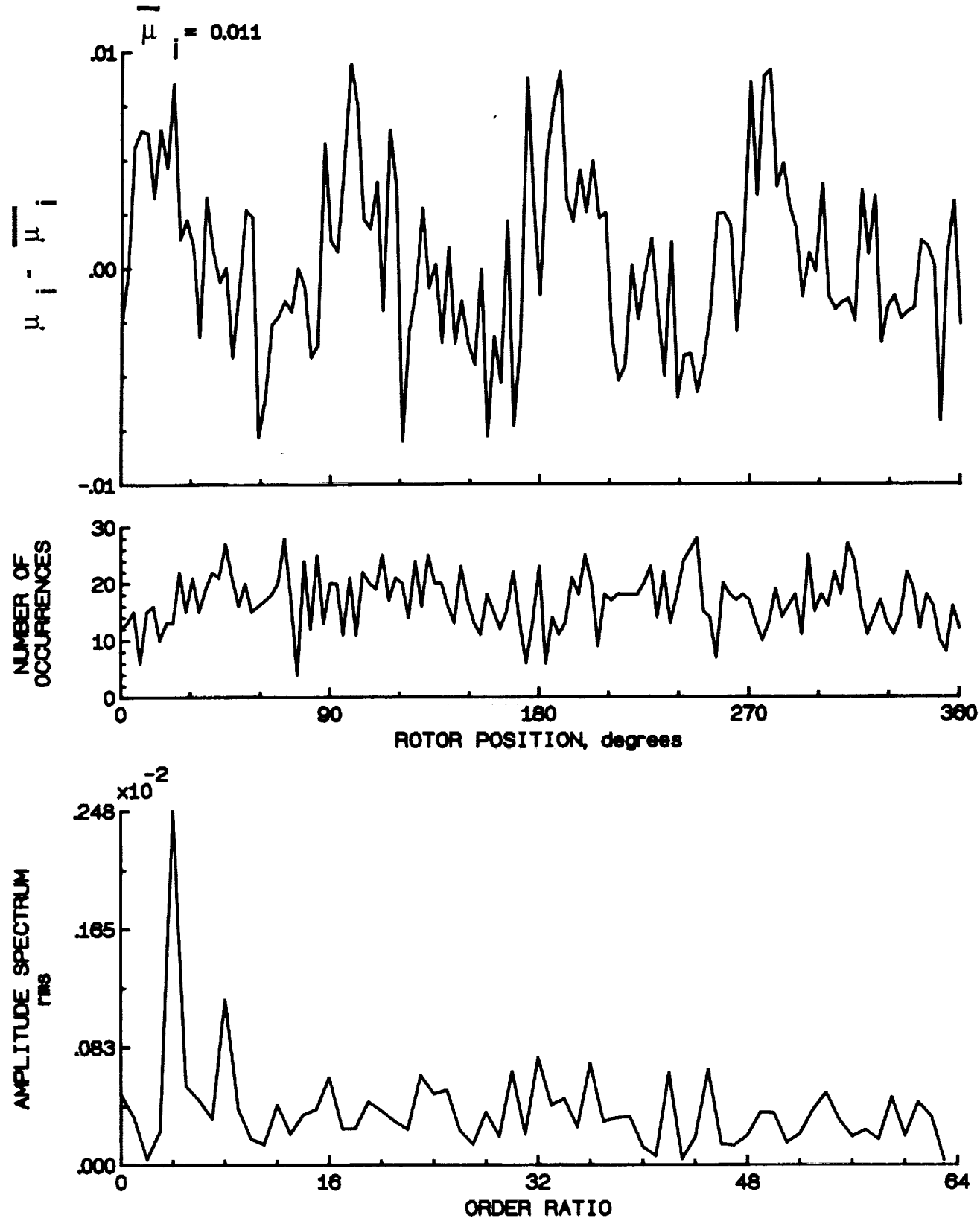


Figure 58.- Induced inflow velocity measured at 90 degrees and r/R of 0.40.

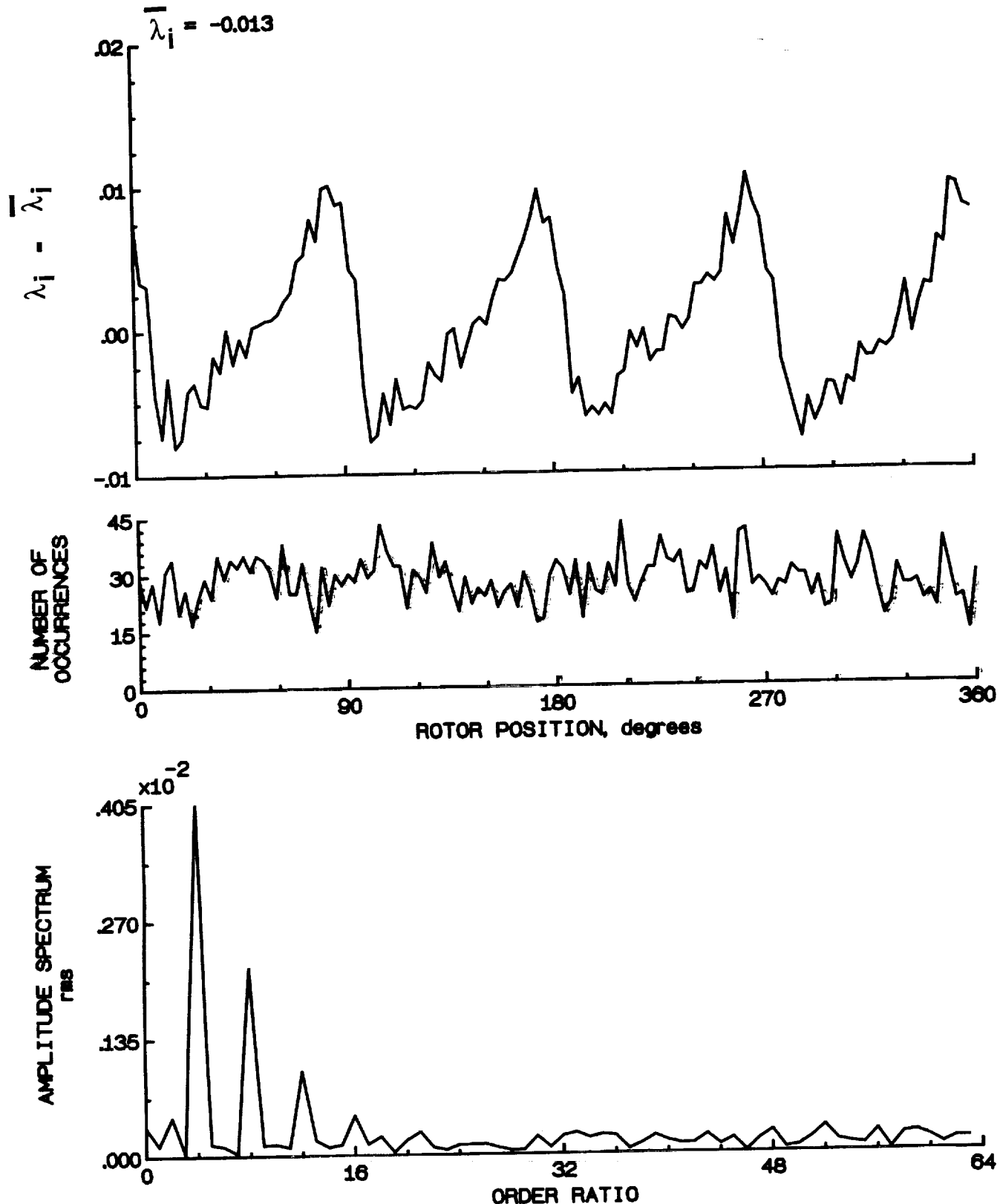


Figure 58.- Concluded.

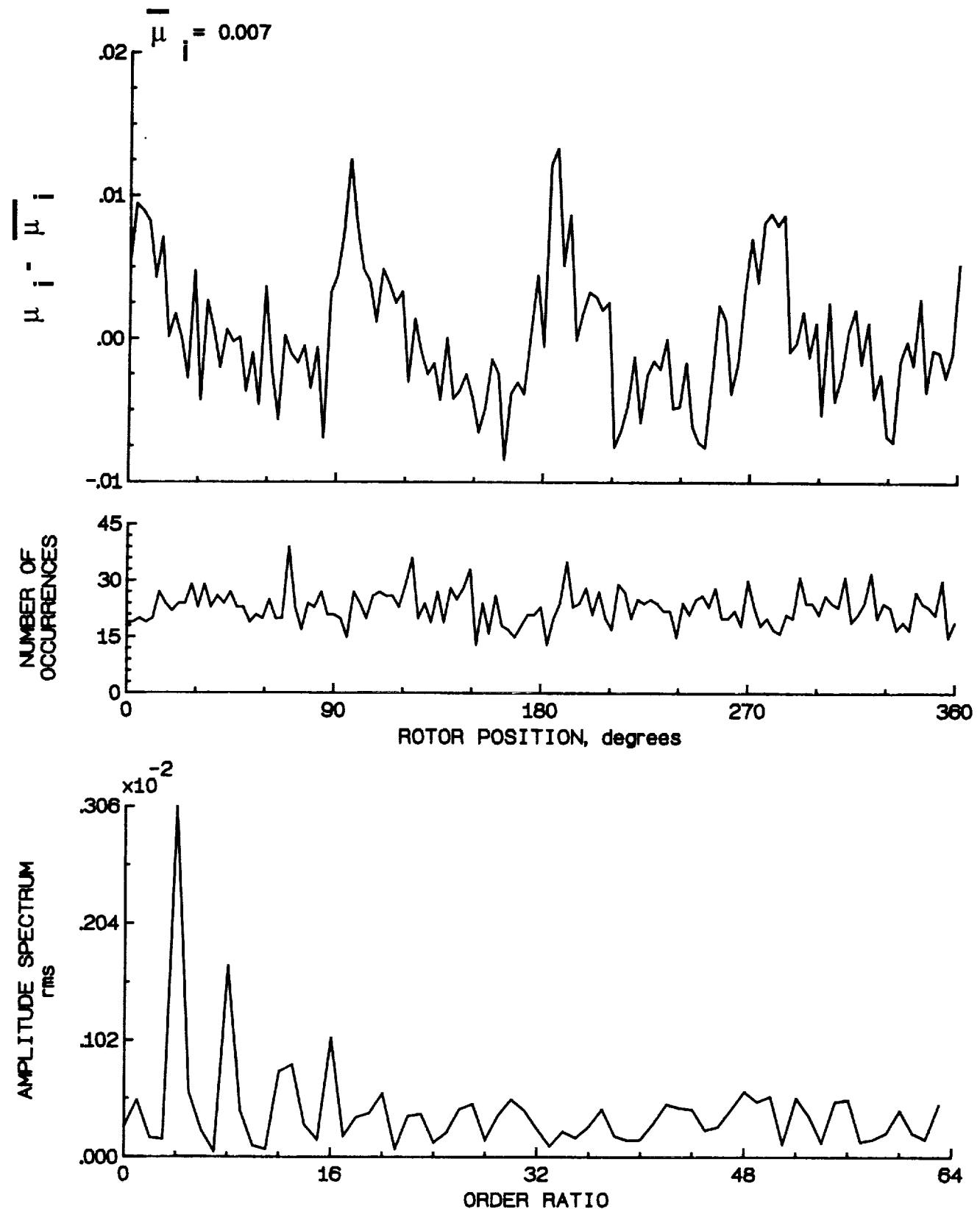


Figure 59.- Induced inflow velocity measured at 90 degrees and r/R of 0.50.

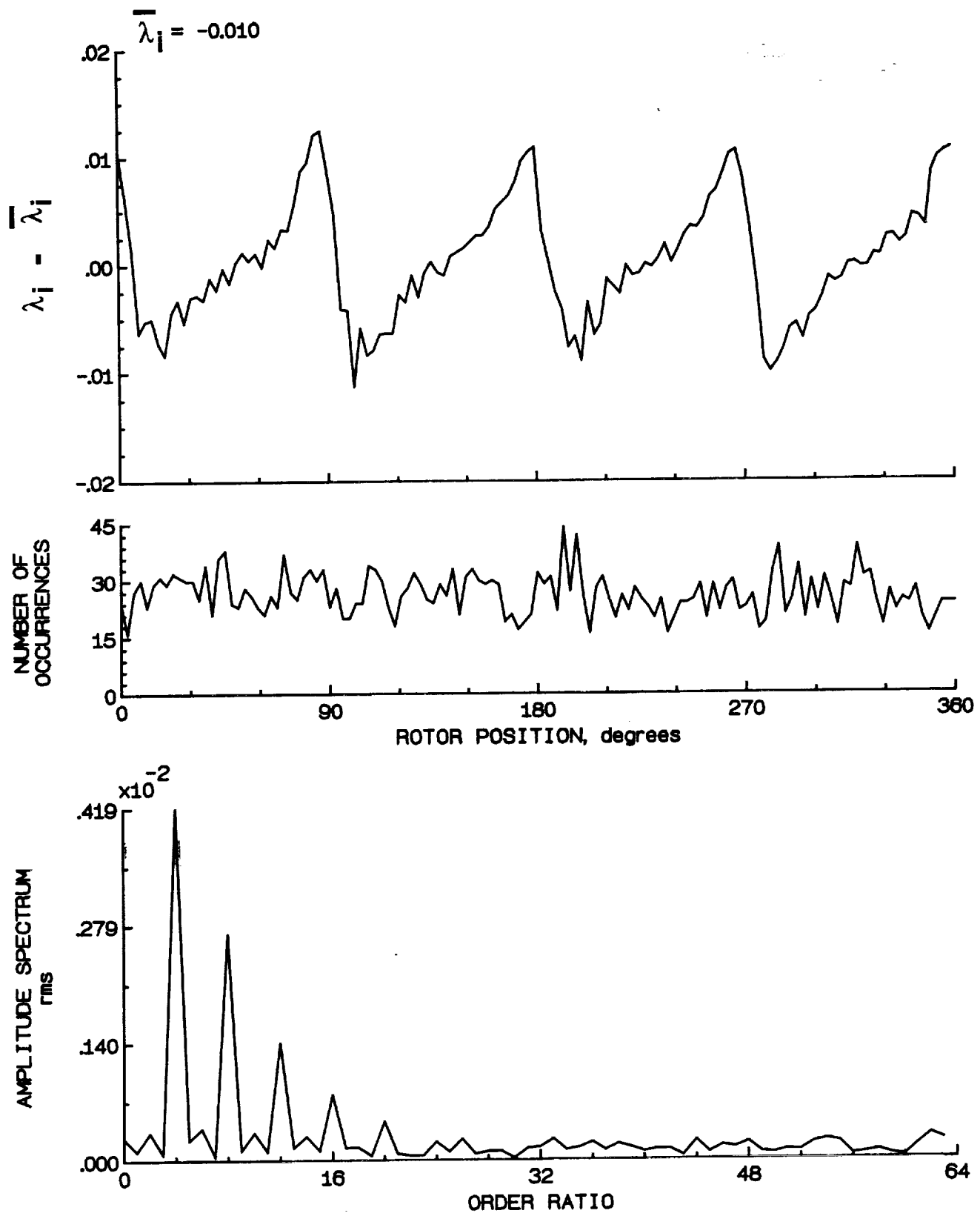


Figure 59.- Concluded.

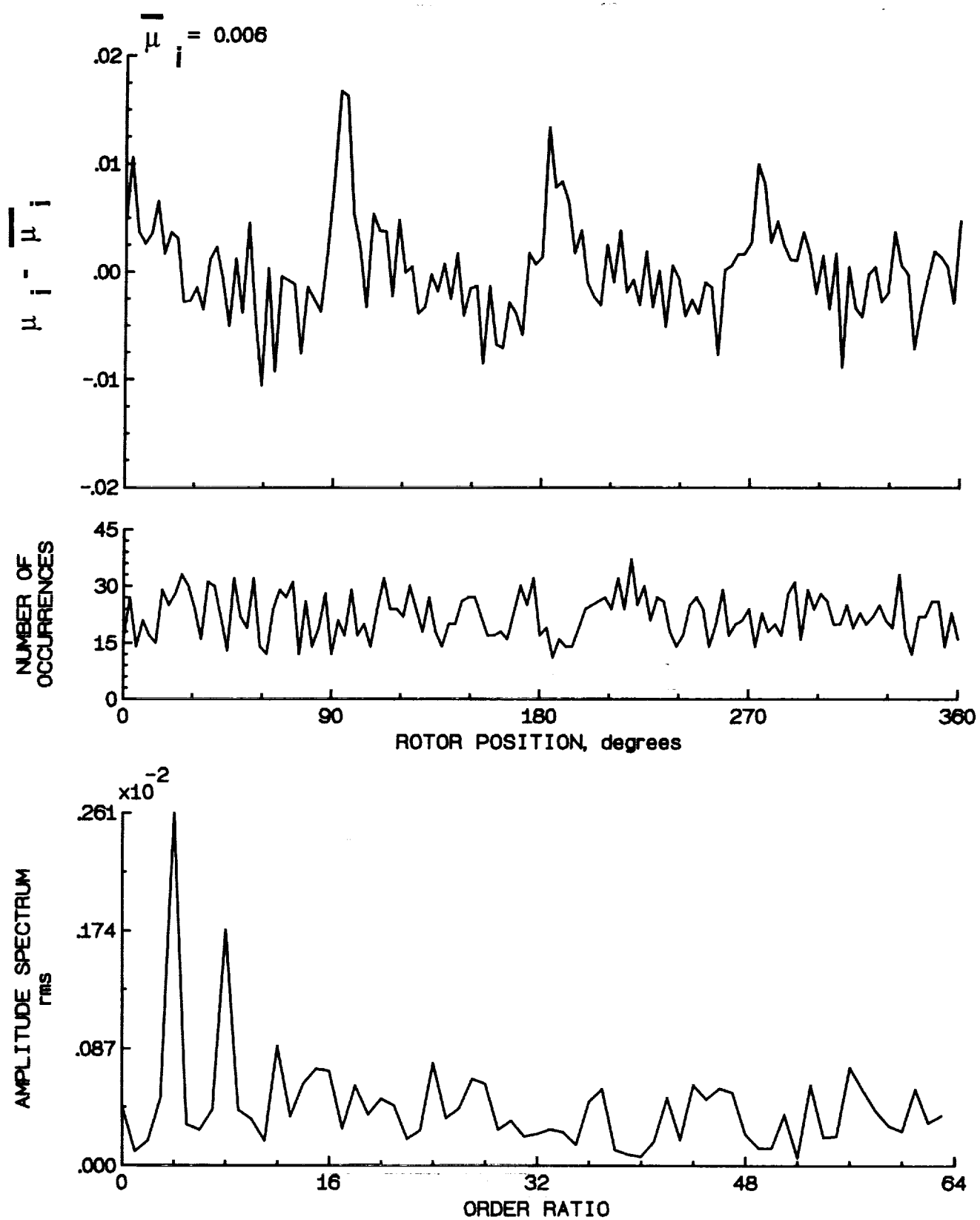


Figure 60.- Induced inflow velocity measured at 90 degrees and r/R of 0.60.

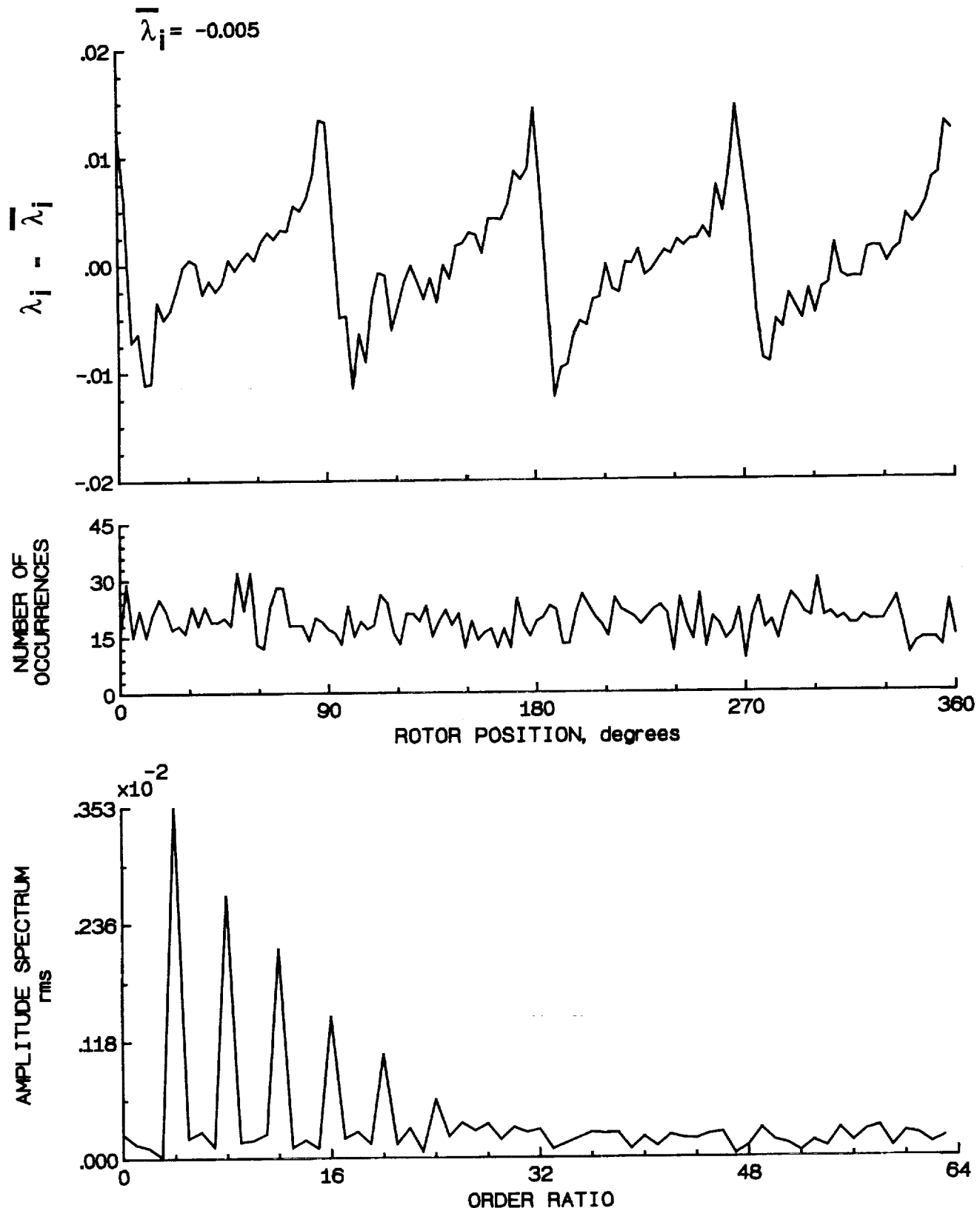


Figure 60.- Concluded.

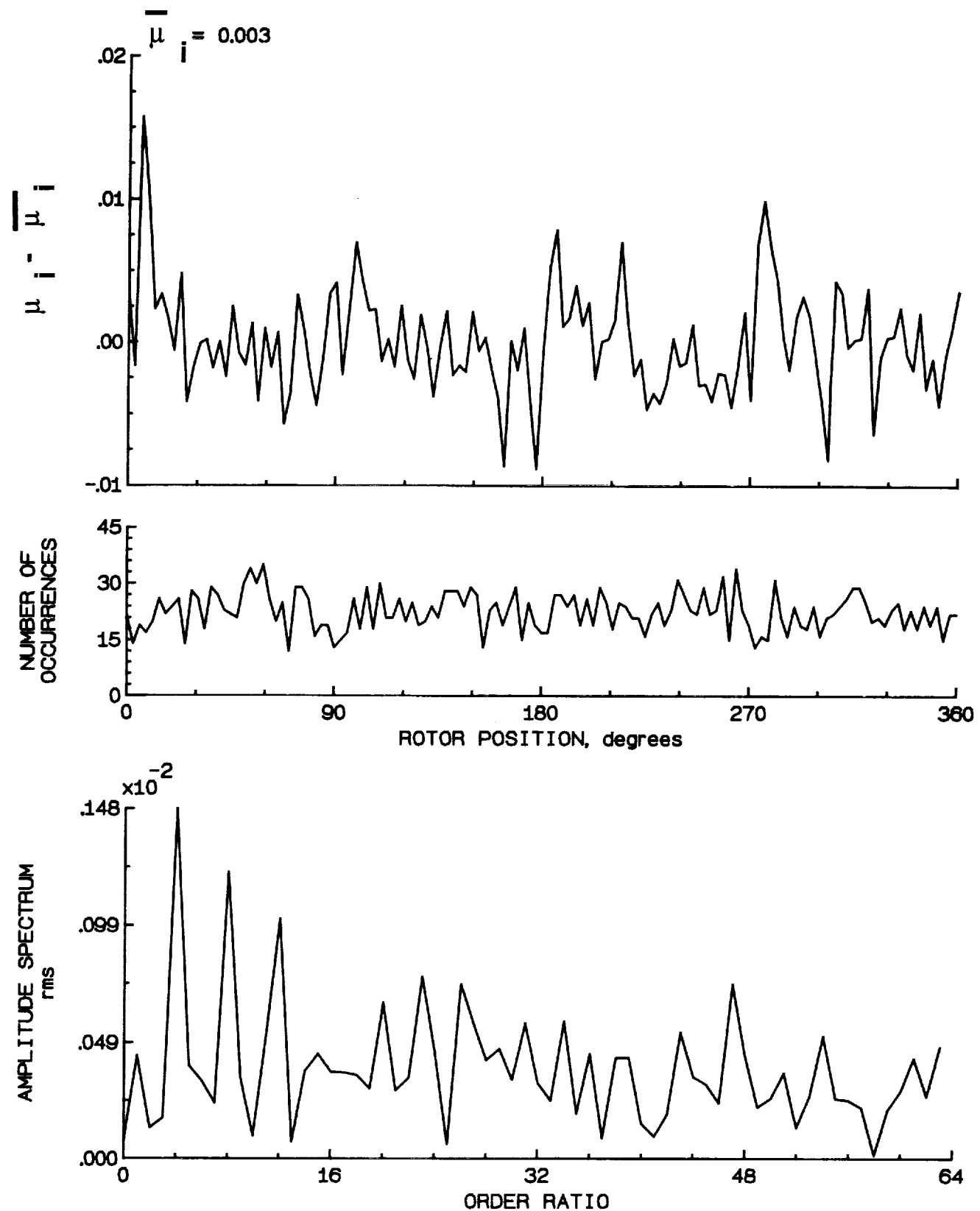


Figure 61.- Induced inflow velocity measured at 90 degrees and r/R of 0.70.

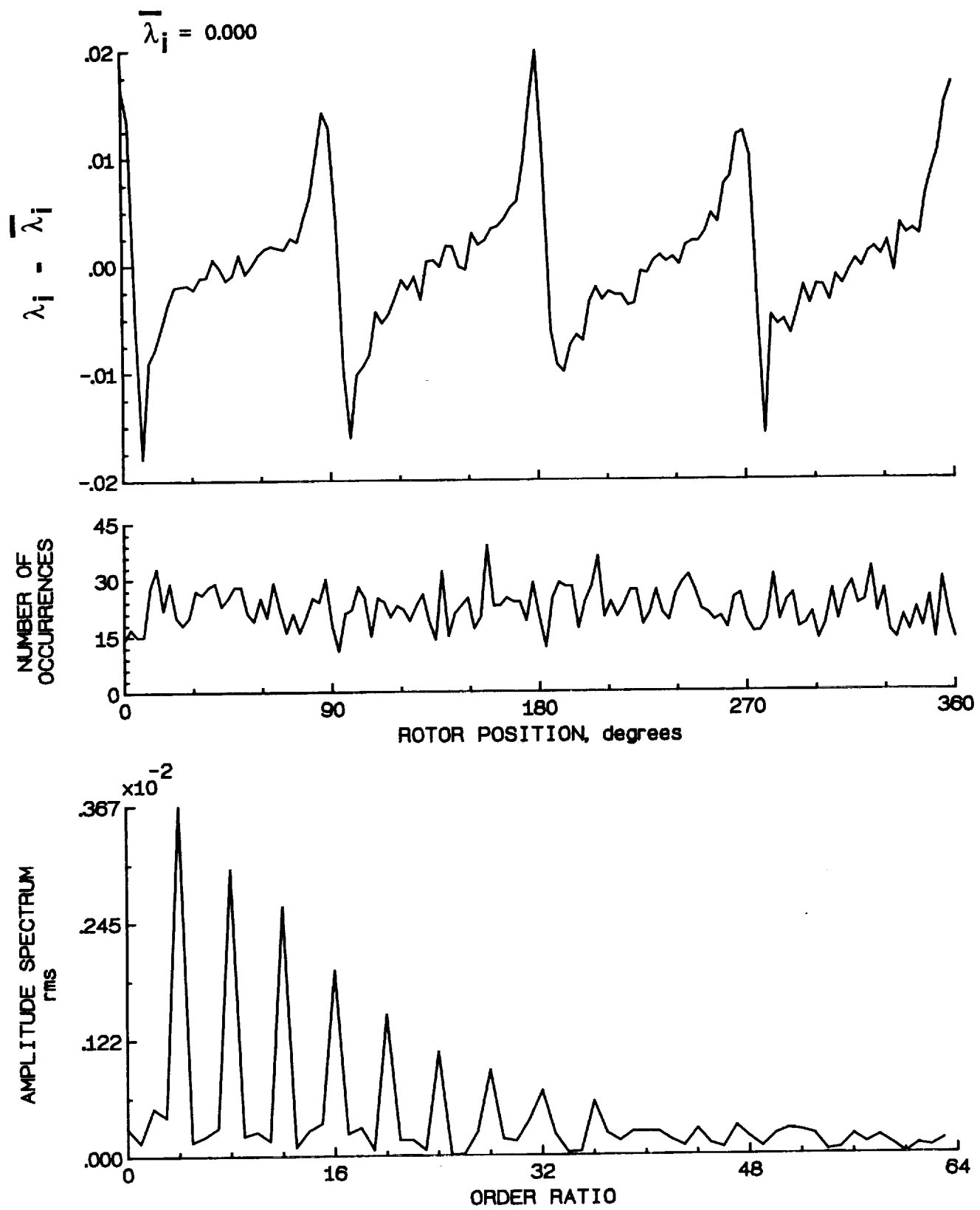


Figure 61.- Concluded.

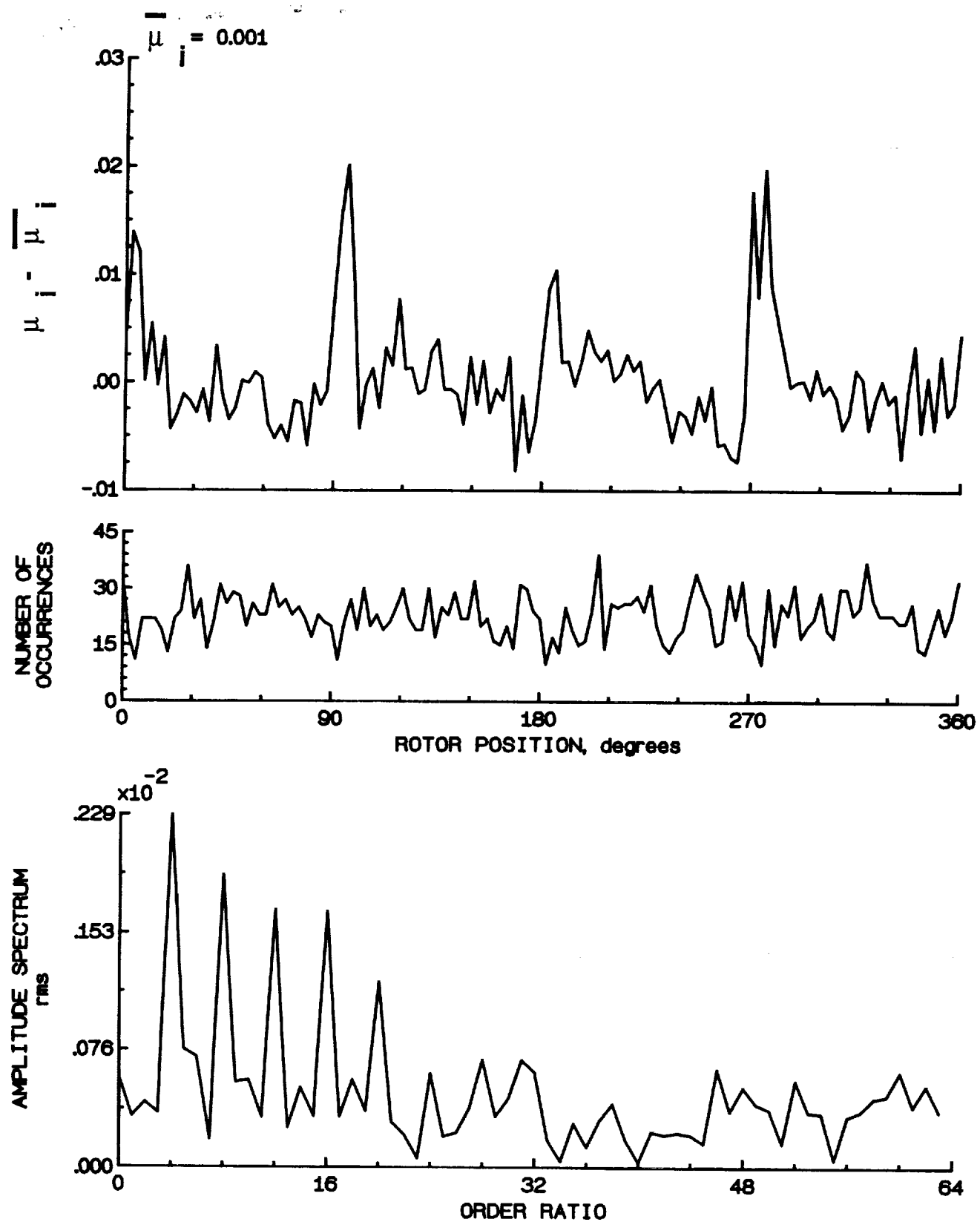


Figure 62.- Induced inflow velocity measured at 90 degrees and r/R of 0.74.

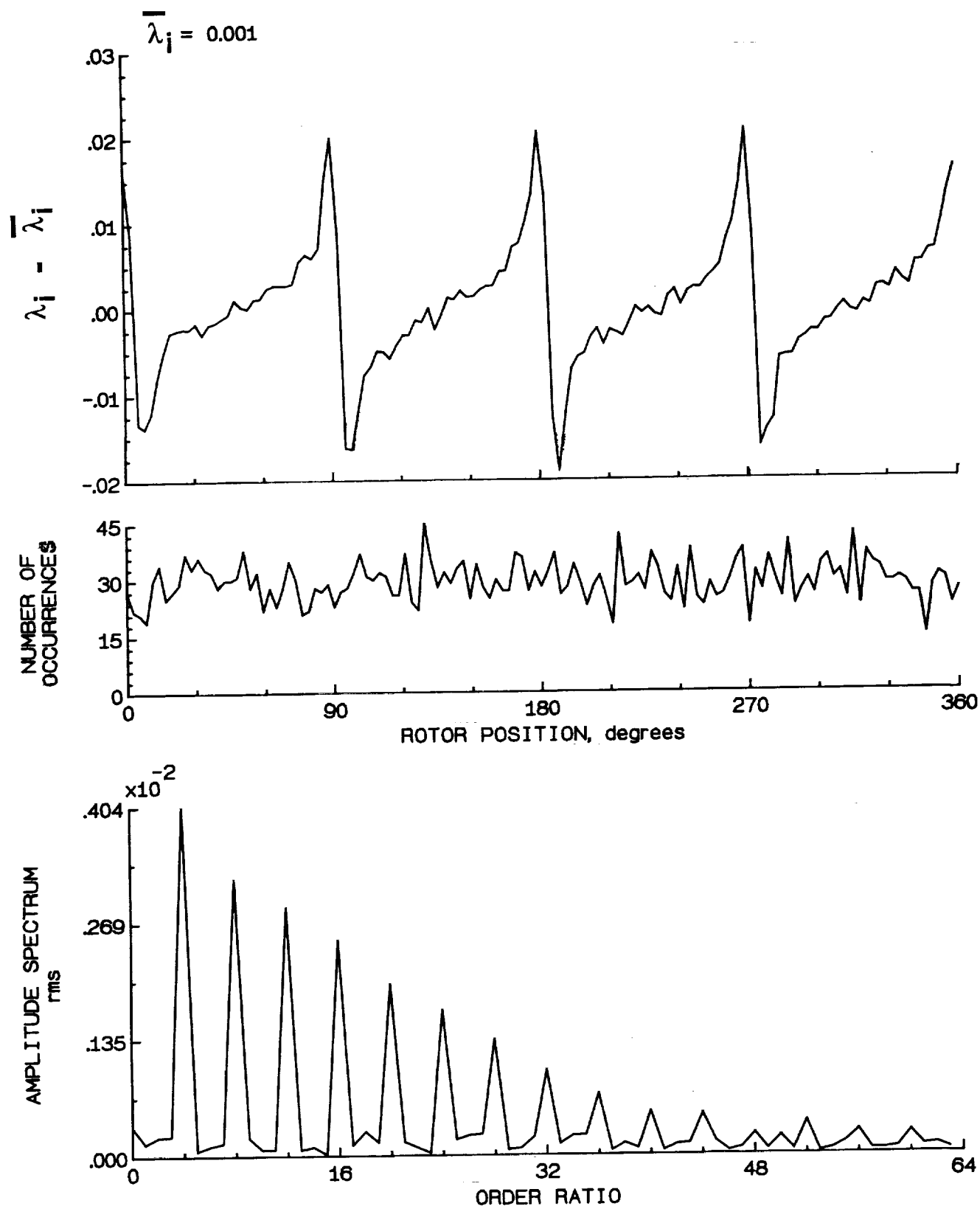


Figure 62.- Concluded.

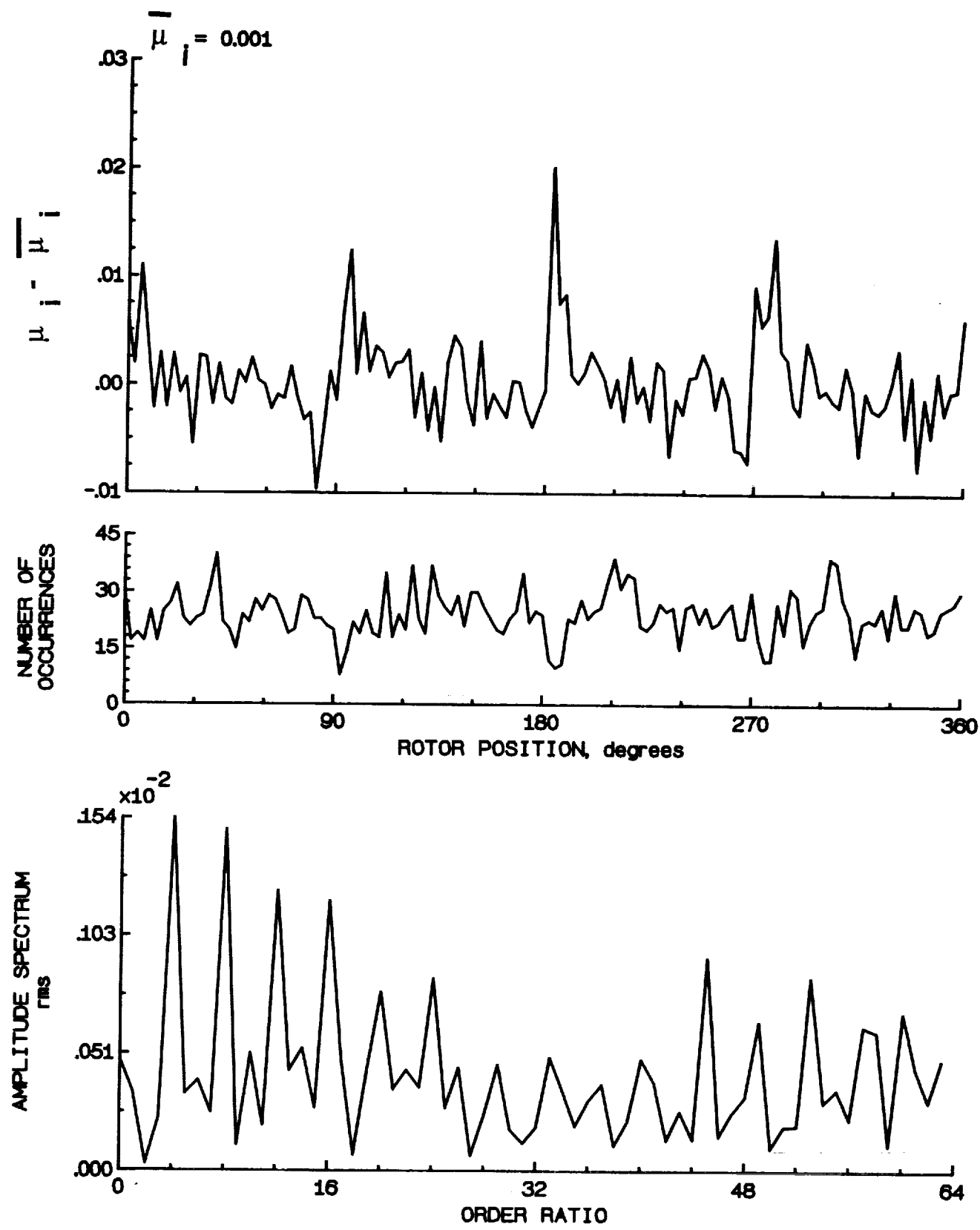


Figure 63.- Induced inflow velocity measured at 90 degrees and r/R of 0.78.

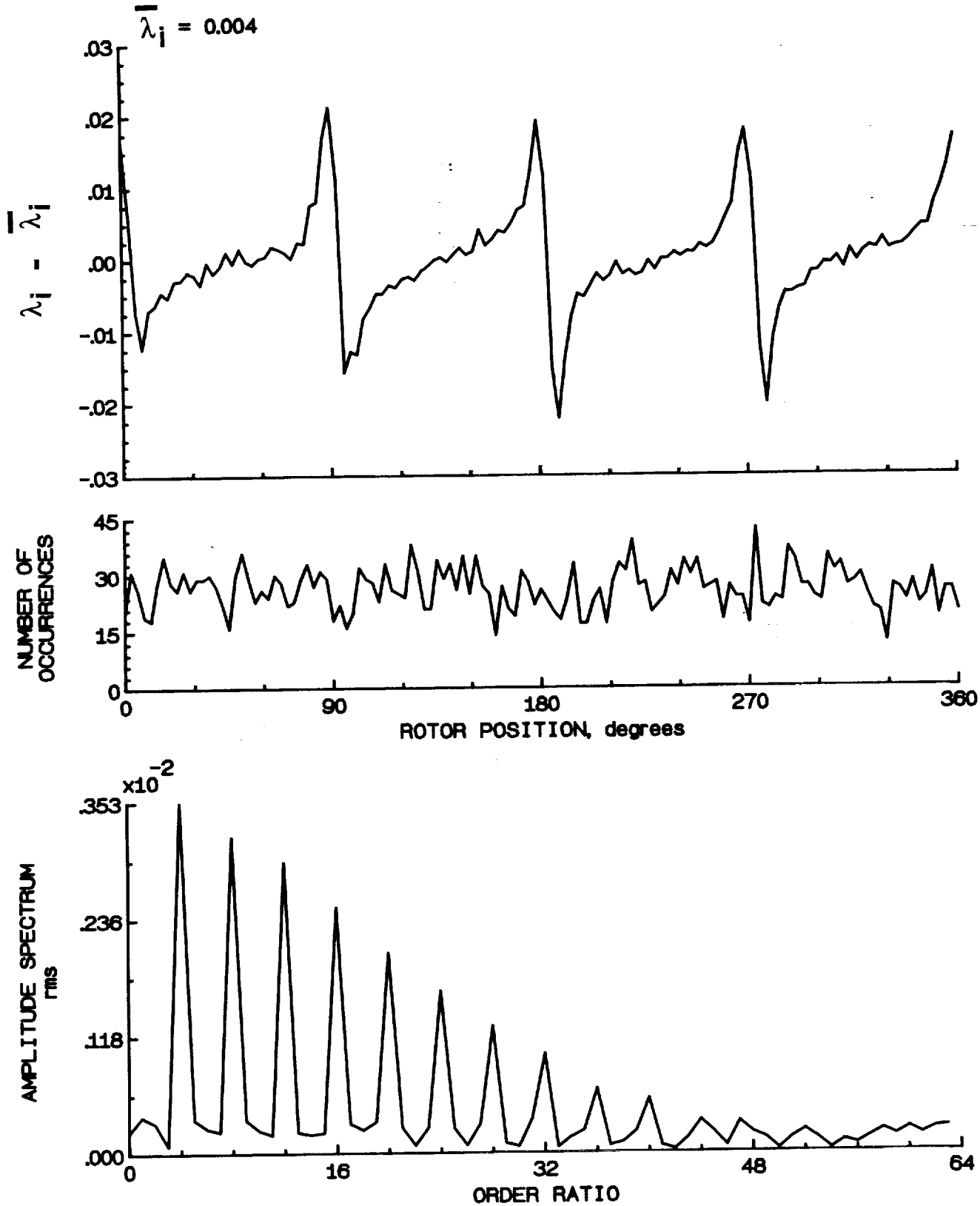


Figure 63.- Concluded.

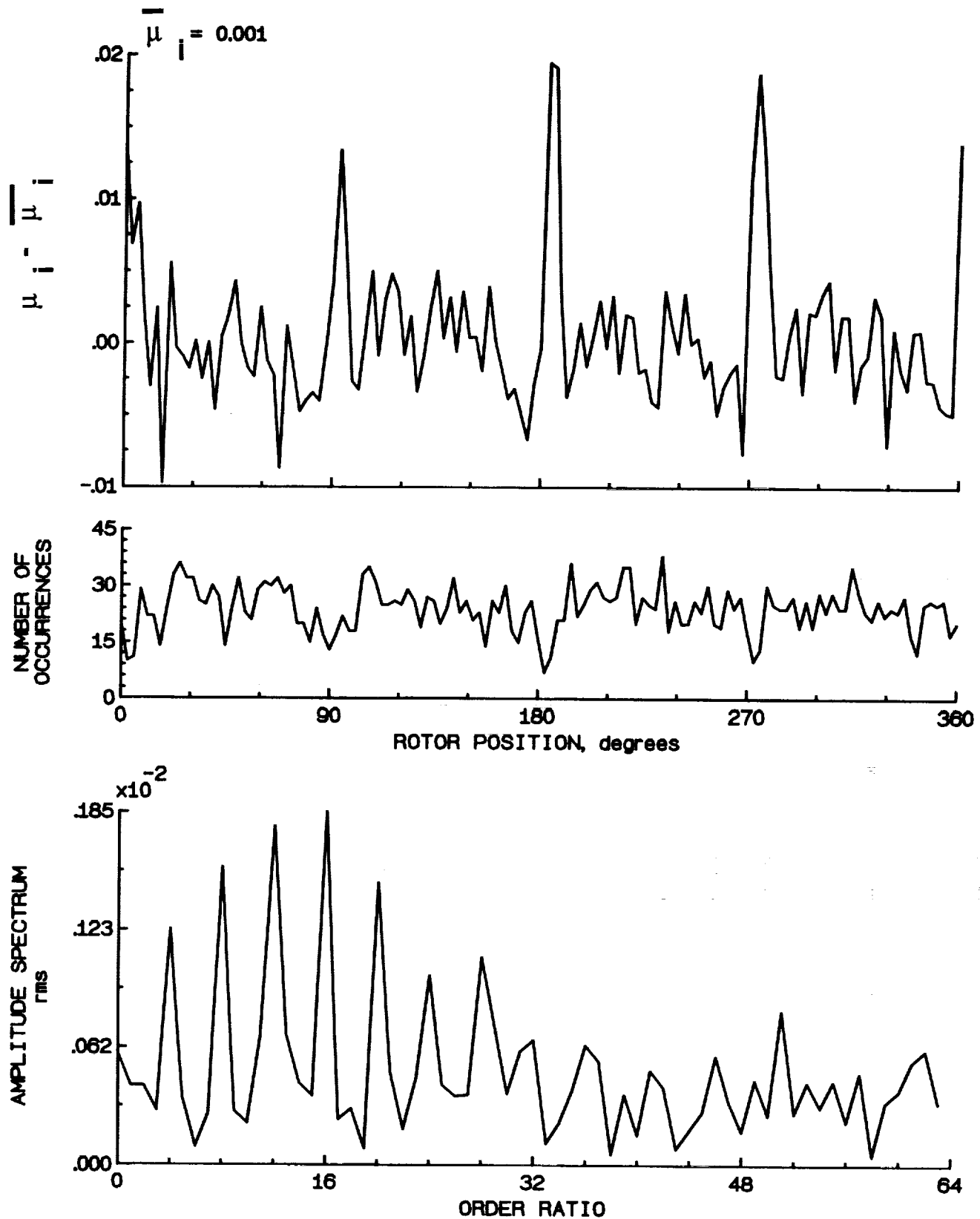


Figure 64.- Induced inflow velocity measured at 90 degrees and r/R of 0.82.

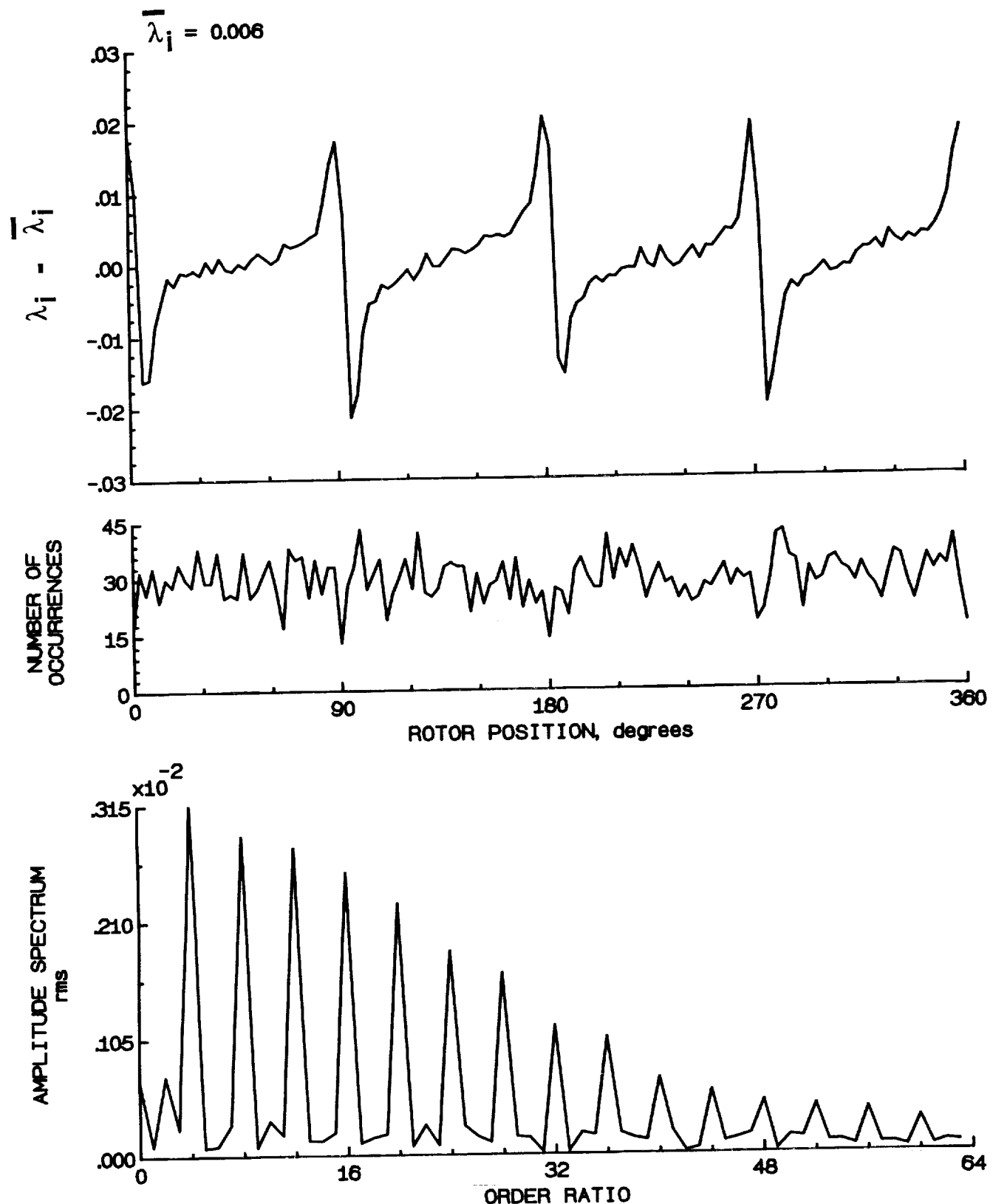


Figure 64.- Concluded.

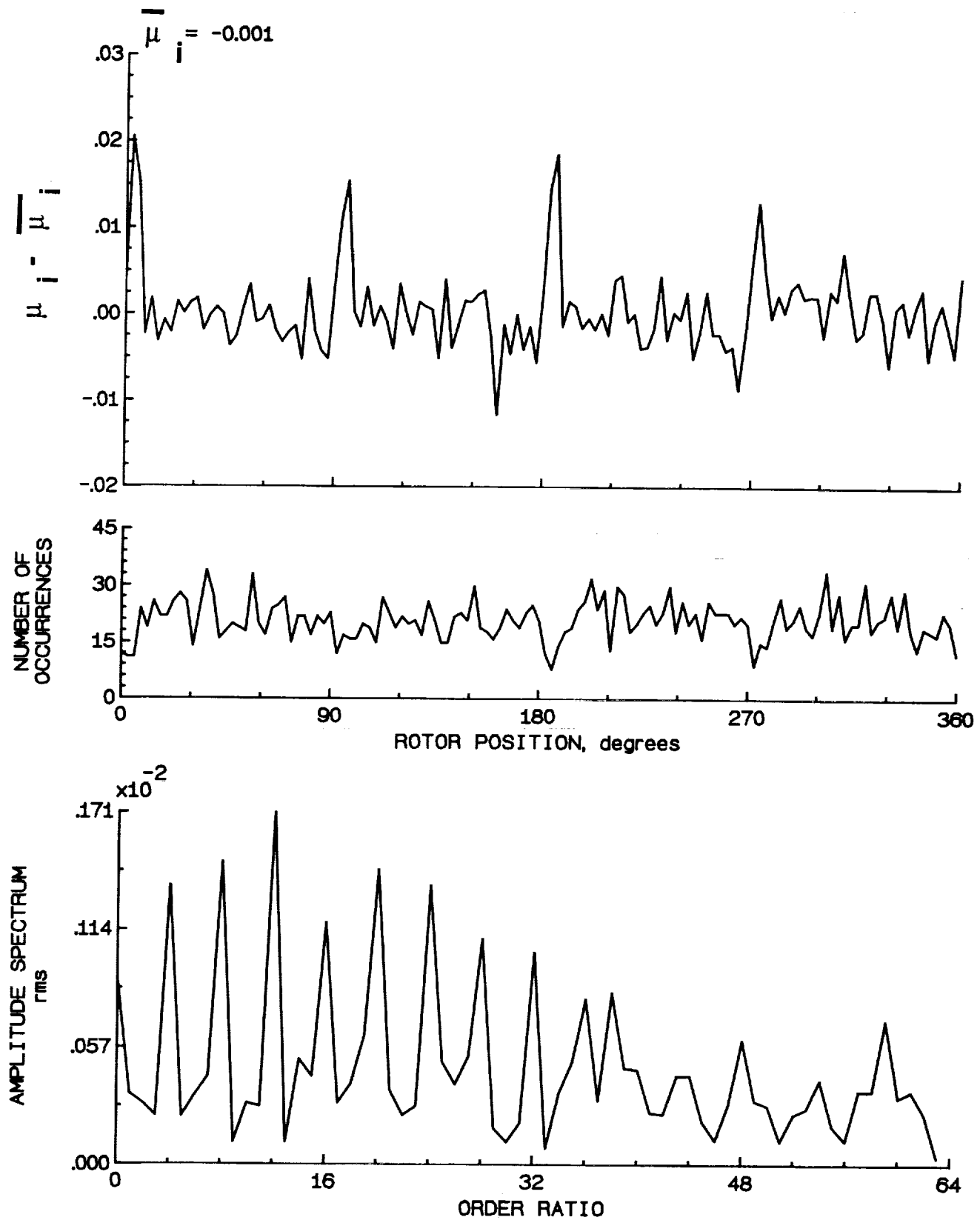


Figure 65.- Induced inflow velocity measured at 90 degrees and r/R of 0.86.

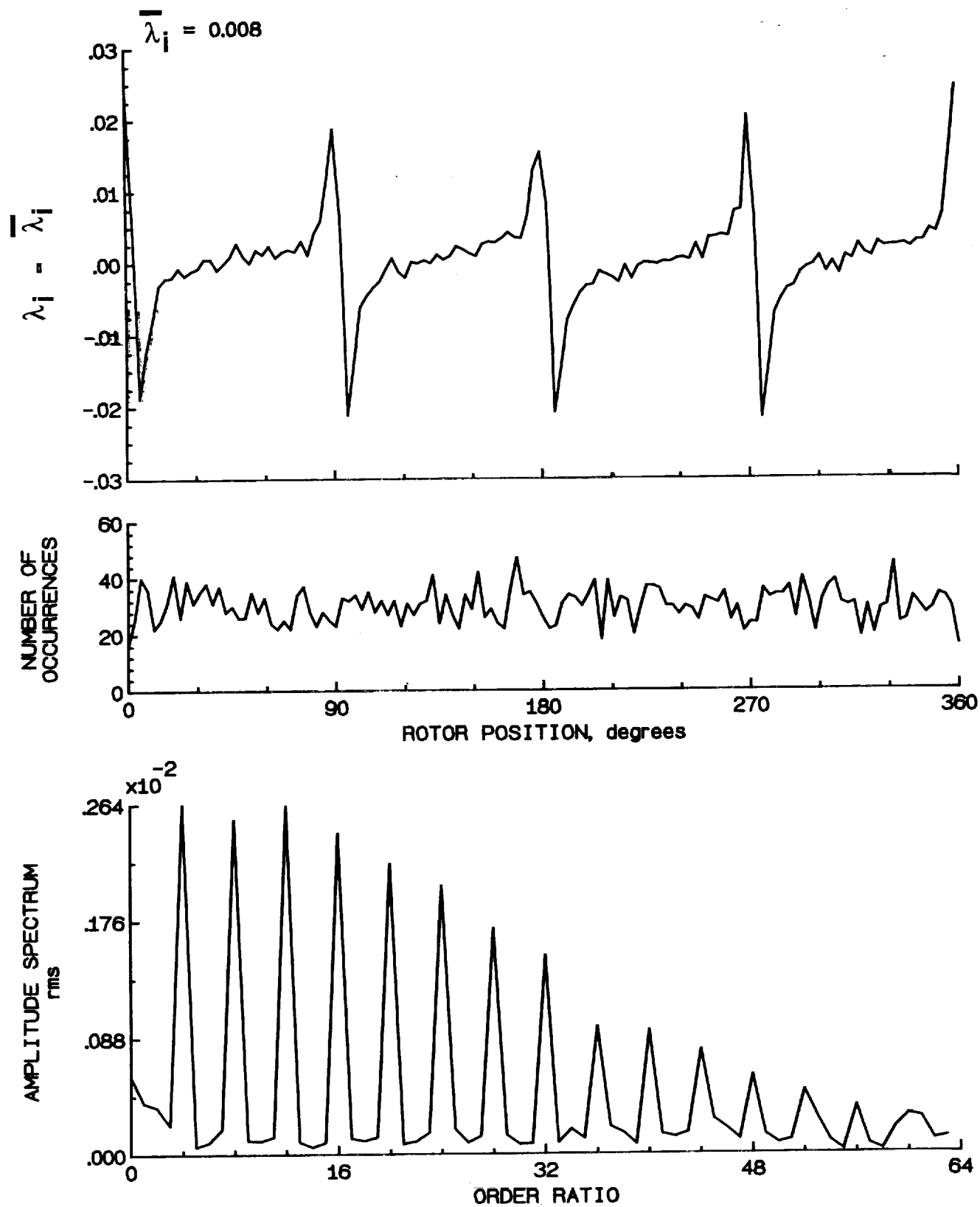


Figure 65.- Concluded.

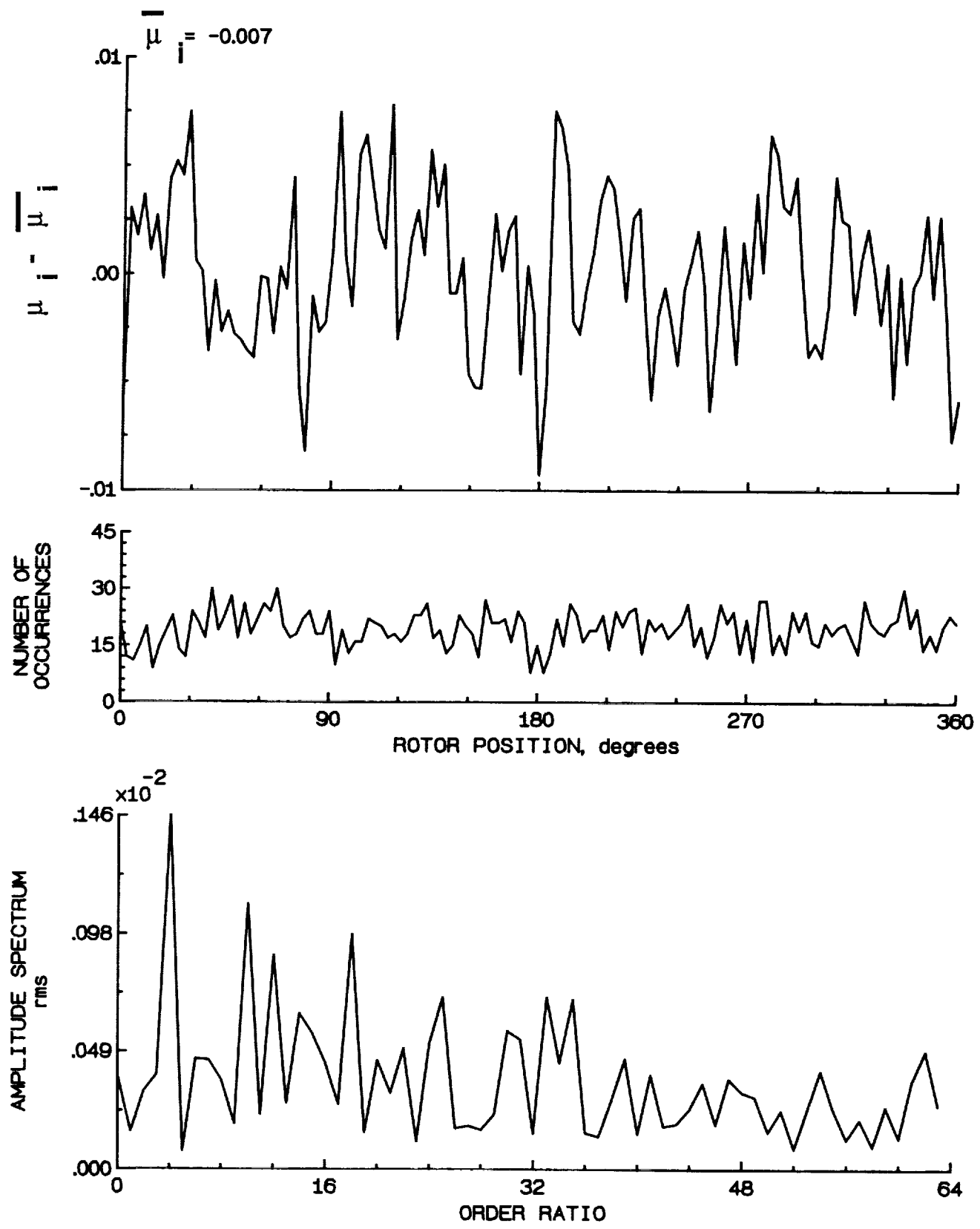


Figure 66.- Induced inflow velocity measured at 90 degrees and r/R of 0.90.

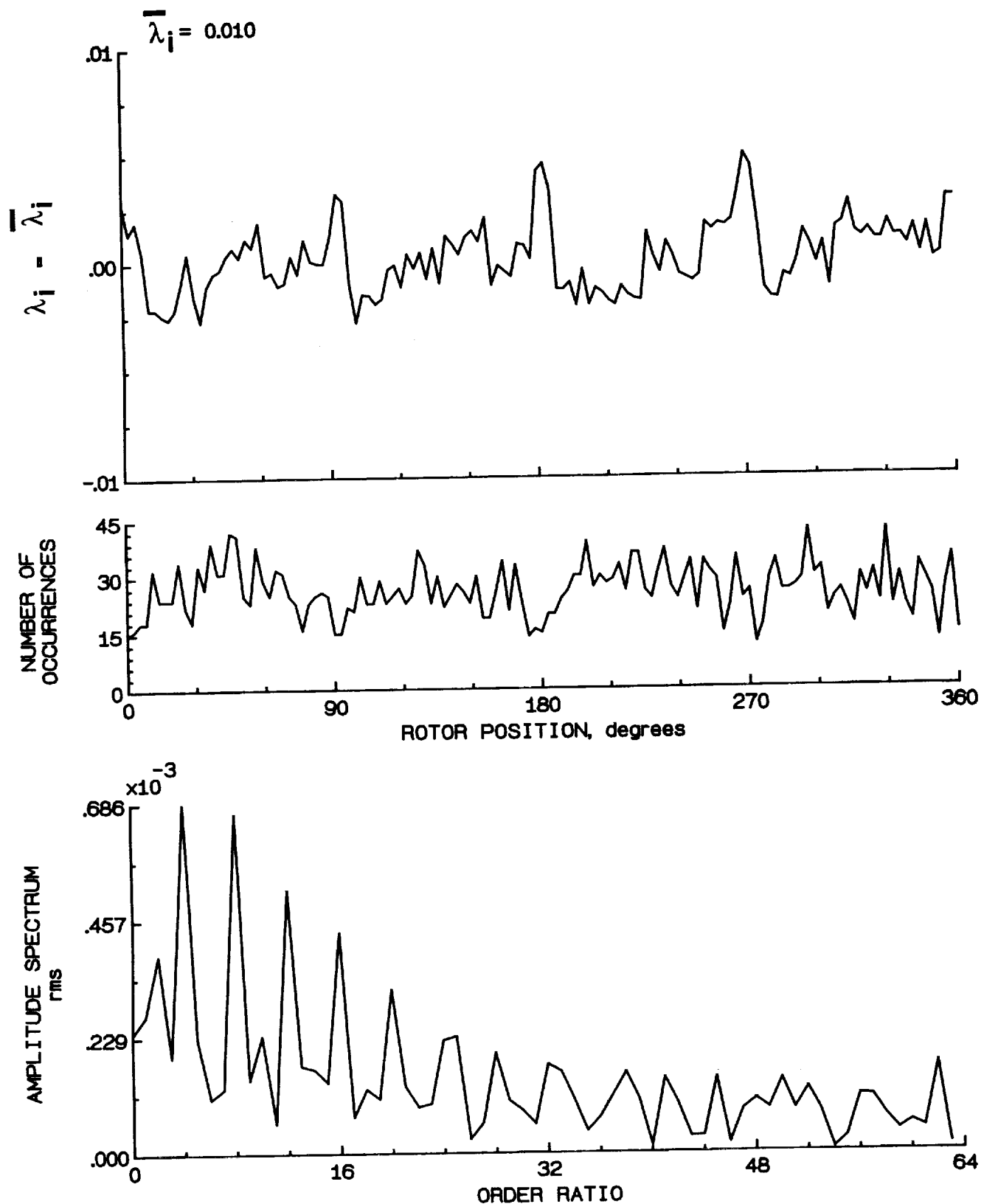


Figure 66.- Concluded.

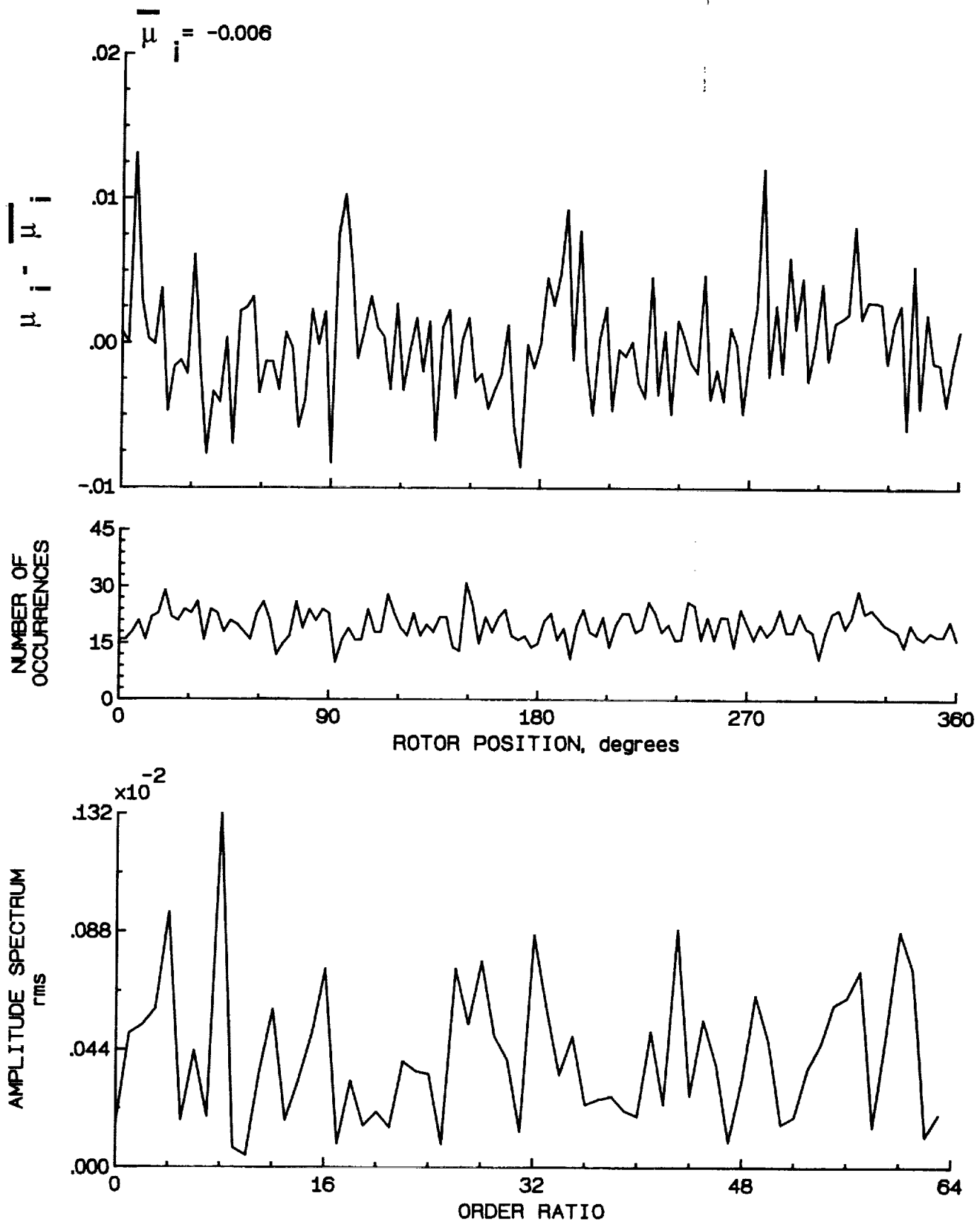


Figure 67.- Induced inflow velocity measured at 90 degrees and r/R of 0.94.

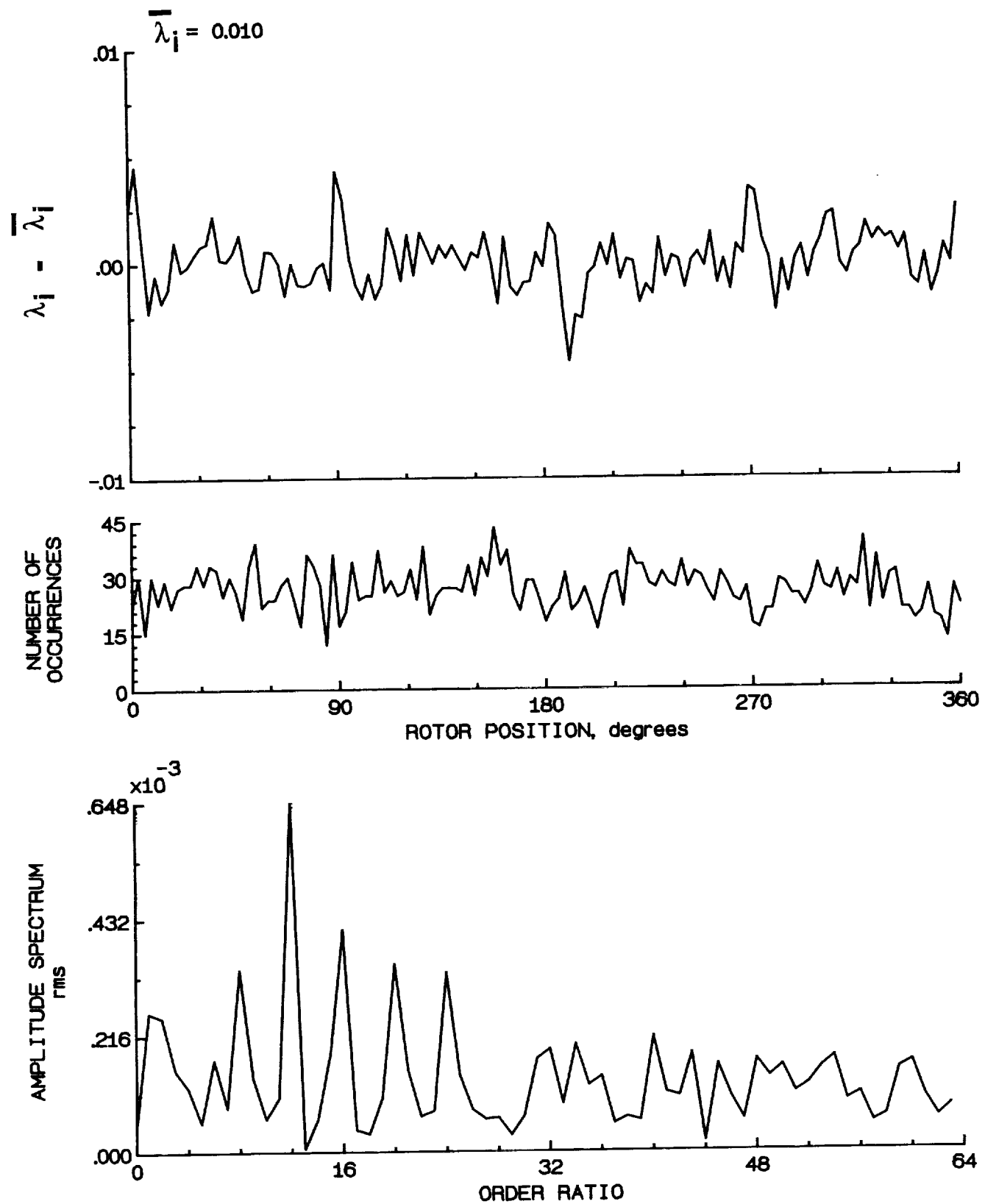


Figure 67.- Concluded.

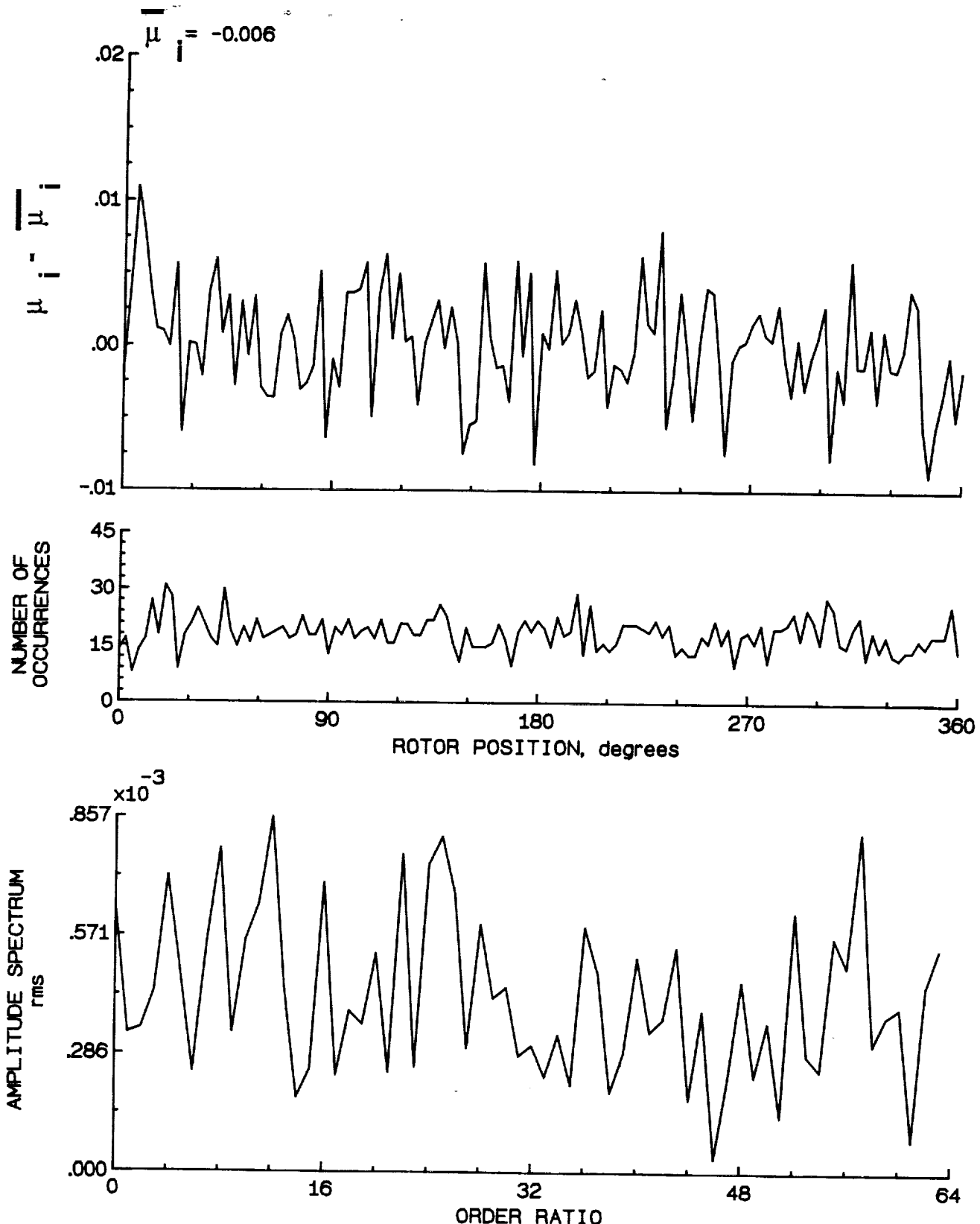


Figure 68.- Induced inflow velocity measured at 90 degrees and r/R of 0.98.

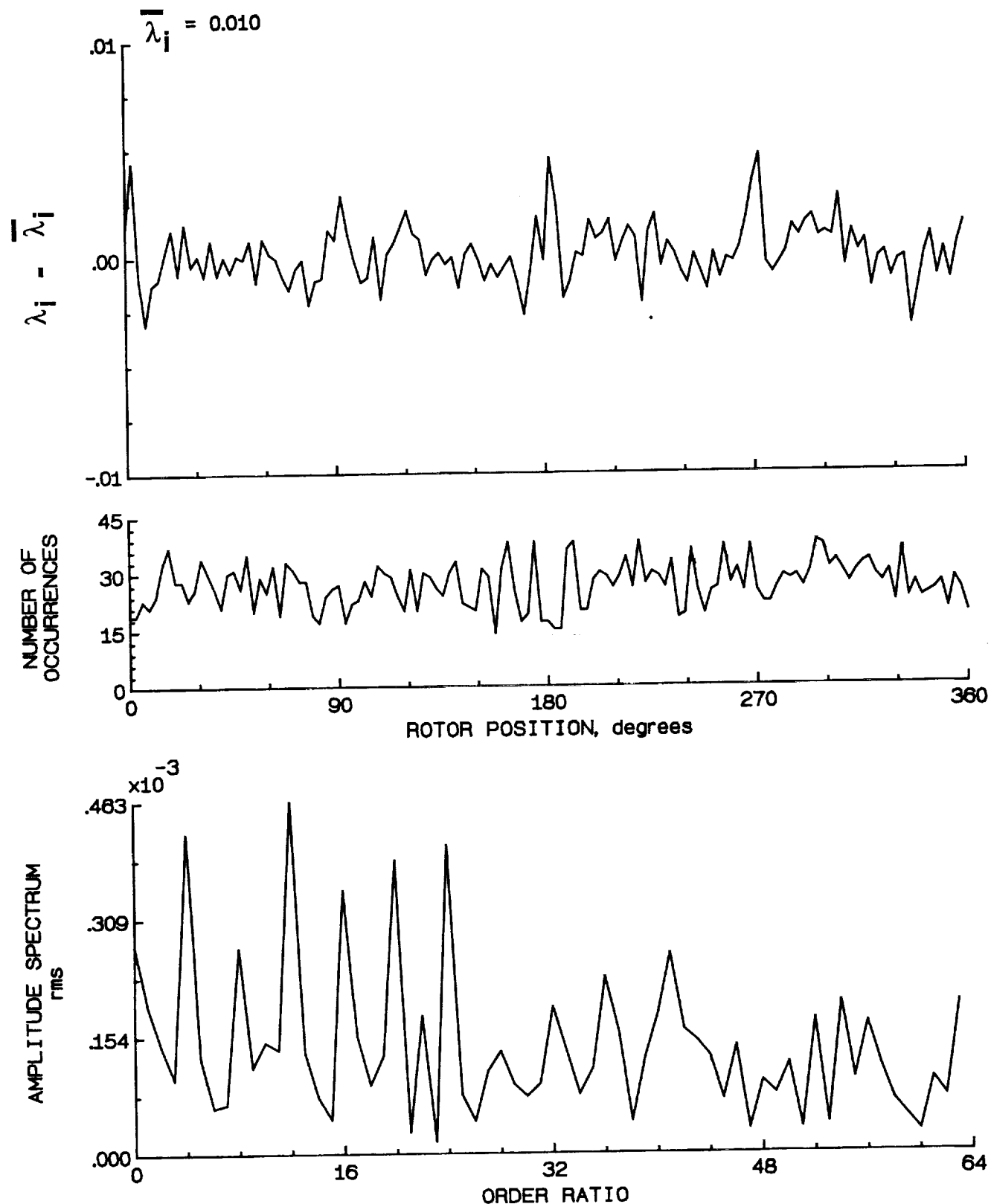


Figure 68.- Concluded.

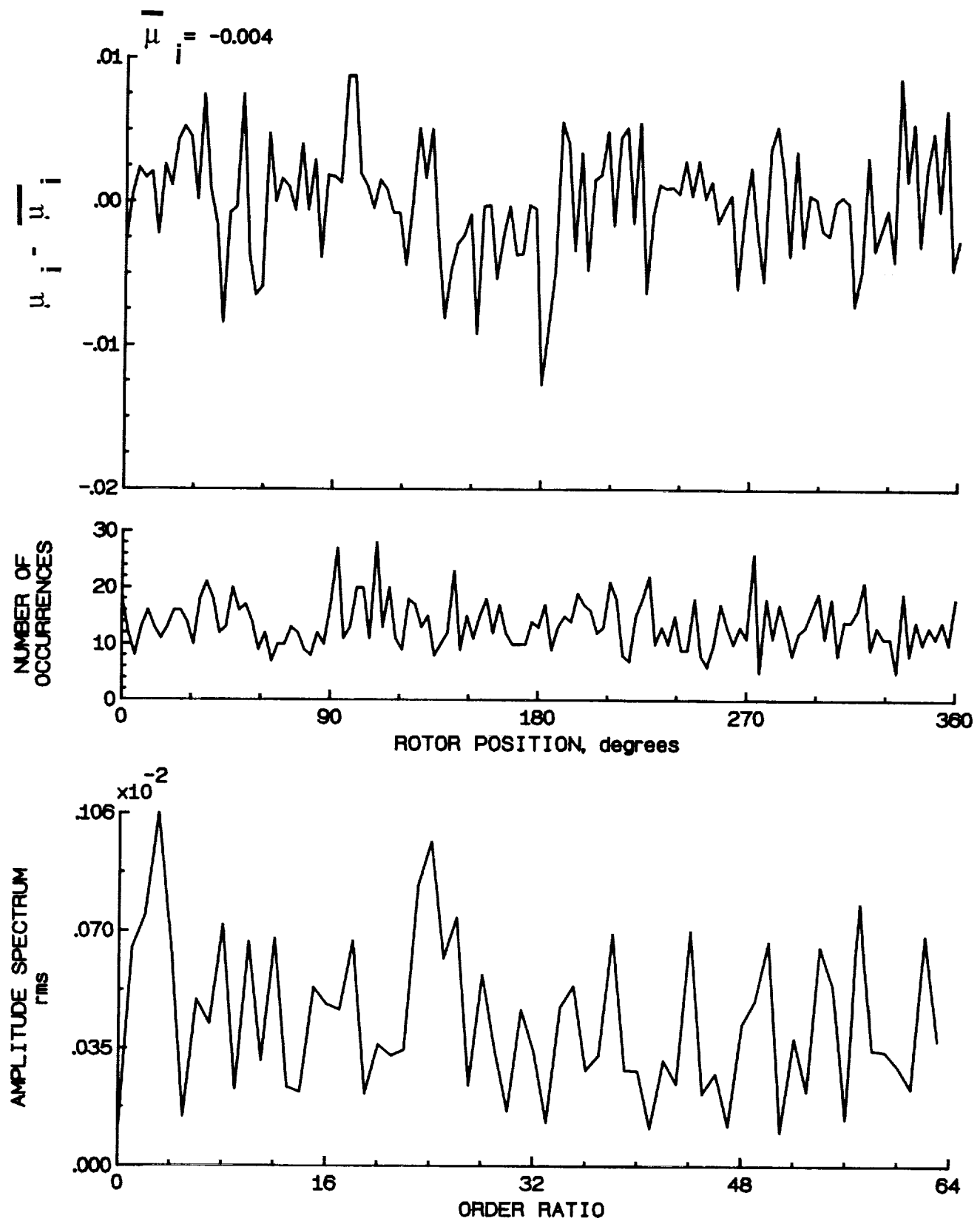


Figure 69.- Induced inflow velocity measured at 90 degrees and r/R of 1.02.

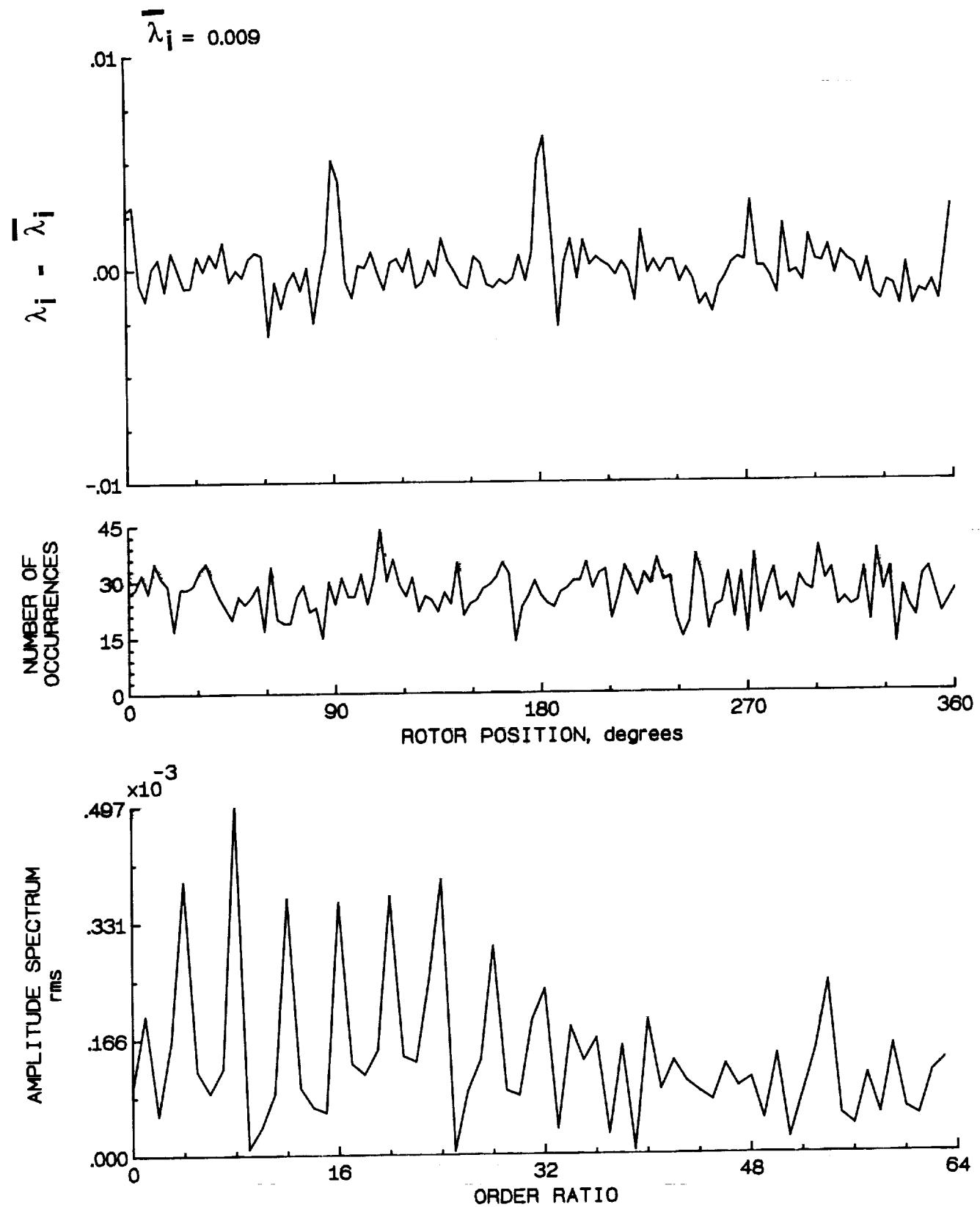


Figure 69.- Concluded.

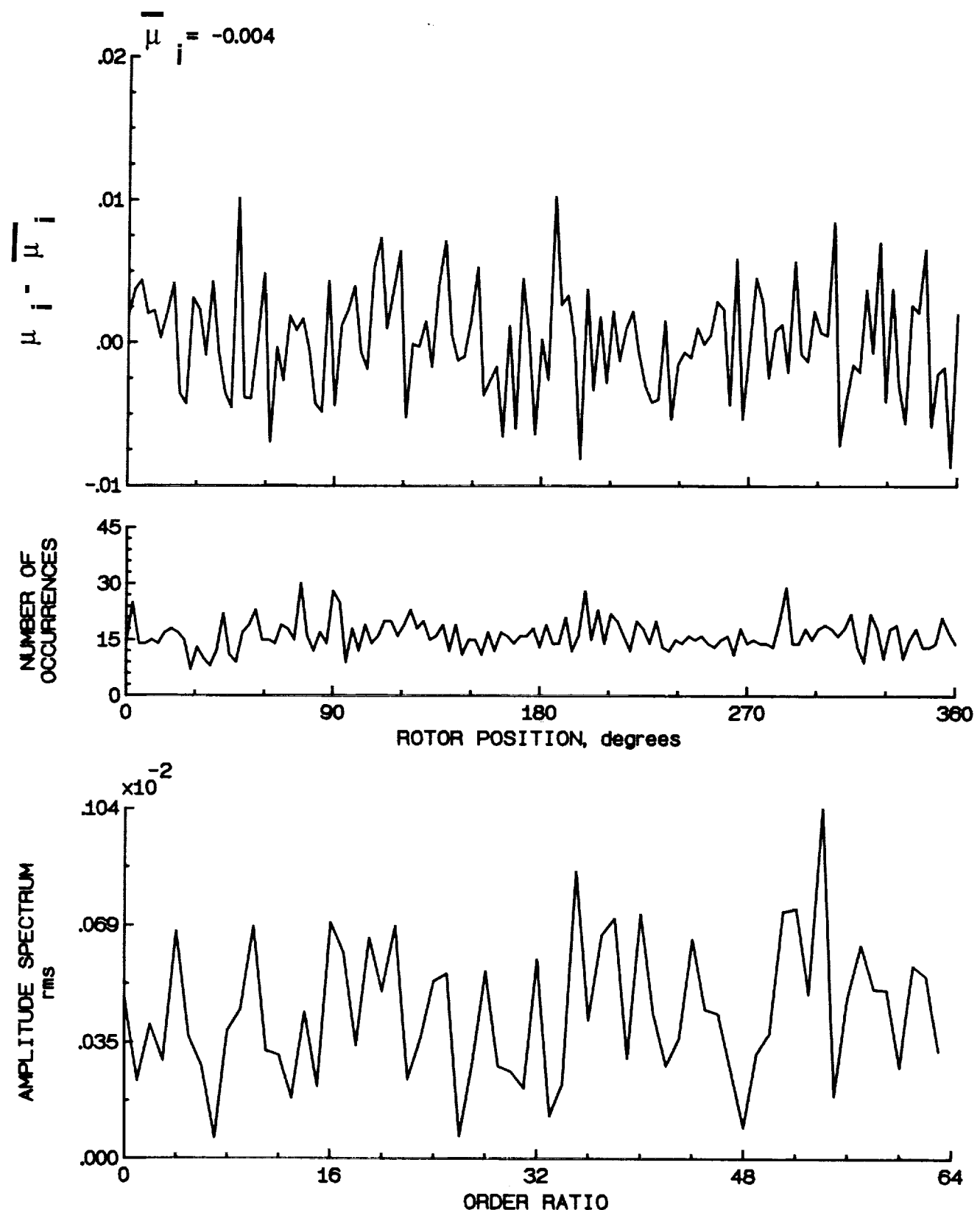


Figure 70.- Induced inflow velocity measured at 90 degrees and r/R of 1.04.

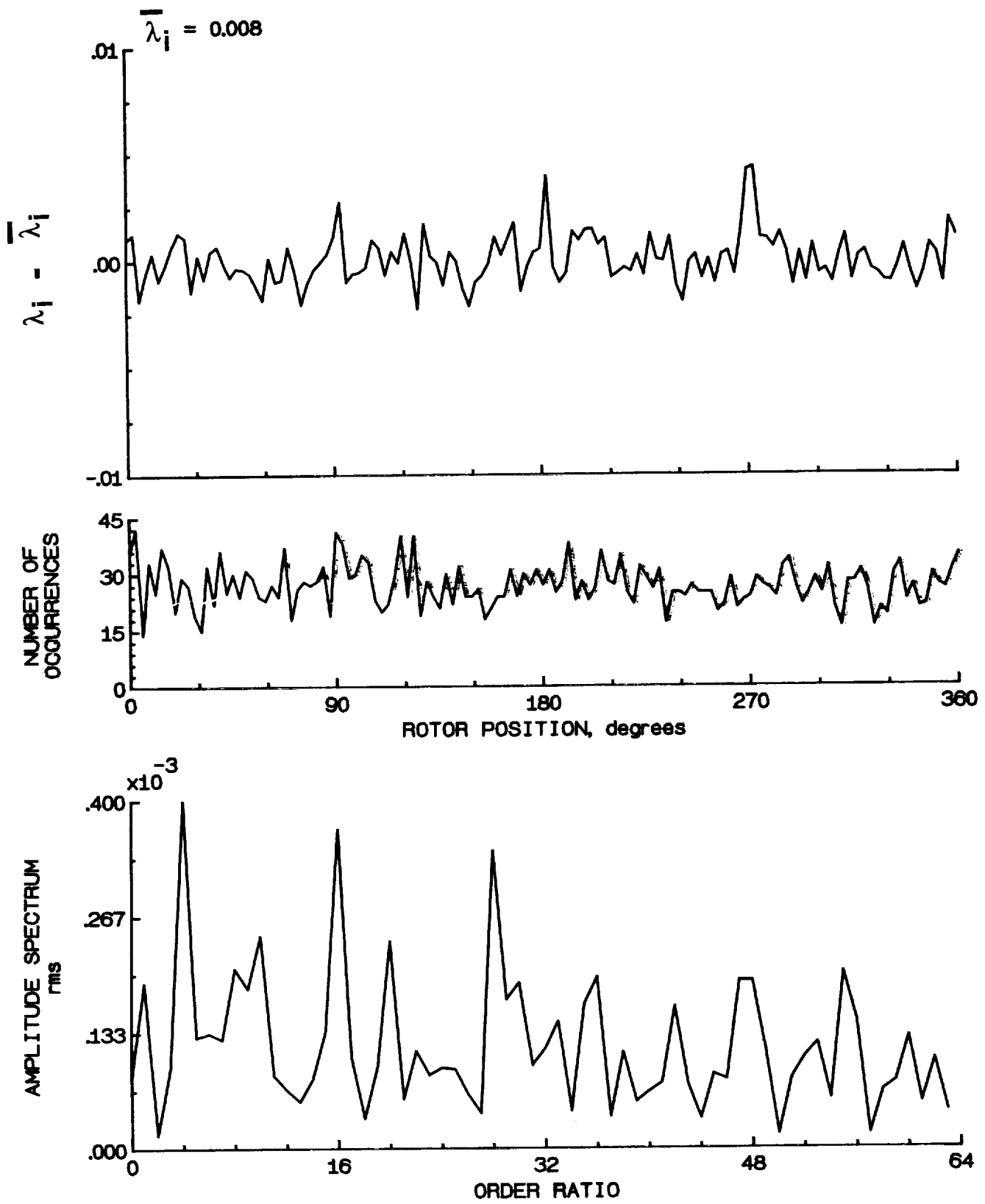


Figure 70.- Concluded.

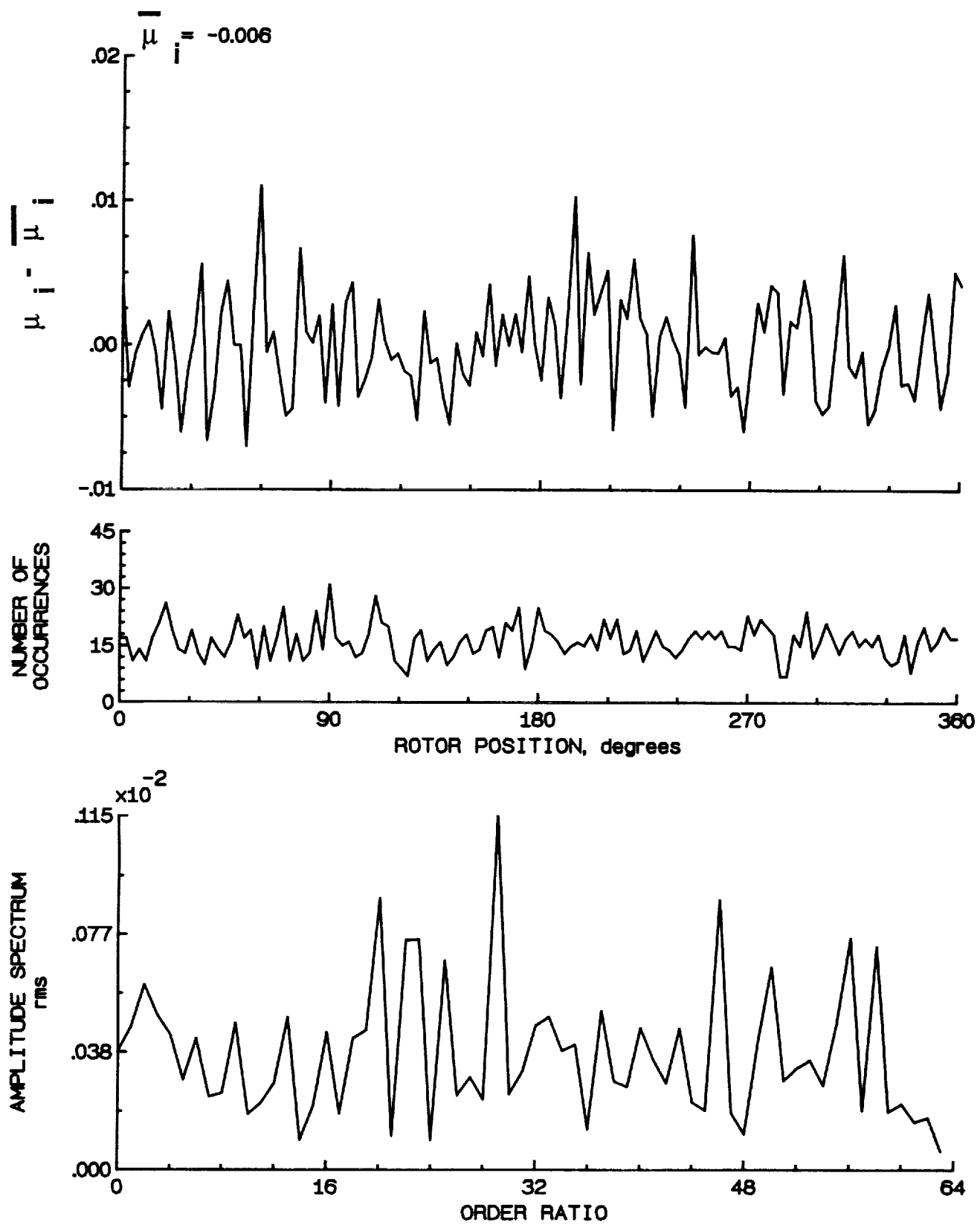


Figure 71.- Induced inflow velocity measured at 90 degrees and r/R of 1.10.

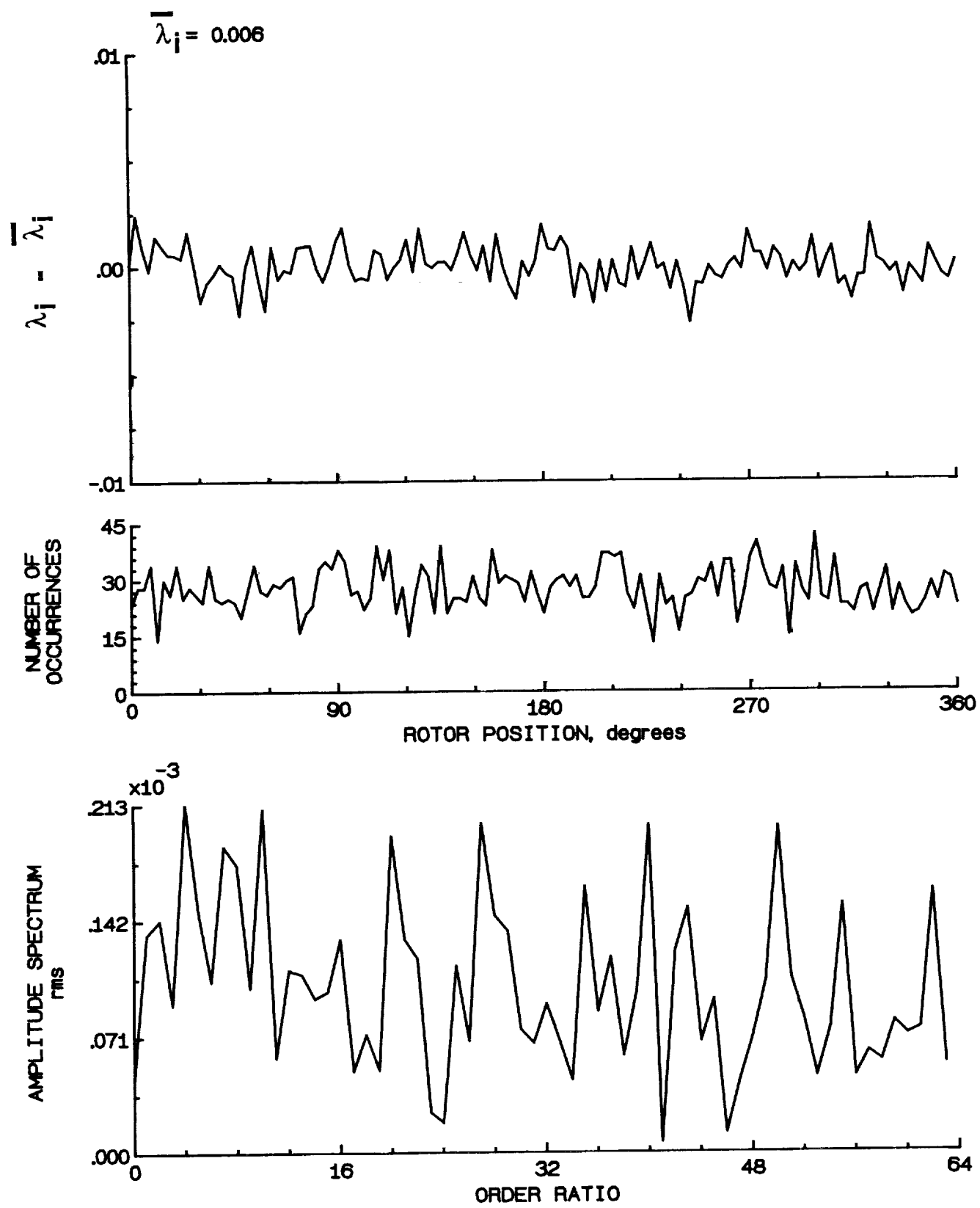


Figure 71.- Concluded.

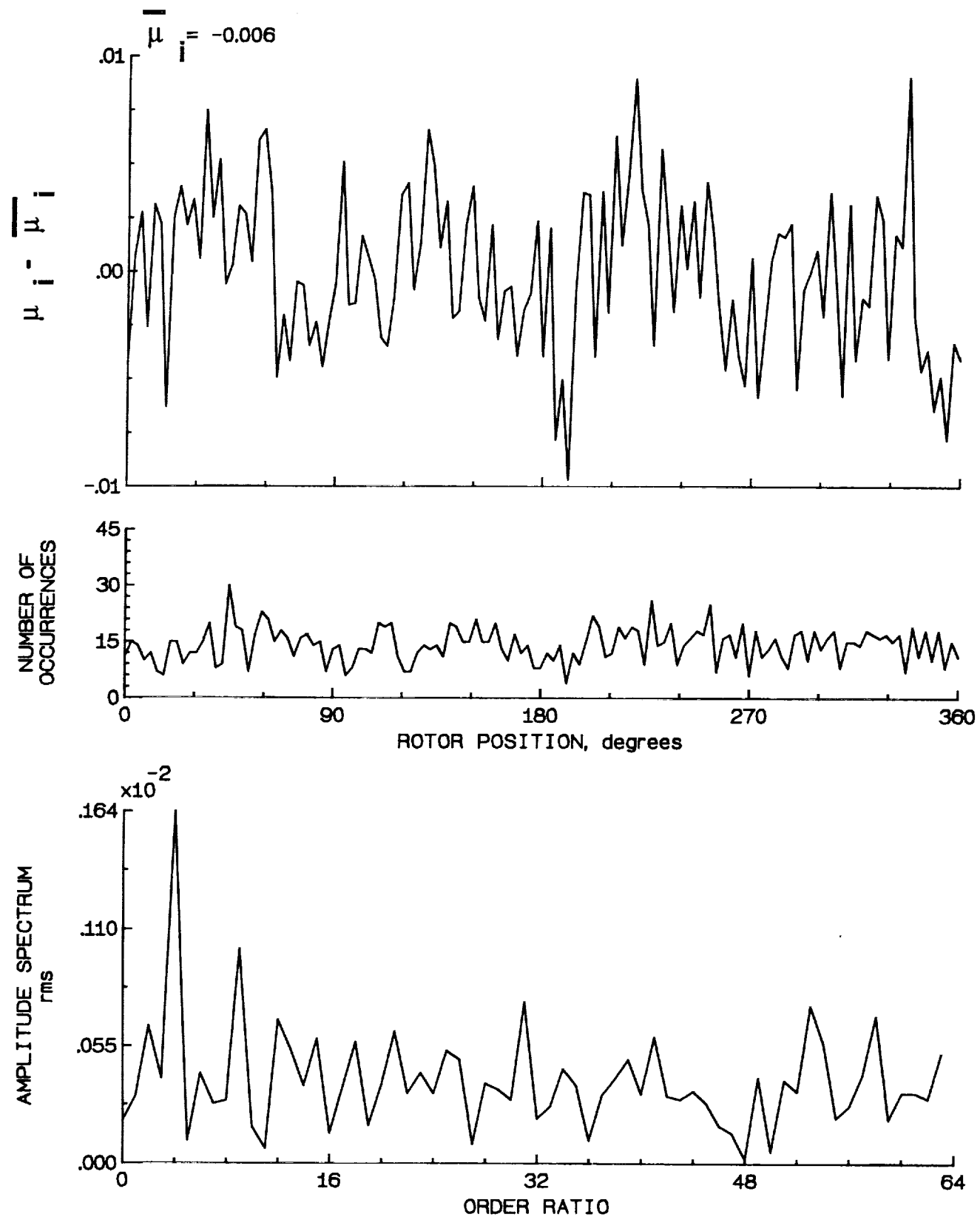


Figure 72.- Induced inflow velocity measured at 120 degrees and r/R of 0.20.

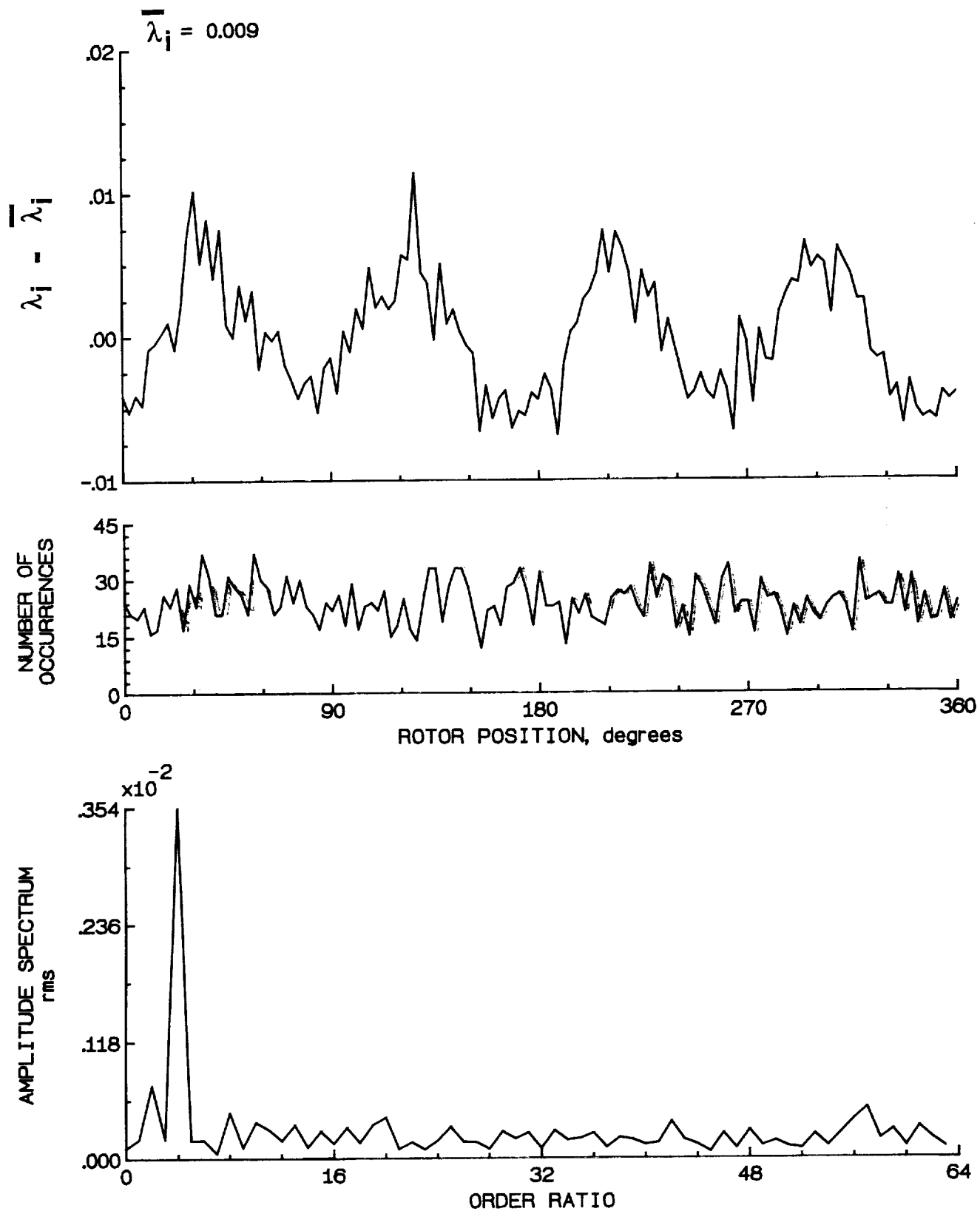


Figure 72.- Concluded.

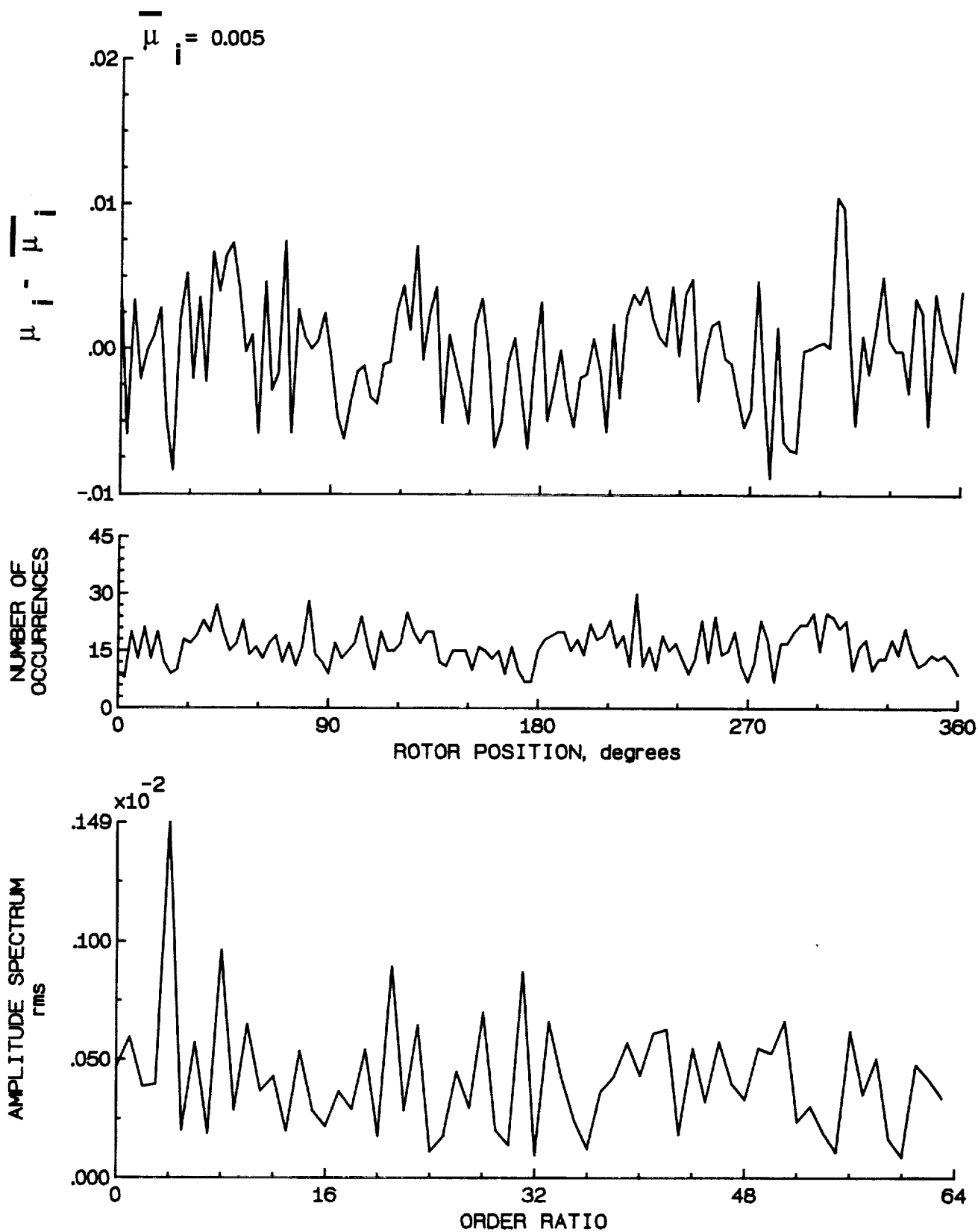


Figure 73.- Induced inflow velocity measured at 120 degrees and r/R of 0.40.

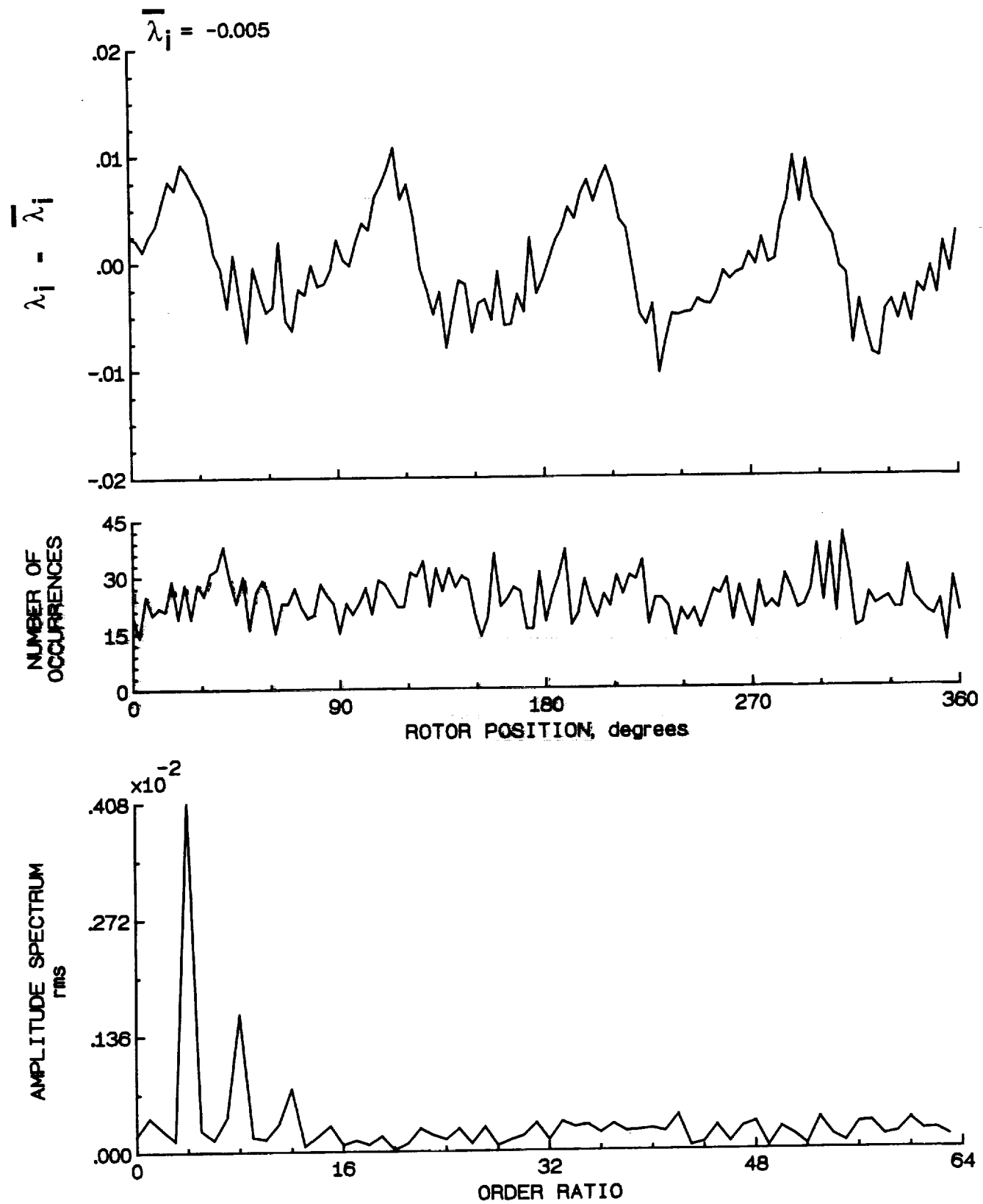


Figure 73.- Concluded.

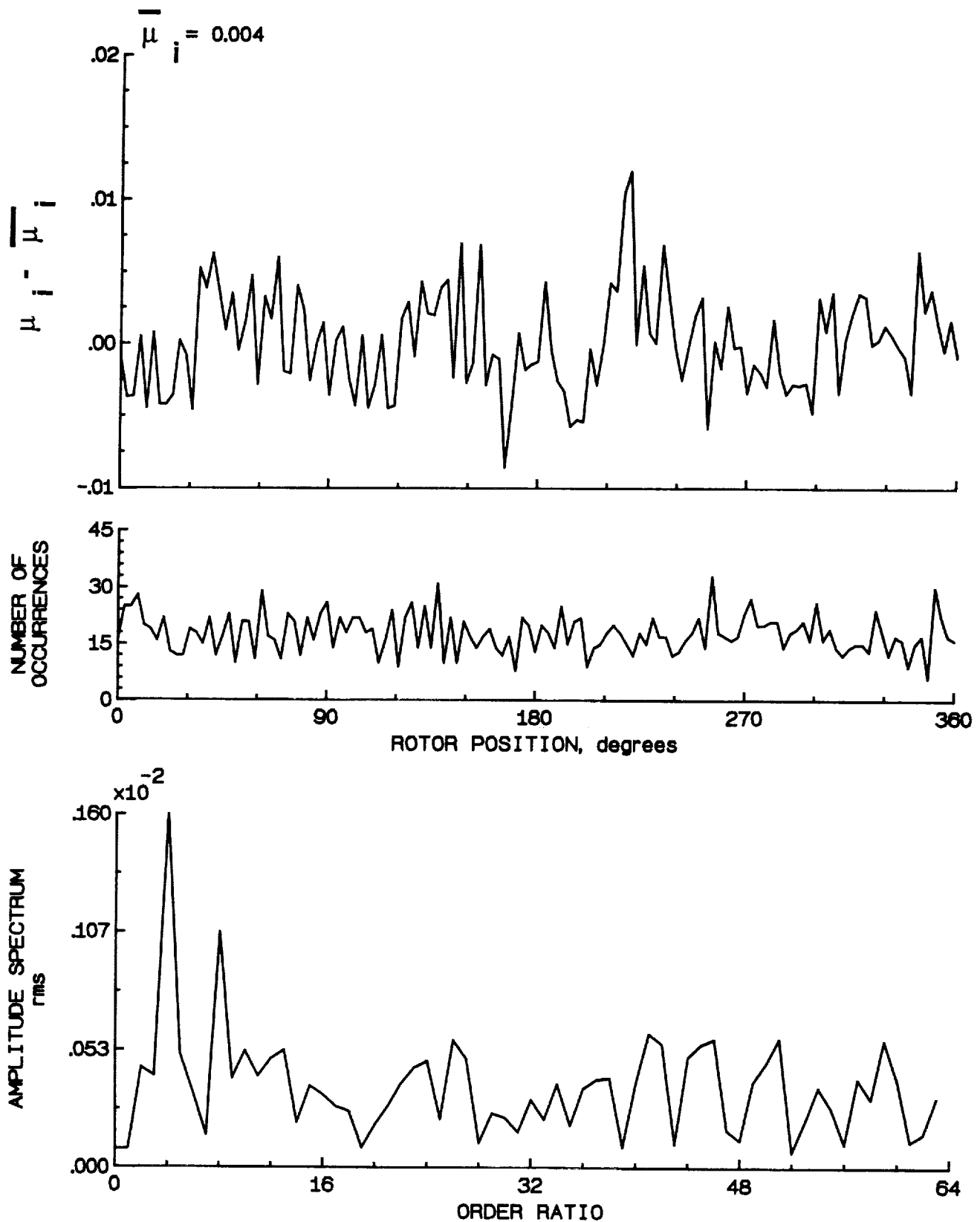


Figure 74.- Induced inflow velocity measured at 120 degrees and r/R of 0.50.

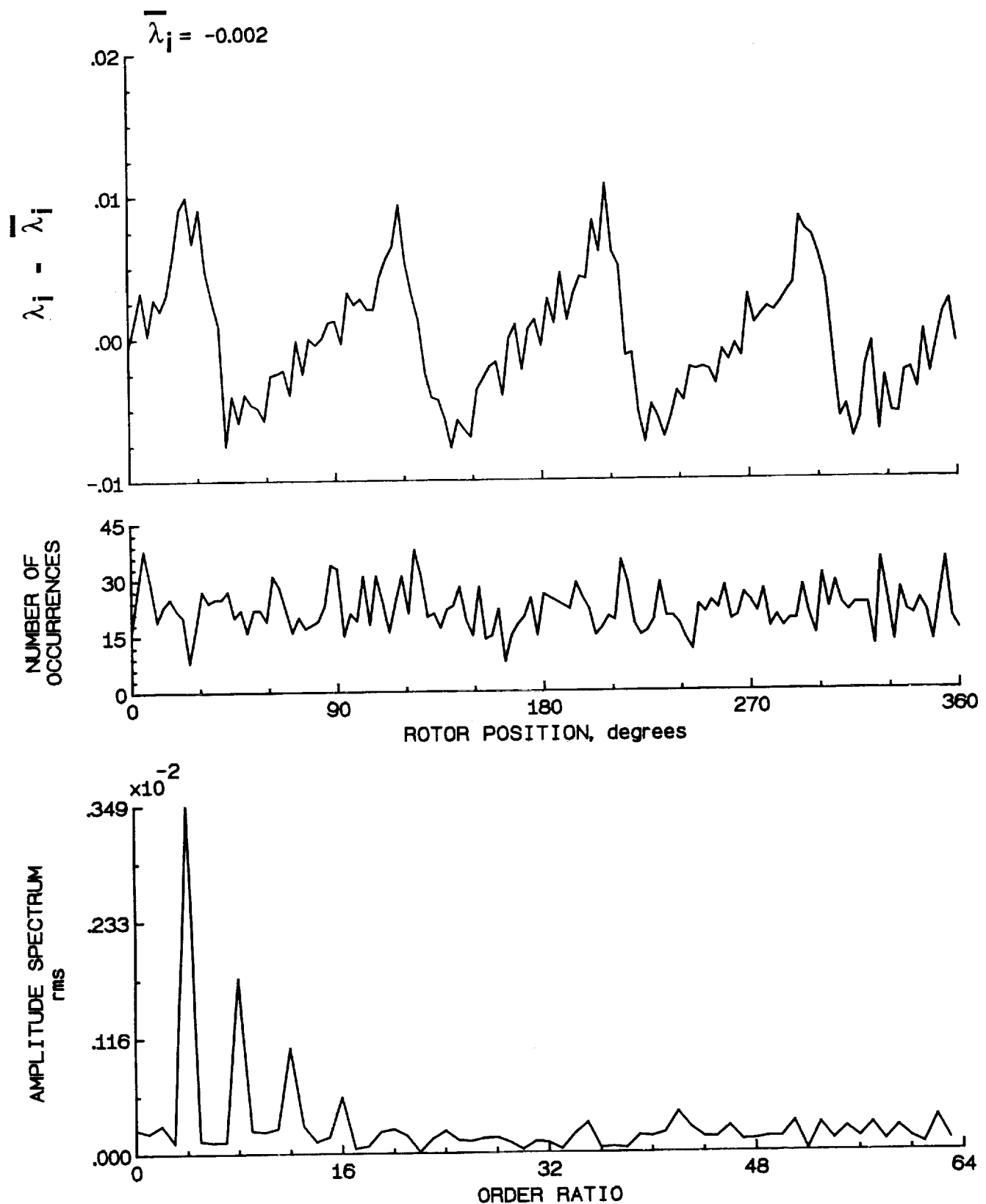


Figure 74.- Concluded.

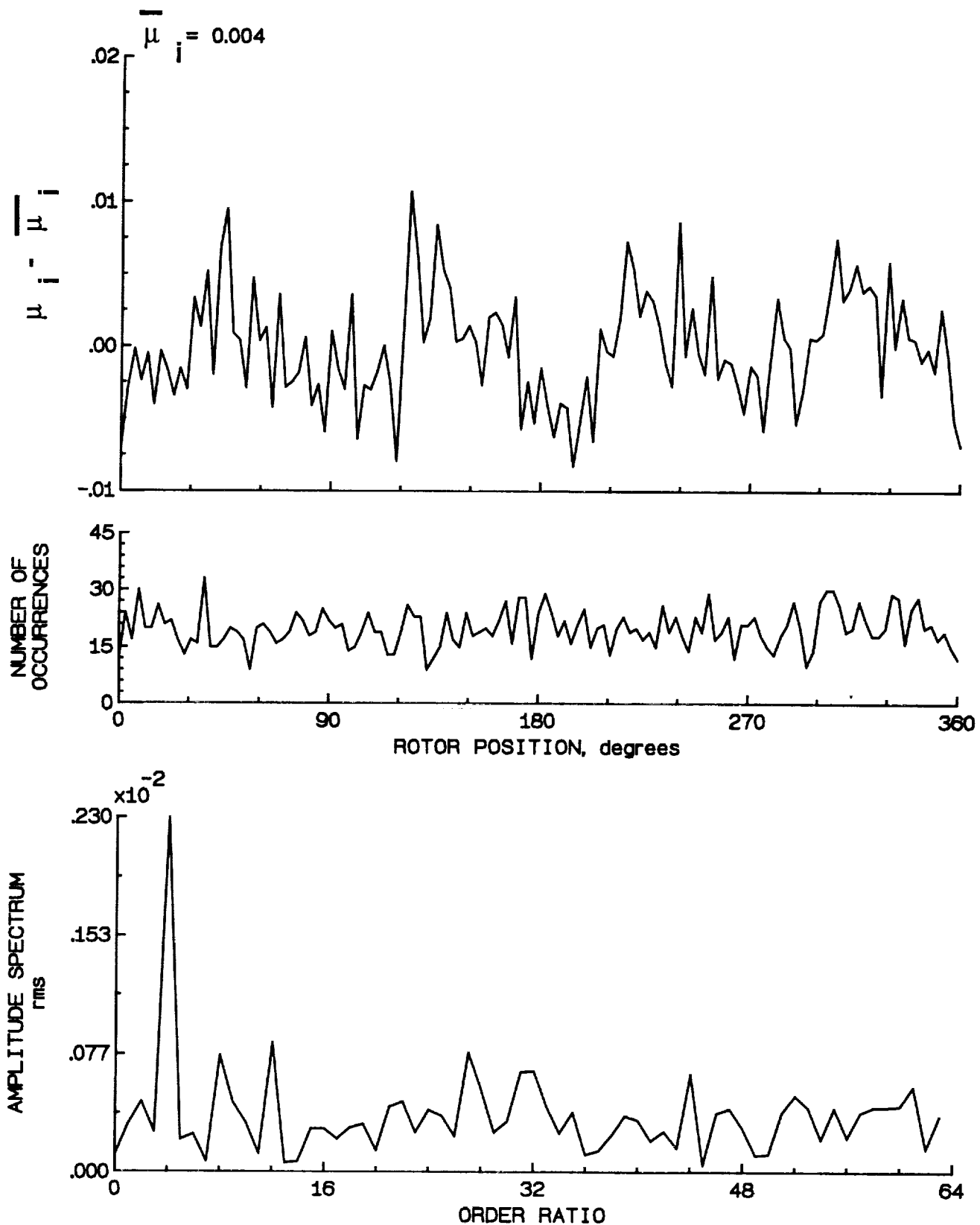


Figure 75.- Induced inflow velocity measured at 120 degrees and r/R of 0.60.

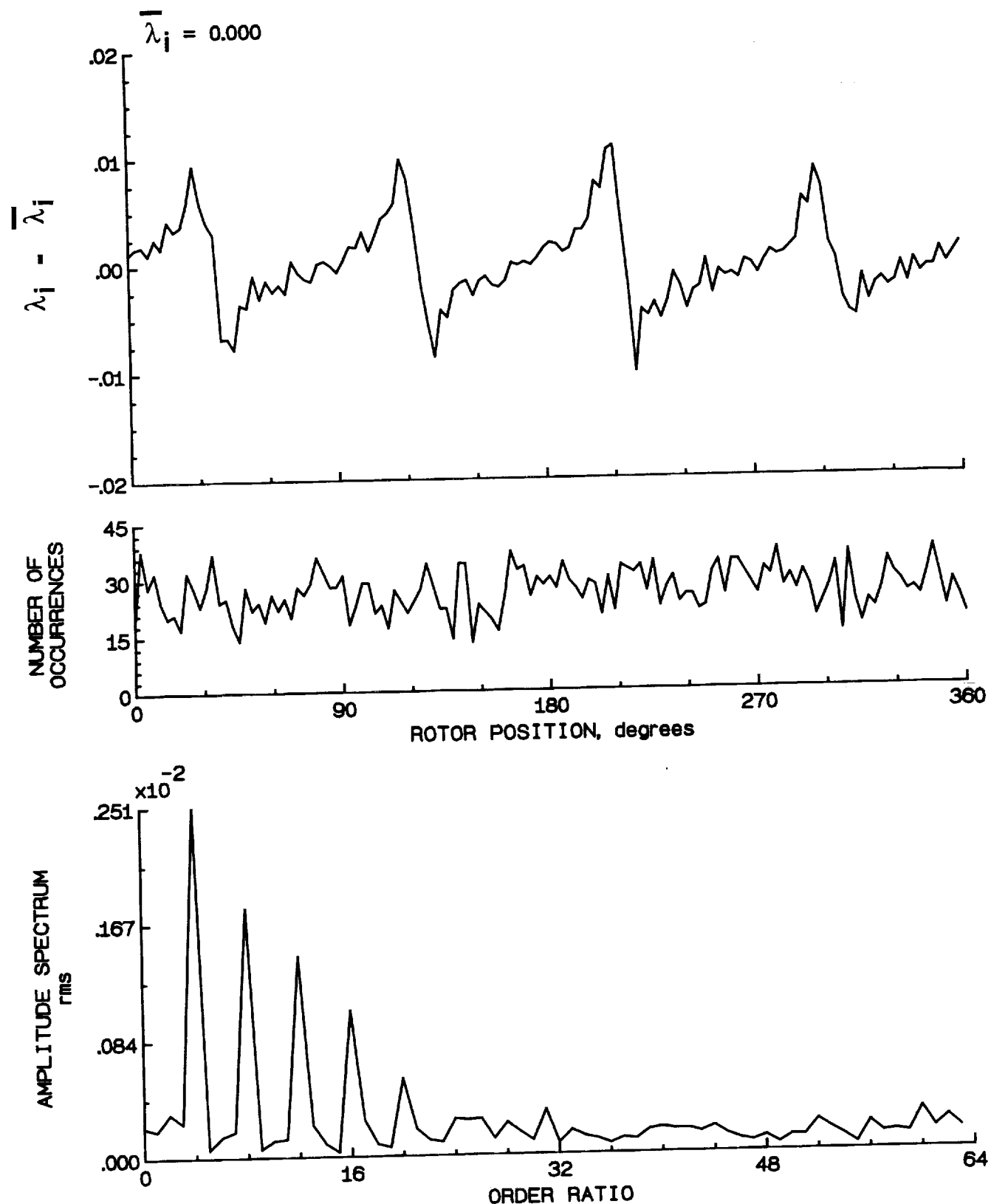


Figure 75.- Concluded.

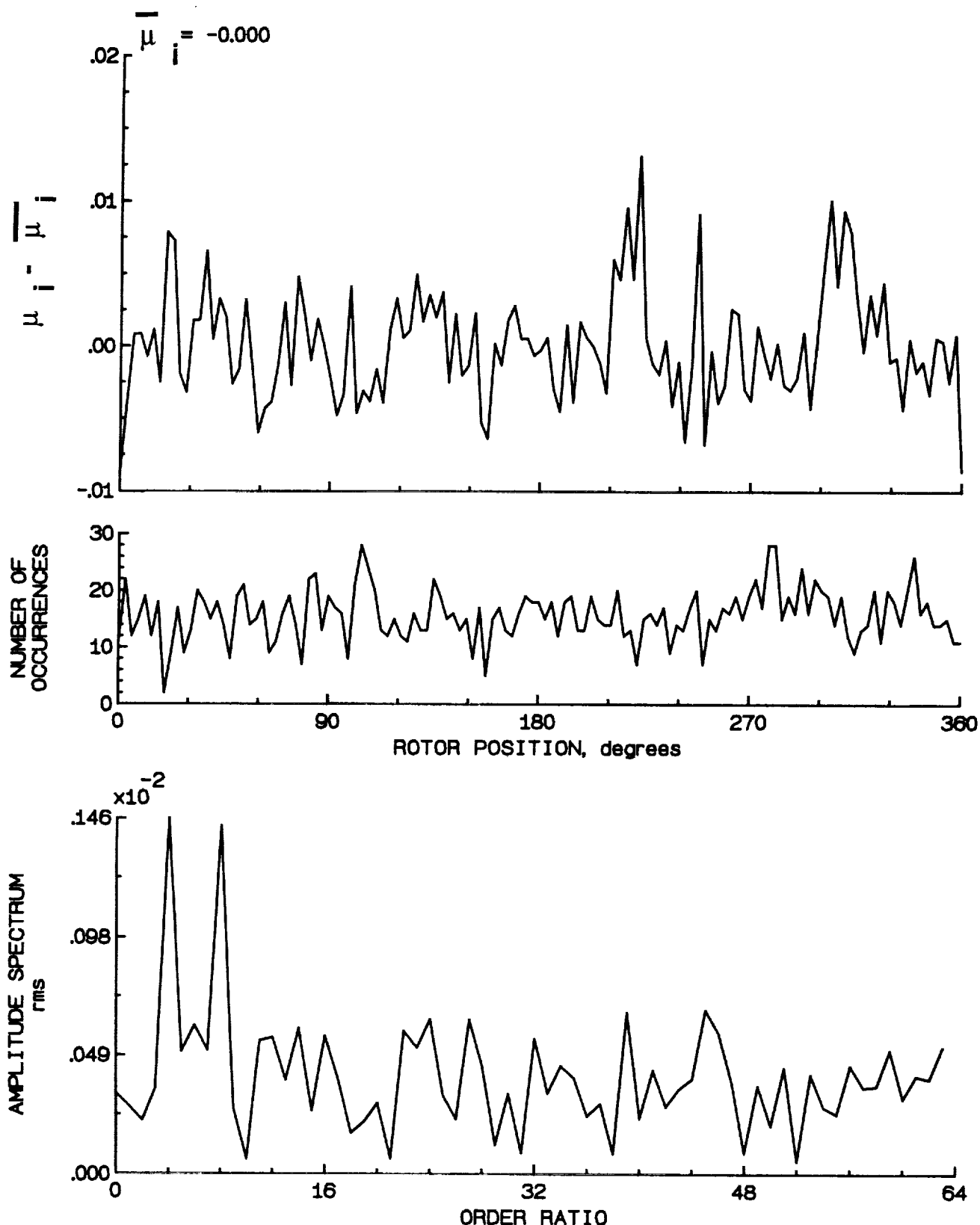


Figure 76.- Induced inflow velocity measured at 120 degrees and r/R of 0.70.

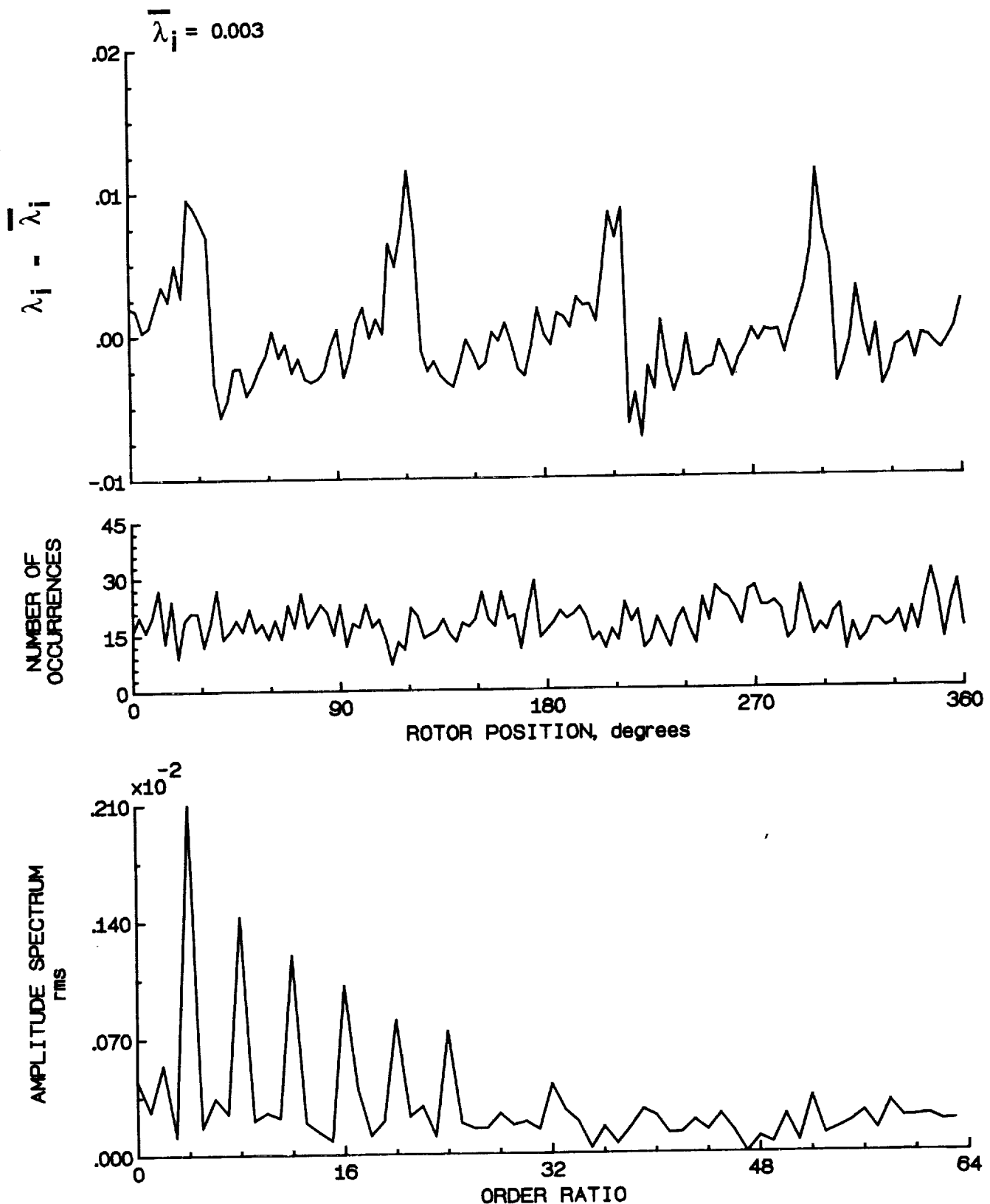


Figure 76.- Concluded.

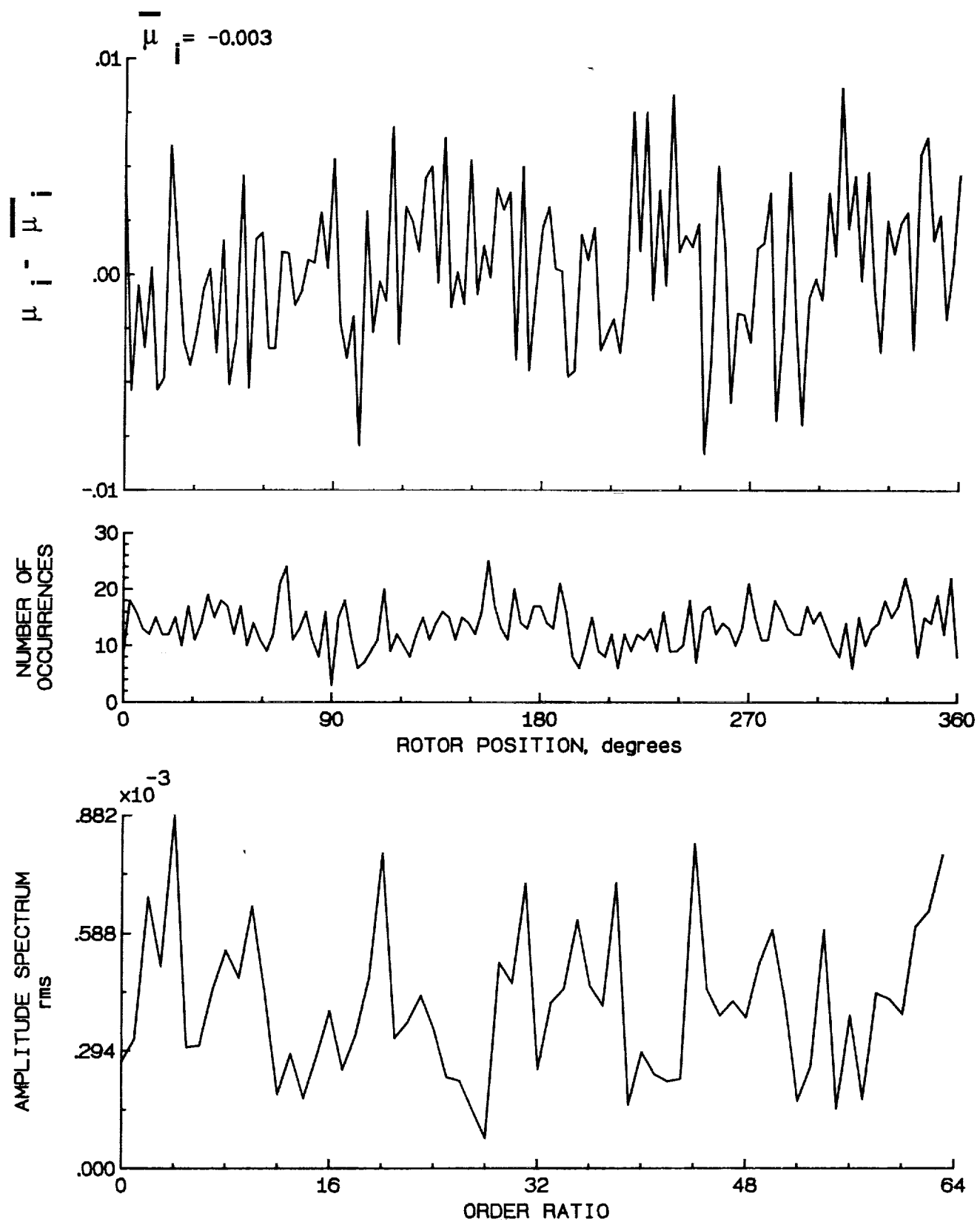


Figure 77.- Induced inflow velocity measured at 120 degrees and r/R of 0.74.

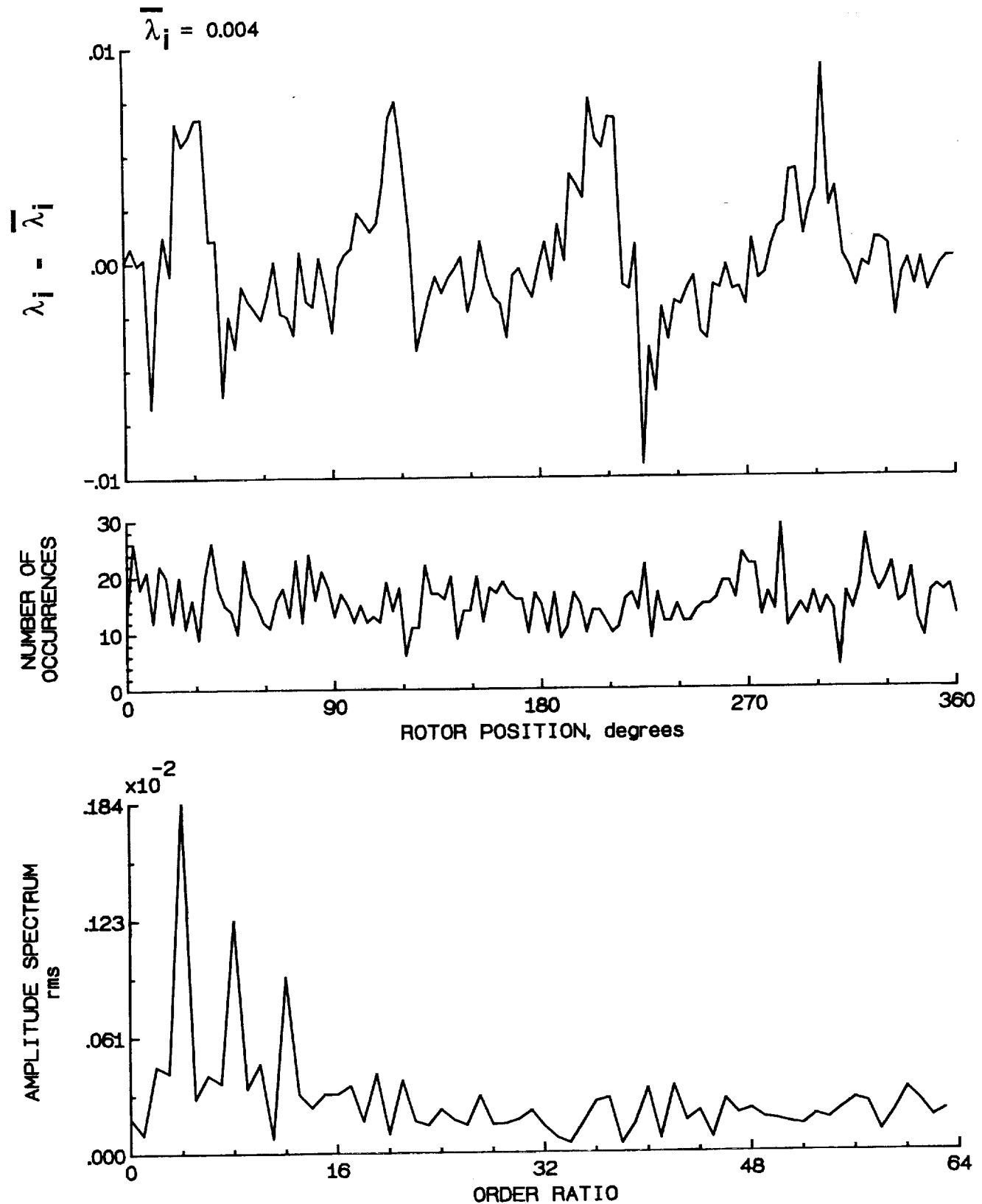


Figure 77.- Concluded.

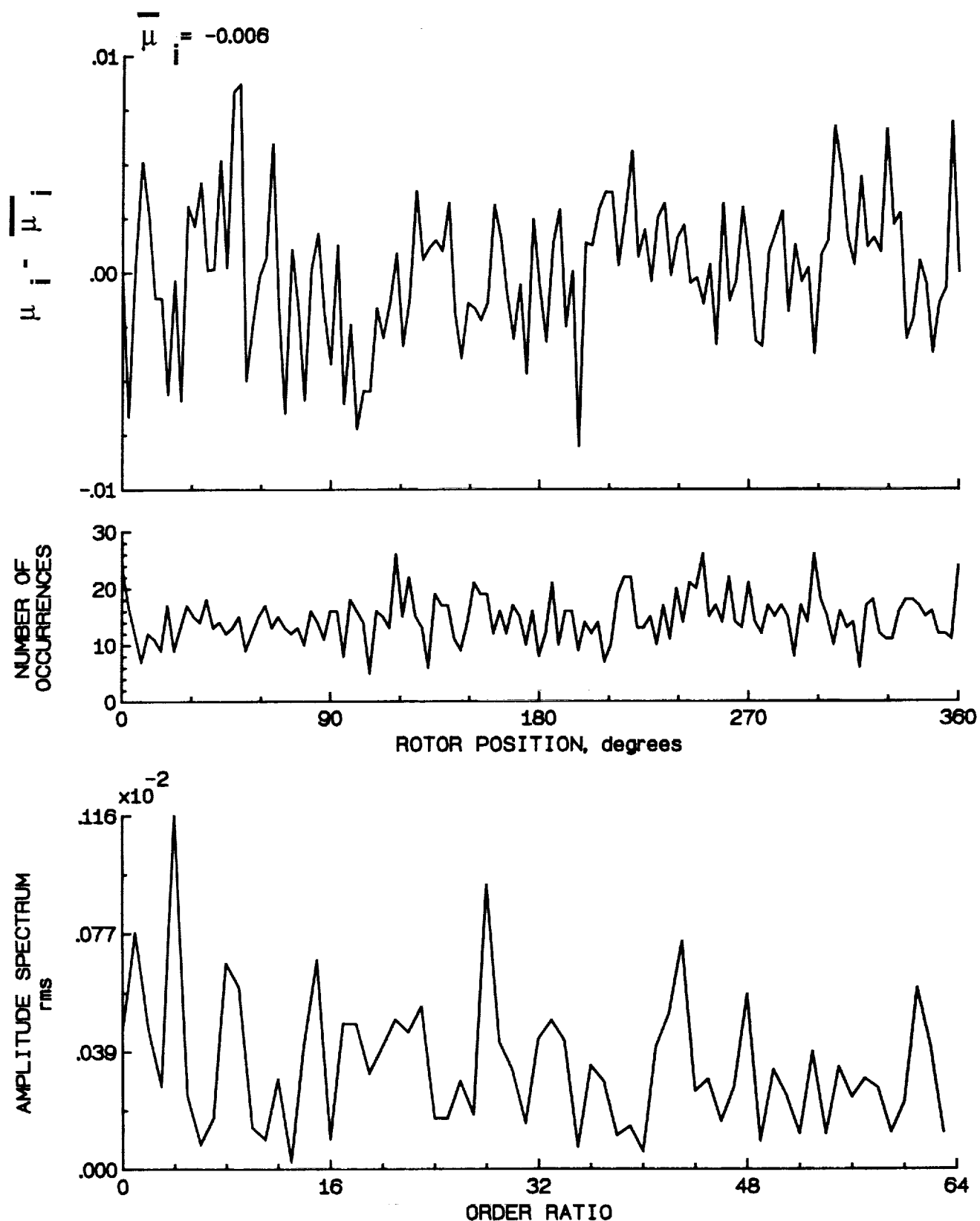


Figure 78.- Induced inflow velocity measured at 120 degrees and r/R of 0.78.

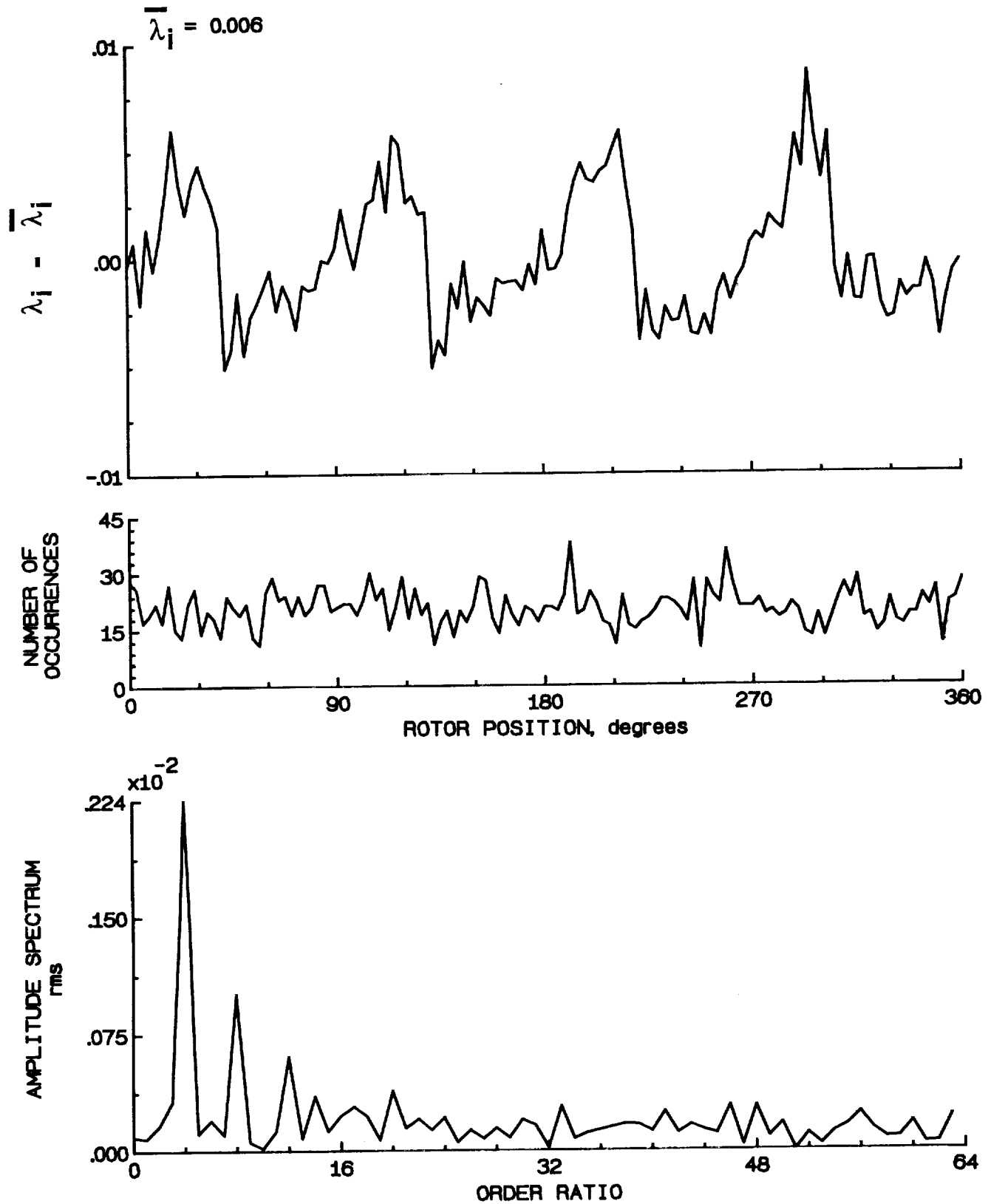


Figure 78.- Concluded.

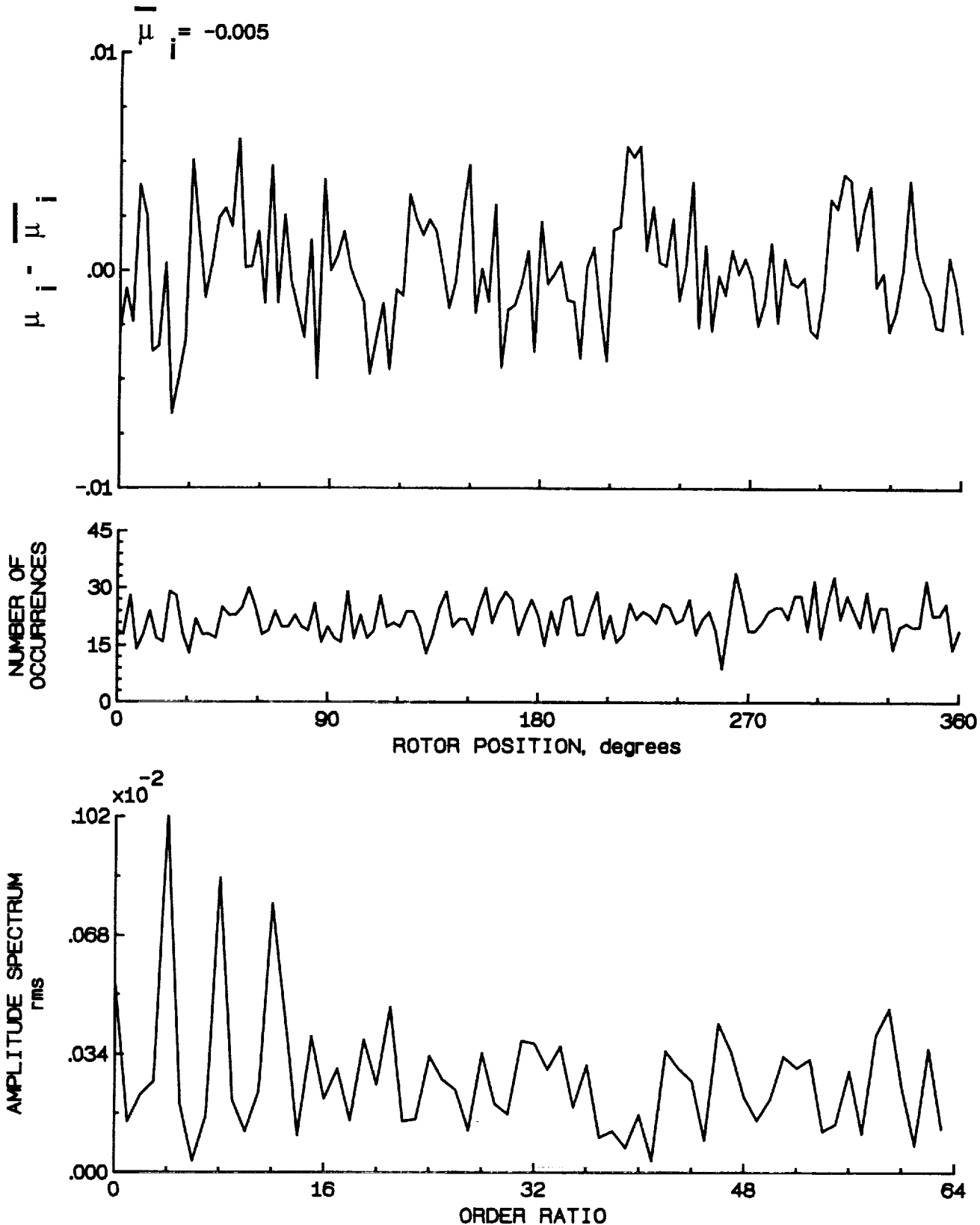


Figure 79.- Induced inflow velocity measured at 120 degrees and r/R of 0.82.

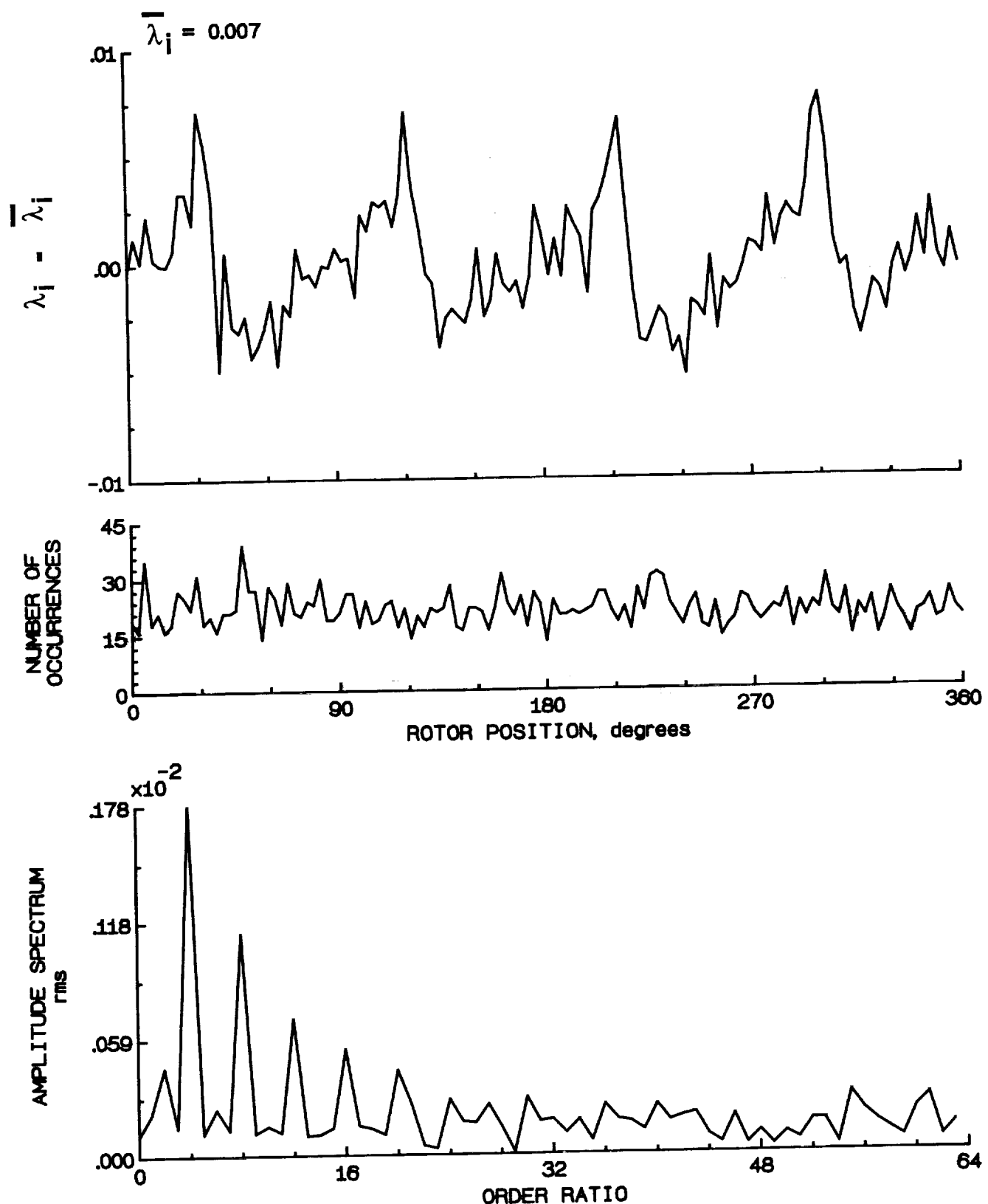


Figure 79.- Concluded.

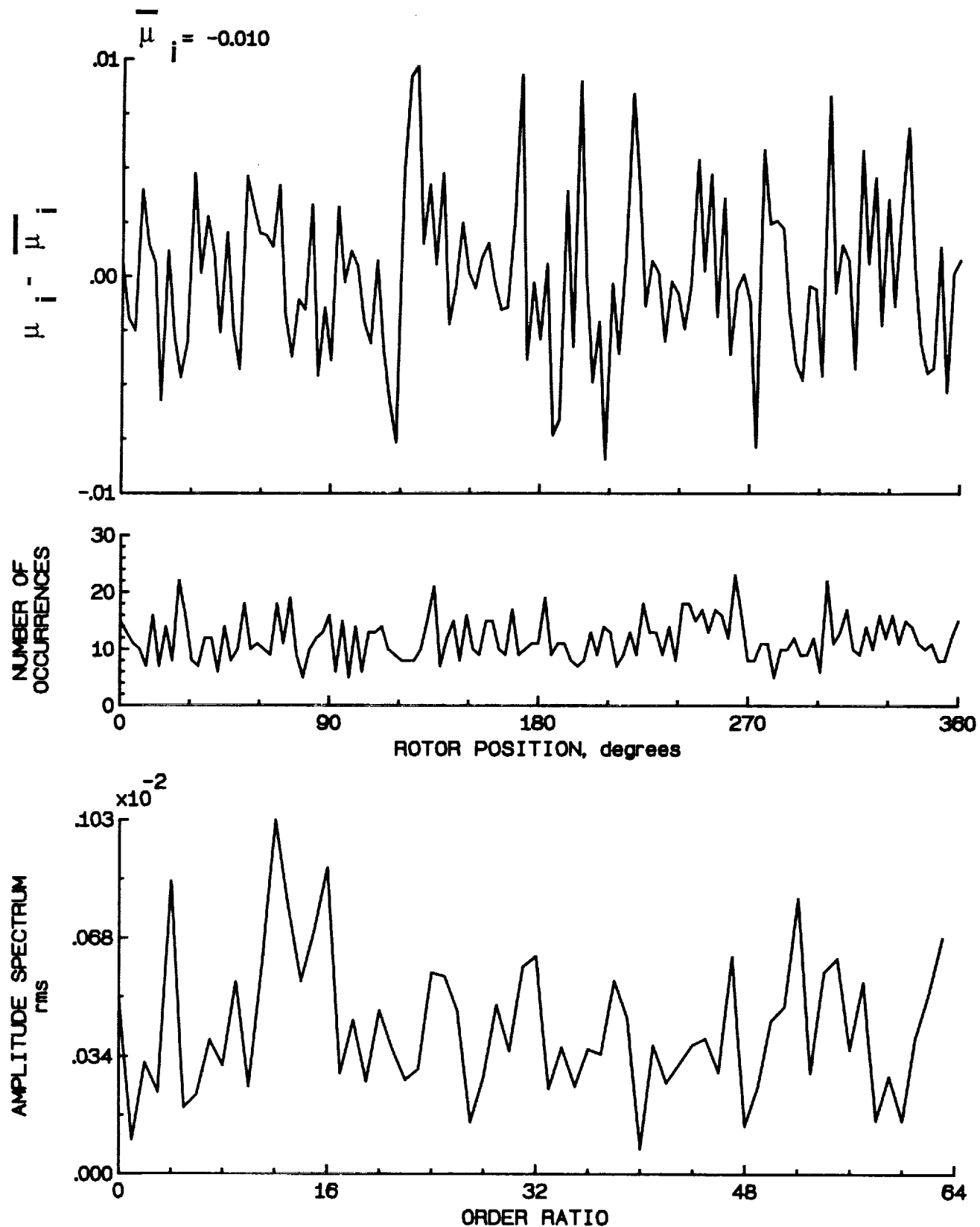


Figure 80.- Induced inflow velocity measured at 120 degrees and r/R of 0.86.

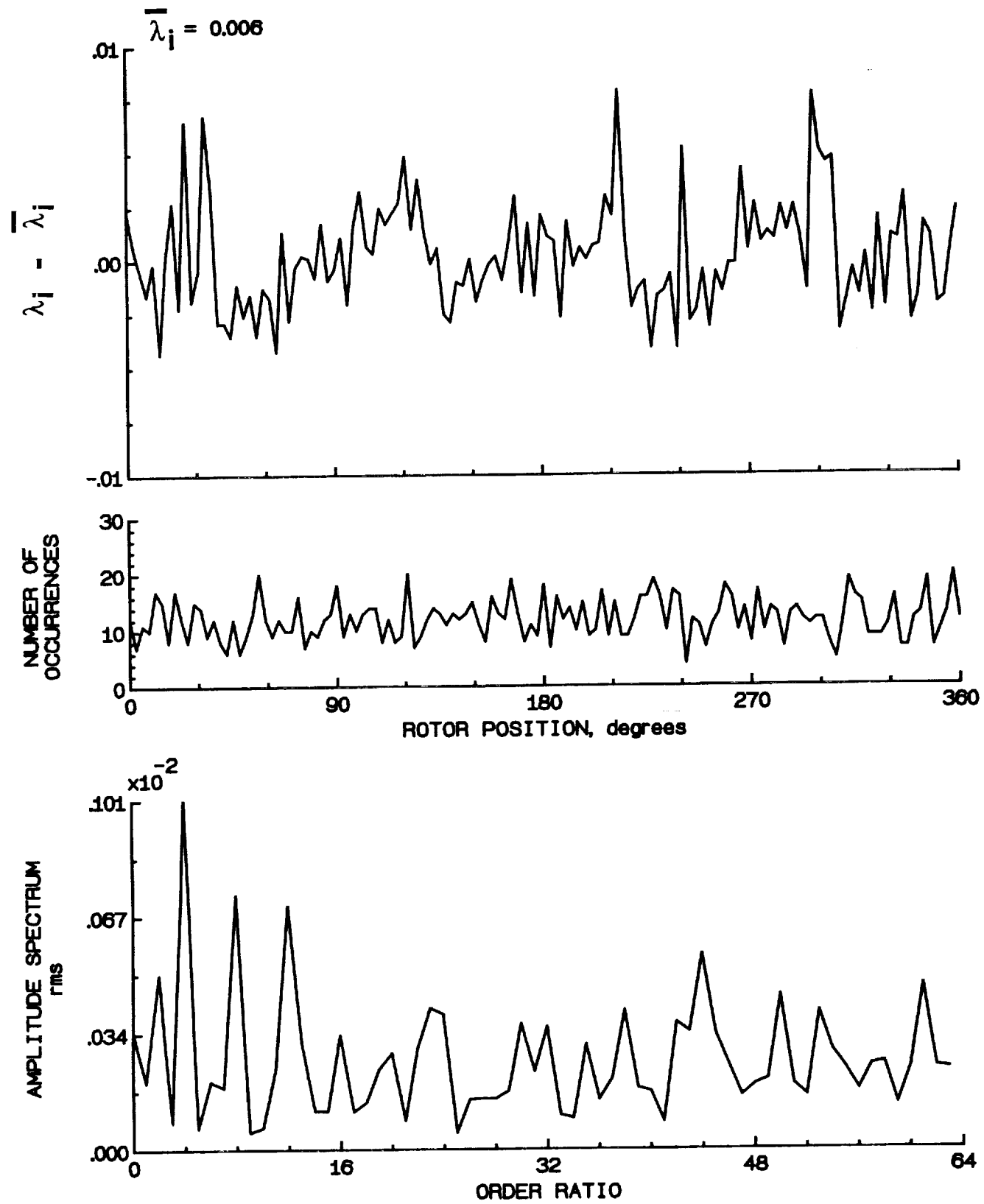


Figure 80.- Concluded.

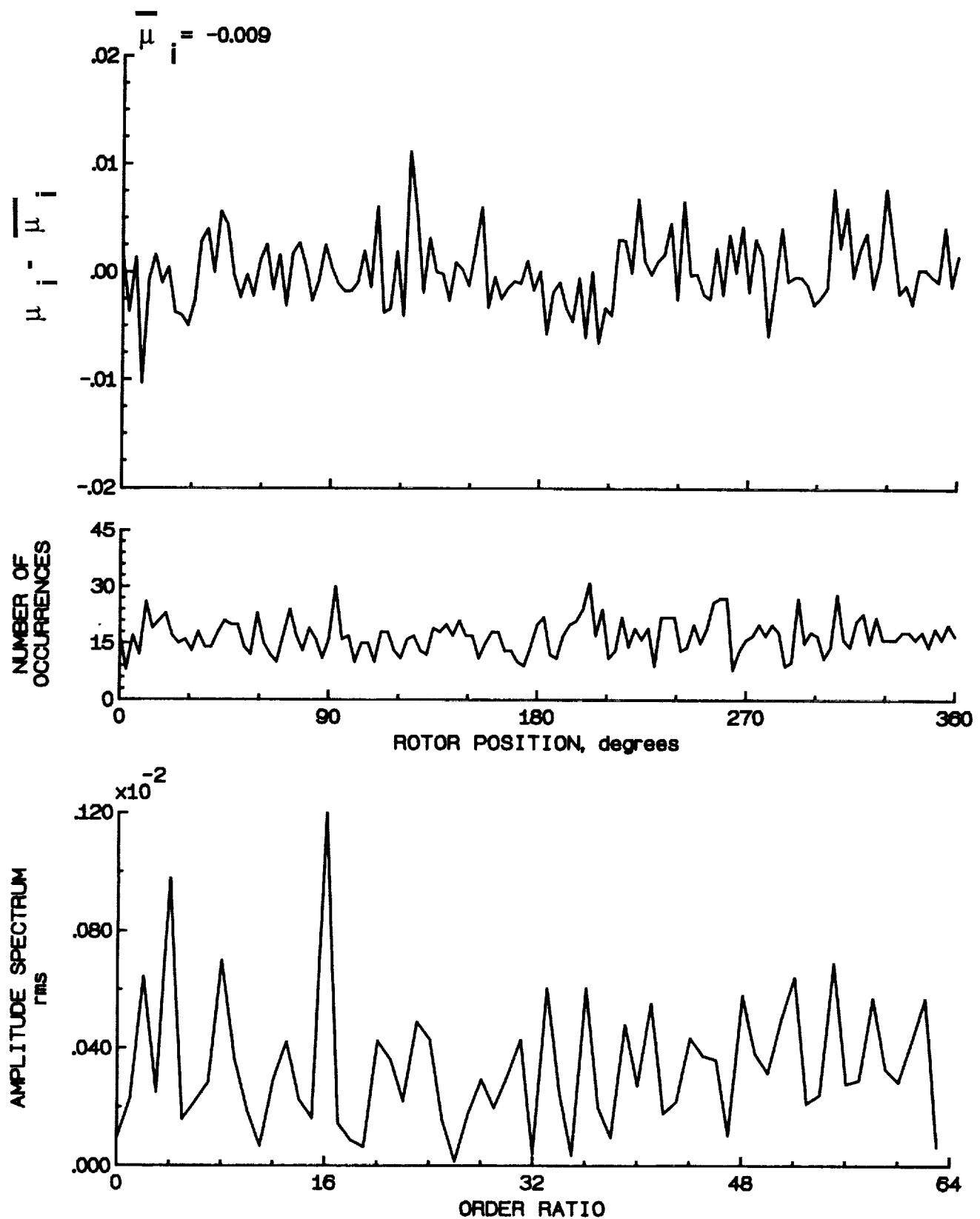


Figure 81.- Induced inflow velocity measured at 120 degrees and r/R of 0.90.

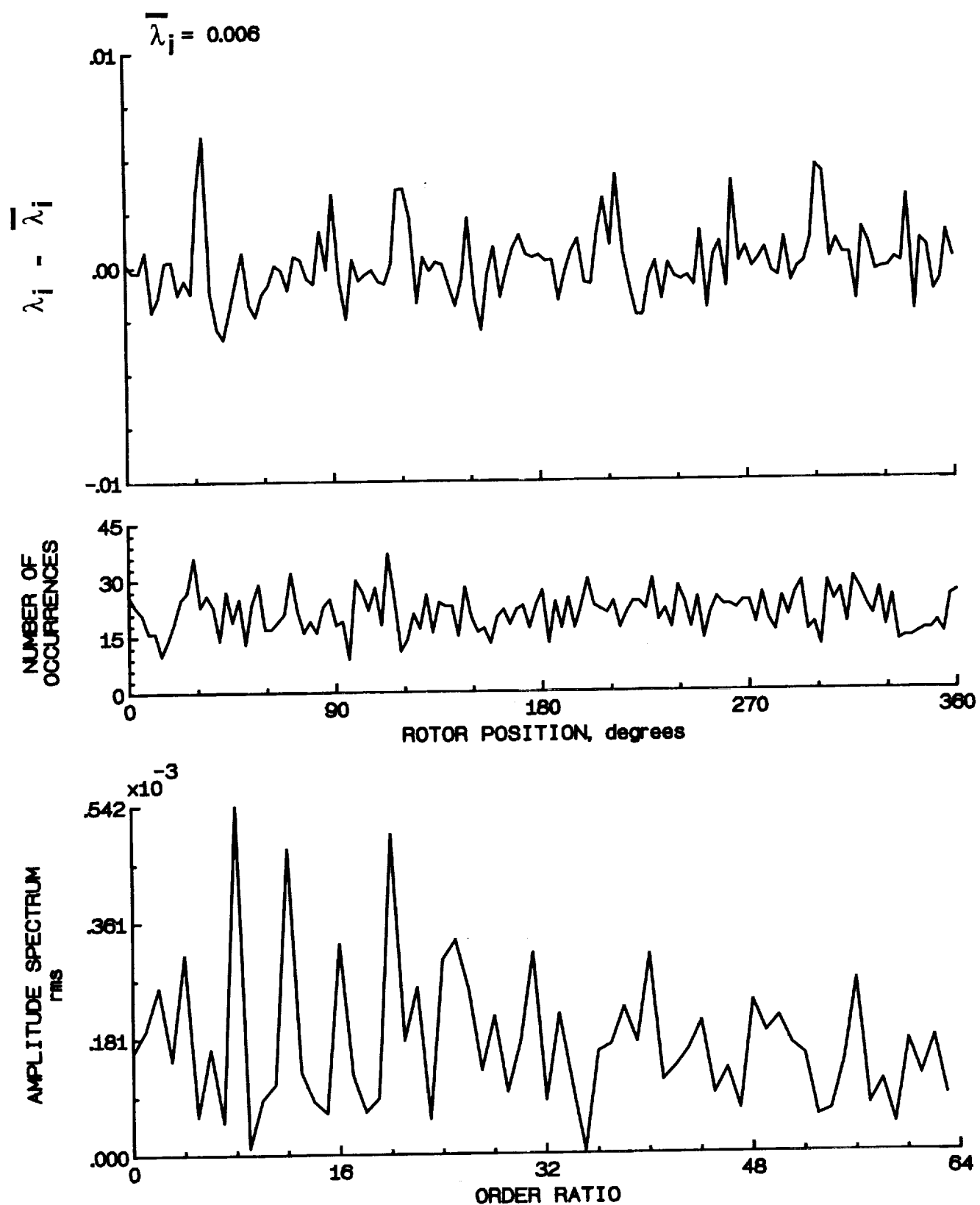


Figure 81.- Concluded.

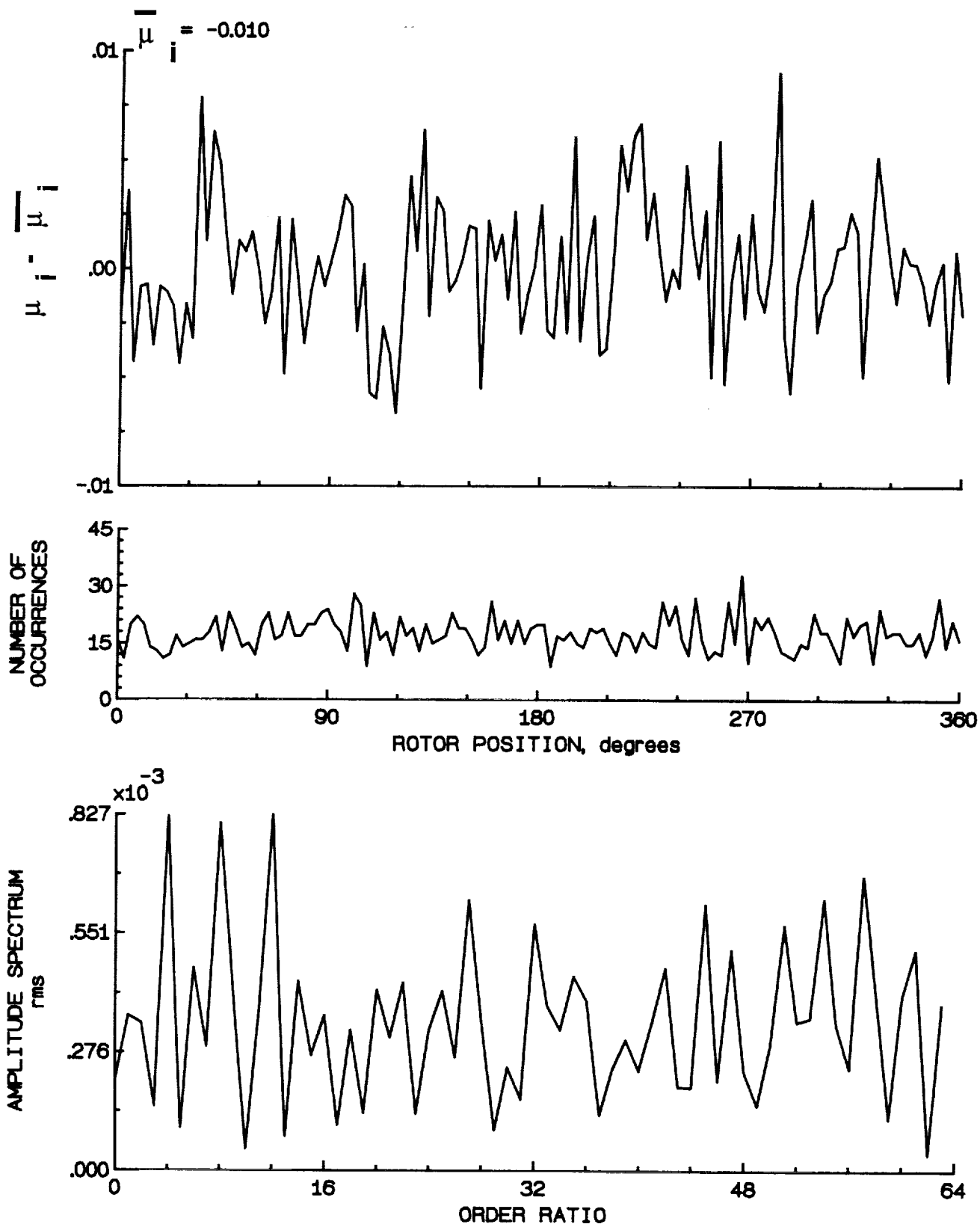


Figure 82.- Induced inflow velocity measured at 120 degrees and r/R of 0.94.

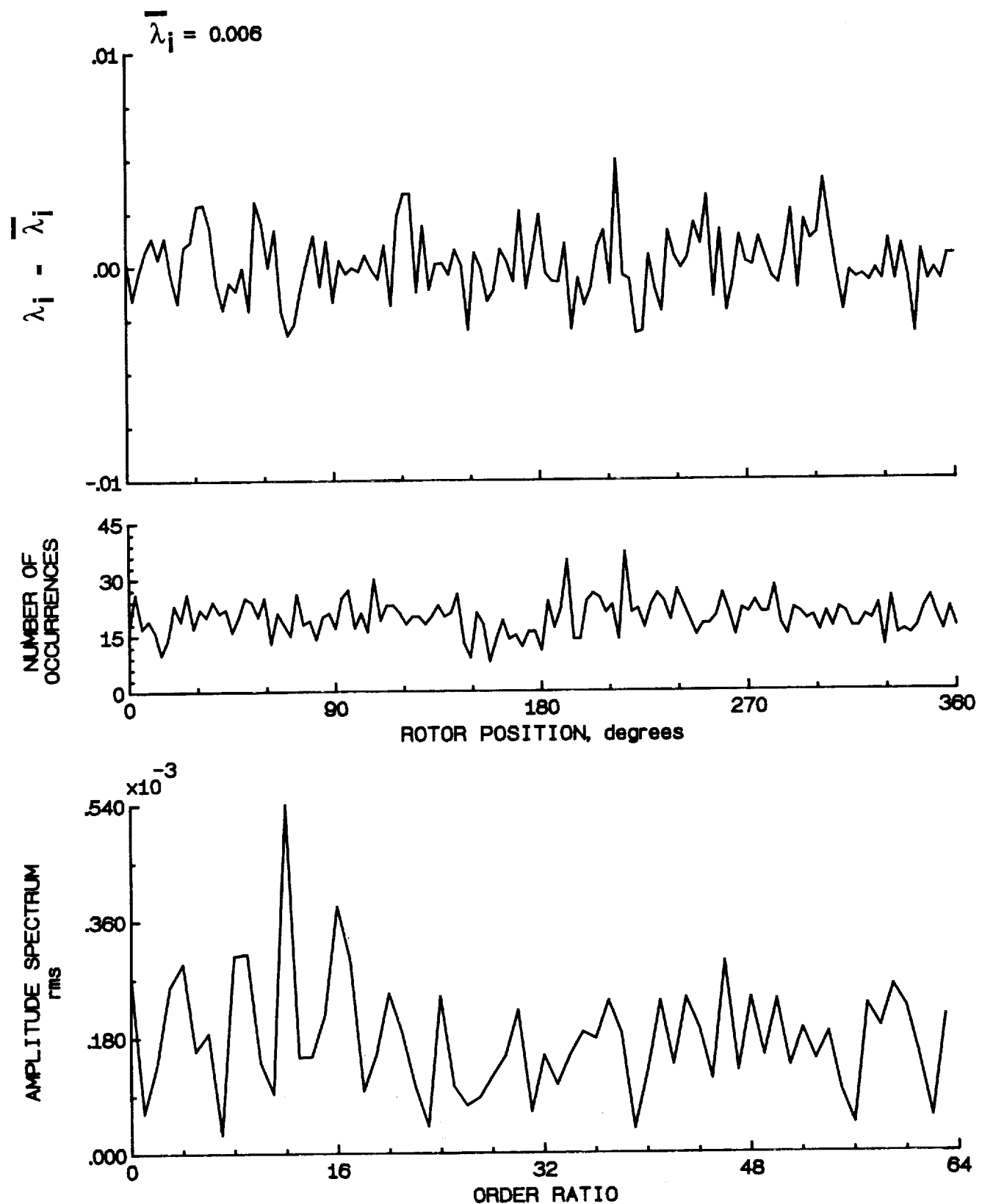


Figure 82.- Concluded.

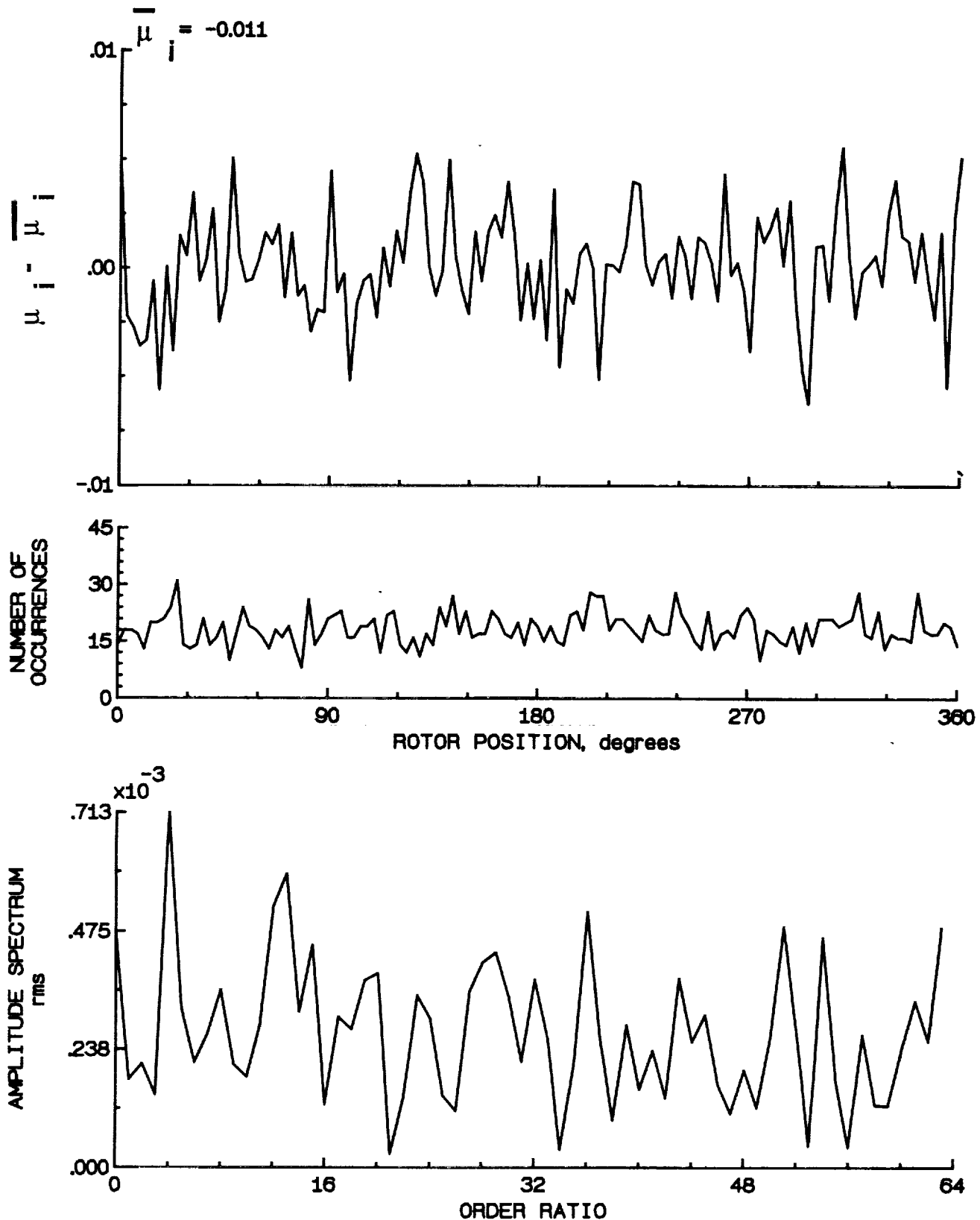


Figure 83.- Induced inflow velocity measured at 120 degrees and r/R of 0.98.

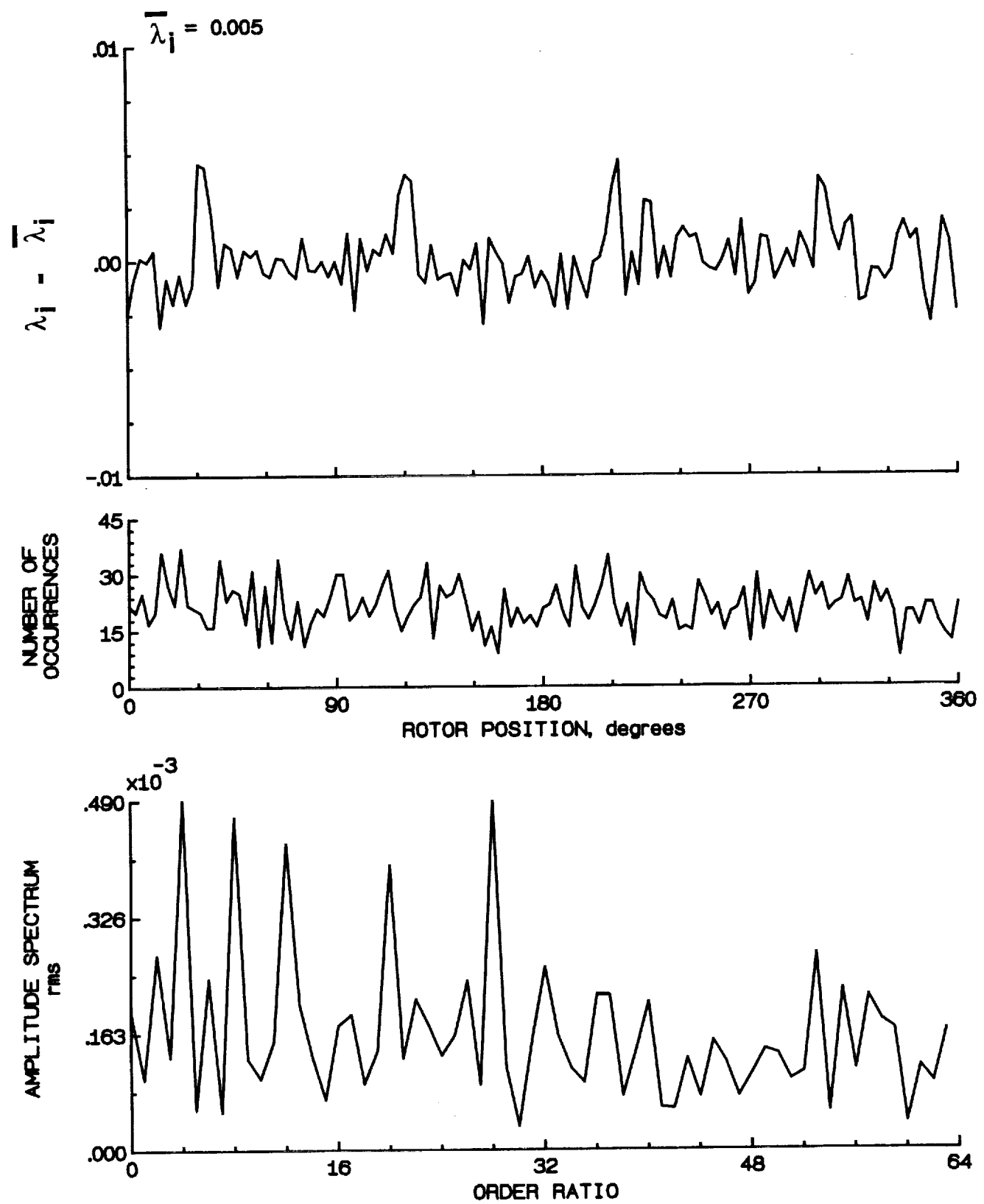


Figure 83.- Concluded.

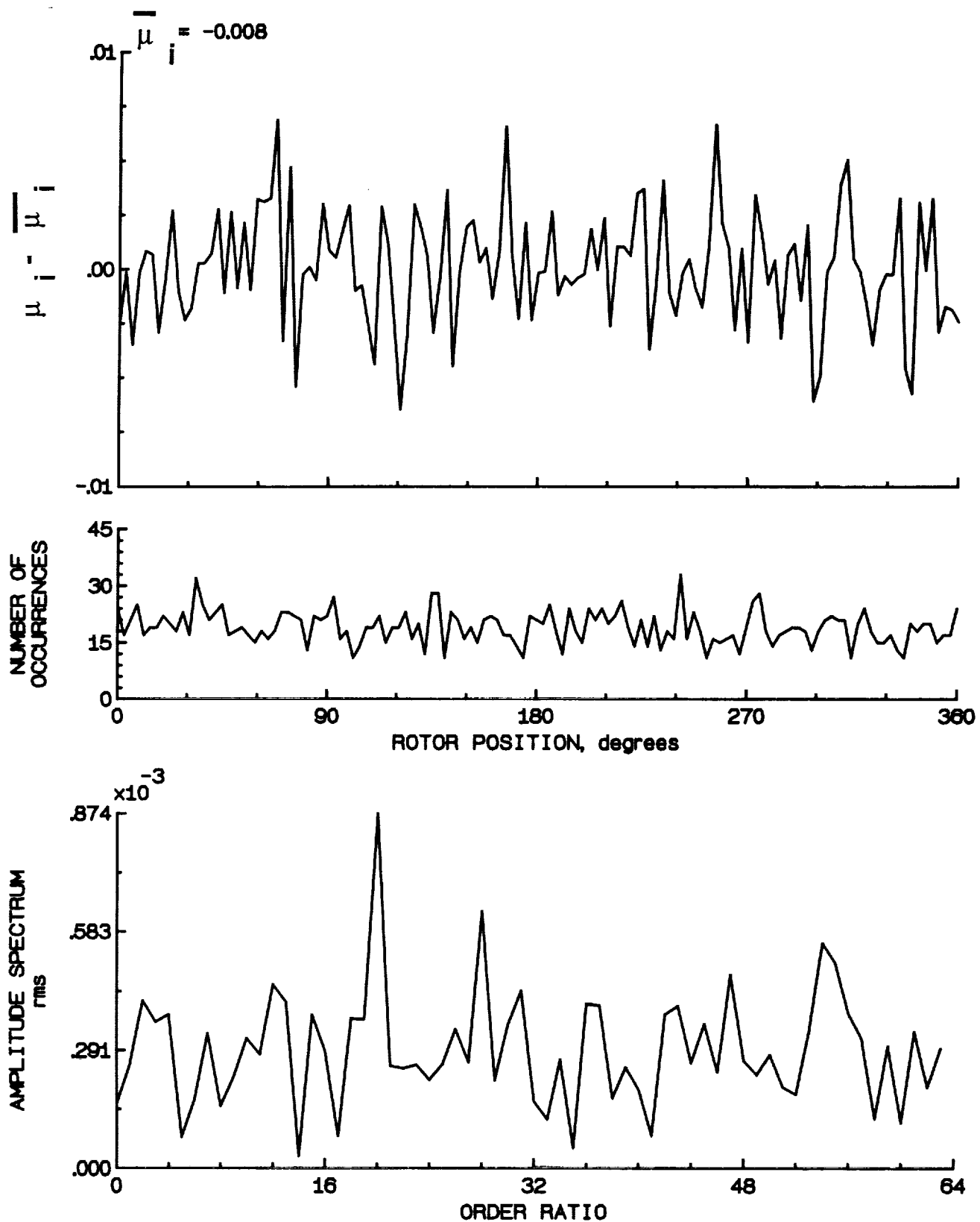


Figure 84.- Induced inflow velocity measured at 120 degrees and r/R of 1.02.

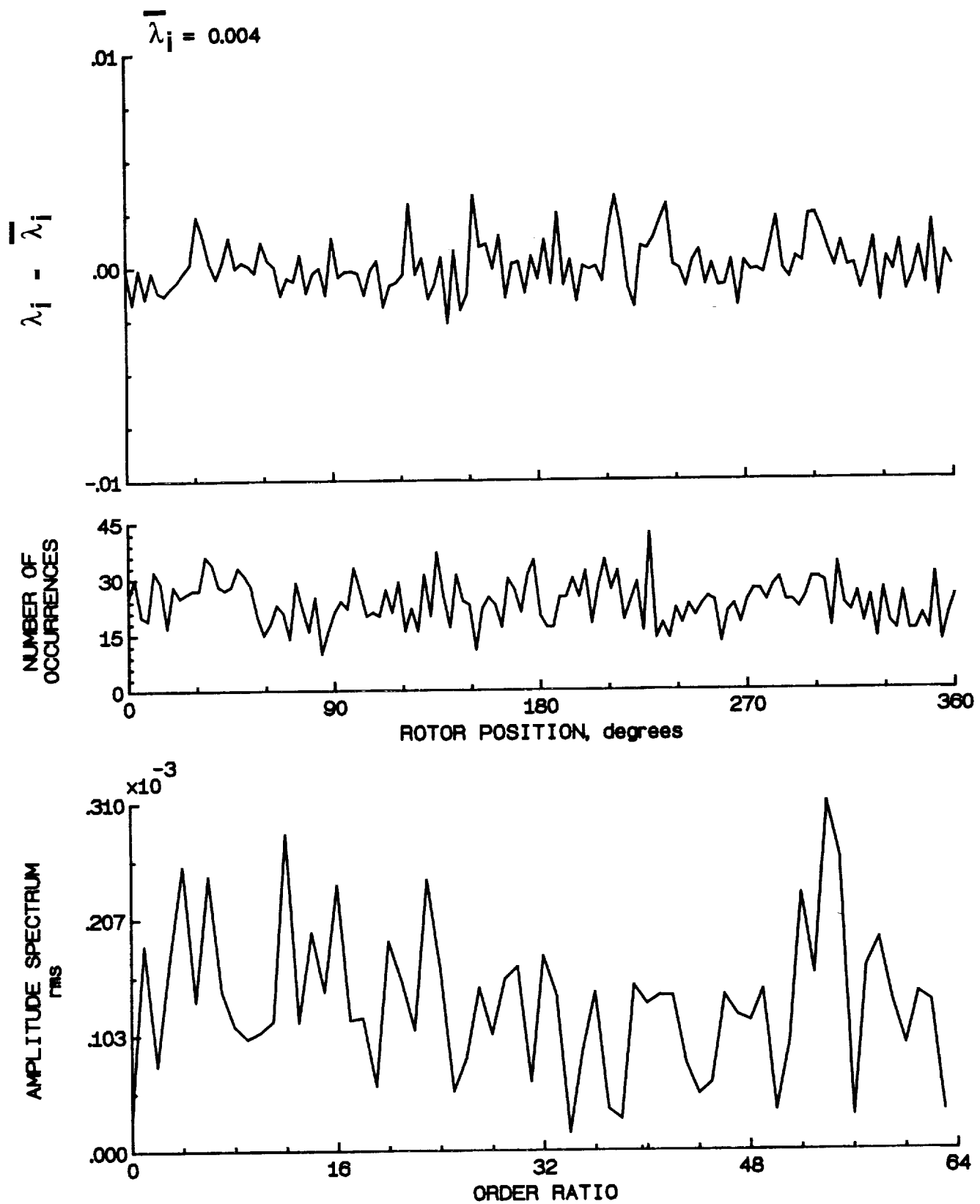


Figure 84.- Concluded.

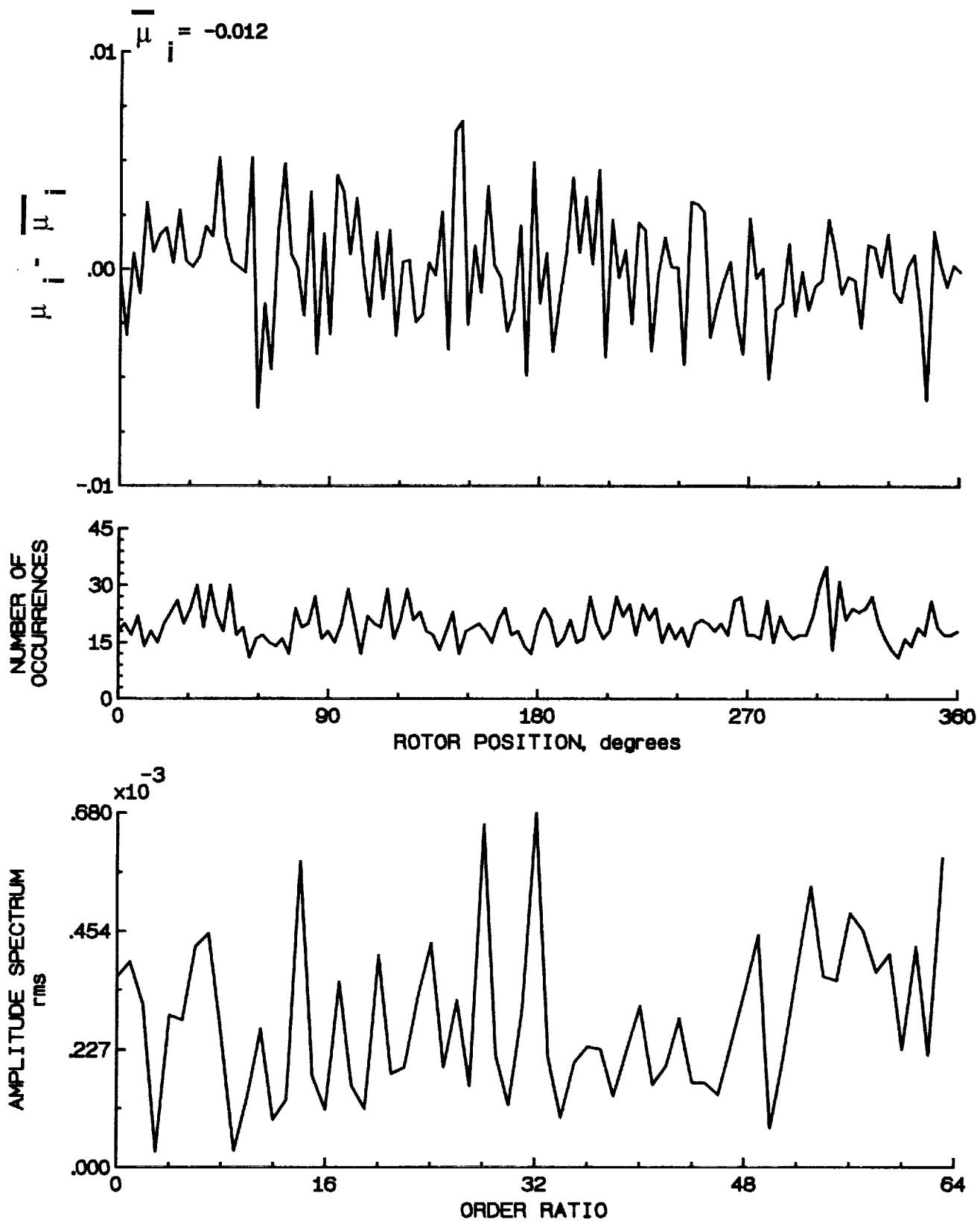


Figure 85.- Induced inflow velocity measured at 120 degrees and r/R of 1.04.

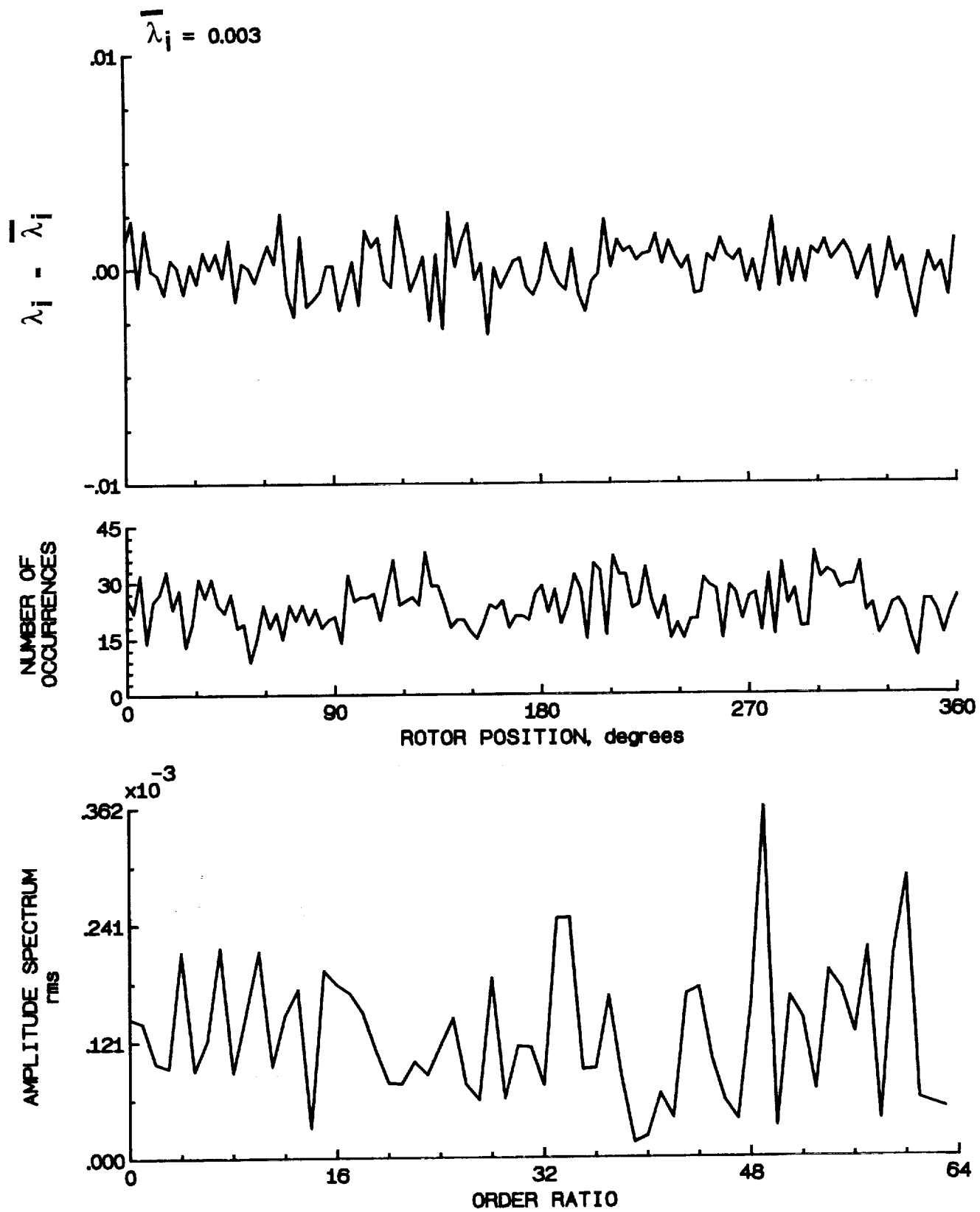


Figure 85.- Concluded.

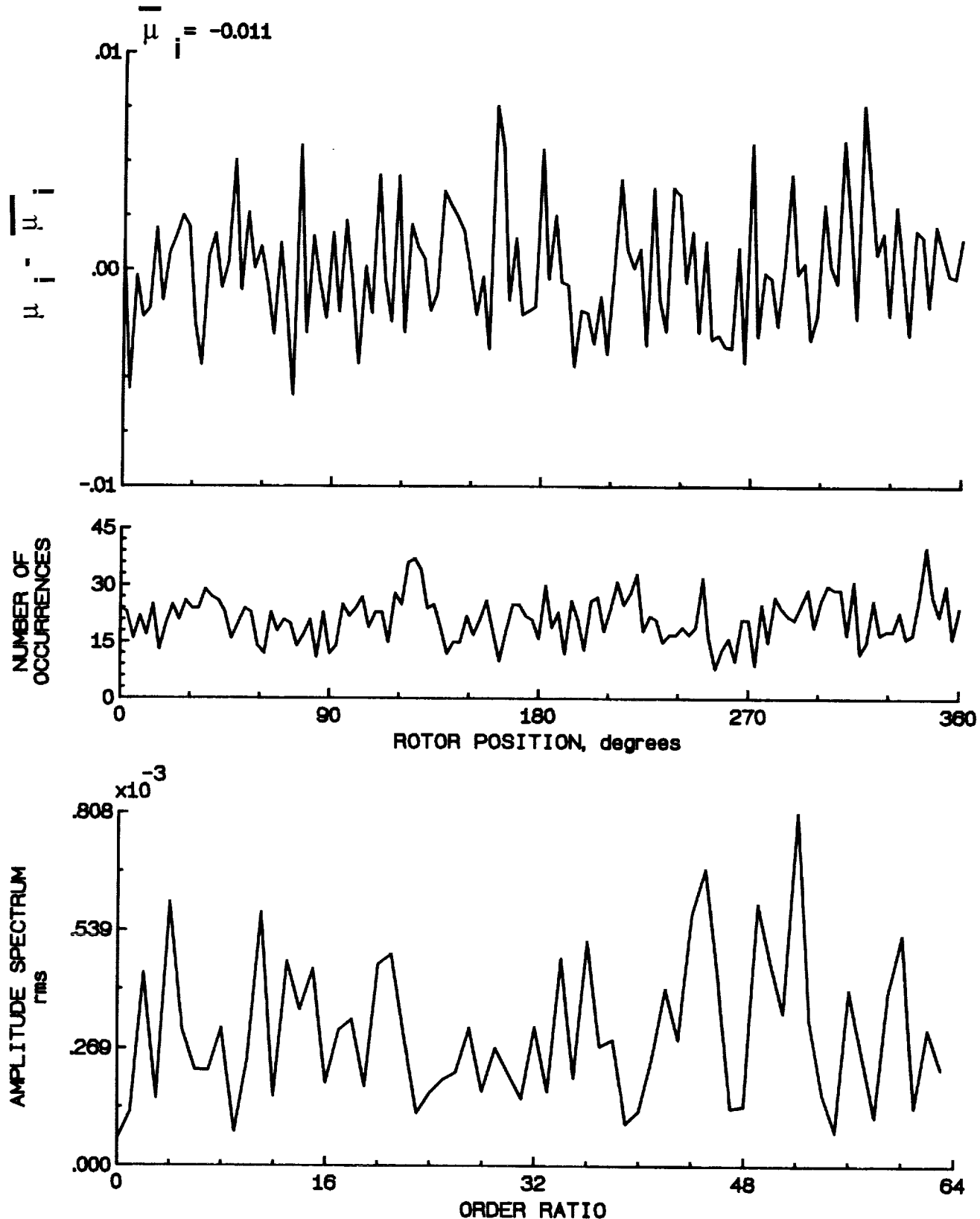


Figure 86.- Induced inflow velocity measured at 120 degrees and r/R of 1.10.

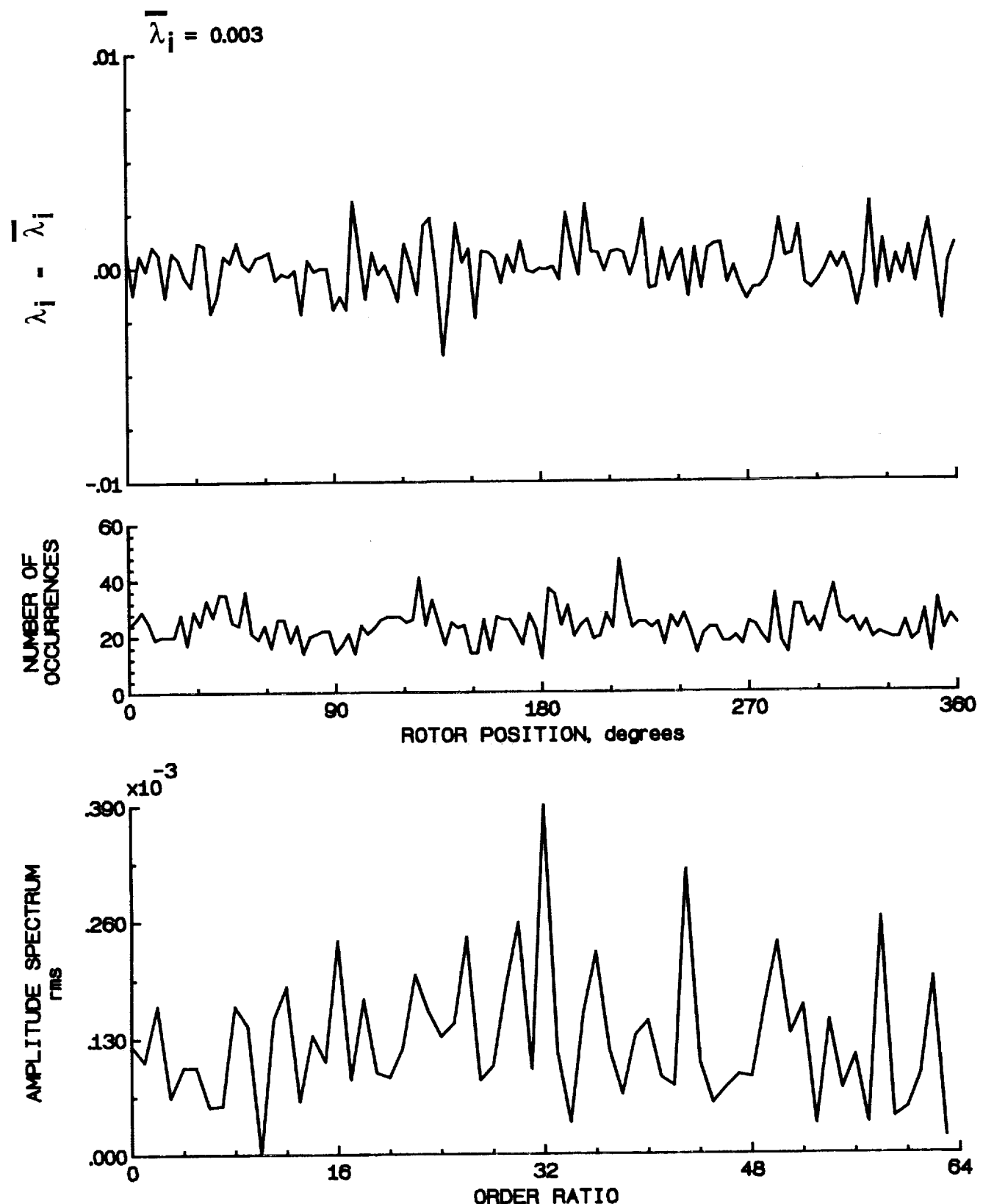


Figure 86.- Concluded.

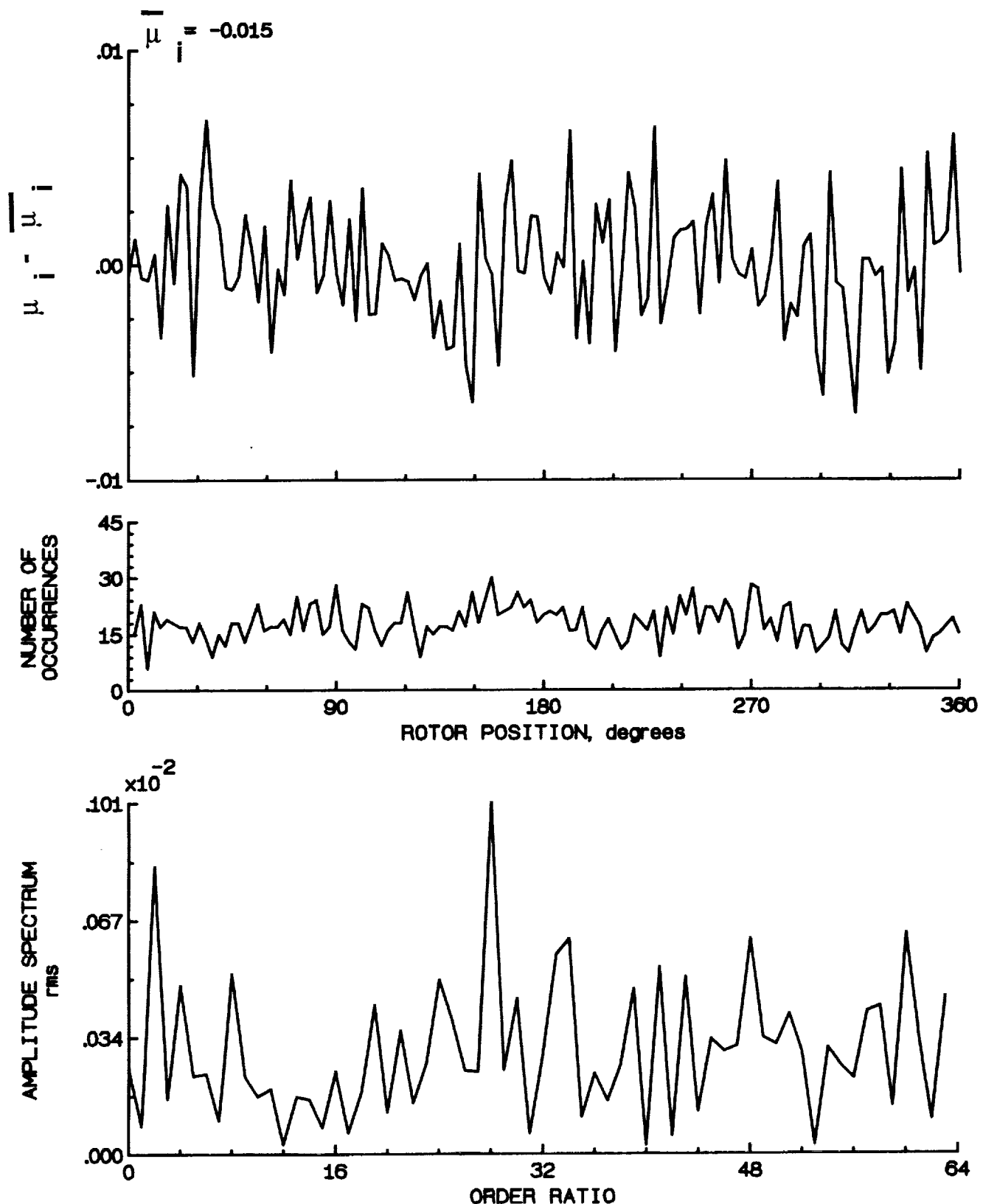


Figure 87.- Induced inflow velocity measured at 150 degrees and r/R of 0.20.

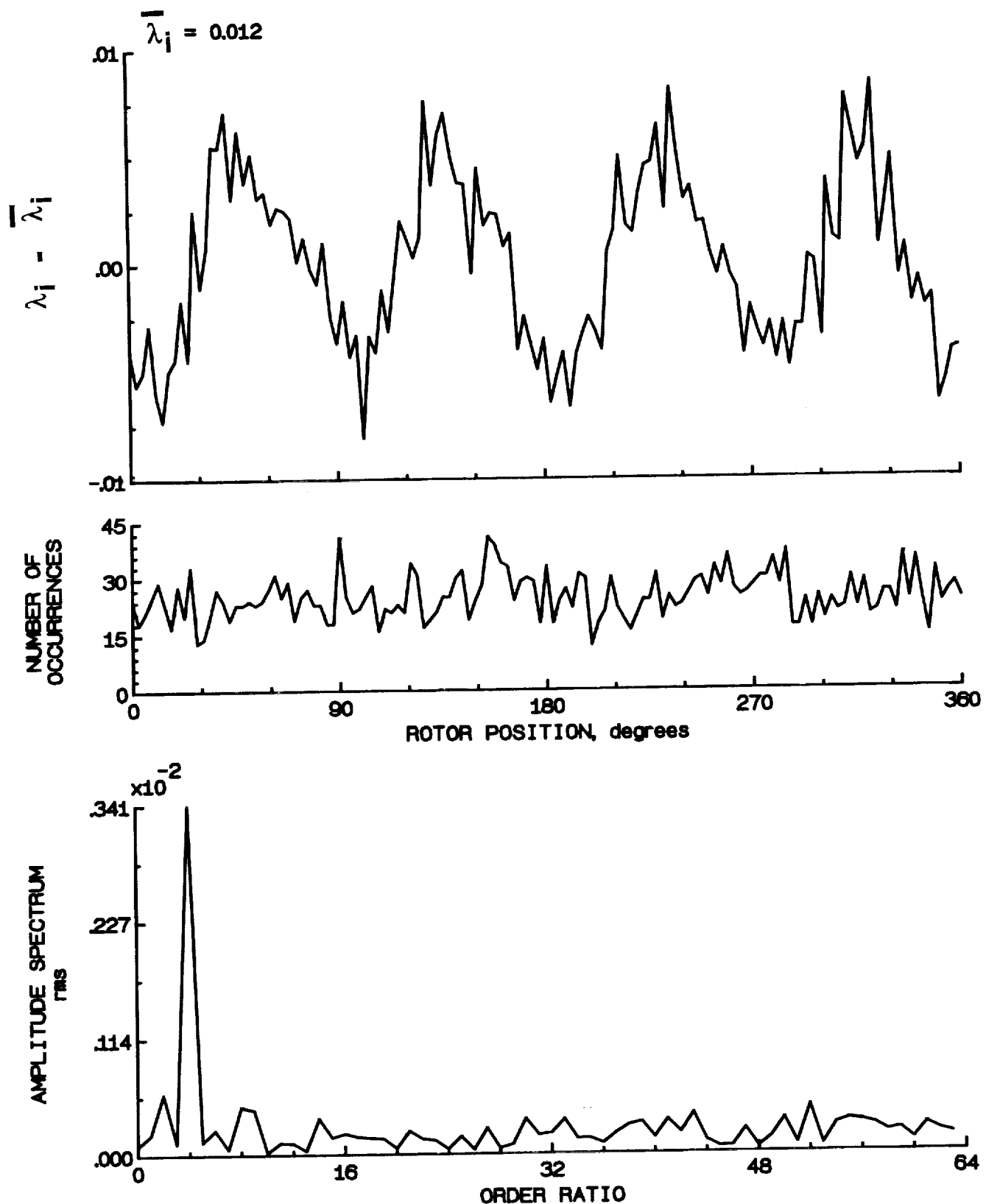


Figure 87.- Concluded.

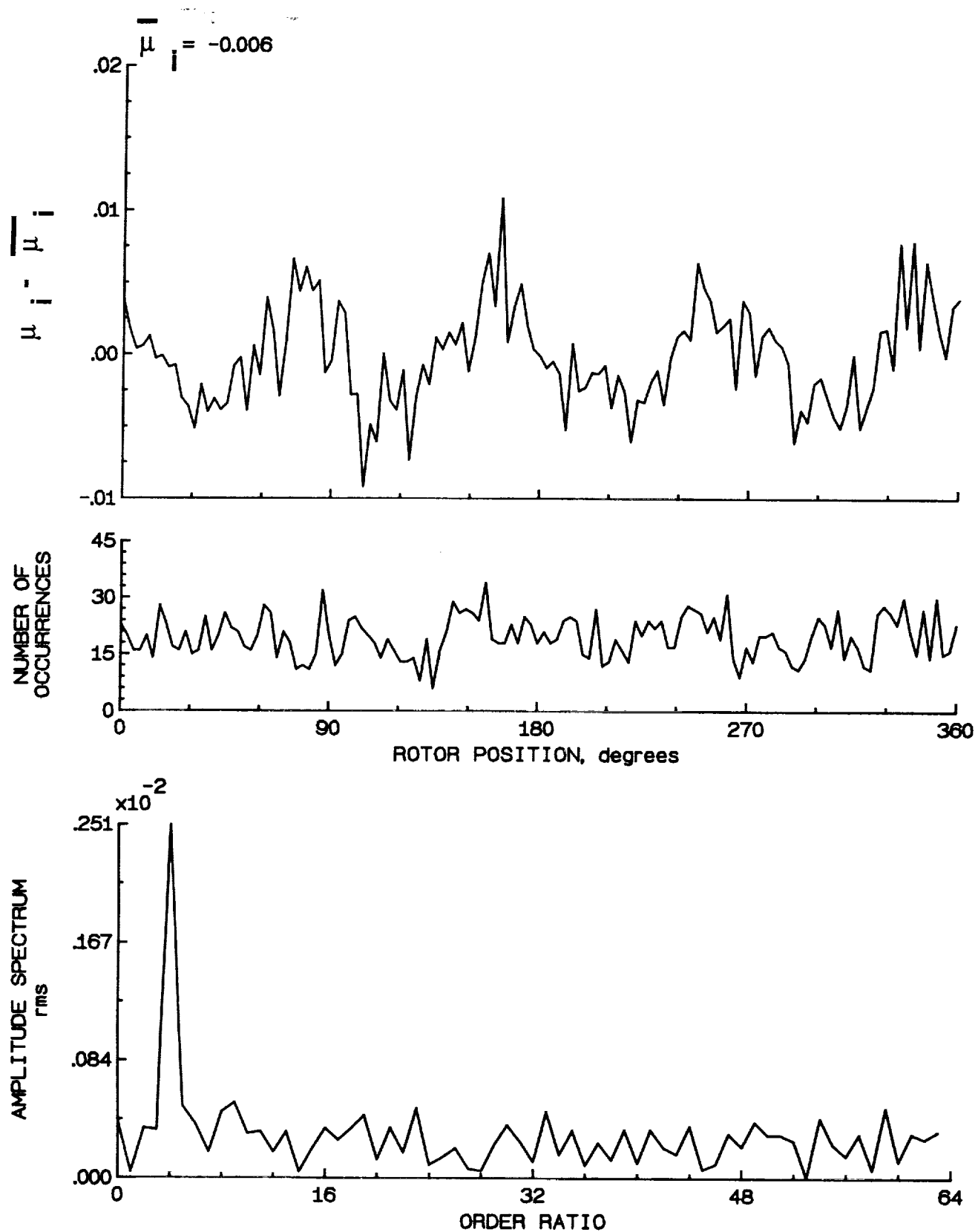


Figure 88.- Induced inflow velocity measured at 150 degrees and r/R of 0.40.

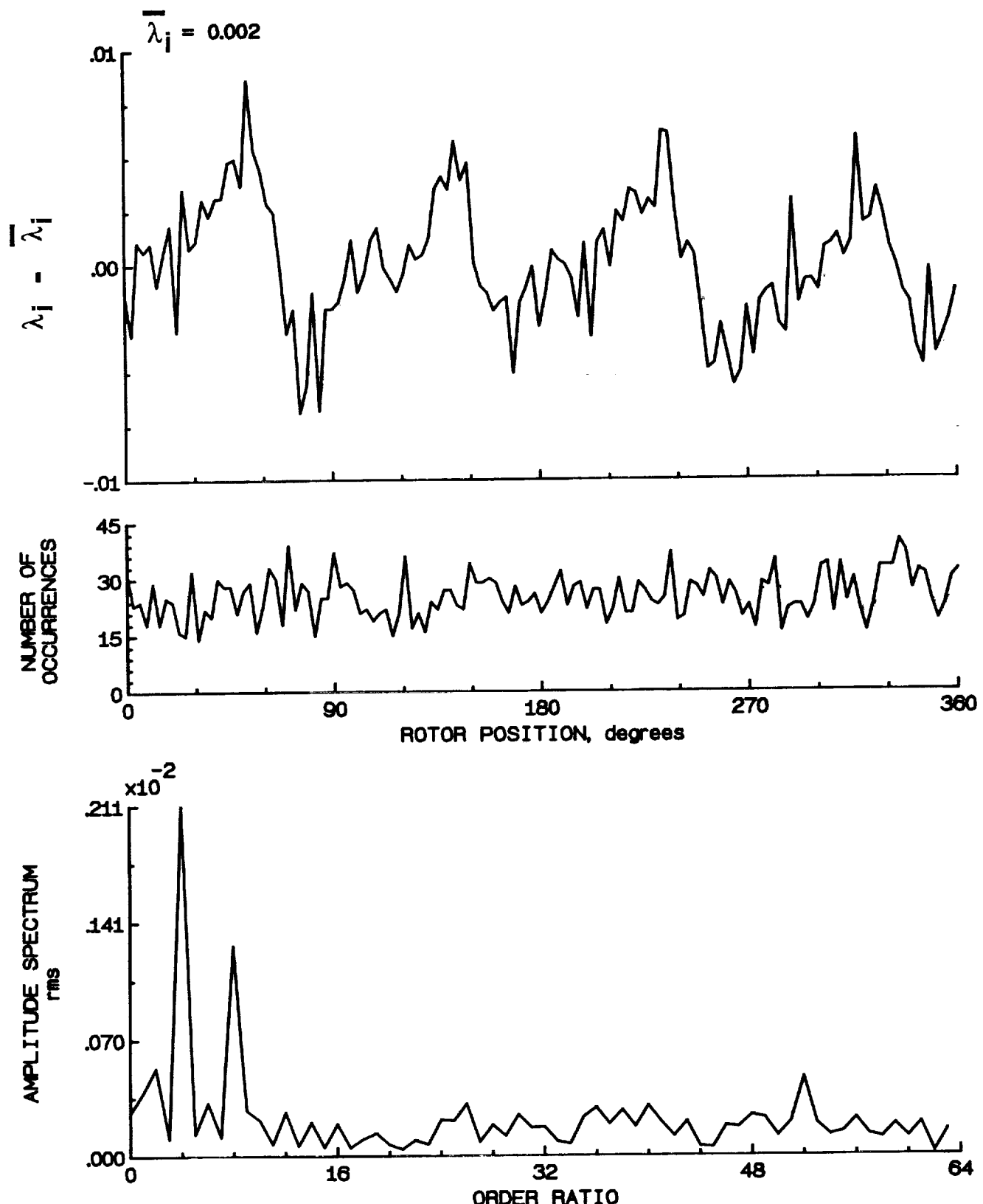


Figure 88.- Concluded.

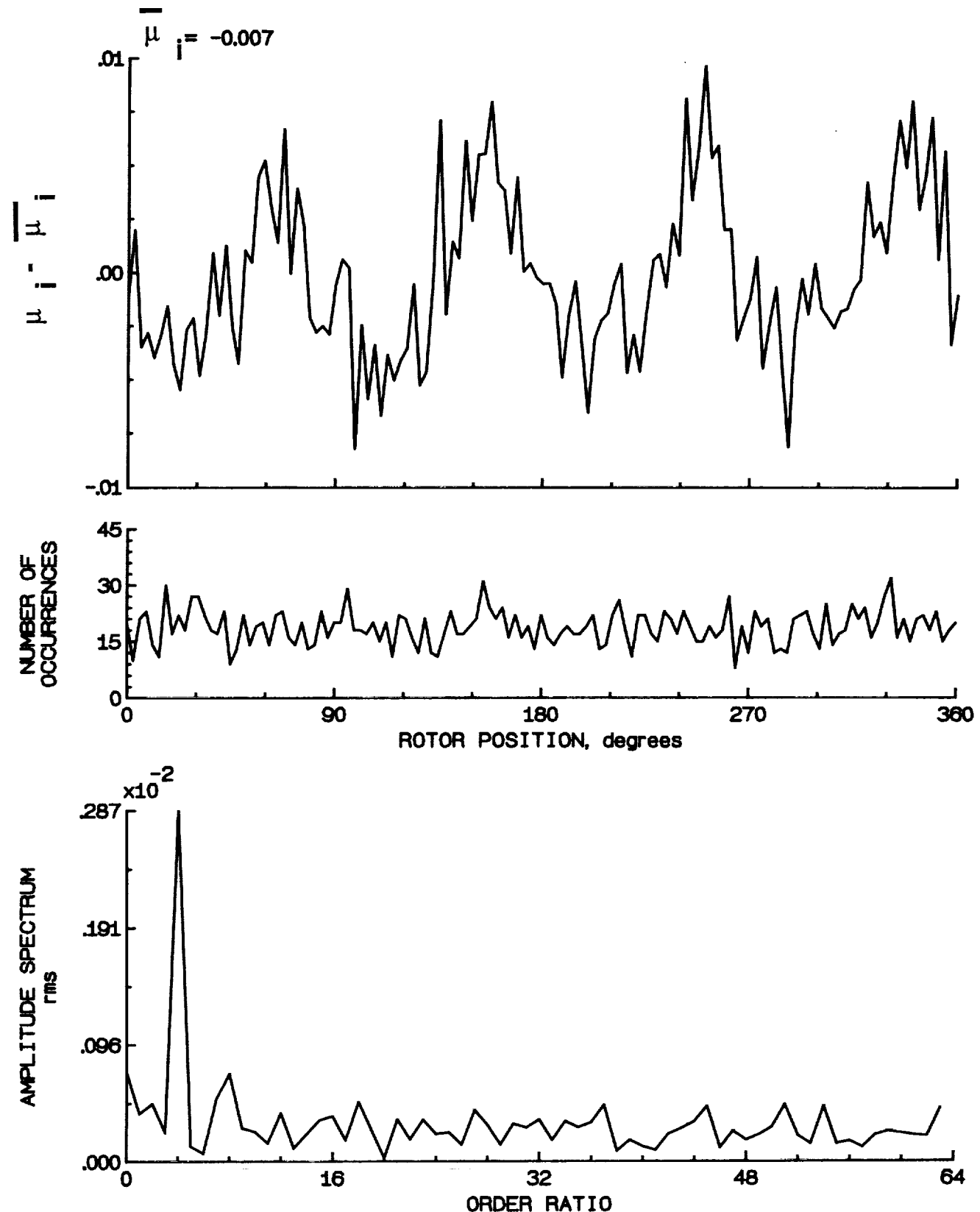


Figure 89.- Induced inflow velocity measured at 150 degrees and r/R of 0.50.

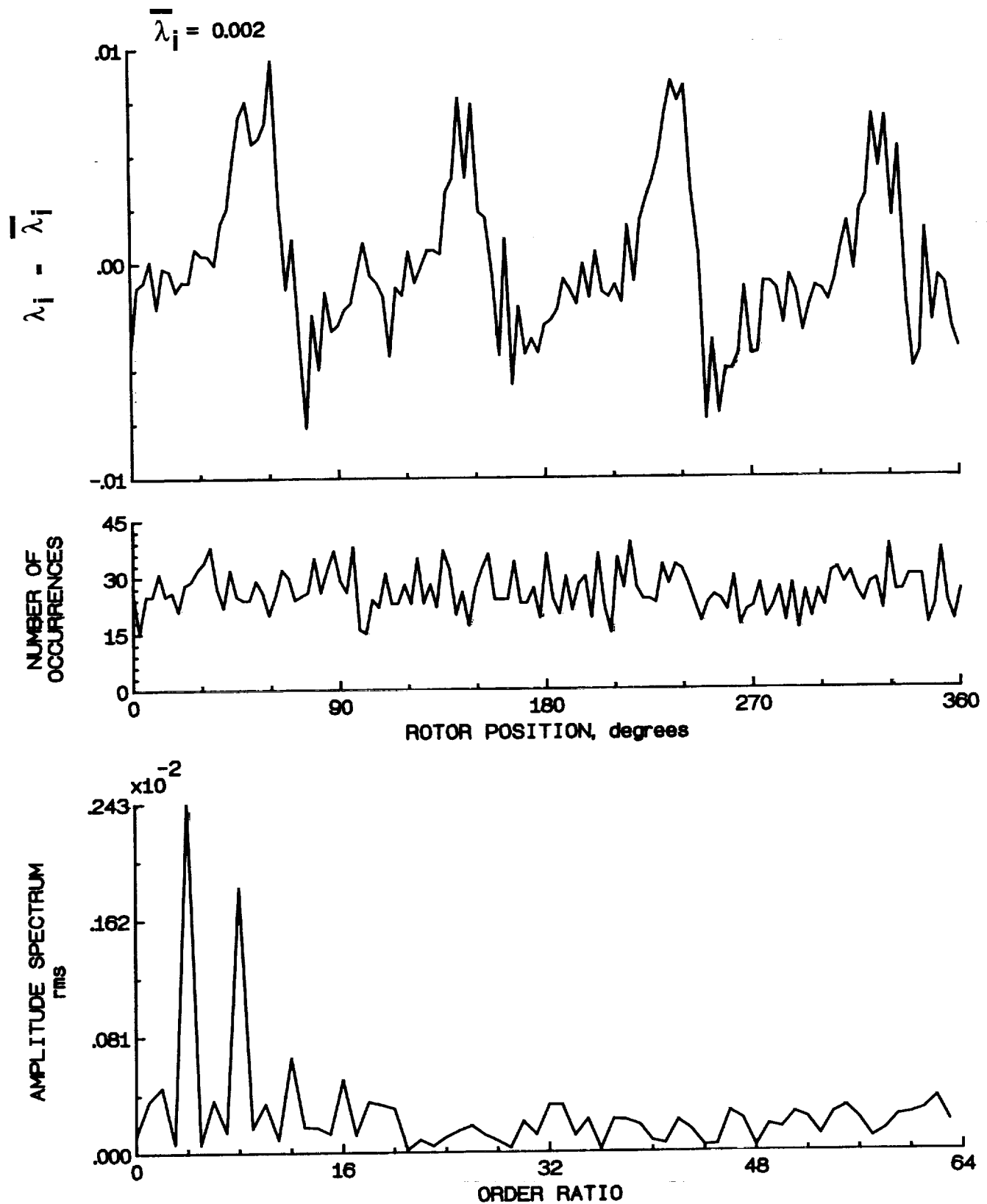


Figure 89.- Concluded.

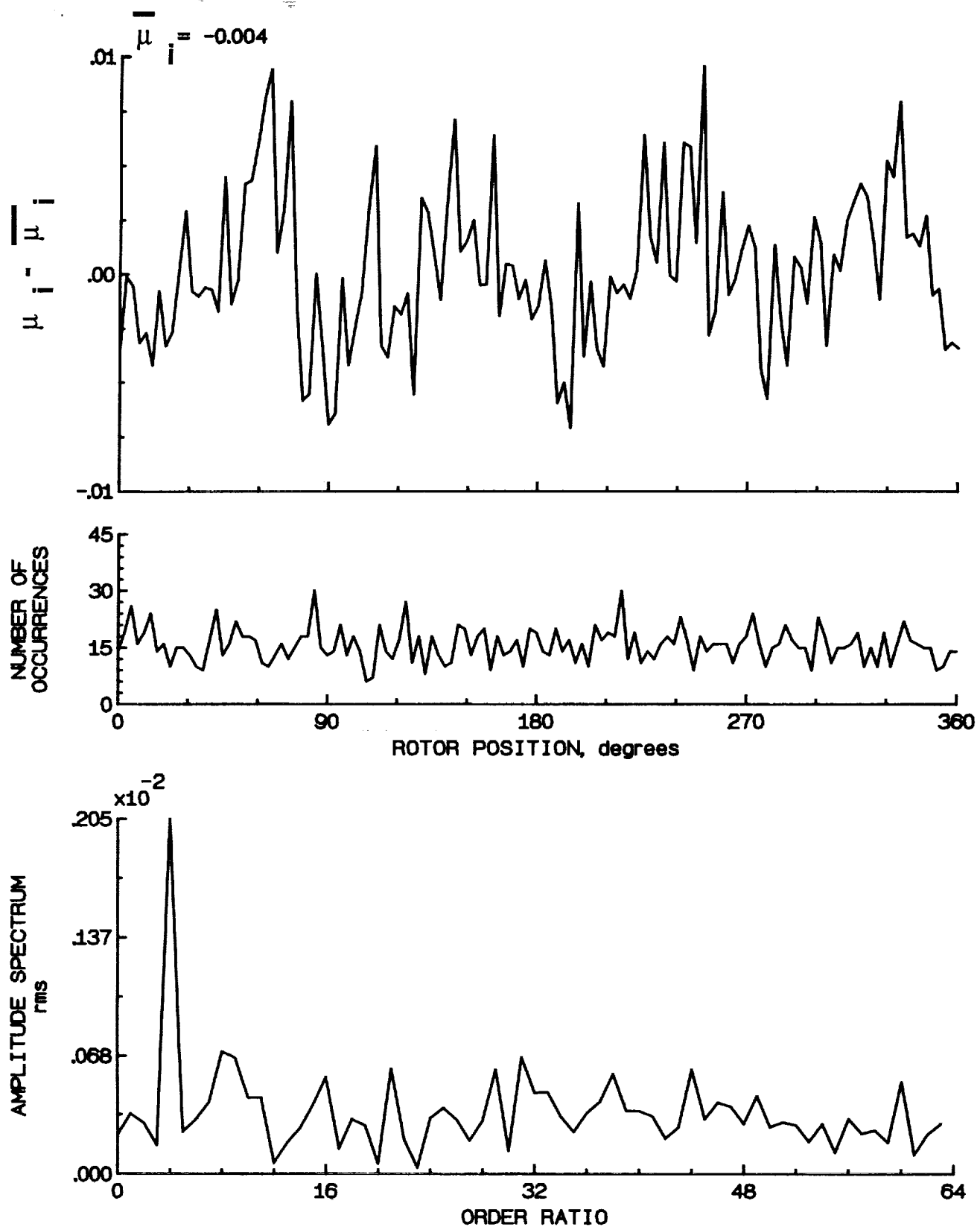


Figure 90.- Induced inflow velocity measured at 150 degrees and r/R of 0.60.

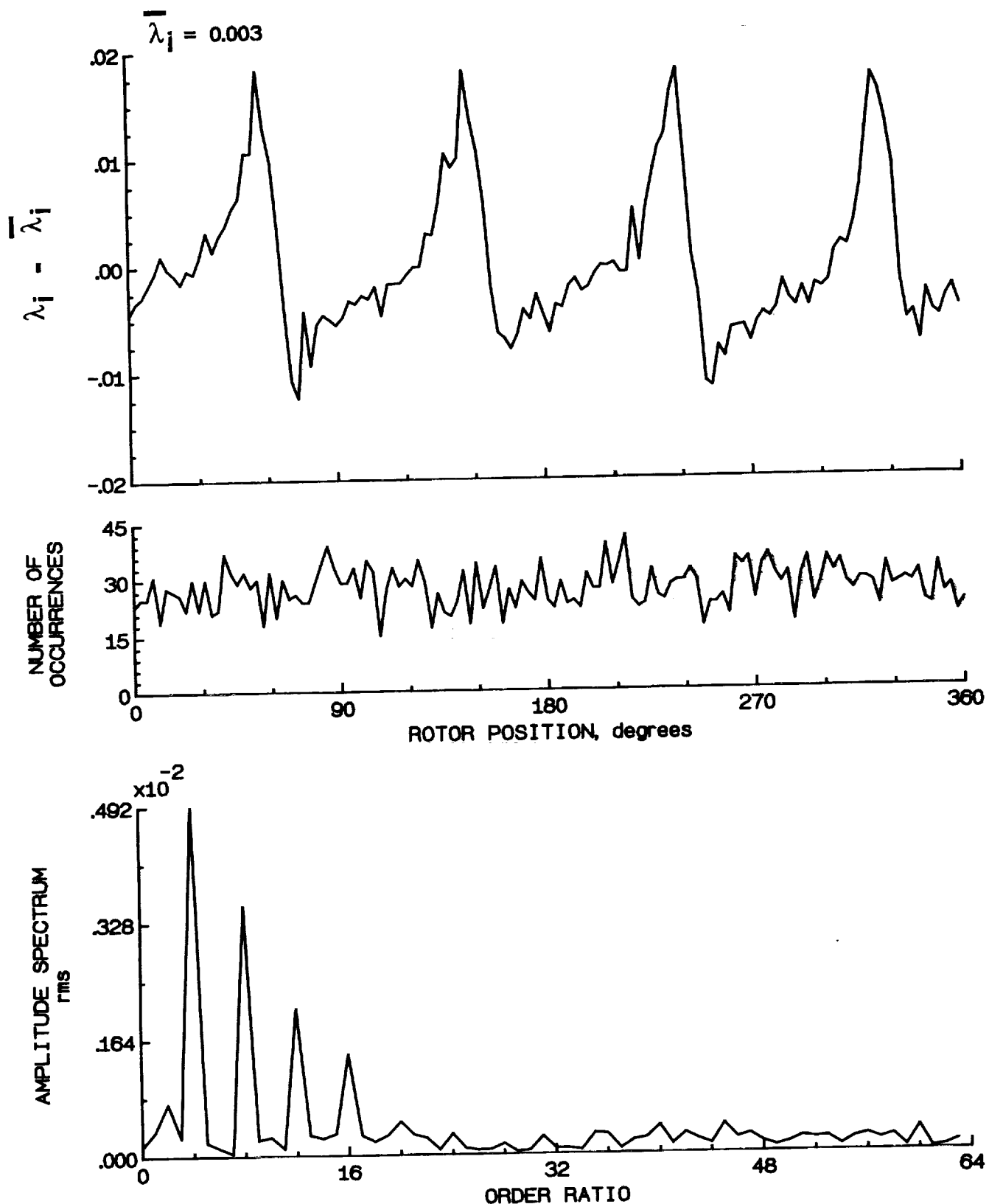


Figure 90.- Concluded.

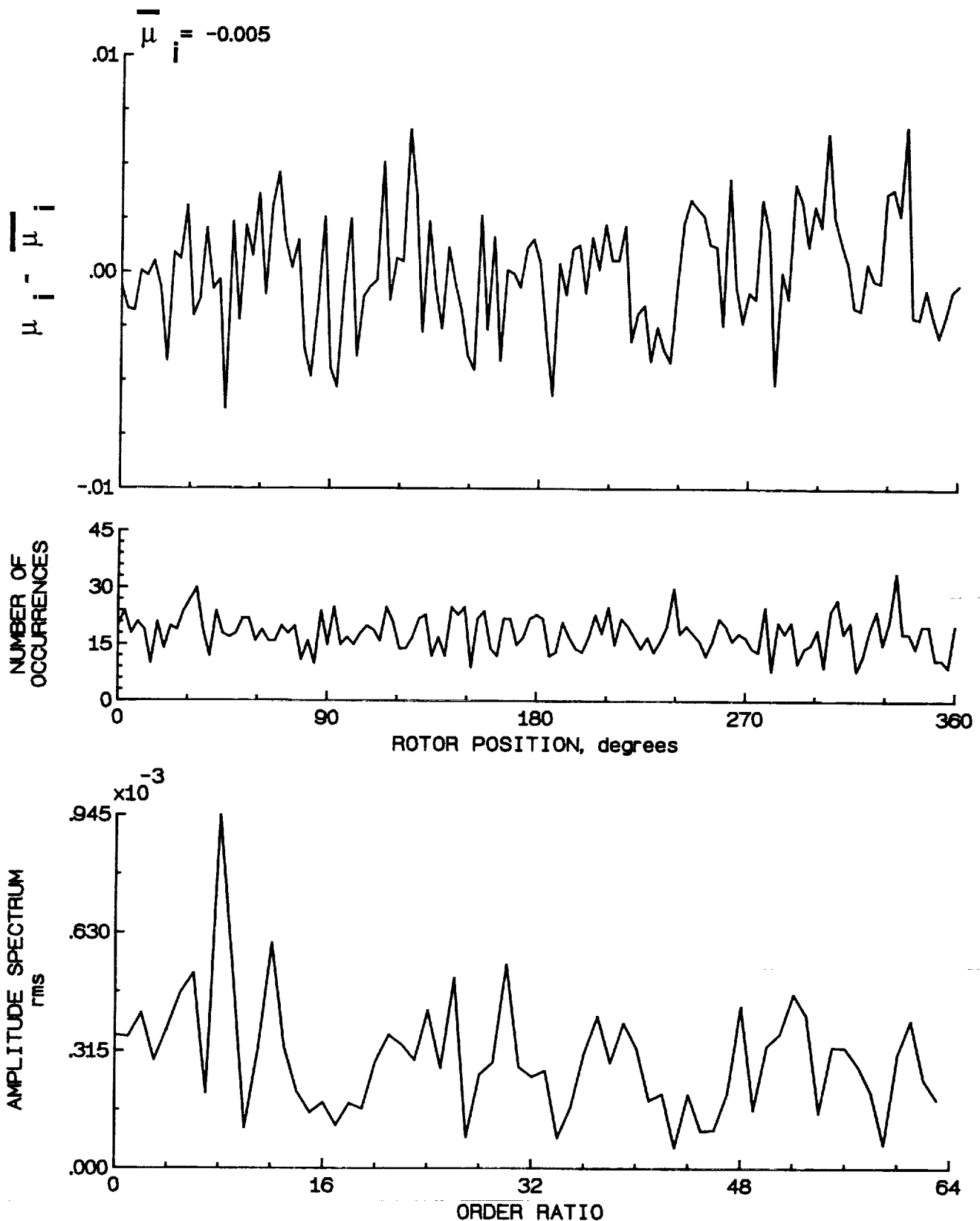


Figure 91.- Induced inflow velocity measured at 150 degrees and r/R of 0.70.

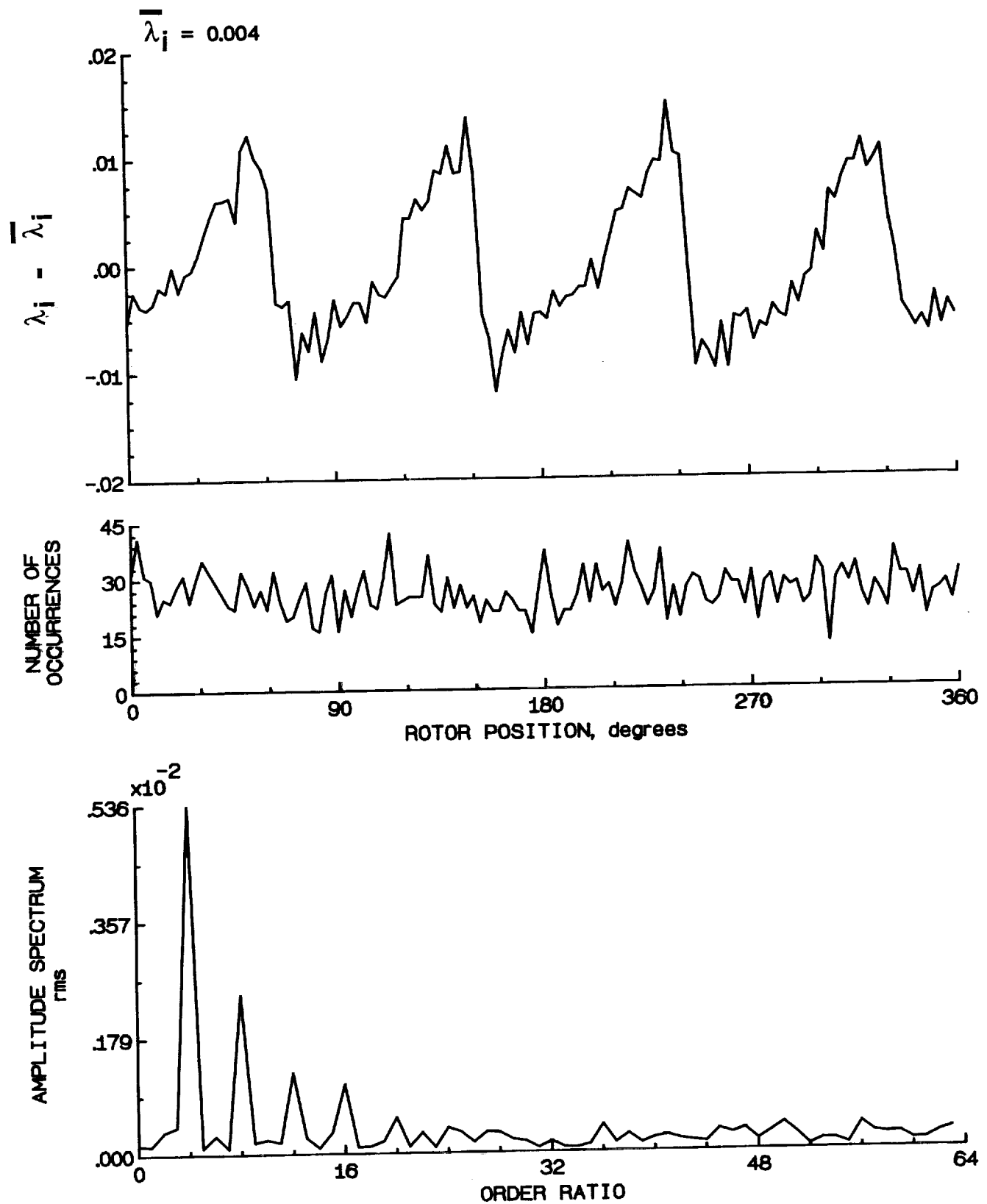


Figure 91.- Concluded.

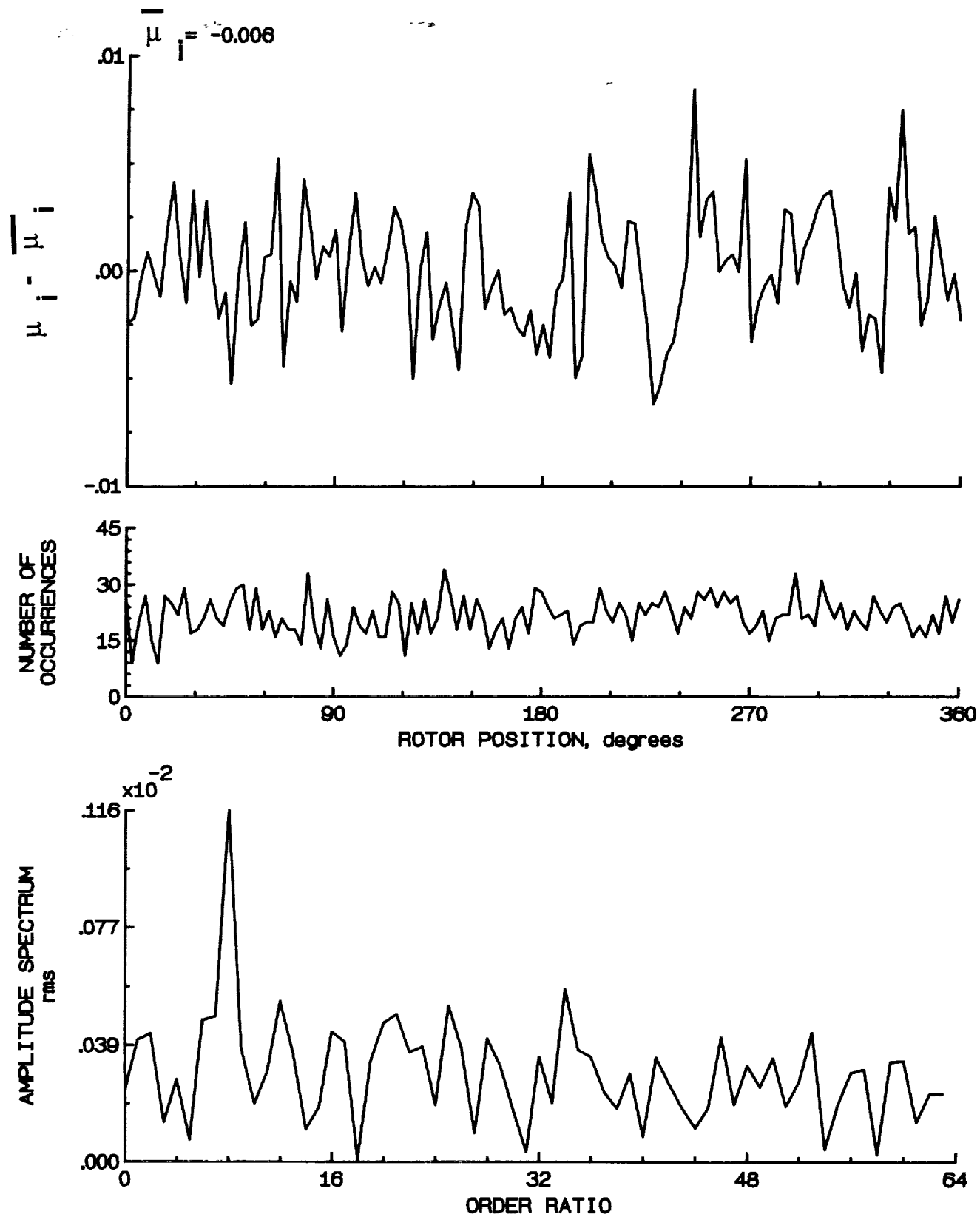


Figure 92.- Induced inflow velocity measured at 150 degrees and r/R of 0.74.

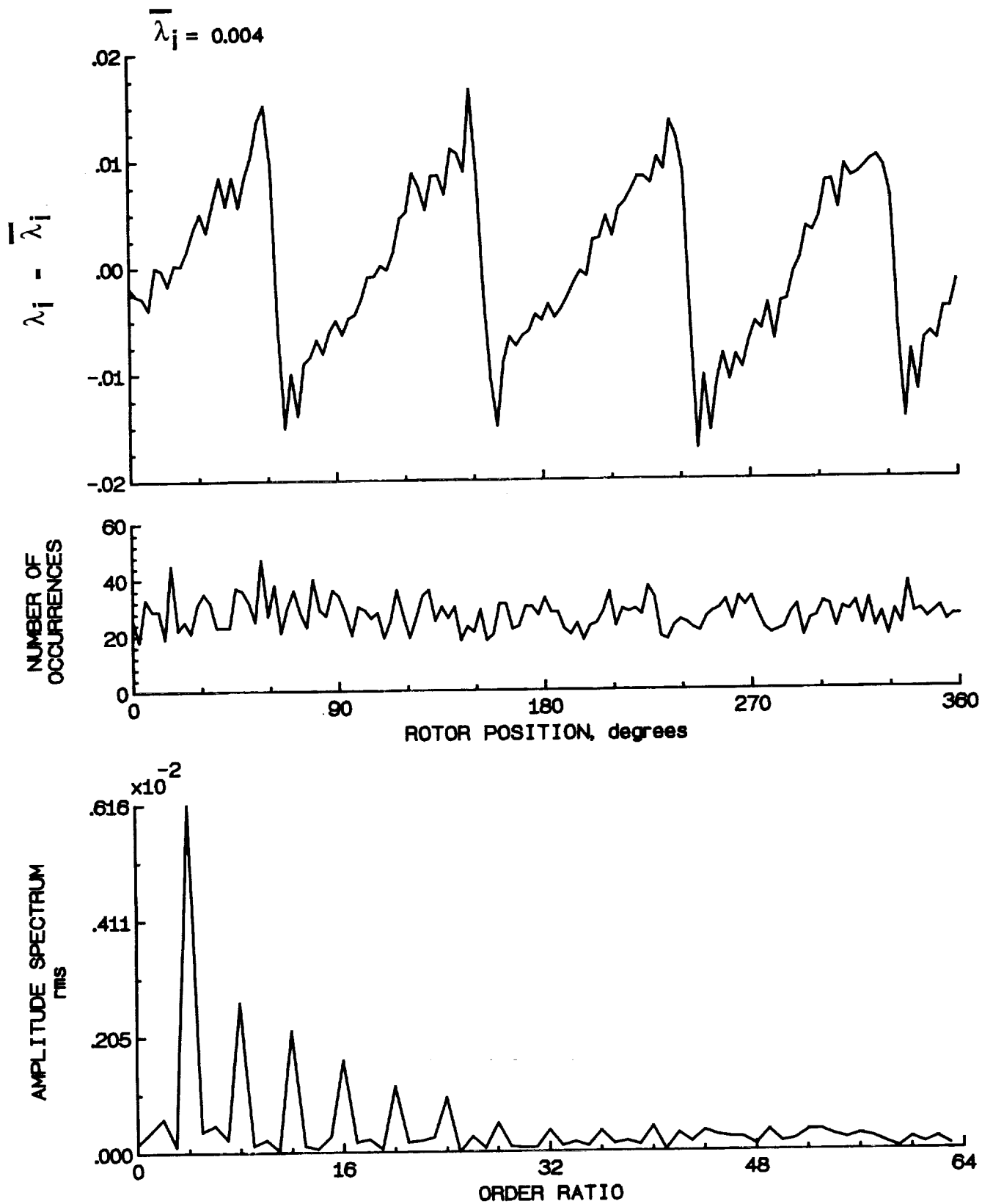


Figure 92.- Concluded.

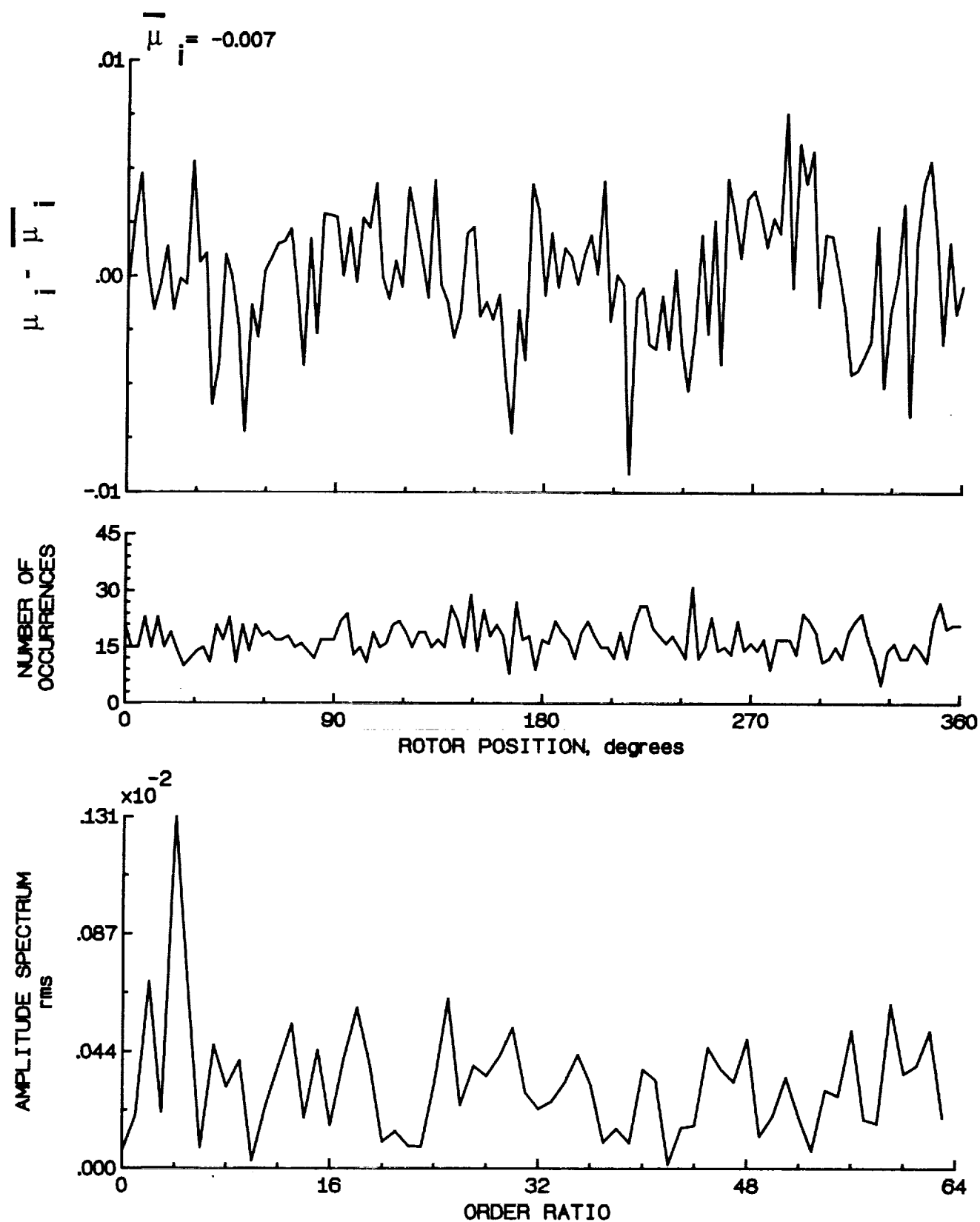


Figure 93.- Induced inflow velocity measured at 150 degrees and r/R of 0.78.

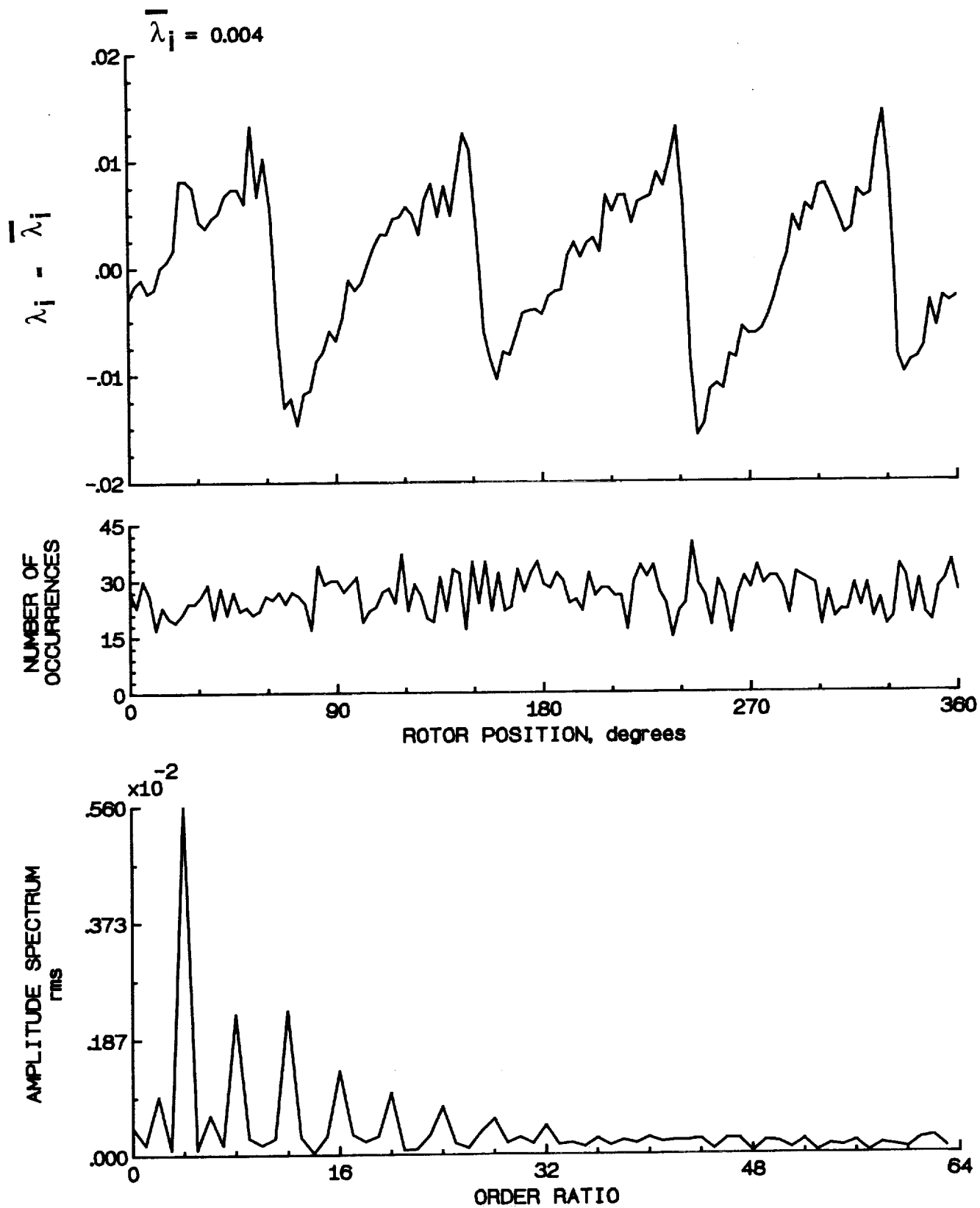


Figure 93.- Concluded.

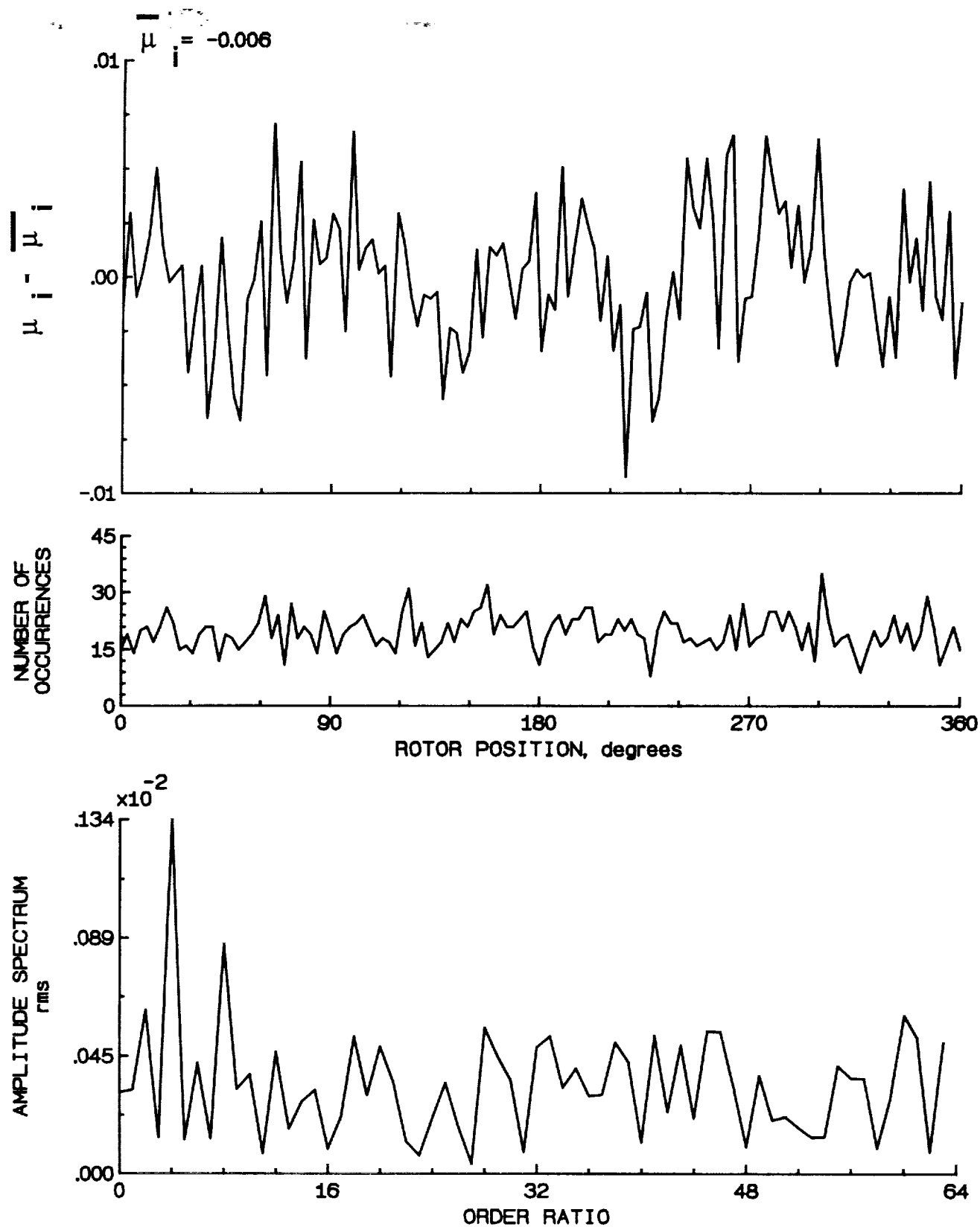


Figure 94.- Induced inflow velocity measured at 150 degrees and r/R of 0.82.

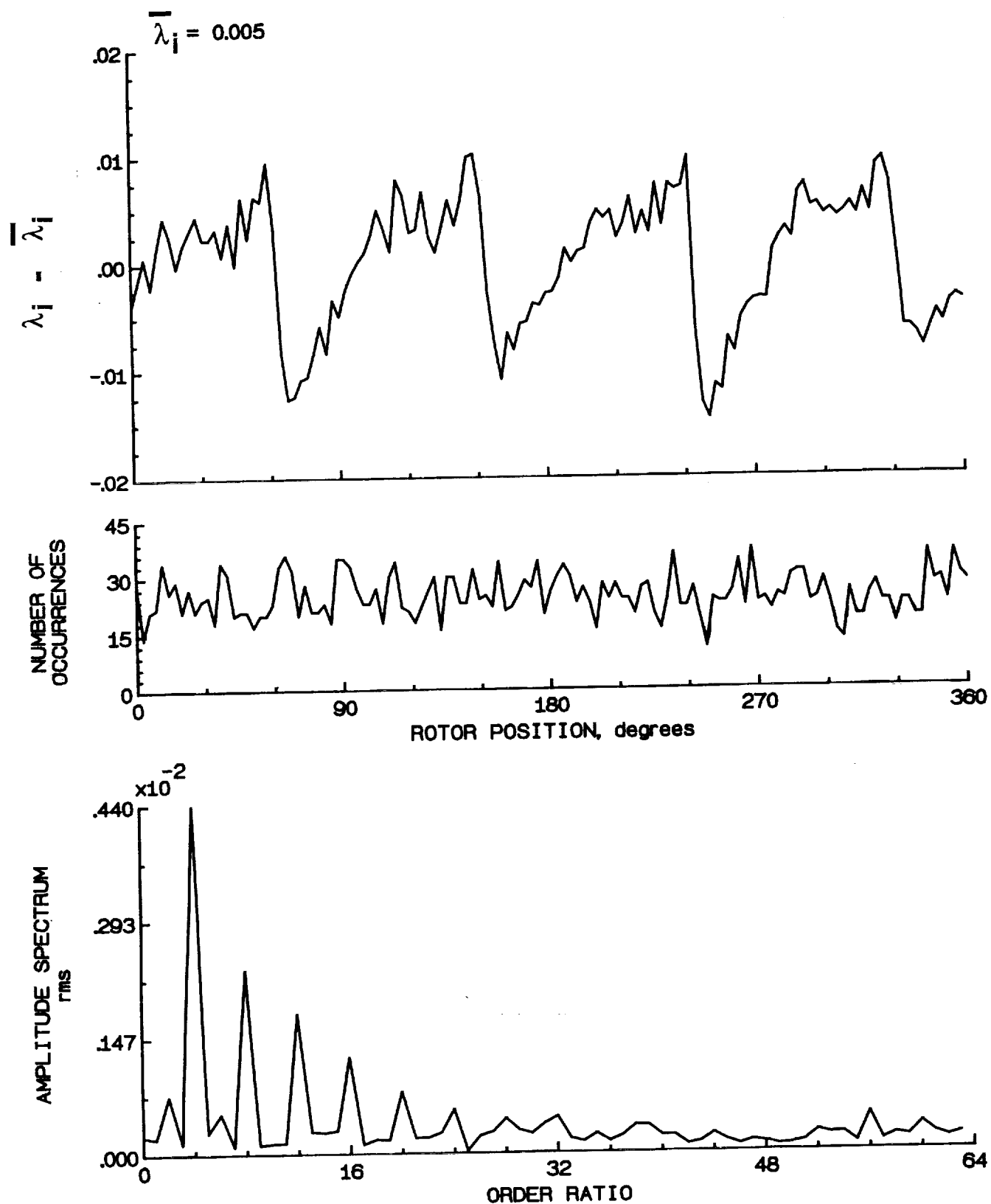


Figure 94.- Concluded.

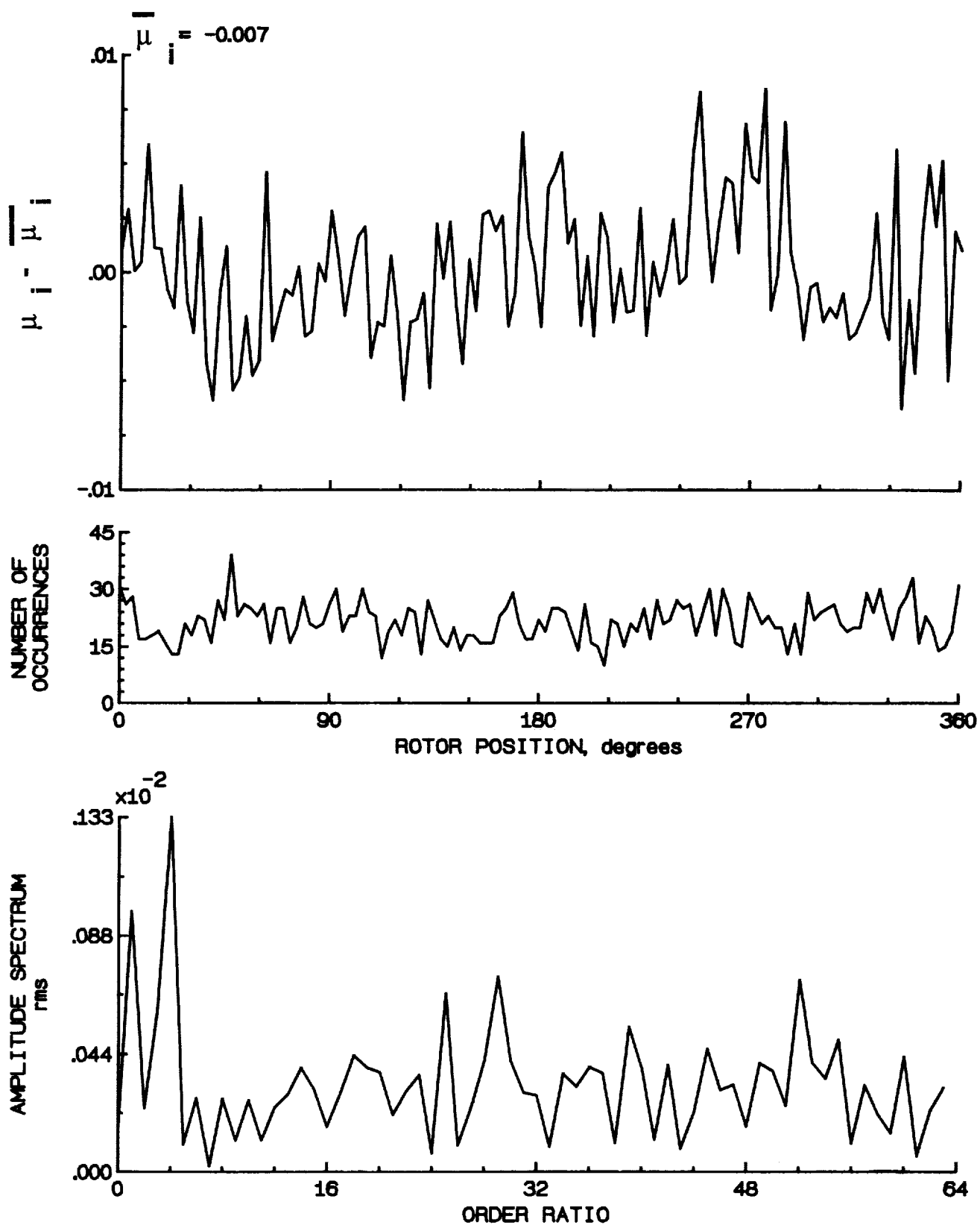


Figure 95.- Induced inflow velocity measured at 150 degrees and r/R of 0.86.

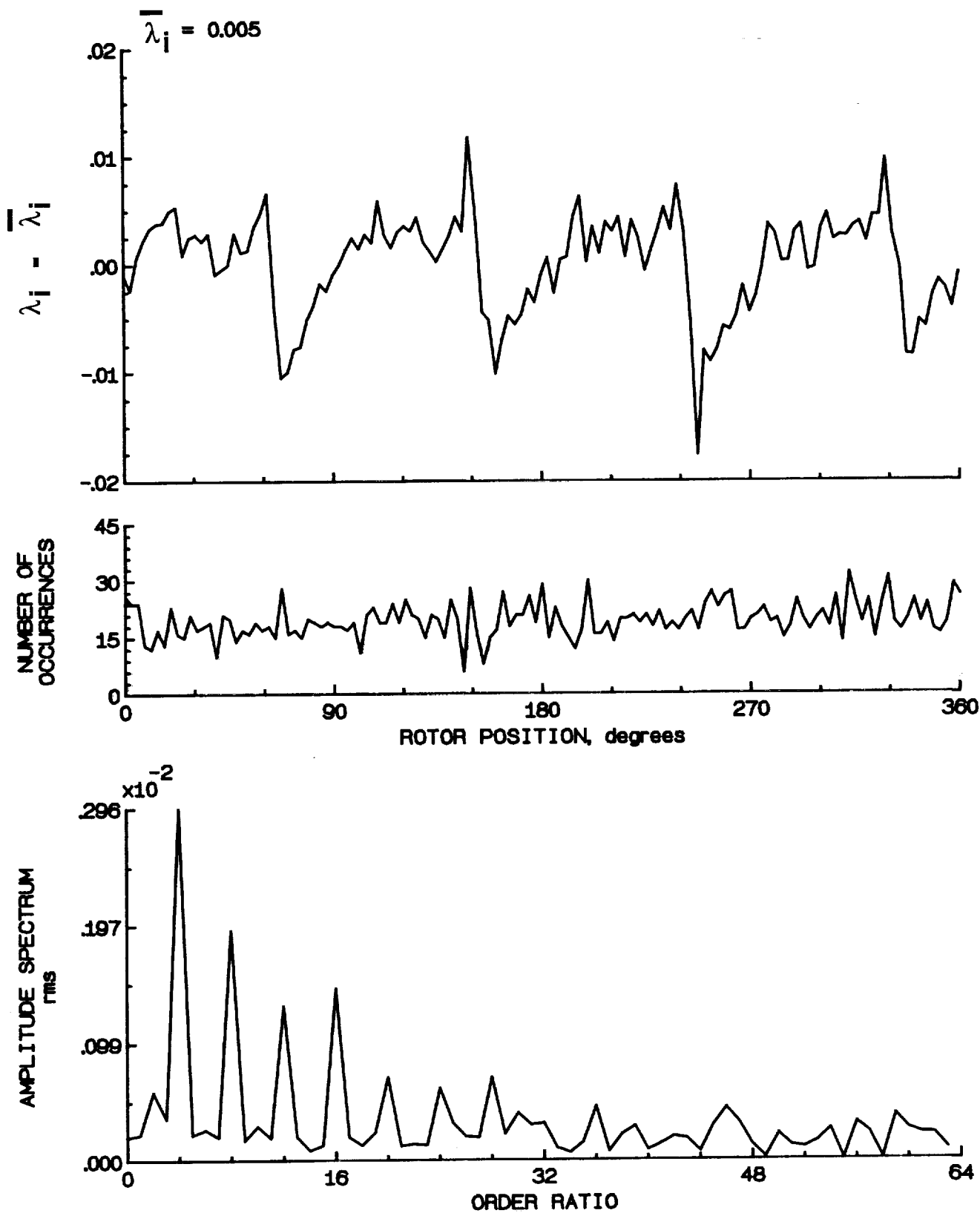


Figure 95.- Concluded.

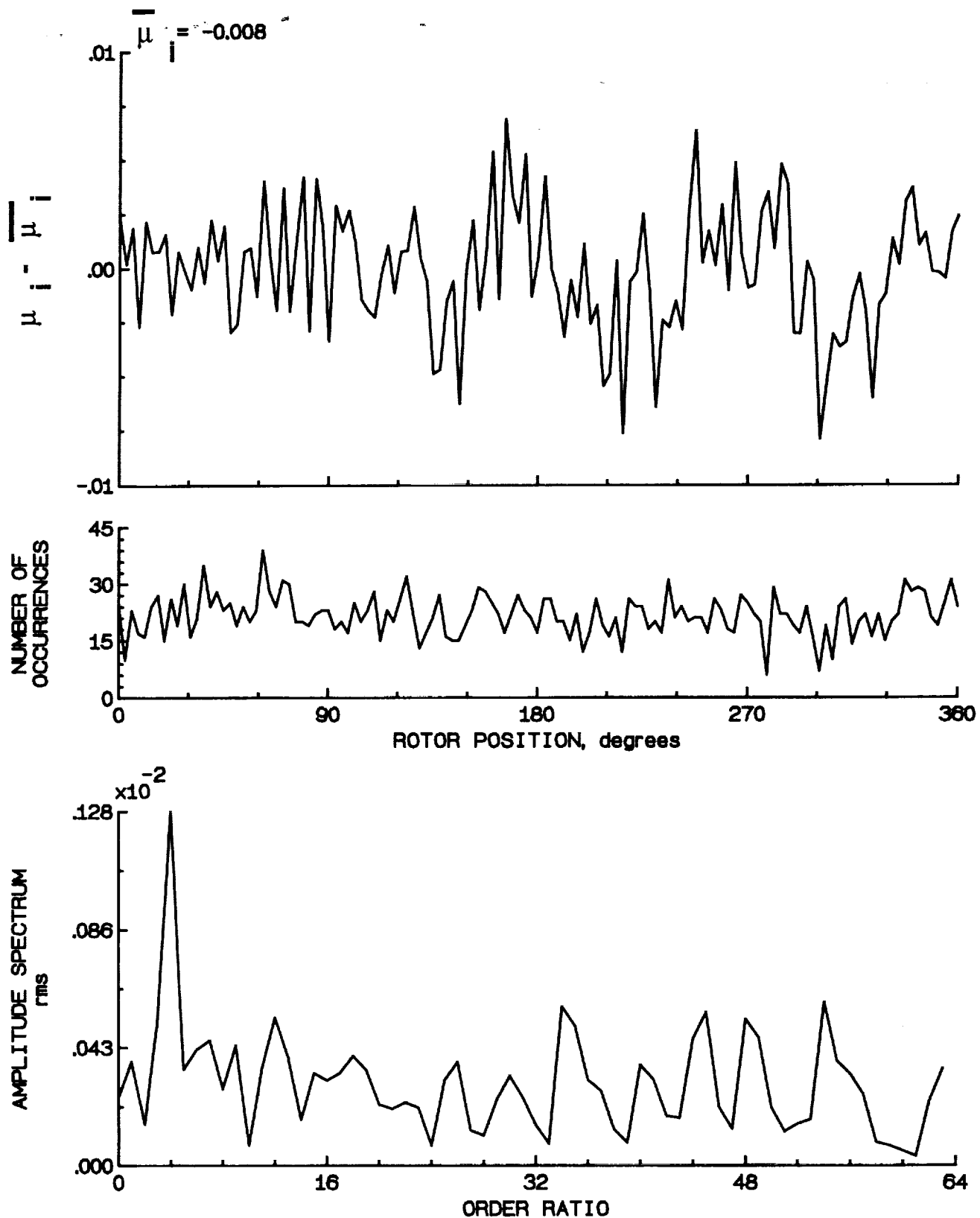


Figure 96.- Induced inflow velocity measured at 150 degrees and r/R of 0.90.

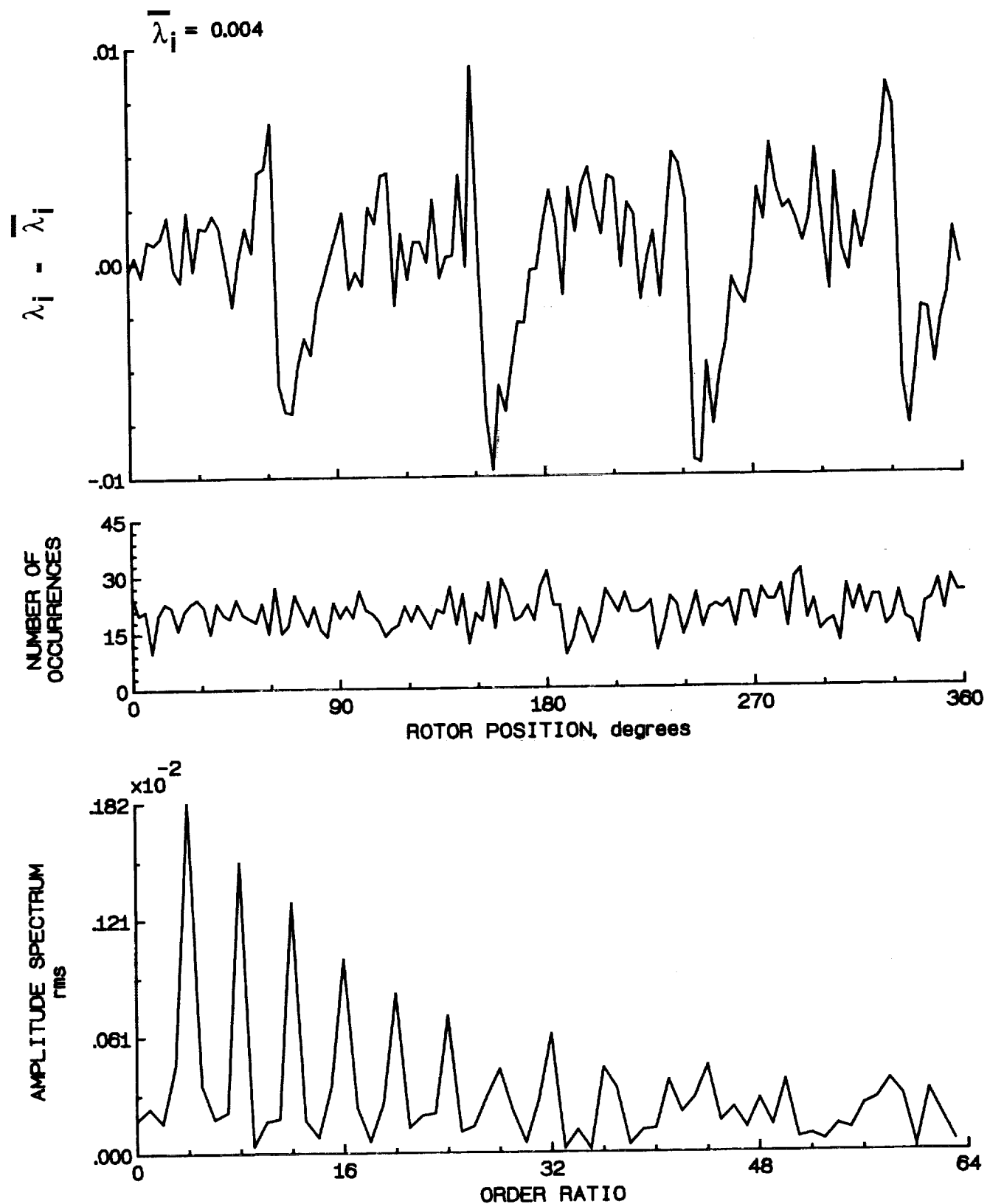


Figure 96.- Concluded.

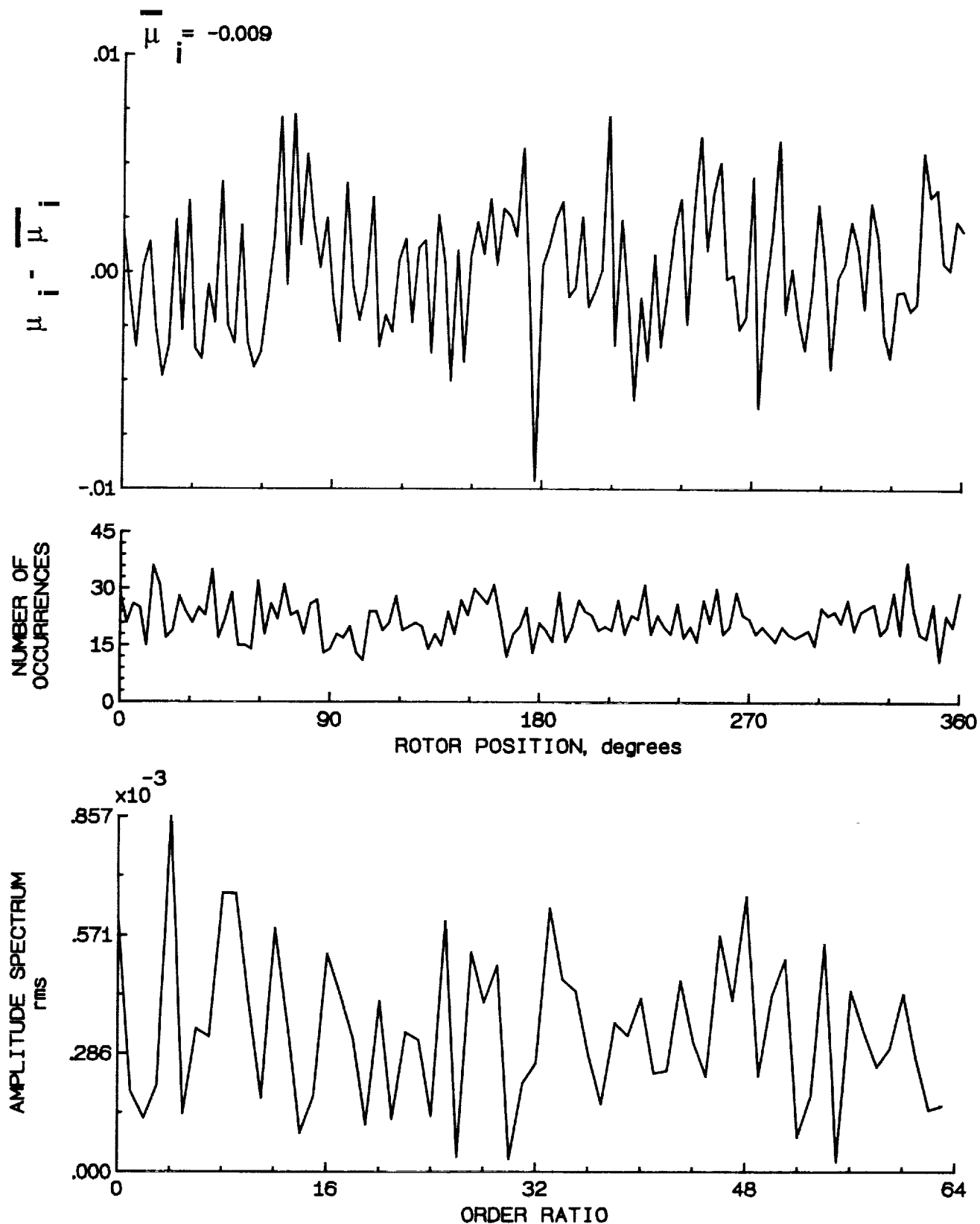


Figure 97.- Induced inflow velocity measured at 150 degrees and r/R of 0.94.

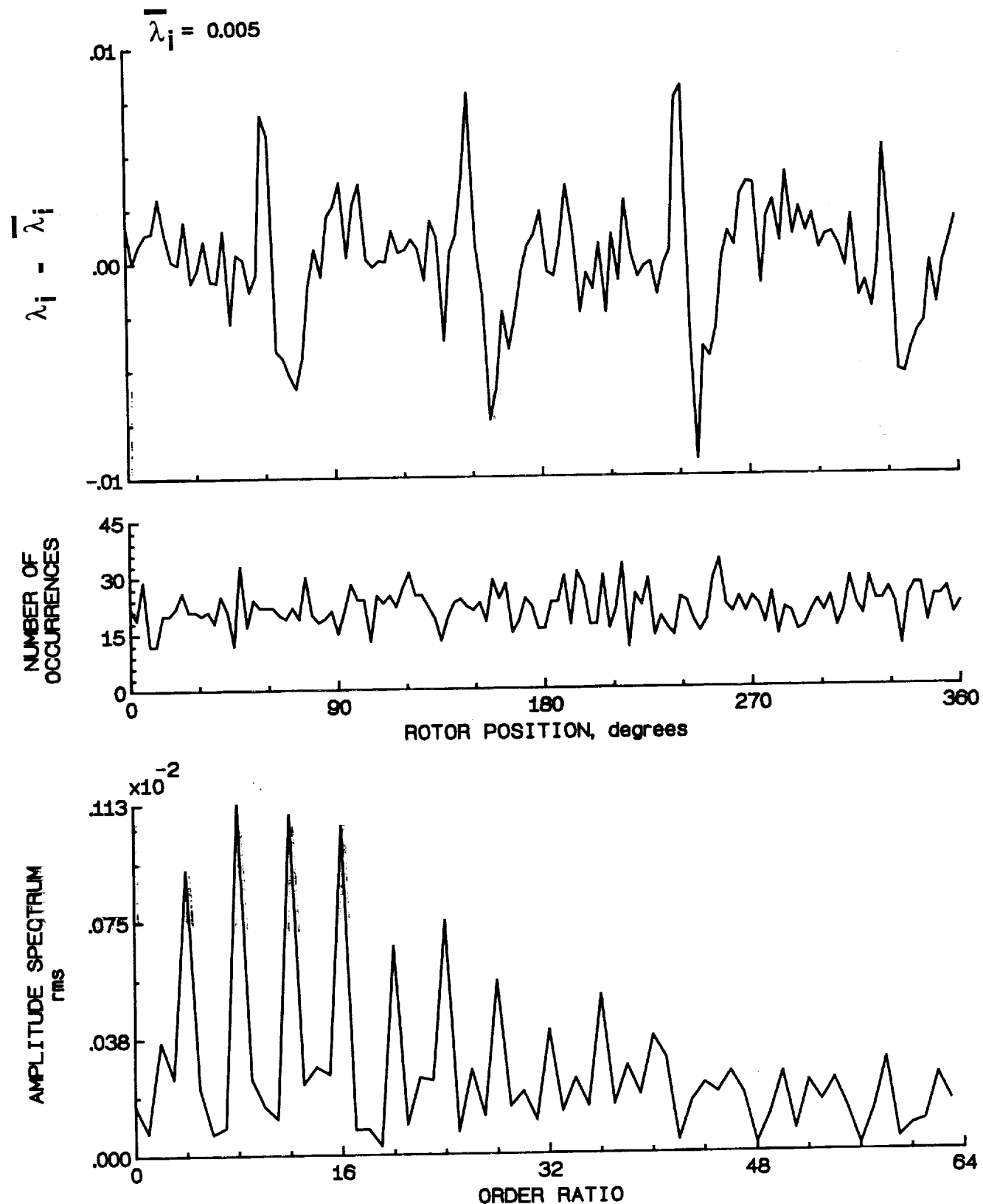


Figure 97.- Concluded.

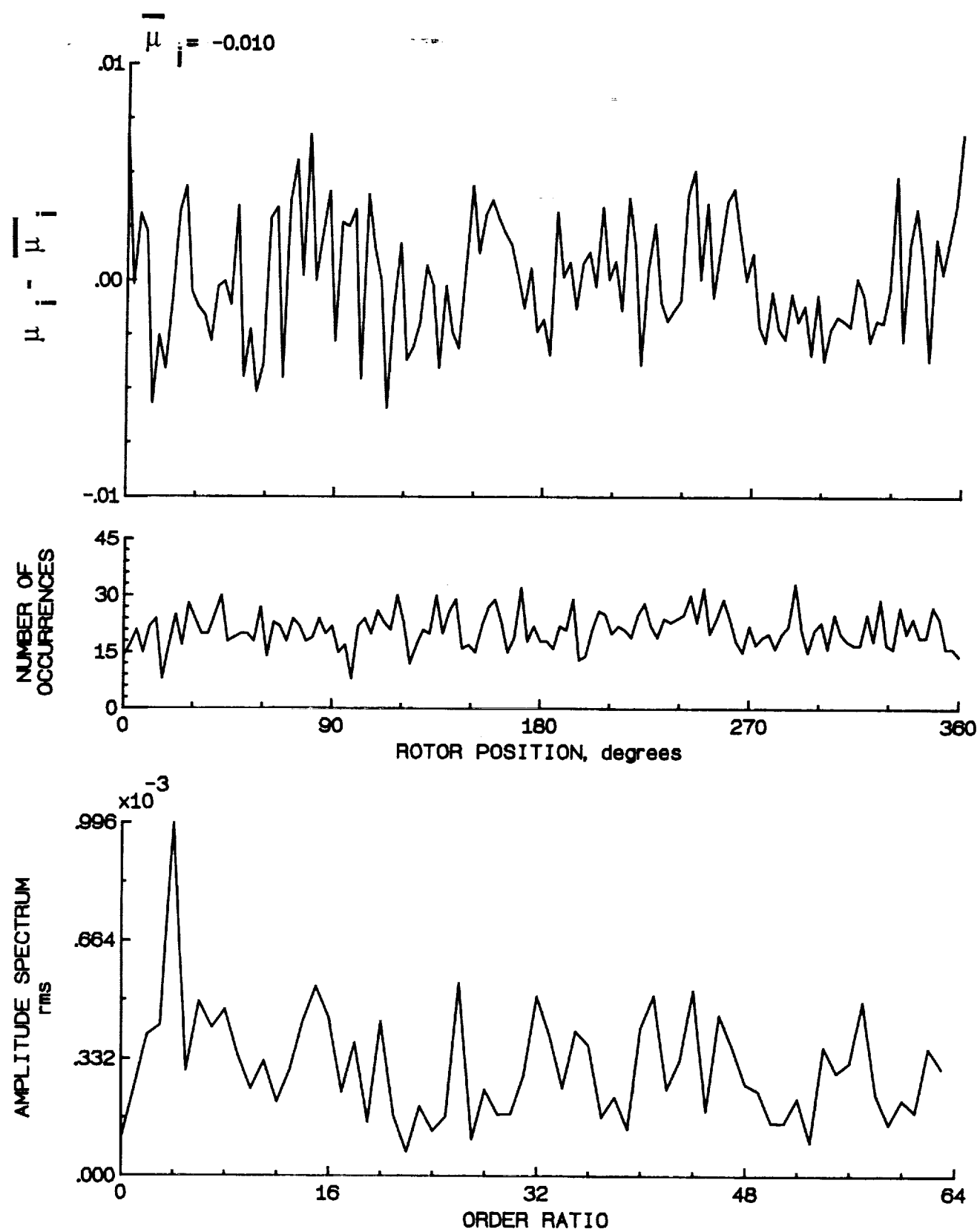


Figure 98.- Induced inflow velocity measured at 150 degrees and r/R of 0.98.

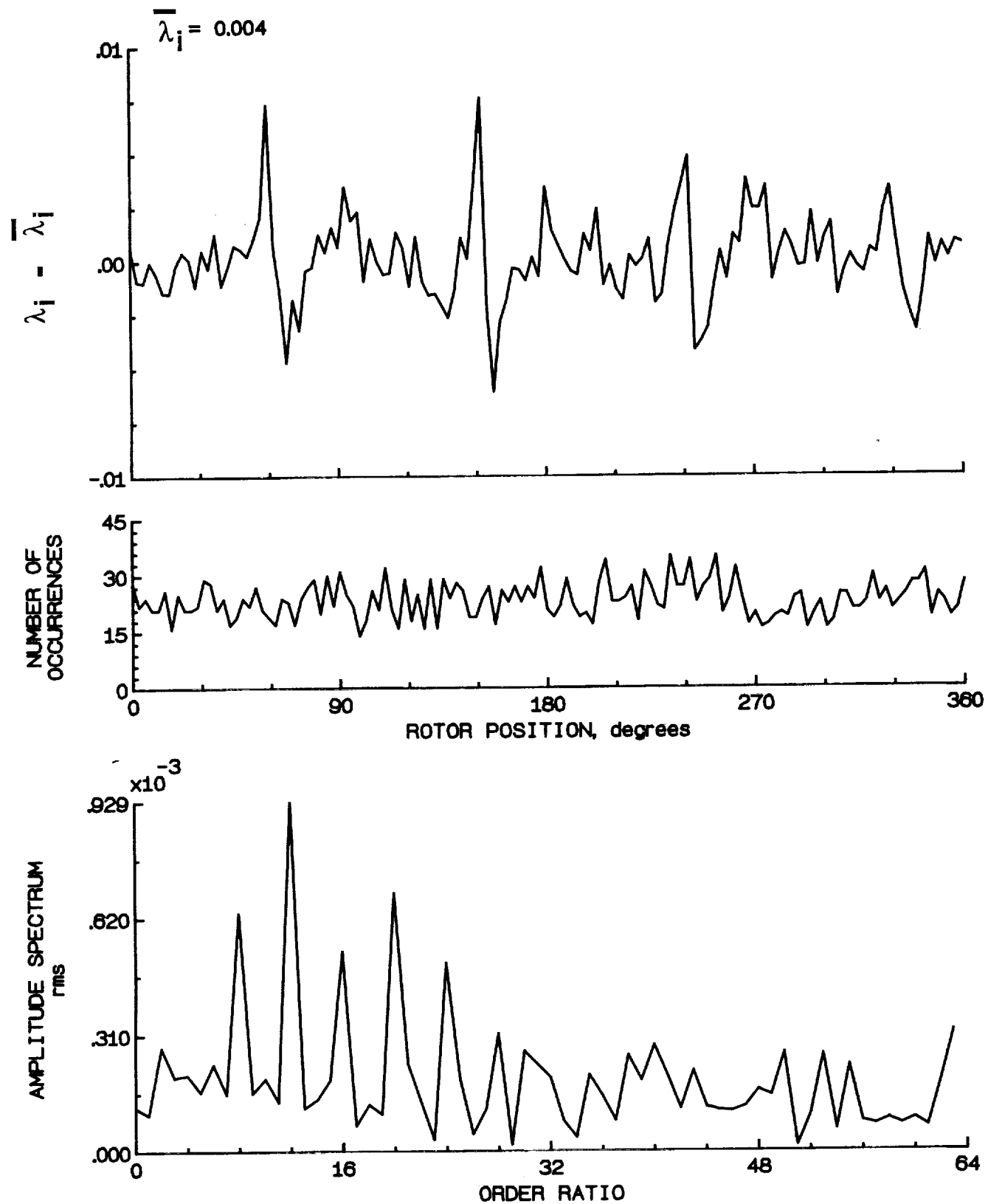


Figure 98.- Concluded.

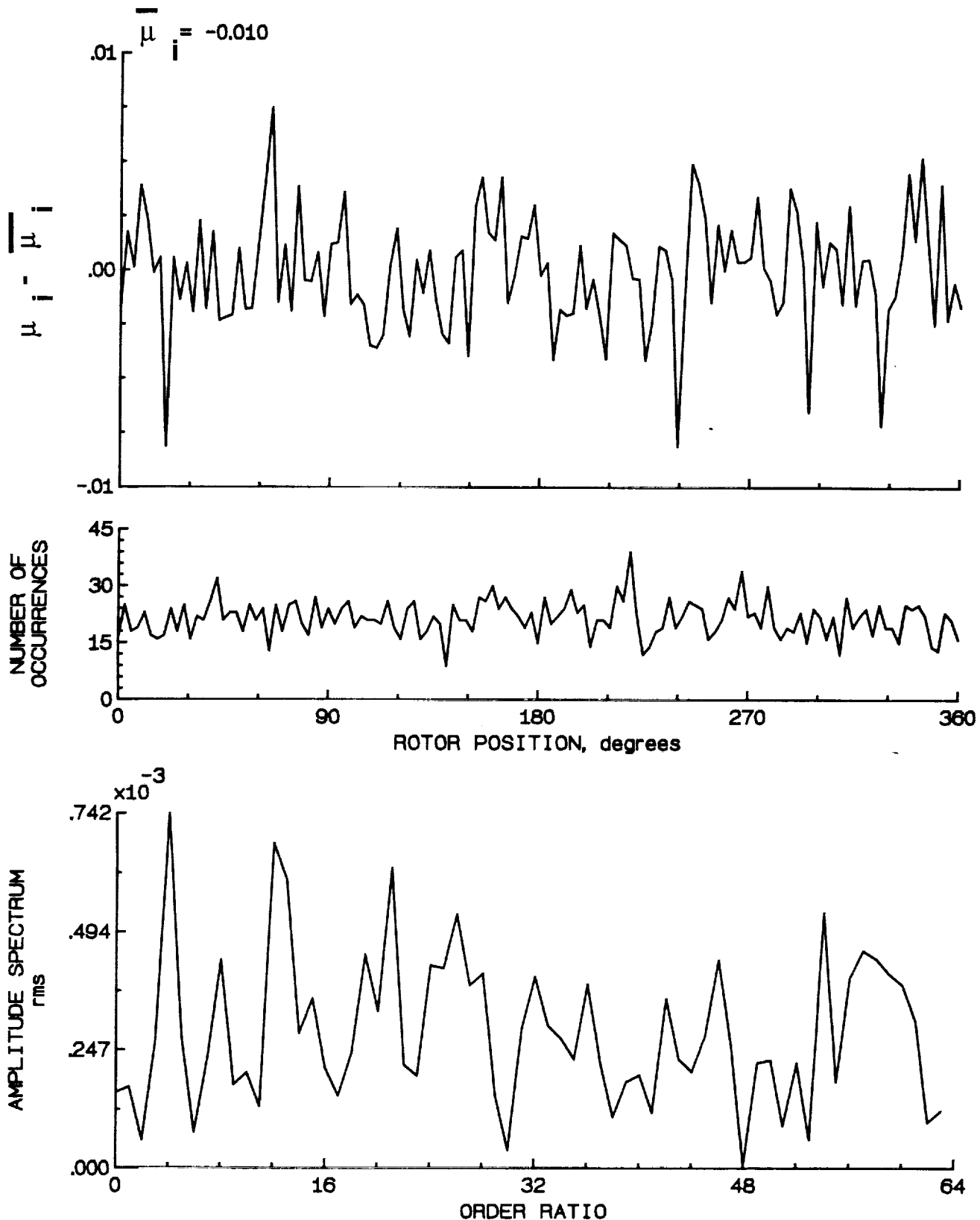


Figure 99.- Induced inflow velocity measured at 150 degrees and r/R of 1.02.

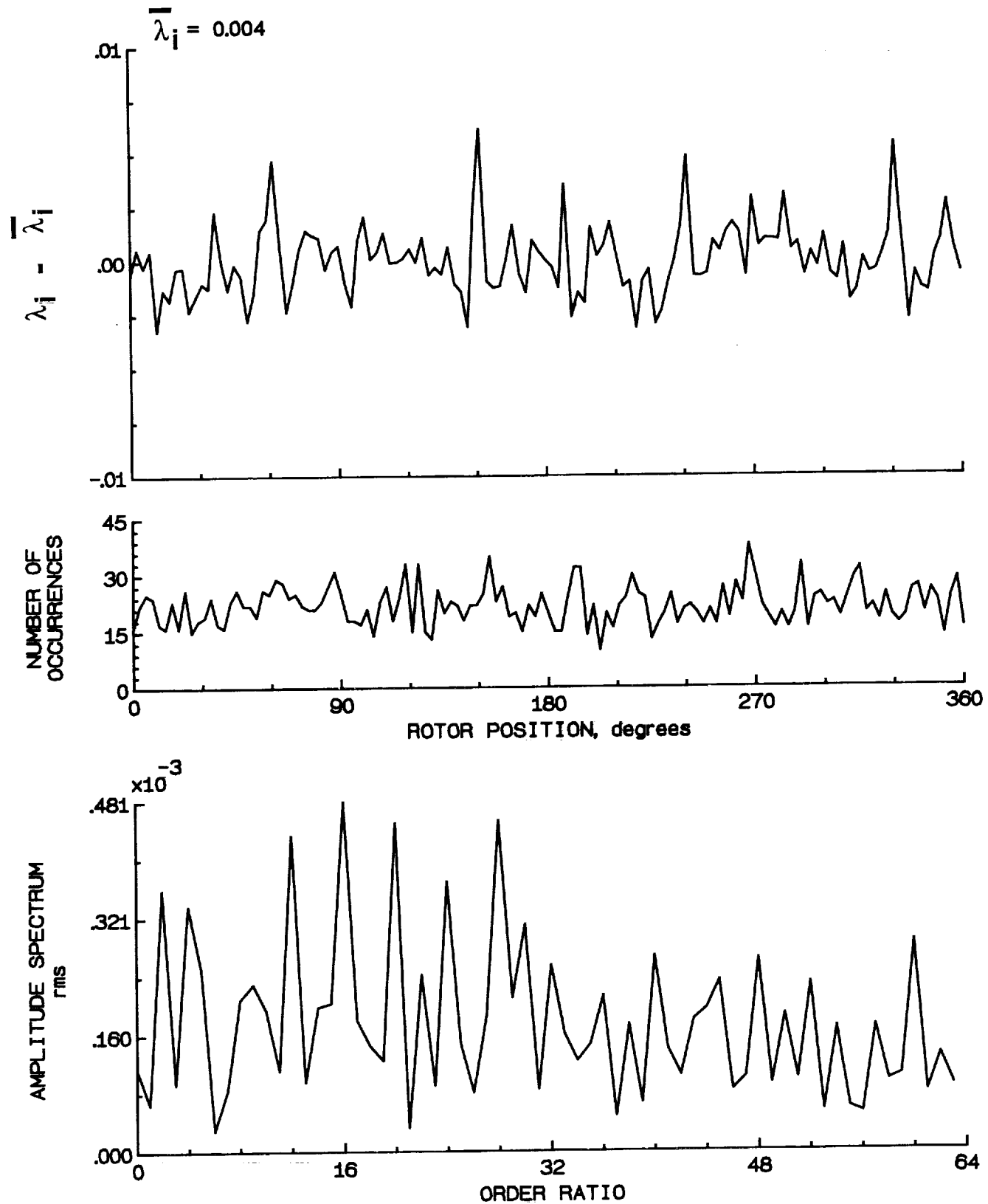


Figure 99.- Concluded.

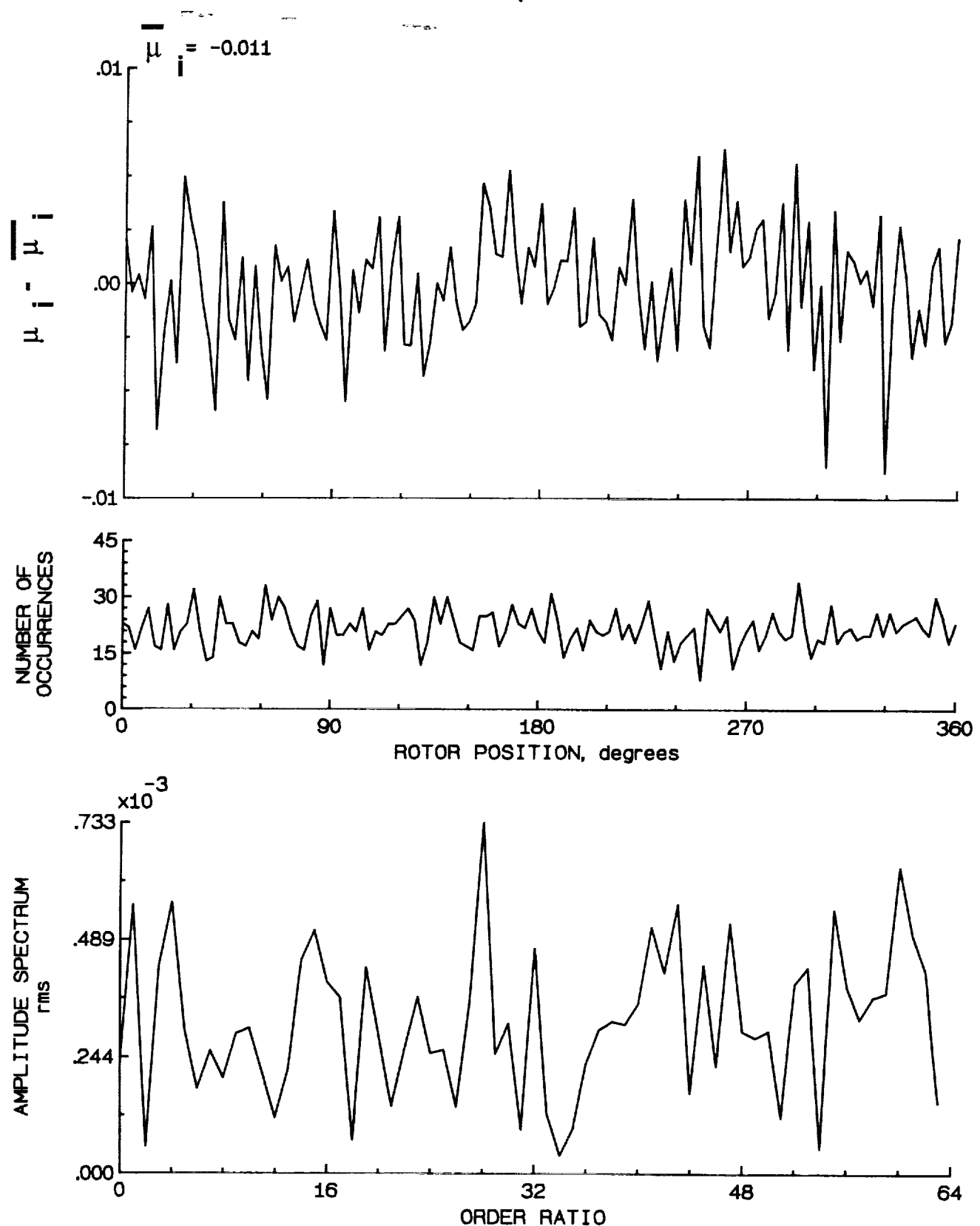


Figure 100.- Induced inflow velocity measured at 150 degrees and r/R of 1.04.

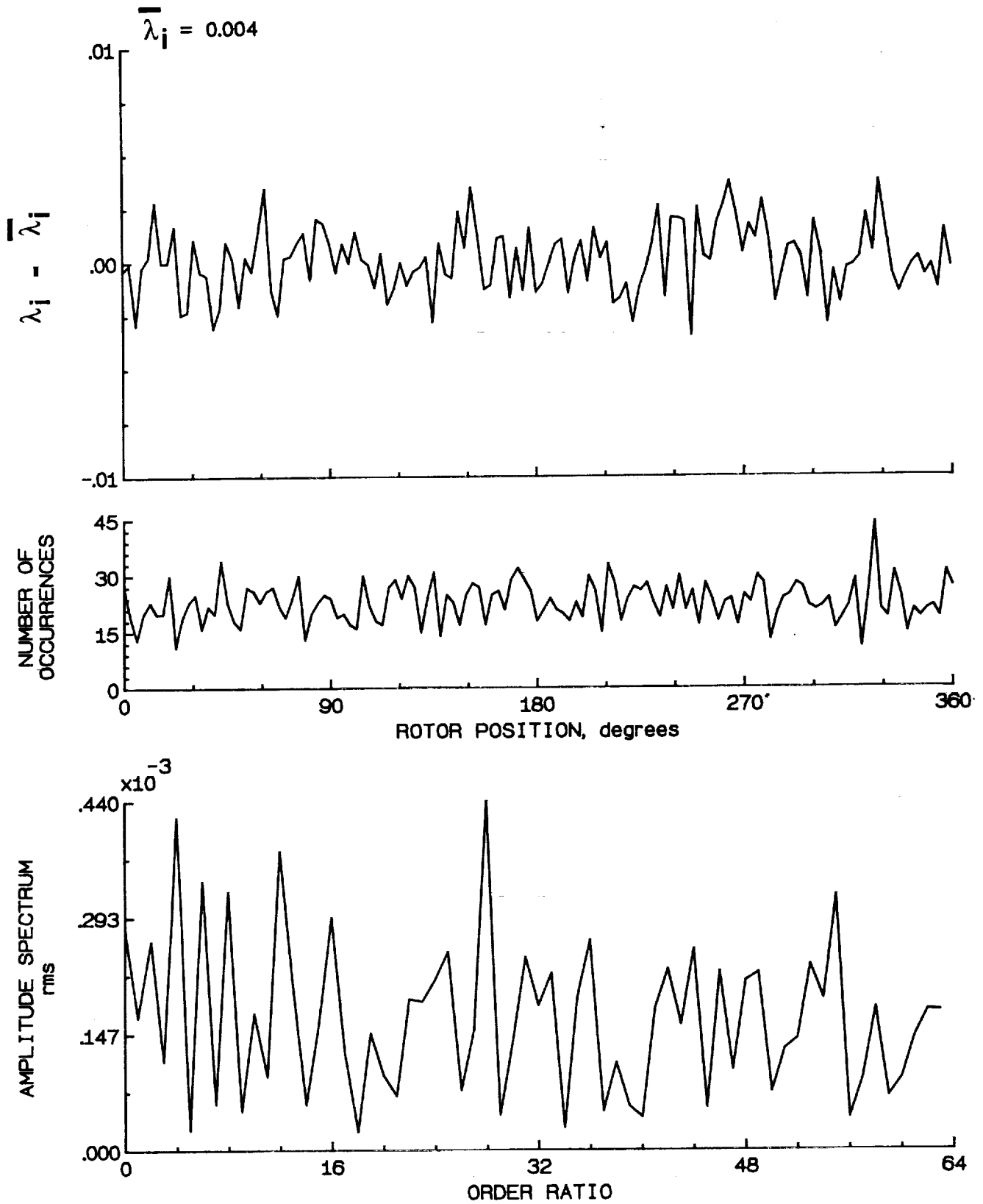


Figure 100.- Concluded.

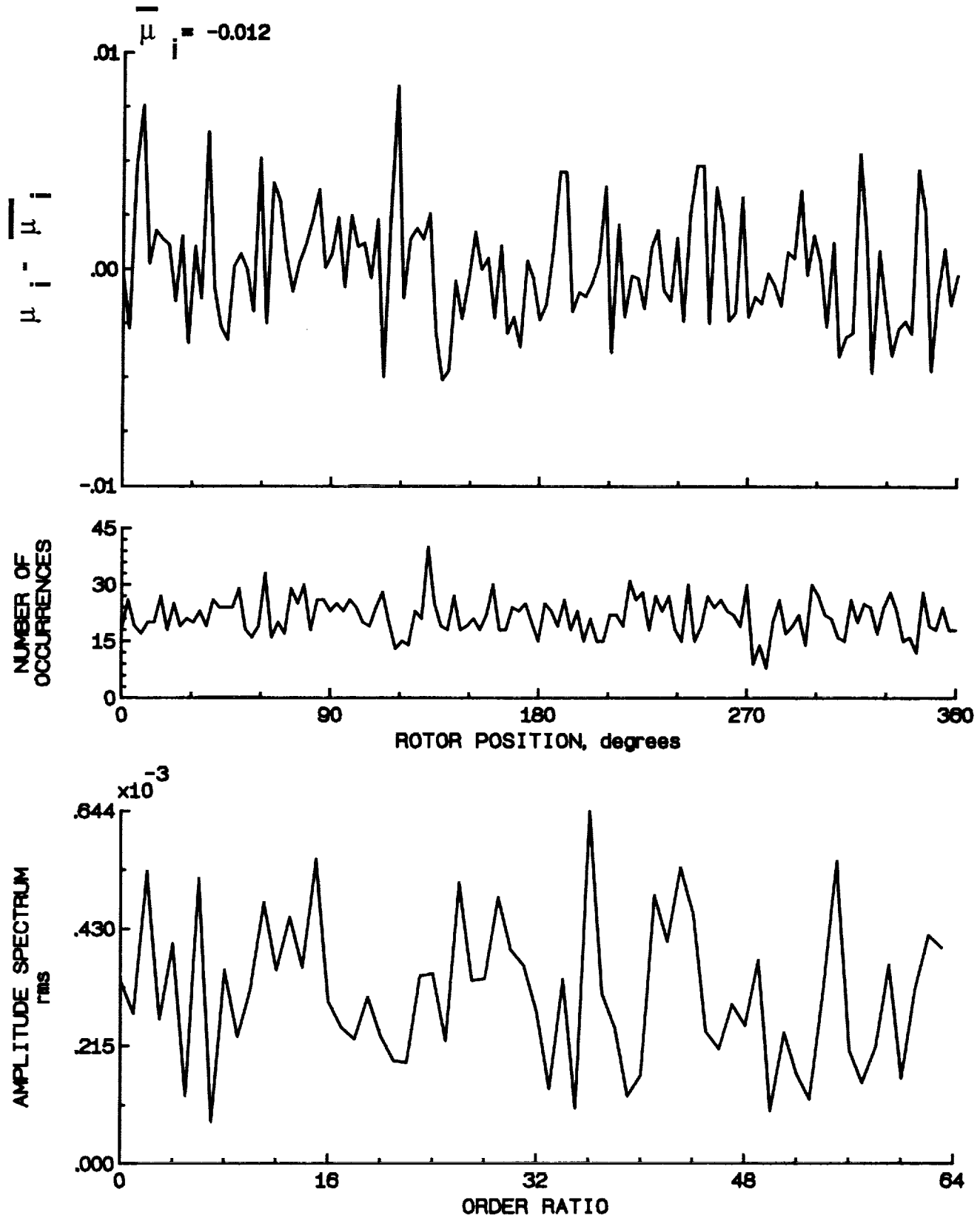


Figure 101.- Induced inflow velocity measured at 150 degrees and r/R of 1.10.

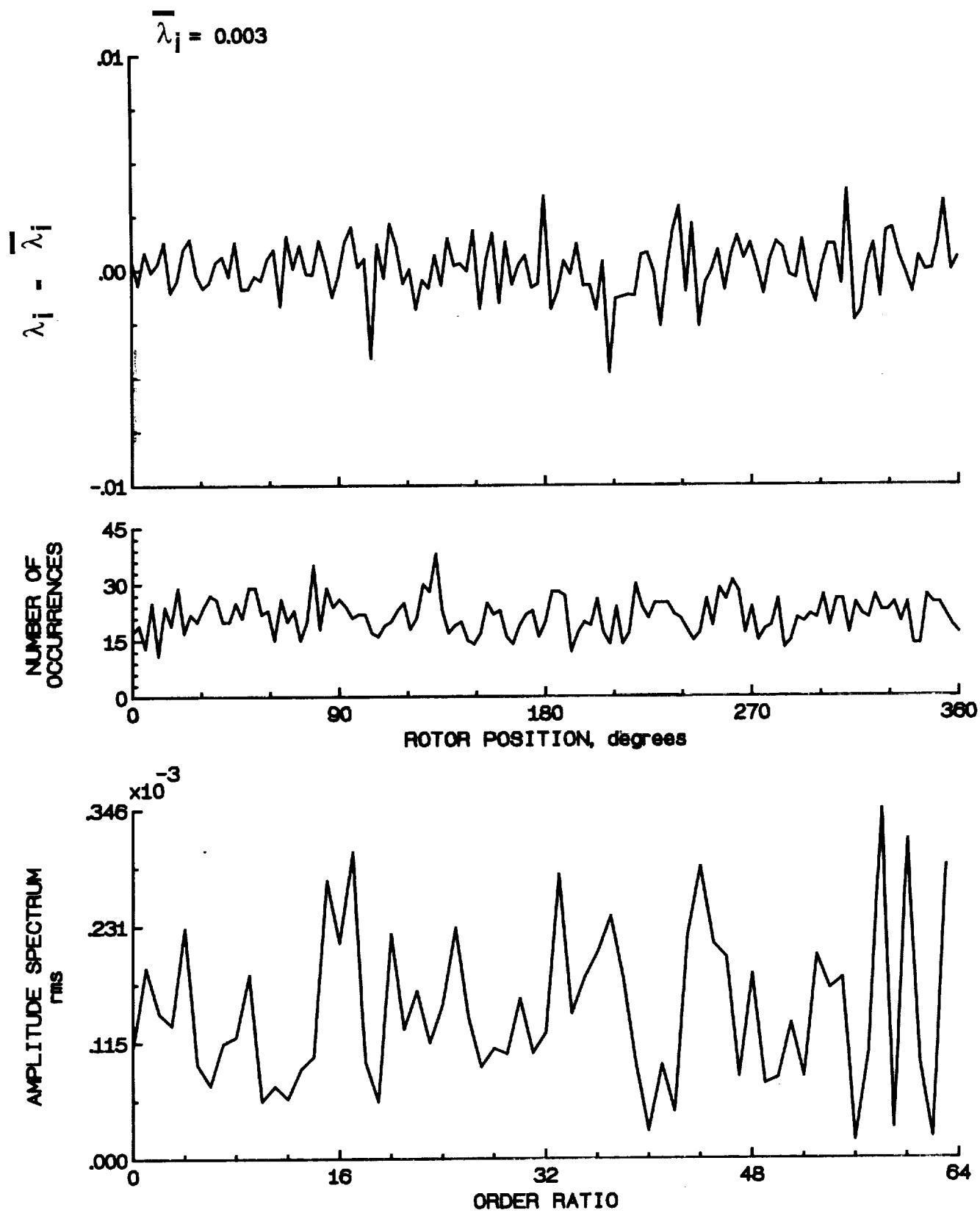


Figure 101.- Concluded.

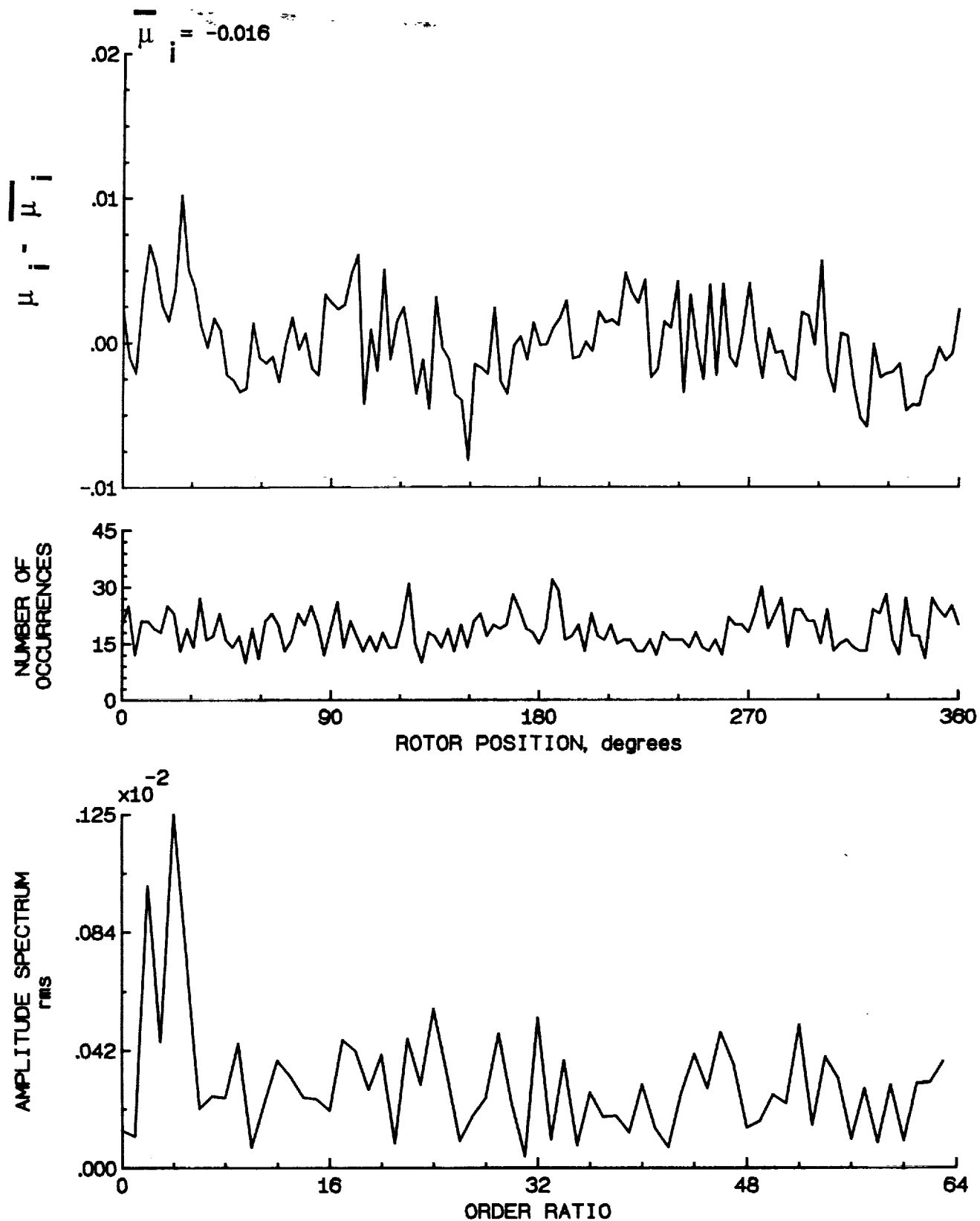


Figure 102.- Induced inflow velocity measured at 180 degrees and r/R of 0.20.

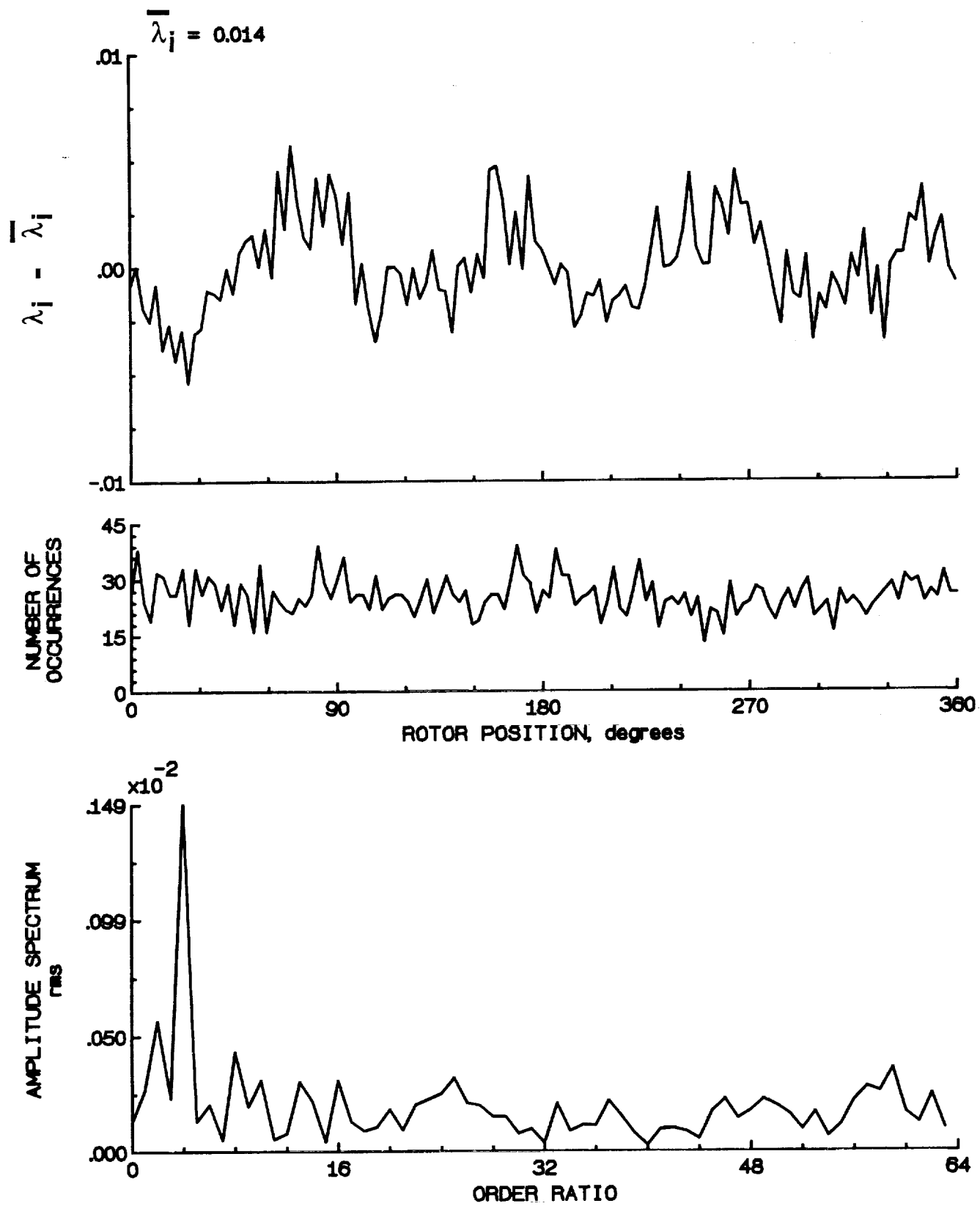


Figure 102.- Concluded.

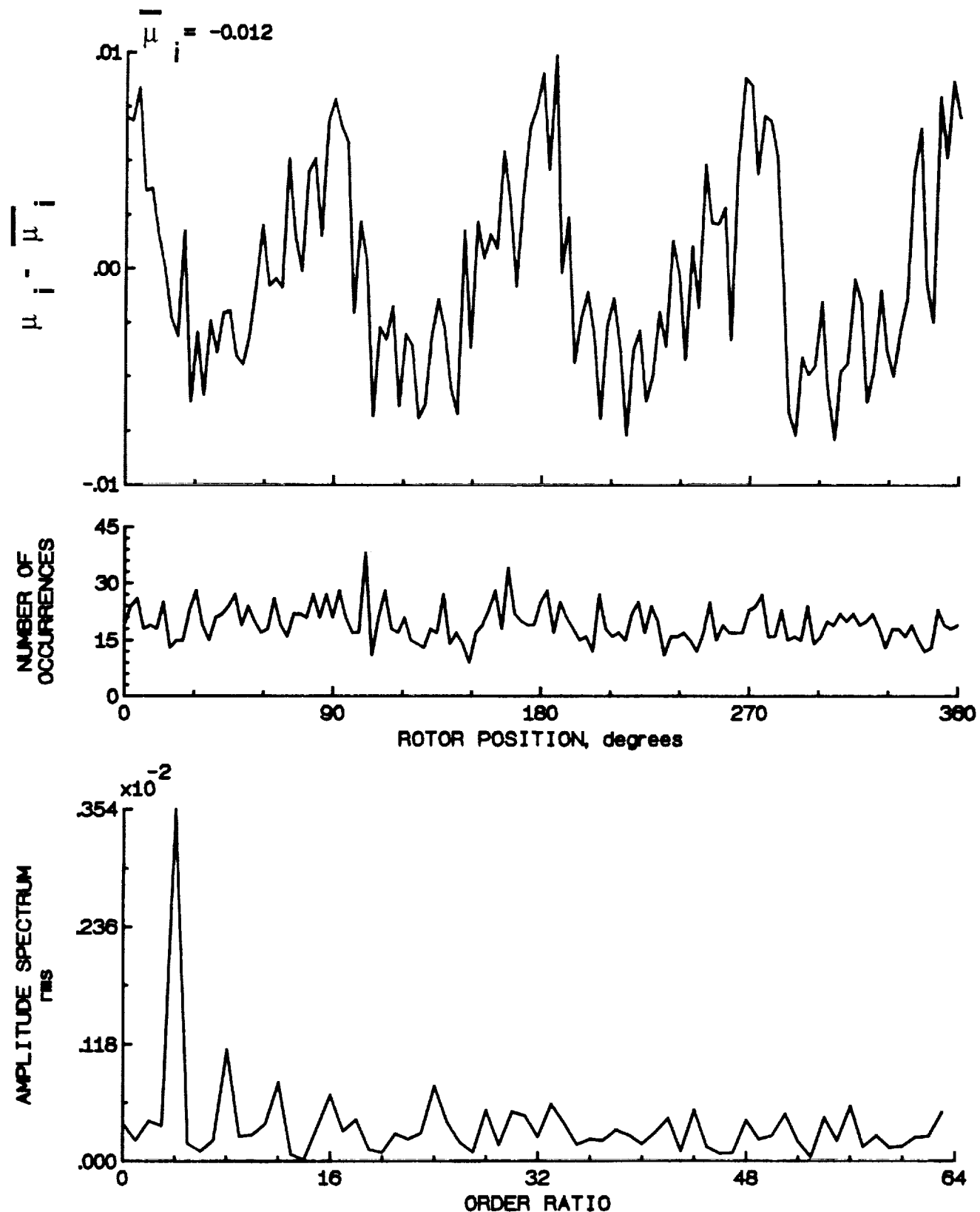


Figure 103.- Induced inflow velocity measured at 180 degrees and r/R of 0.40.

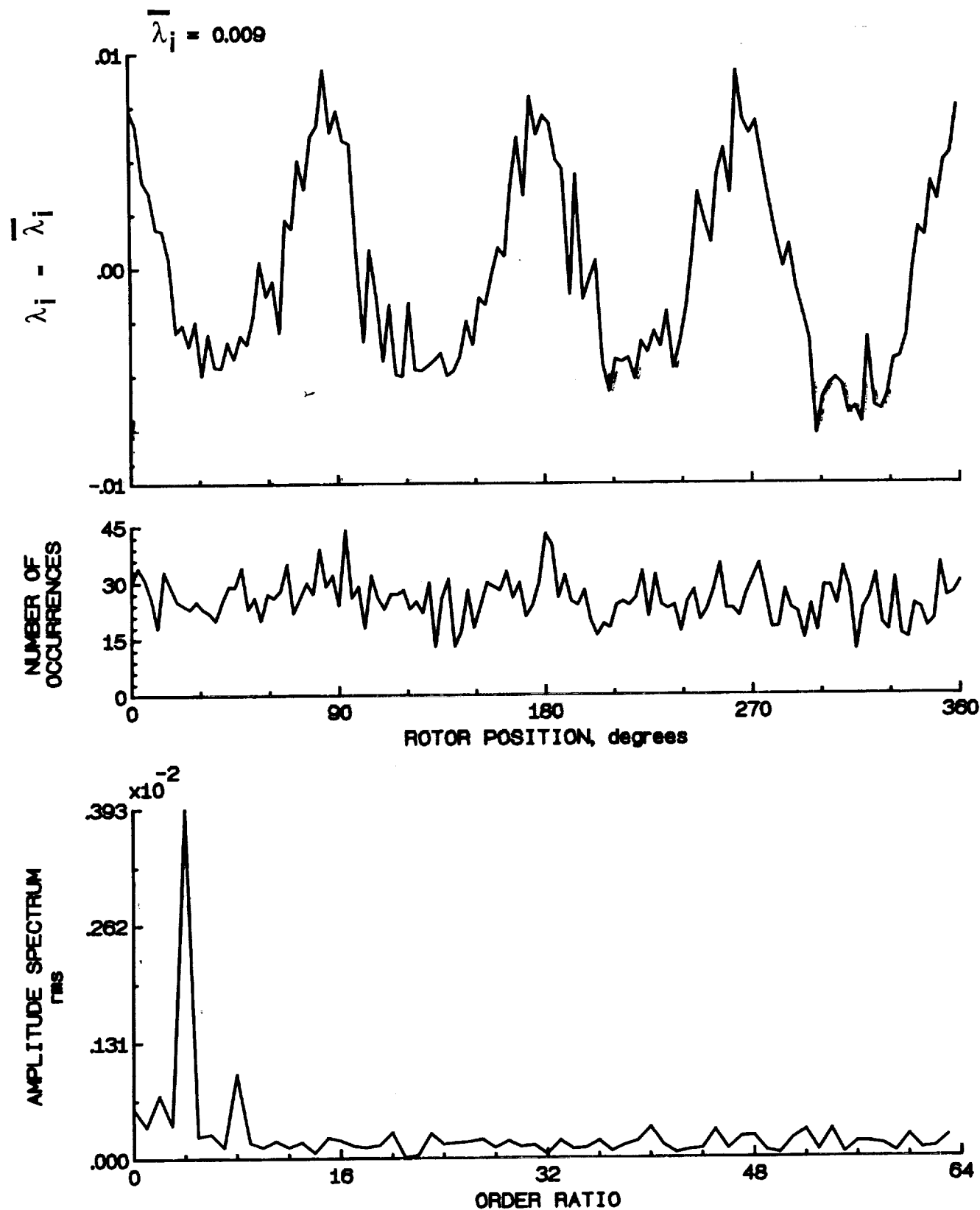


Figure 103.- Concluded.

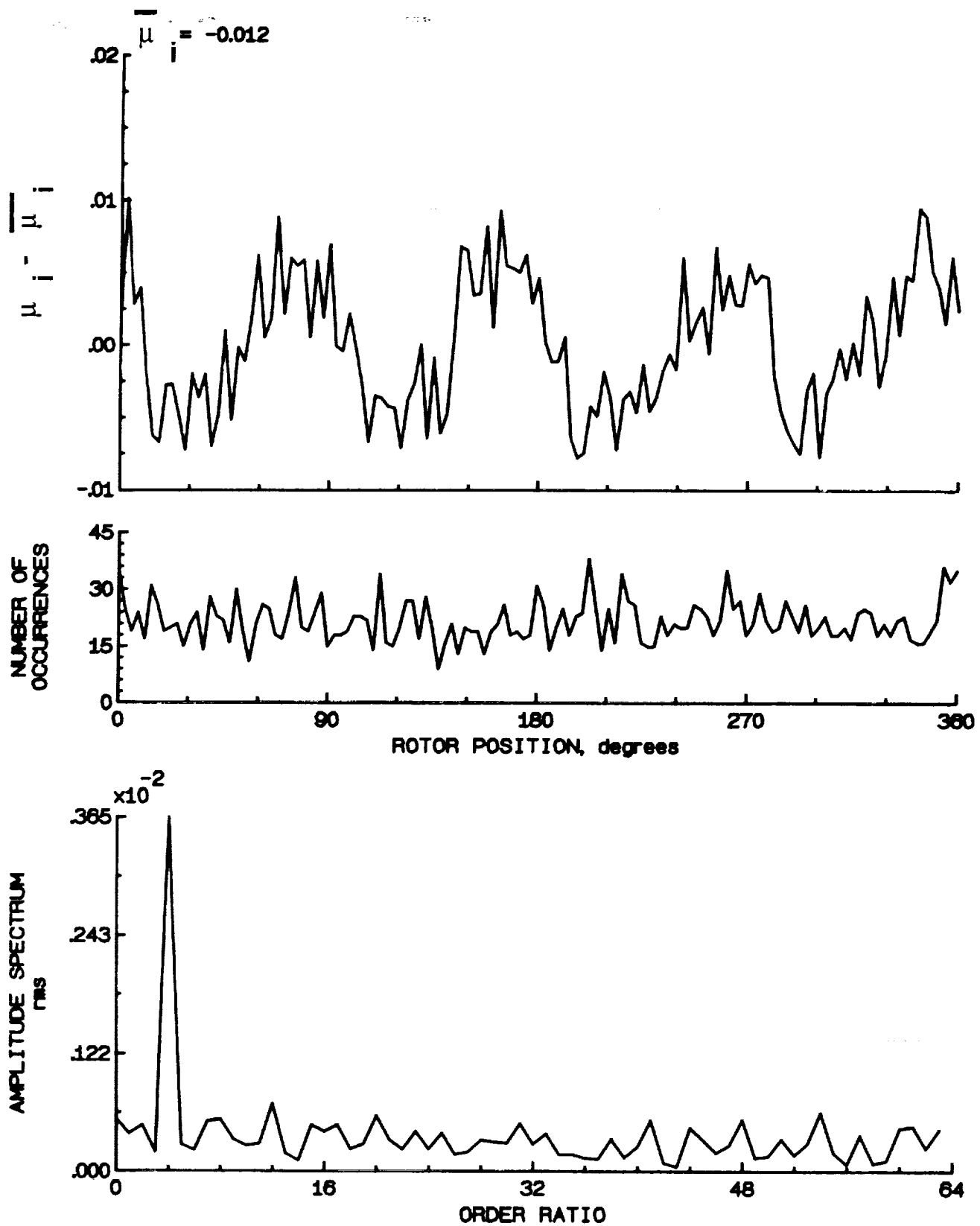


Figure 104.- Induced inflow velocity measured at 180 degrees and r/R of 0.50.

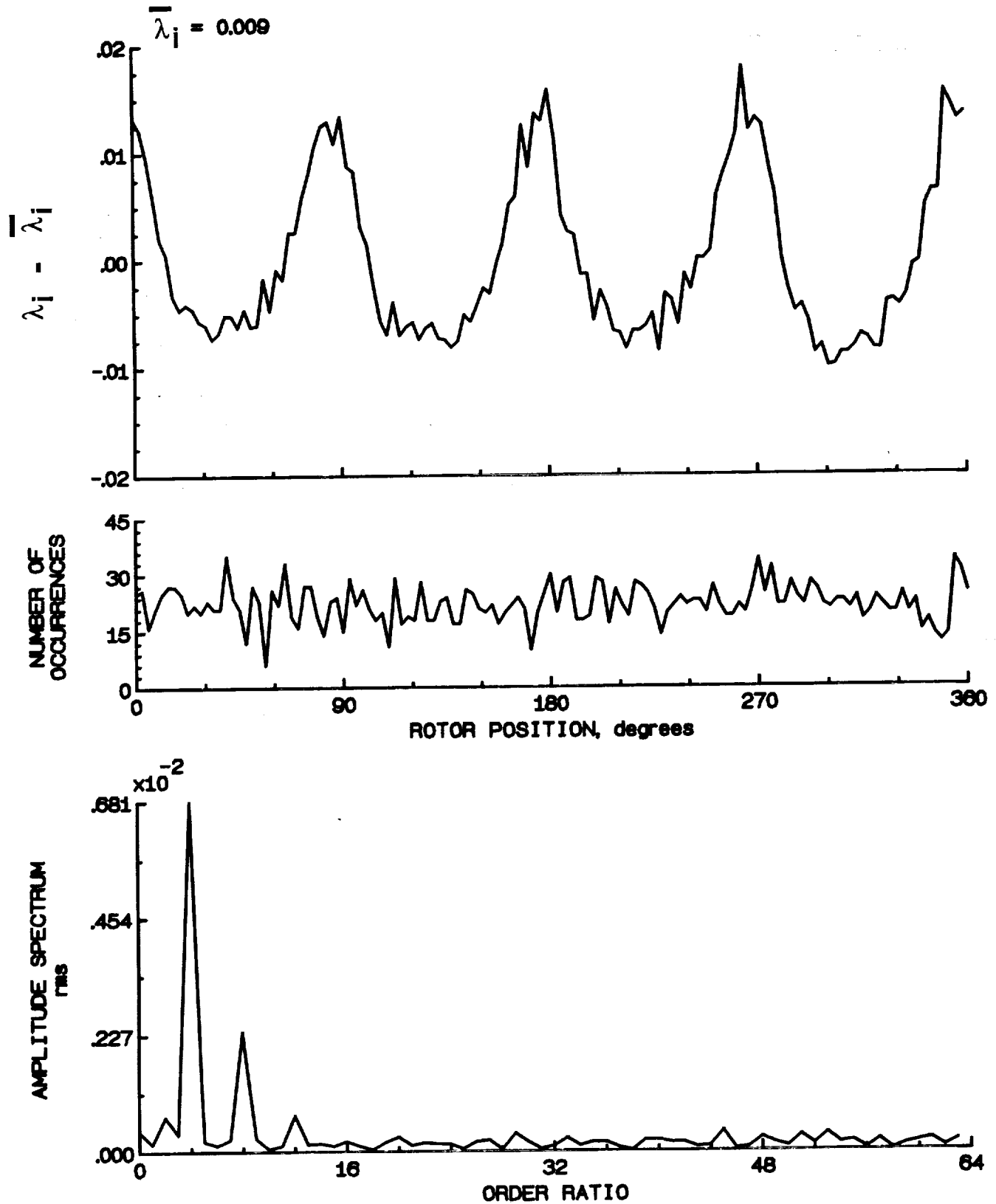


Figure 104.- Concluded.

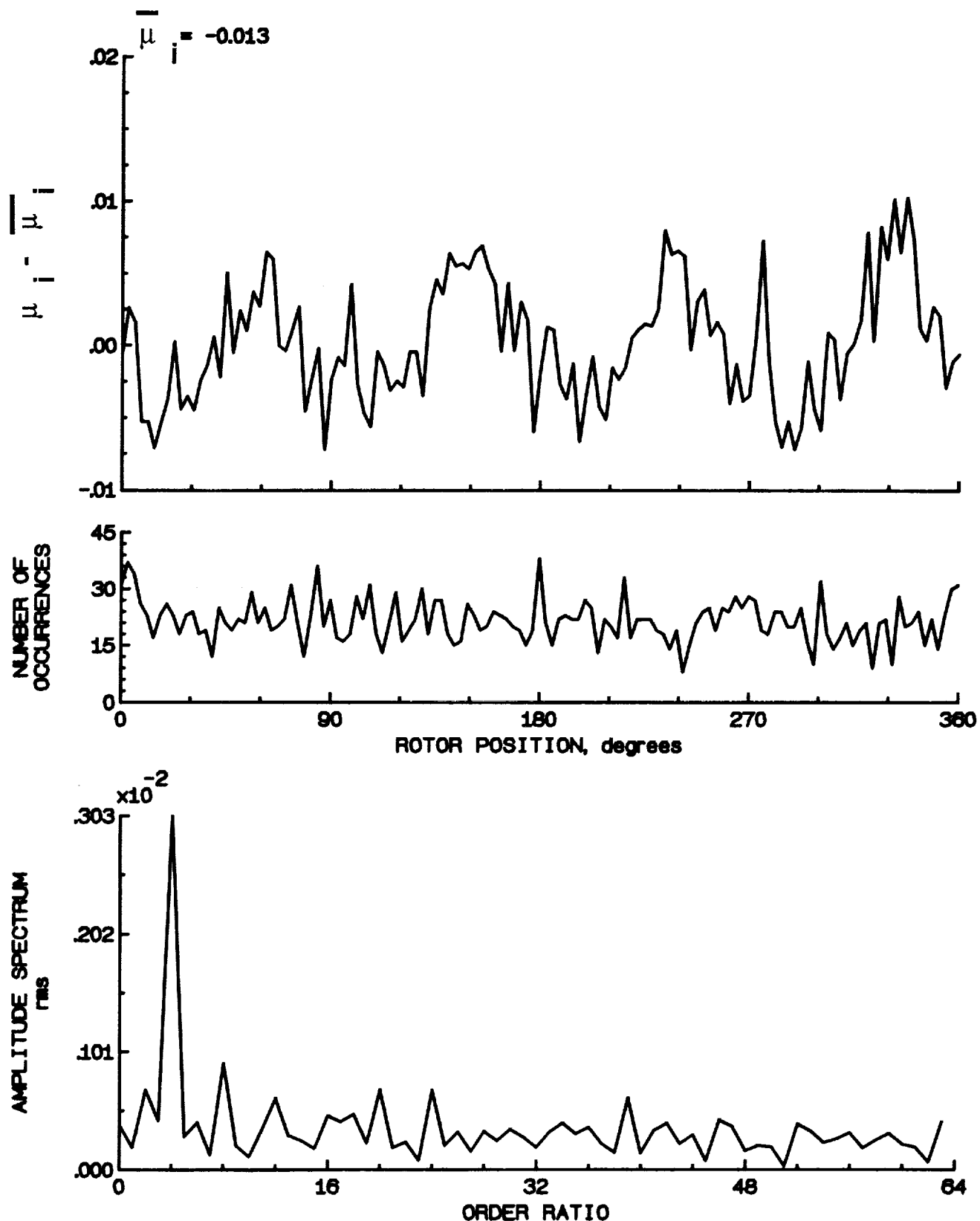


Figure 105.- Induced inflow velocity measured at 180 degrees and r/R of 0.60.

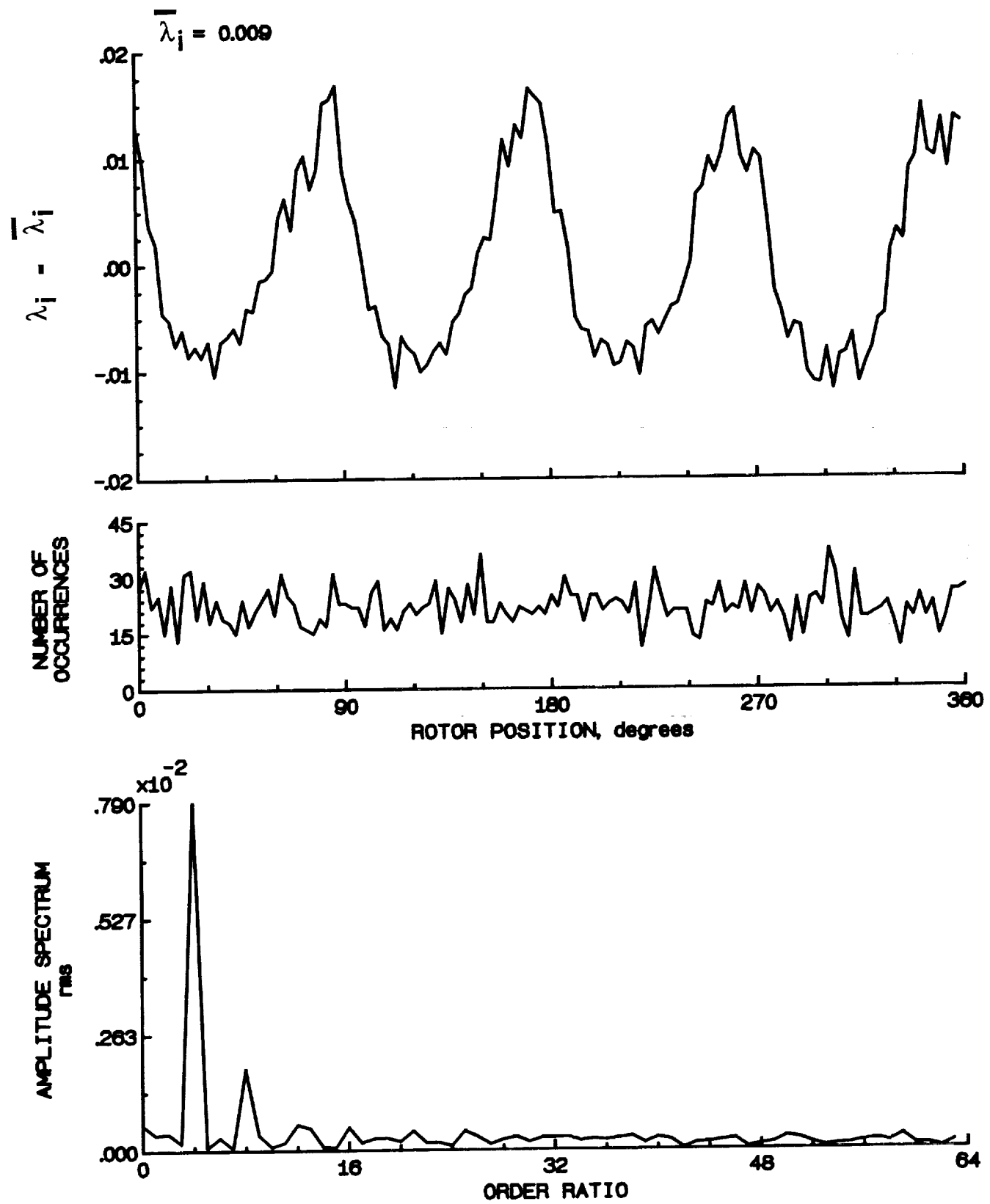


Figure 105.- Concluded.

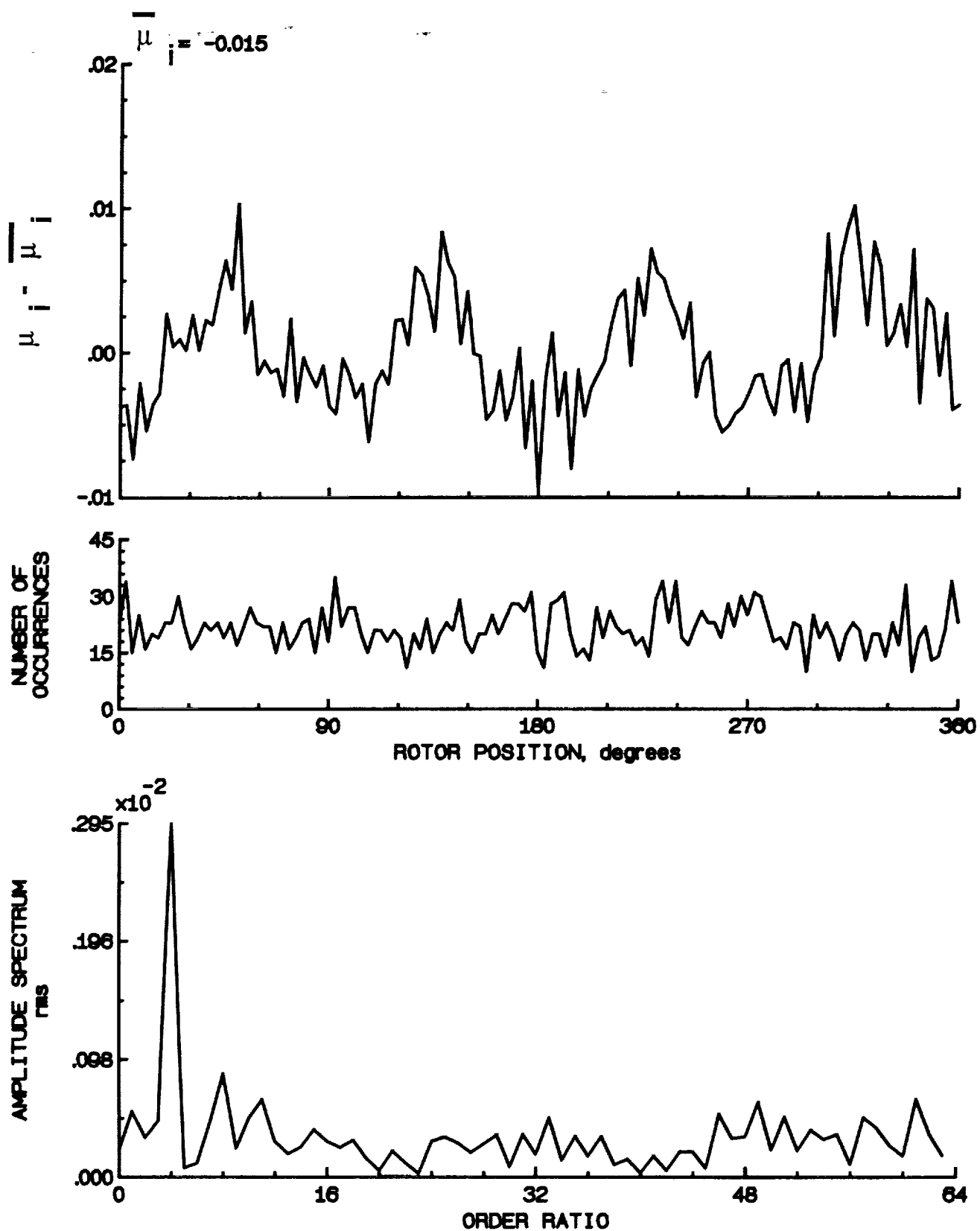


Figure 106.- Induced inflow velocity measured at 180 degrees and r/R of 0.70.

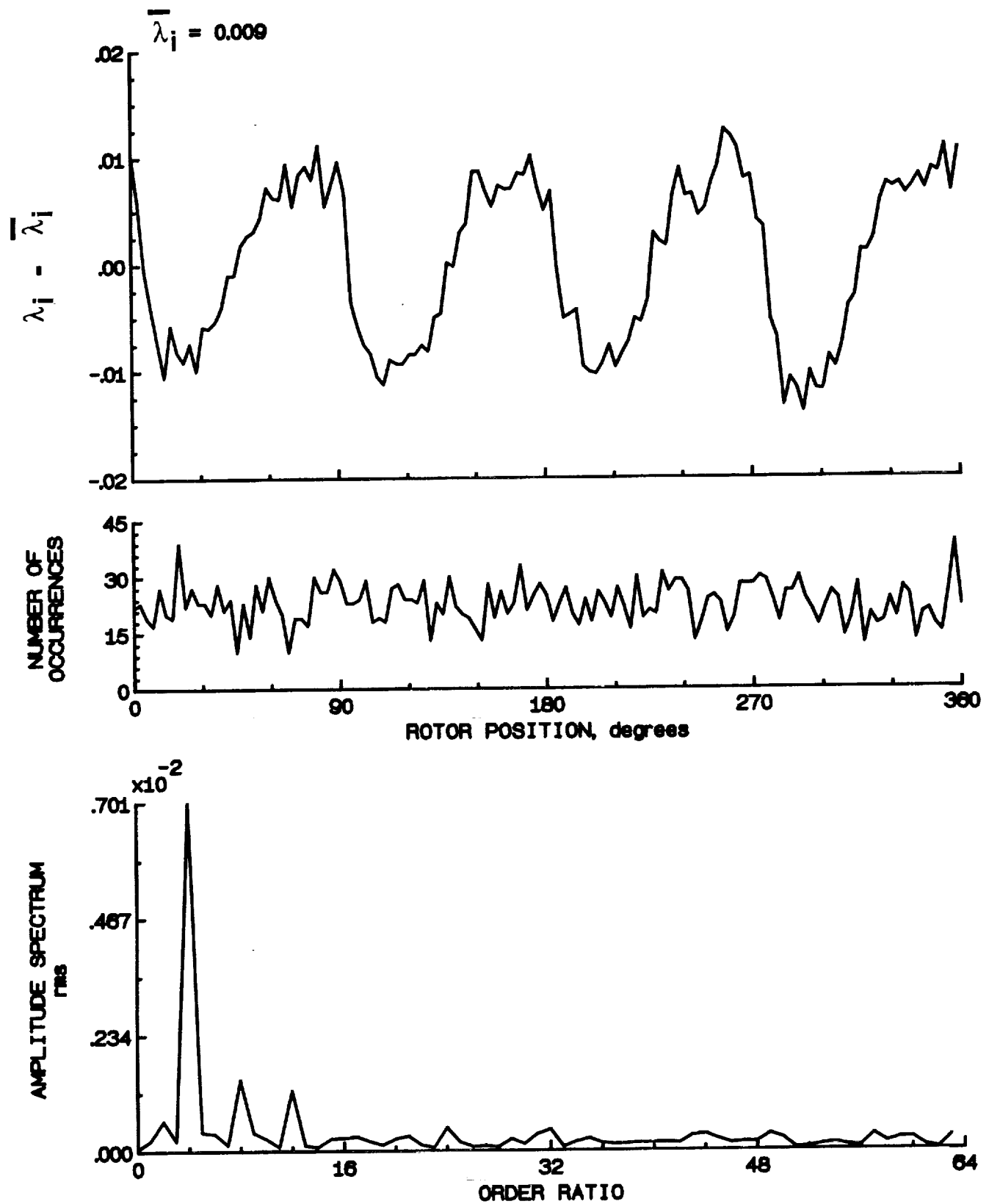


Figure 106.- Concluded.

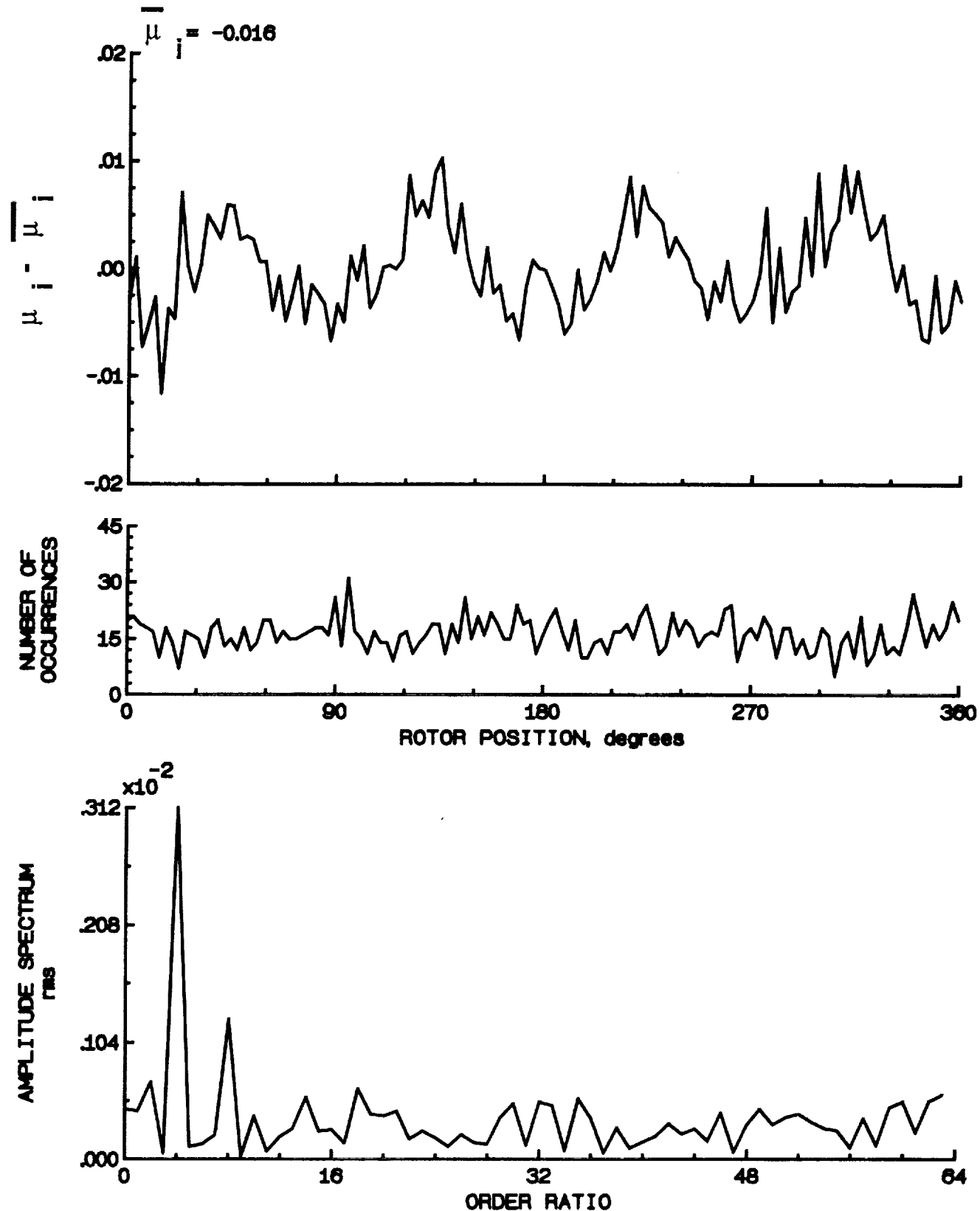


Figure 107.- Induced inflow velocity measured at 180 degrees and r/R of 0.74.

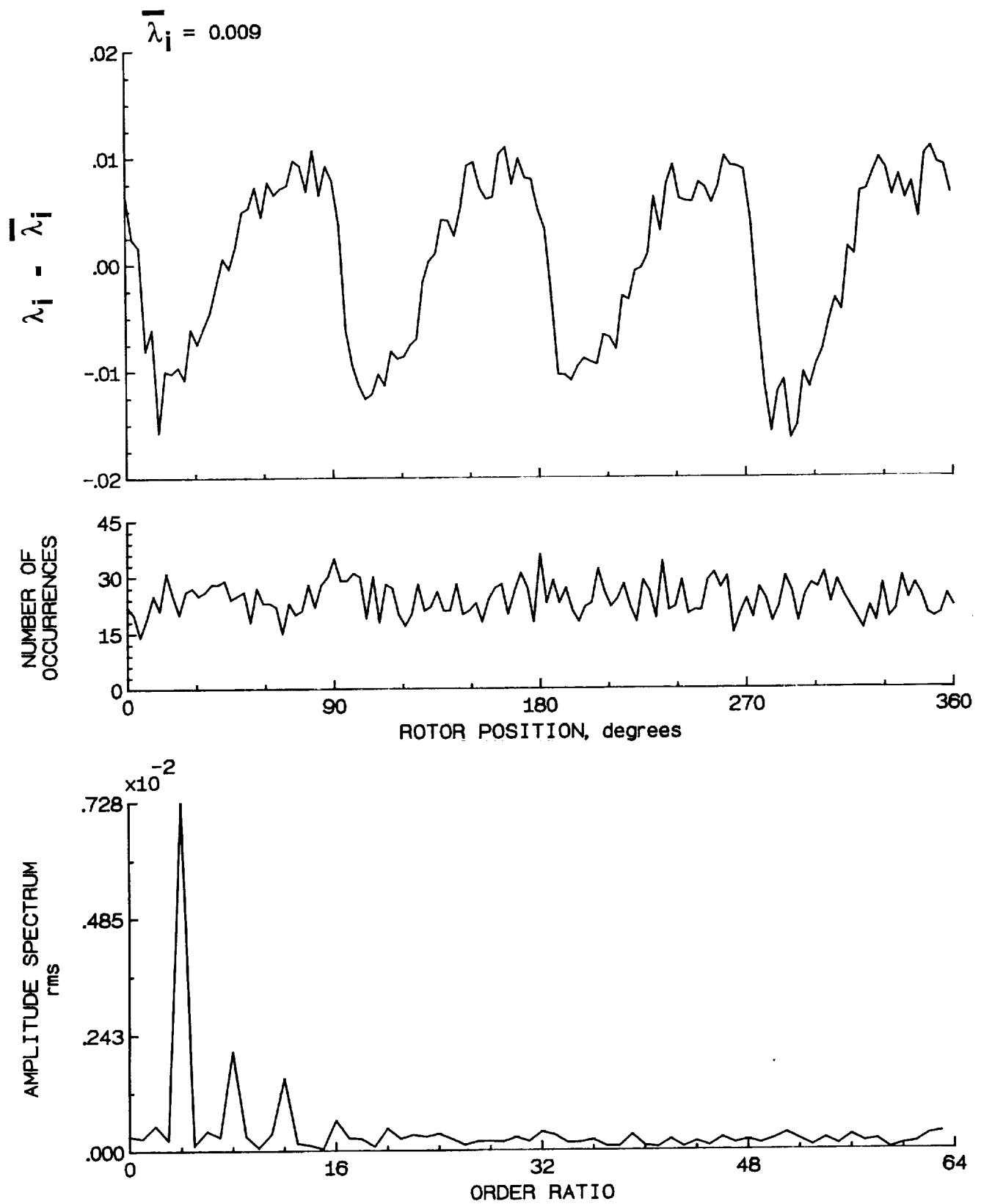


Figure 107.- Concluded.

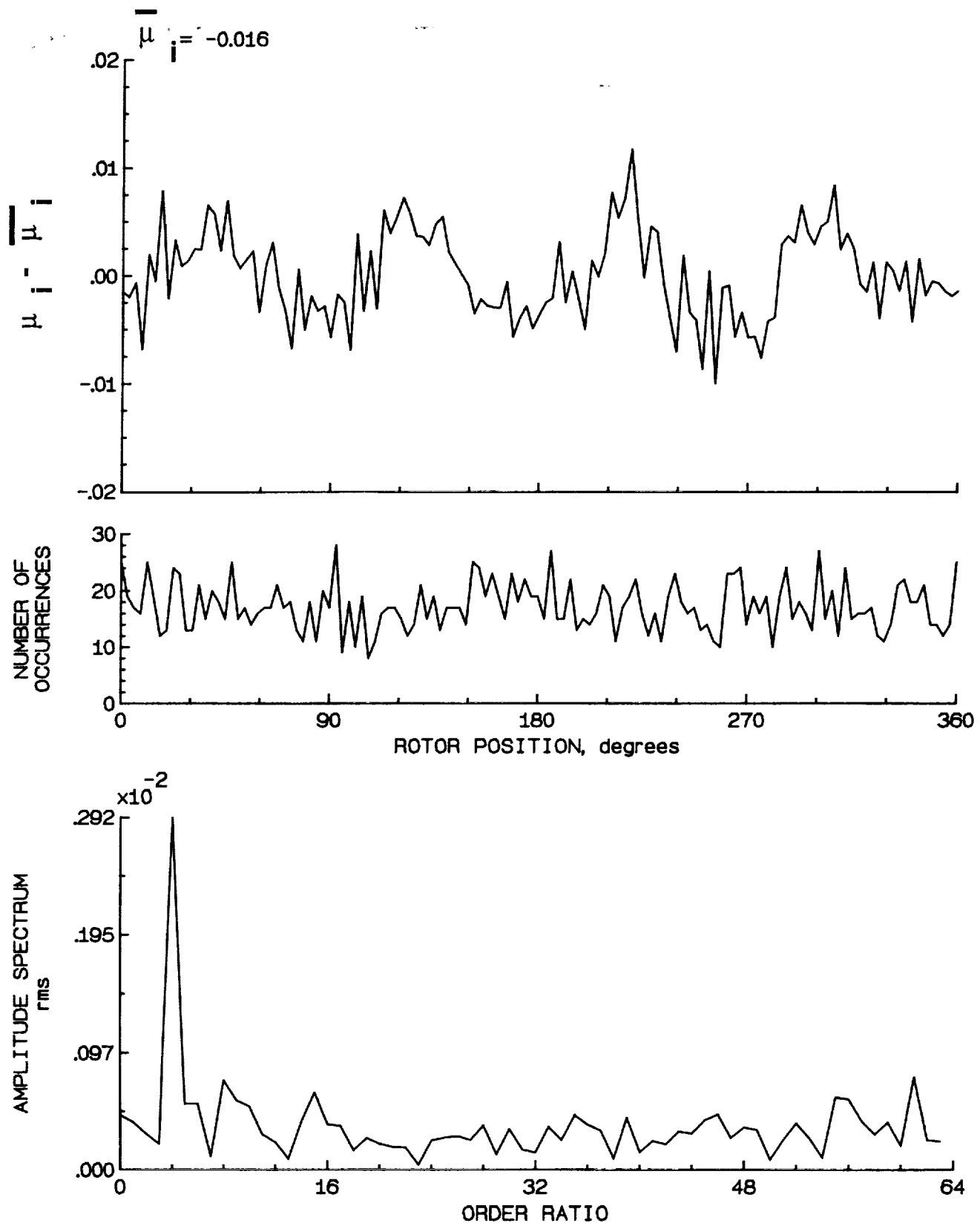


Figure 108.- Induced inflow velocity measured at 180 degrees and r/R of 0.78.

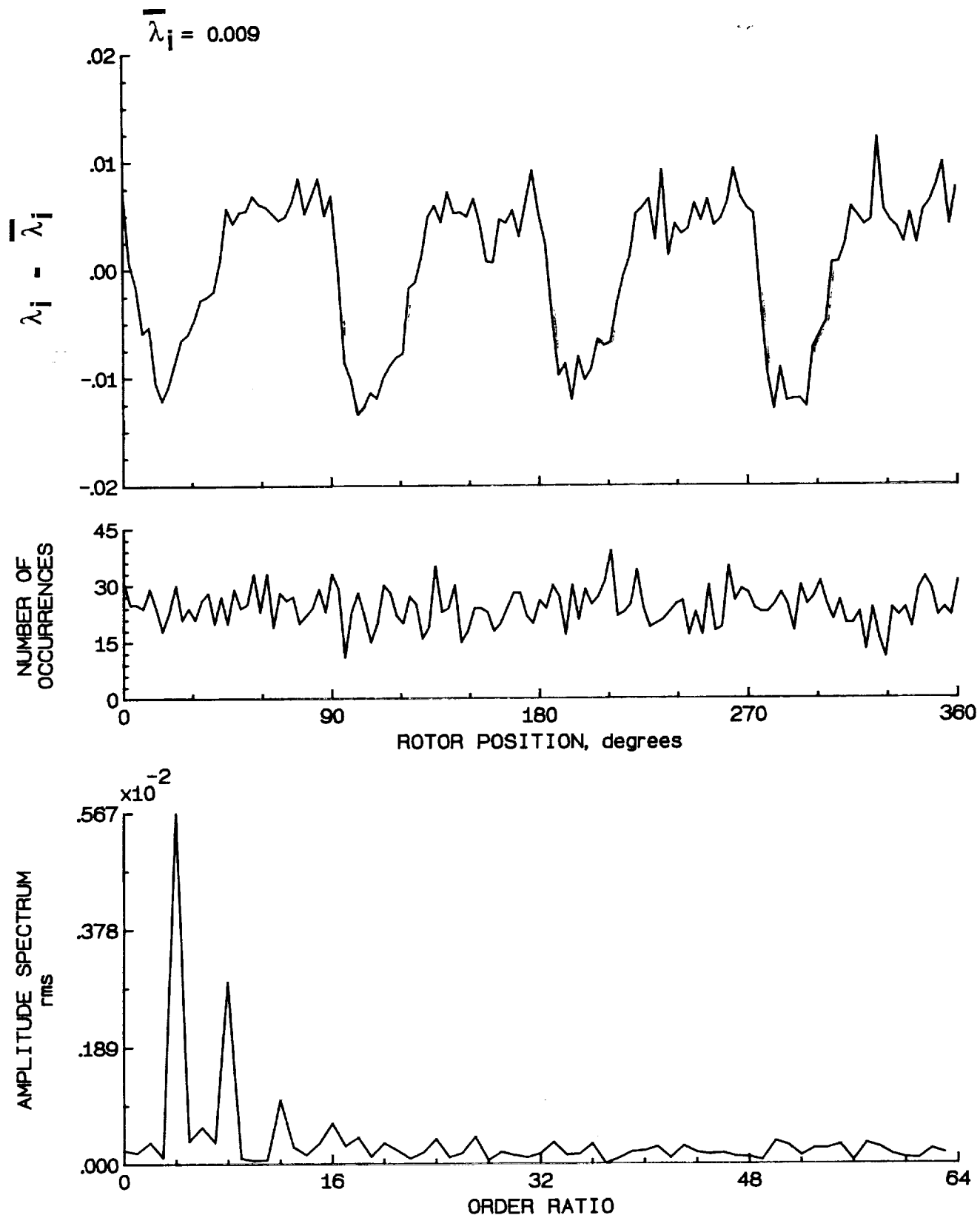


Figure 108.- Concluded.

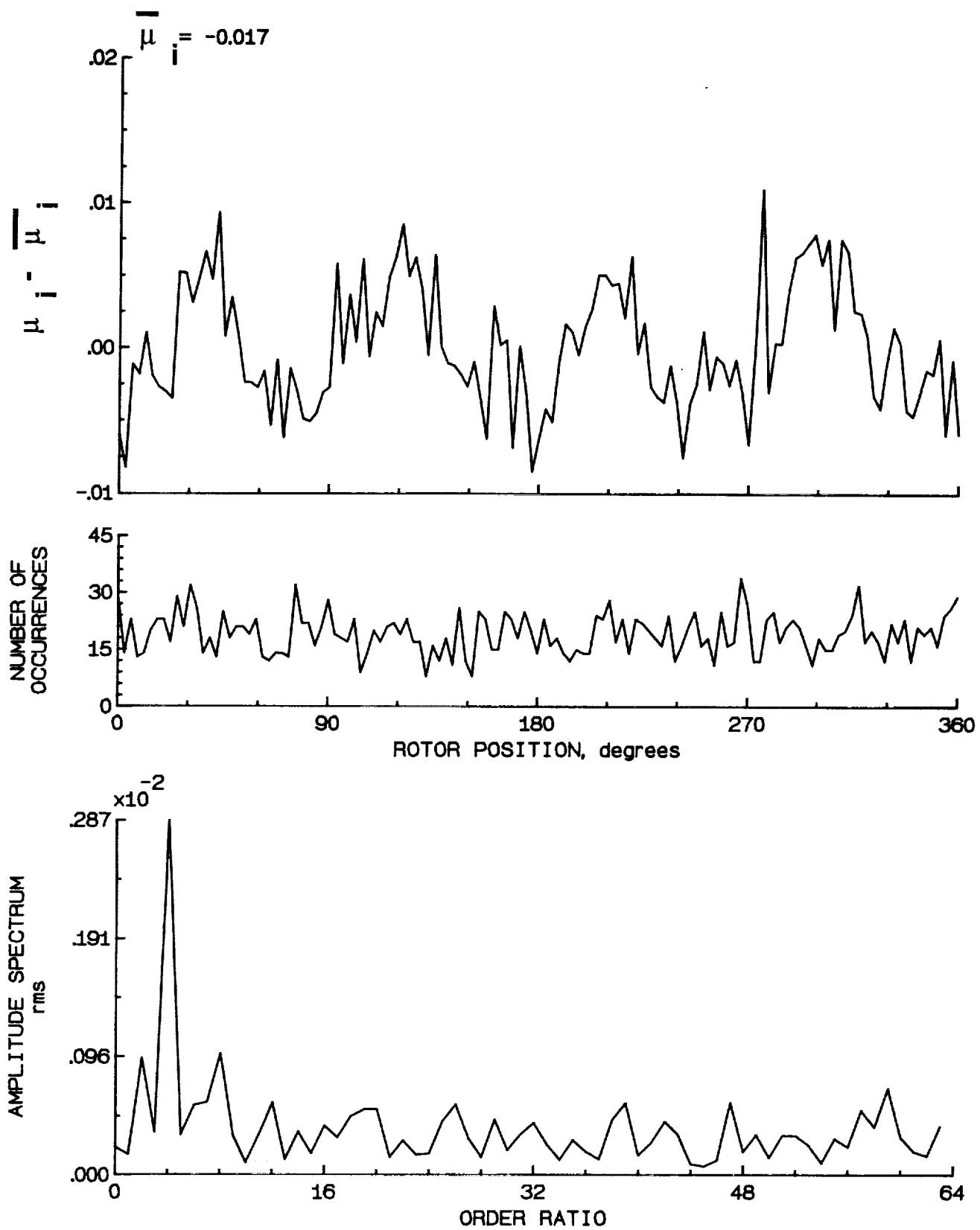


Figure 109.- Induced inflow velocity measured at 180 degrees and r/R of 0.82.

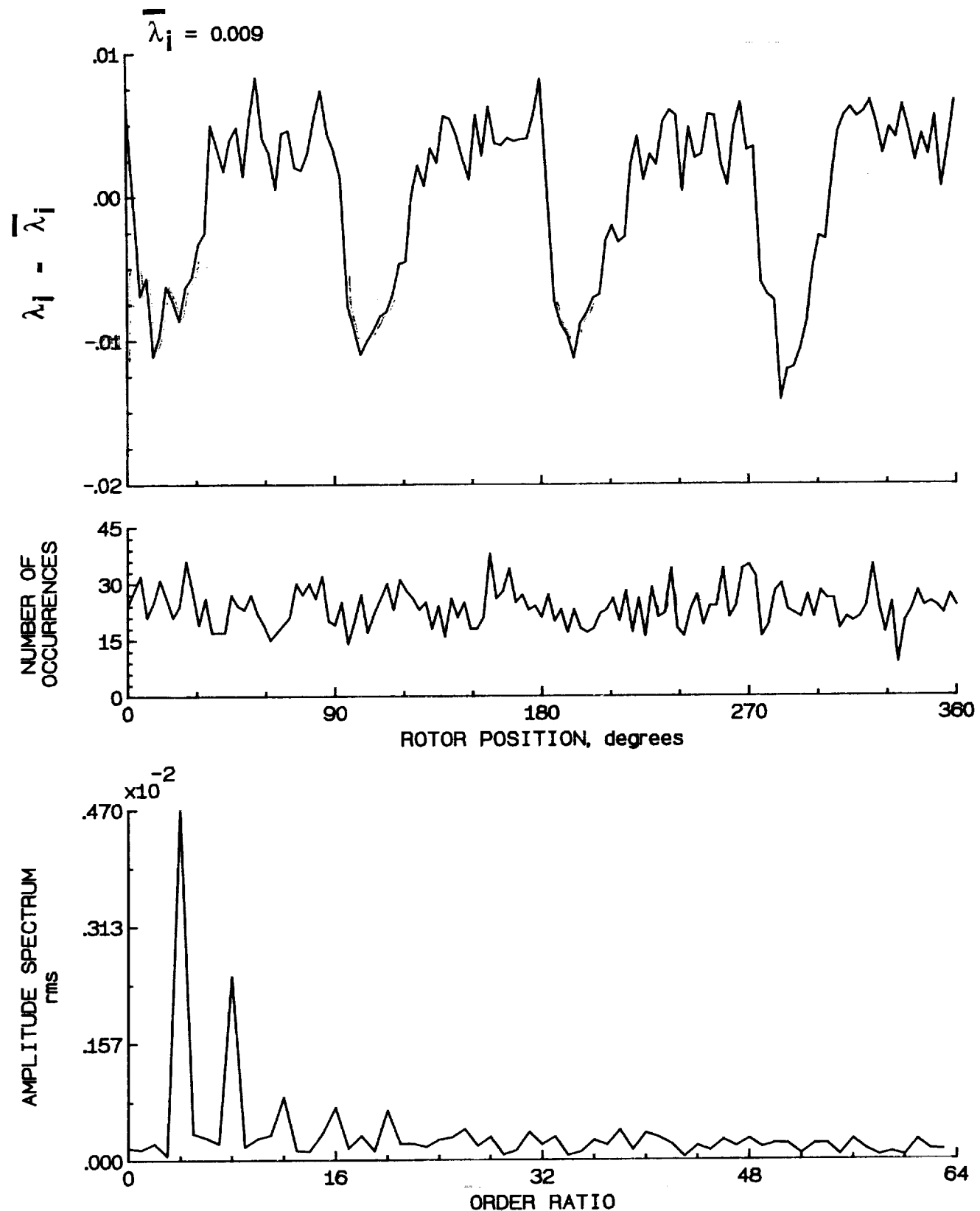


Figure 109.- Concluded.

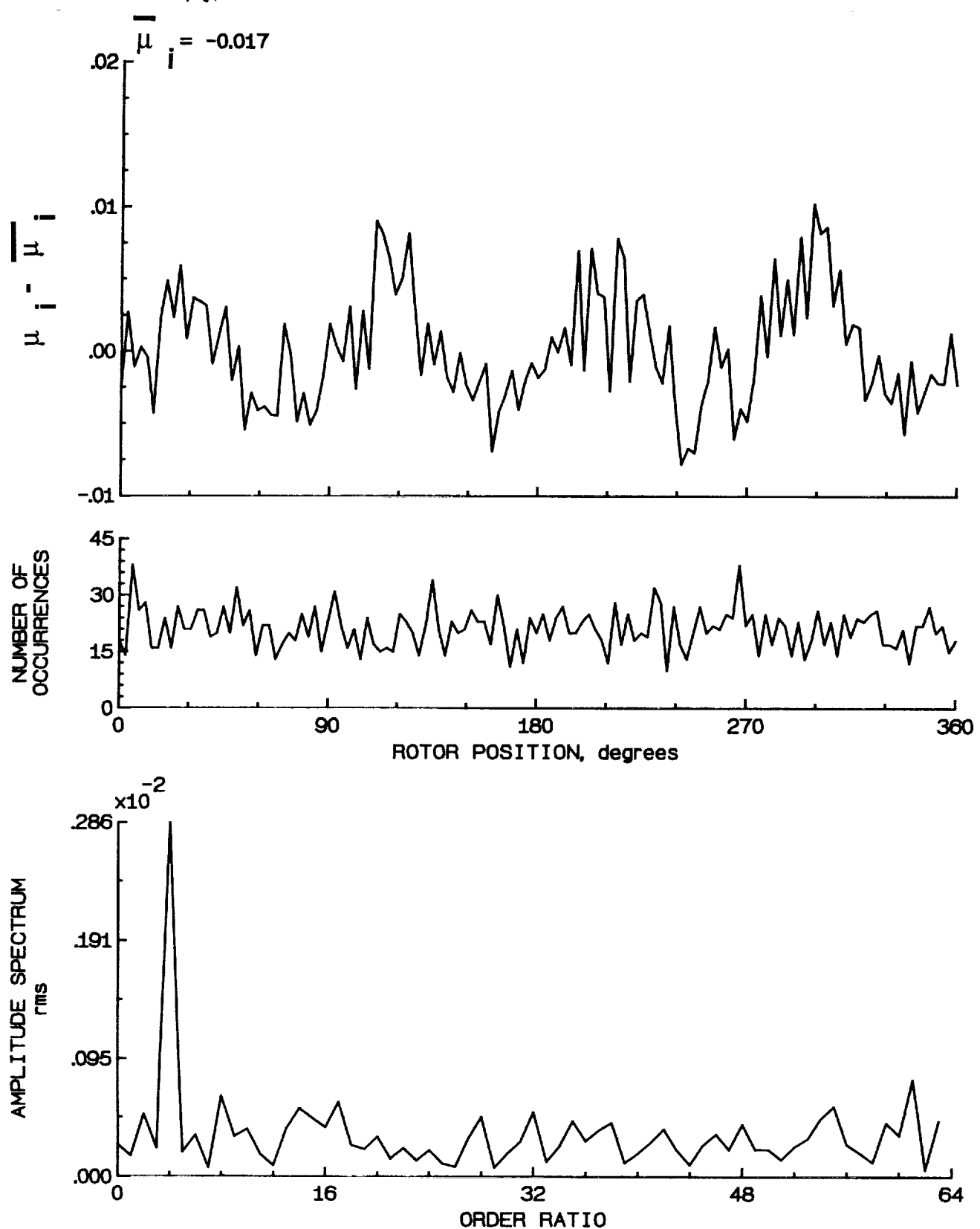


Figure 110.- Induced inflow velocity measured at 180 degrees and r/R of 0.86.

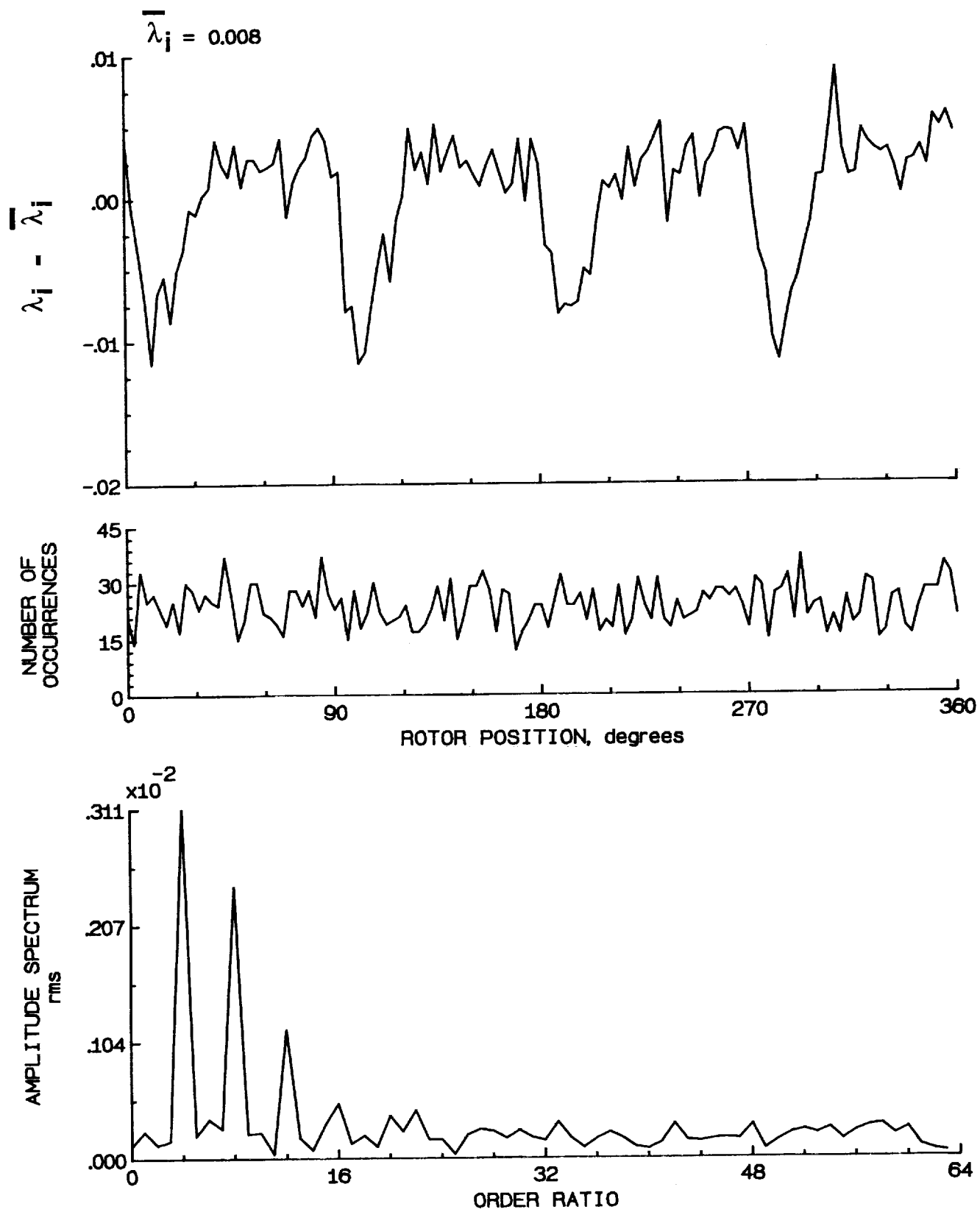


Figure 110.- Concluded.

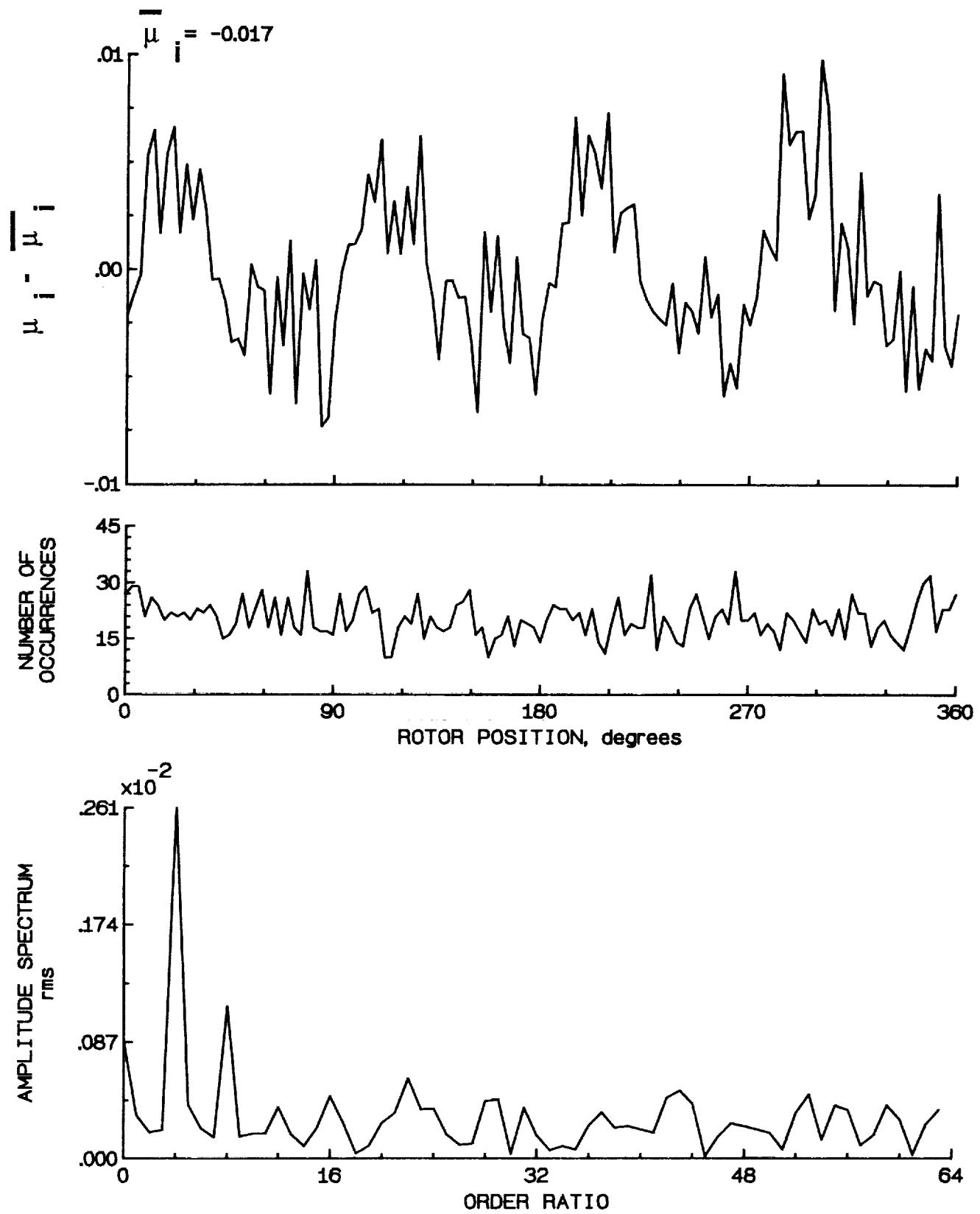


Figure 111.- Induced inflow velocity measured at 180 degrees and r/R of 0.90.

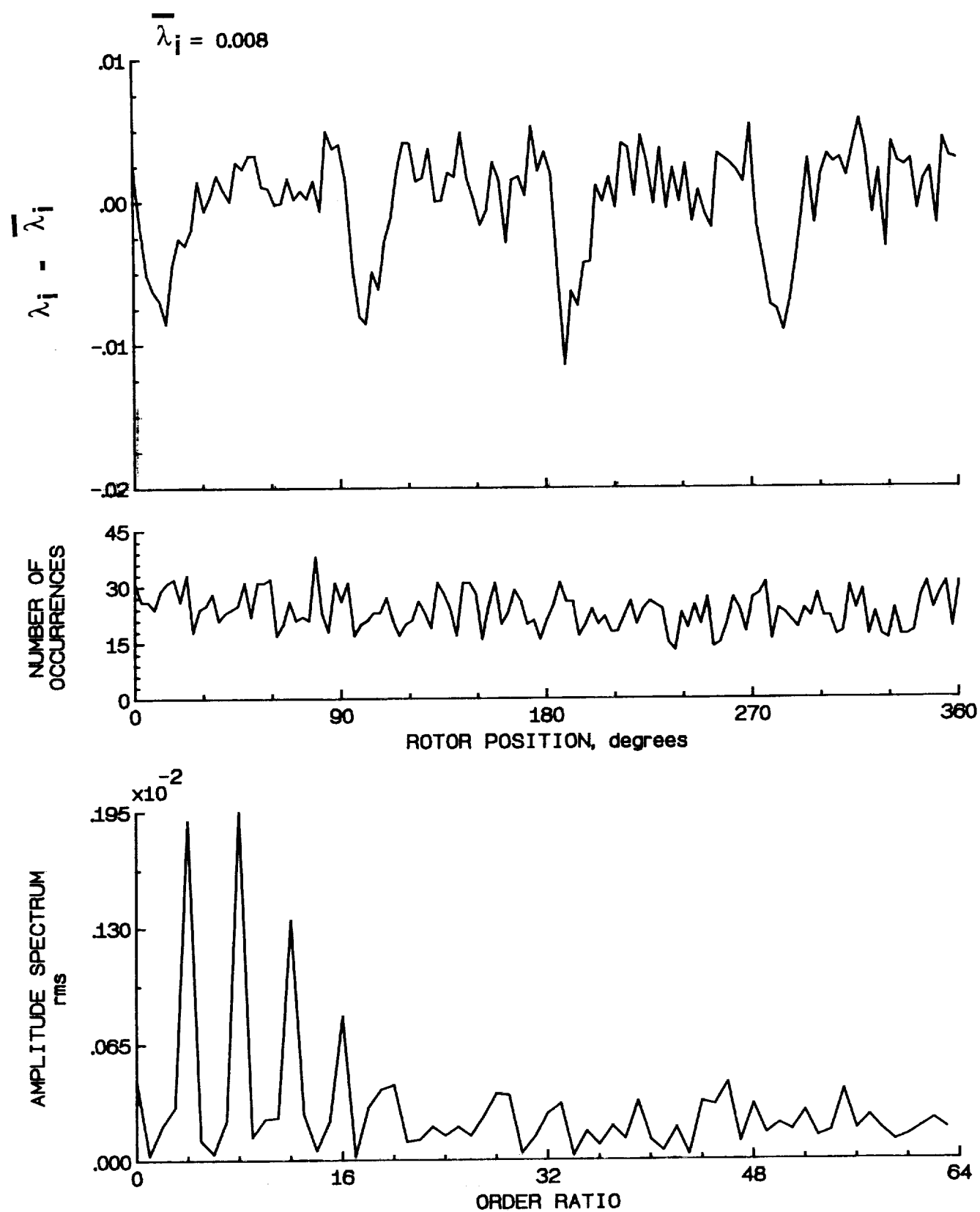


Figure 111.- Concluded.

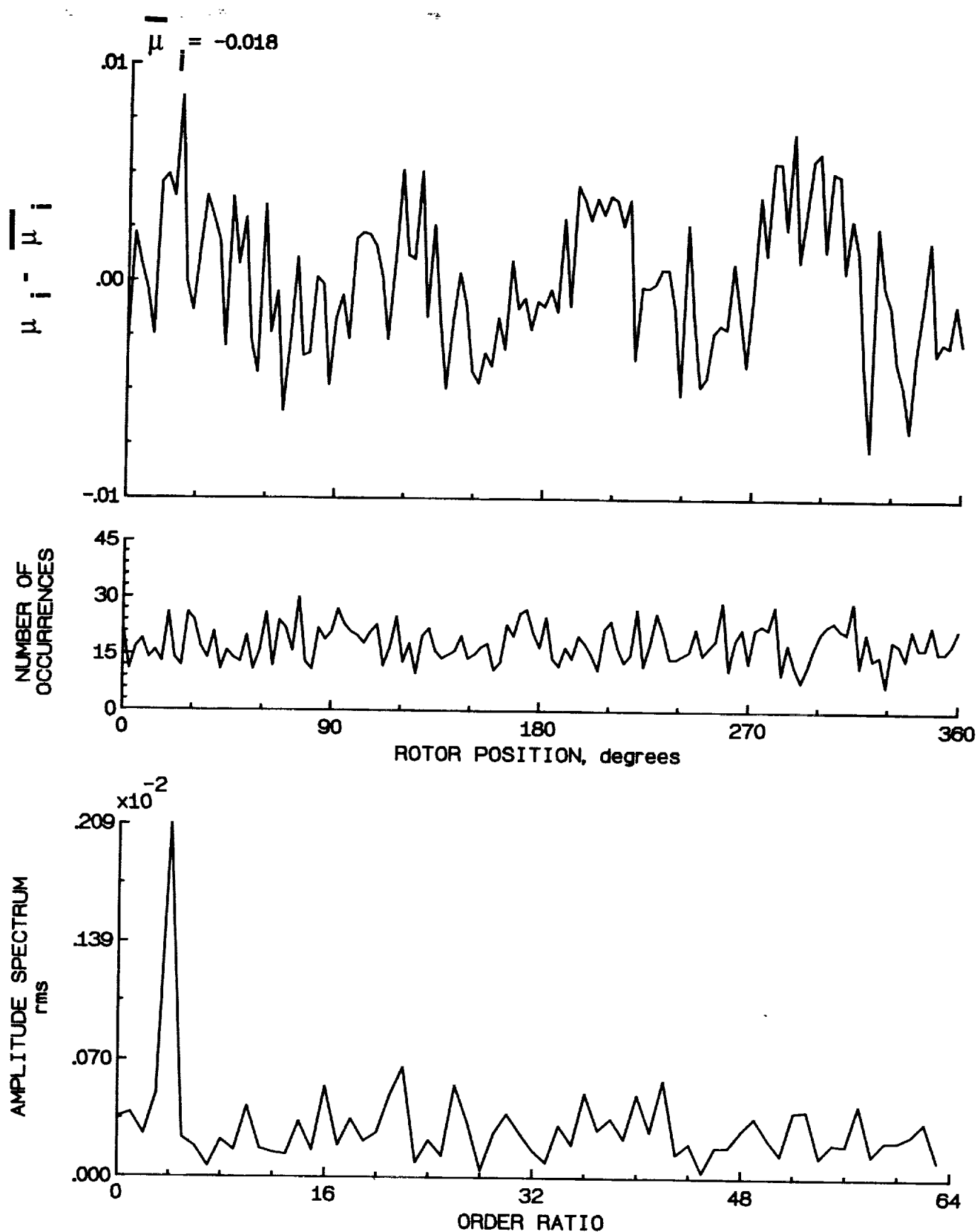


Figure 112.- Induced inflow velocity measured at 180 degrees and r/R of 0.94.

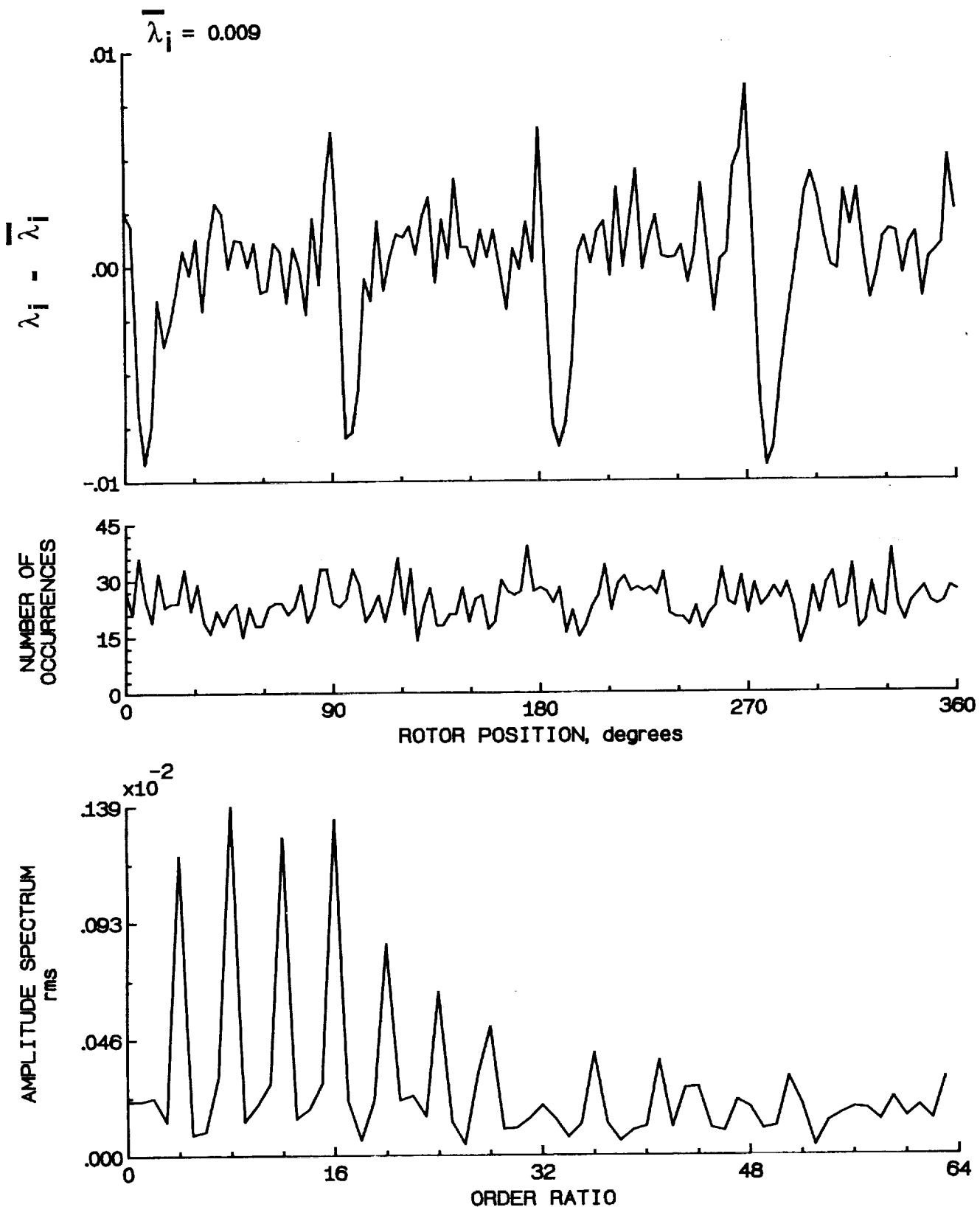


Figure 112.- Concluded.

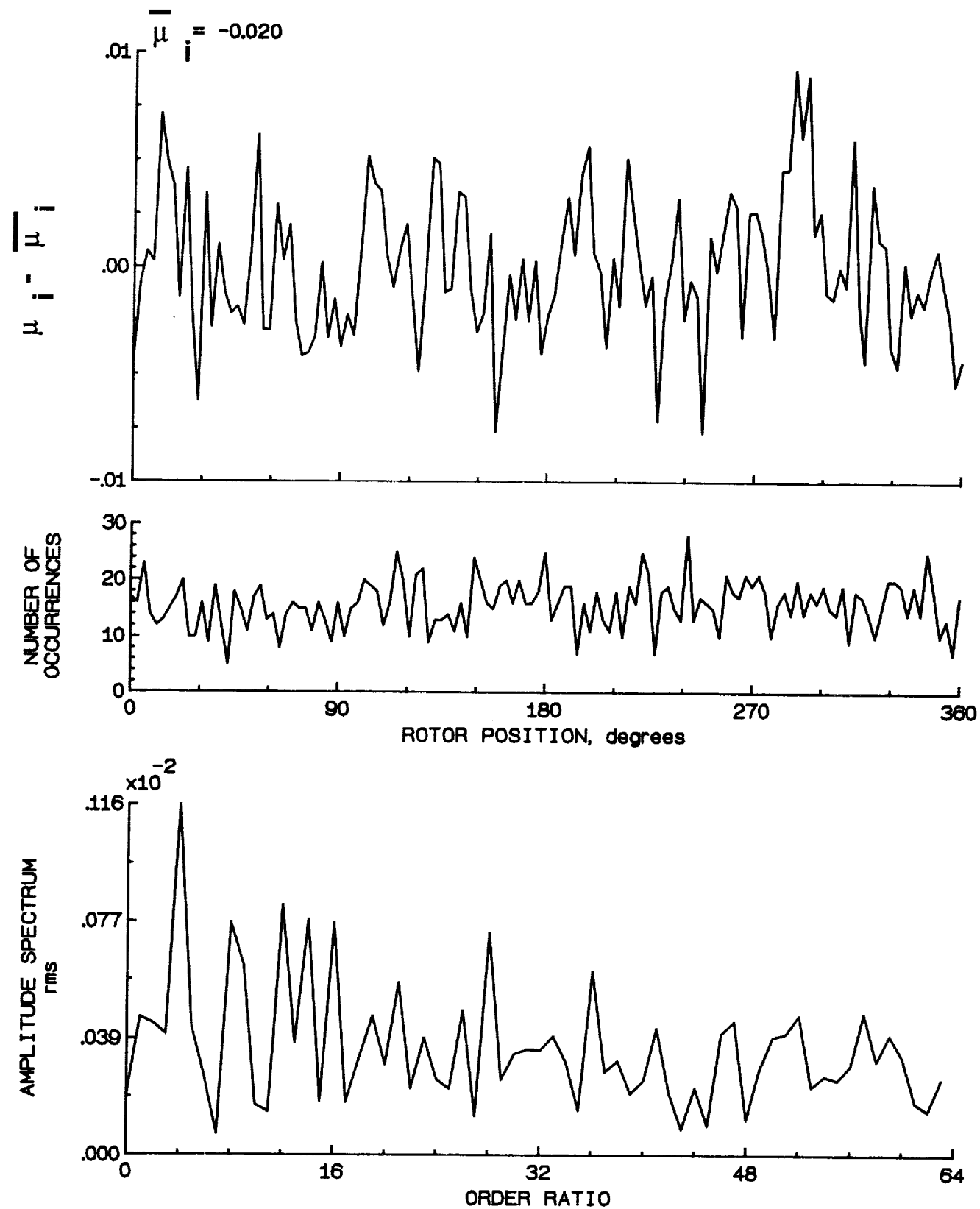


Figure 113.- Induced inflow velocity measured at 180 degrees and r/R of 0.98.

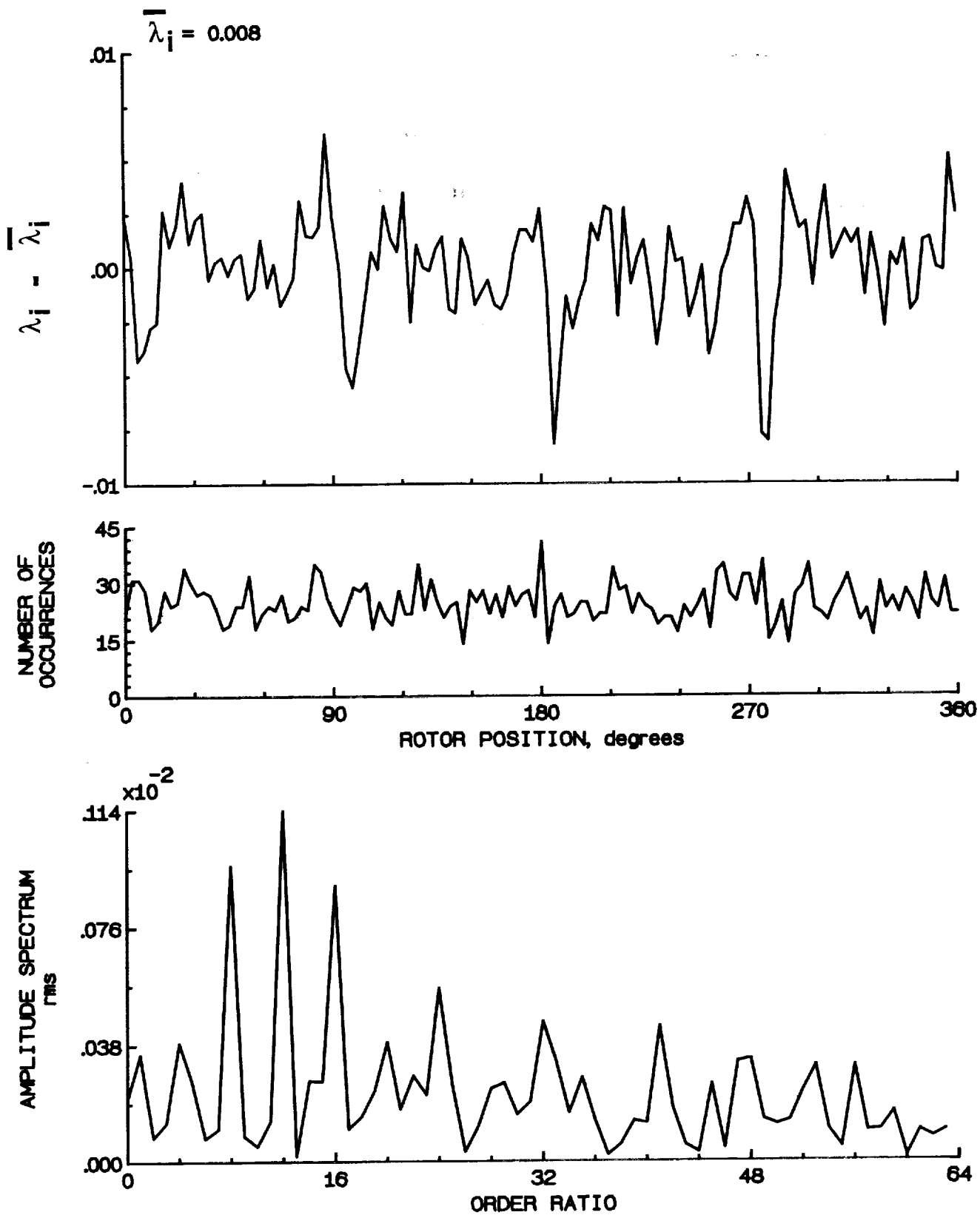


Figure 113.- Concluded.

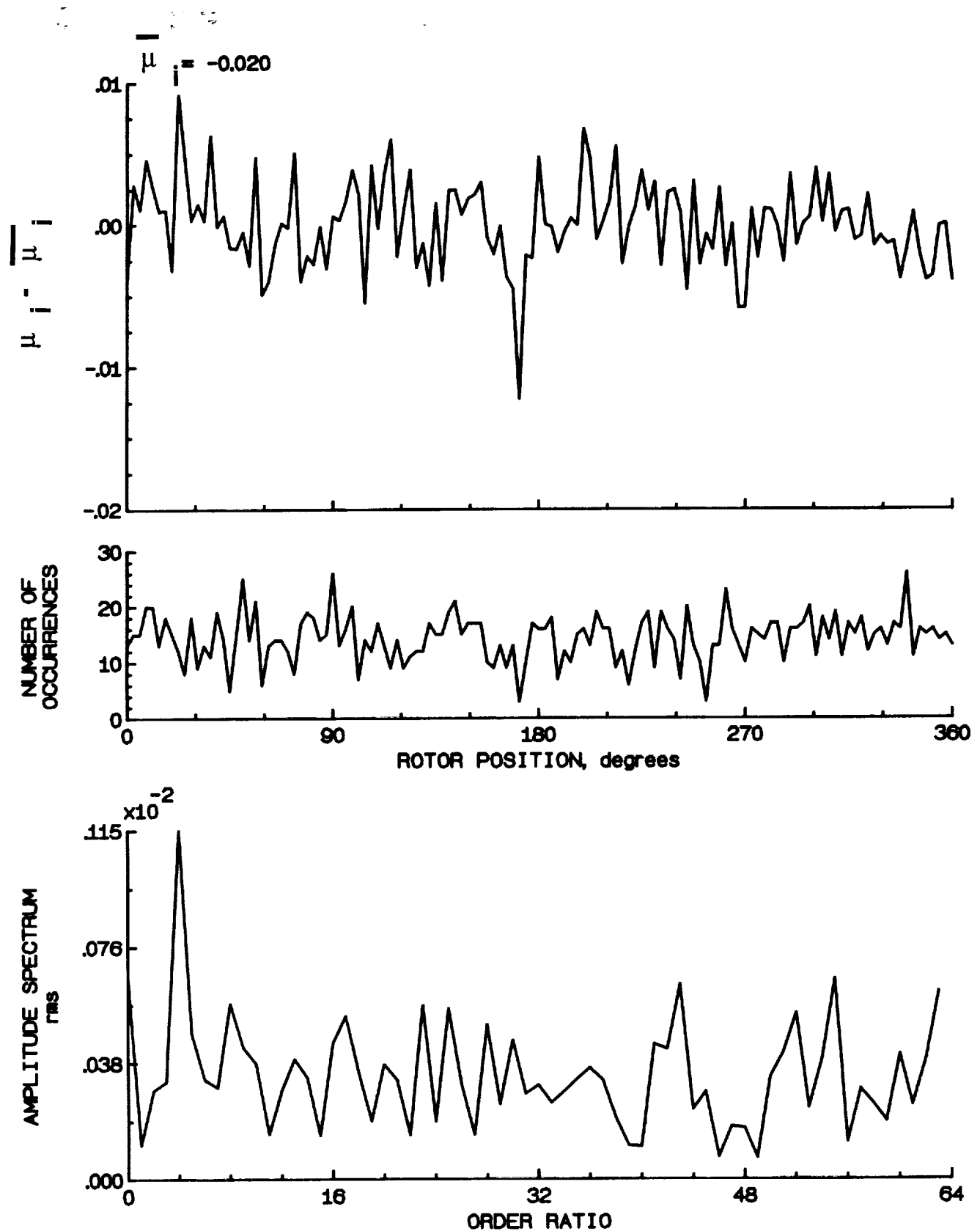


Figure 114.- Induced inflow velocity measured at 180 degrees and r/R of 1.02.

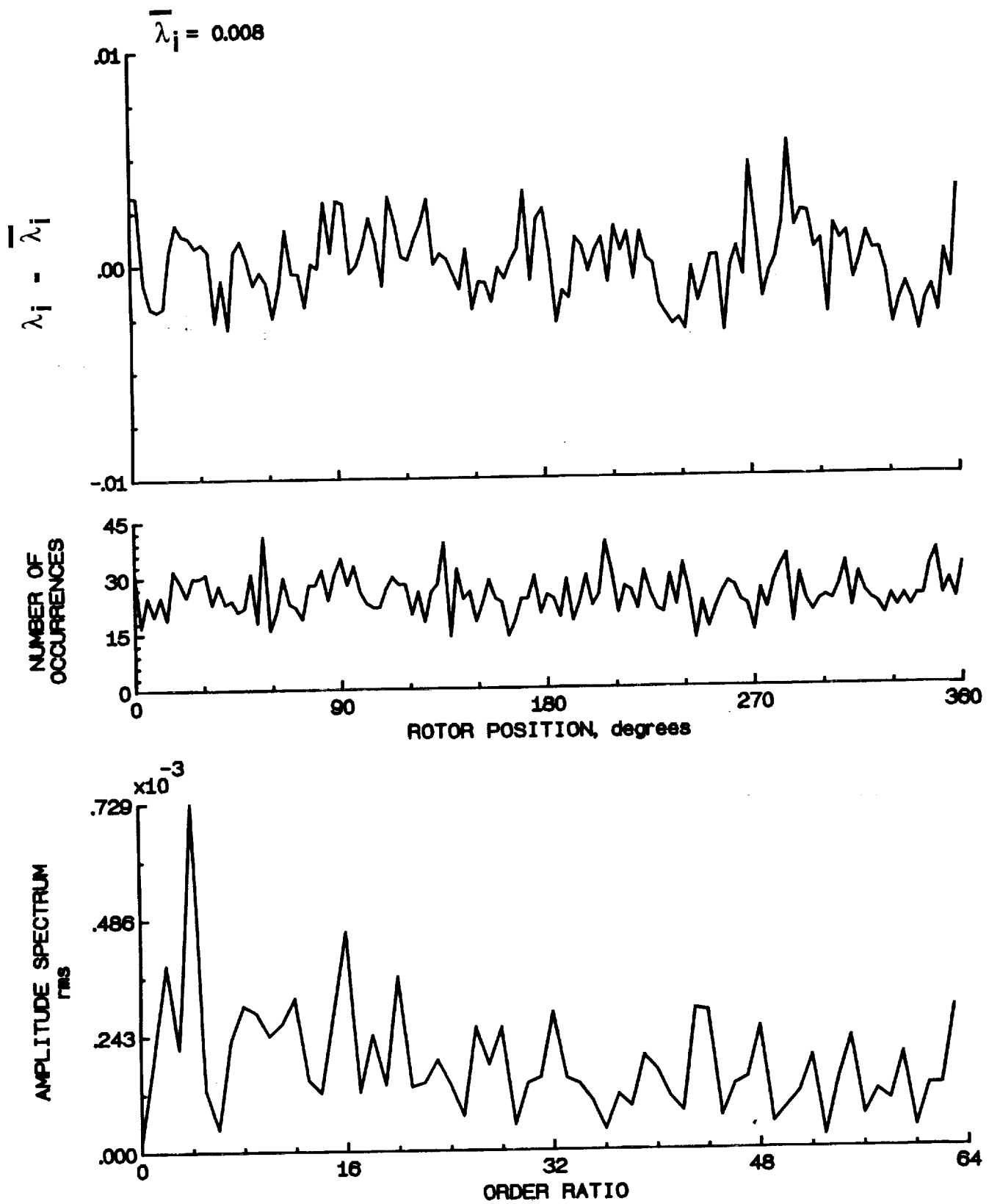


Figure 114.- Concluded.

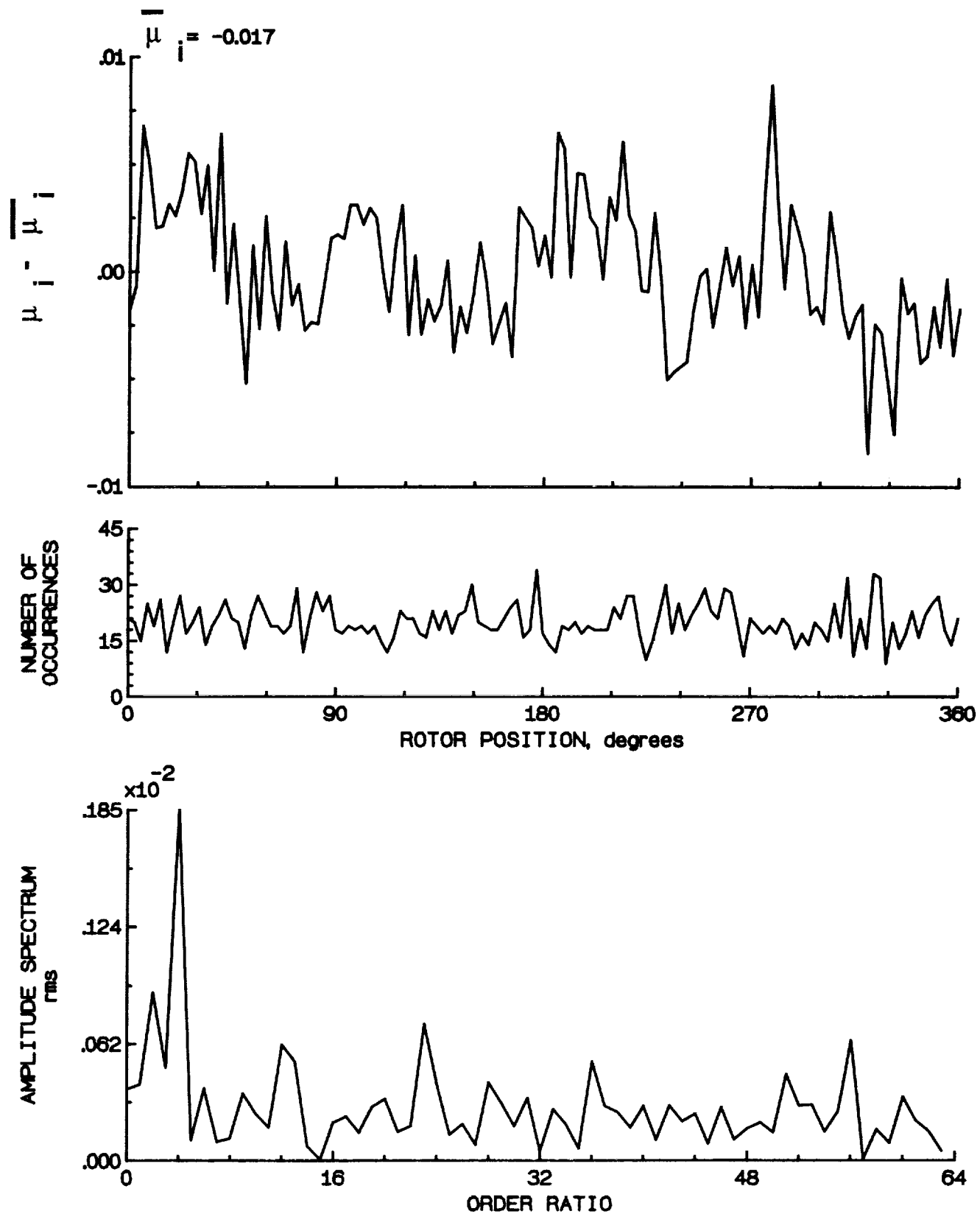


Figure 115.- Induced inflow velocity measured at 210 degrees and r/R of 0.20.

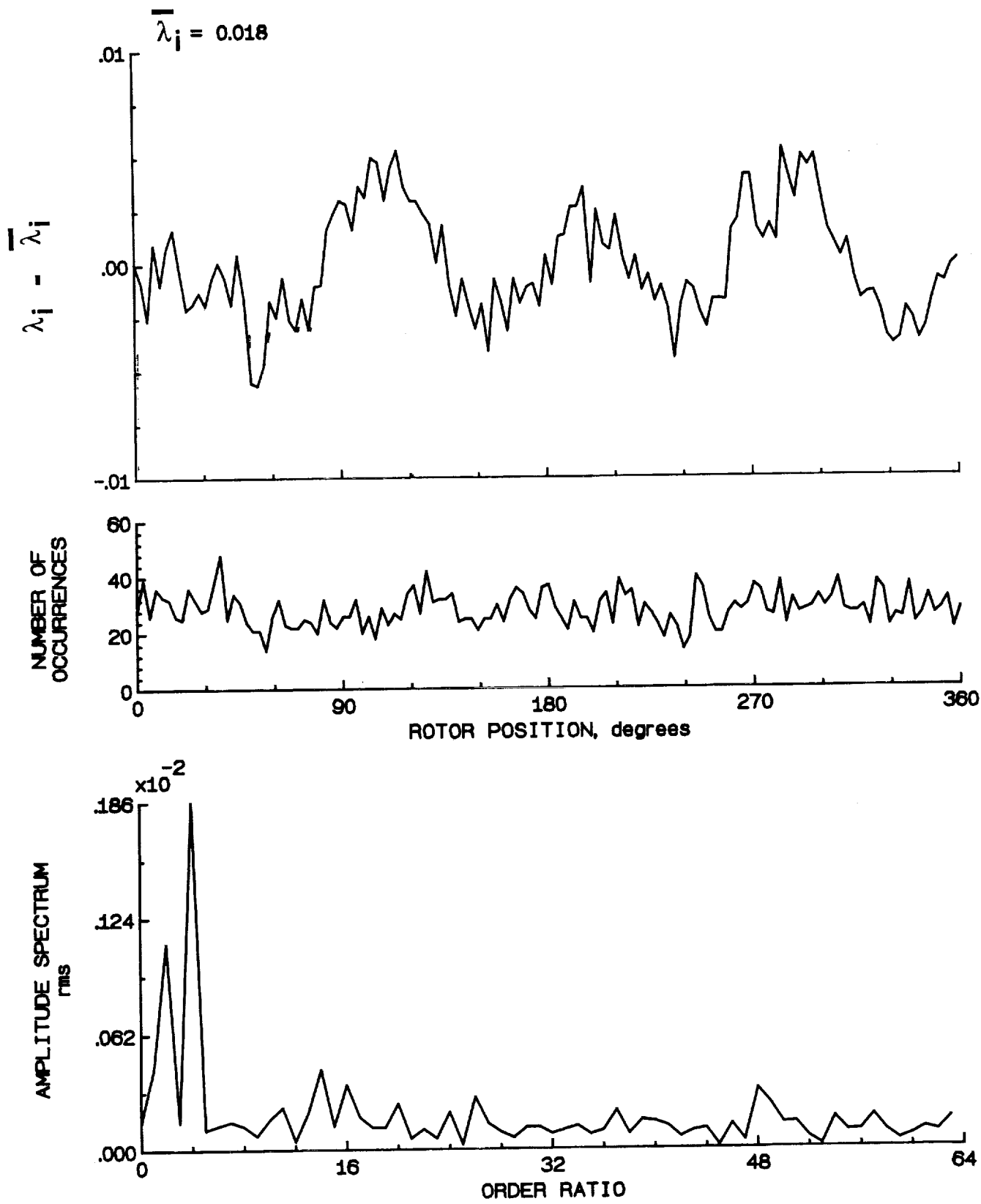


Figure 115.- Concluded.

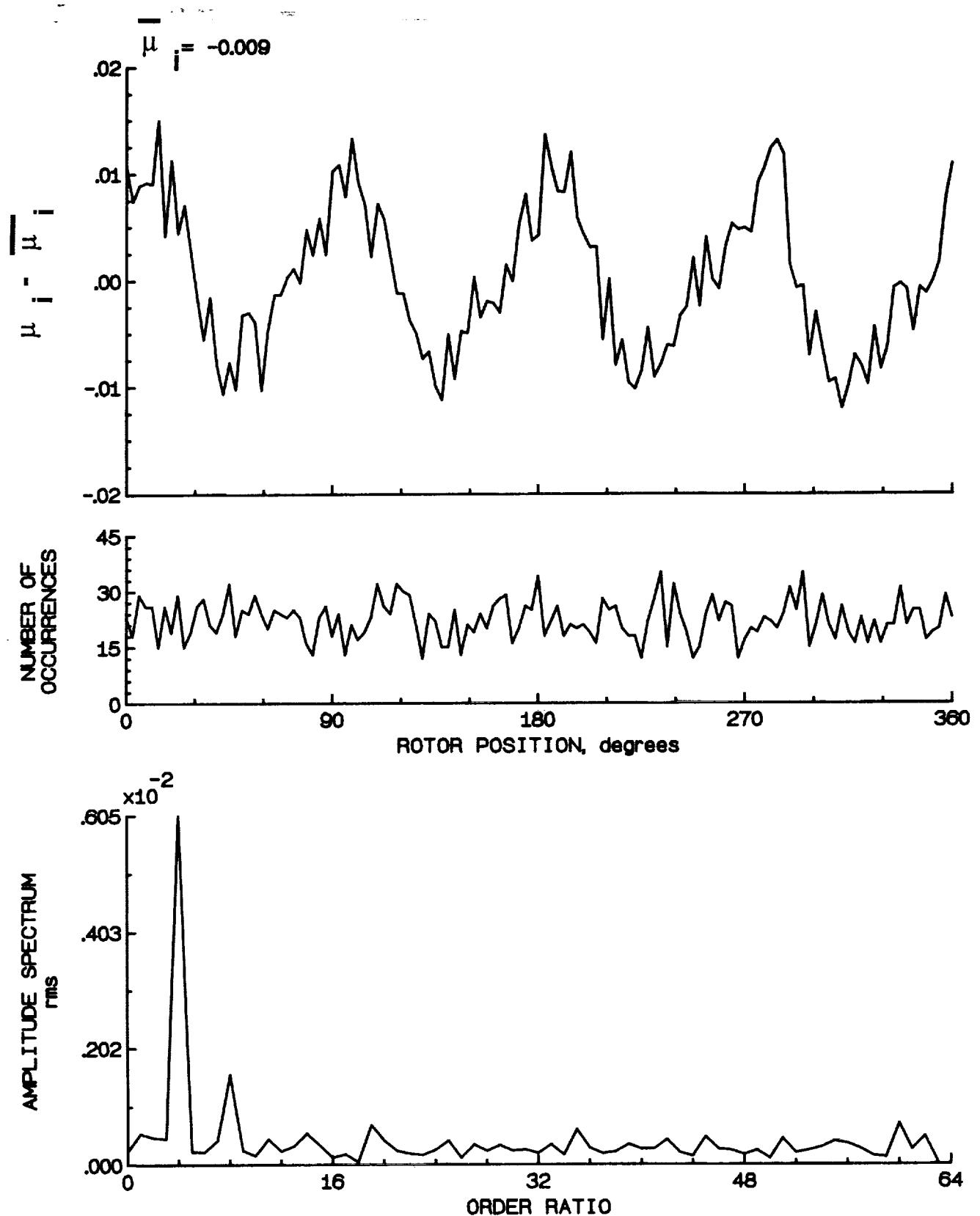


Figure 116.- Induced inflow velocity measured at 210 degrees and r/R of 0.40.

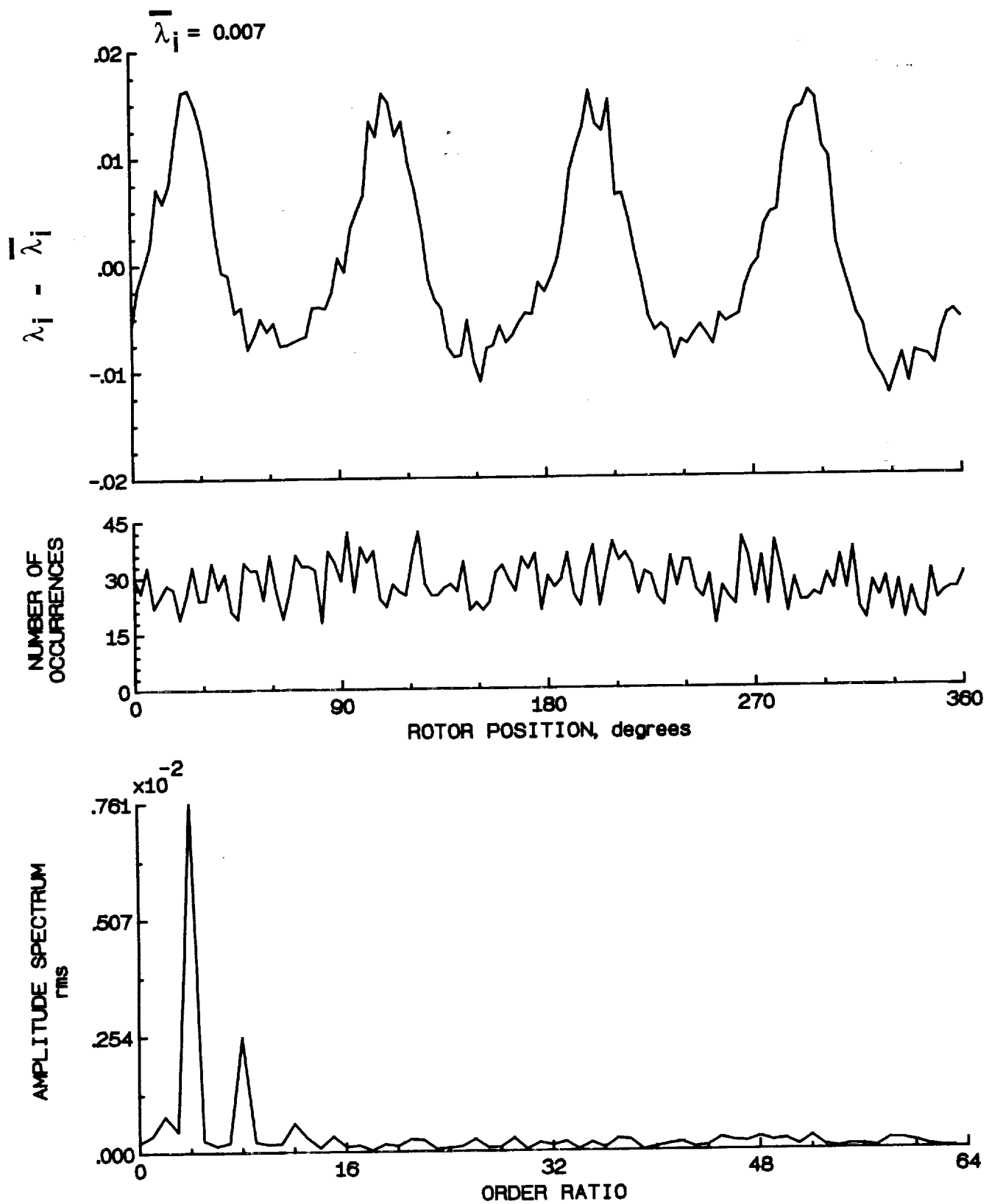


Figure 116.- Concluded.

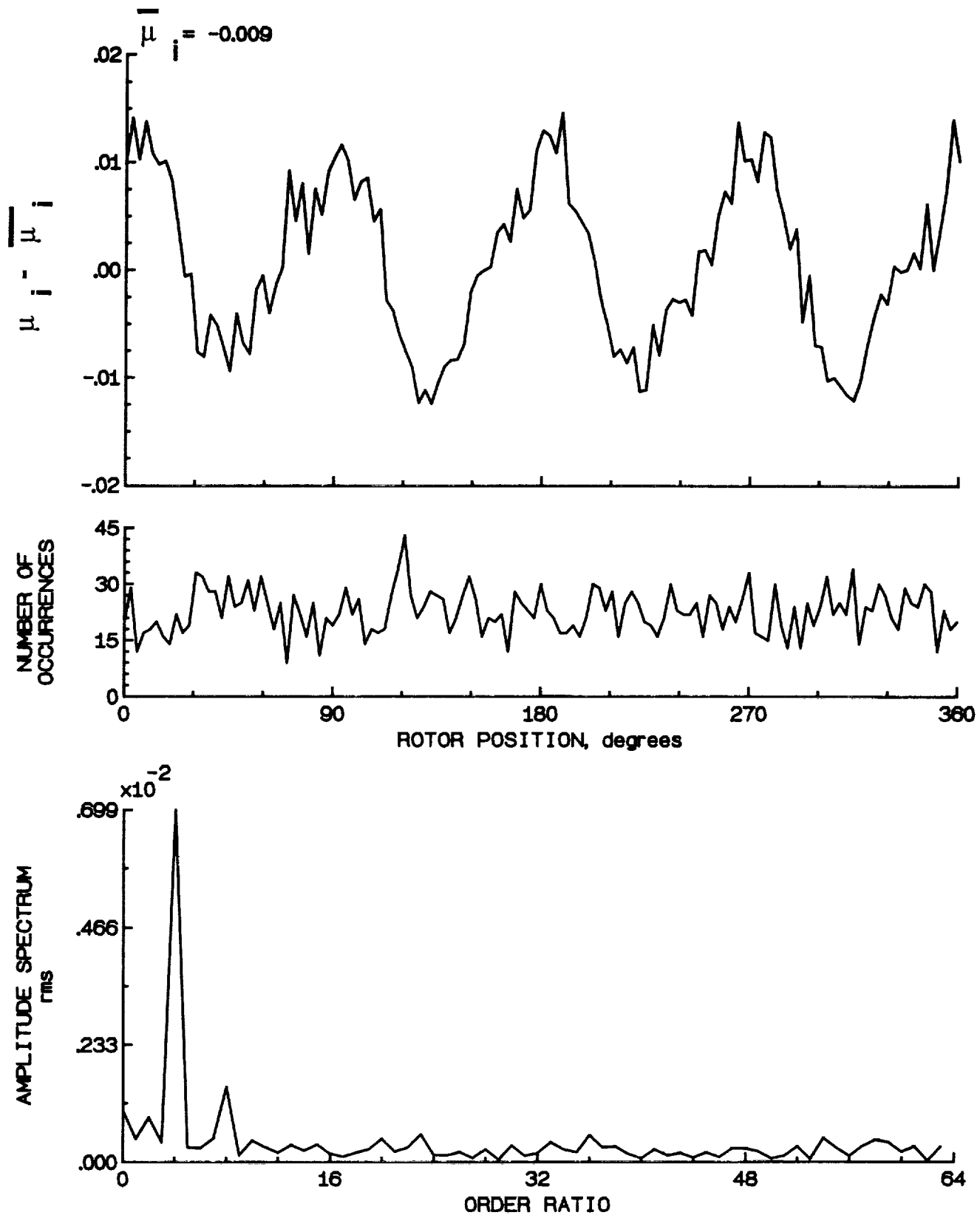


Figure 117.- Induced inflow velocity measured at 210 degrees and r/R of 0.50.

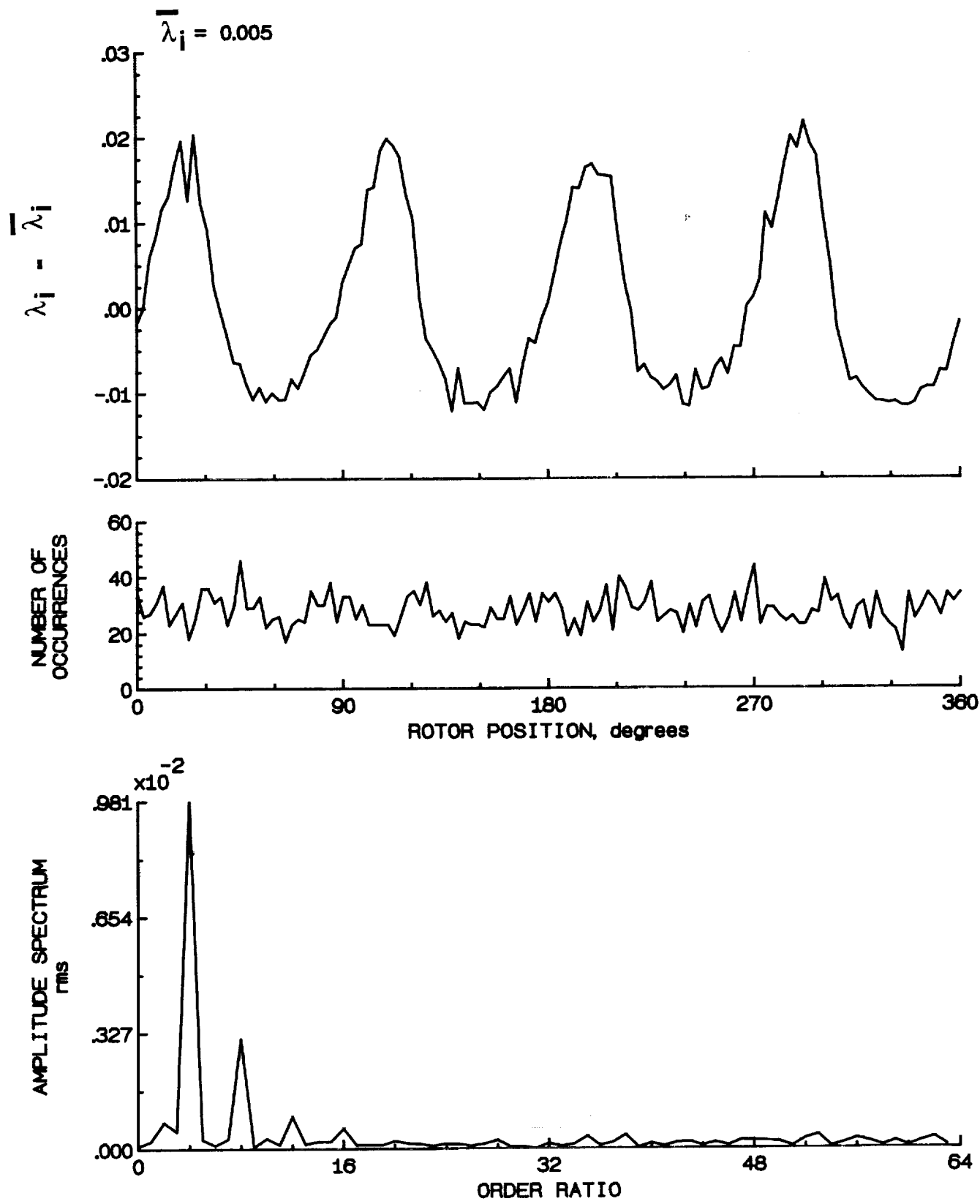


Figure 117.- Concluded.

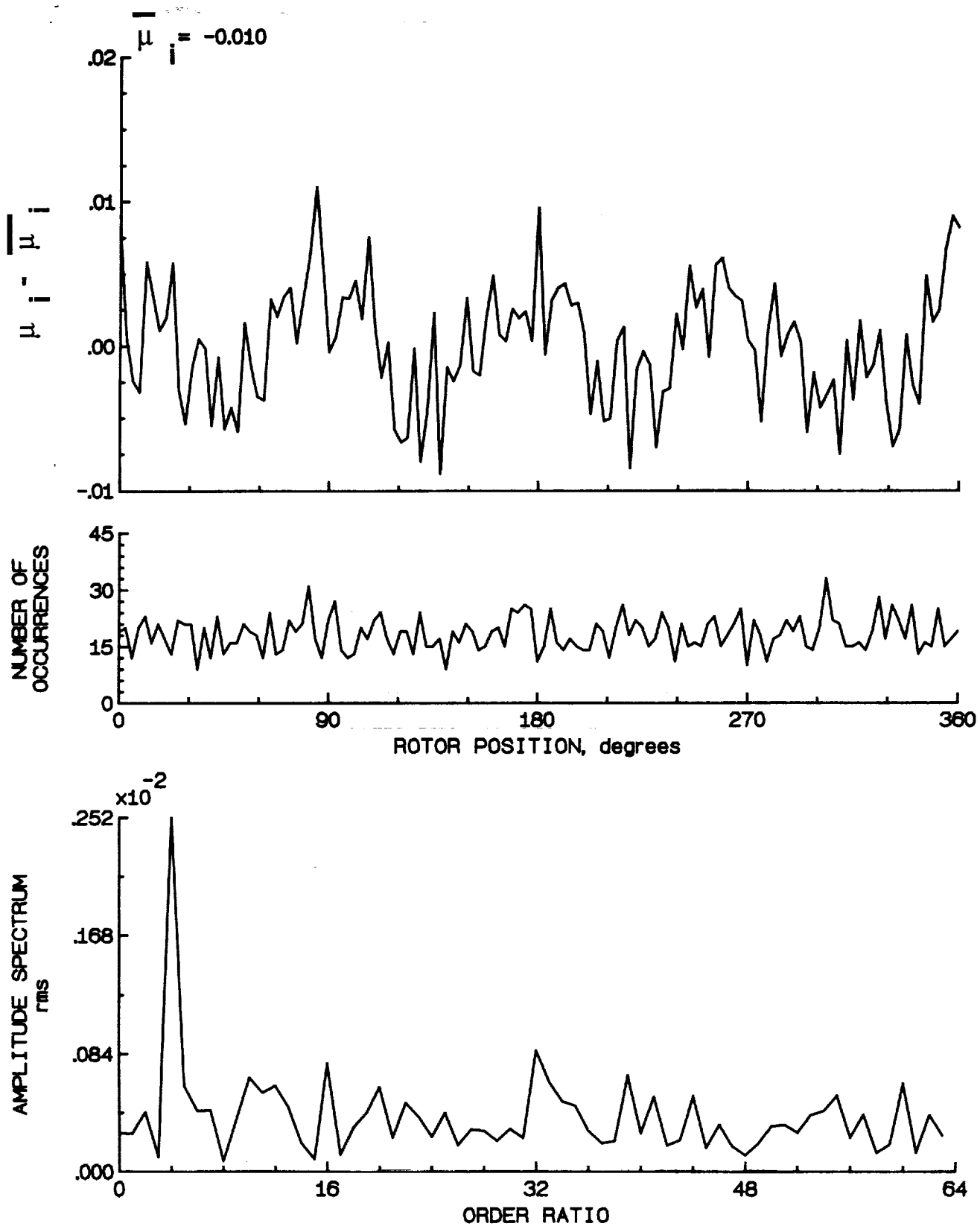


Figure 118.- Induced inflow velocity measured at 210 degrees and r/R of 0.60.

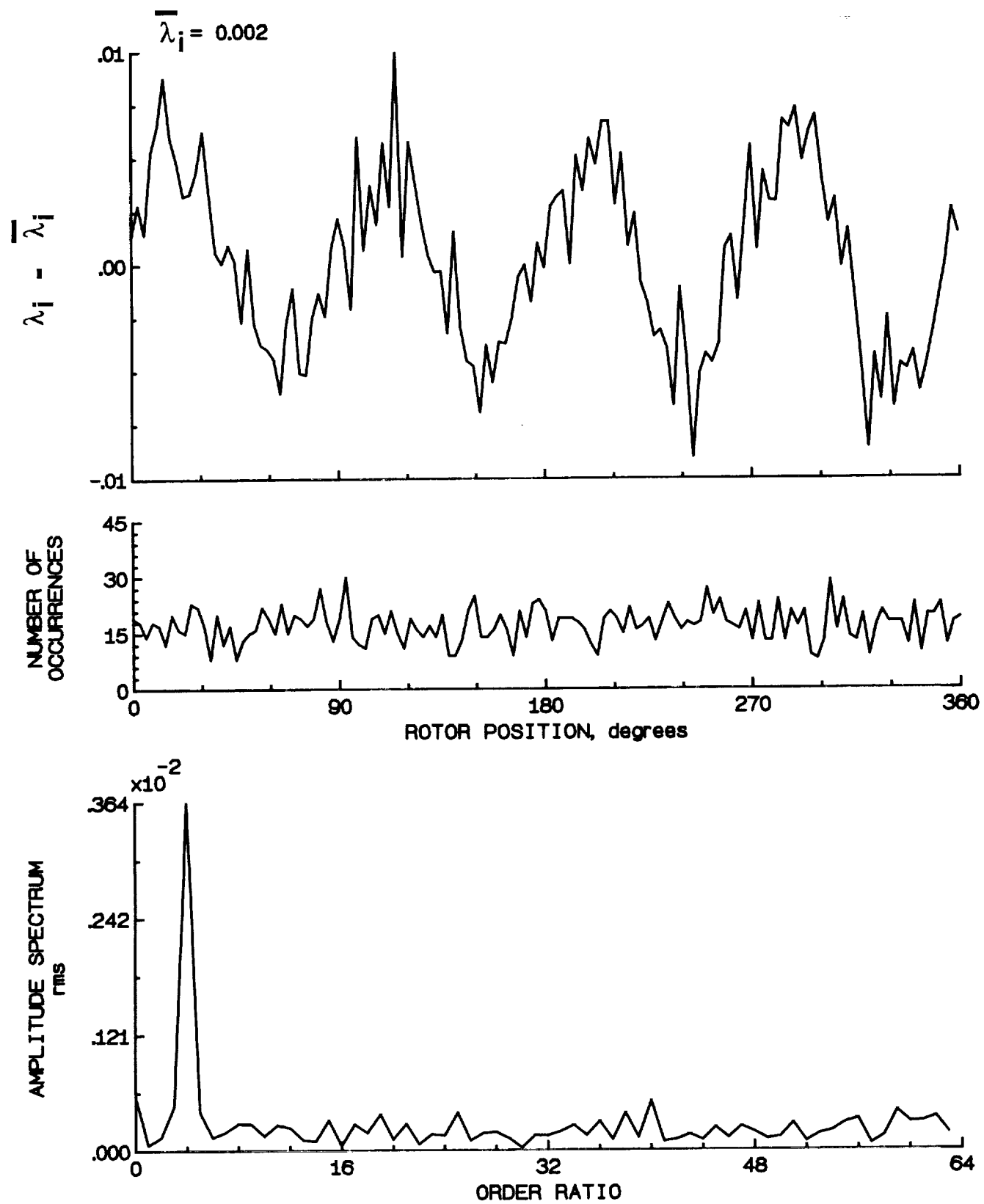


Figure 118.- Concluded.

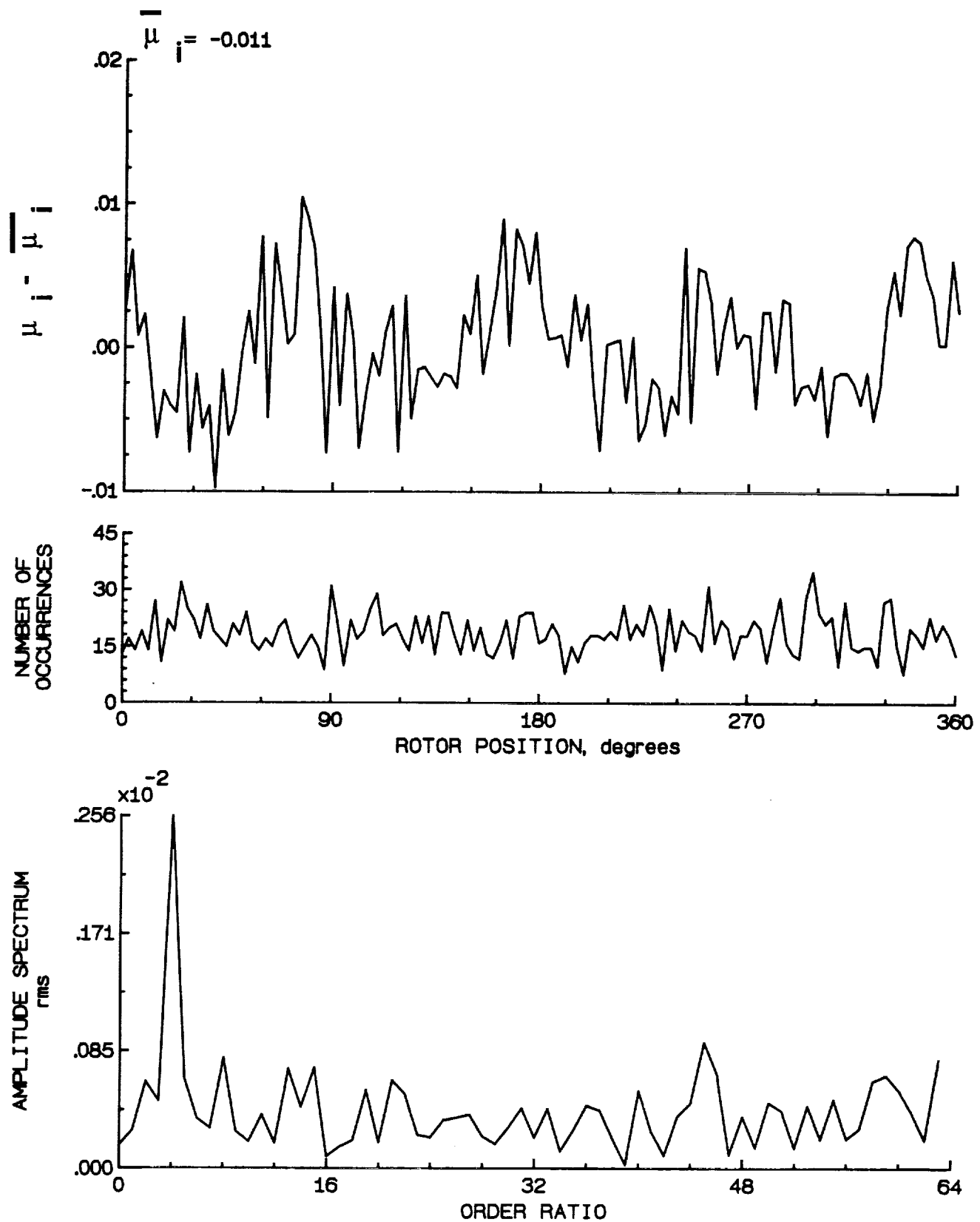


Figure 119.- Induced inflow velocity measured at 210 degrees and r/R of 0.70.

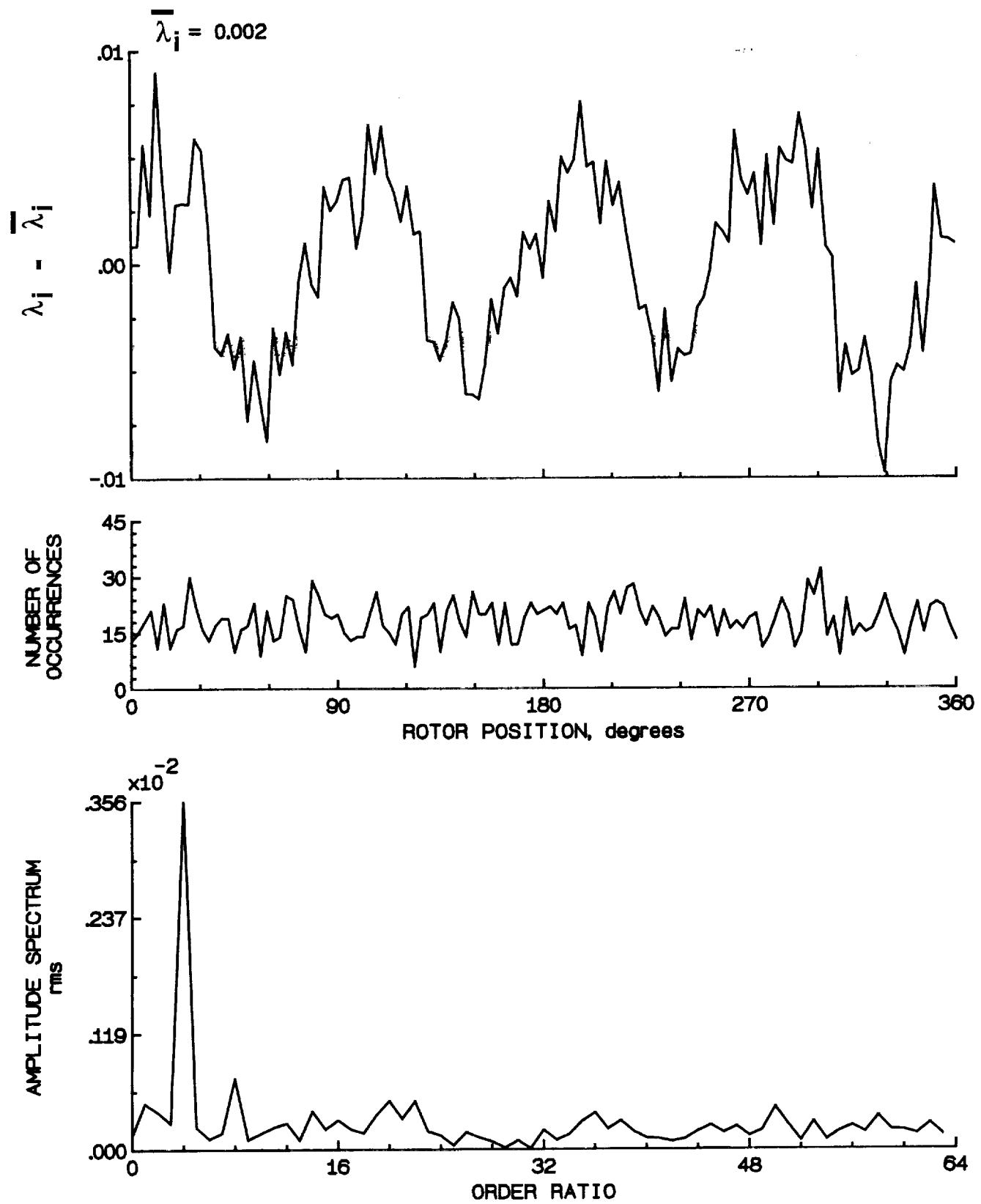


Figure 119.- Concluded.

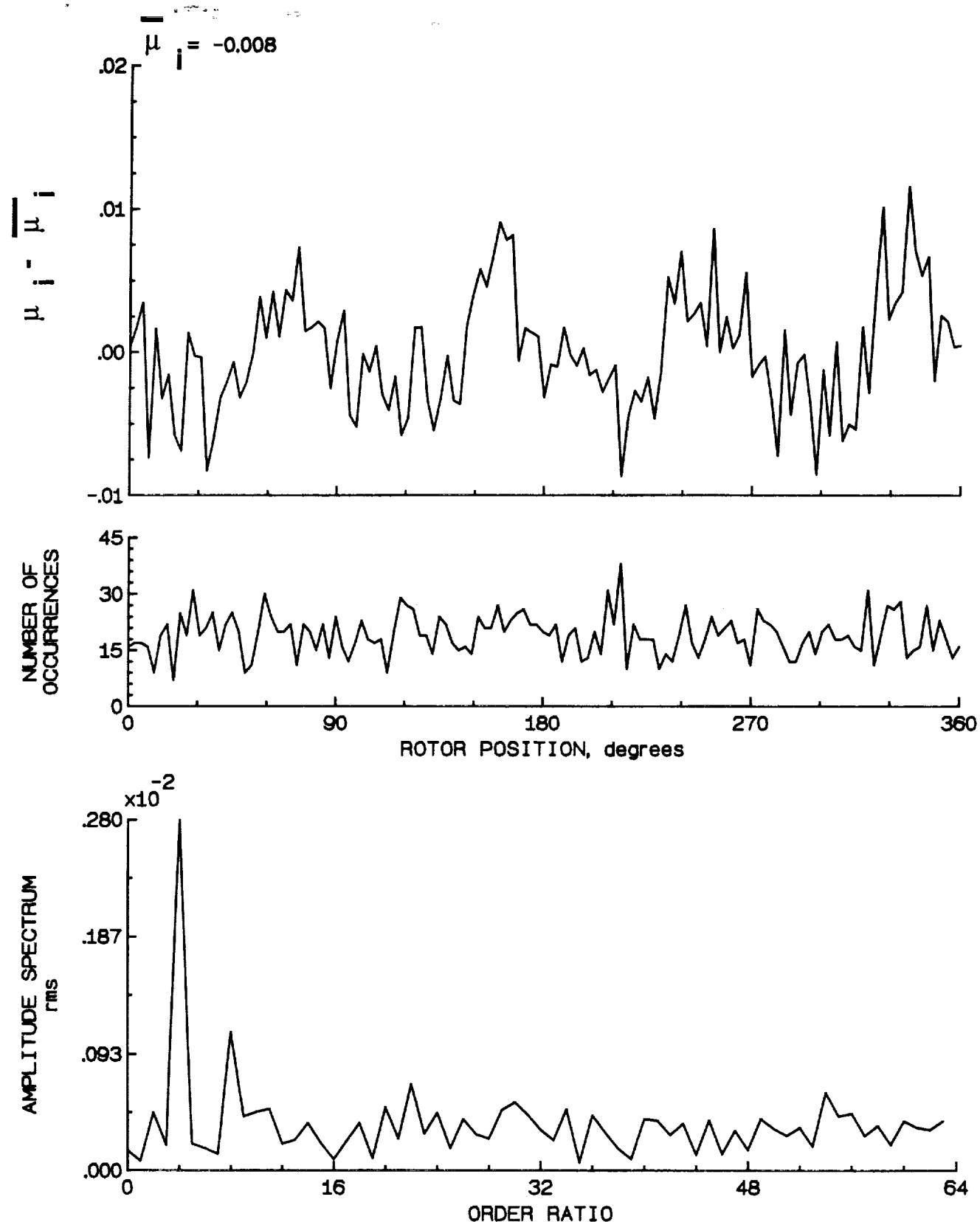


Figure 120.- Induced inflow velocity measured at 210 degrees and r/R of 0.74.

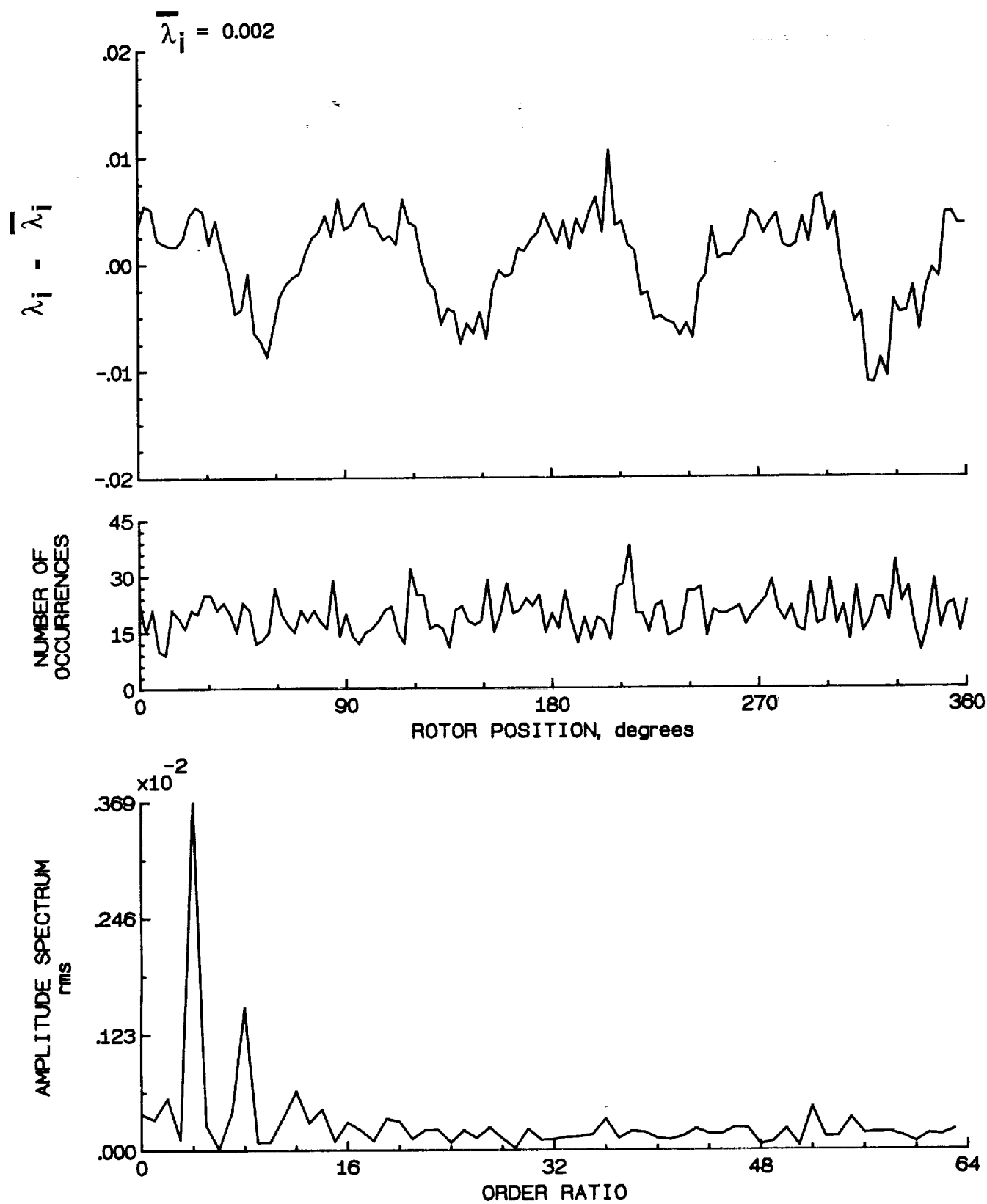


Figure 120.- Concluded.

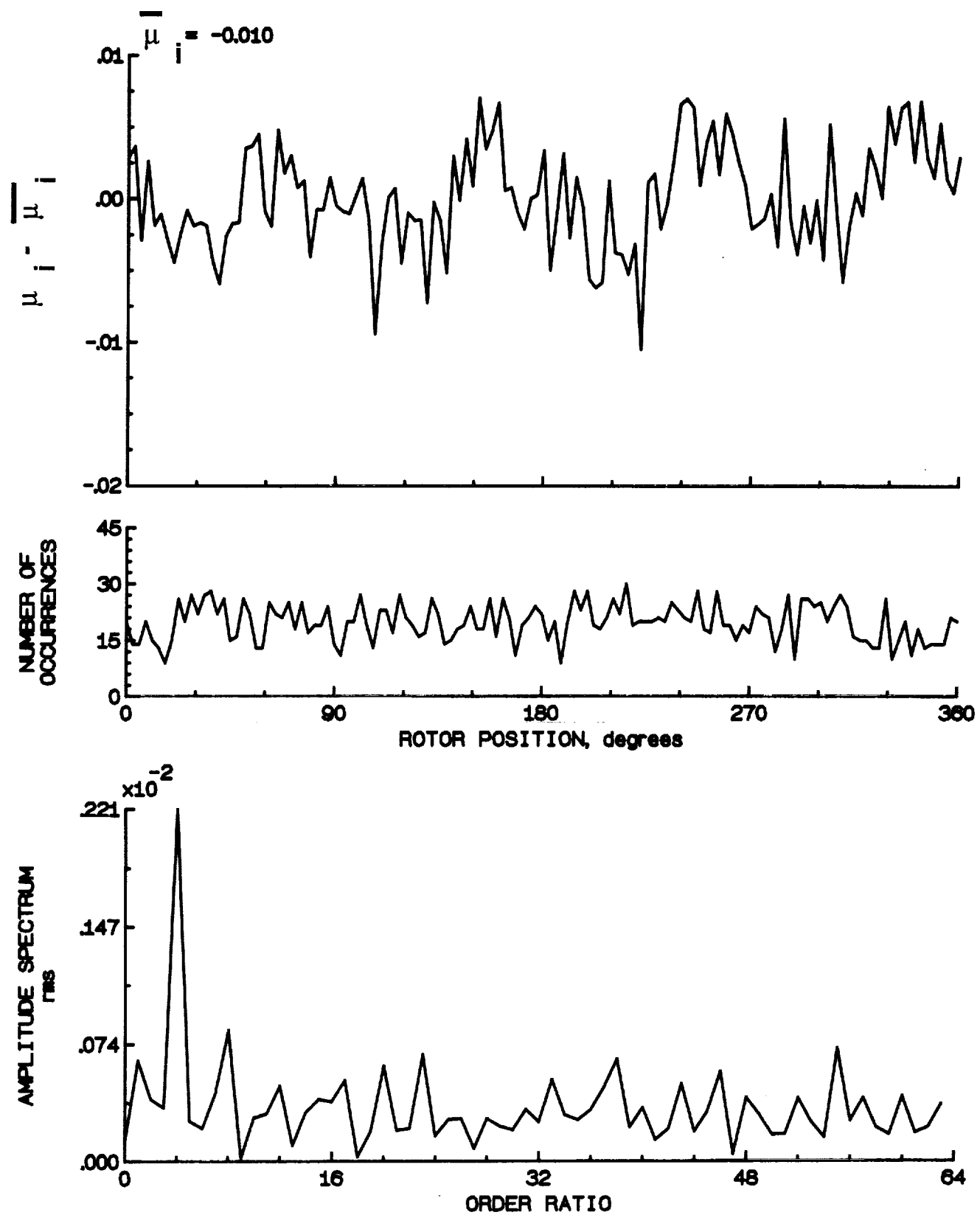


Figure 121.- Induced inflow velocity measured at 210 degrees and r/R of 0.78.

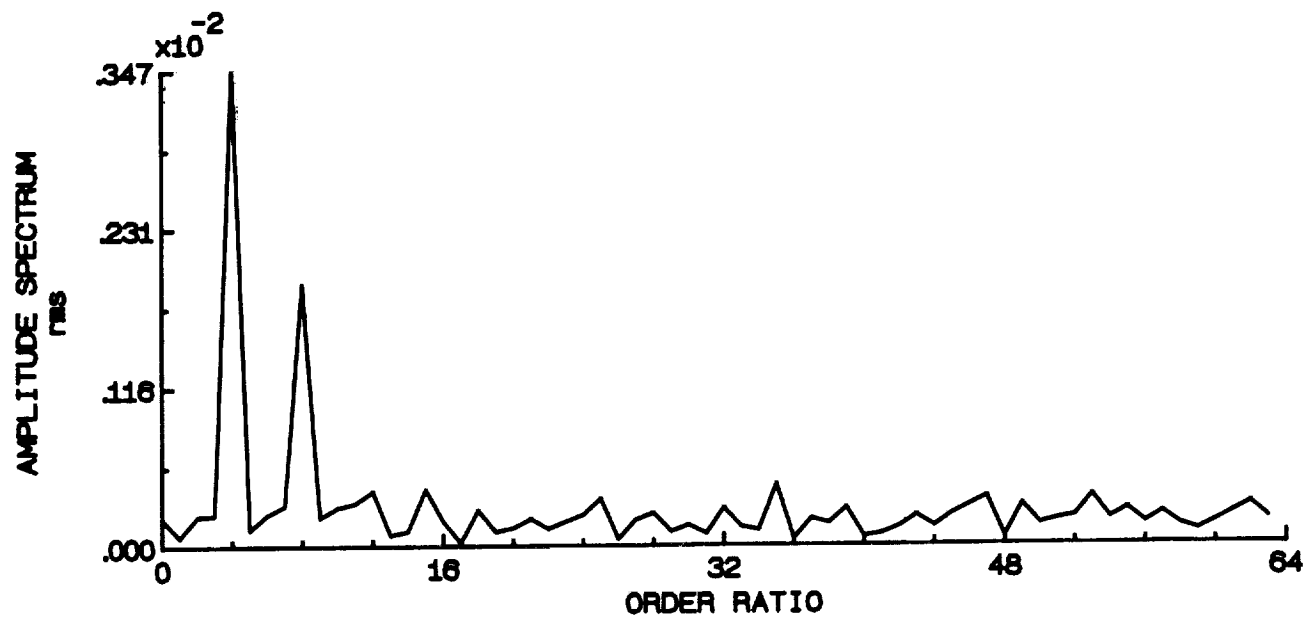
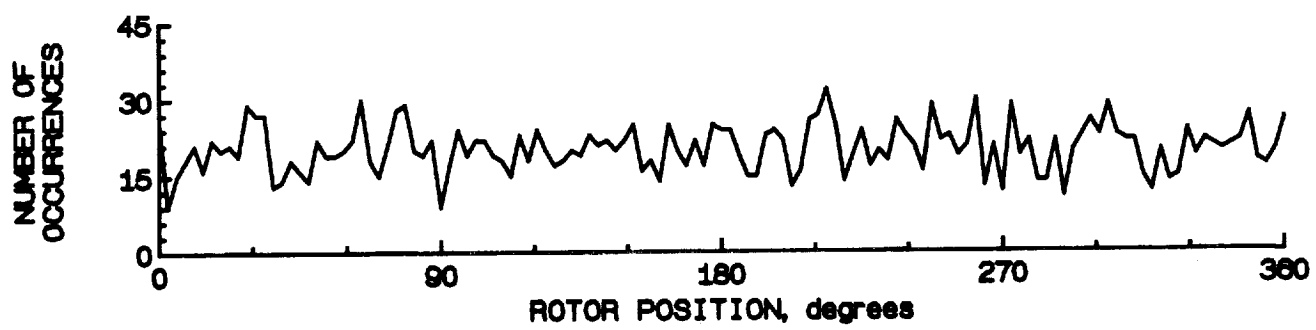
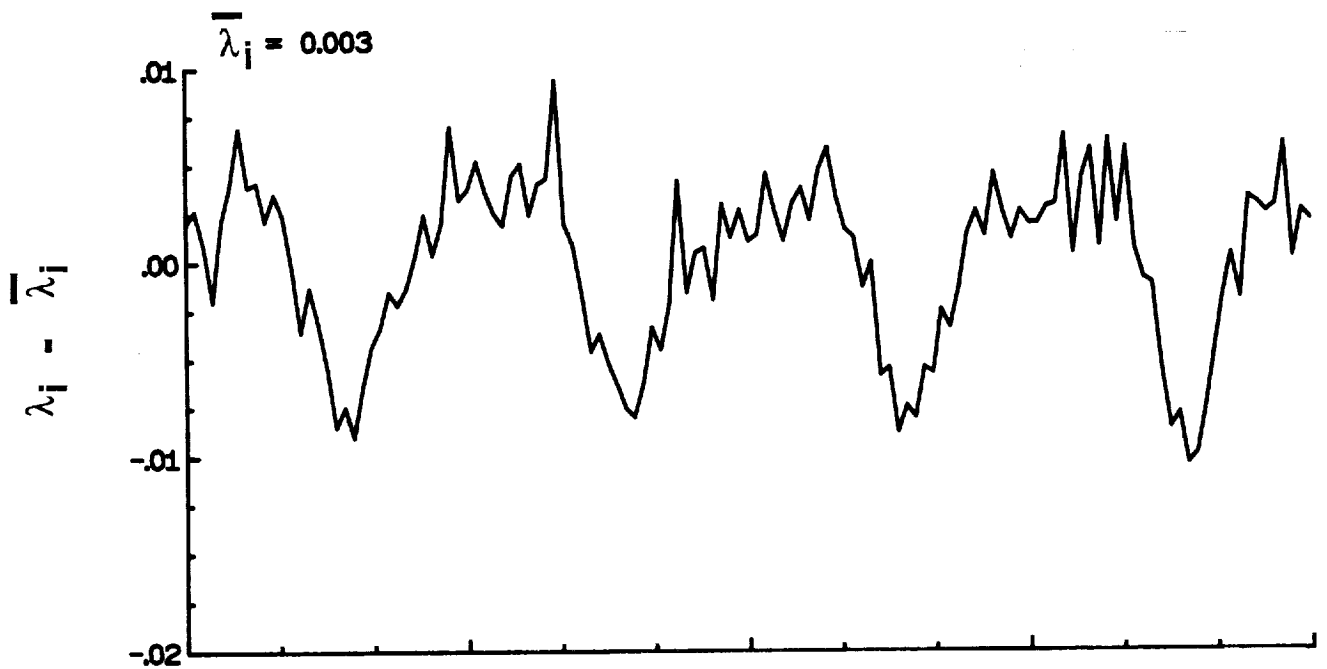


Figure 121.- Concluded.

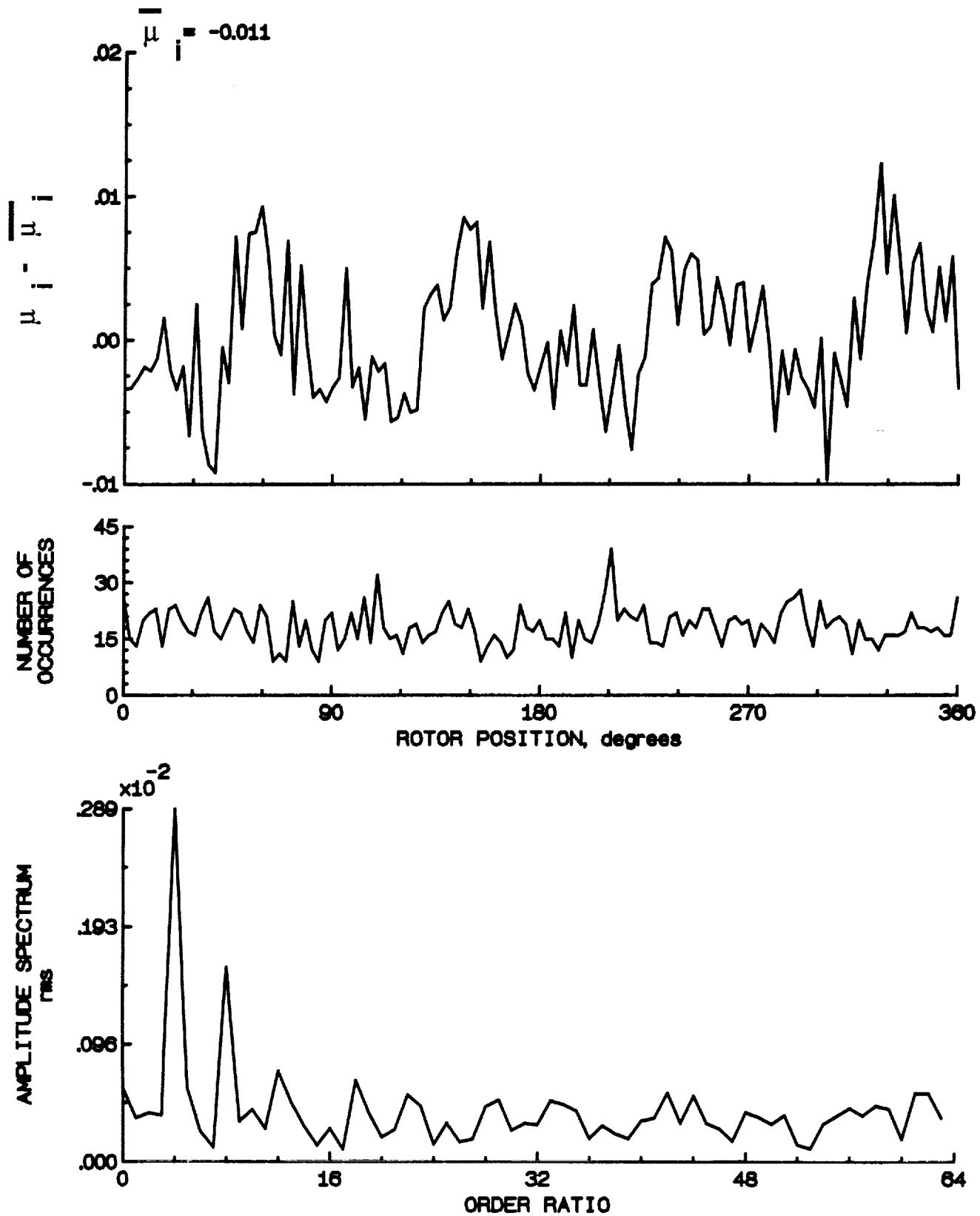


Figure 122.- Induced inflow velocity measured at 210 degrees and r/R of 0.82.

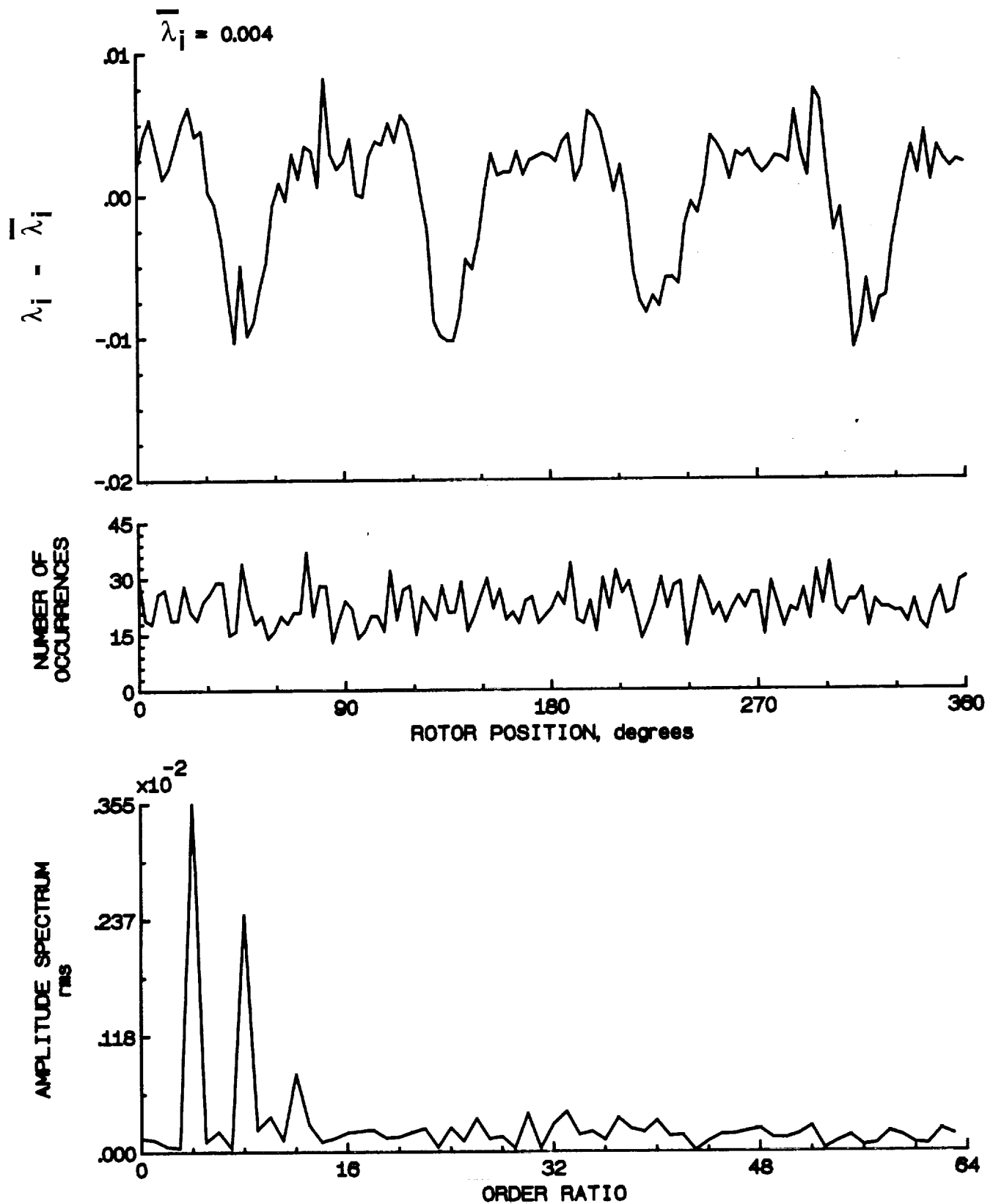


Figure 122.- Concluded.

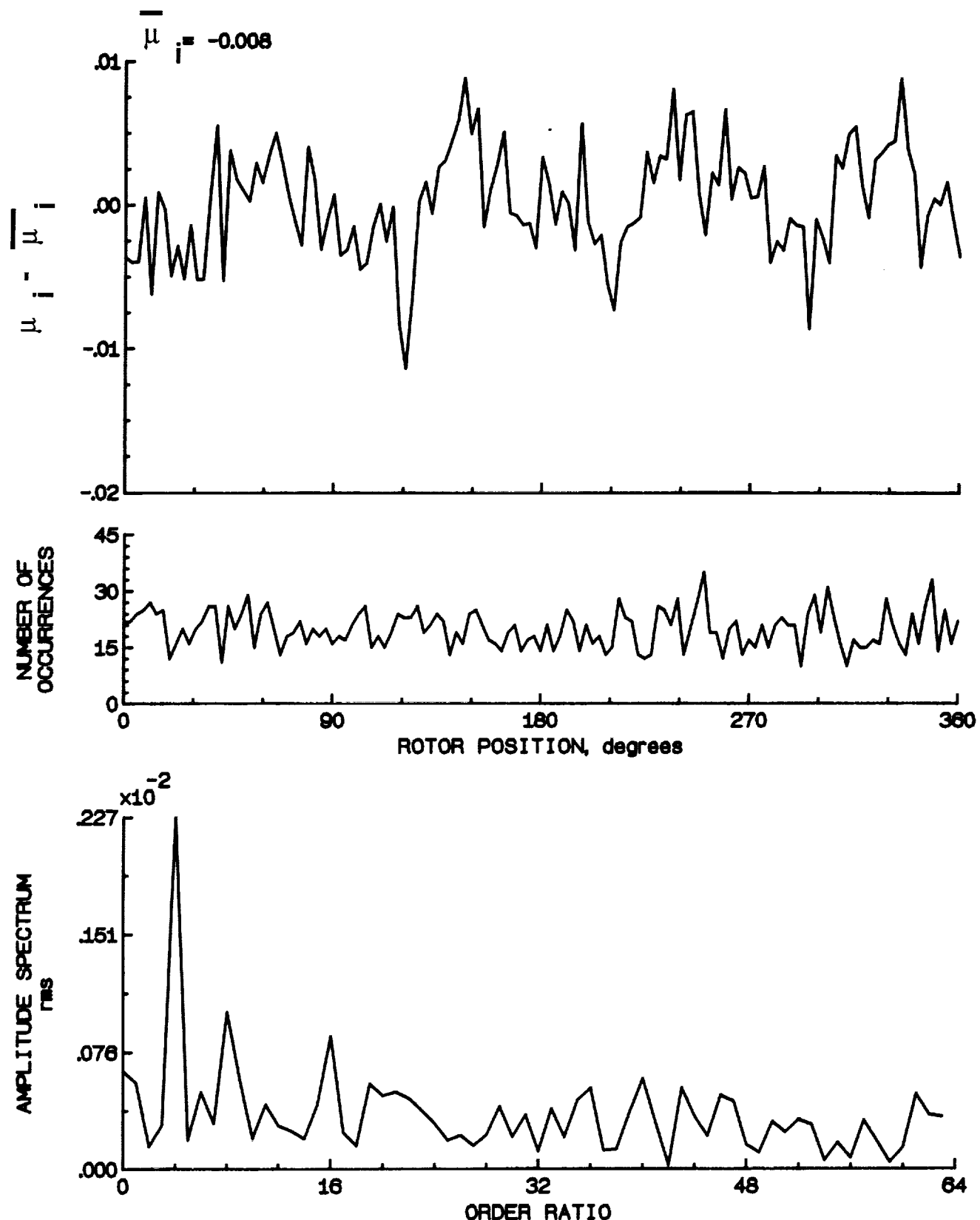


Figure 123.- Induced inflow velocity measured at 210 degrees and r/R of 0.86.

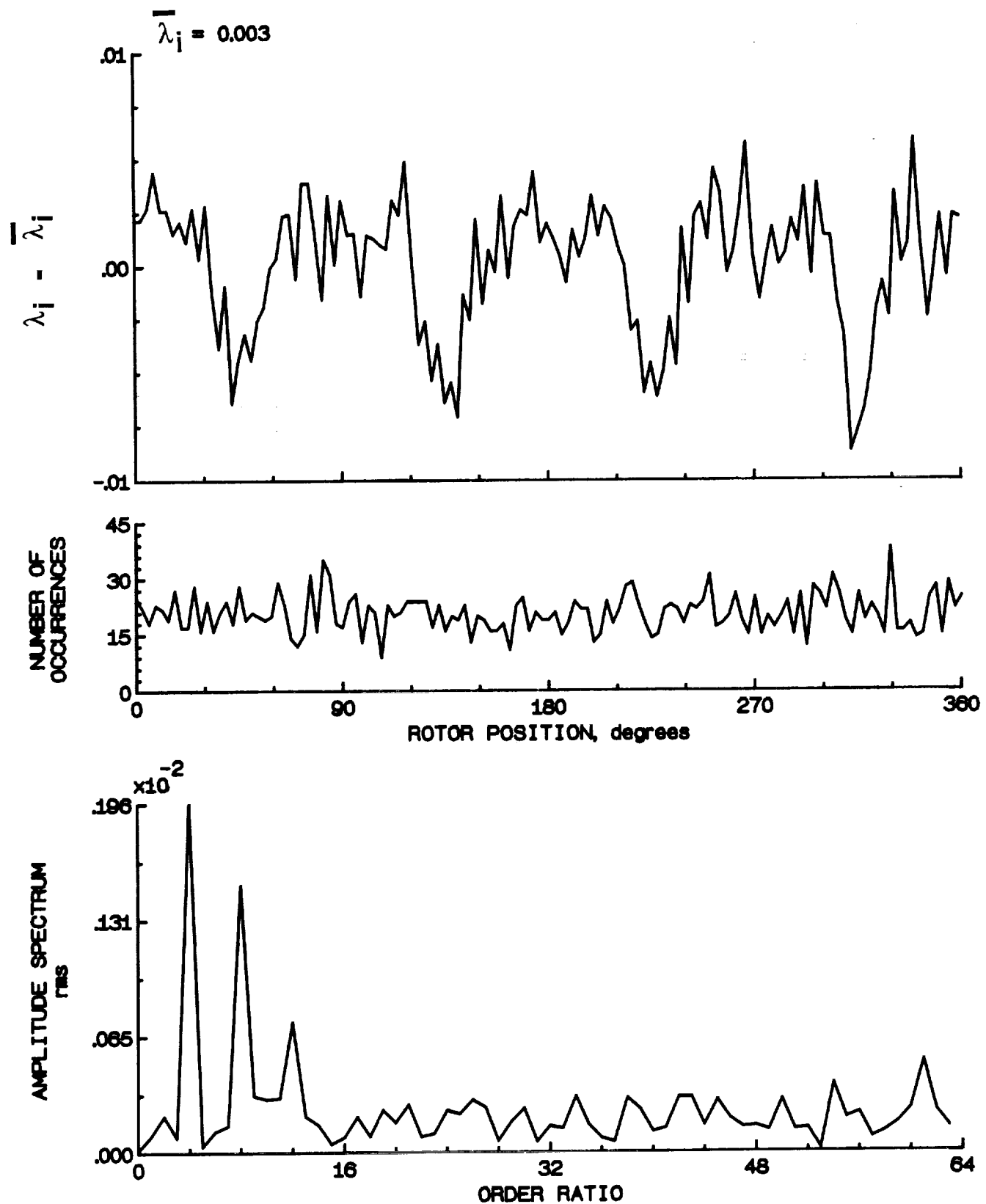


Figure 123.- Concluded.

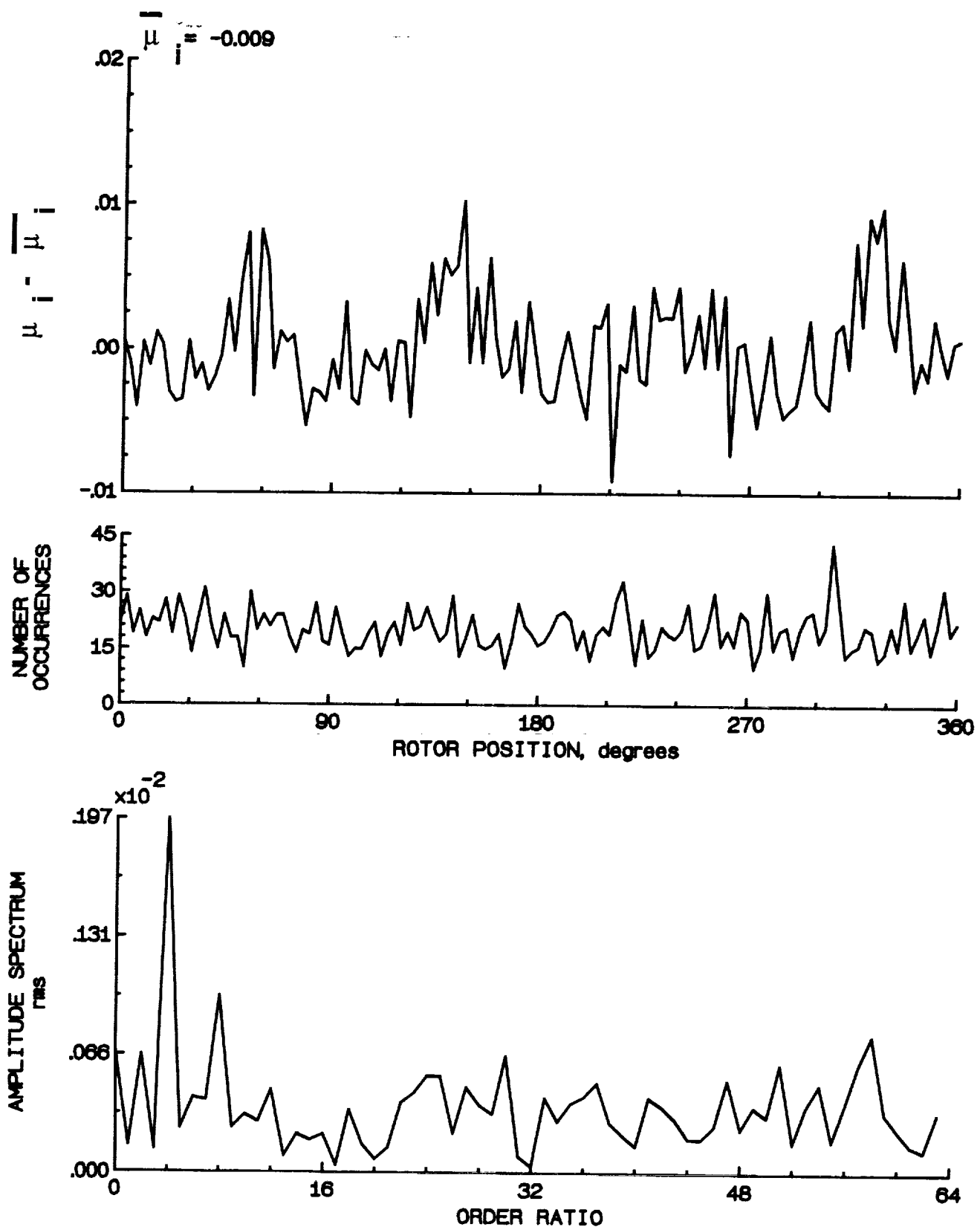


Figure 124.- Induced inflow velocity measured at 210 degrees and r/R of 0.90.

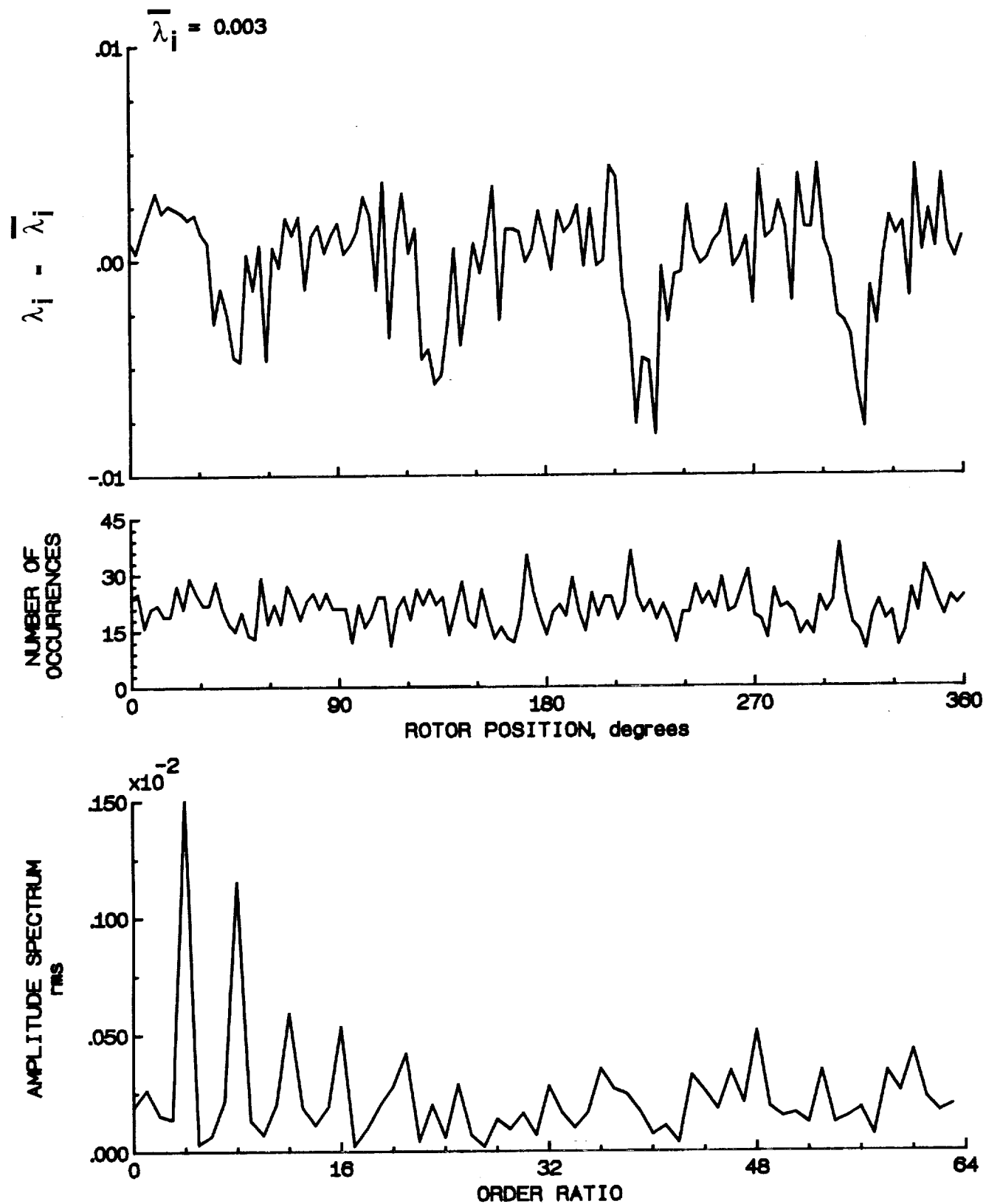


Figure 124.- Concluded.

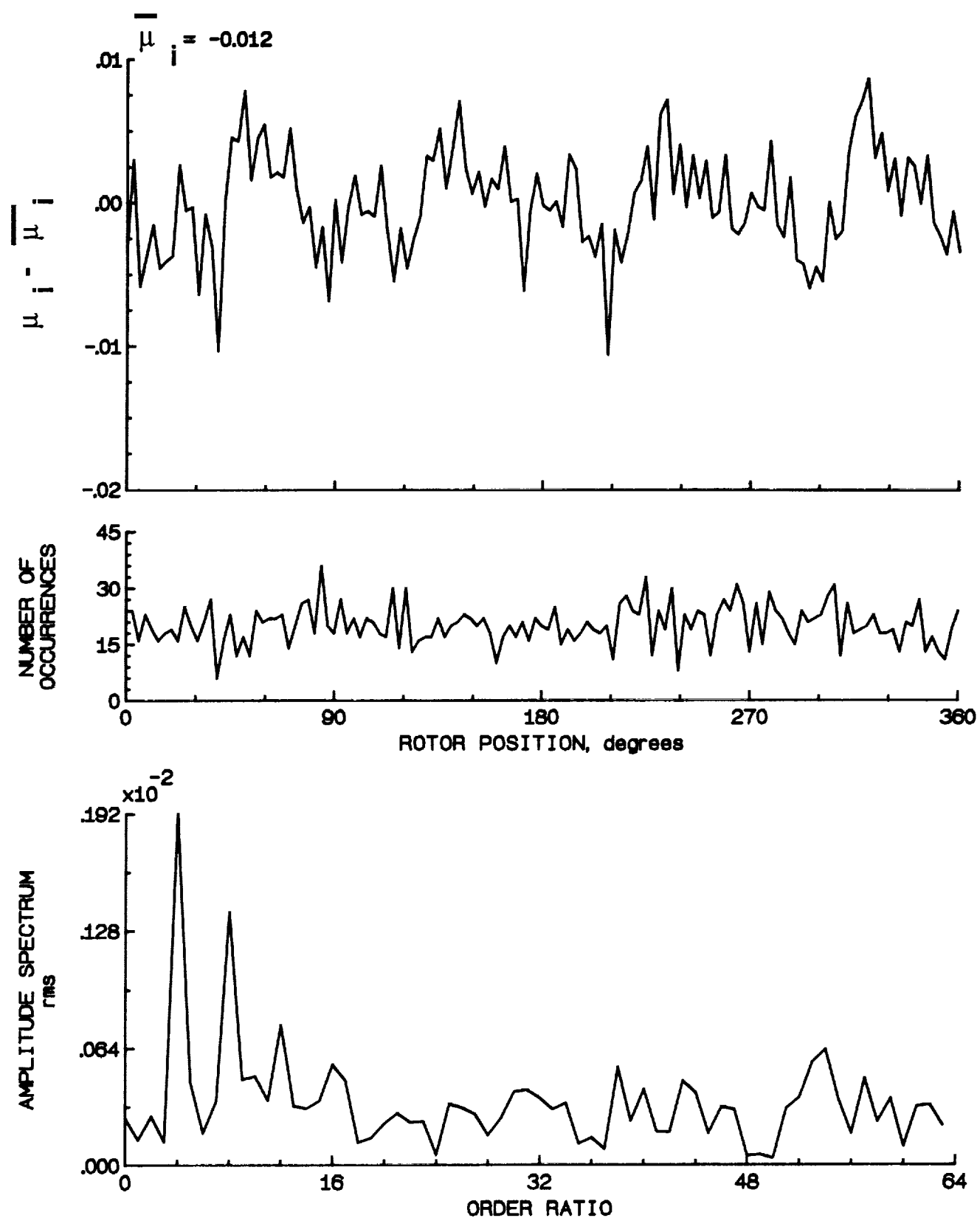


Figure 125.- Induced inflow velocity measured at 210 degrees and r/R of 0.94.

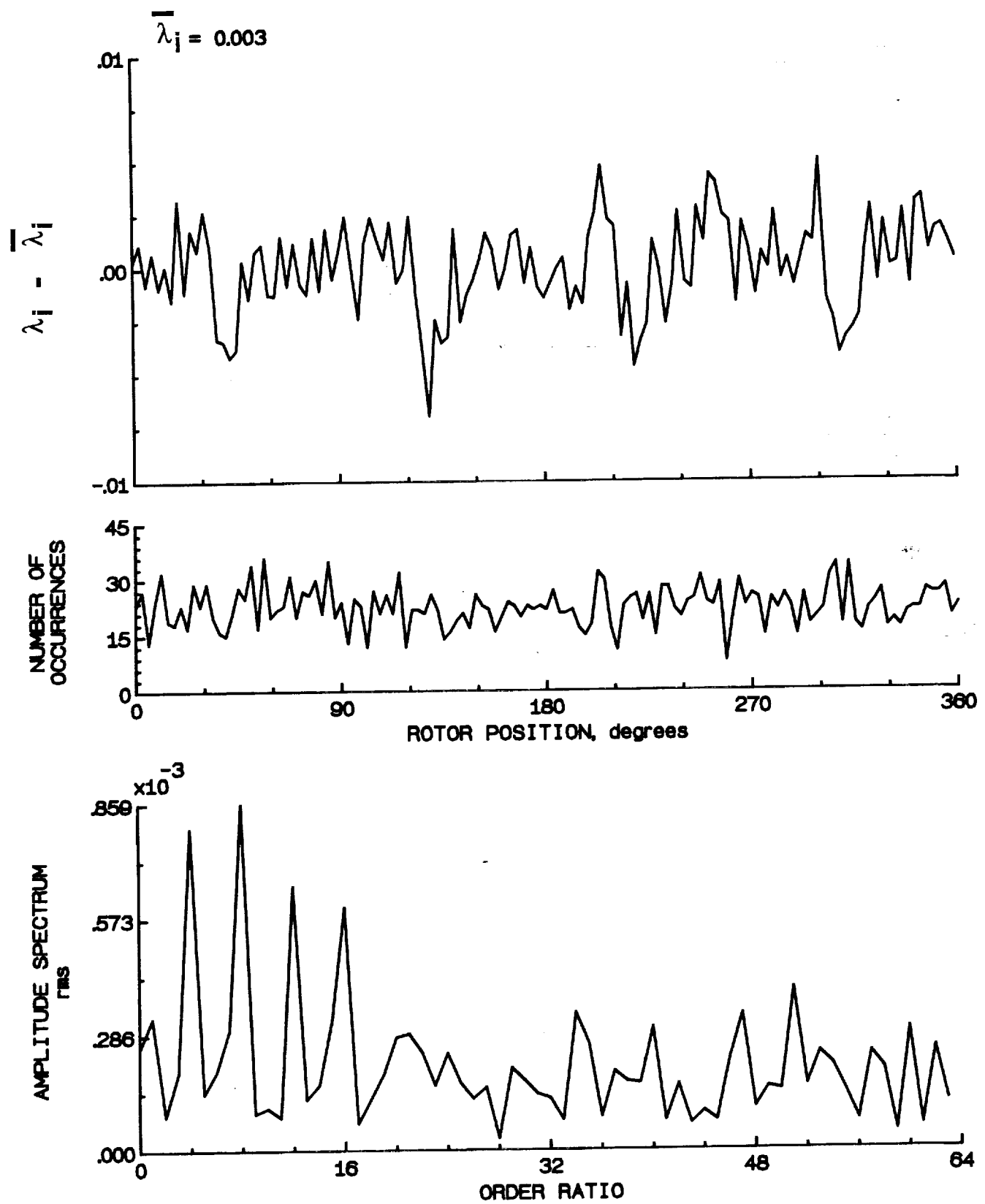


Figure 125.- Concluded.

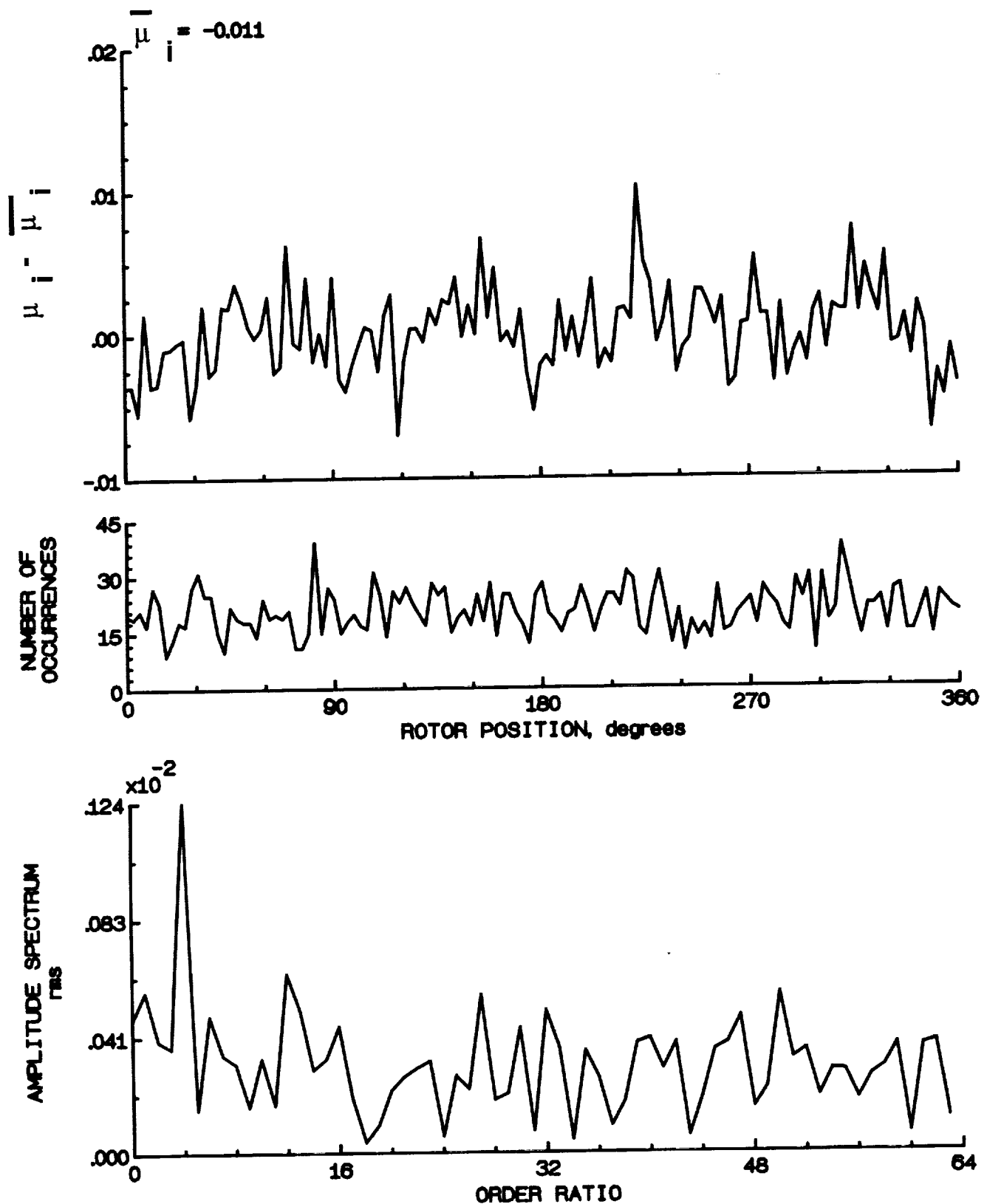


Figure 126.- Induced inflow velocity measured at 210 degrees and r/R of 0.98.

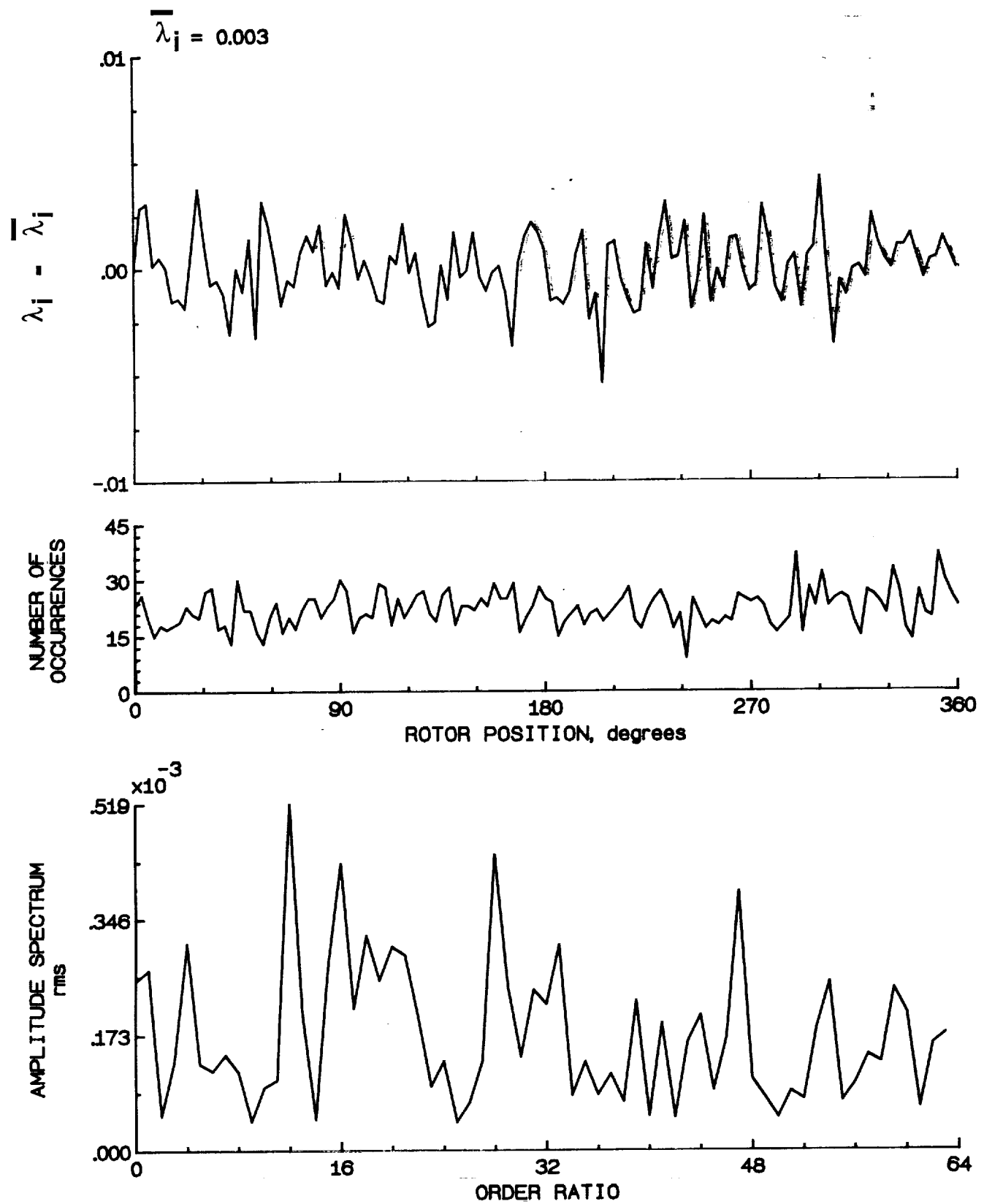


Figure 126.- Concluded.

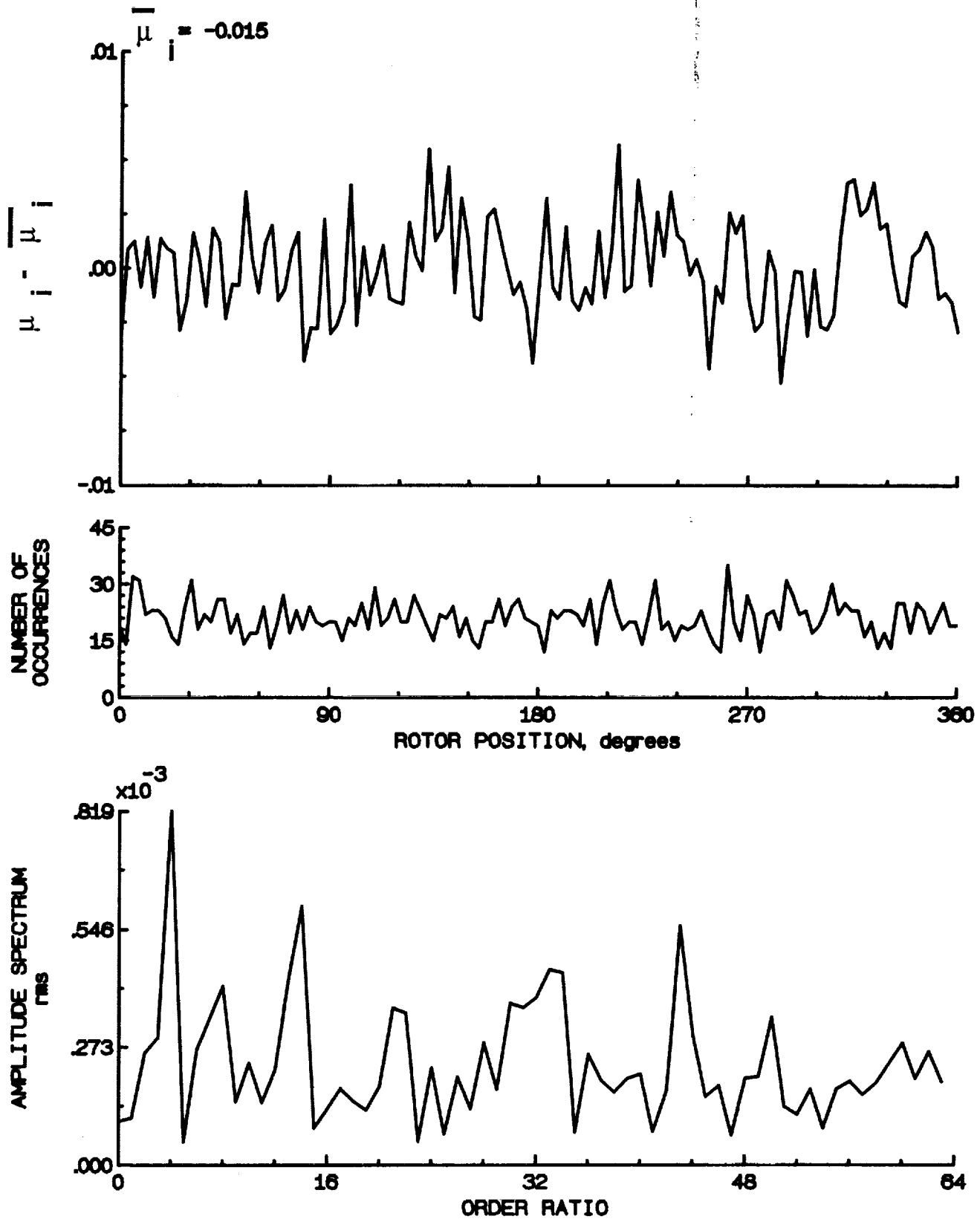


Figure 127.- Induced inflow velocity measured at 210 degrees and r/R of 1.02.

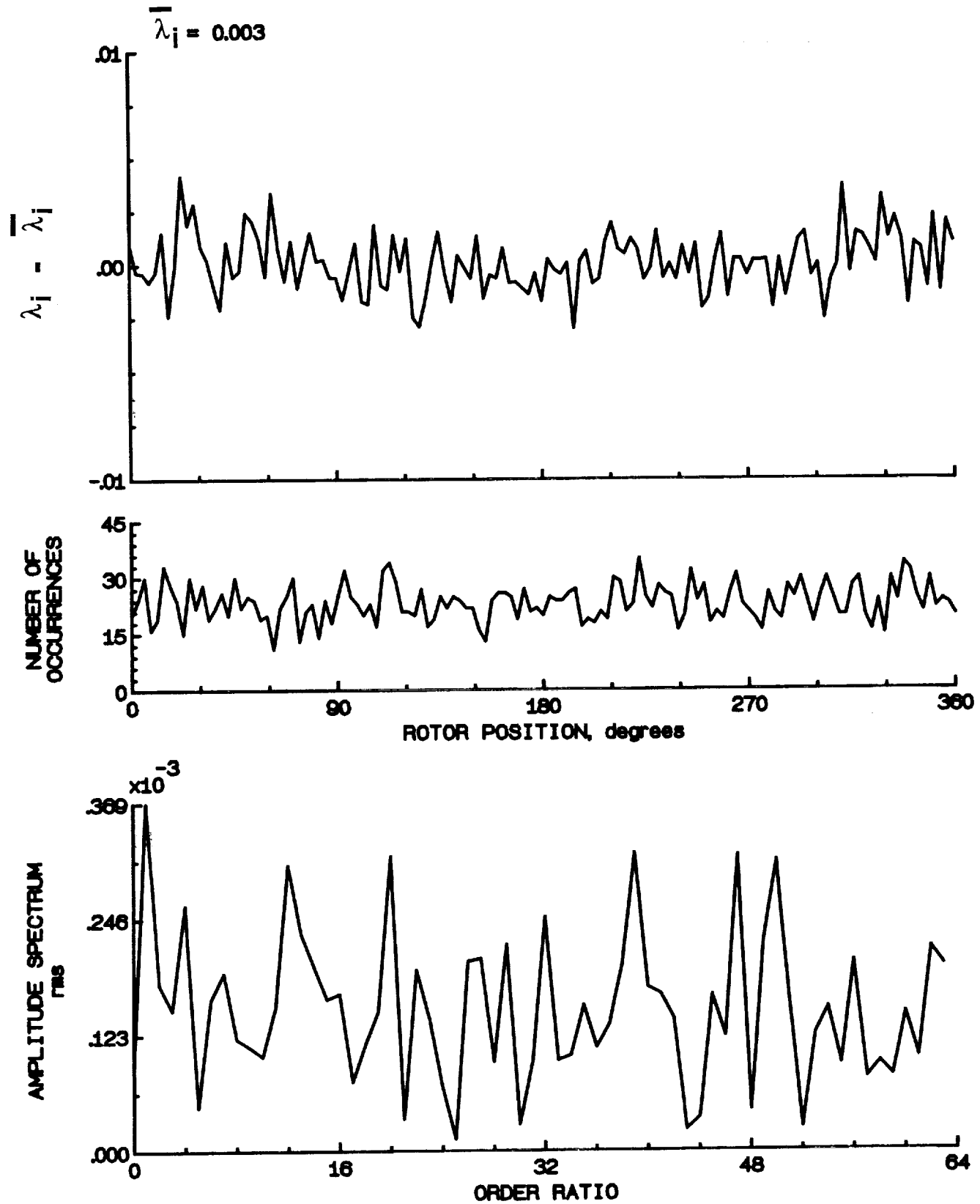


Figure 127.- Concluded.

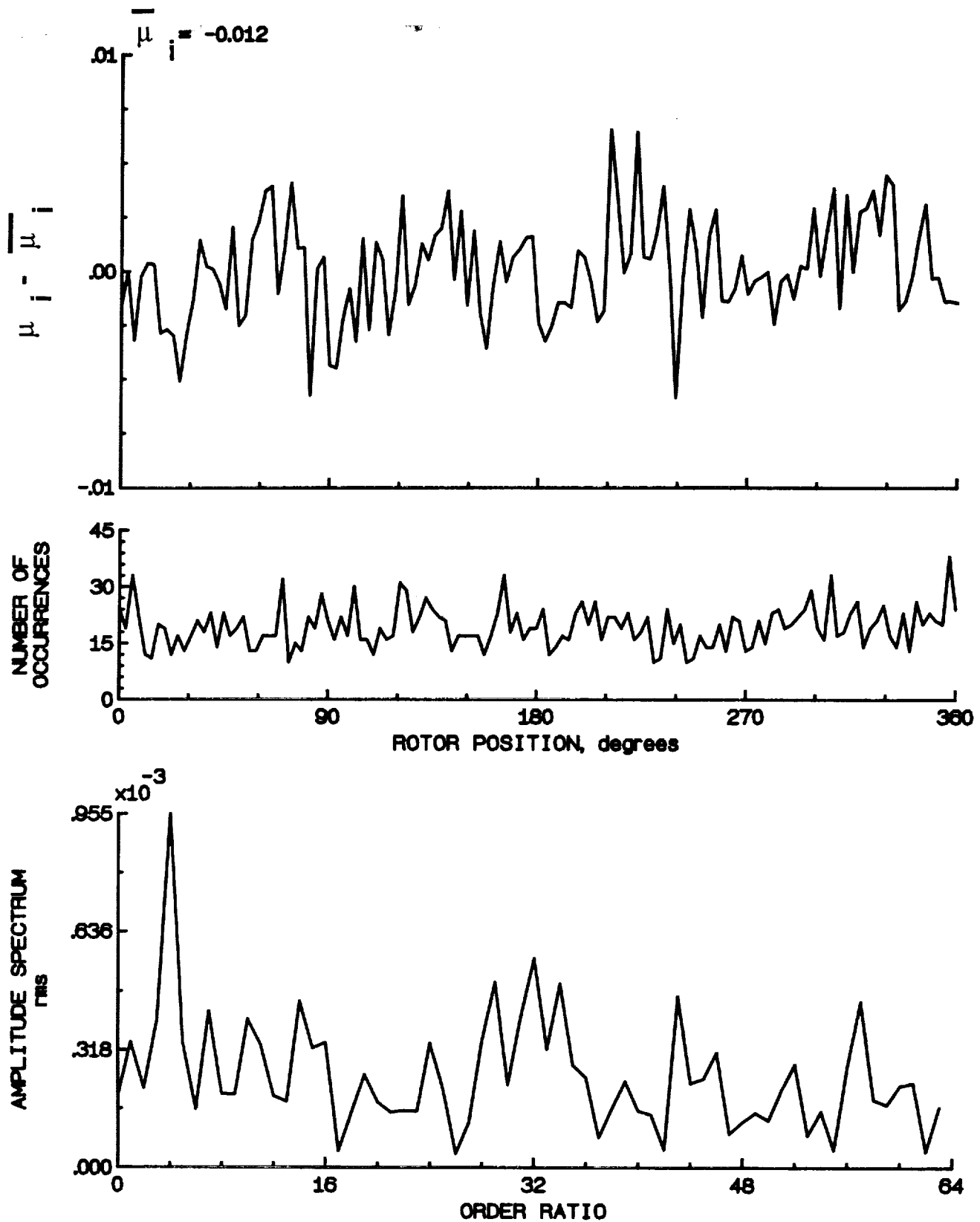


Figure 128.- Induced inflow velocity measured at 210 degrees and r/R of 1.04.

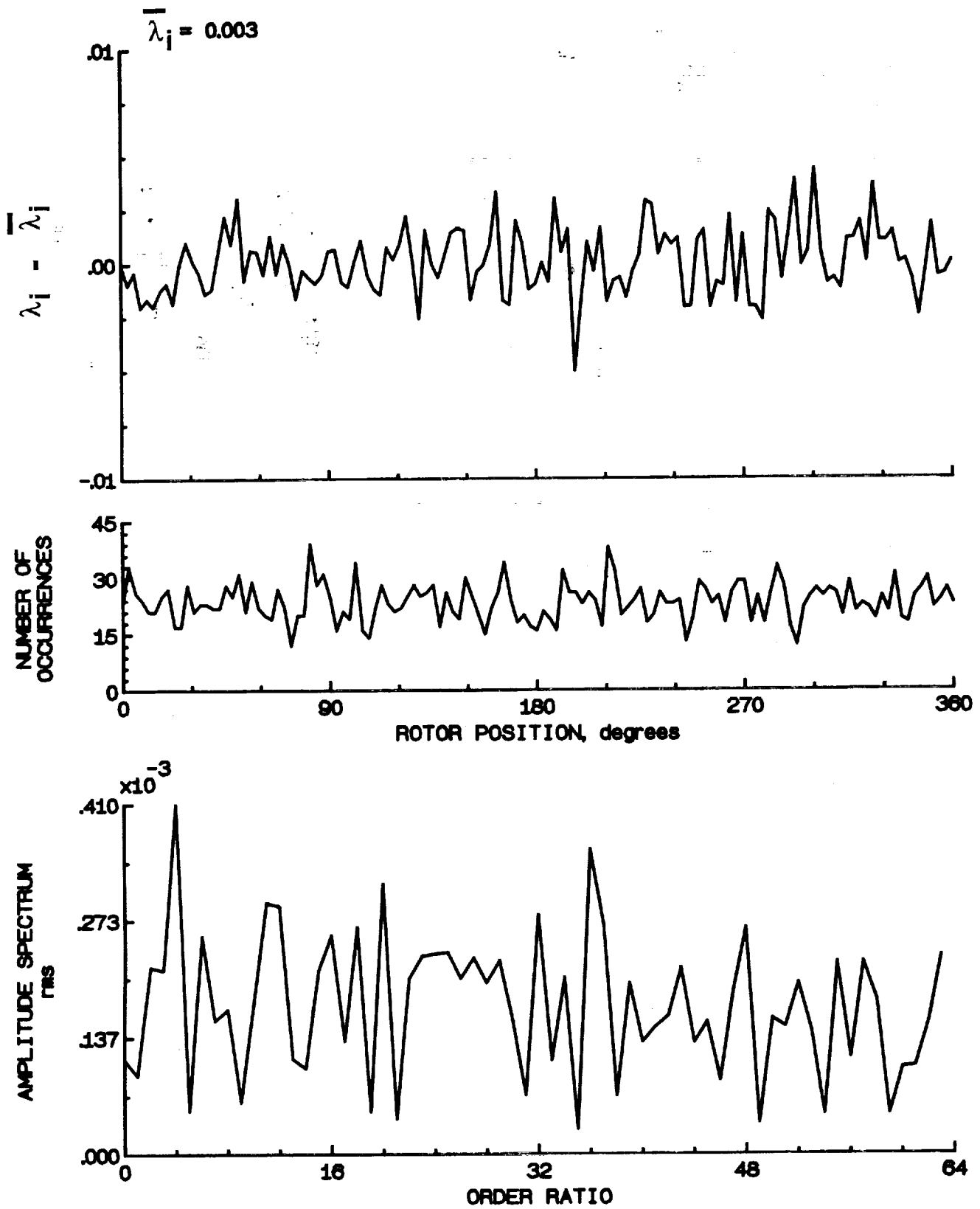


Figure 128.- Concluded.

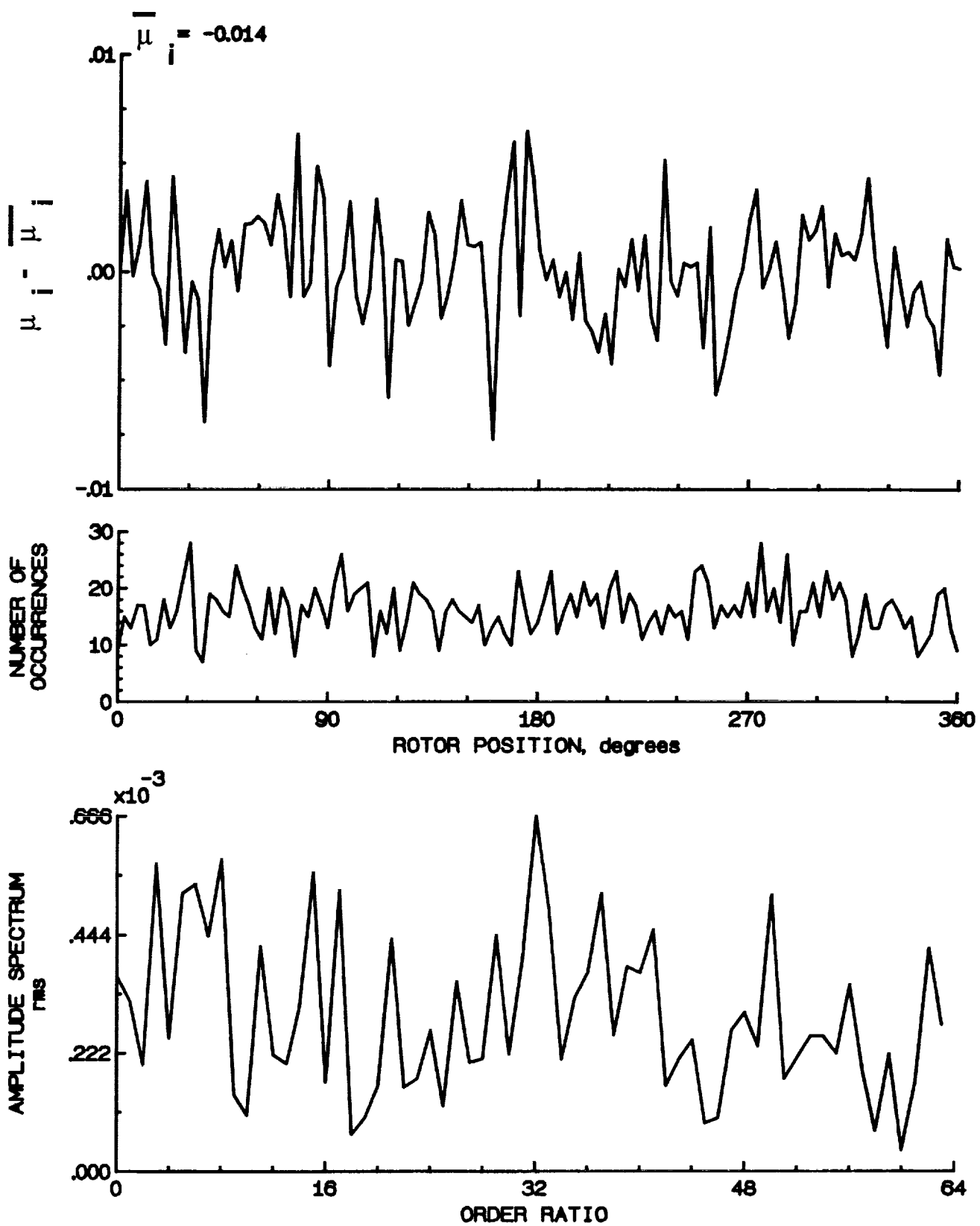


Figure 129.- Induced inflow velocity measured at 210 degrees and r/R of 1.10.

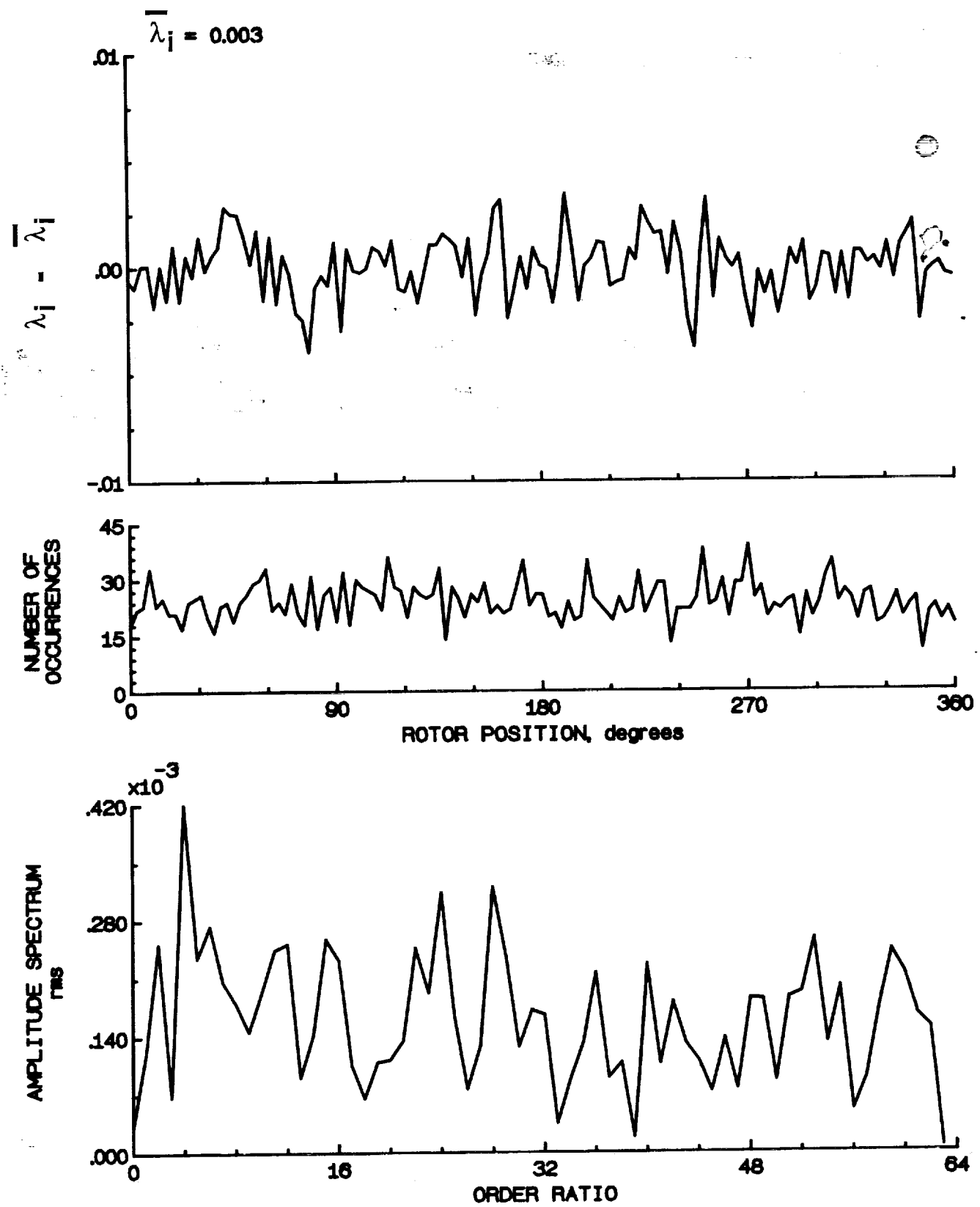


Figure 129.- Concluded.

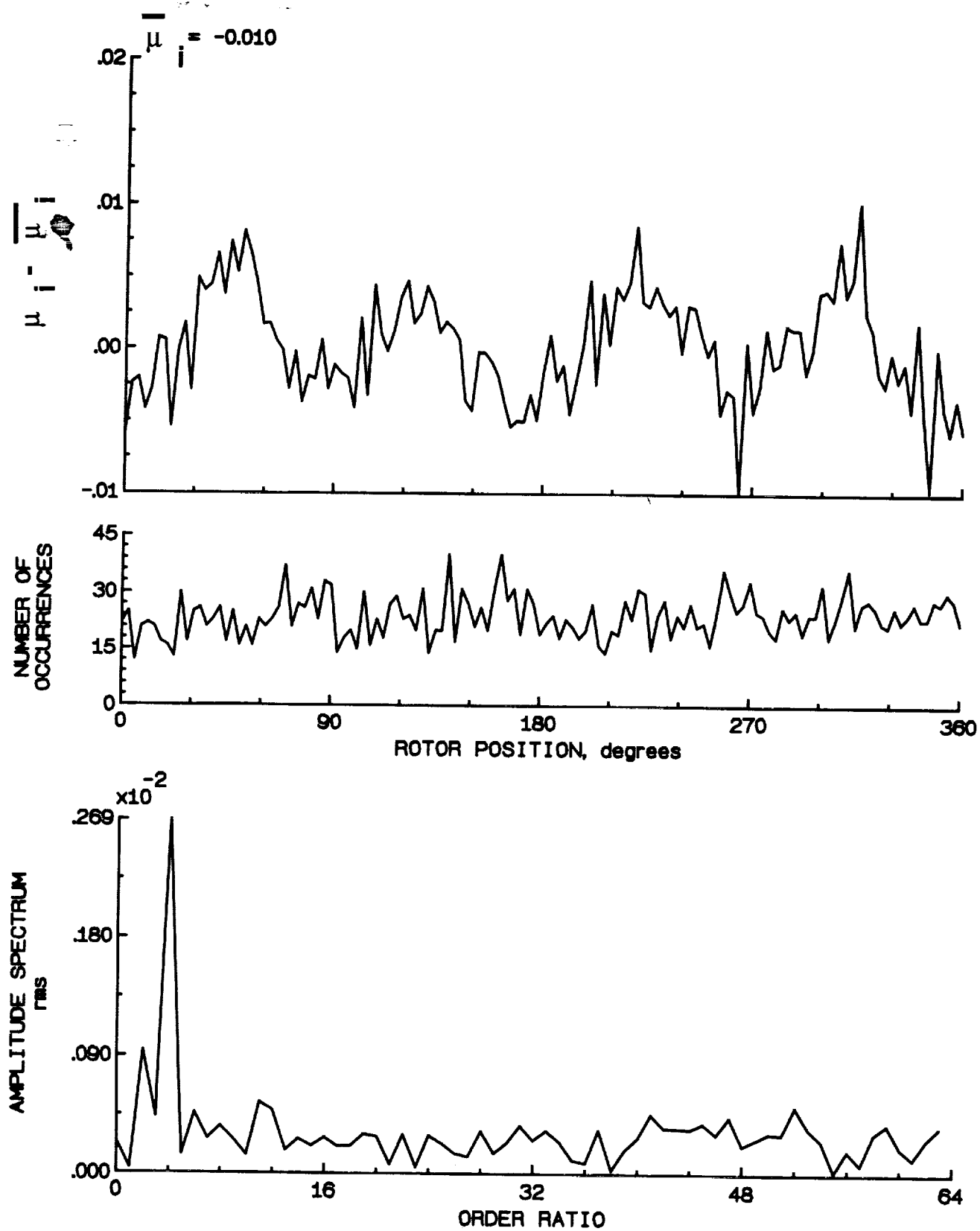


Figure 130.- Induced inflow velocity measured at 240 degrees and r/R of 0.20.

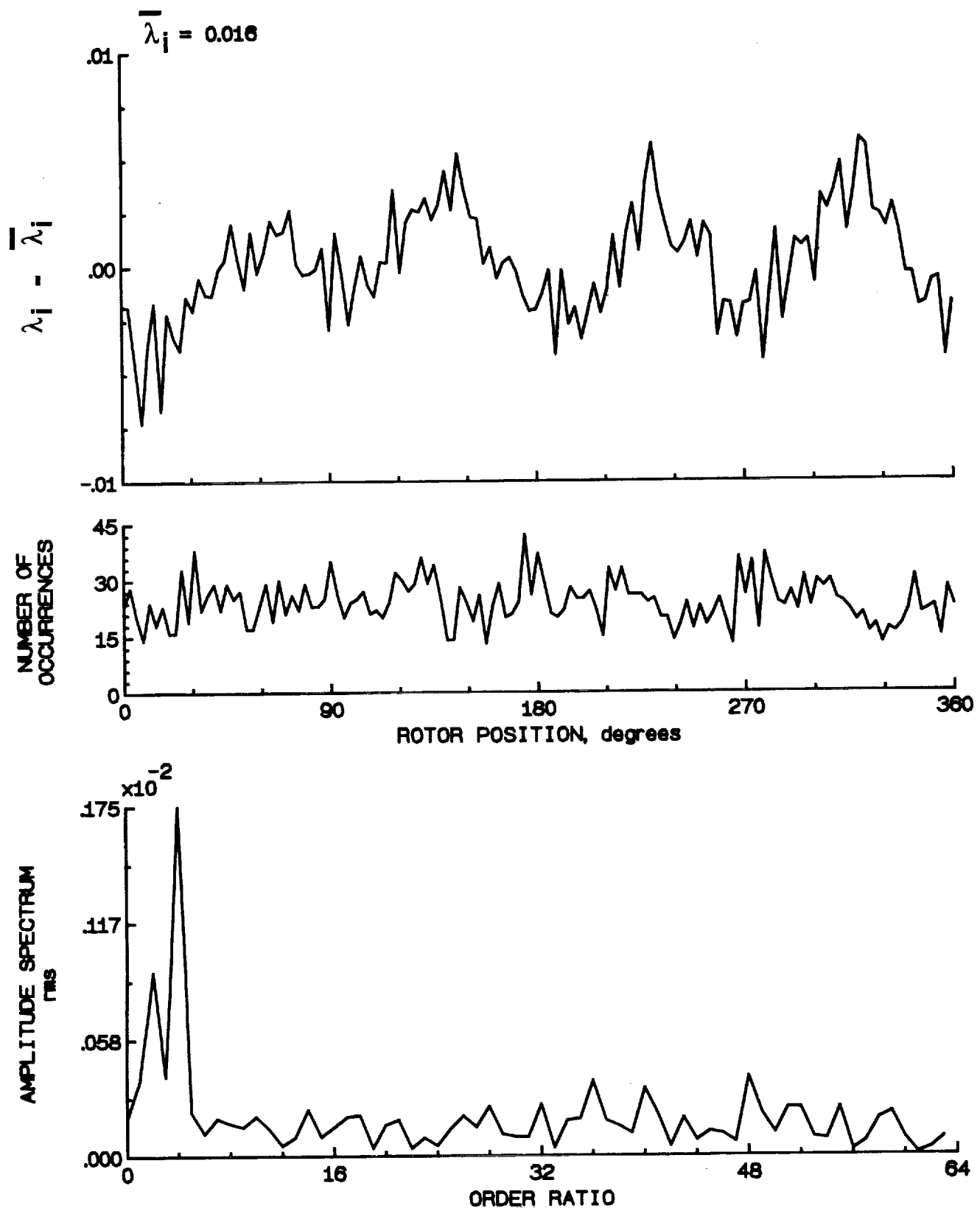


Figure 130.- Concluded.

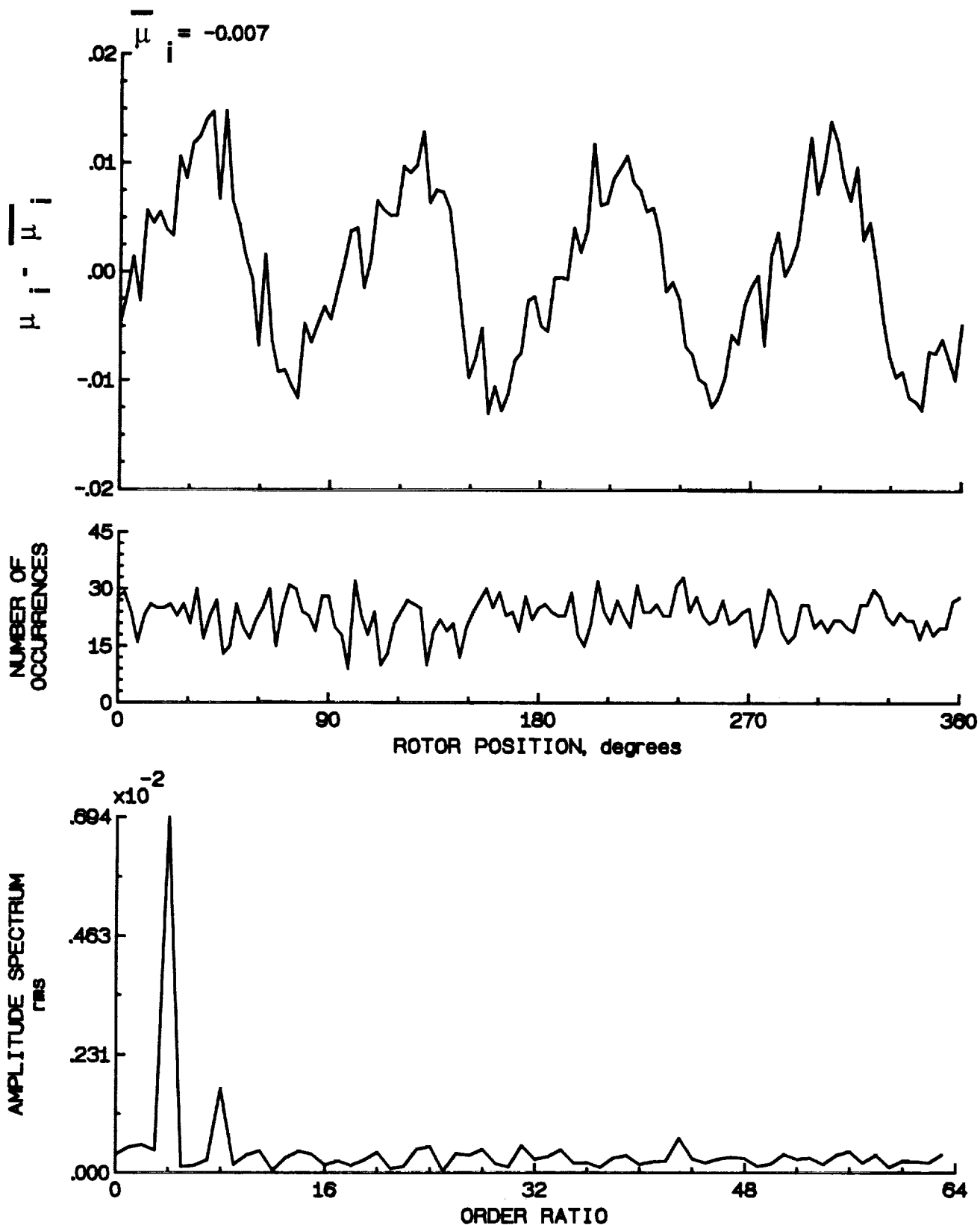


Figure 131.- Induced inflow velocity measured at 240 degrees and r/R of 0.40.

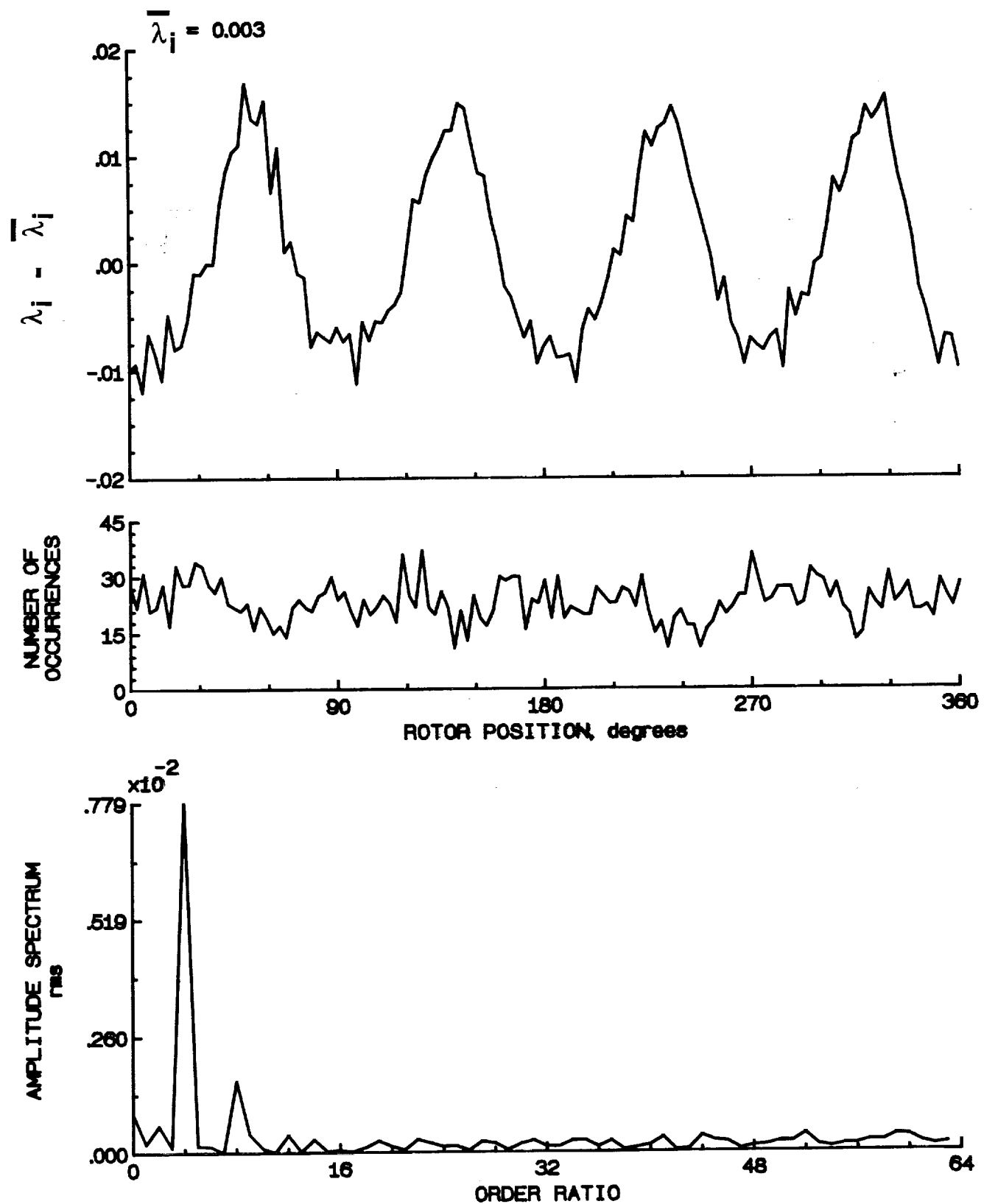


Figure 131.- Concluded.

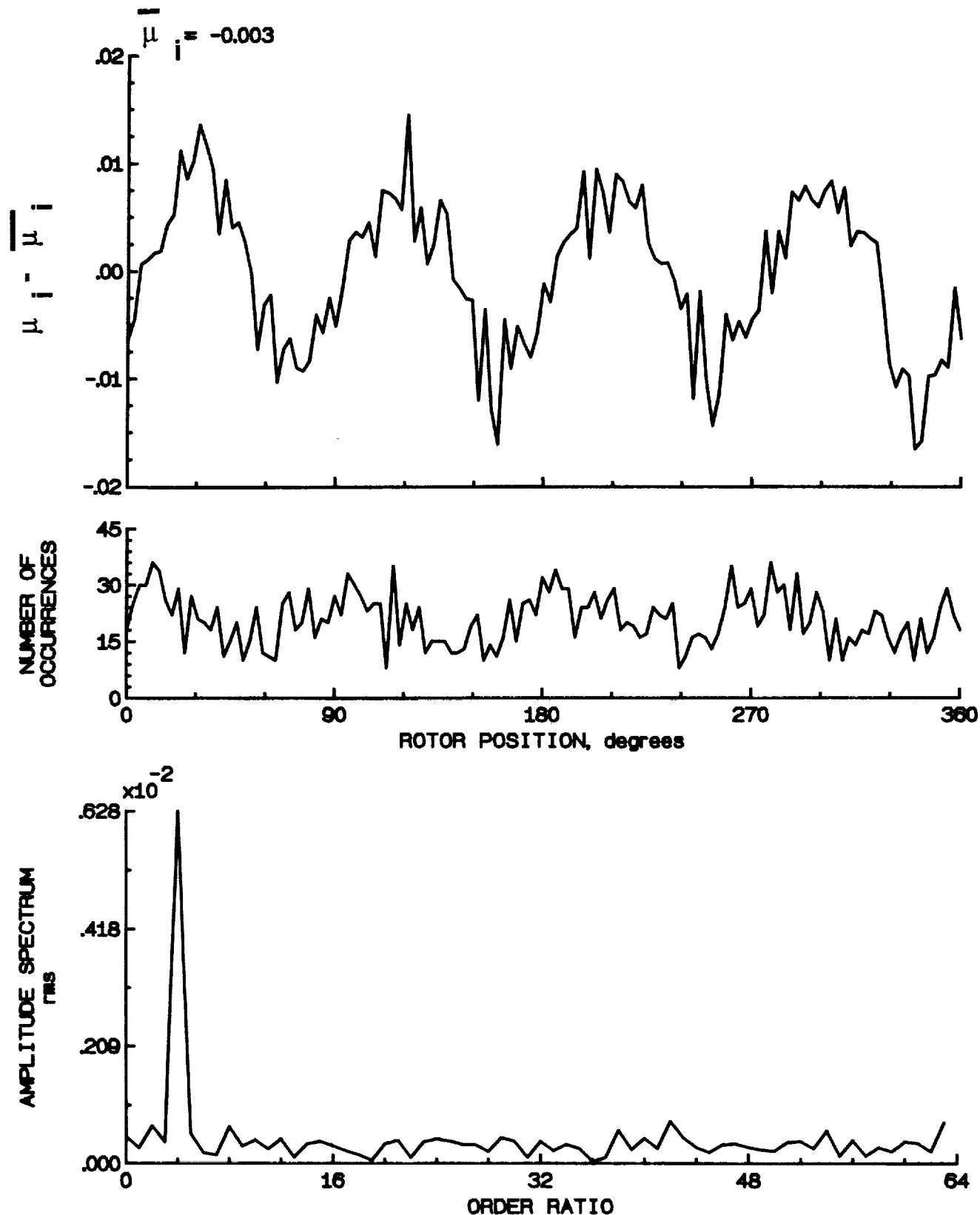


Figure 132.- Induced inflow velocity measured at 240 degrees and r/R of 0.50.

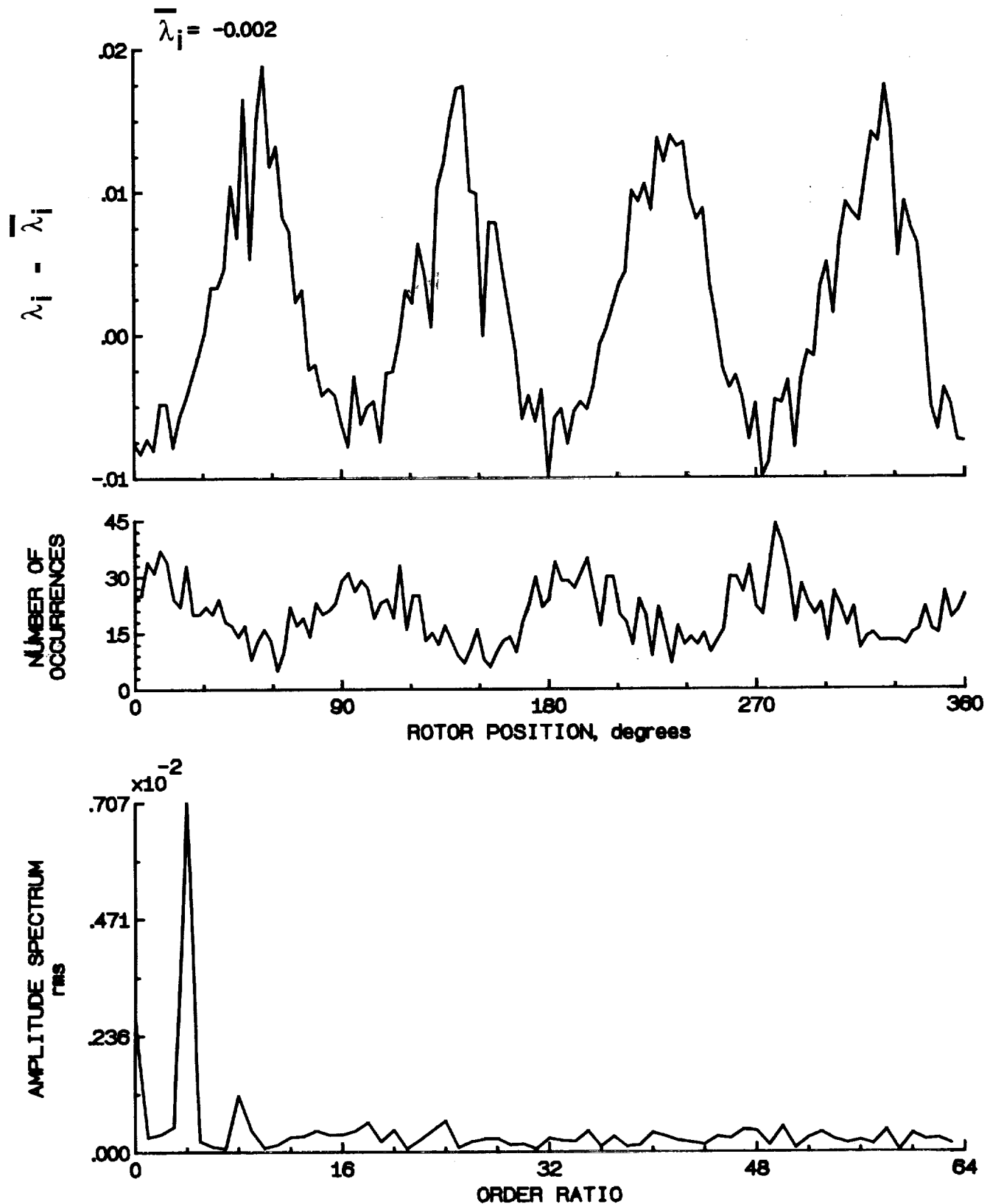


Figure 132.- Concluded.

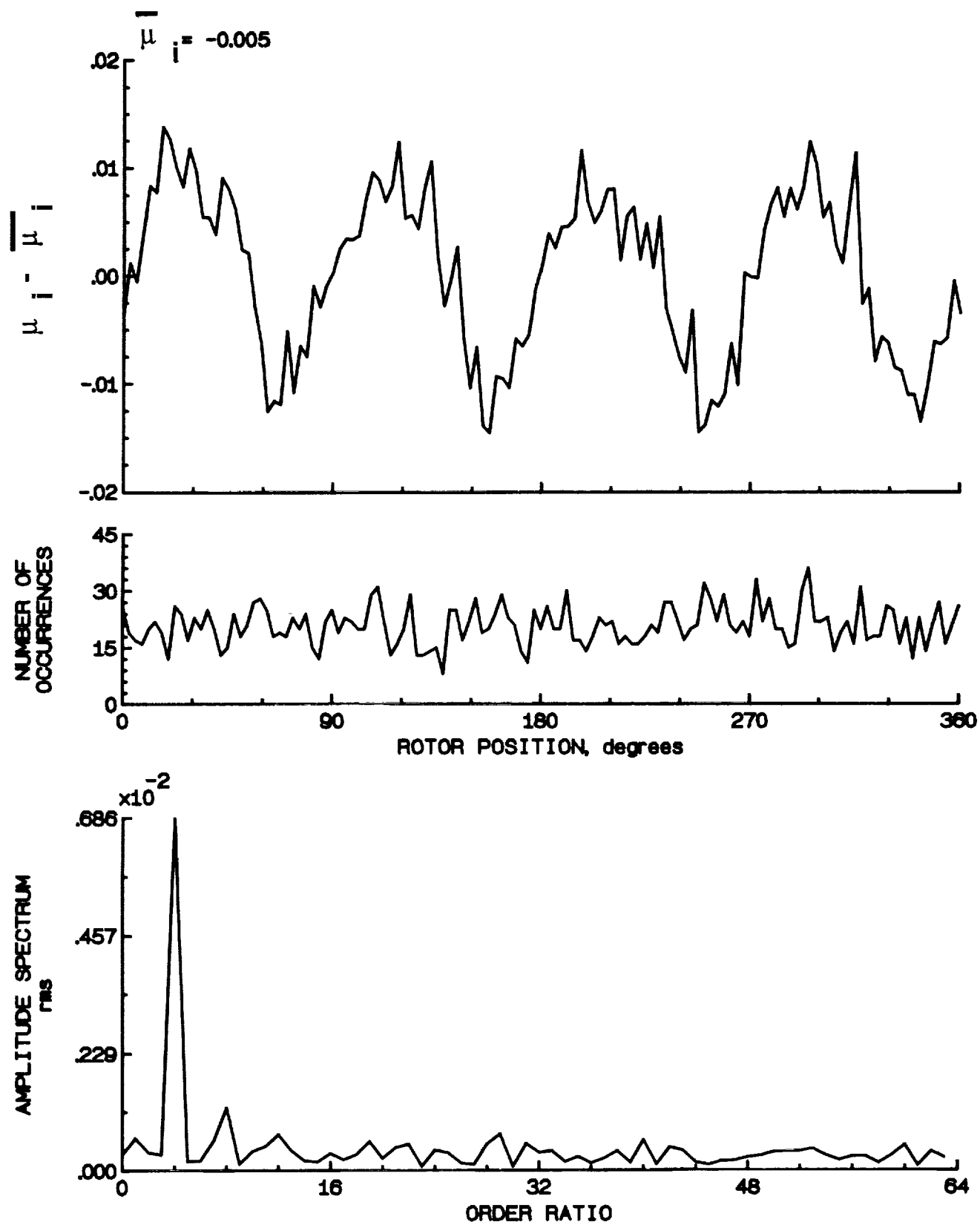


Figure 133.- Induced inflow velocity measured at 240 degrees and r/R of 0.60.

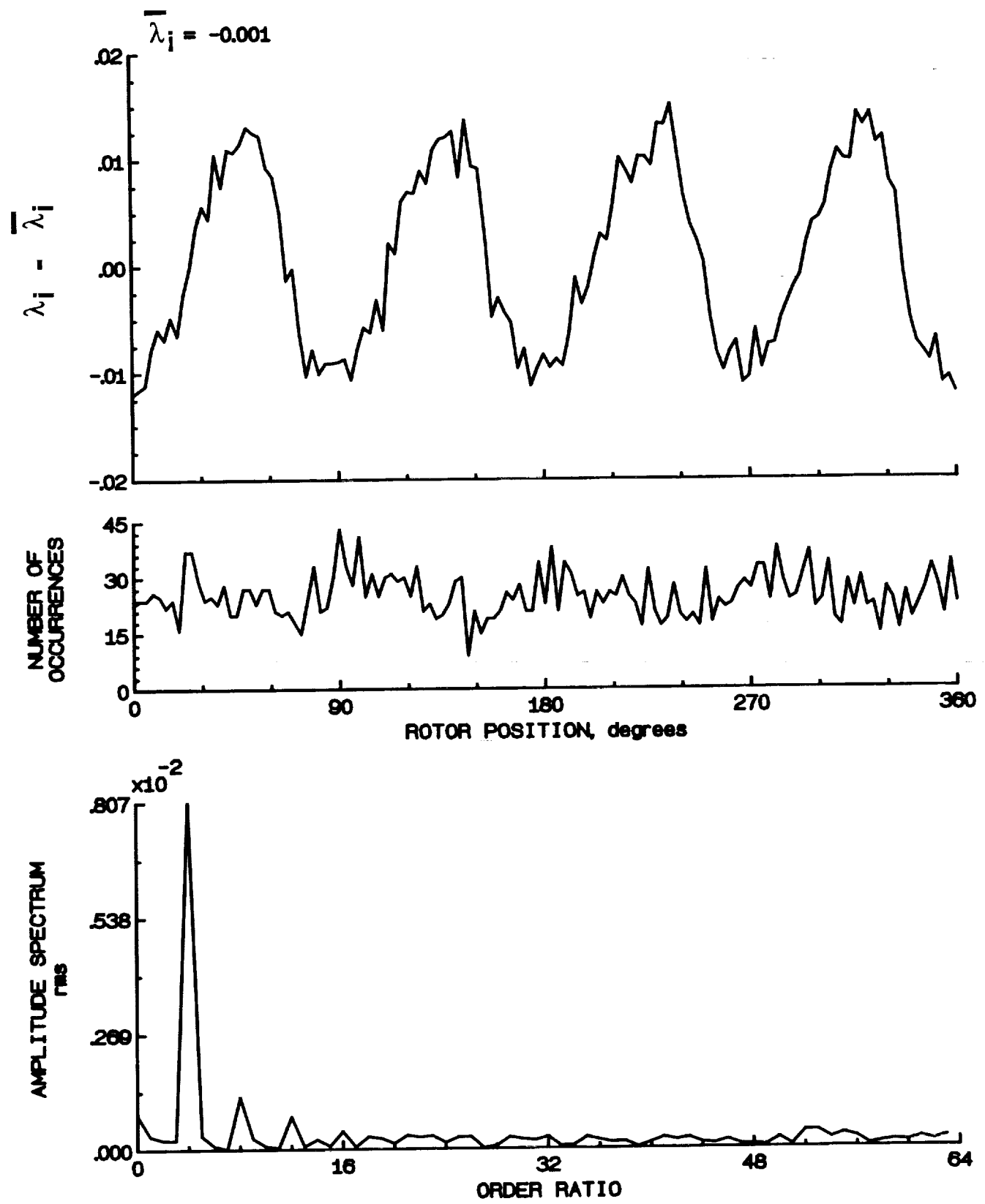


Figure 133.- Concluded.

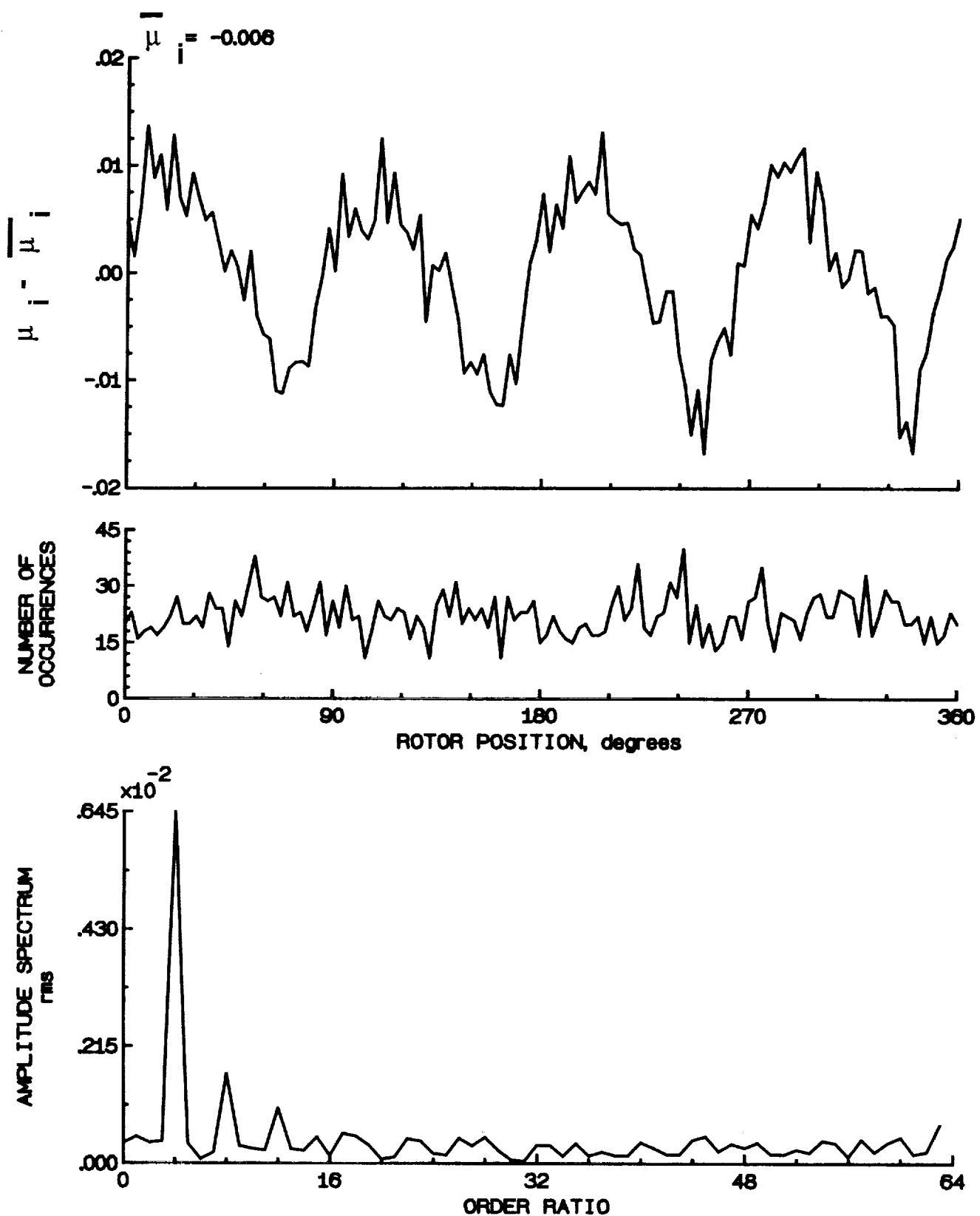


Figure 134.- Induced inflow velocity measured at 240 degrees and r/R of 0.70.

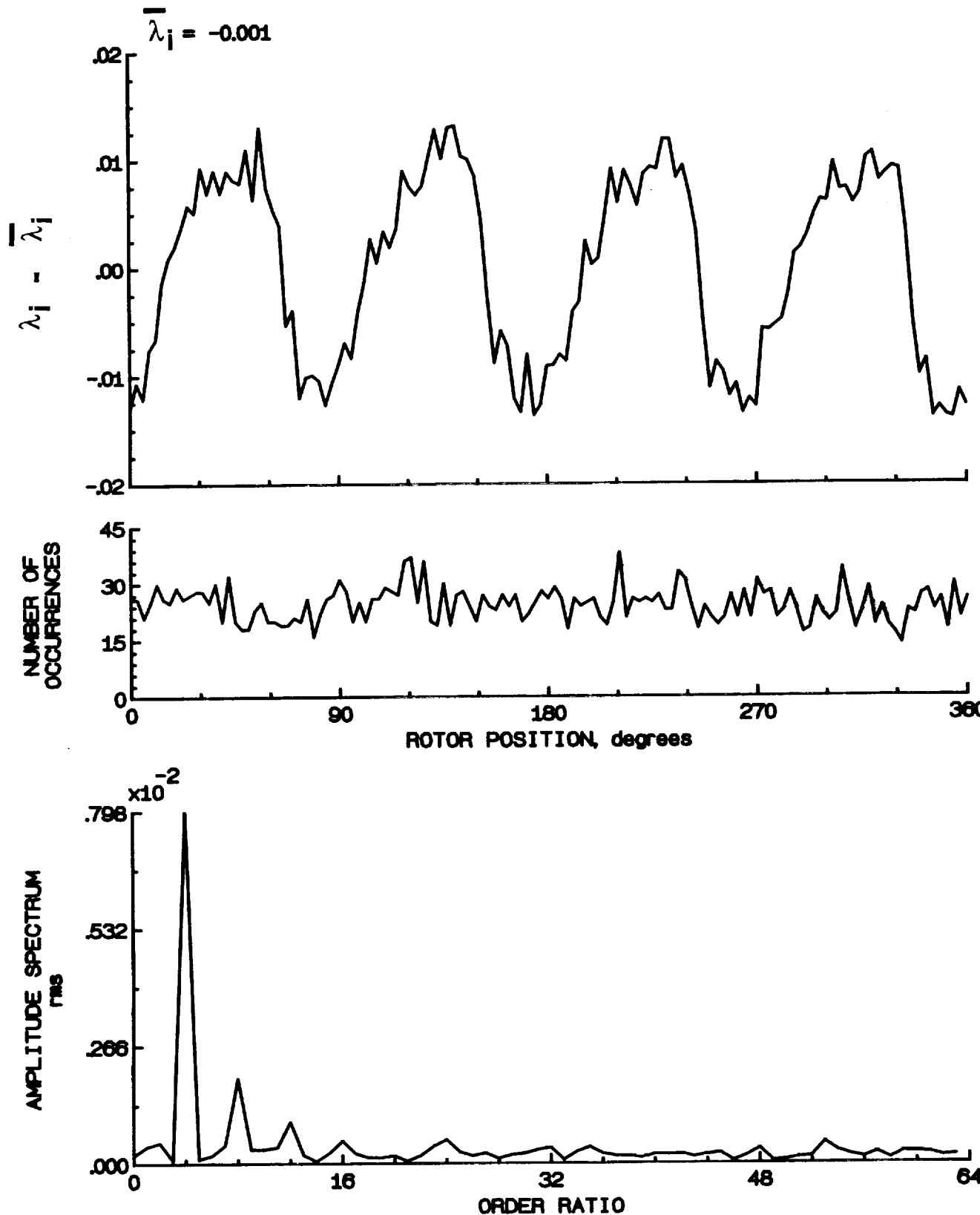


Figure 134.- Concluded.

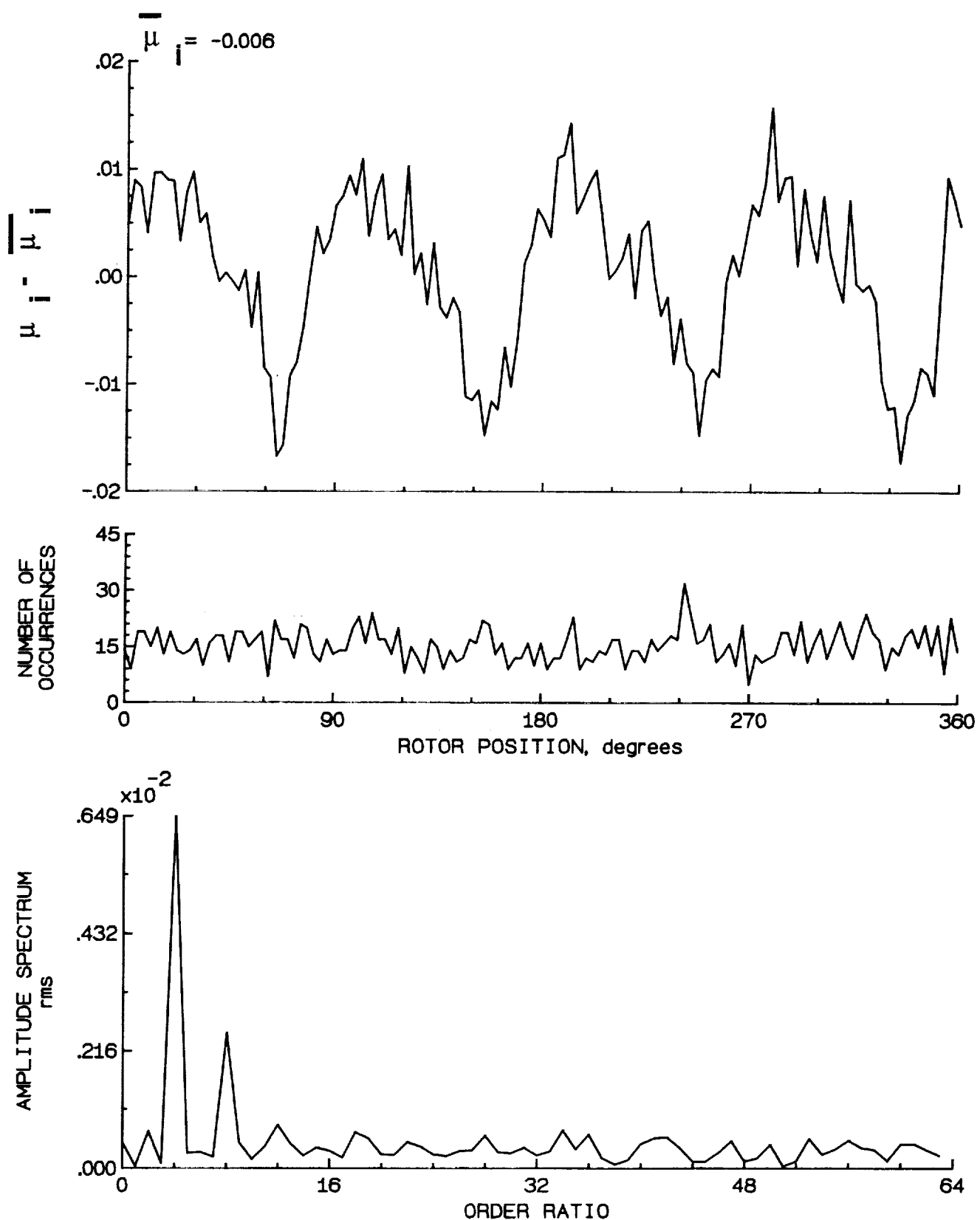


Figure 135.- Induced inflow velocity measured at 240 degrees and r/R of 0.74.

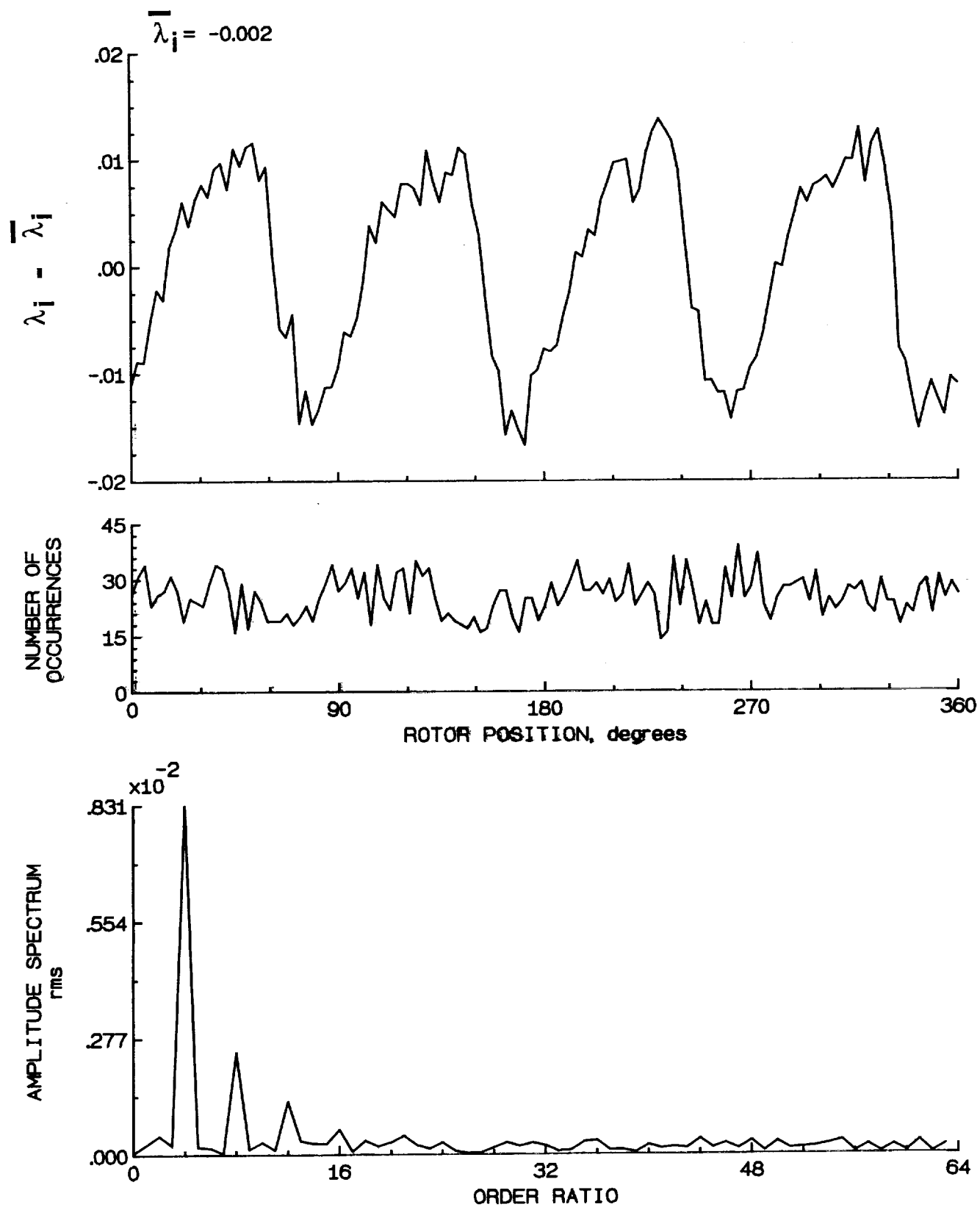


Figure 135.- Concluded.

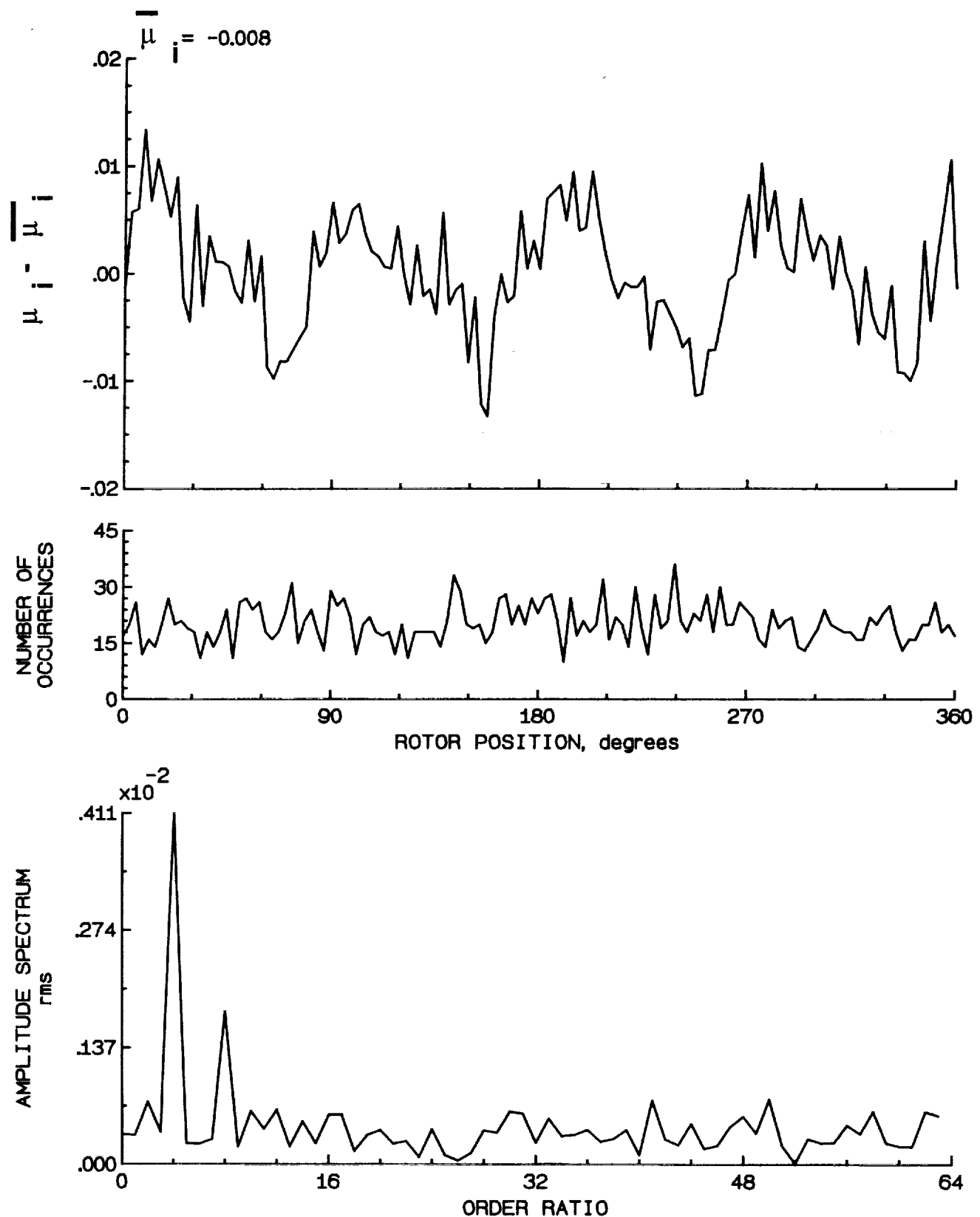


Figure 136.- Induced inflow velocity measured at 240 degrees and r/R of 0.78.

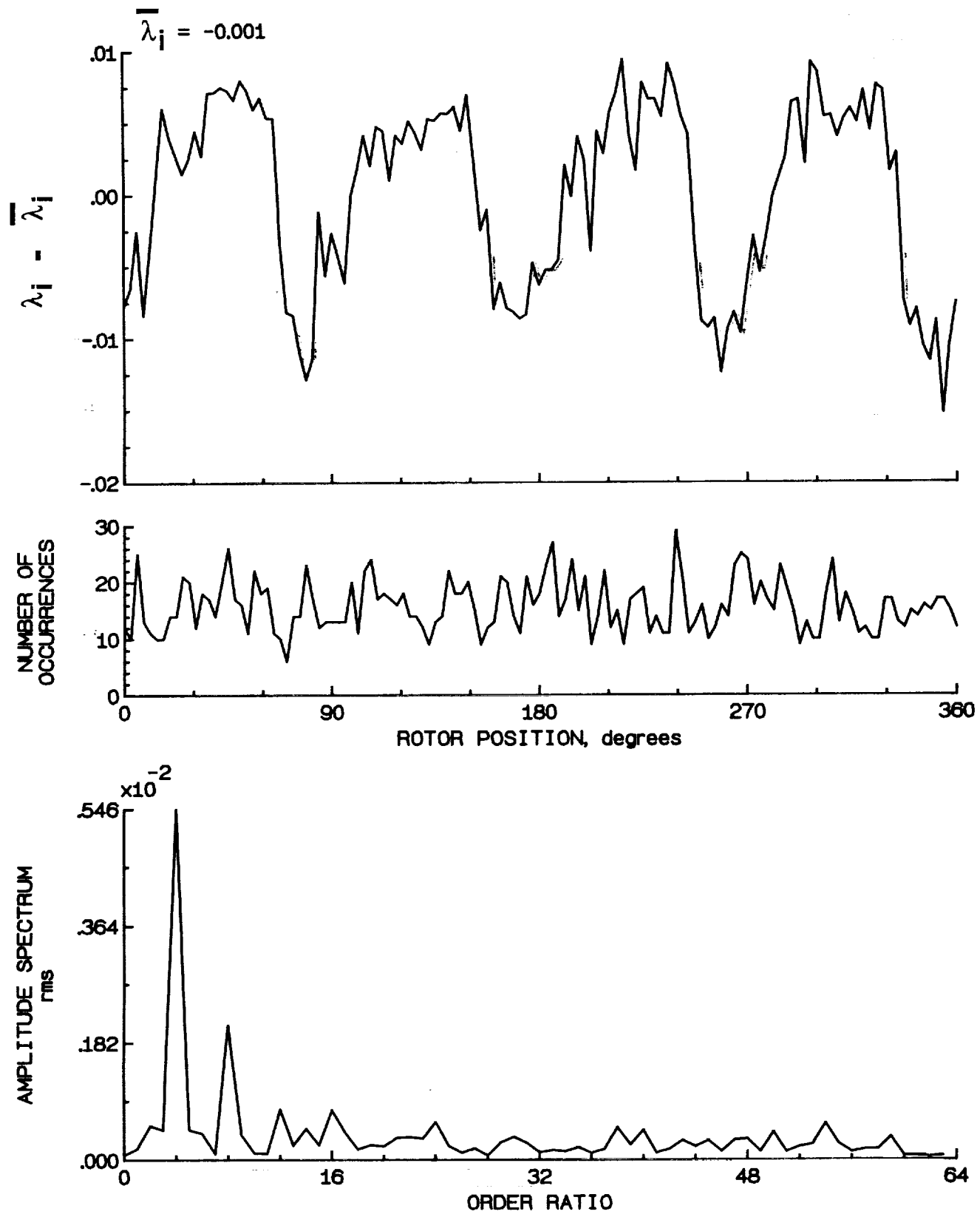


Figure 136.- Concluded.

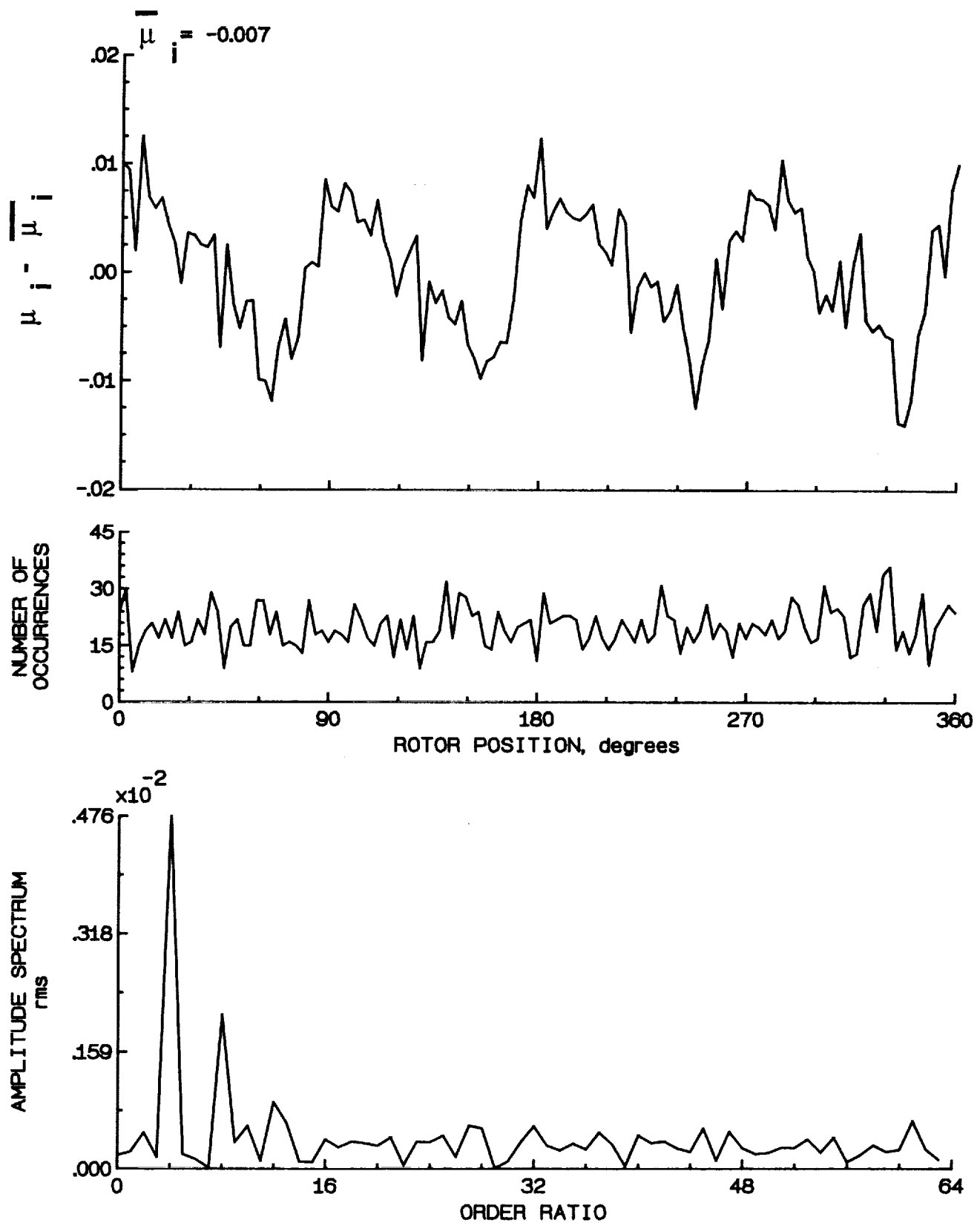


Figure 137.- Induced inflow velocity measured at 240 degrees and r/R of 0.82.

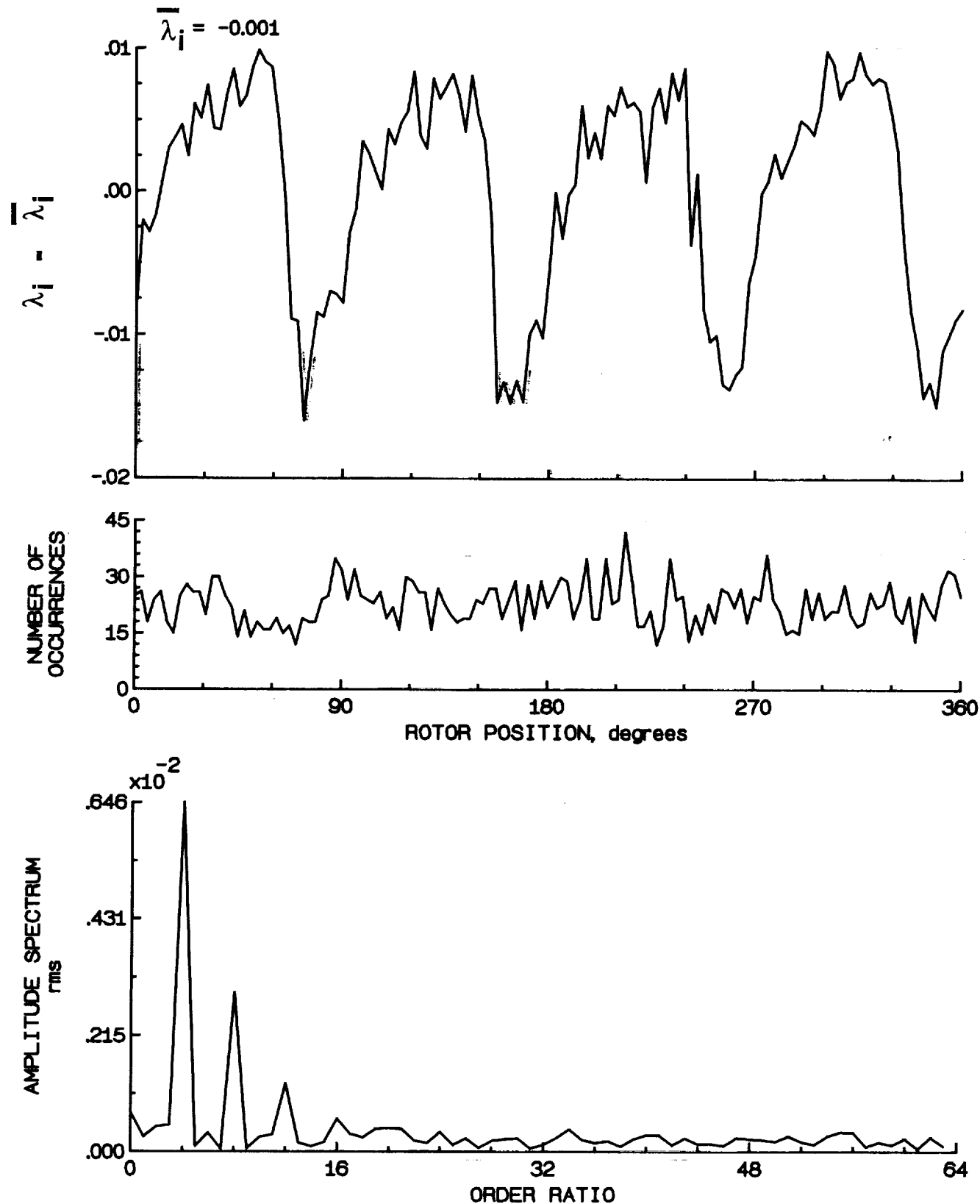


Figure 137.- Concluded.

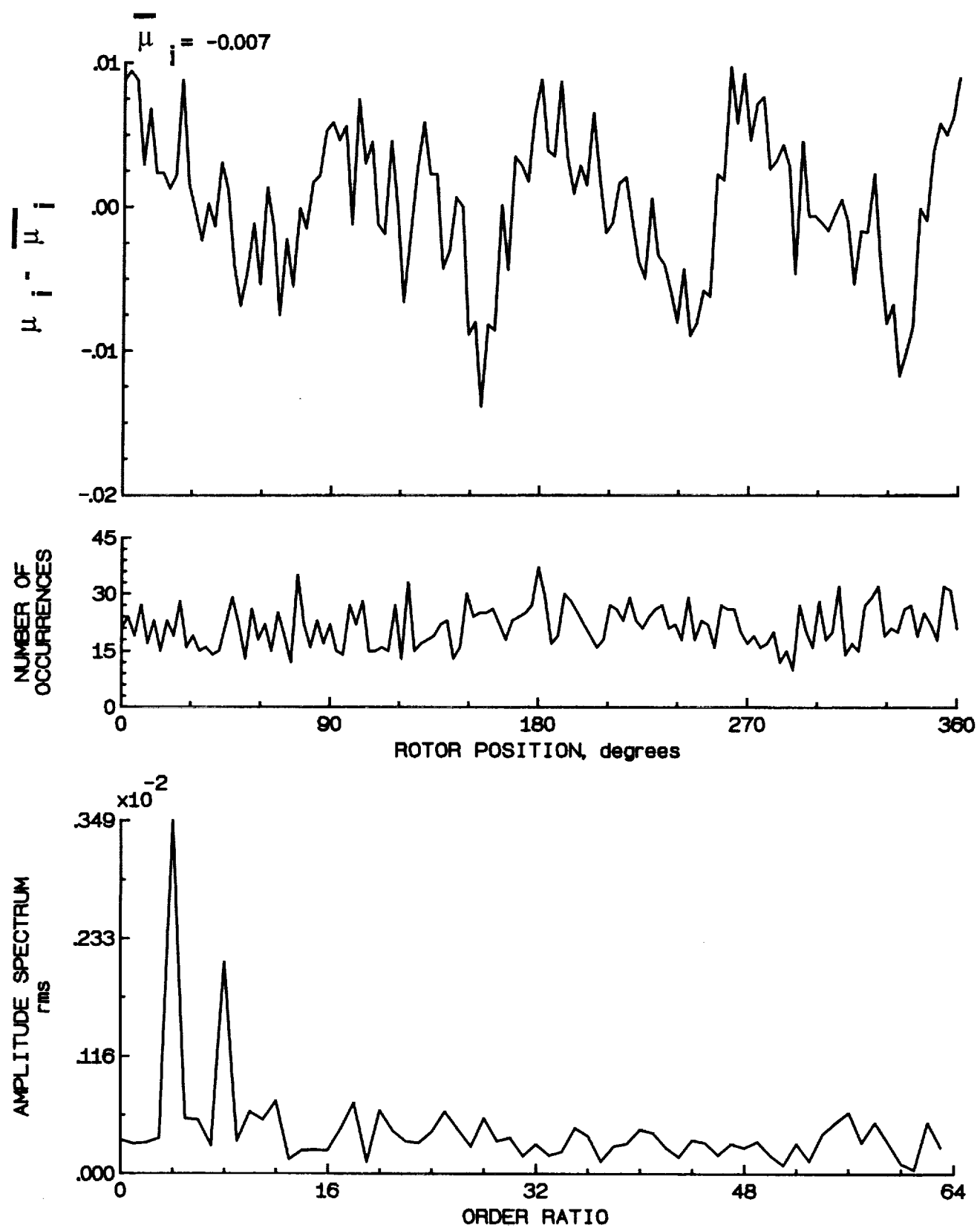


Figure 138.- Induced inflow velocity measured at 240 degrees and r/R of 0.86.

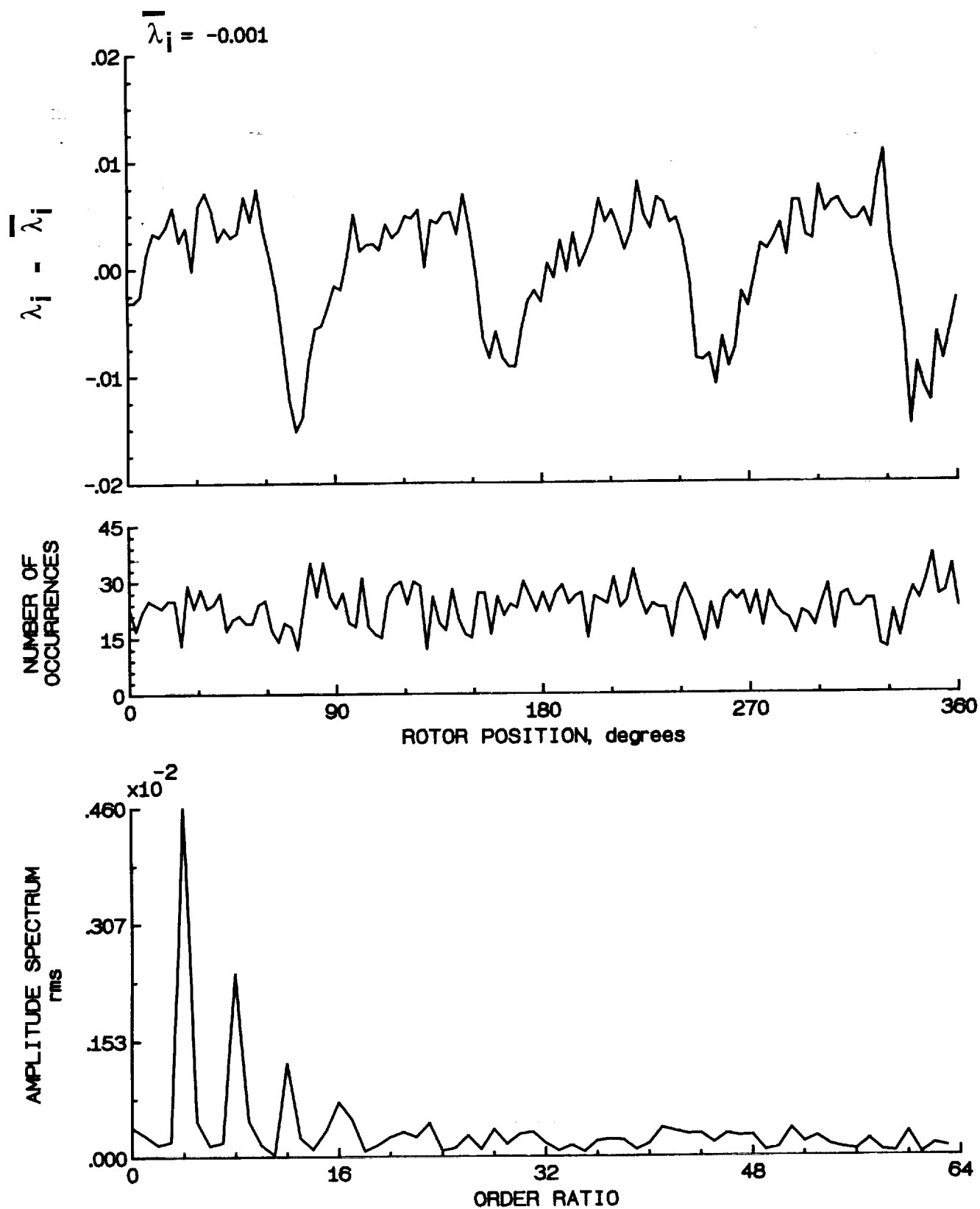


Figure 138.- Concluded.

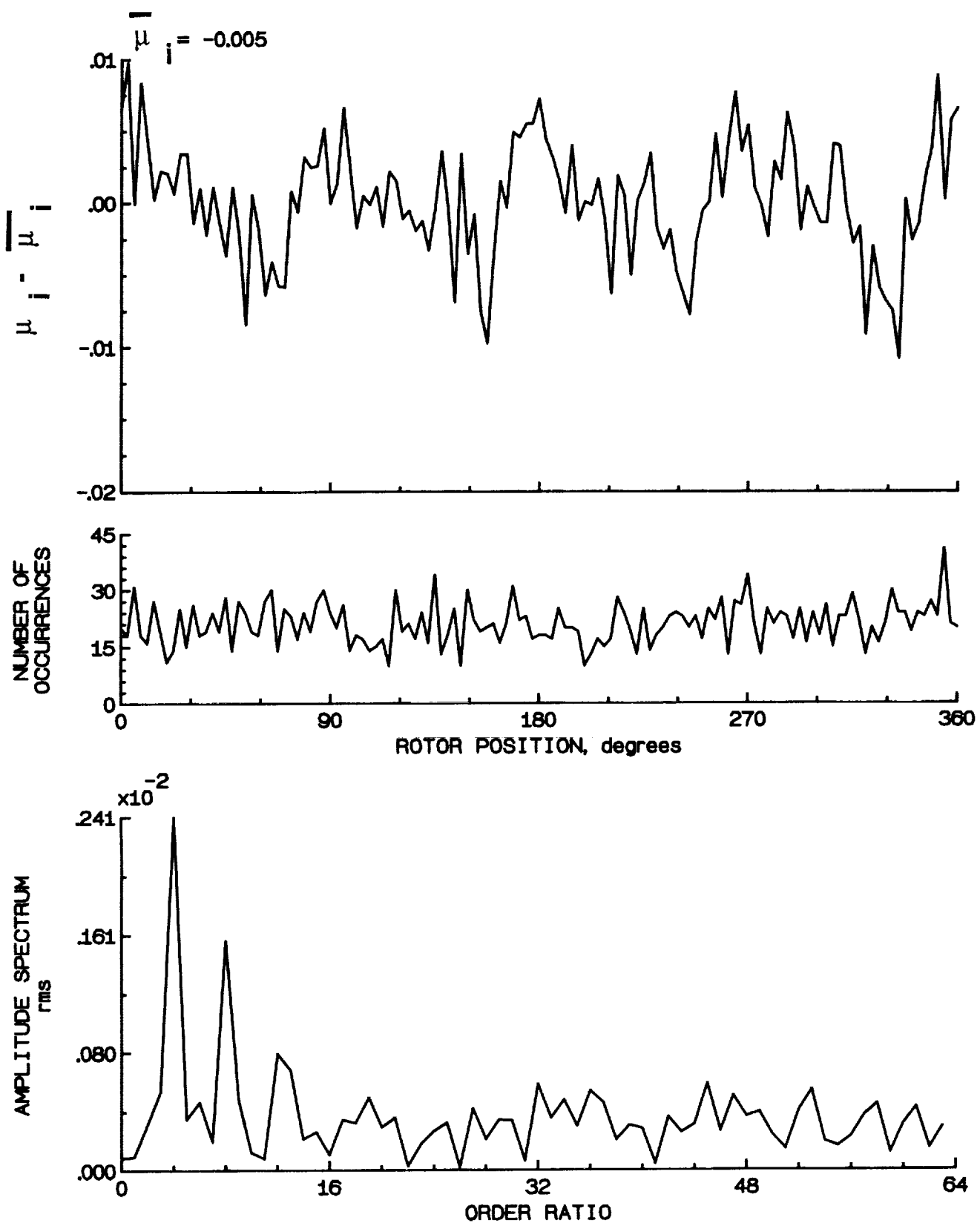


Figure 139.- Induced inflow velocity measured at 240 degrees and r/R of 0.90.

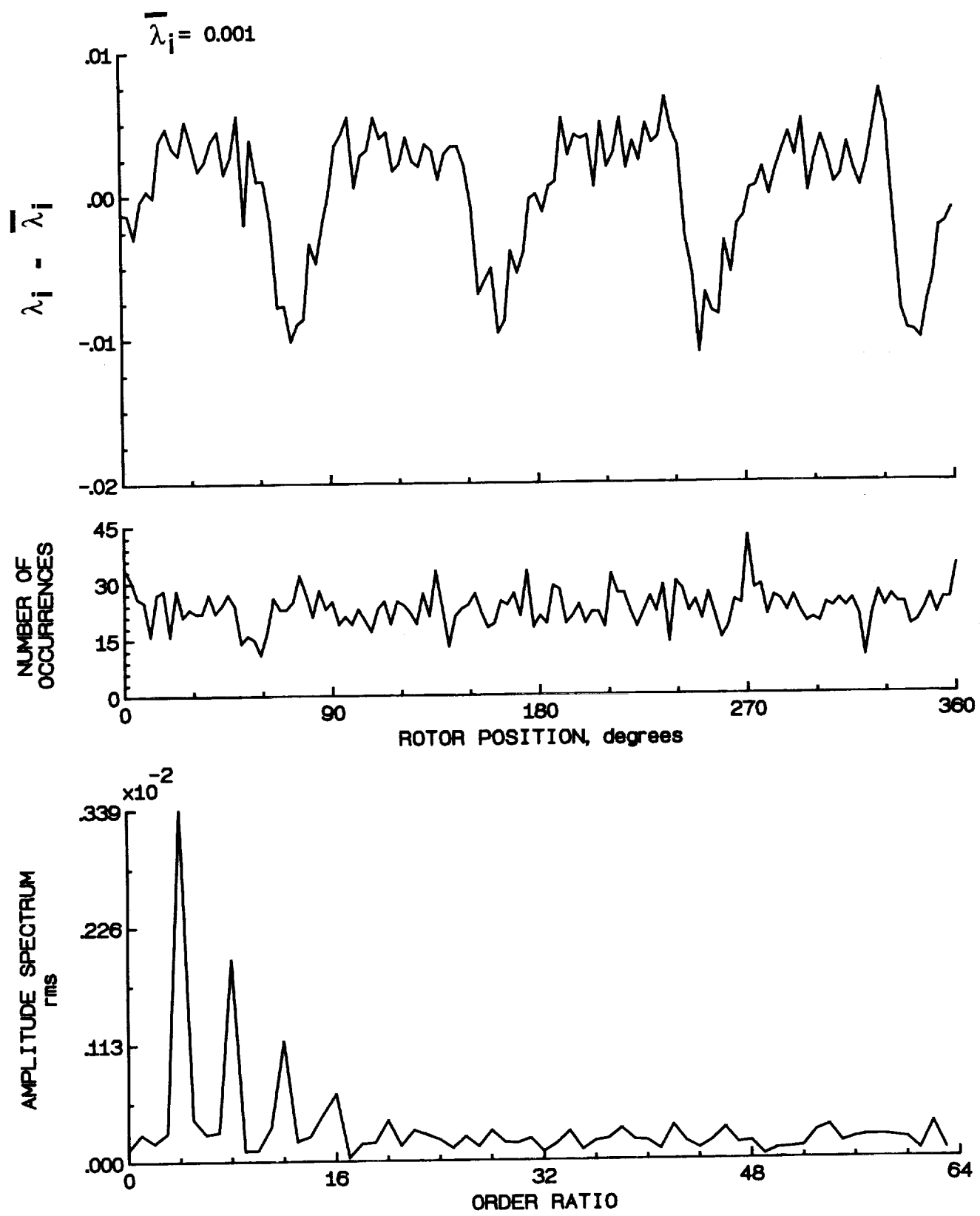


Figure 139.- Concluded.

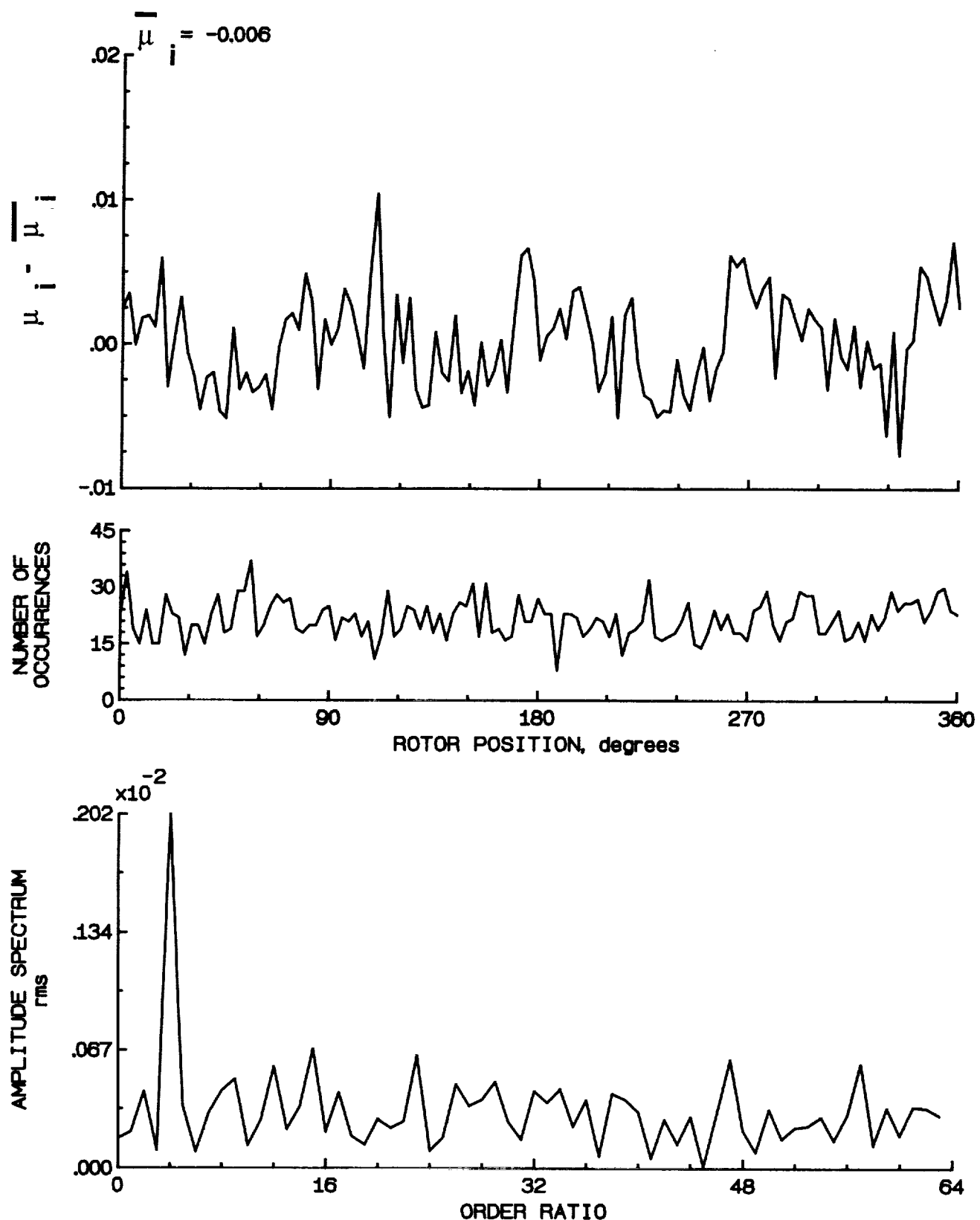


Figure 140.- Induced inflow velocity measured at 240 degrees and r/R of 0.94.

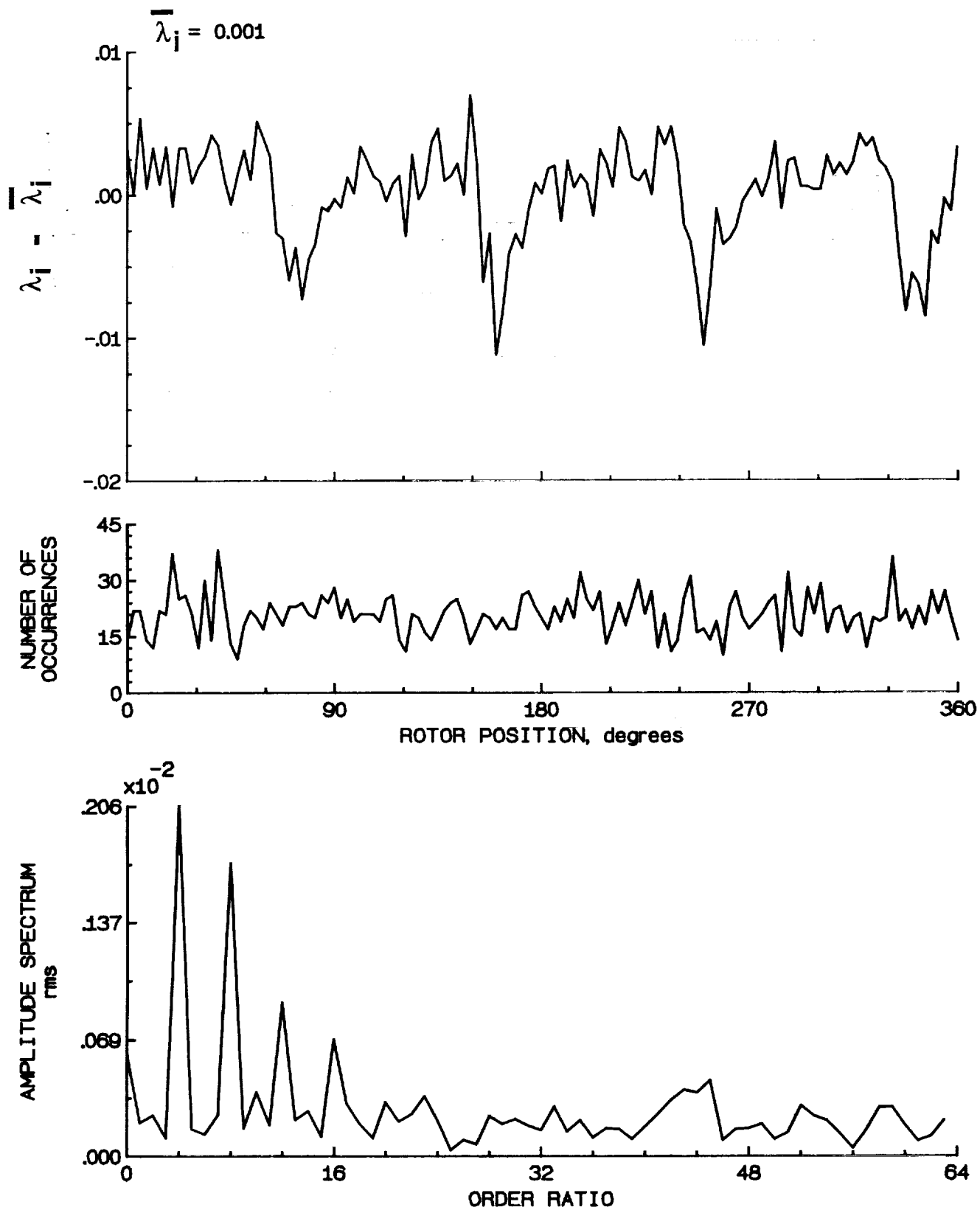


Figure 140.- Concluded.

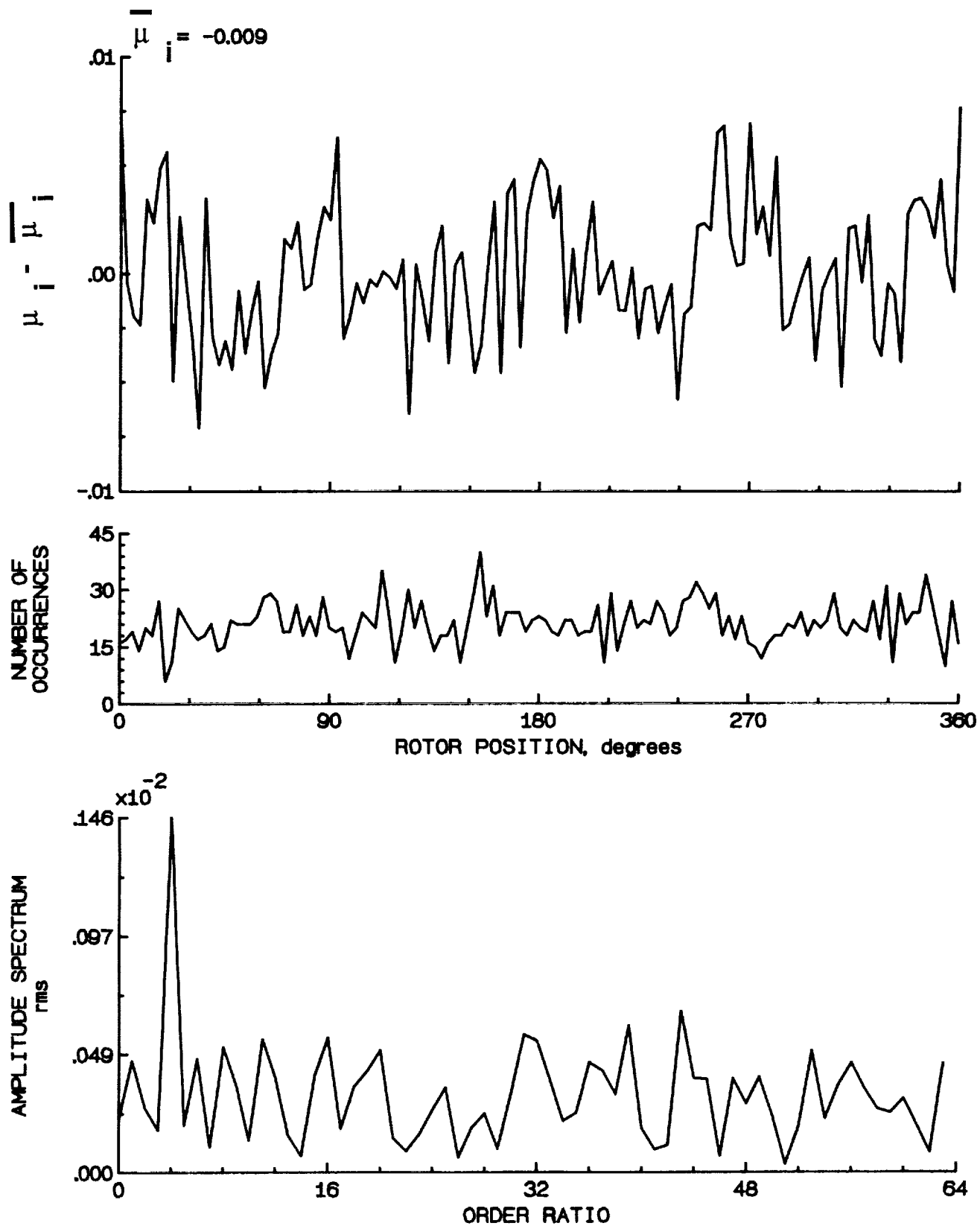


Figure 141.- Induced inflow velocity measured at 240 degrees and r/R of 0.98.

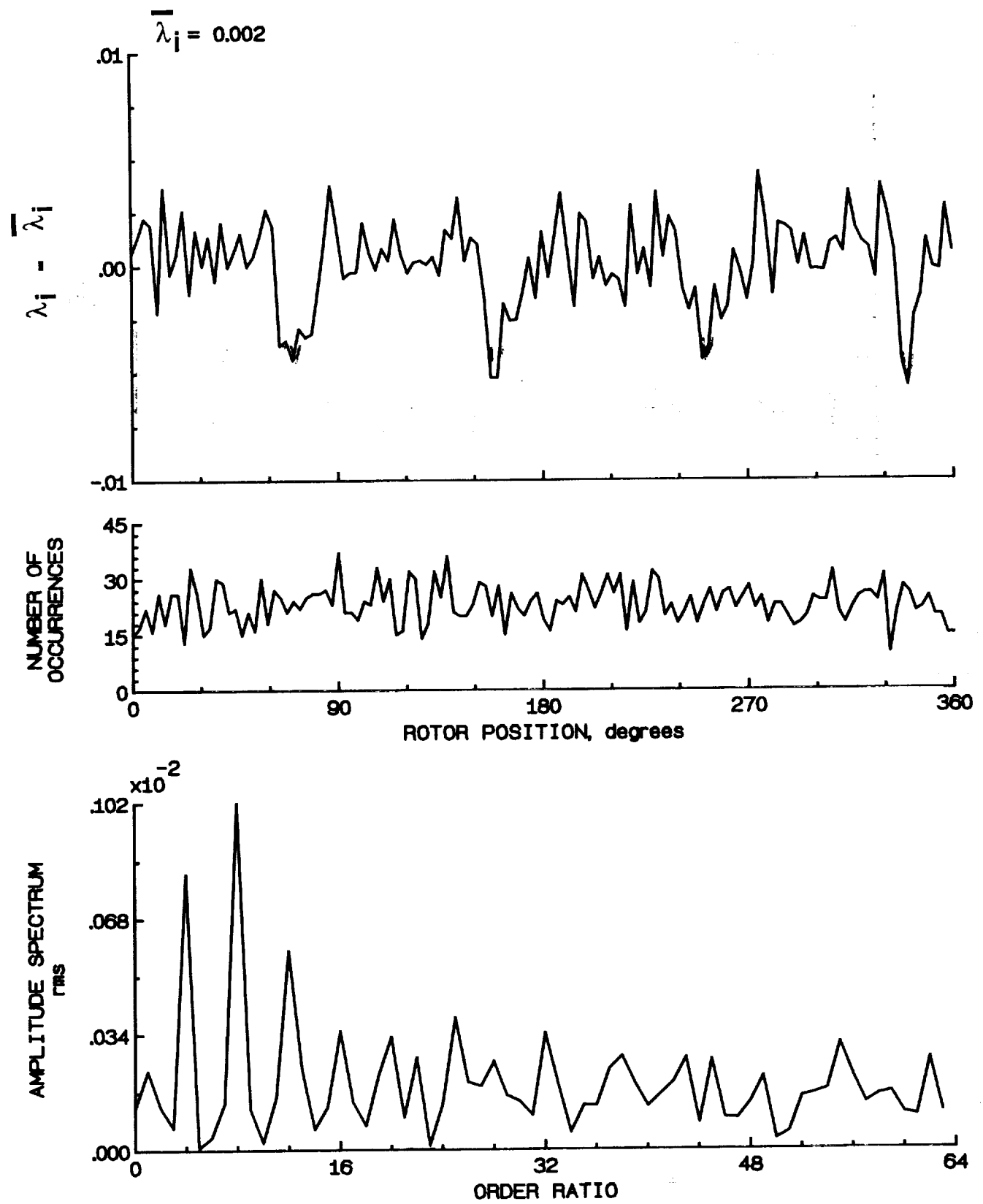


Figure 141.- Concluded.

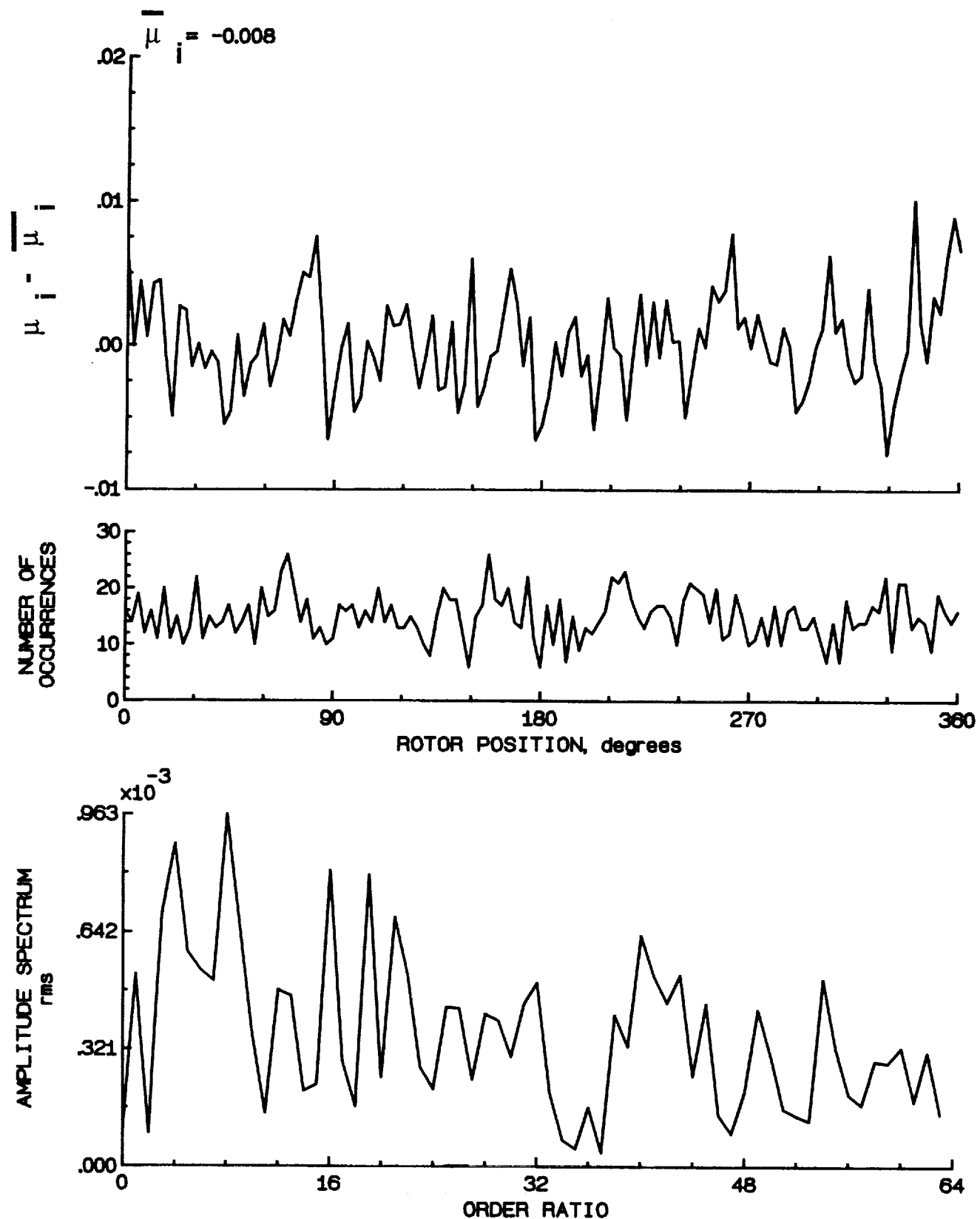


Figure 142.- Induced inflow velocity measured at 240 degrees and r/R of 1.02.

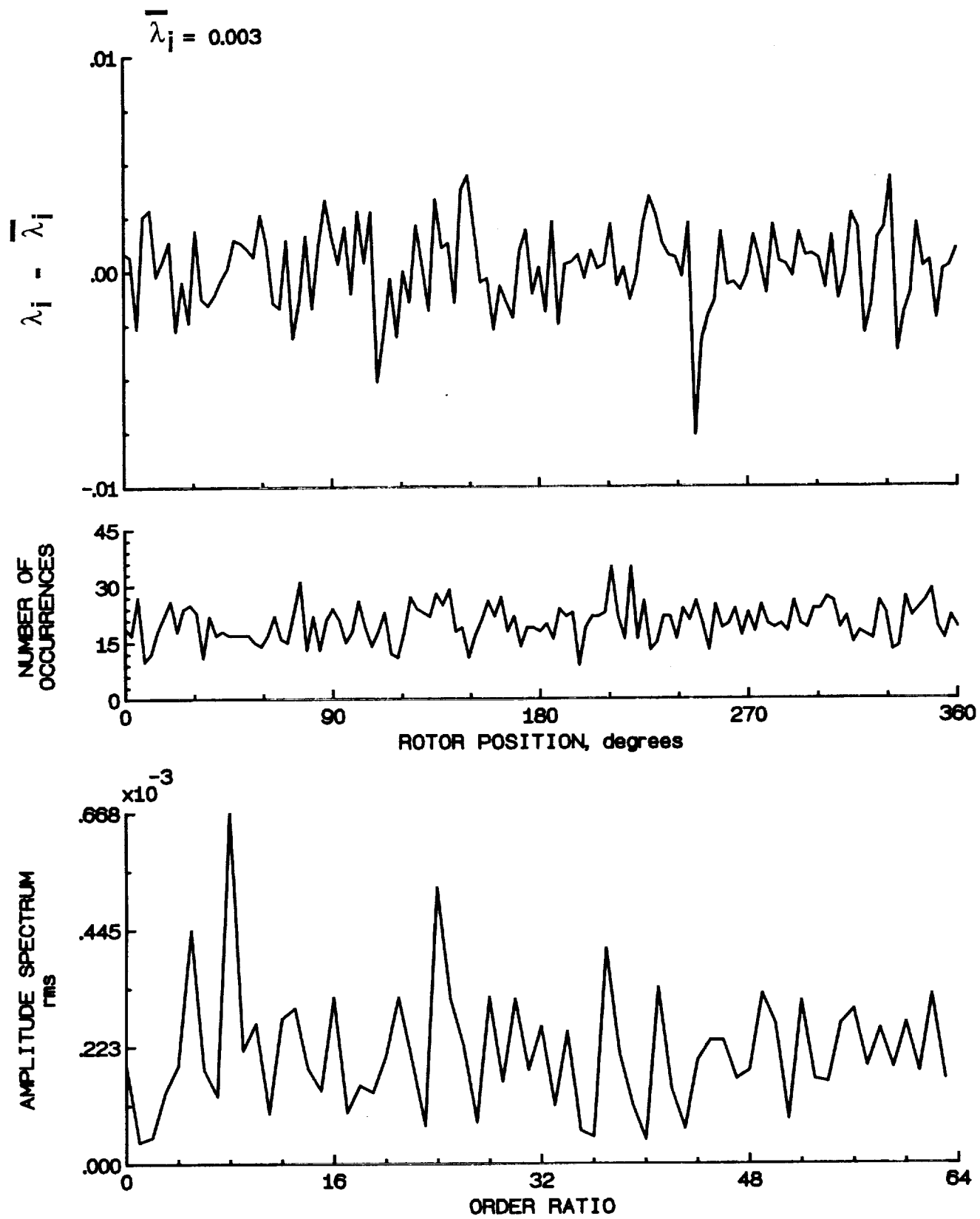


Figure 142.- Concluded.

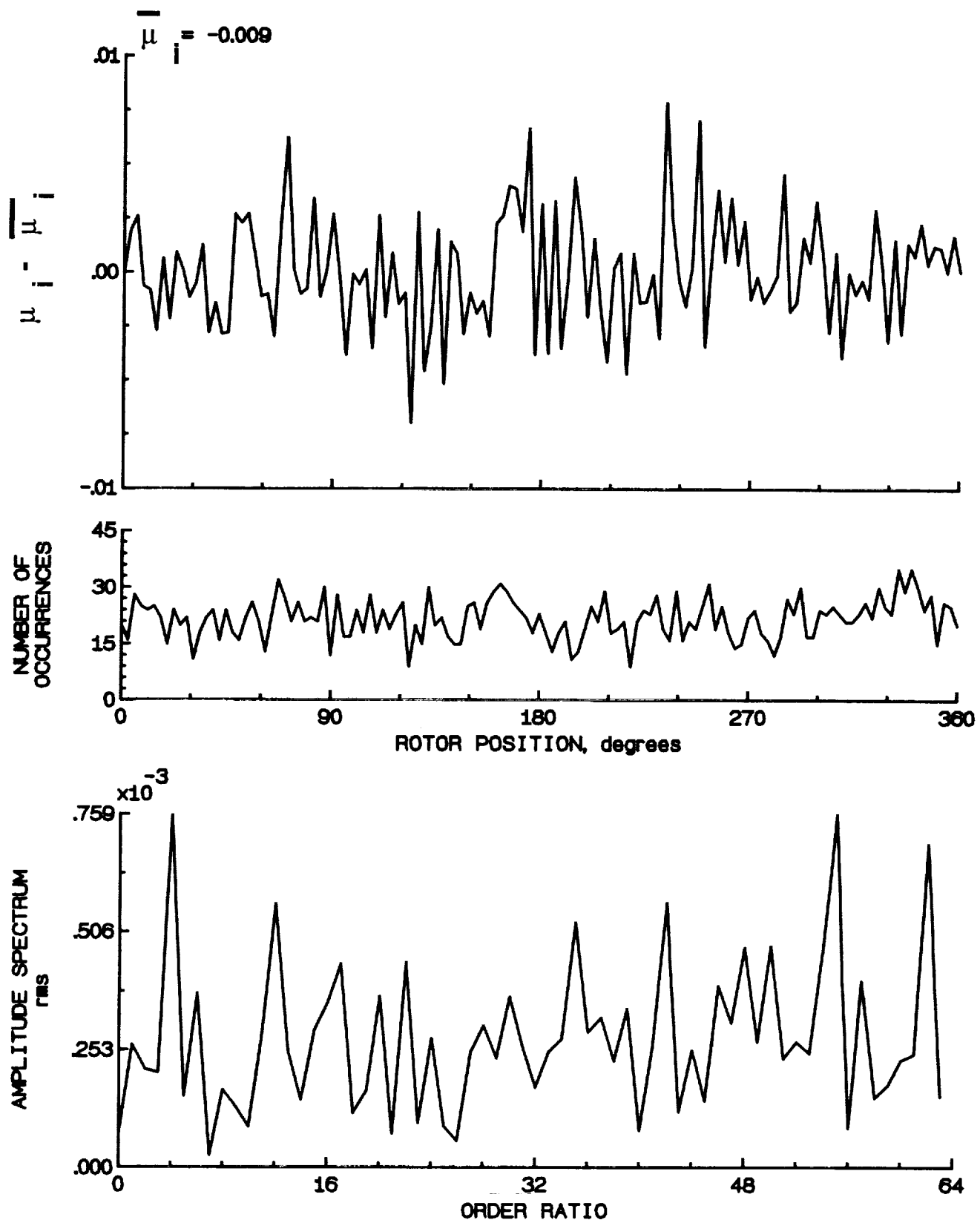


Figure 143.- Induced inflow velocity measured at 240 degrees and r/R of 1.04.

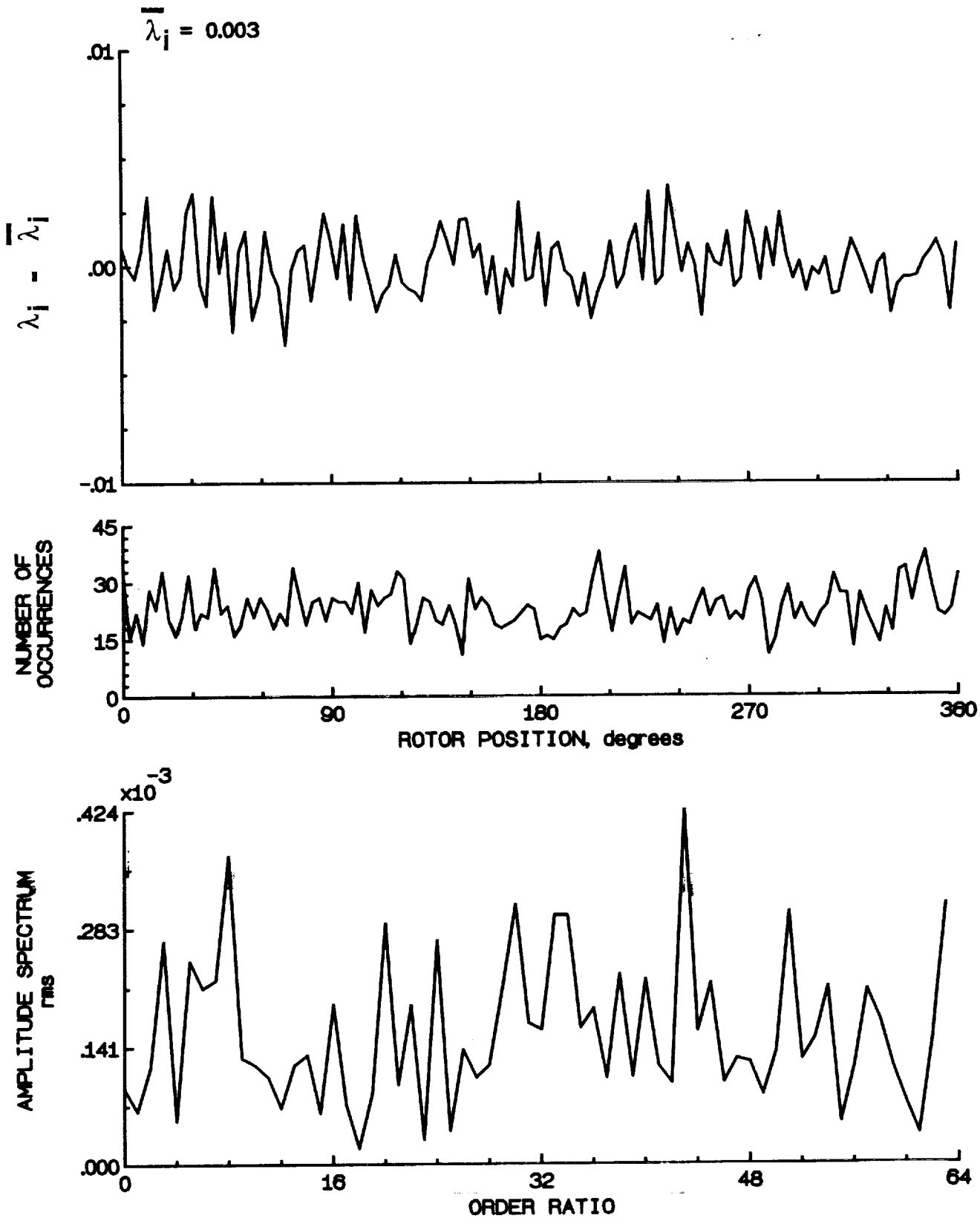


Figure 143.- Concluded.

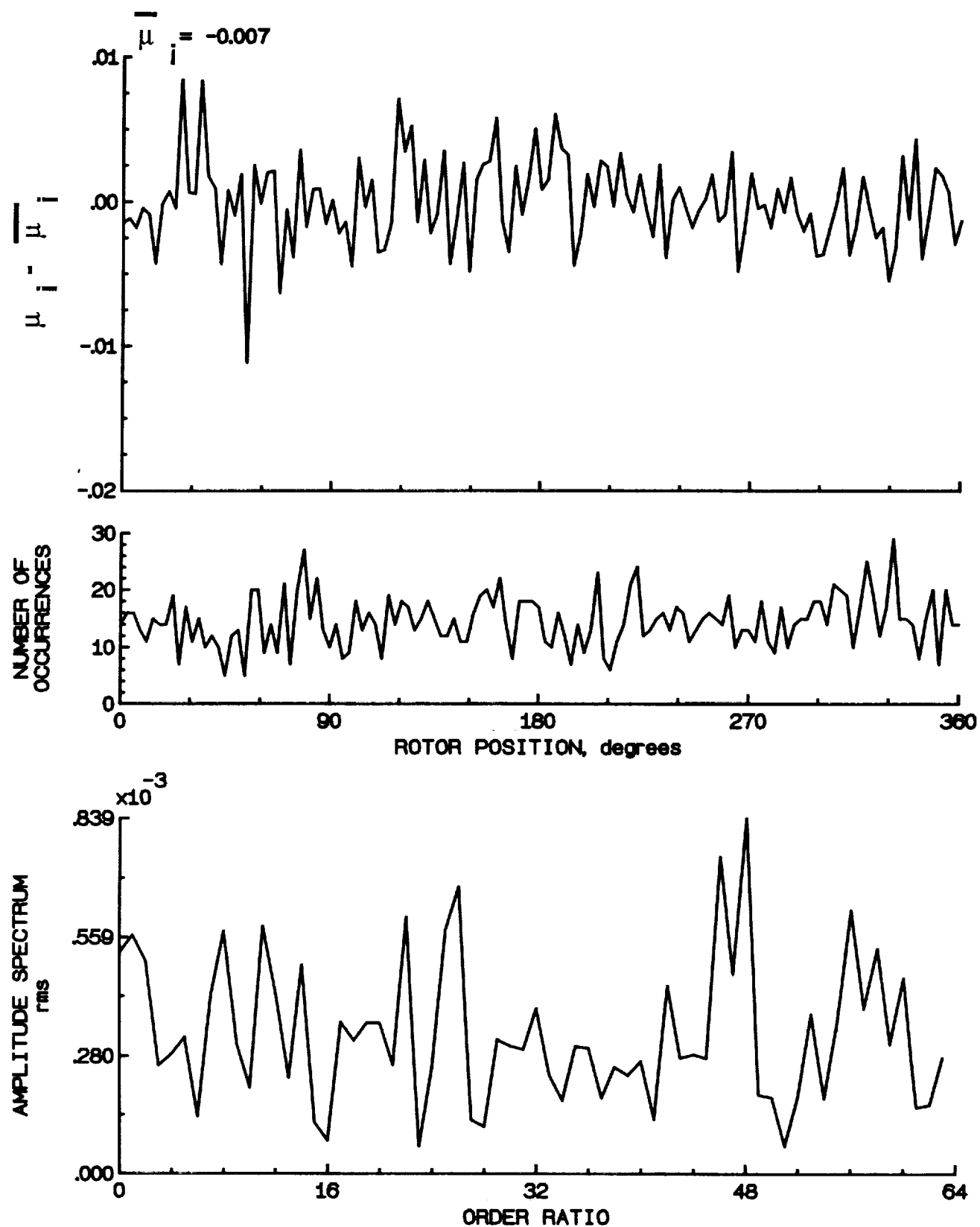


Figure 144.- Induced inflow velocity measured at 240 degrees and r/R of 1.10.

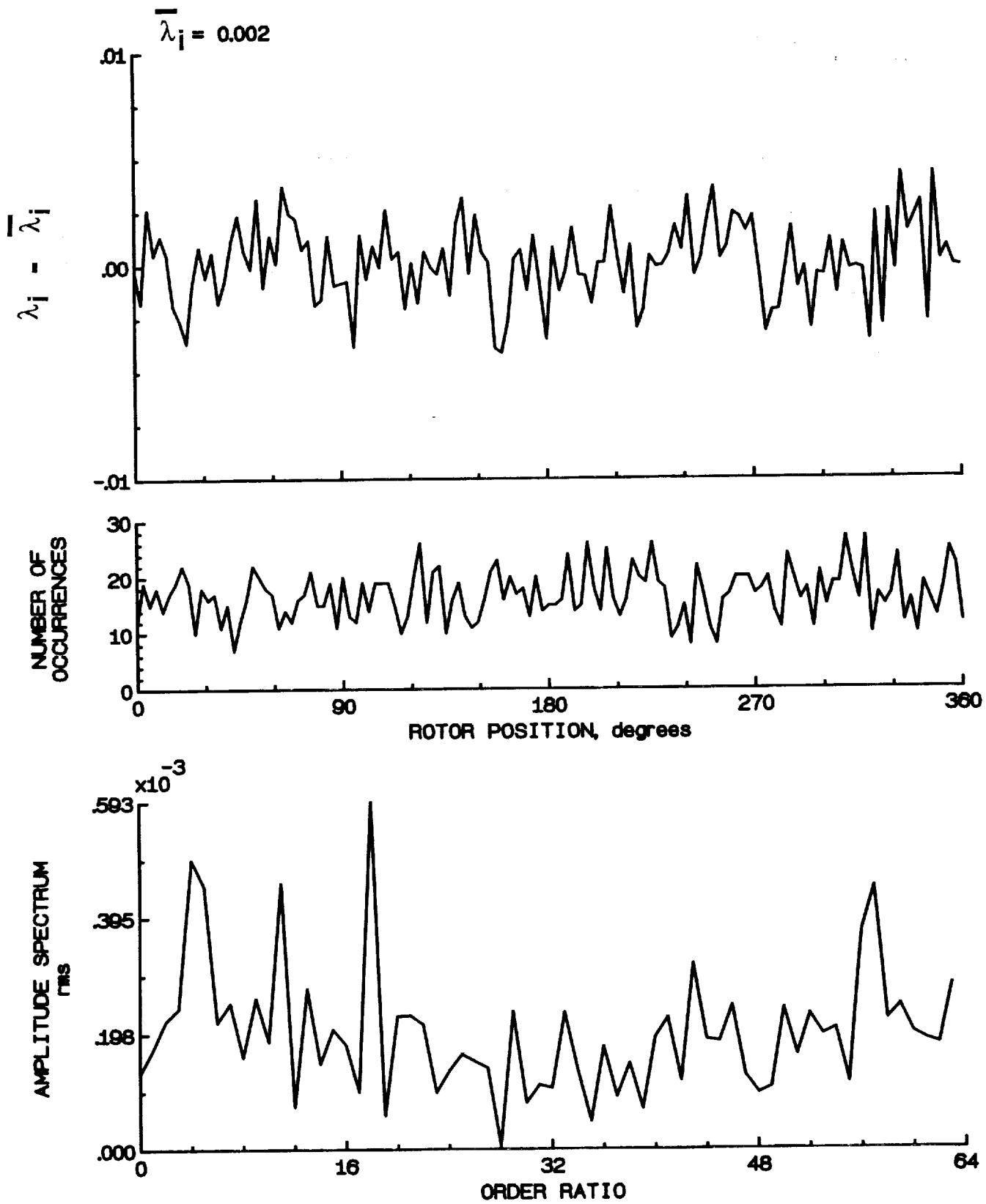


Figure 144.- Concluded.

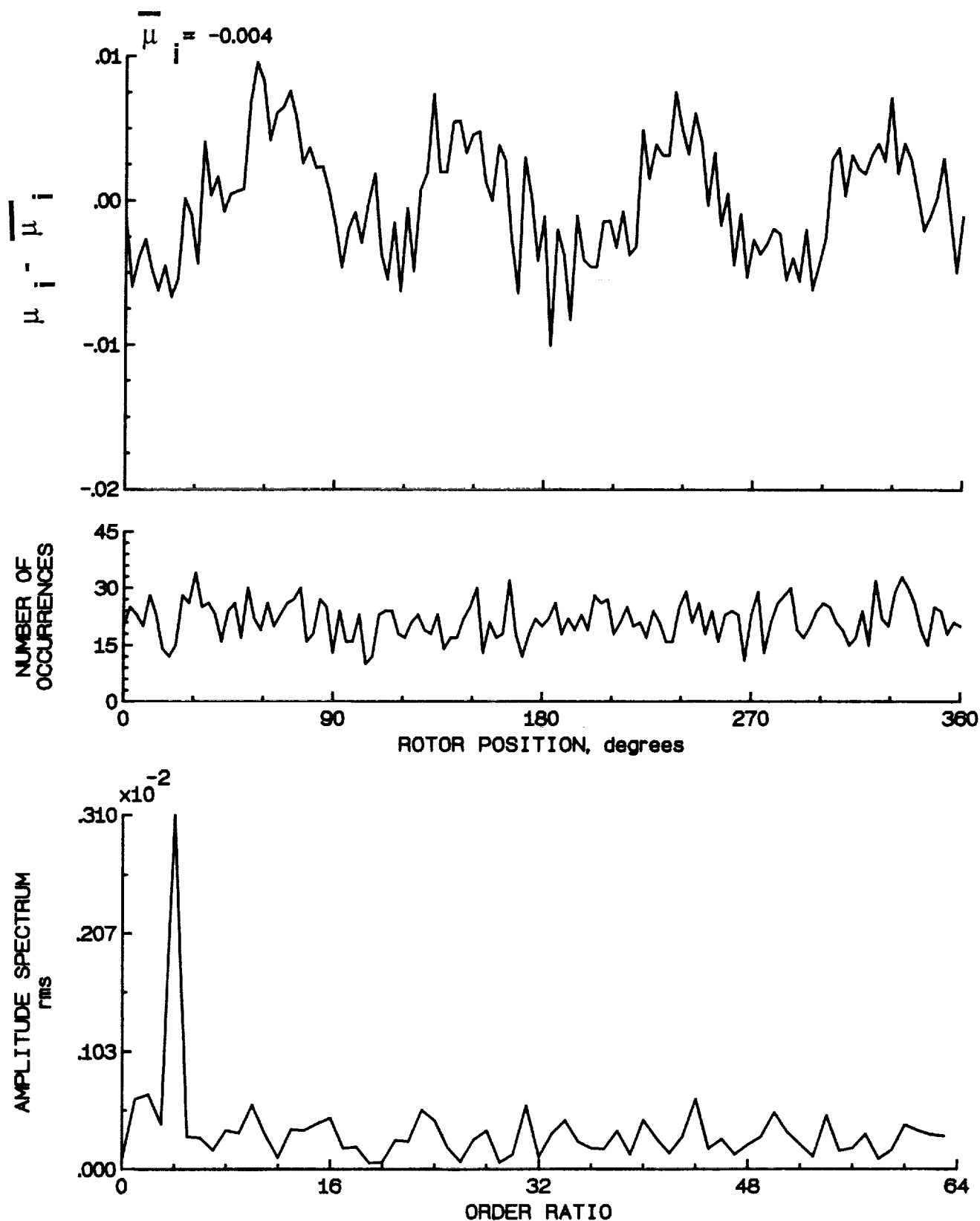


Figure 145.- Induced inflow velocity measured at 270 degrees and r/R of 0.20.

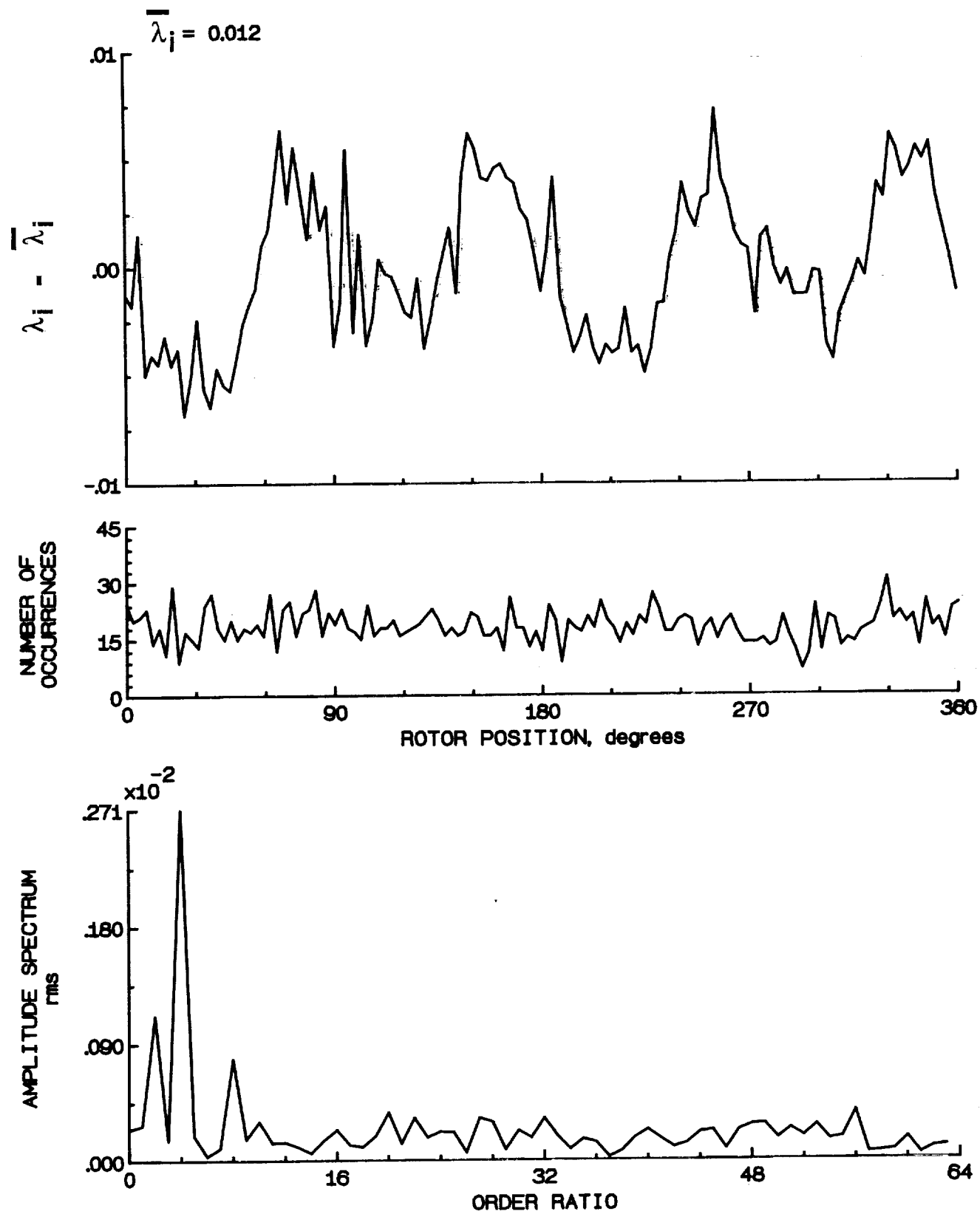


Figure 145.- Concluded.

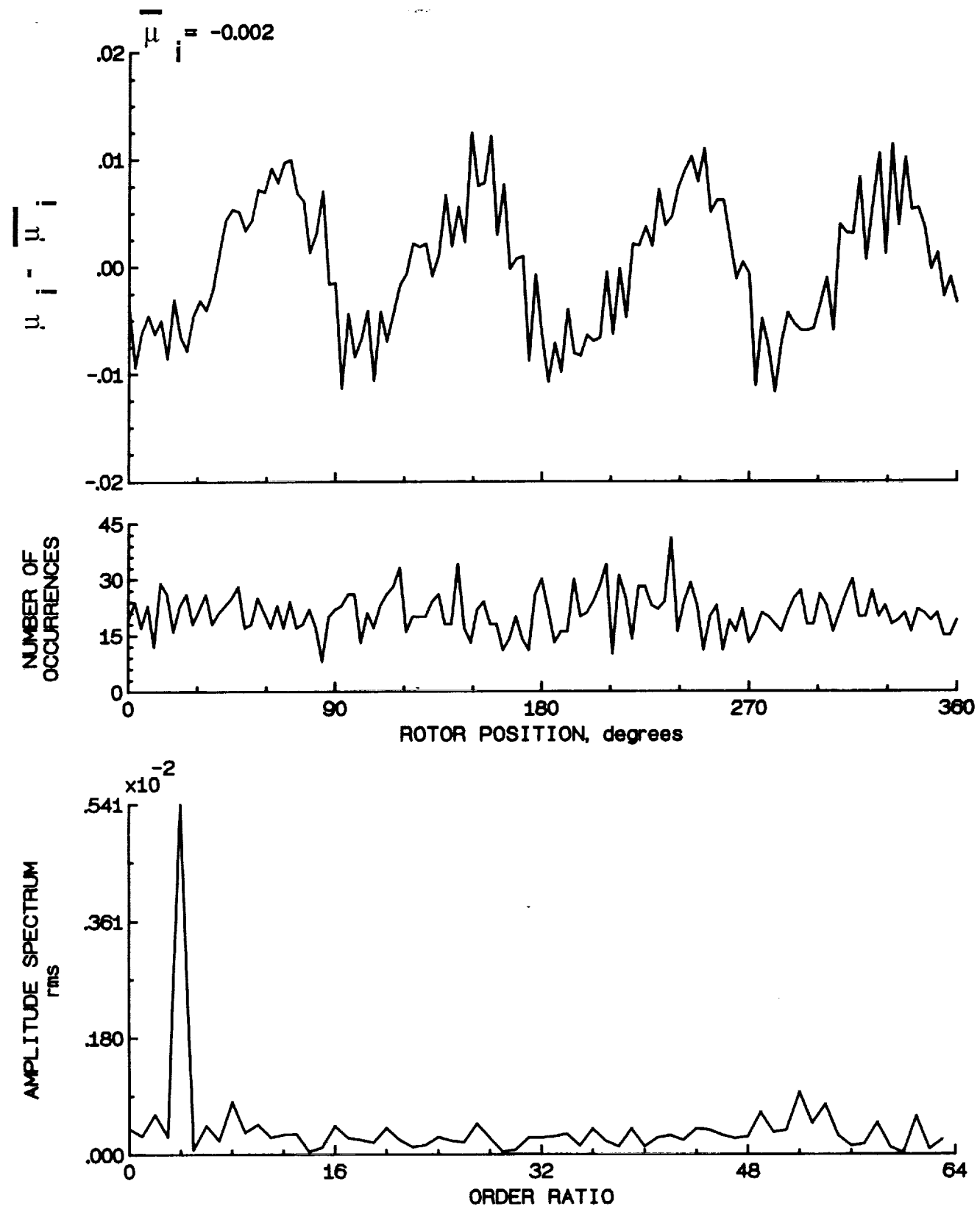


Figure 146.- Induced inflow velocity measured at 270 degrees and r/R of 0.40.

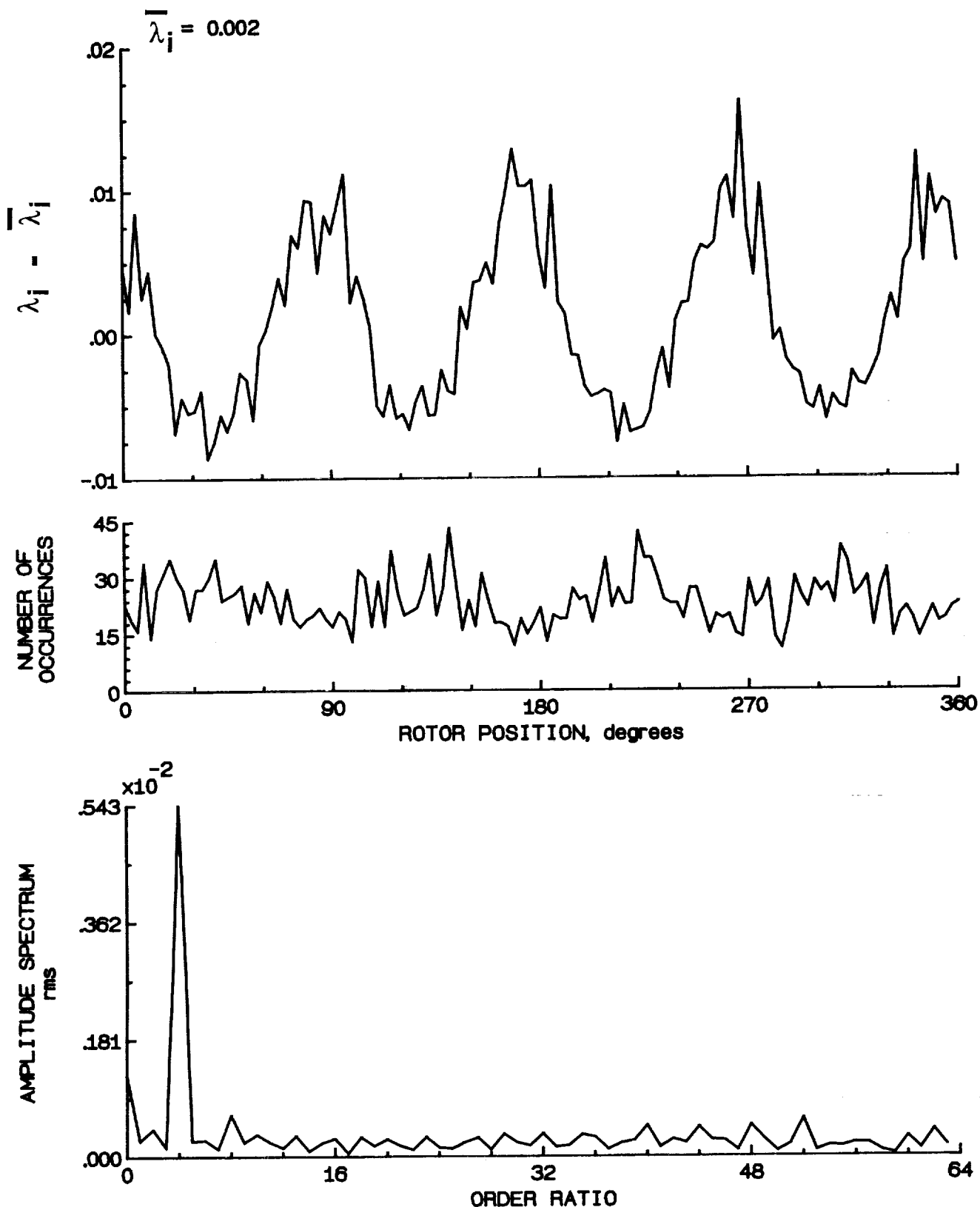


Figure 146.- Concluded.

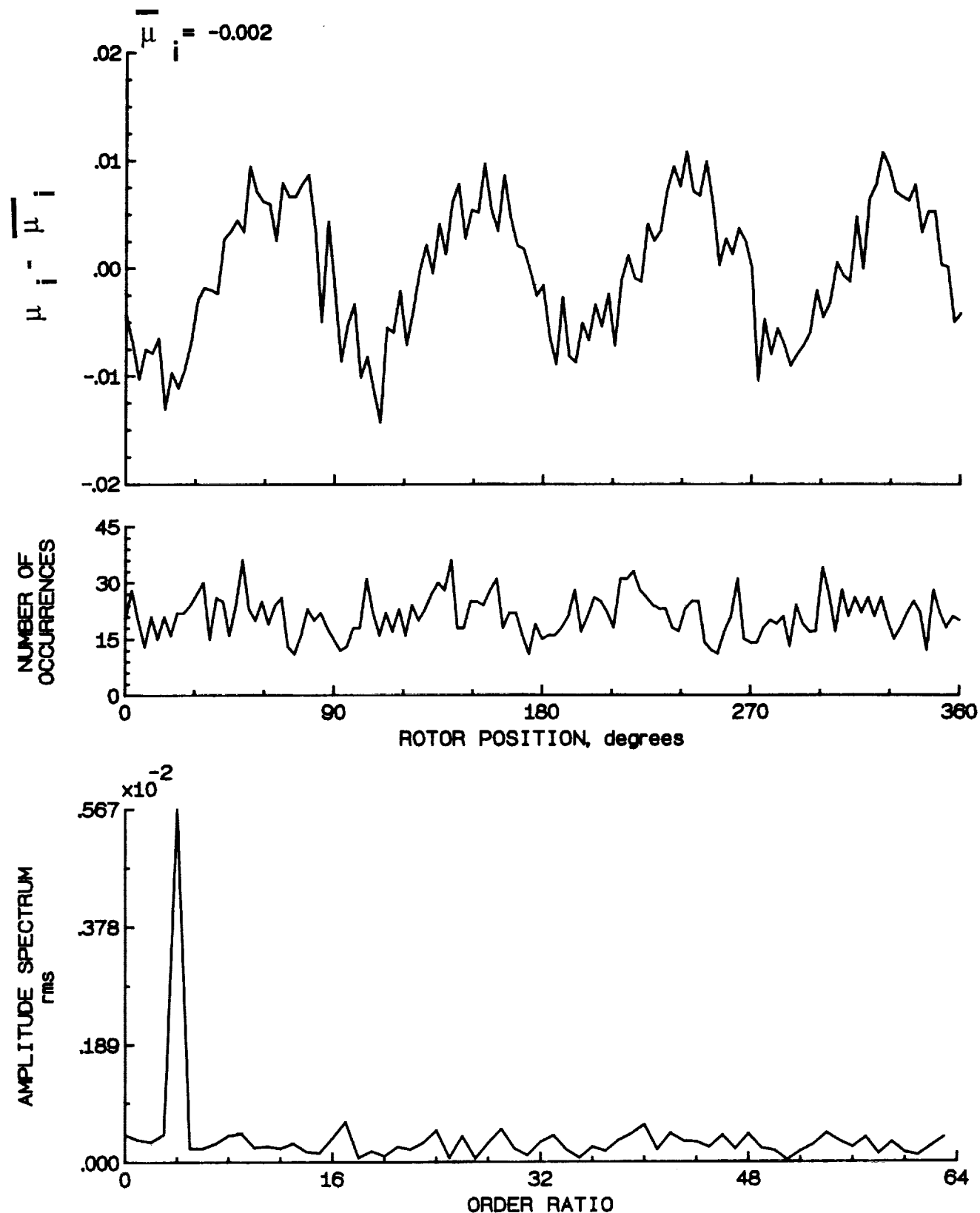


Figure 147.- Induced inflow velocity measured at 270 degrees and r/R of 0.50.

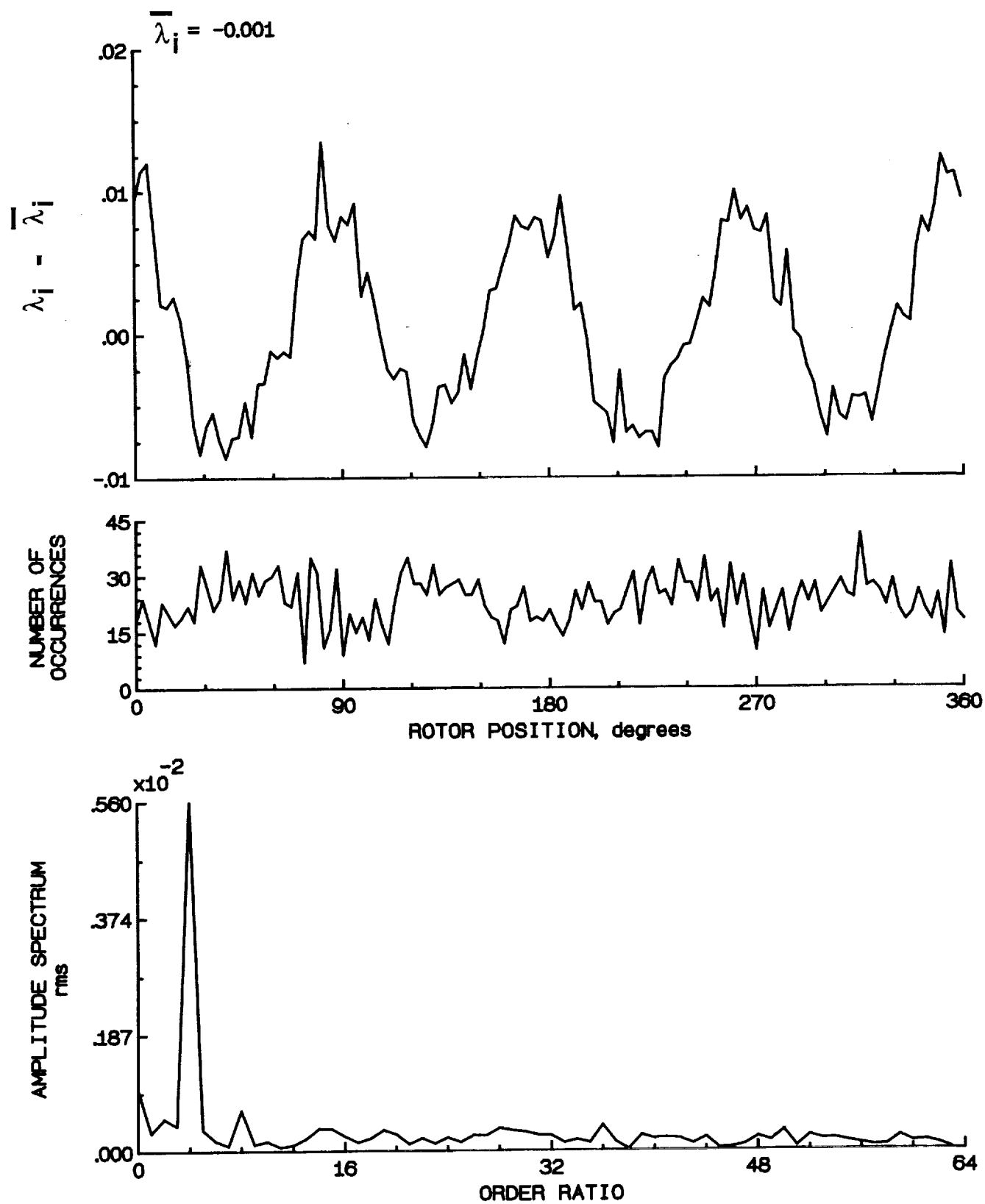


Figure 147.- Concluded.

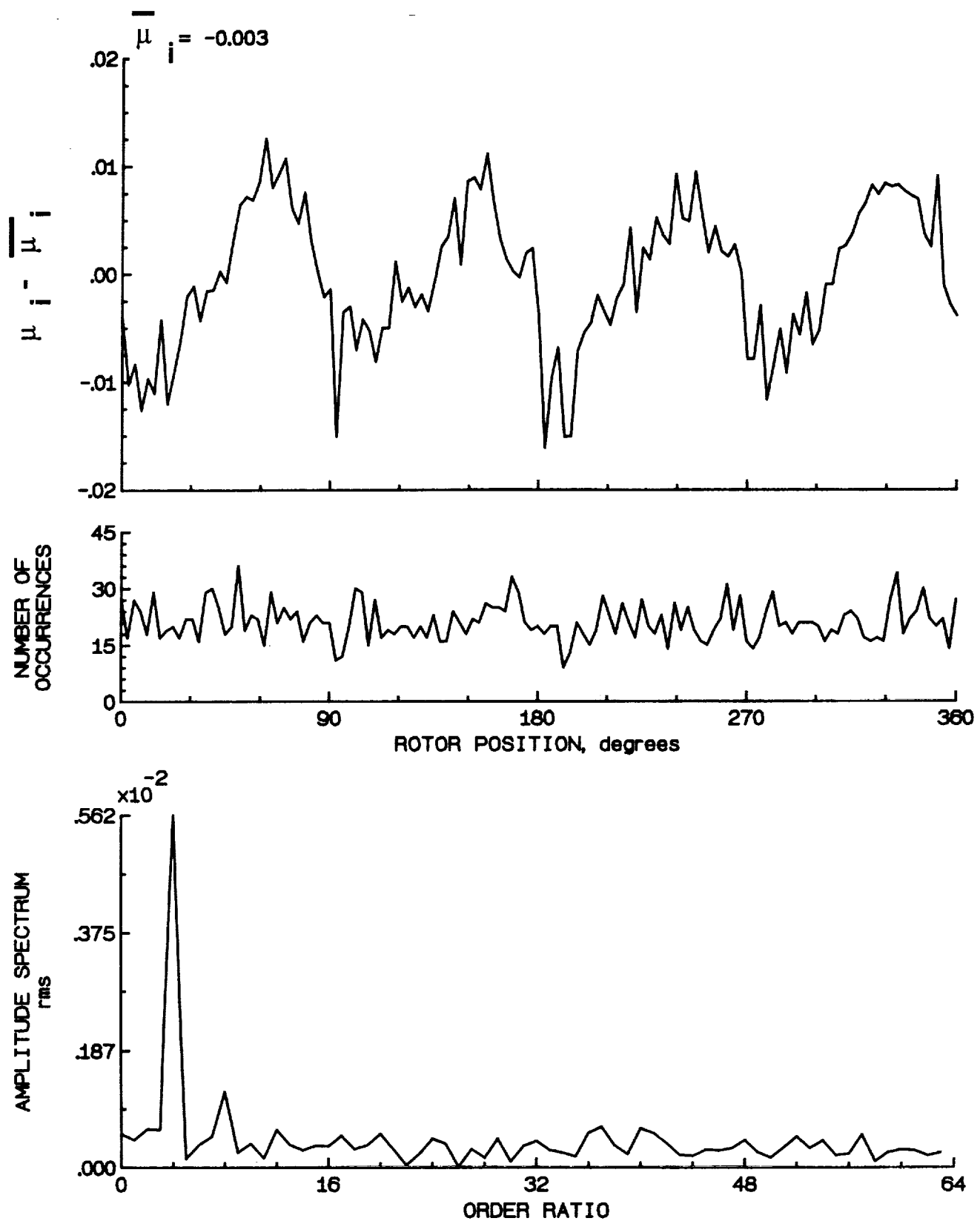


Figure 148.- Induced inflow velocity measured at 270 degrees and r/R of 0.60.

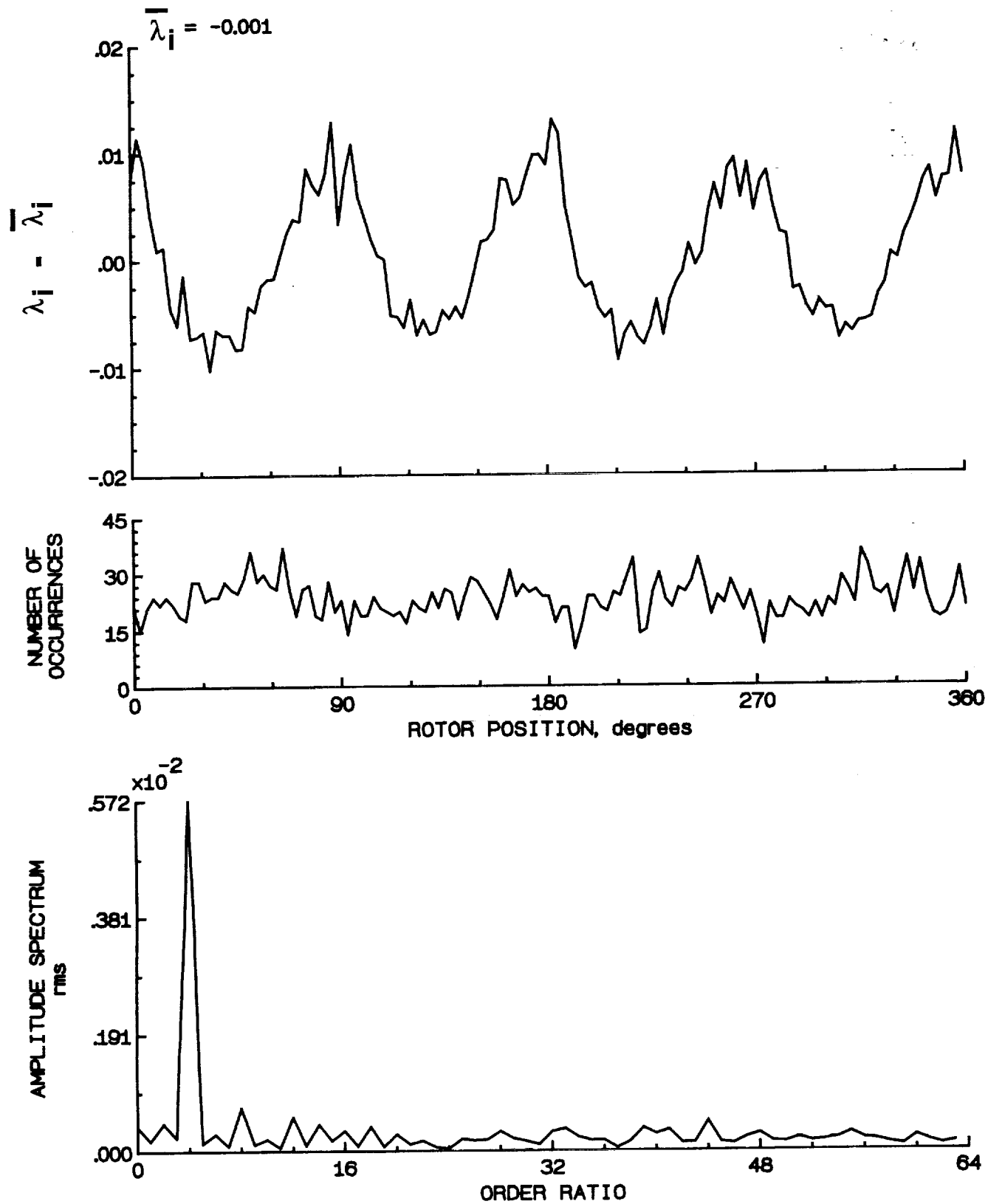


Figure 148.- Concluded.

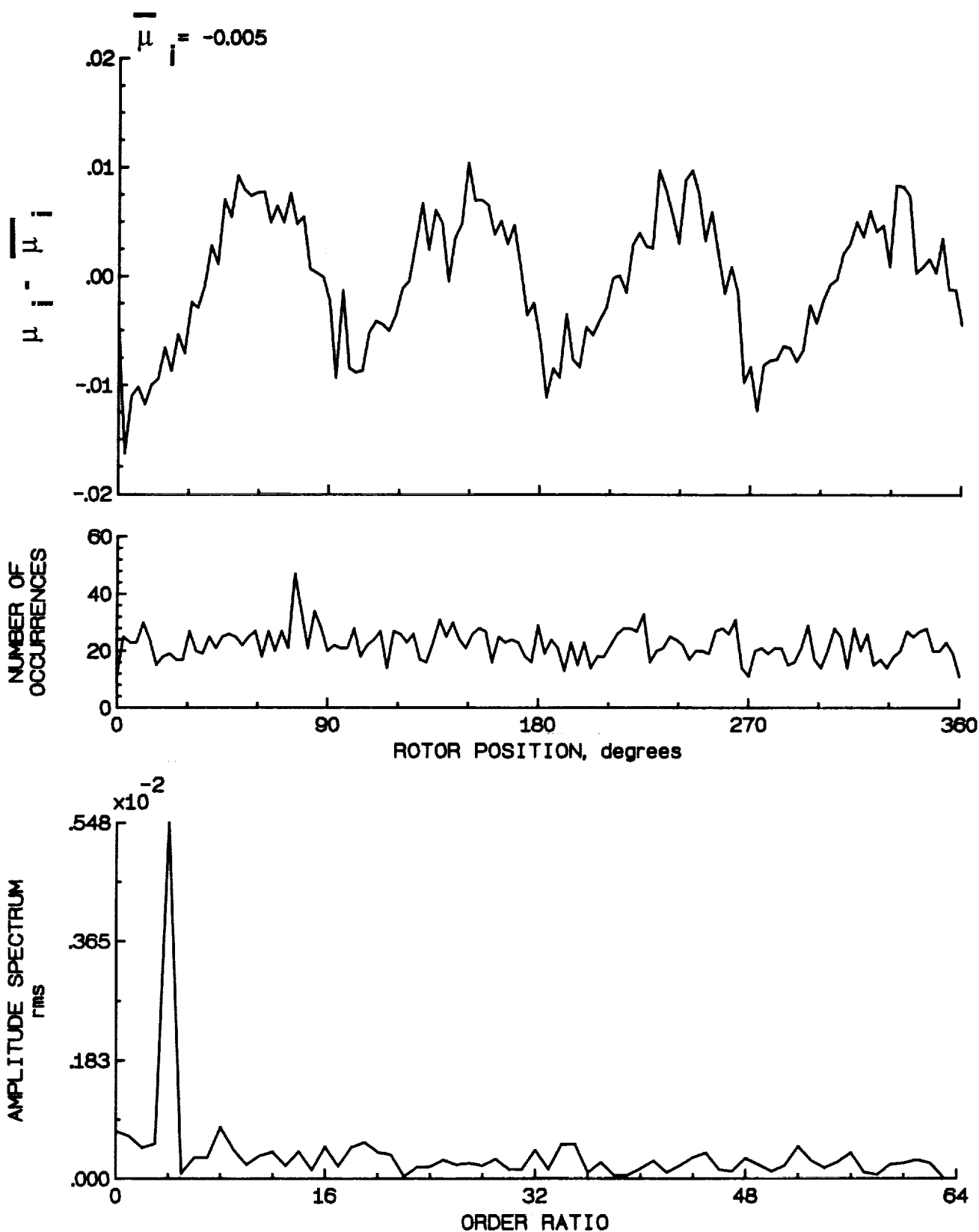


Figure 149.- Induced inflow velocity measured at 270 degrees and r/R of 0.70.

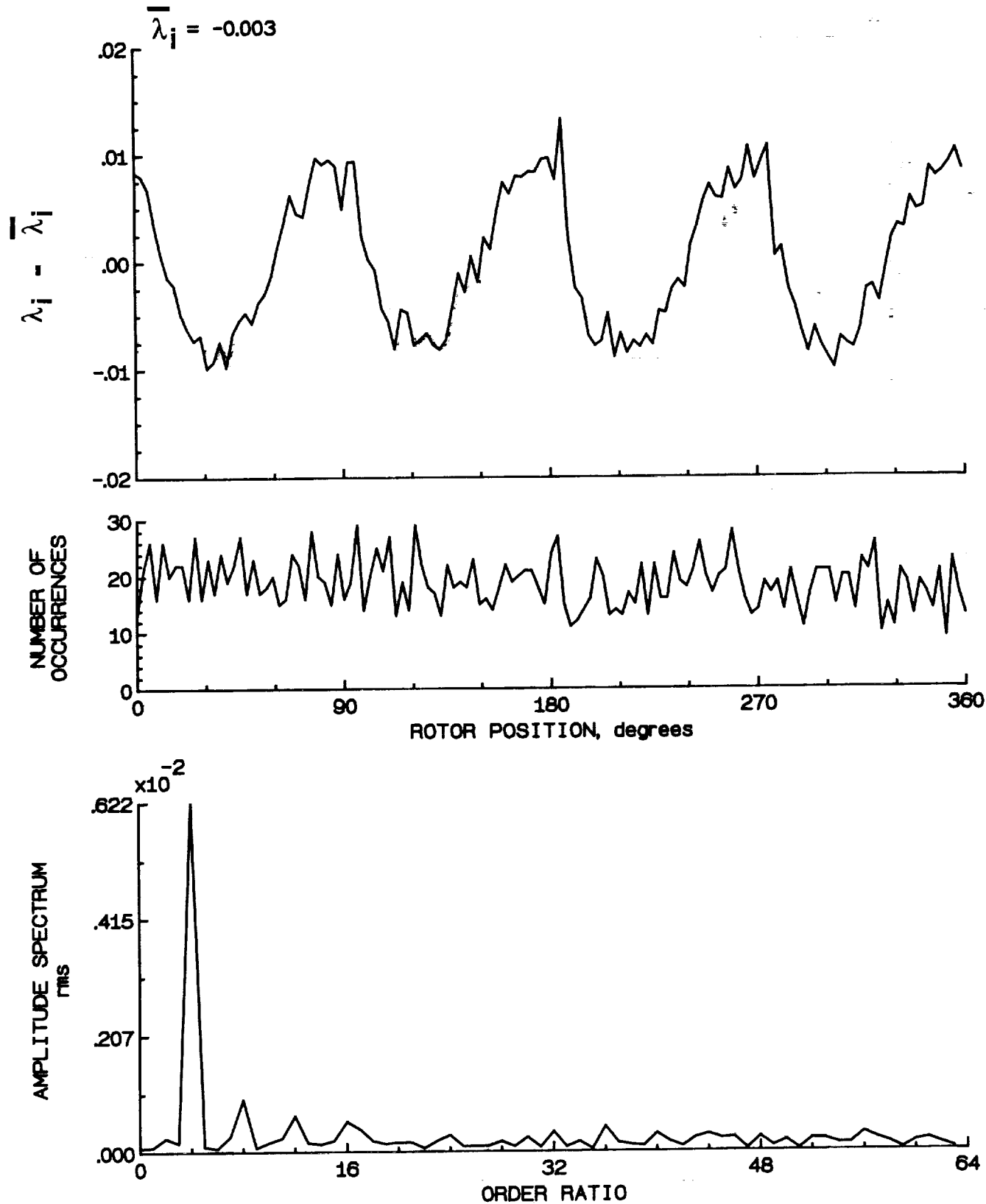


Figure 149.- Concluded.

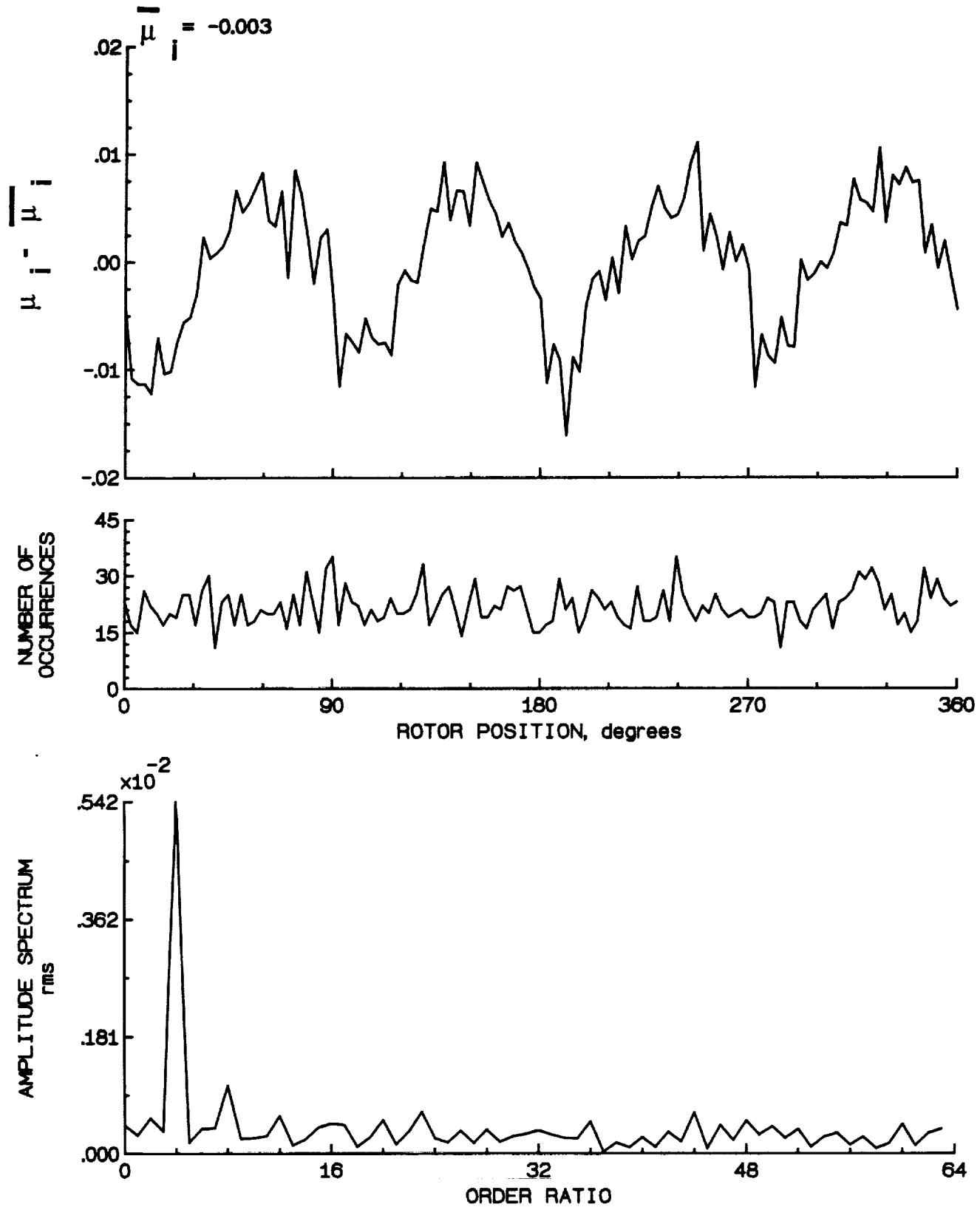


Figure 150.- Induced inflow velocity measured at 270 degrees and r/R of 0.74.

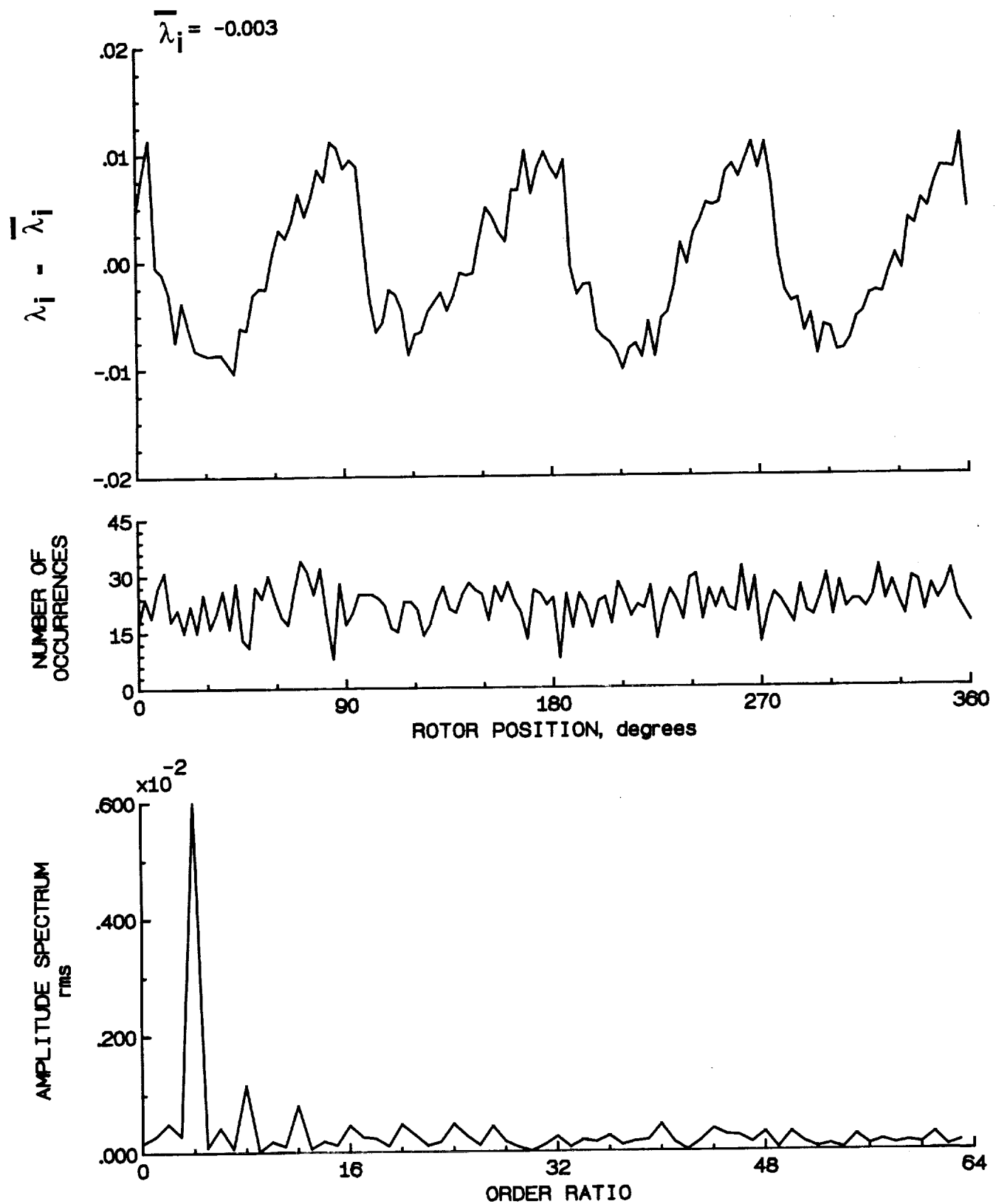


Figure 150.- Concluded.

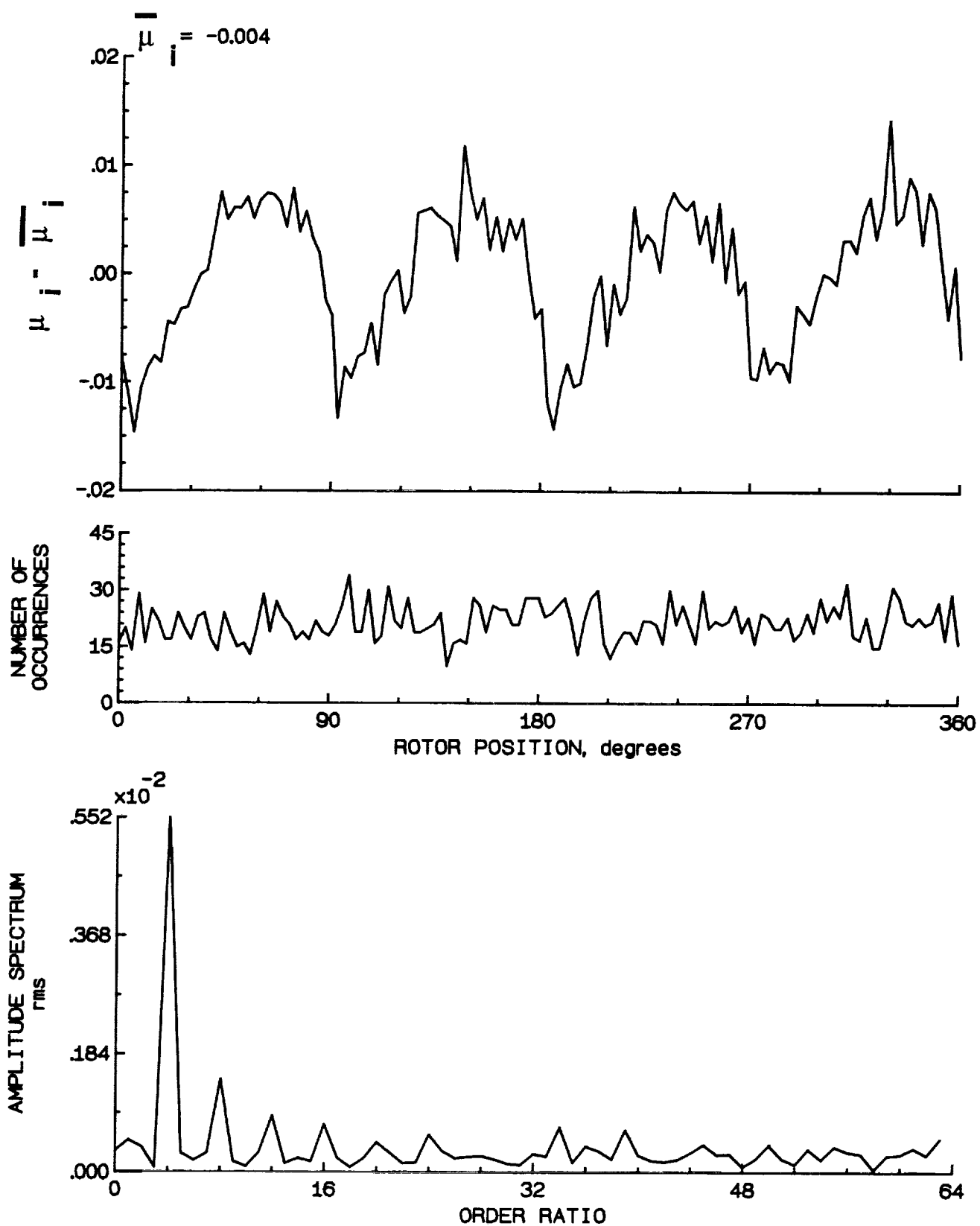


Figure 151.- Induced inflow velocity measured at 270 degrees and r/R of 0.78.

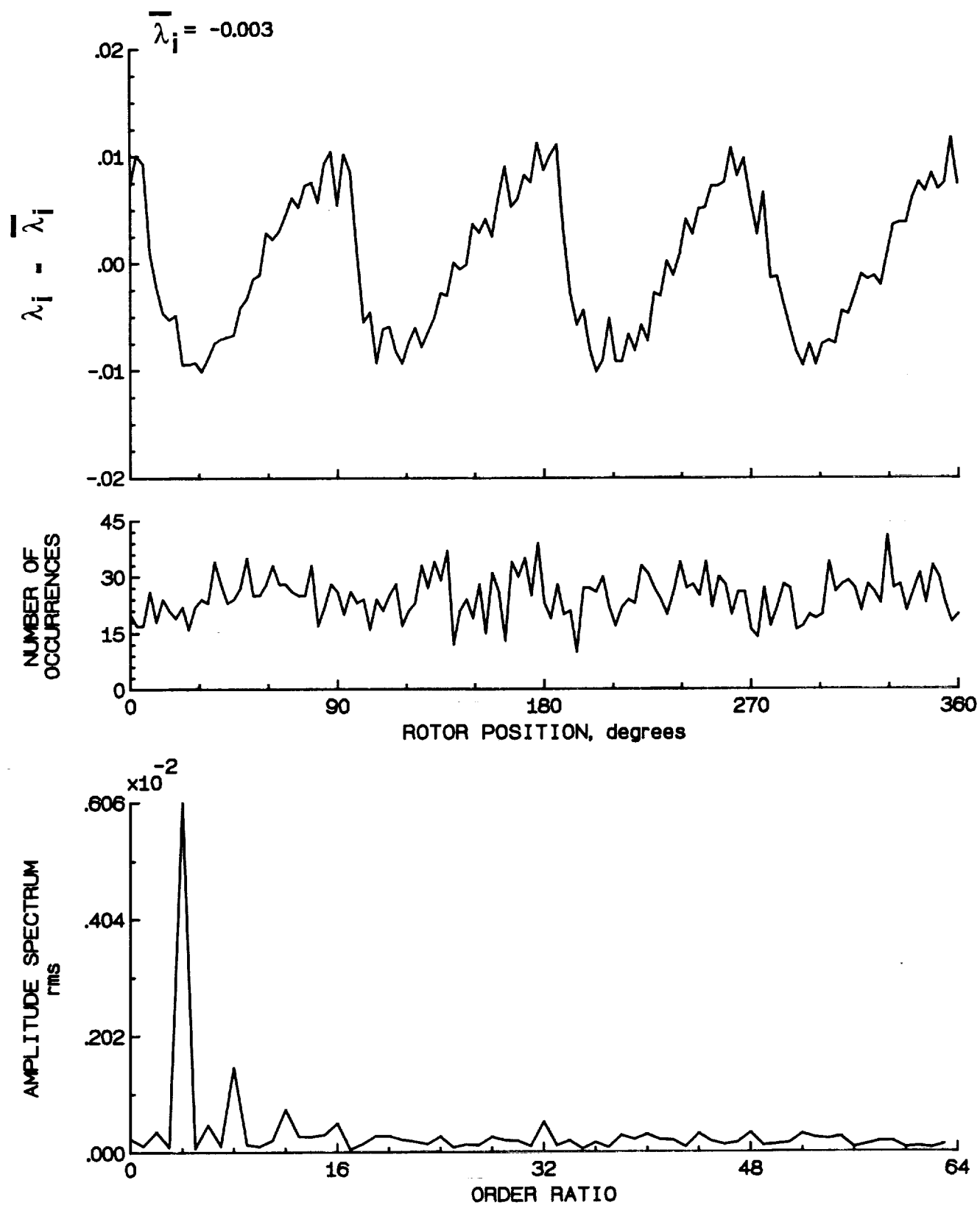


Figure 151.- Concluded.

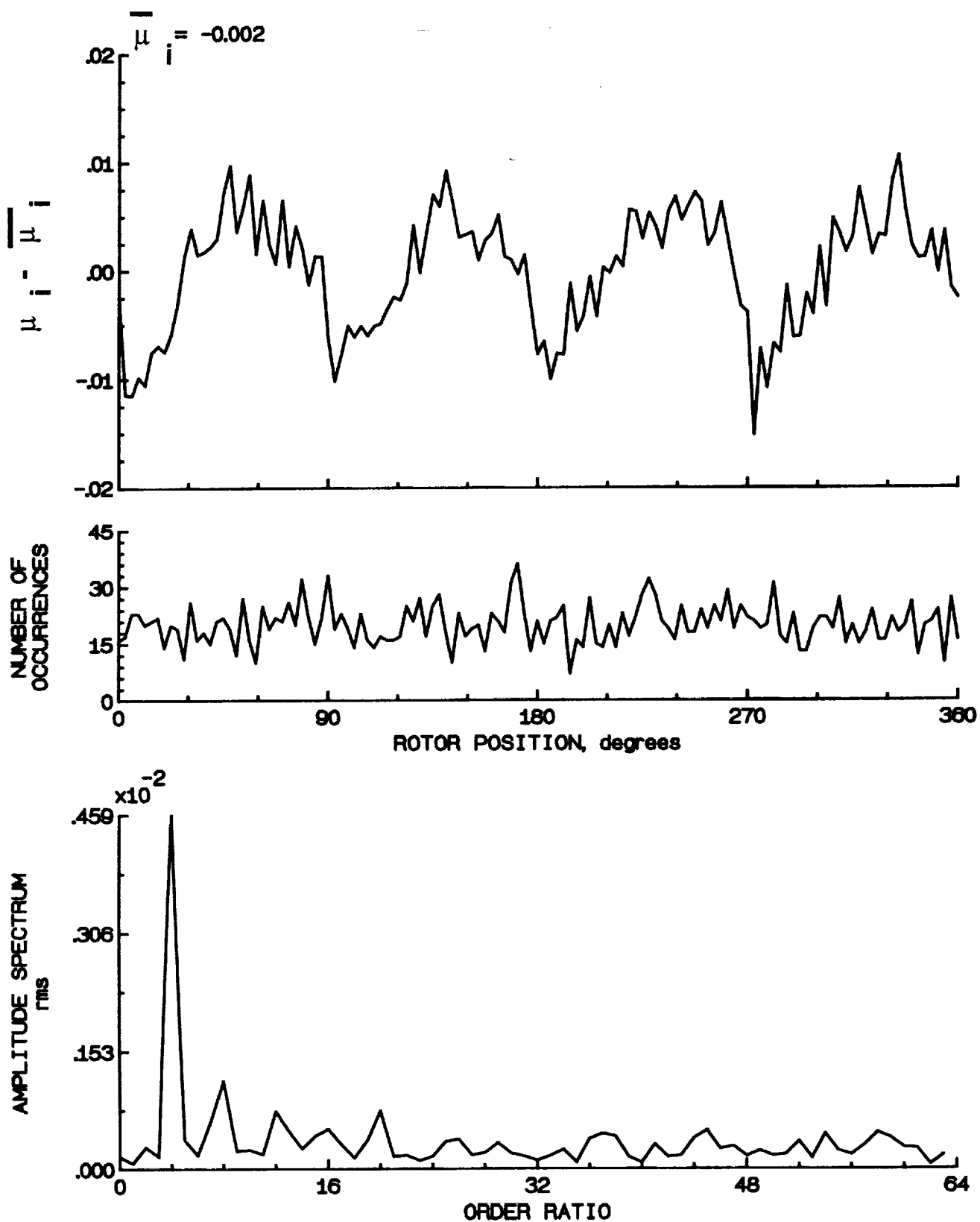


Figure 152.- Induced inflow velocity measured at 270 degrees and r/R of 0.82.

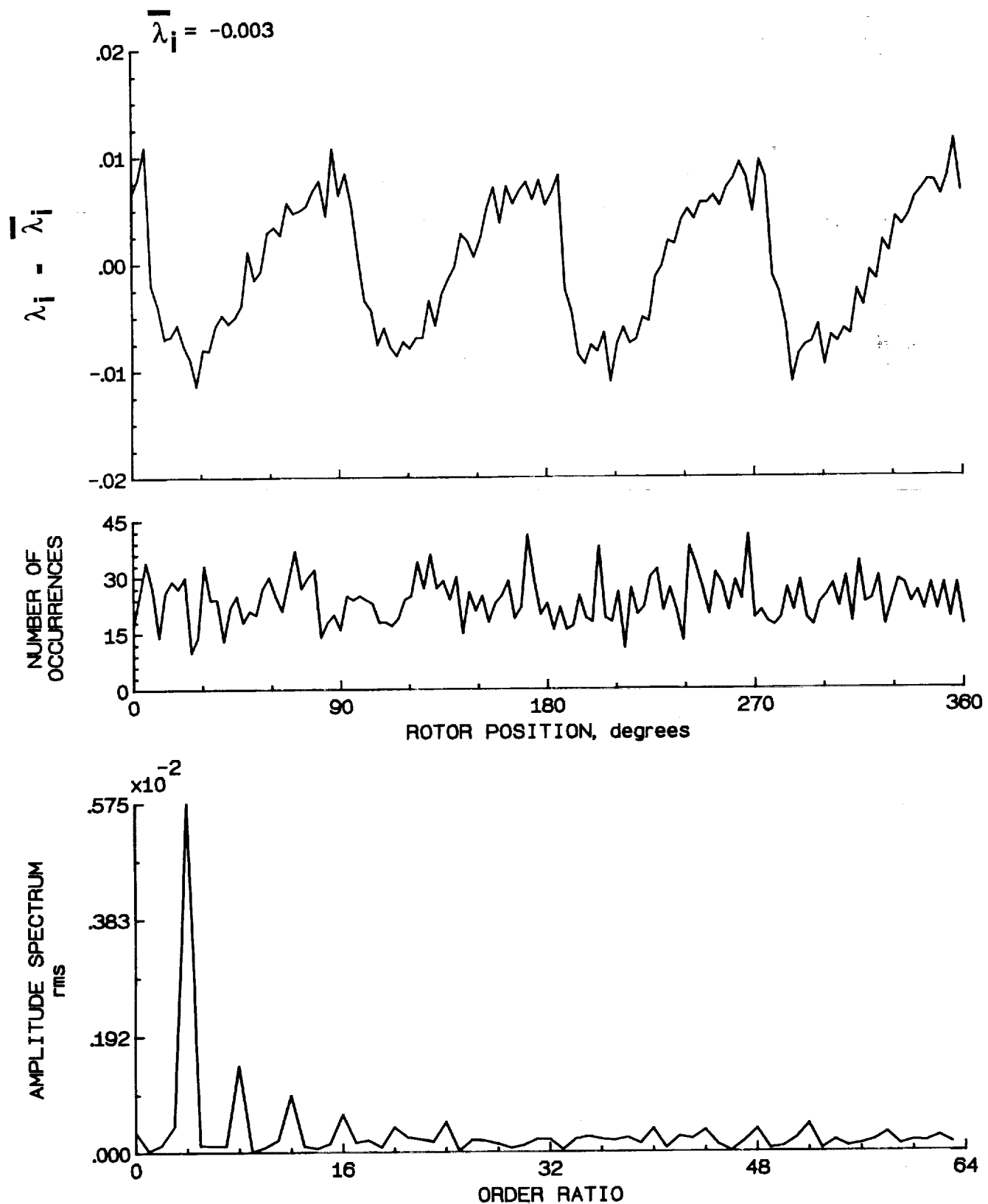


Figure 152.- Concluded.

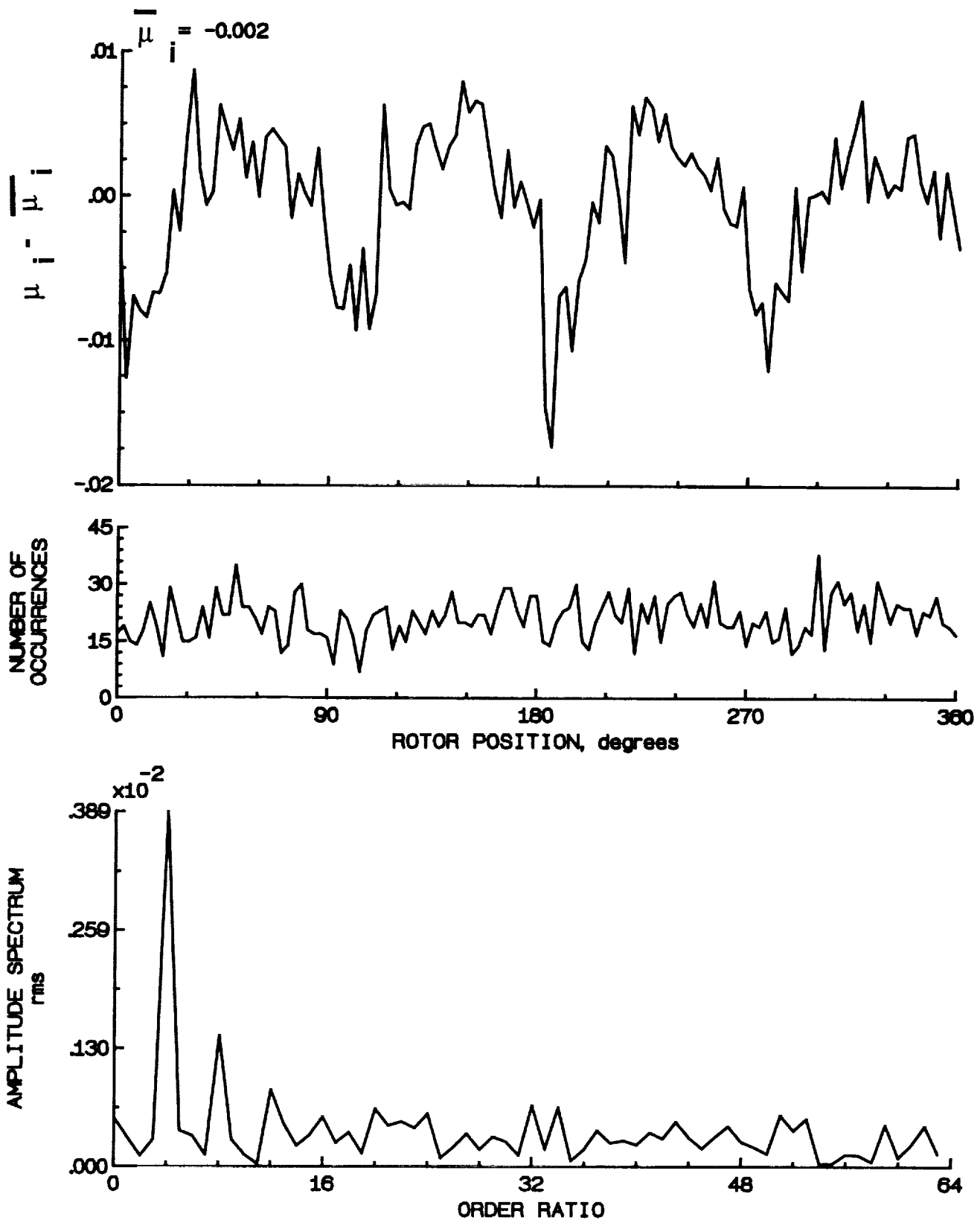


Figure 153.- Induced inflow velocity measured at 270 degrees and r/R of 0.86.

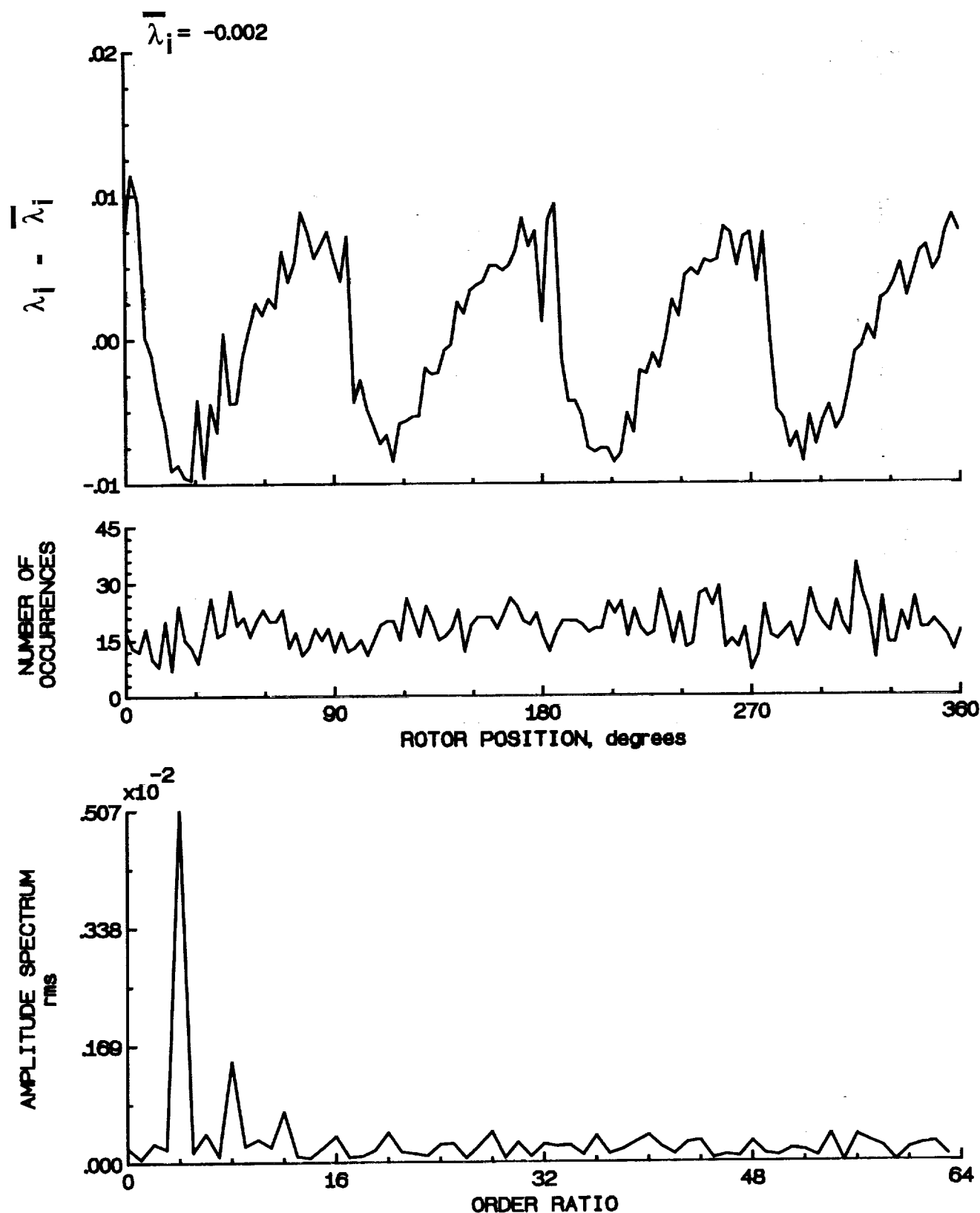


Figure 153.- Concluded.

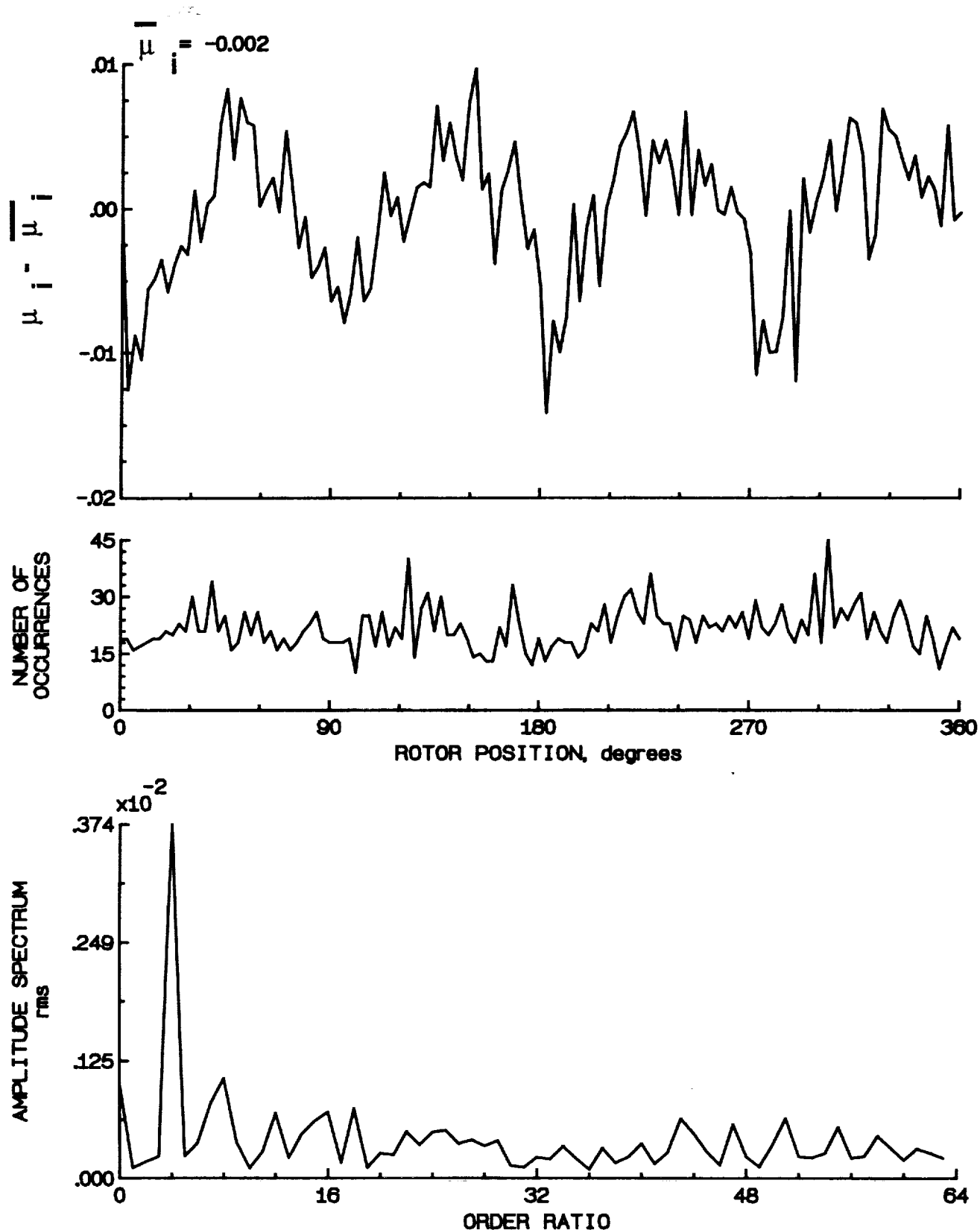


Figure 154.- Induced inflow velocity measured at 270 degrees and r/R of 0.90.

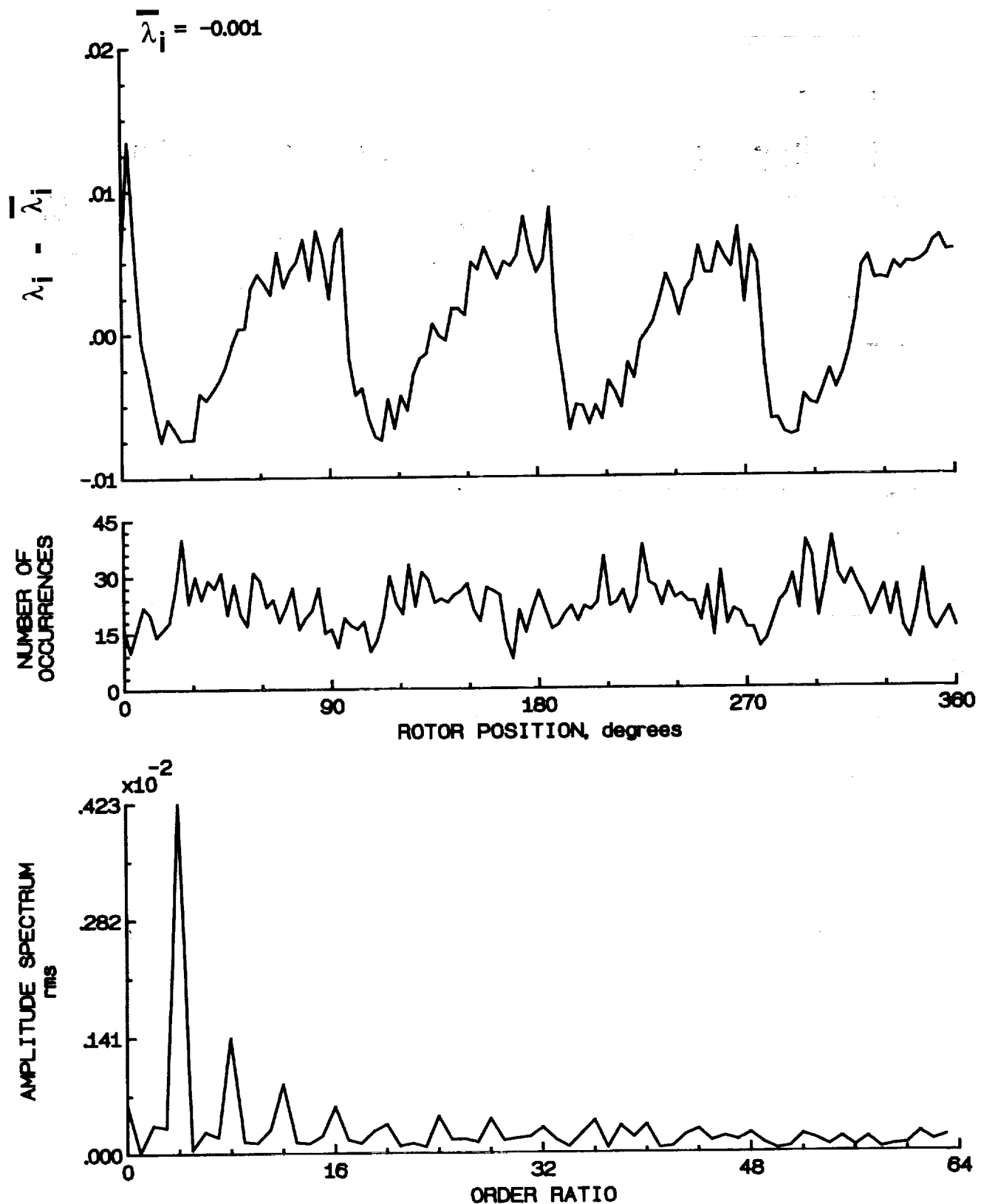


Figure 154.- Concluded.

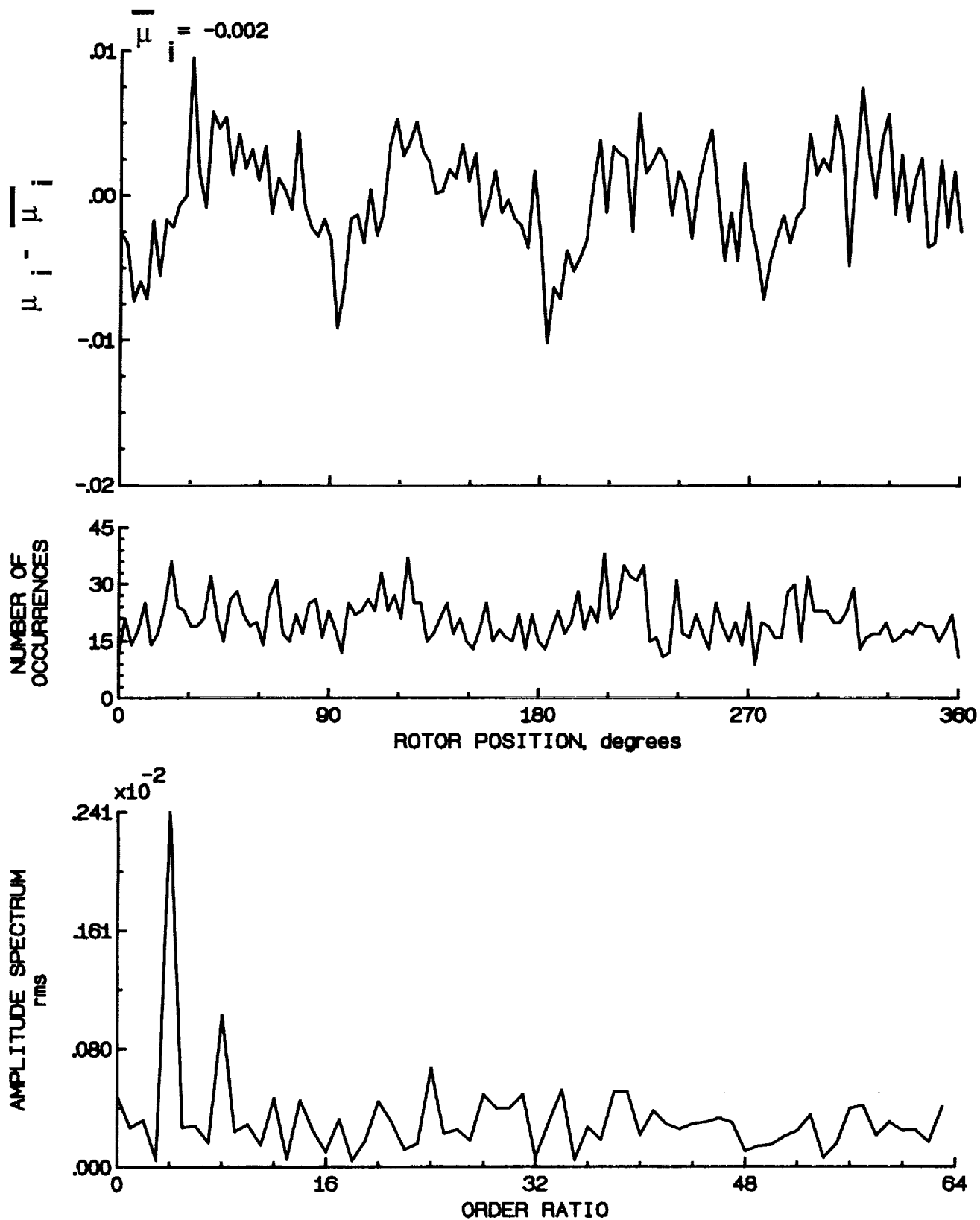


Figure 155.- Induced inflow velocity measured at 270 degrees and r/R of 0.94.

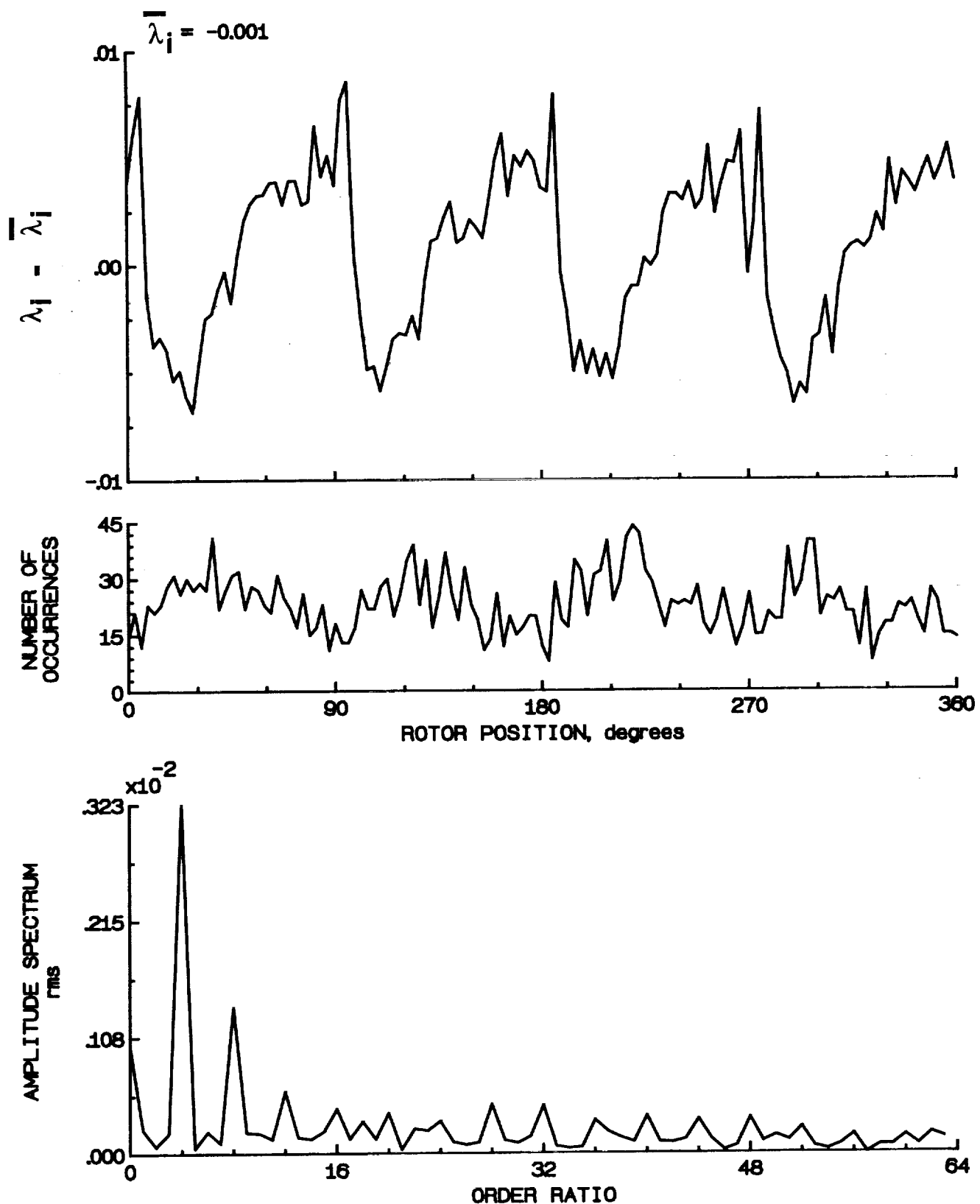


Figure 155.- Concluded.

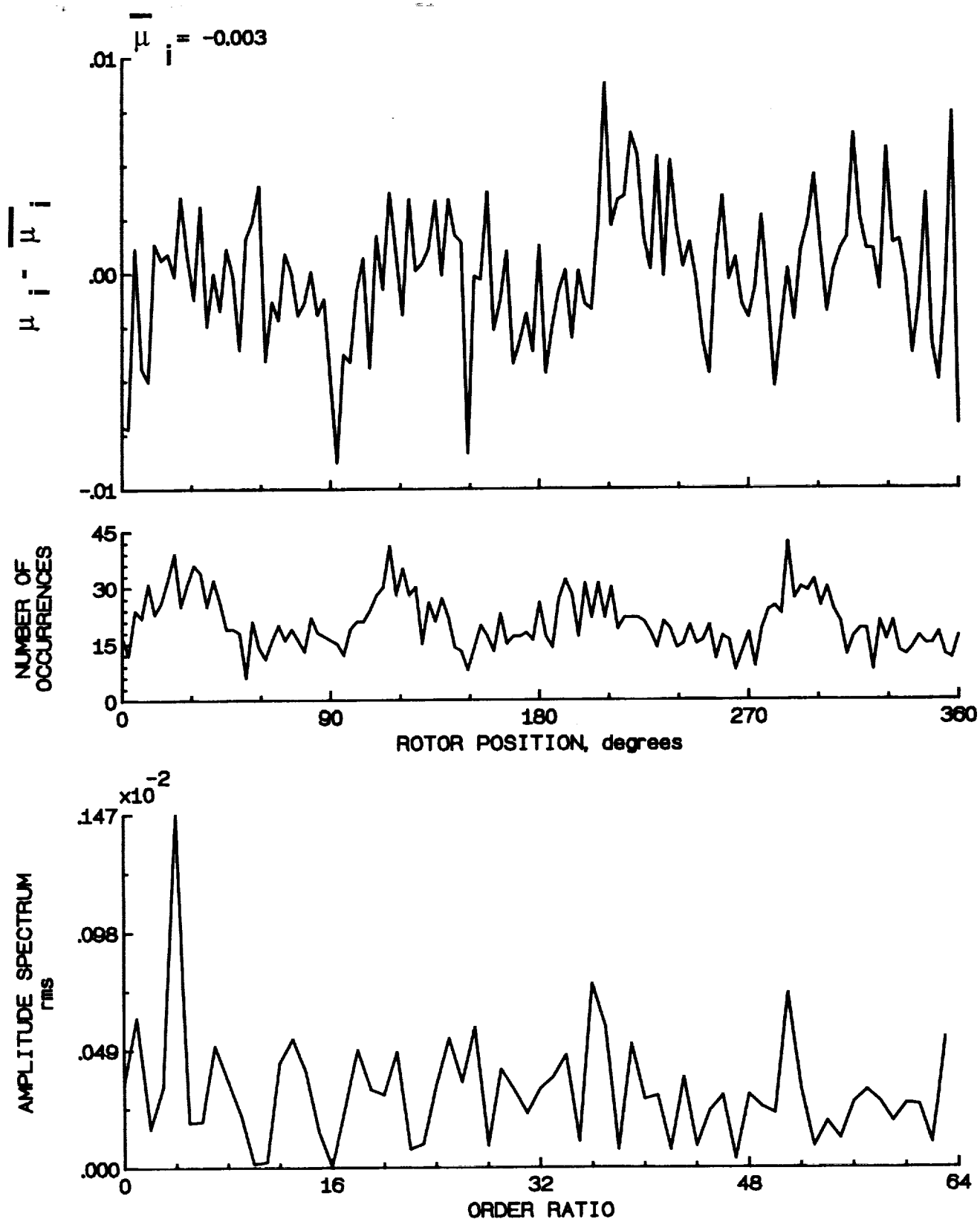


Figure 156.- Induced inflow velocity measured at 270 degrees and r/R of 0.98.

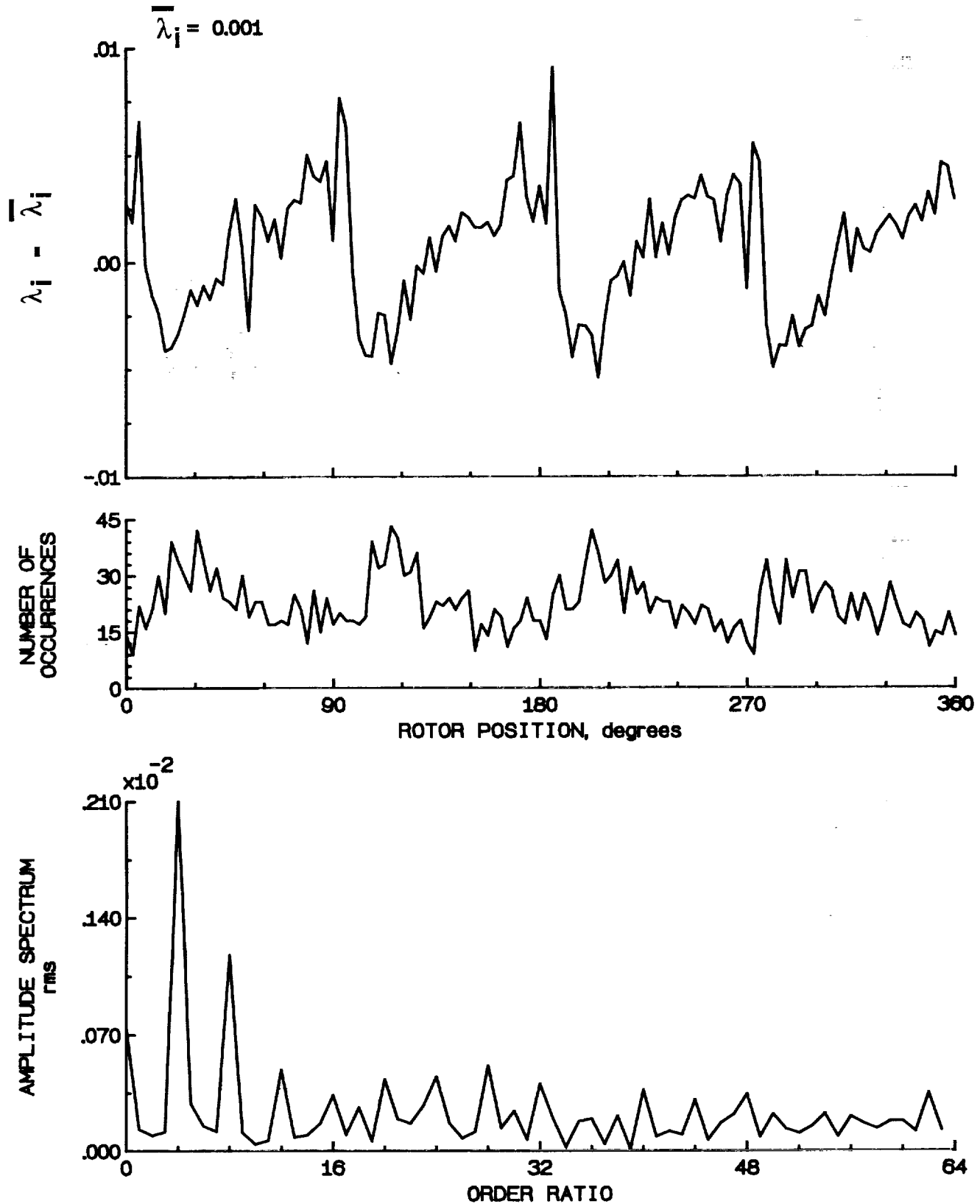


Figure 156.- Concluded.

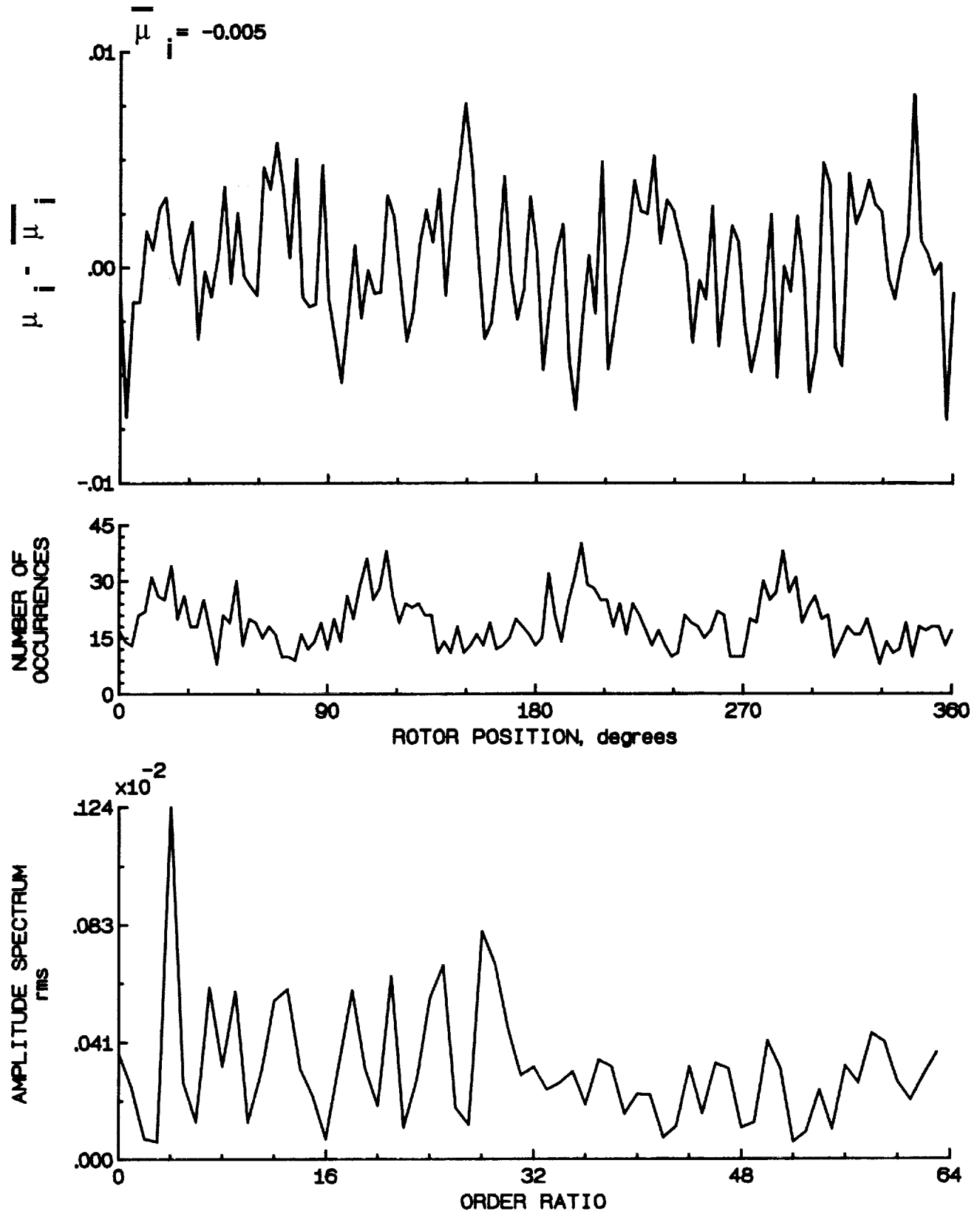


Figure 157.- Induced inflow velocity measured at 270 degrees and r/R of 1.02.

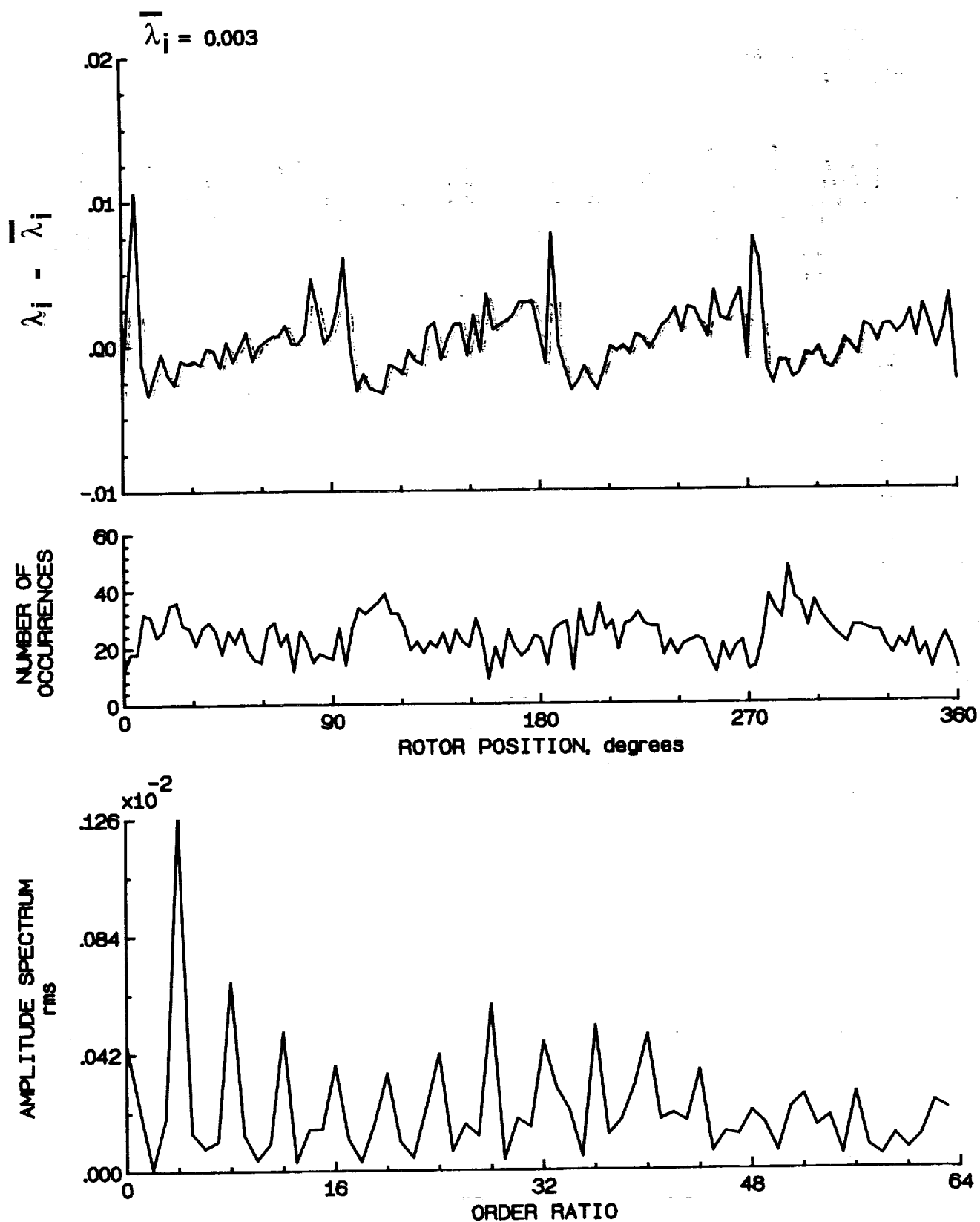


Figure 157.- Concluded.

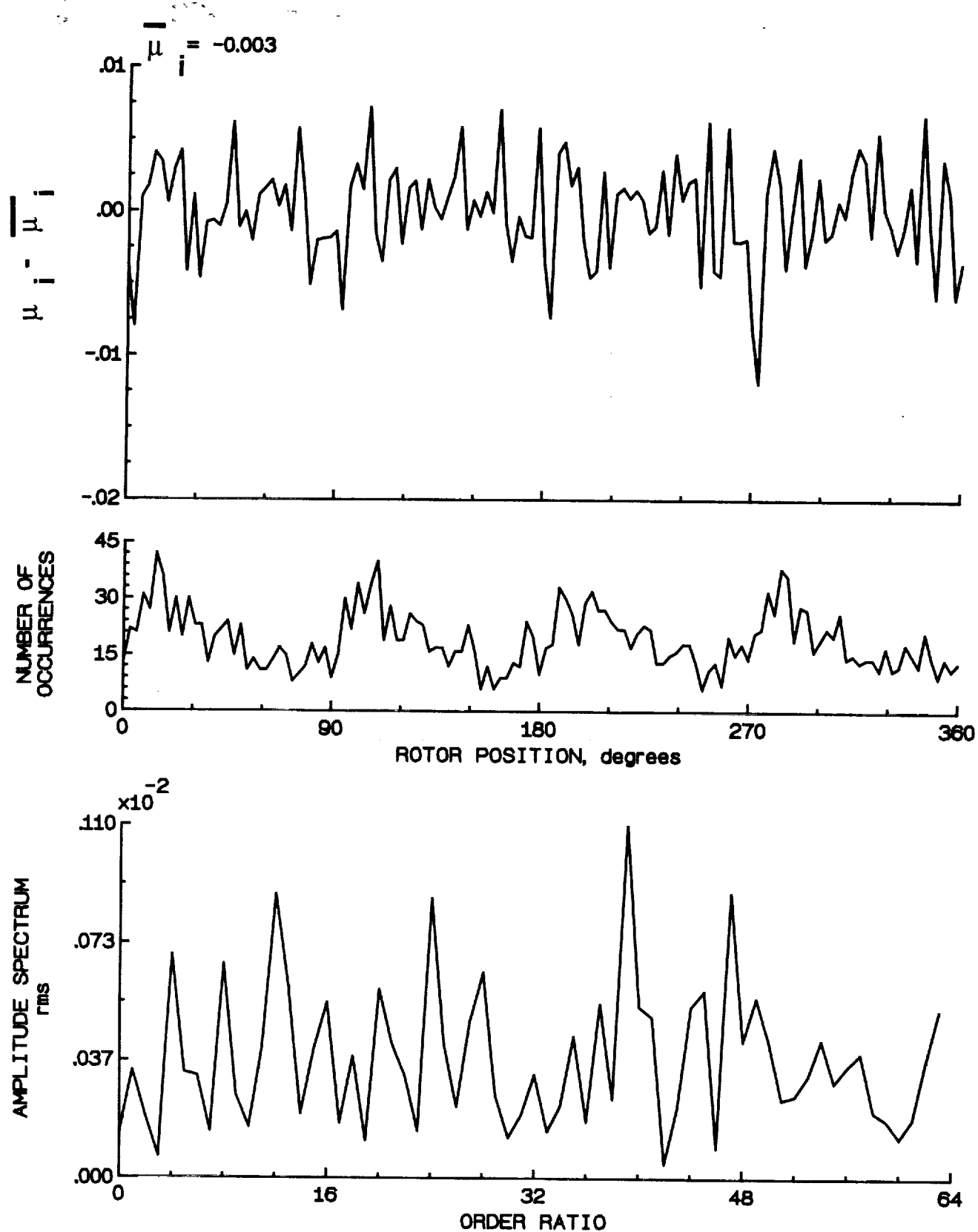


Figure 158.- Induced inflow velocity measured at 270 degrees and r/R of 1.04.

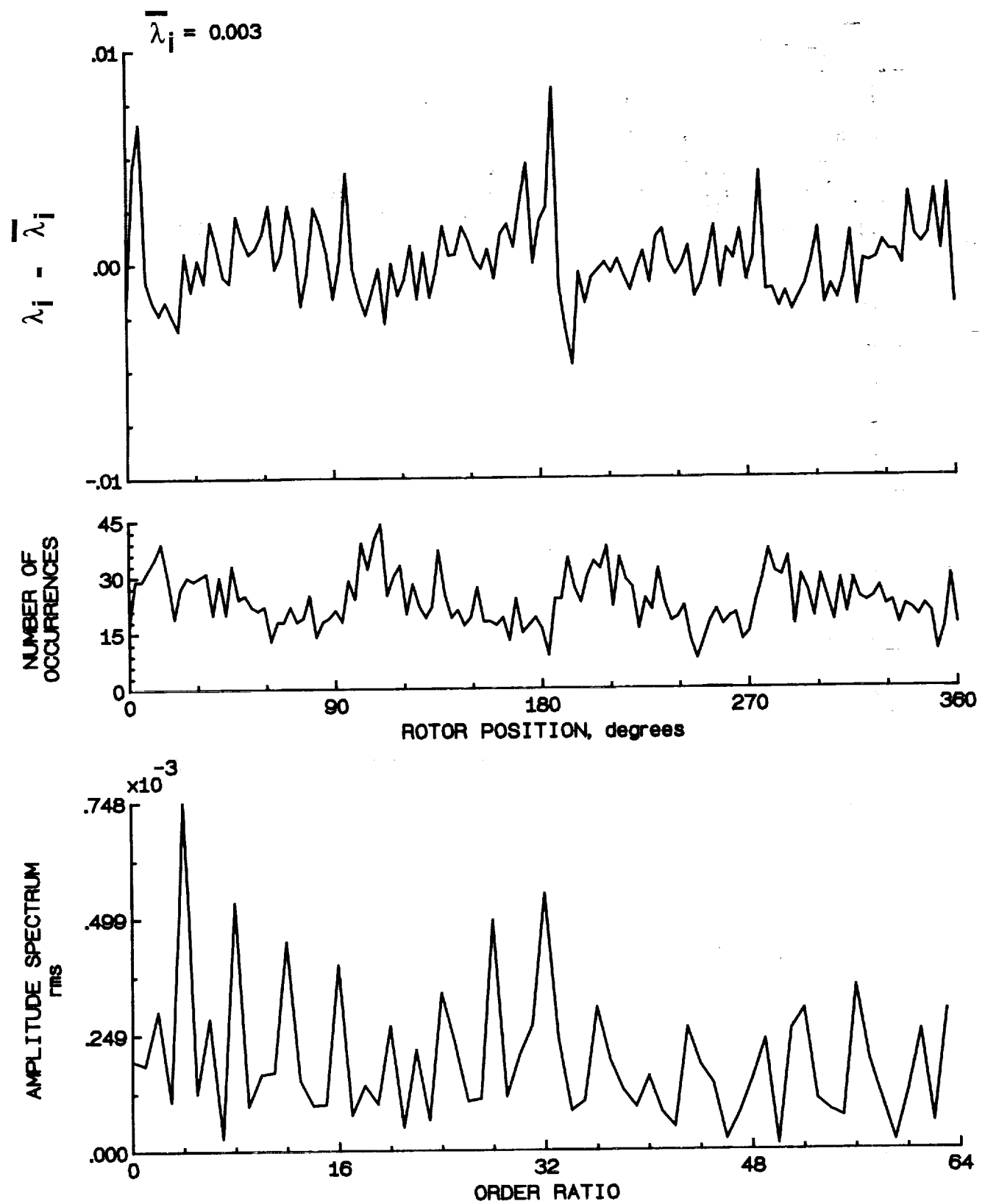


Figure 158.- Concluded.

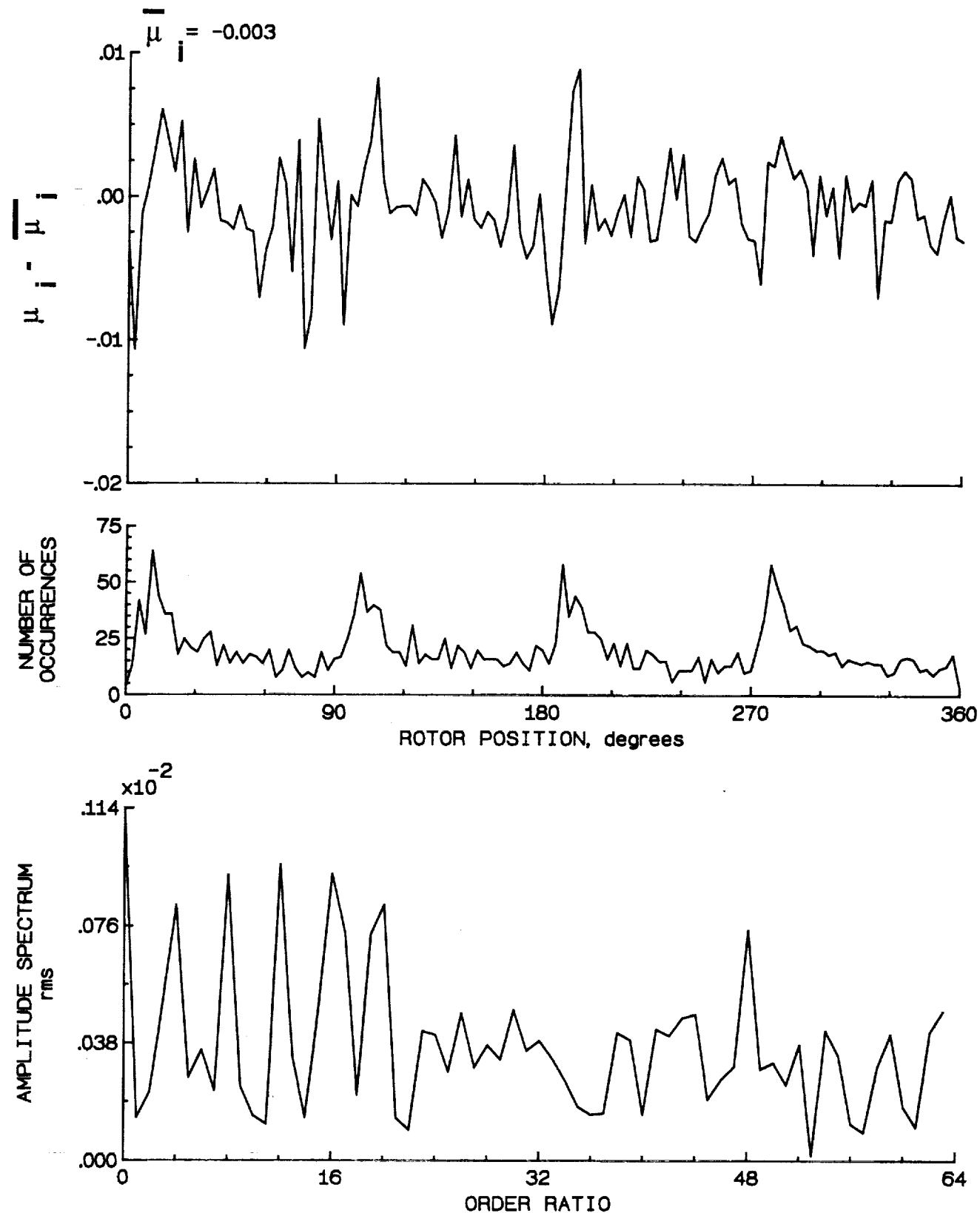


Figure 159.- Induced inflow velocity measured at 270 degrees and r/R of 1.10.

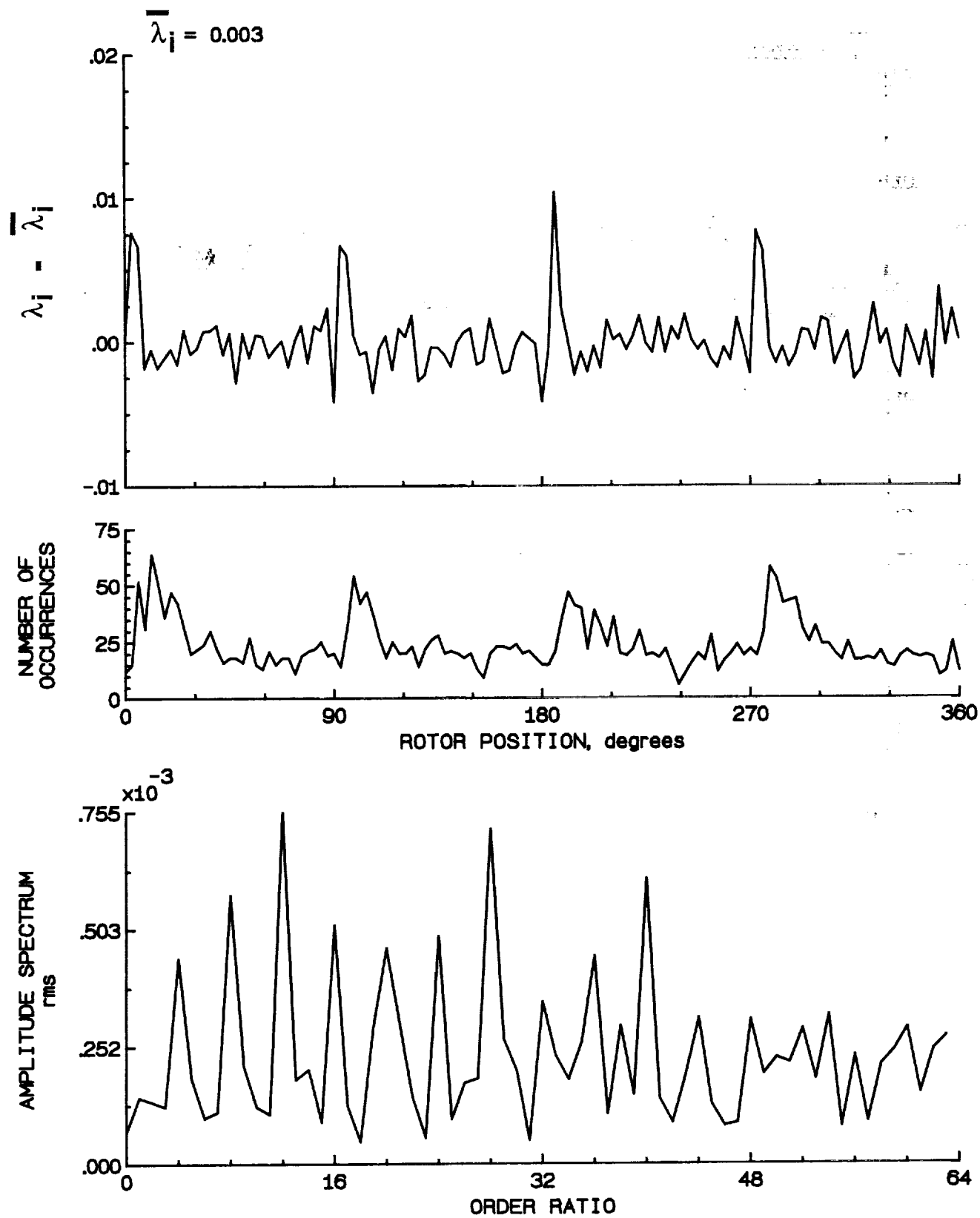


Figure 159.- Concluded.

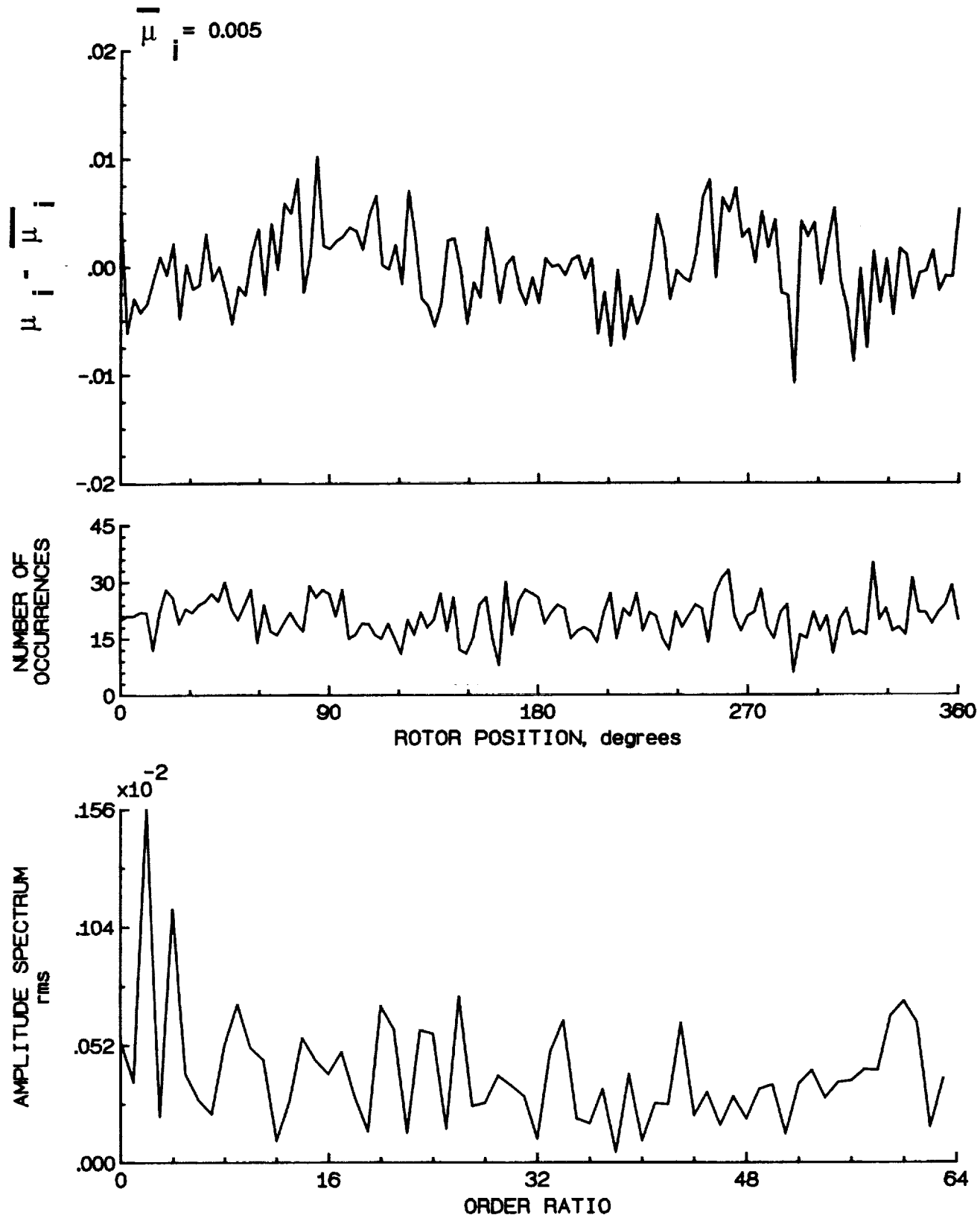


Figure 160.- Induced inflow velocity measured at 300 degrees and r/R of 0.20.

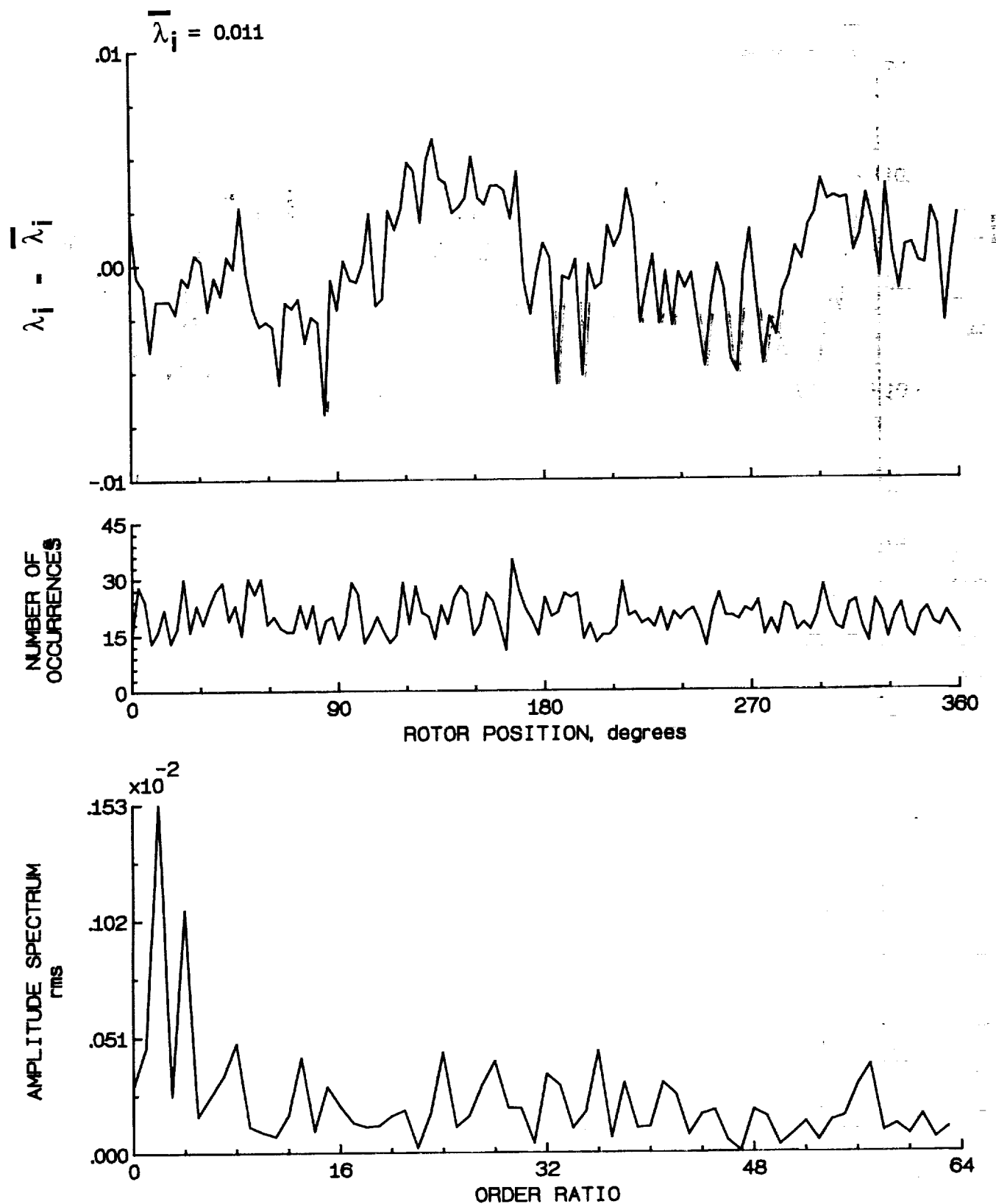


Figure 160.- Concluded.

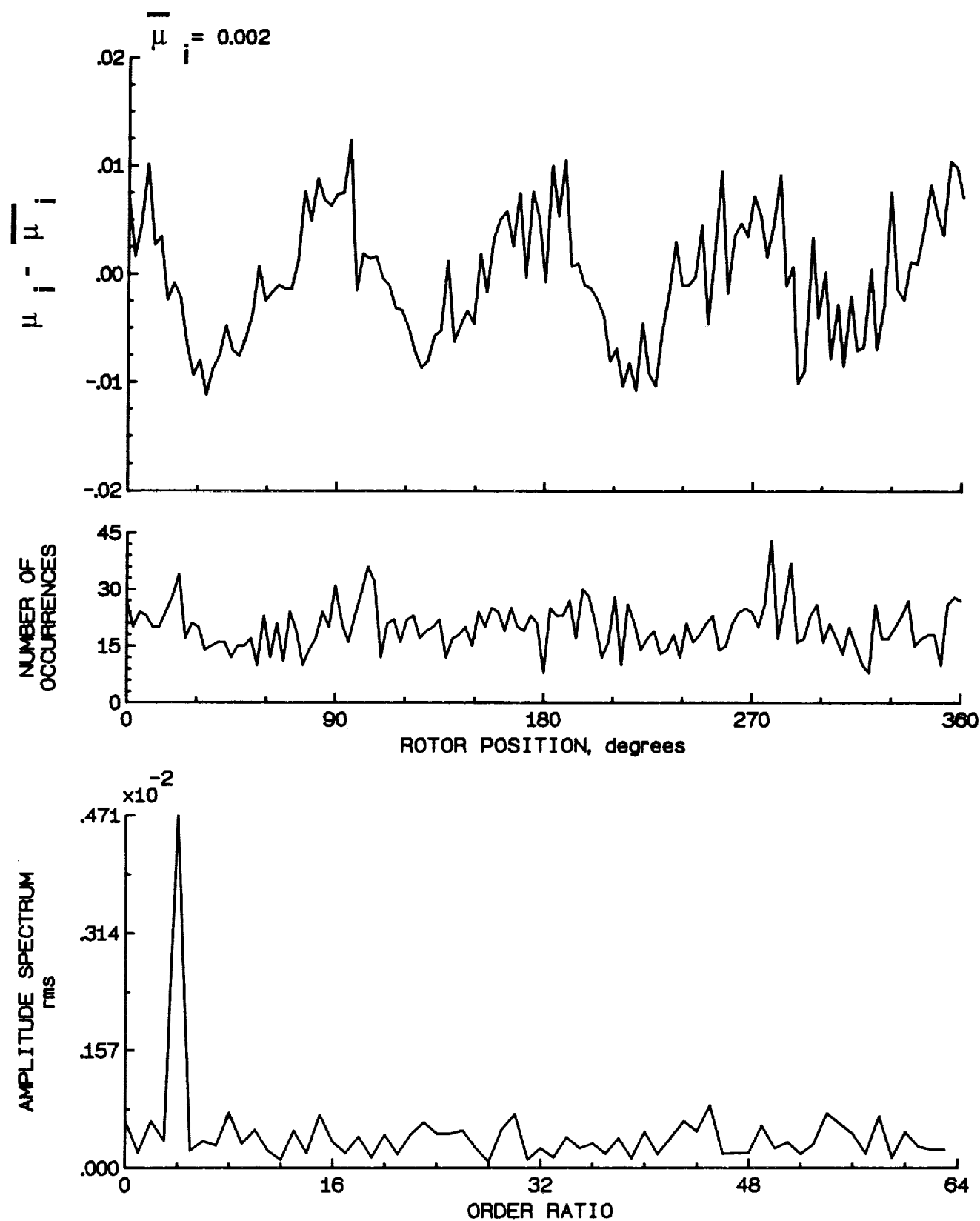


Figure 161.- Induced inflow velocity measured at 300 degrees and r/R of 0.40.

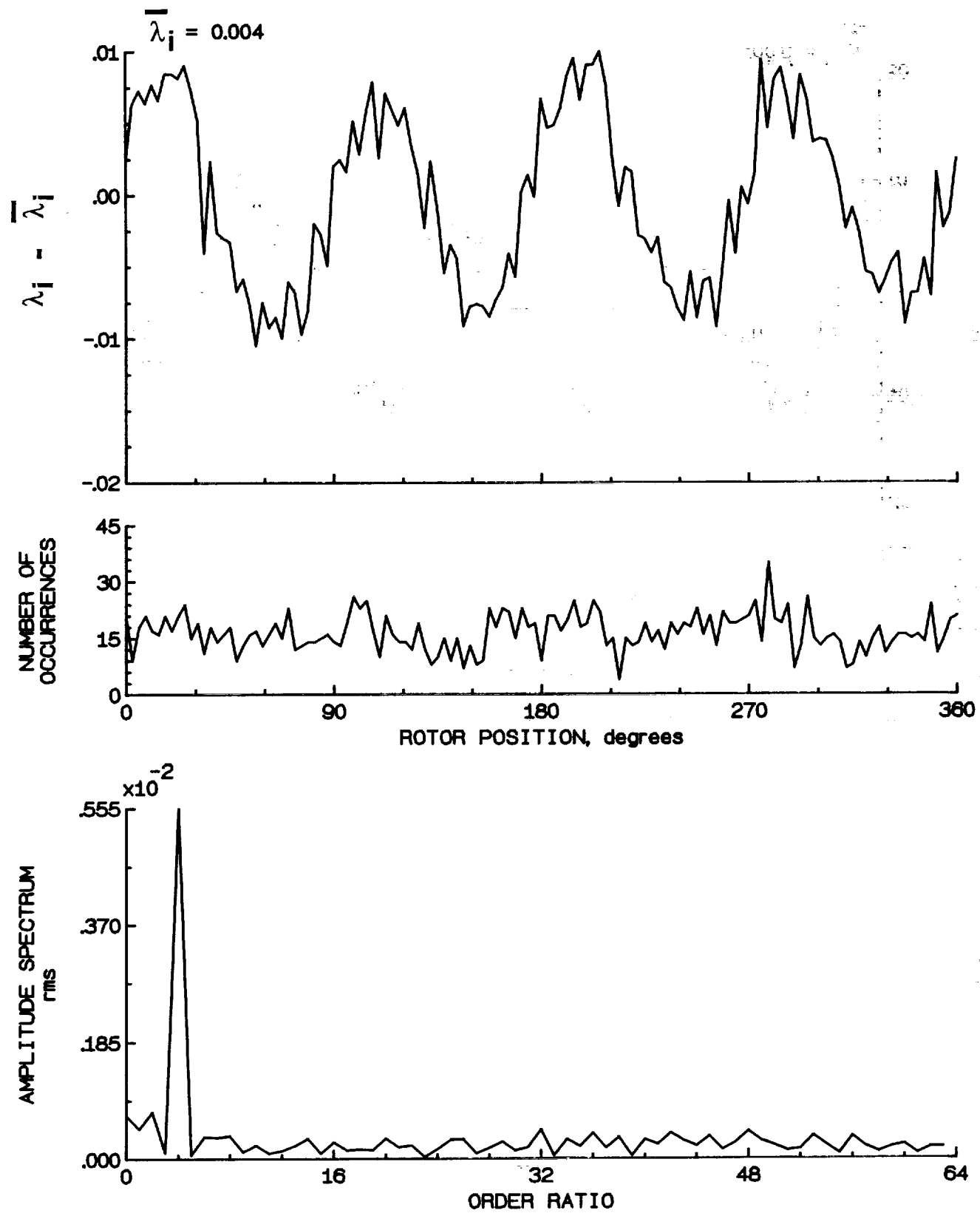


Figure 161.- Concluded.

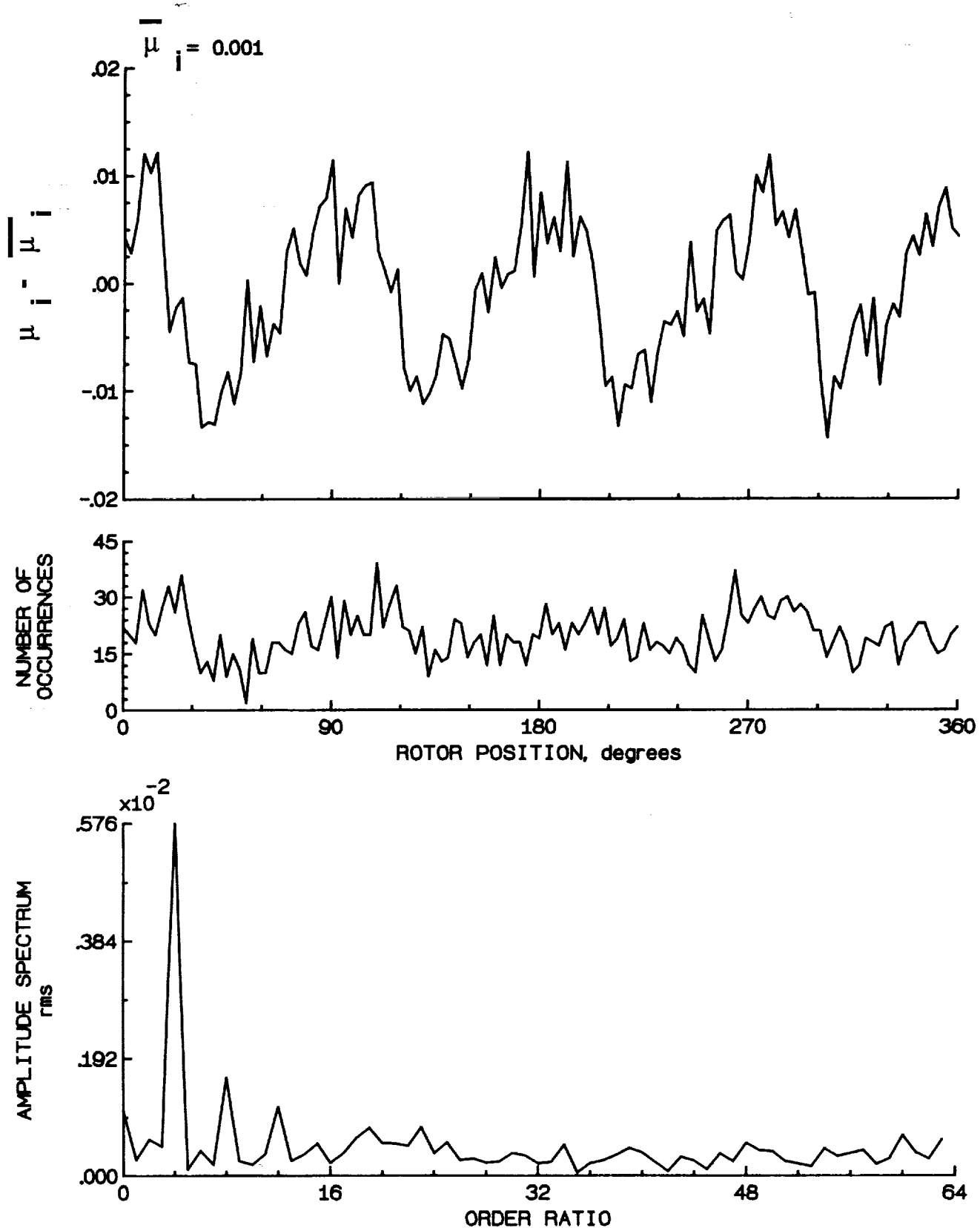


Figure 162.- Induced inflow velocity measured at 300 degrees and r/R of 0.50.

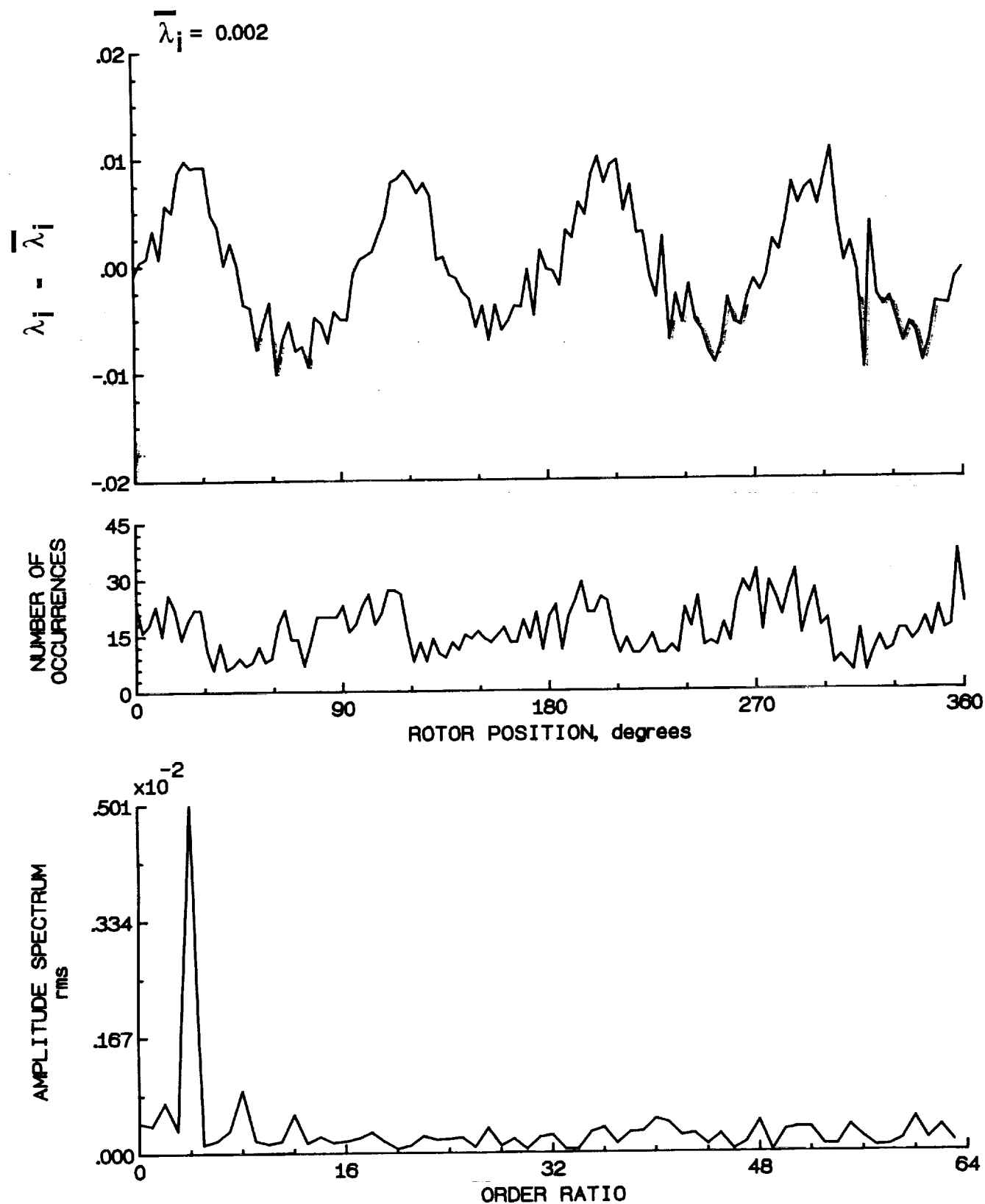


Figure 162.- Concluded.

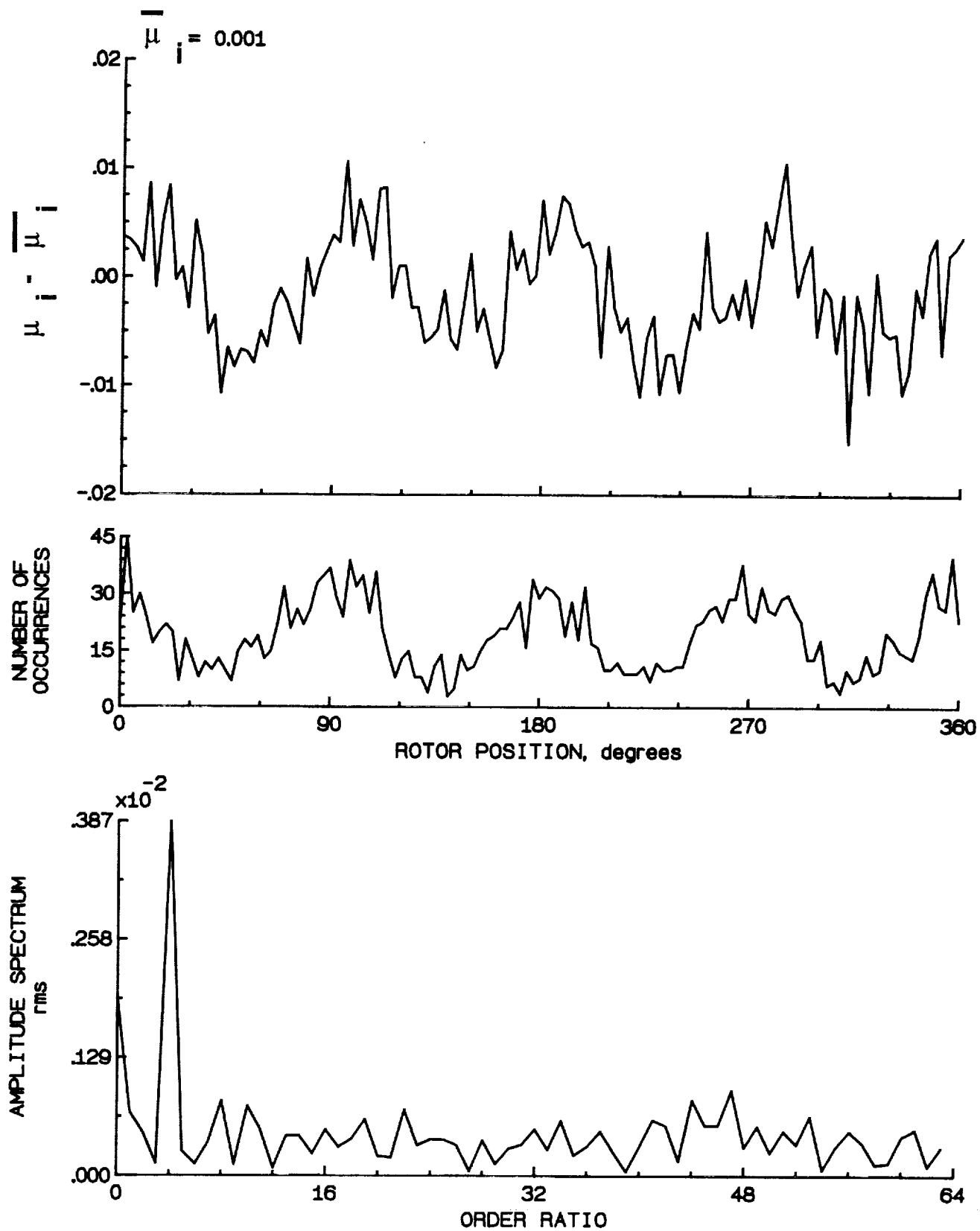


Figure 163.- Induced inflow velocity measured at 300 degrees and r/R of 0.60.

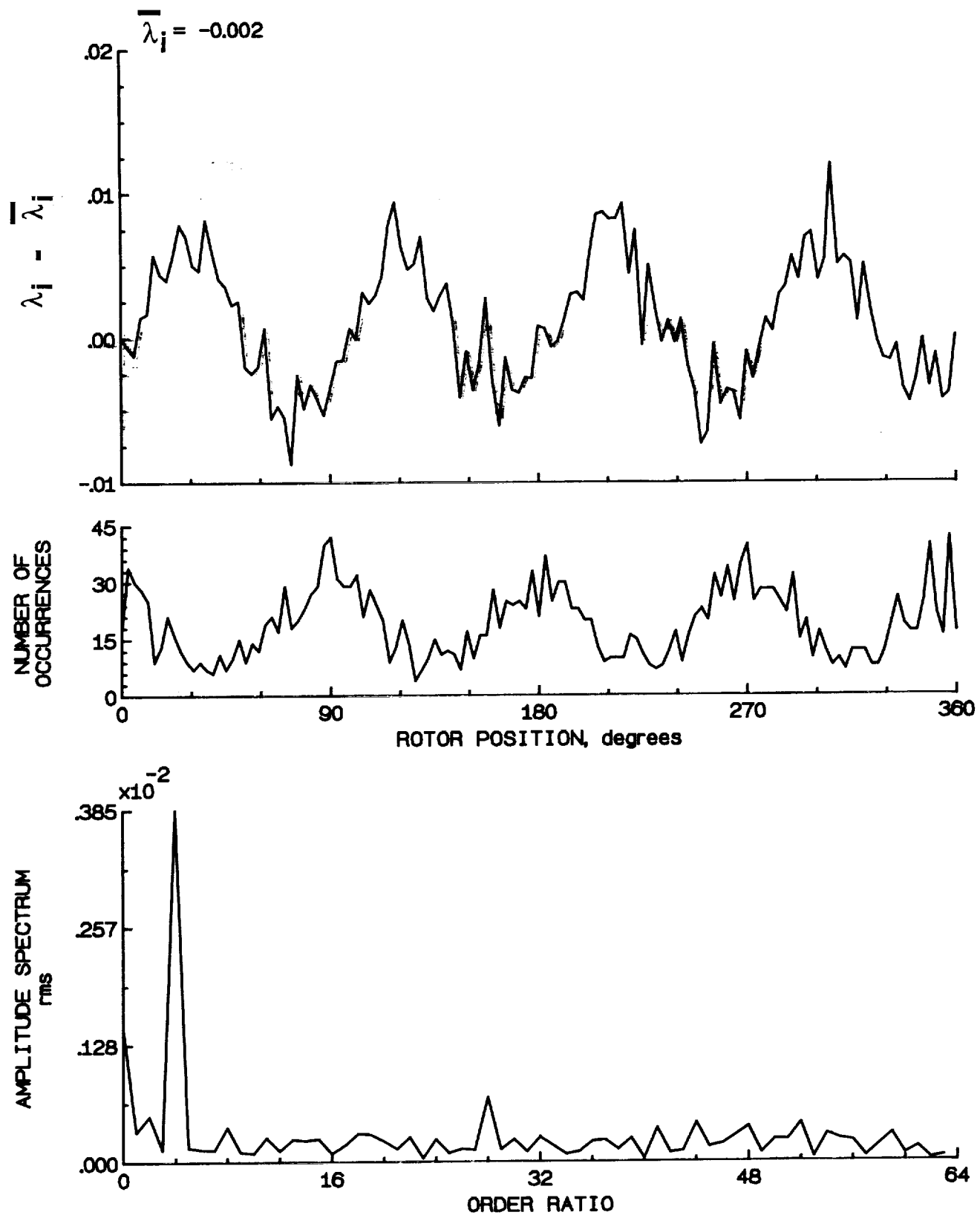


Figure 163.- Concluded.

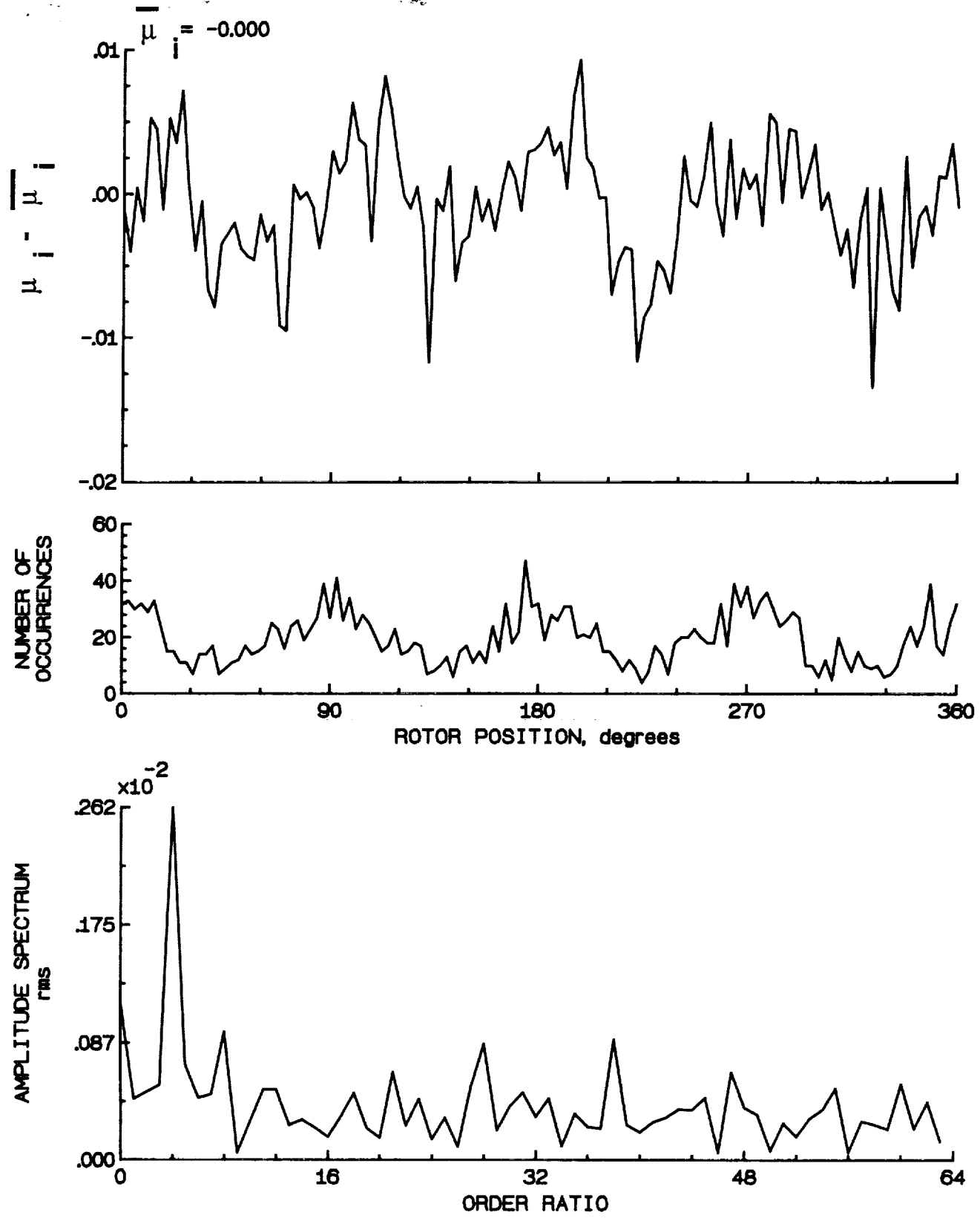


Figure 164.- Induced inflow velocity measured at 300 degrees and r/R of 0.70.

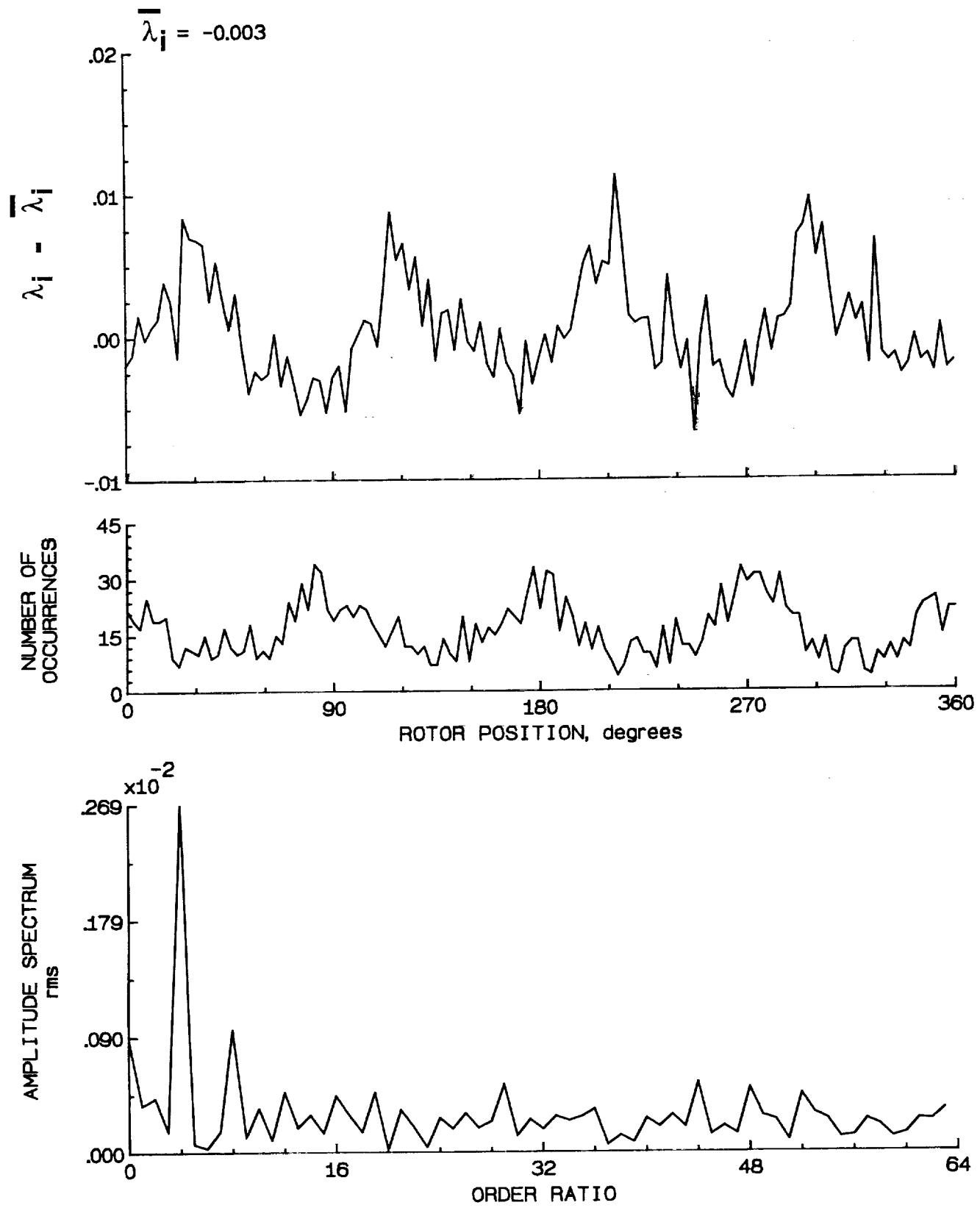


Figure 164.- Concluded.

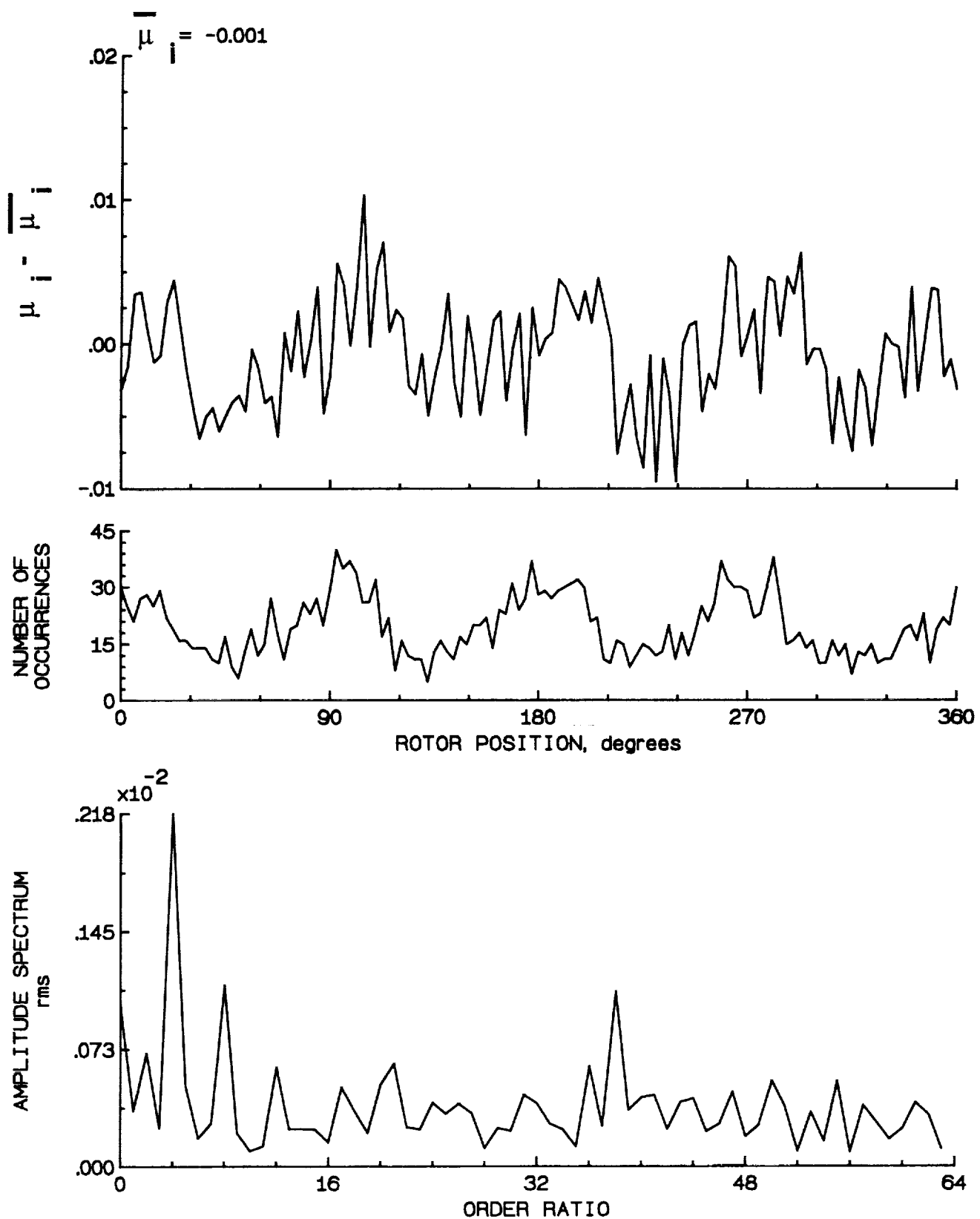


Figure 165.- Induced inflow velocity measured at 300 degrees and r/R of 0.74.

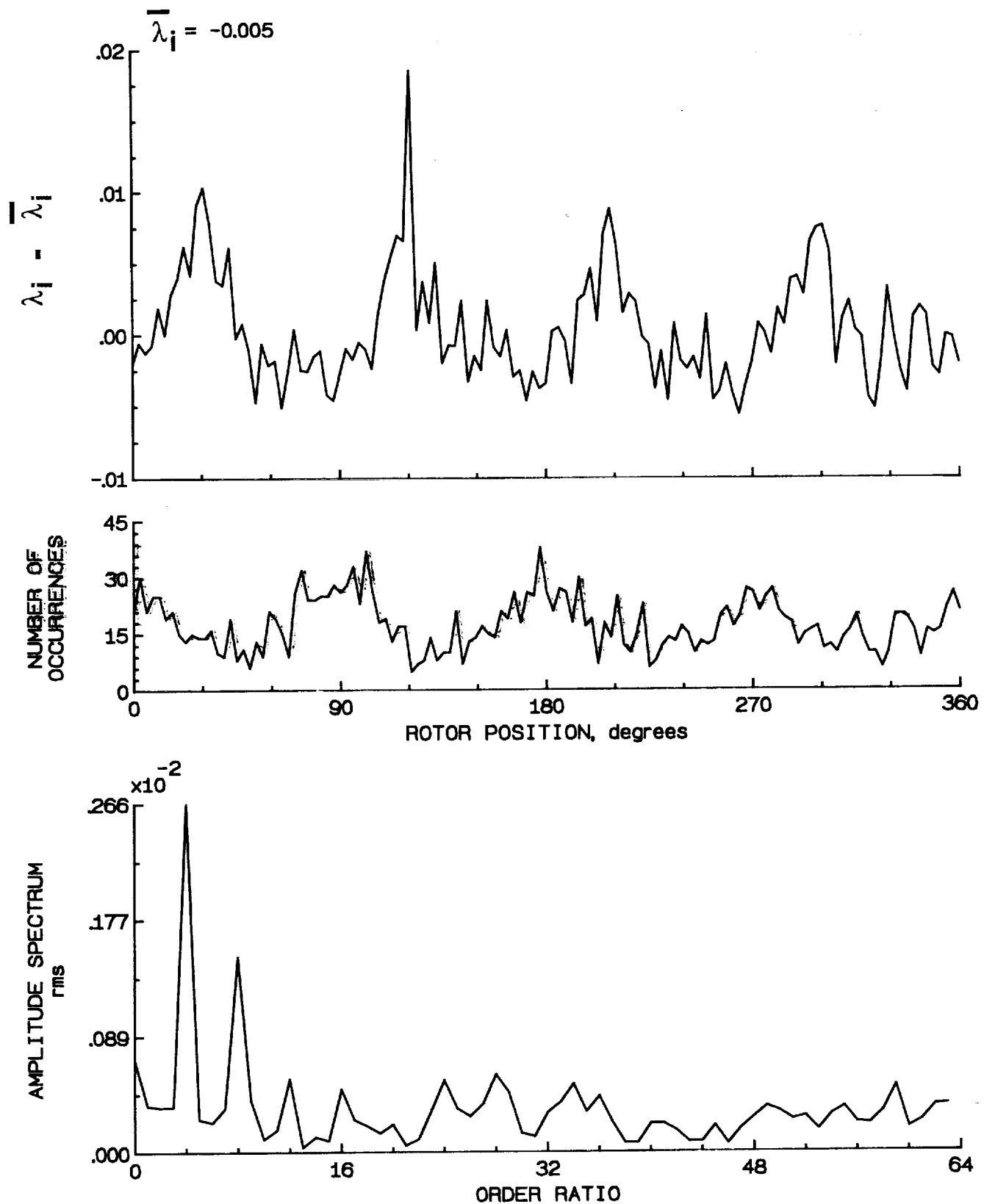


Figure 165.- Concluded.

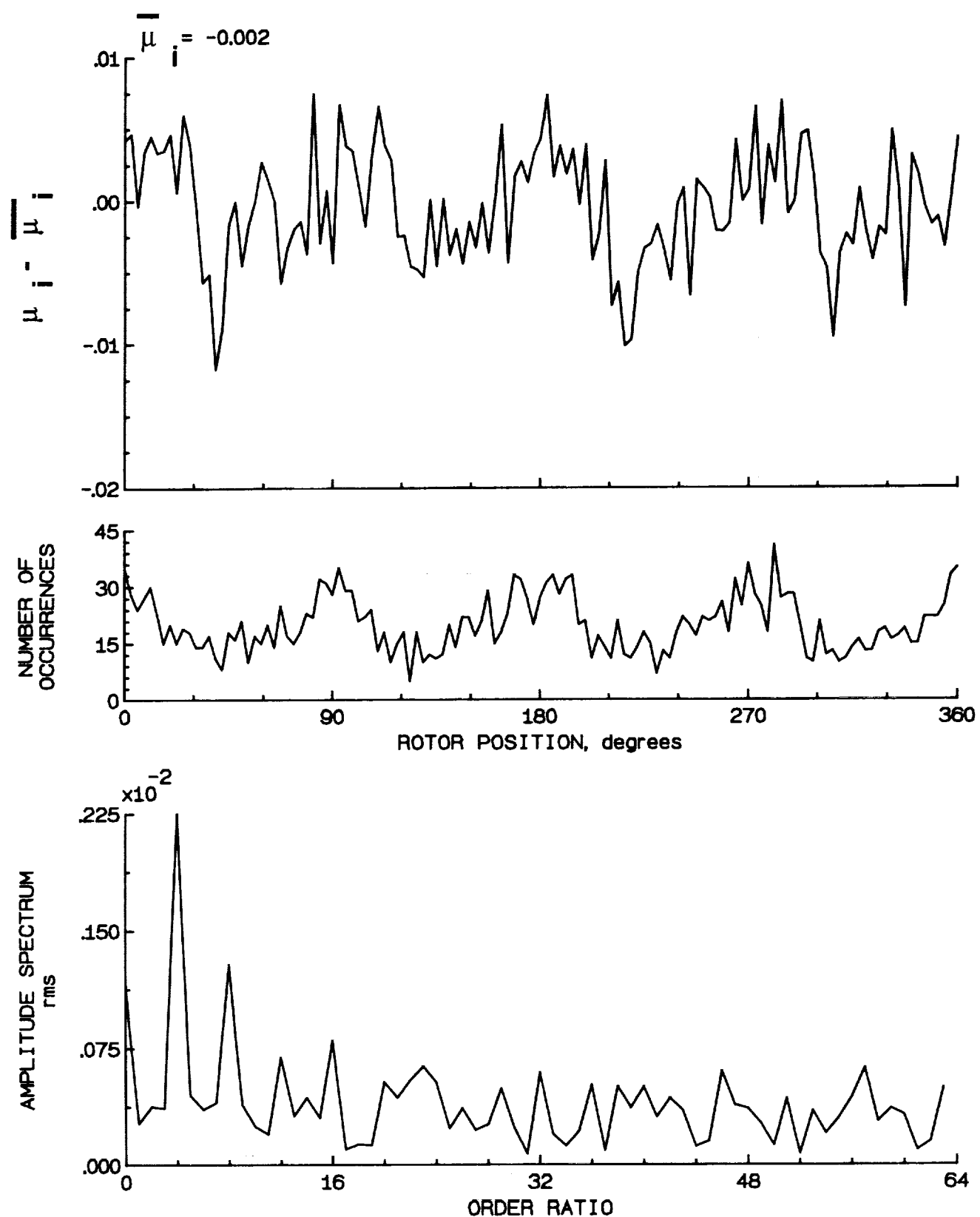


Figure 166.- Induced inflow velocity measured at 300 degrees and r/R of 0.78.

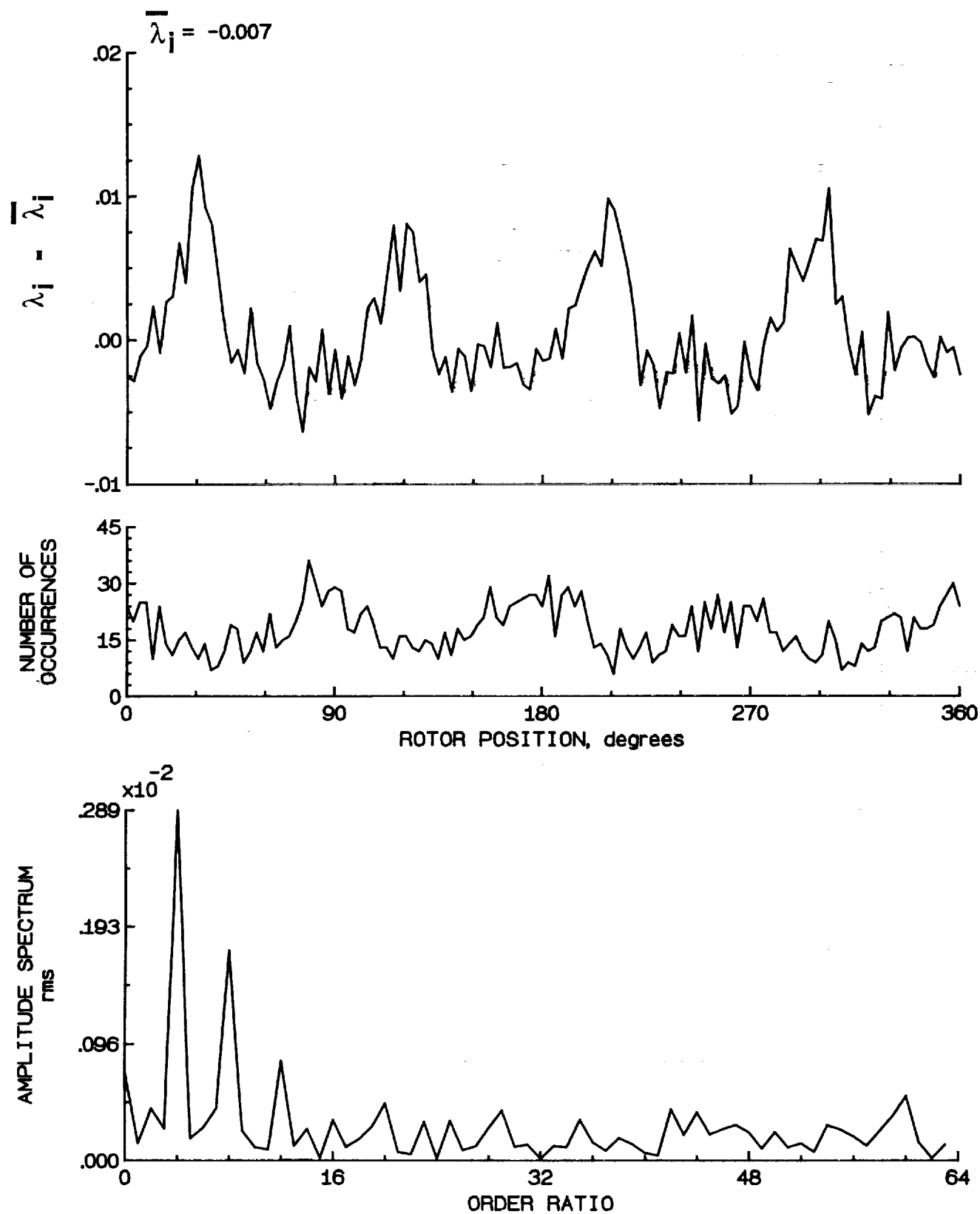


Figure 166.- Concluded.

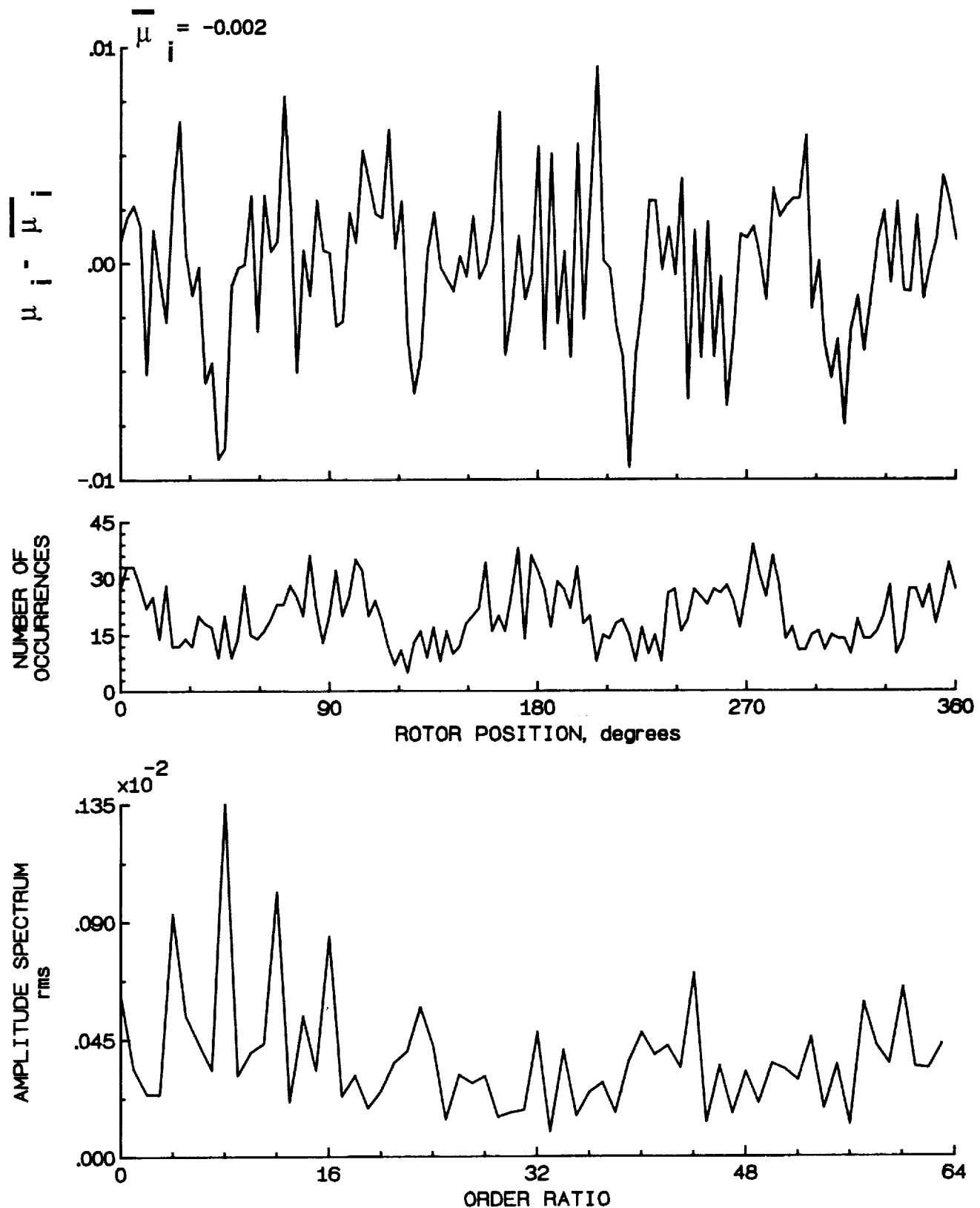


Figure 167.- Induced inflow velocity measured at 300 degrees and r/R of 0.82.

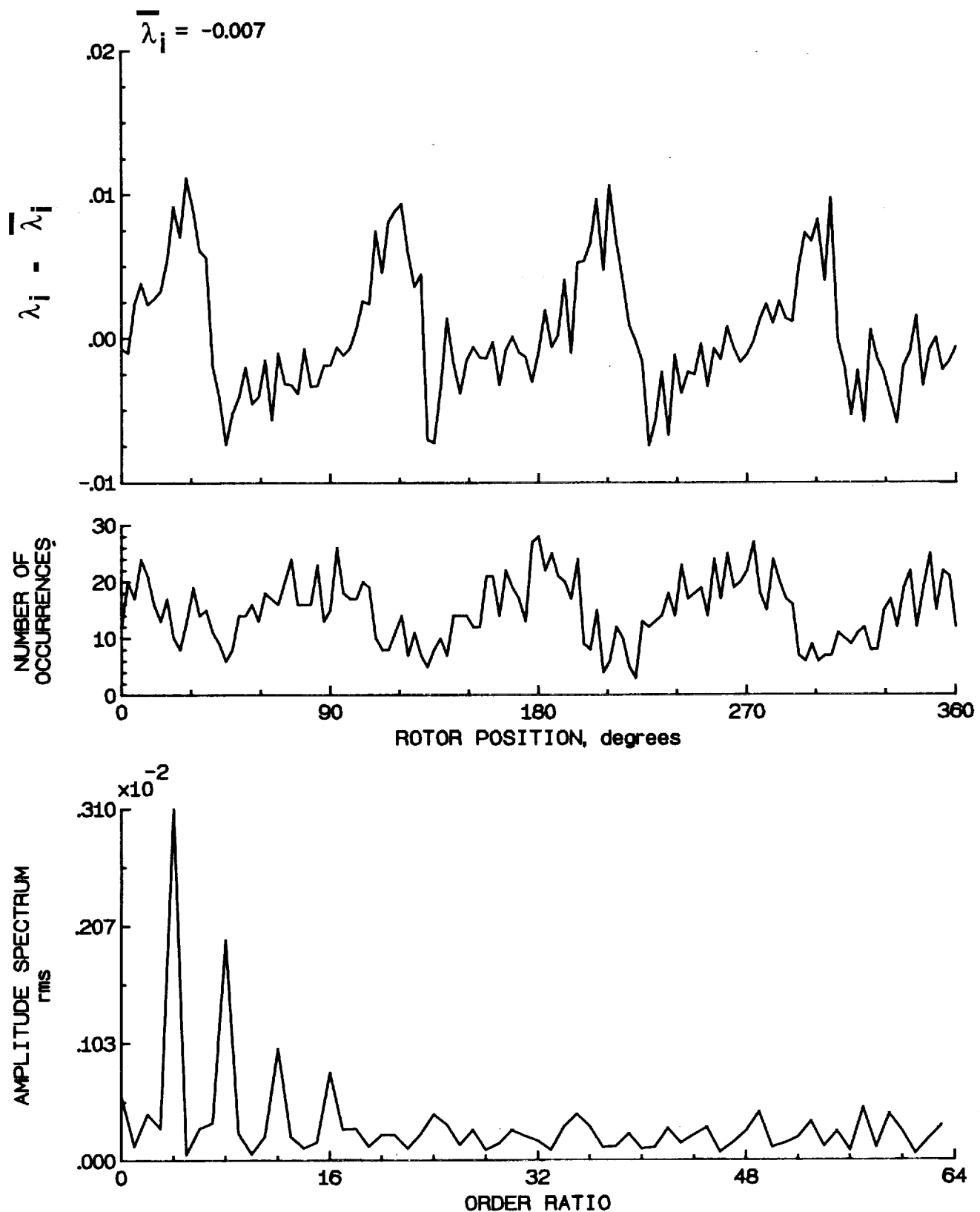


Figure 167.- Concluded.

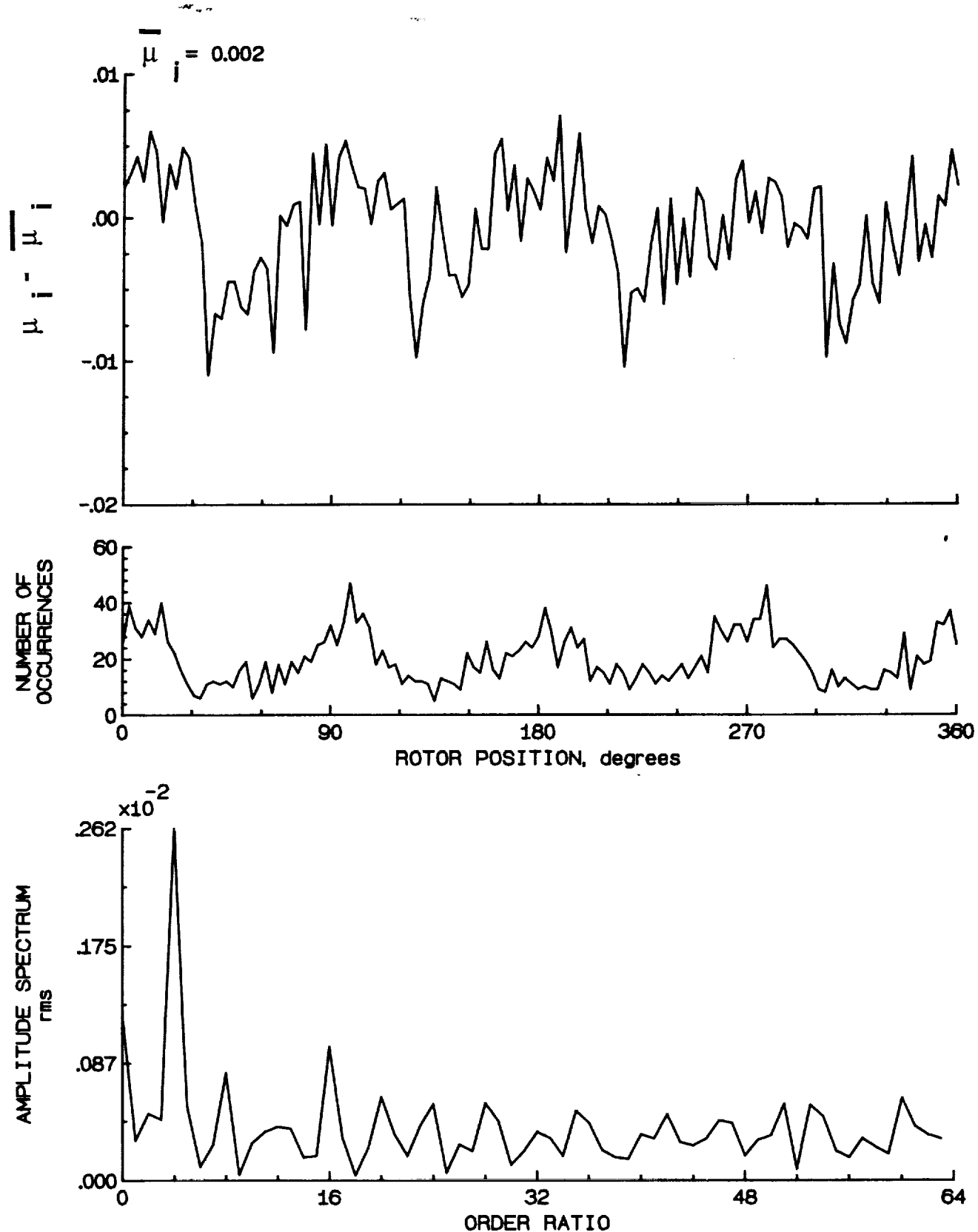


Figure 168.- Induced inflow velocity measured at 300 degrees and r/R of 0.86.

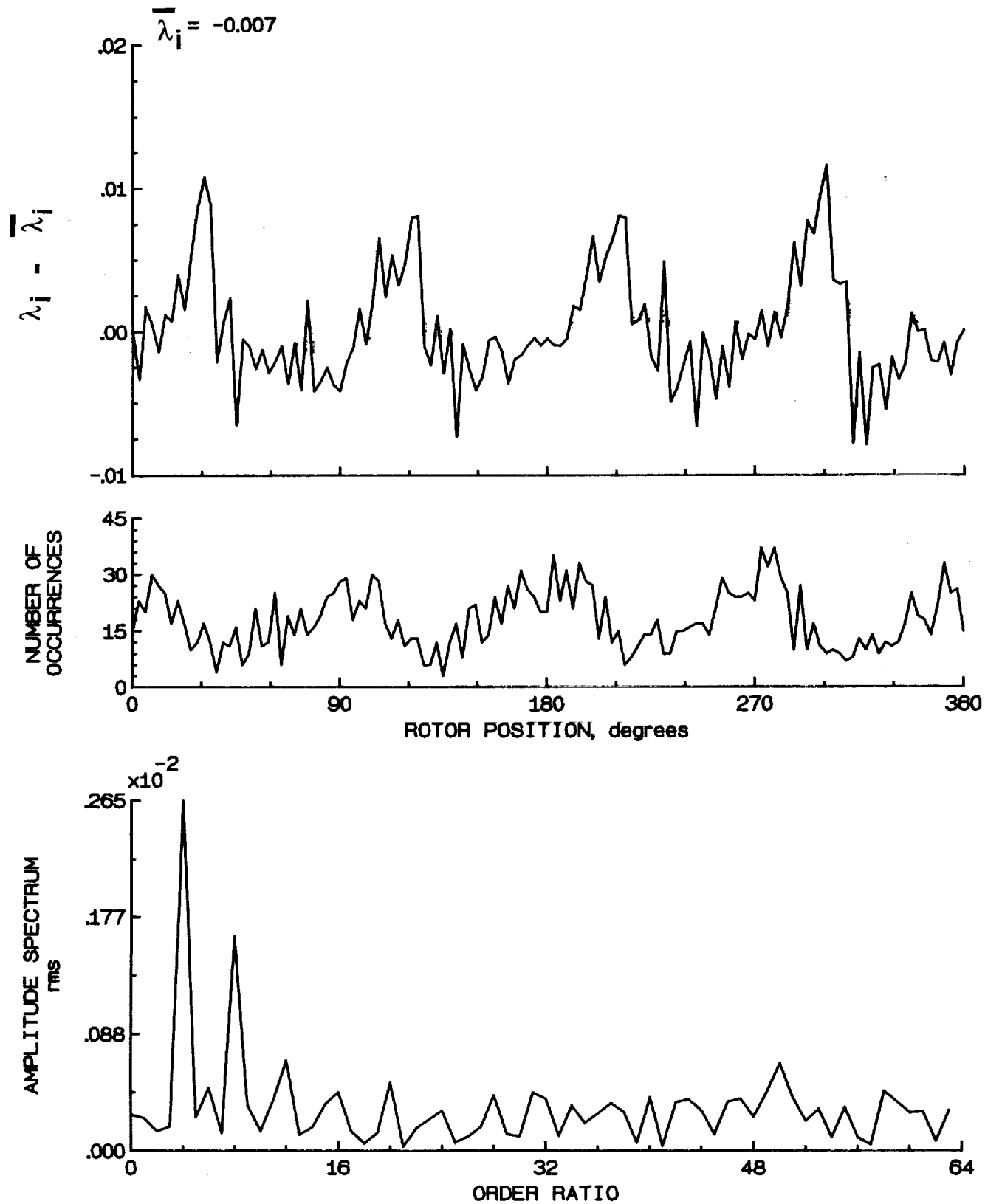


Figure 168.- Concluded.

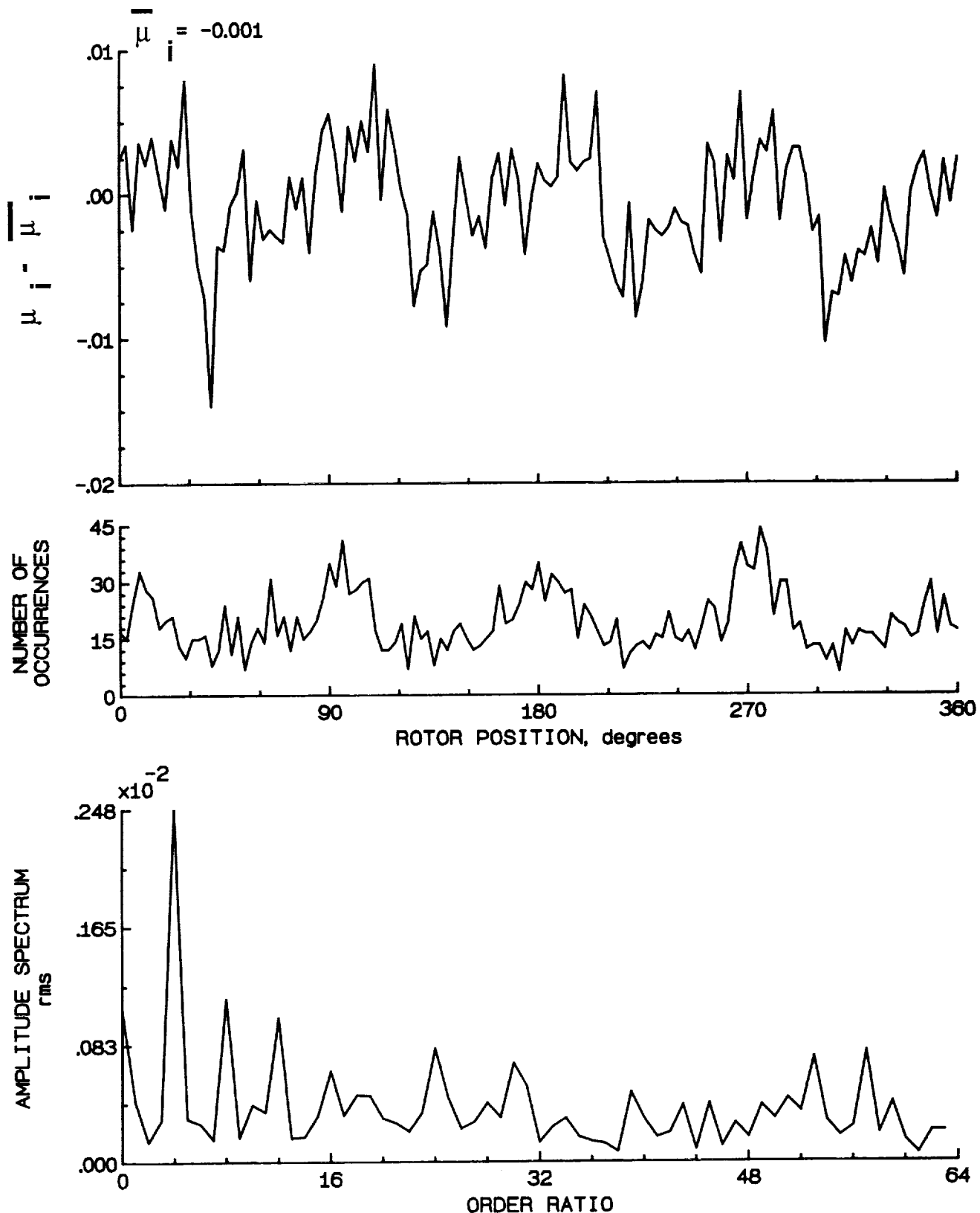


Figure 169.- Induced inflow velocity measured at 300 degrees and r/R of 0.90.

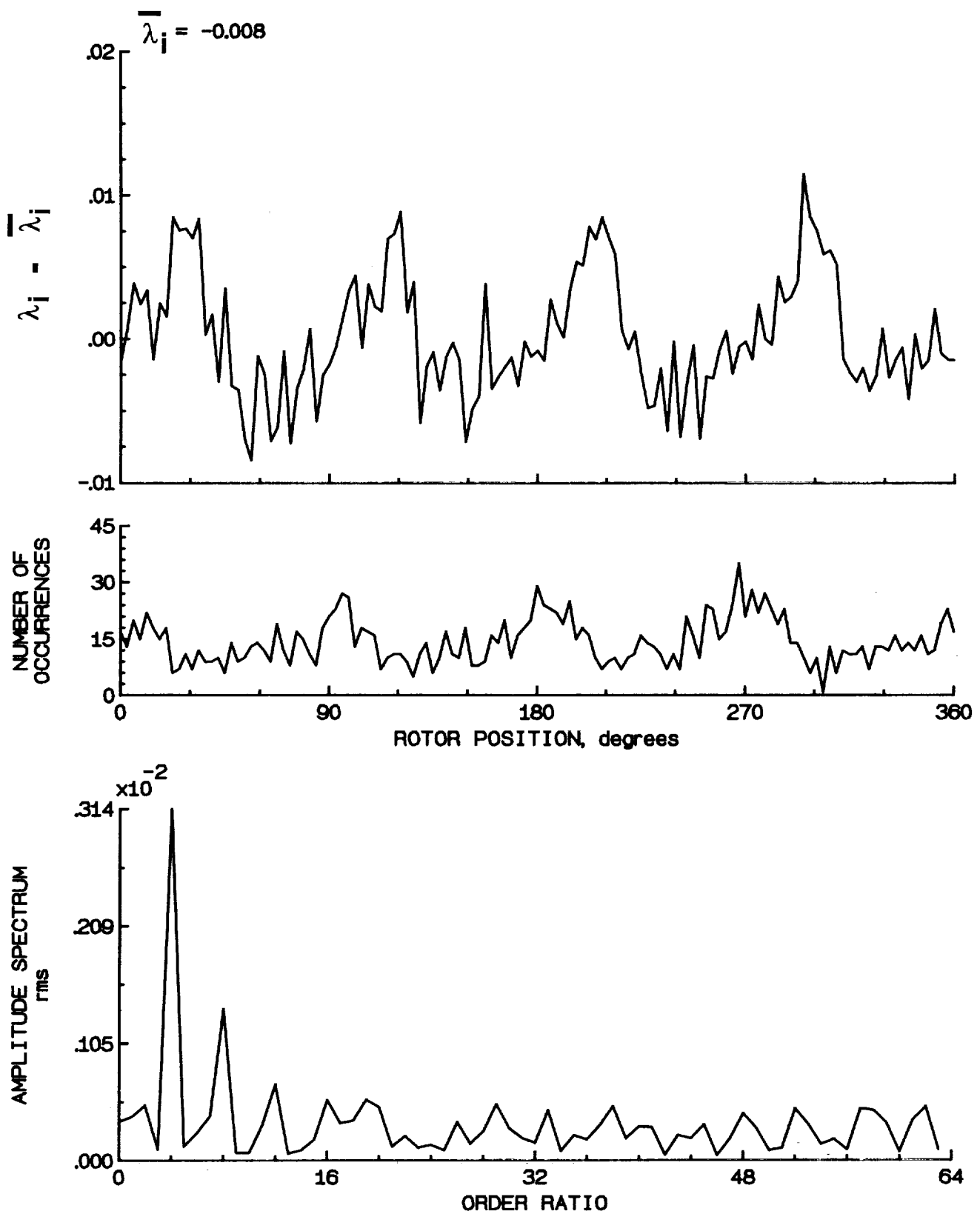


Figure 169.- Concluded.

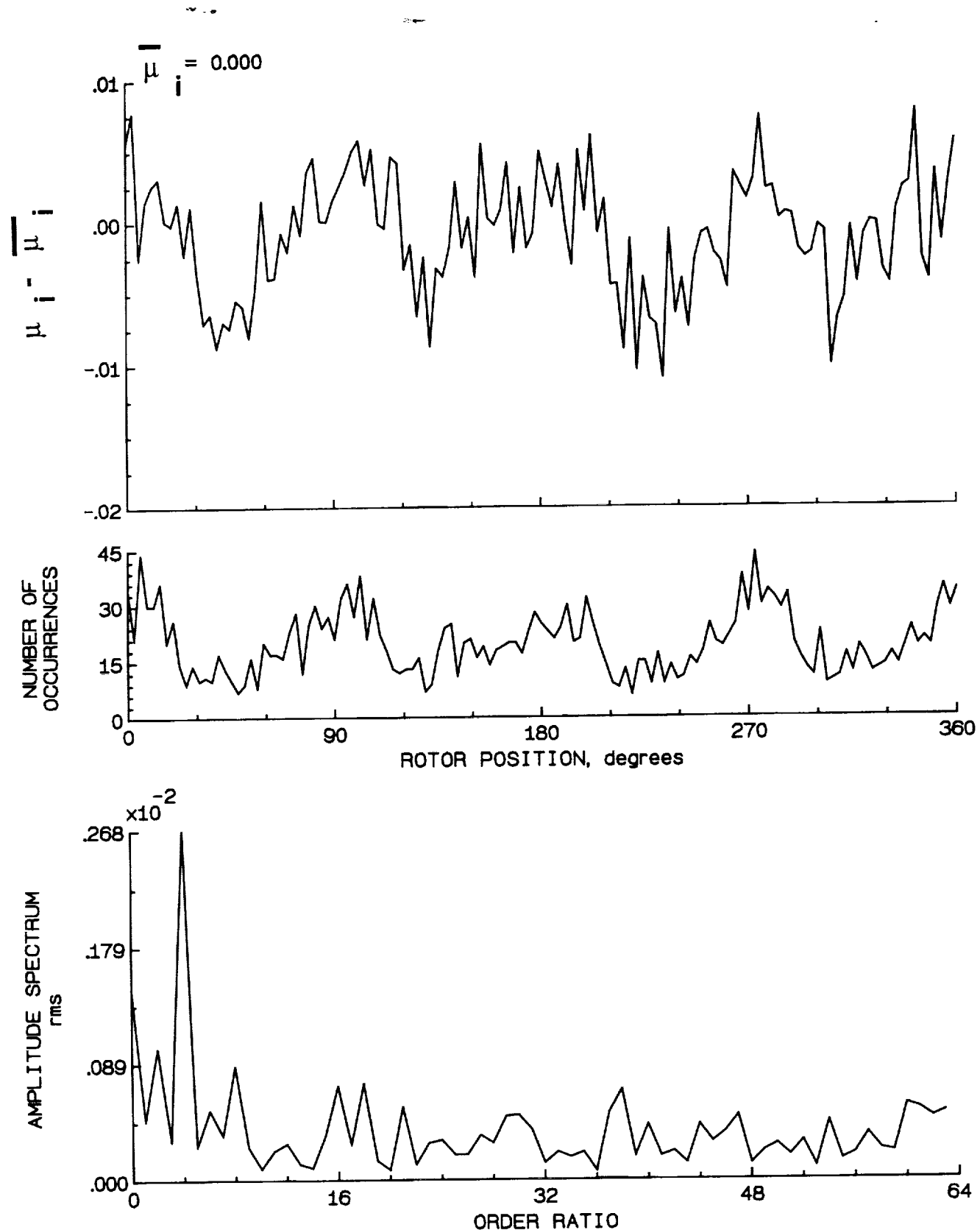


Figure 170.- Induced inflow velocity measured at 300 degrees and r/R of 0.94.

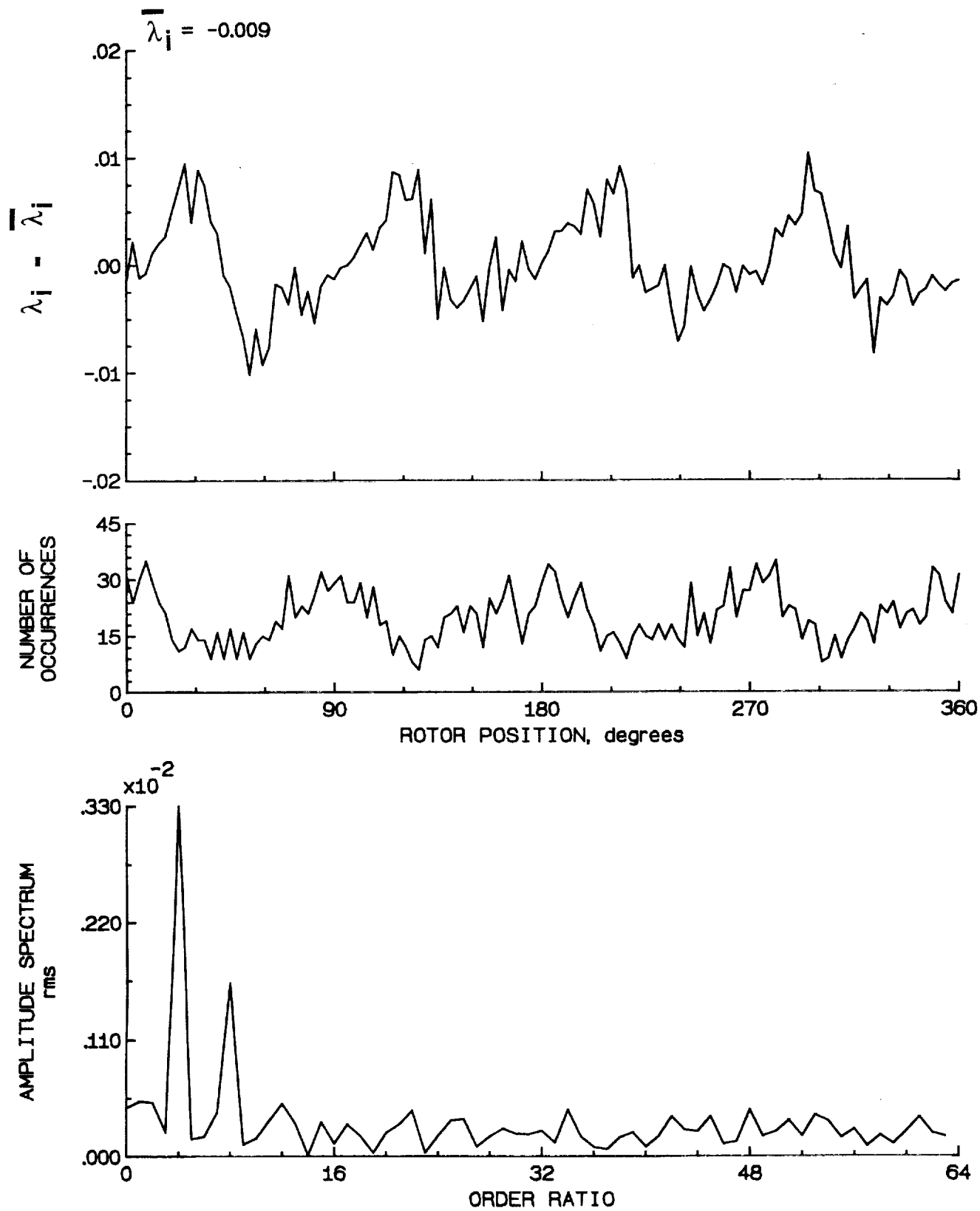


Figure 170.- Concluded.

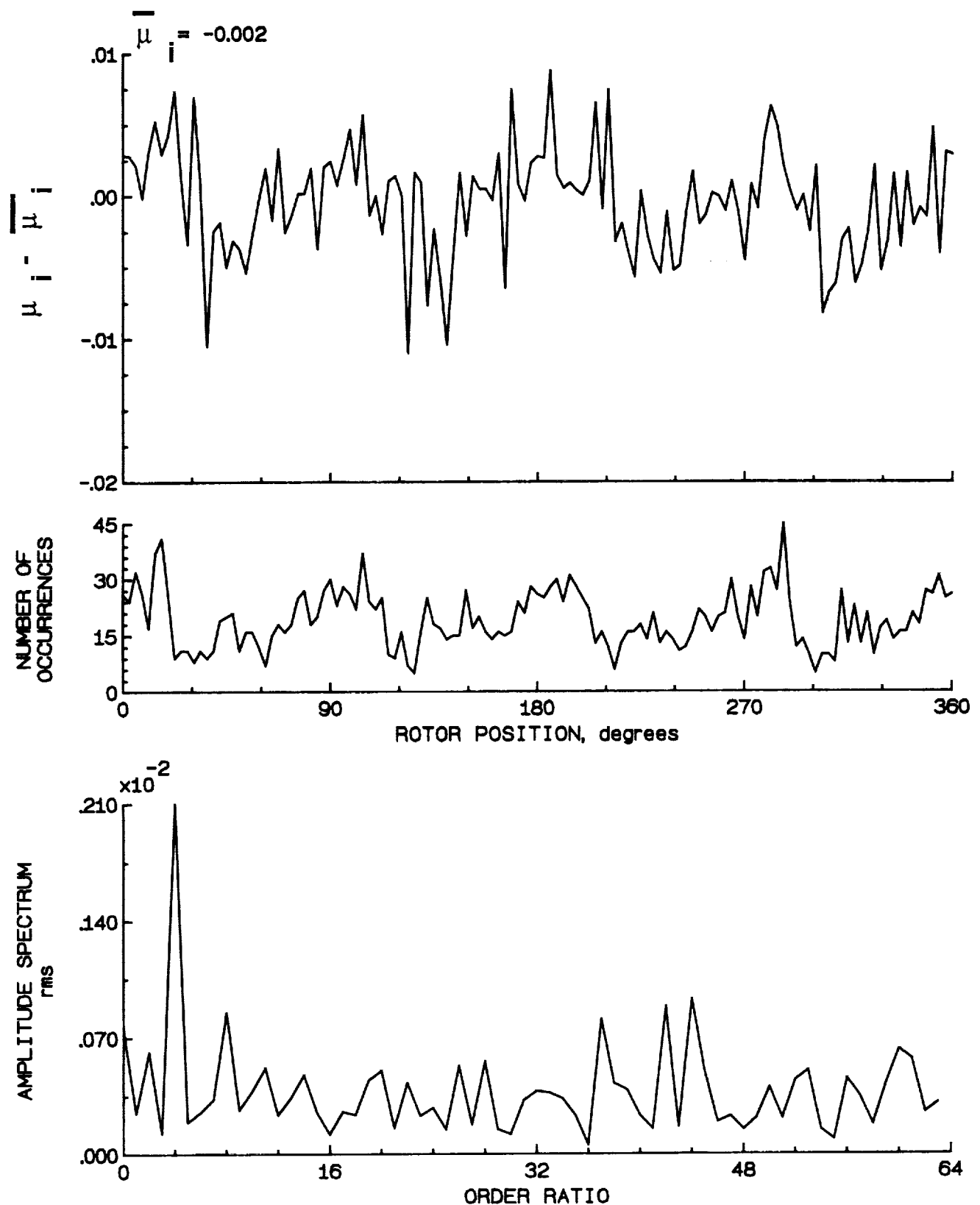


Figure 171.- Induced inflow velocity measured at 300 degrees and r/R of 0.98.

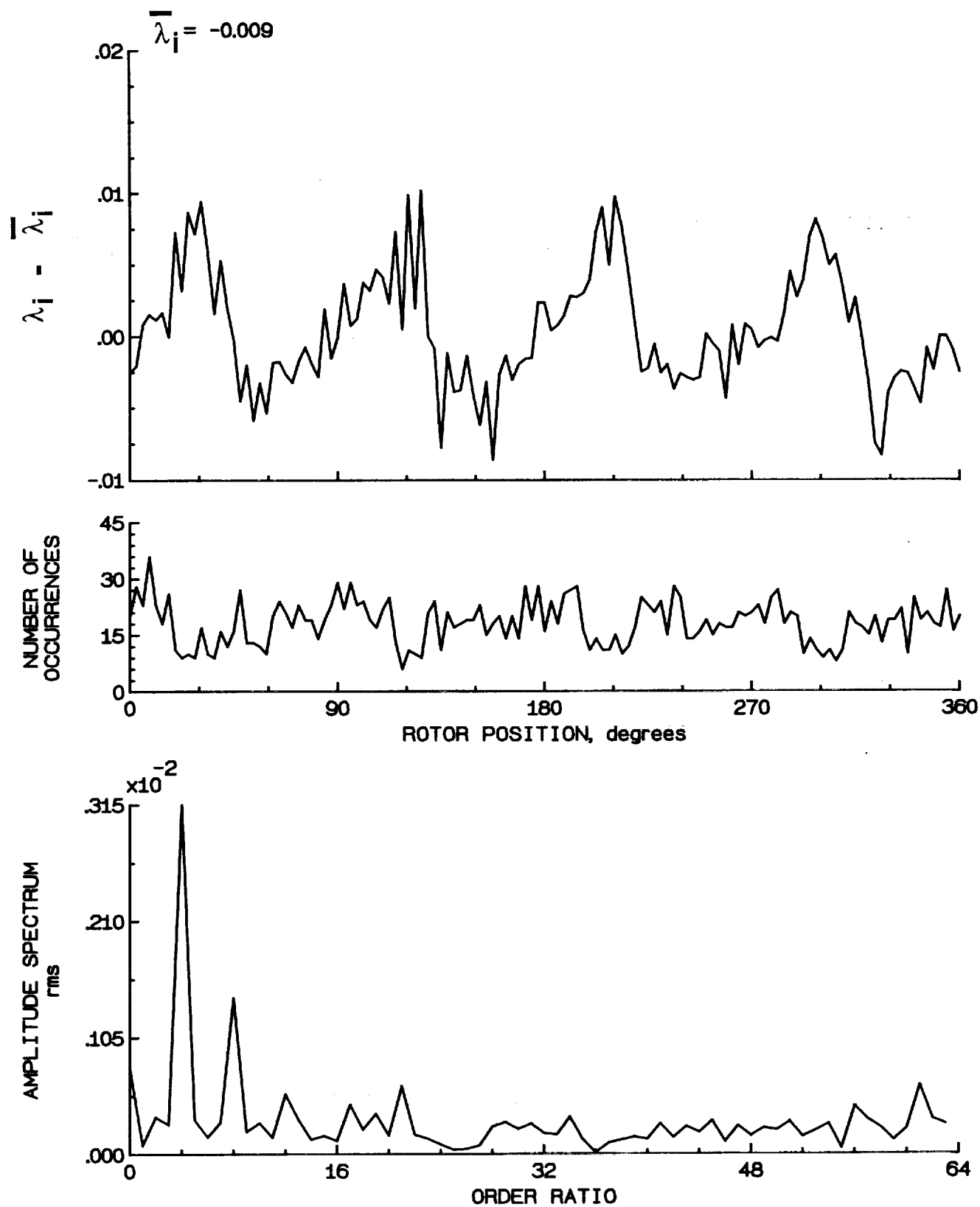


Figure 171.- Concluded.

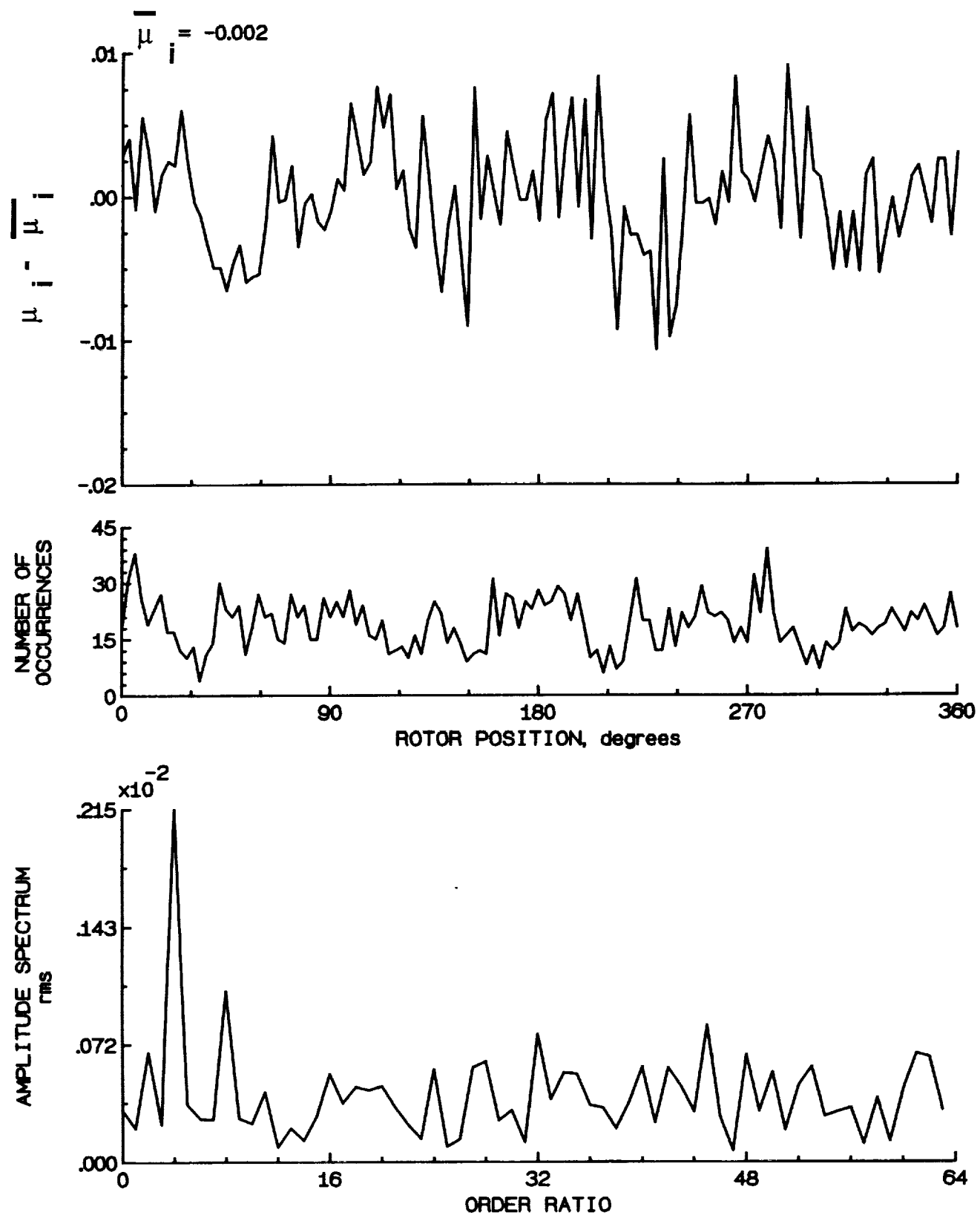


Figure 172.- Induced inflow velocity measured at 300 degrees and r/R of 1.02.

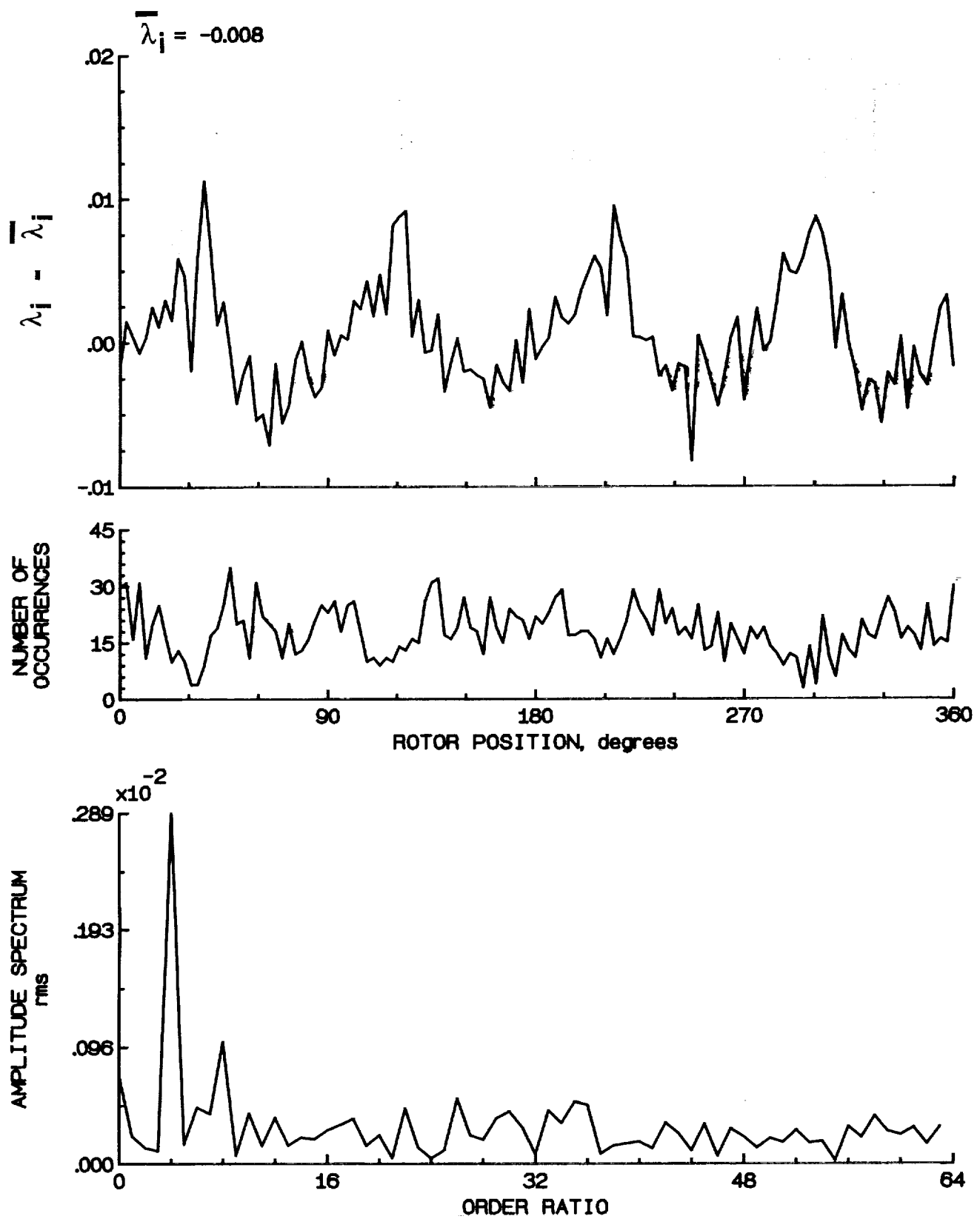


Figure 172.- Concluded.

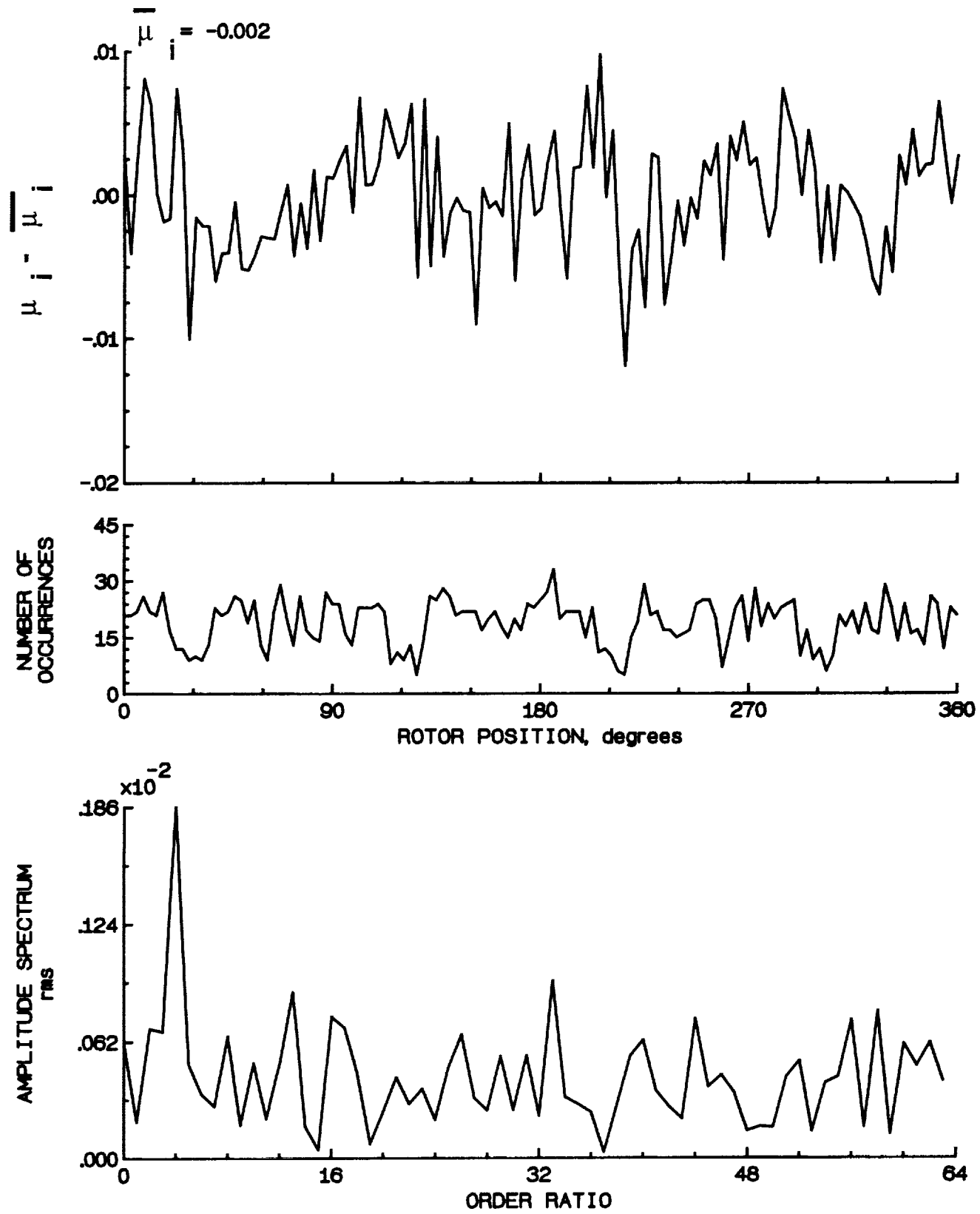


Figure 173.- Induced inflow velocity measured at 300 degrees and r/R of 1.04.

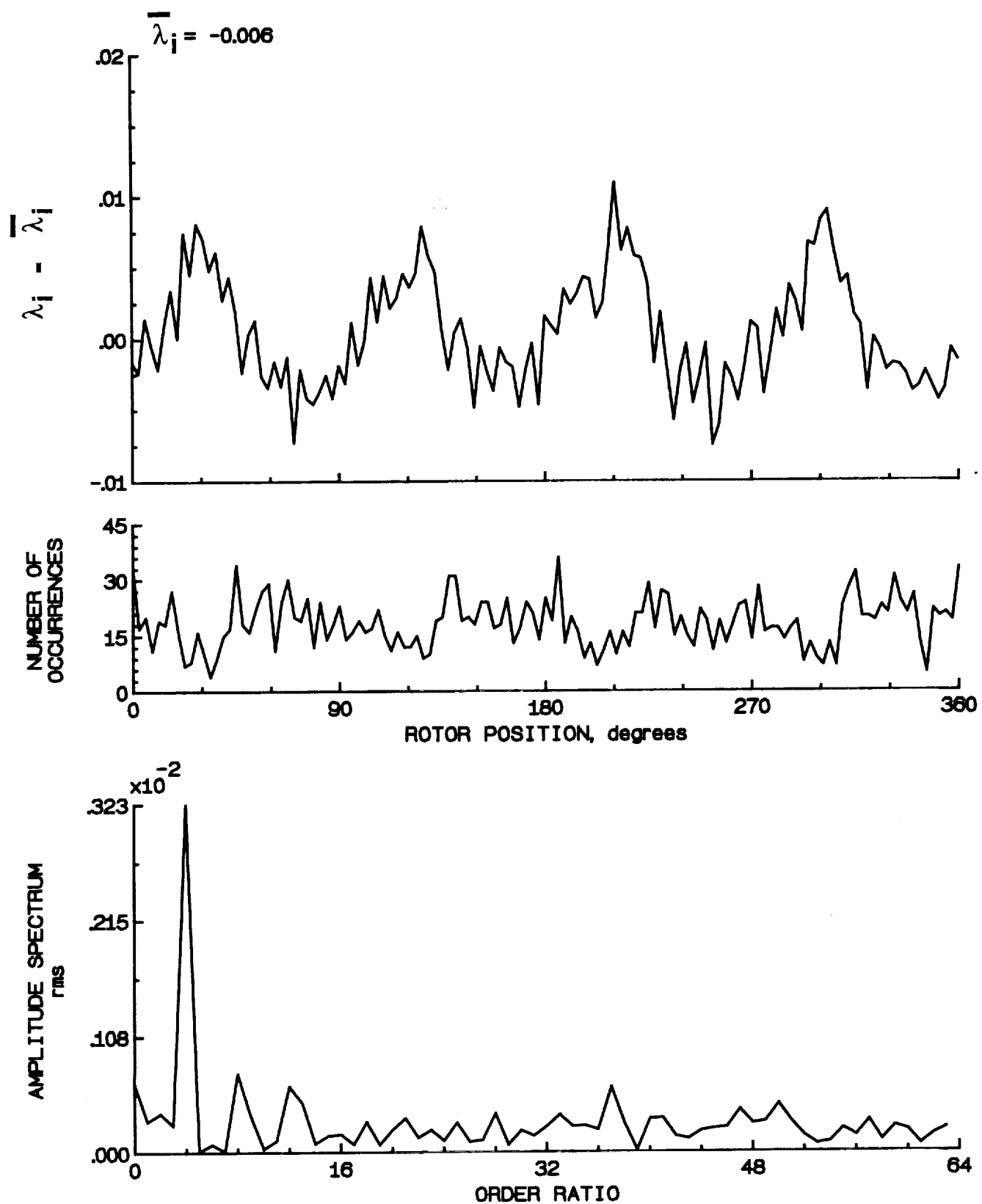


Figure 173.- Concluded.

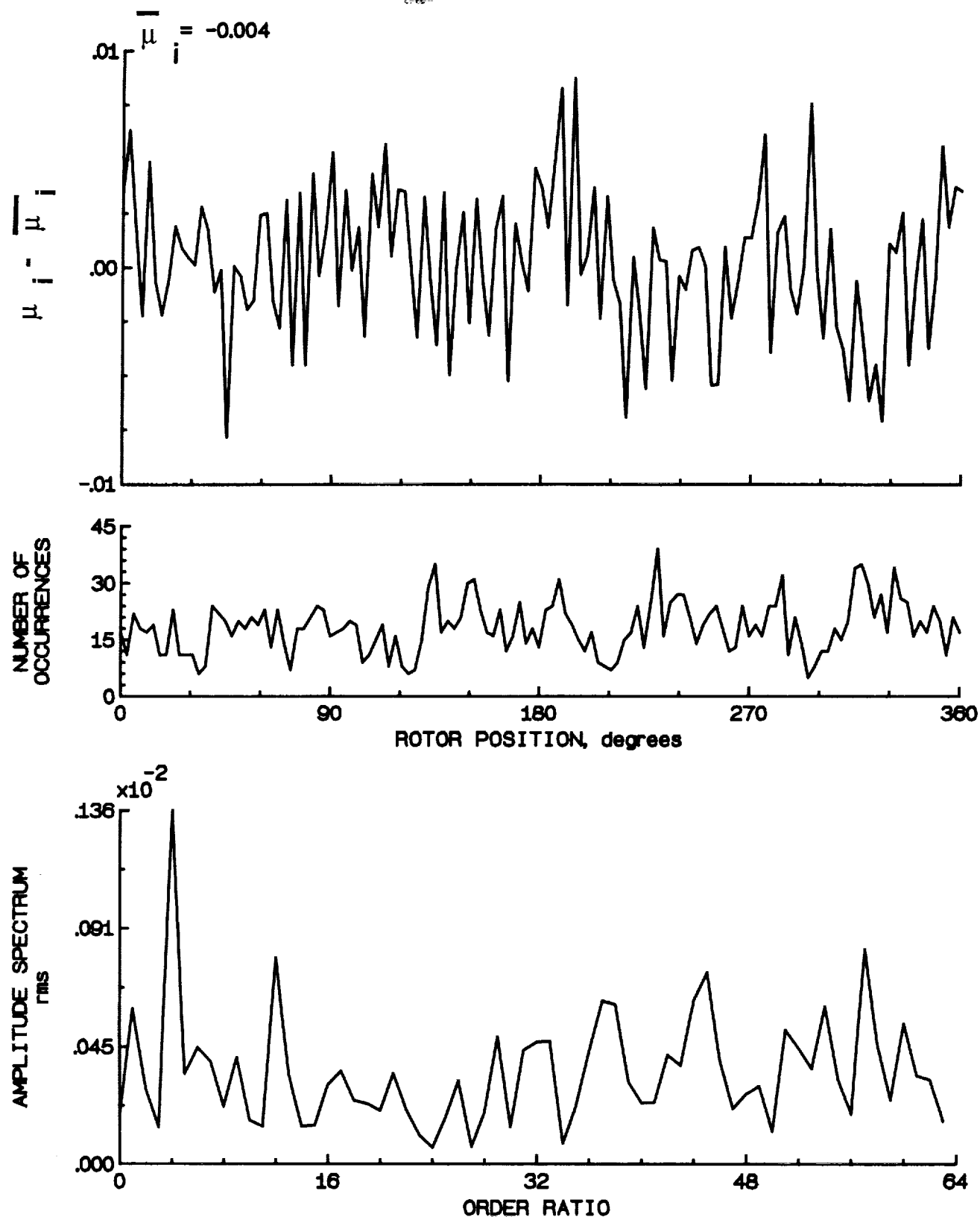


Figure 174.- Induced inflow velocity measured at 300 degrees and r/R of 1.10.

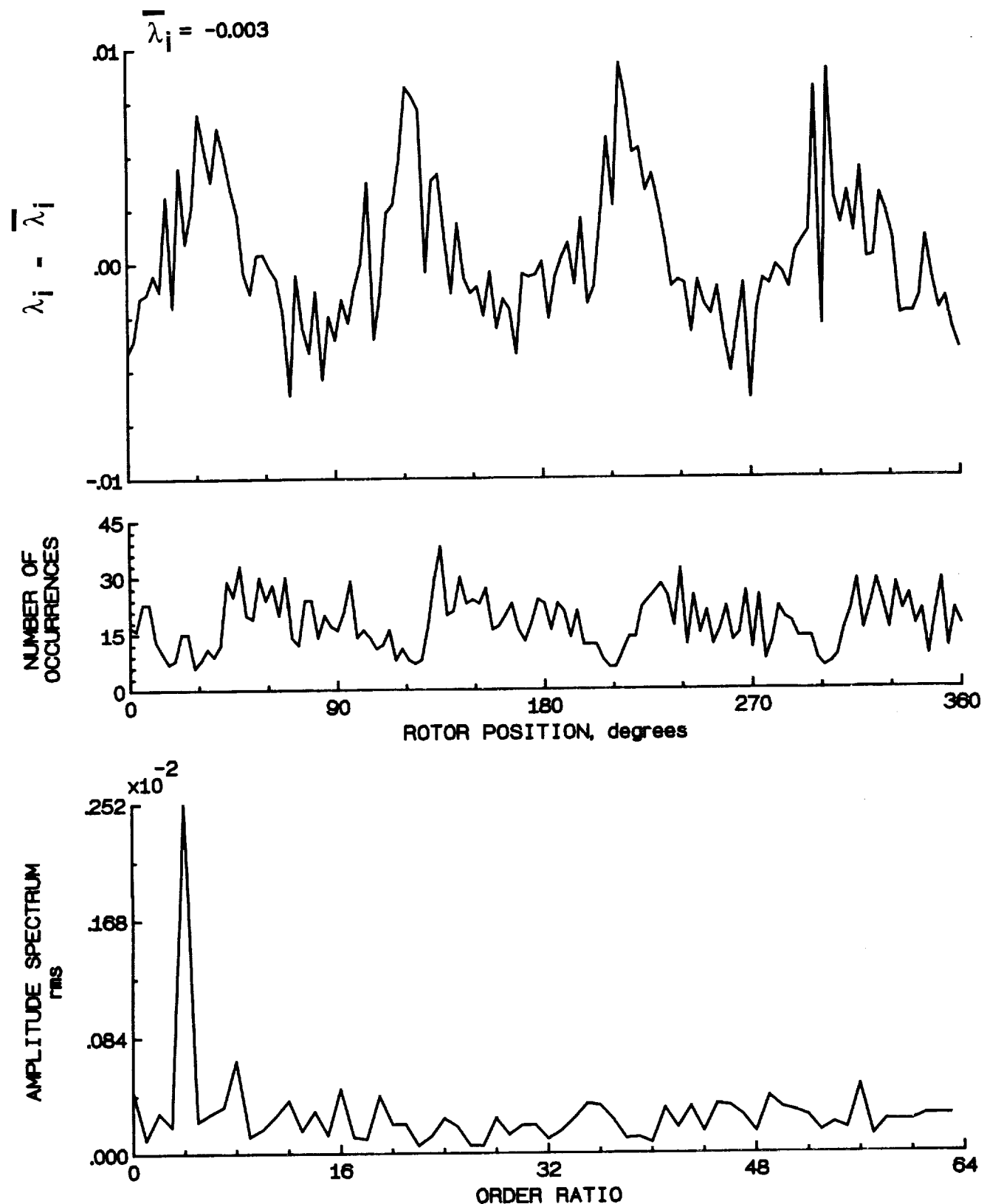


Figure 174.- Concluded.

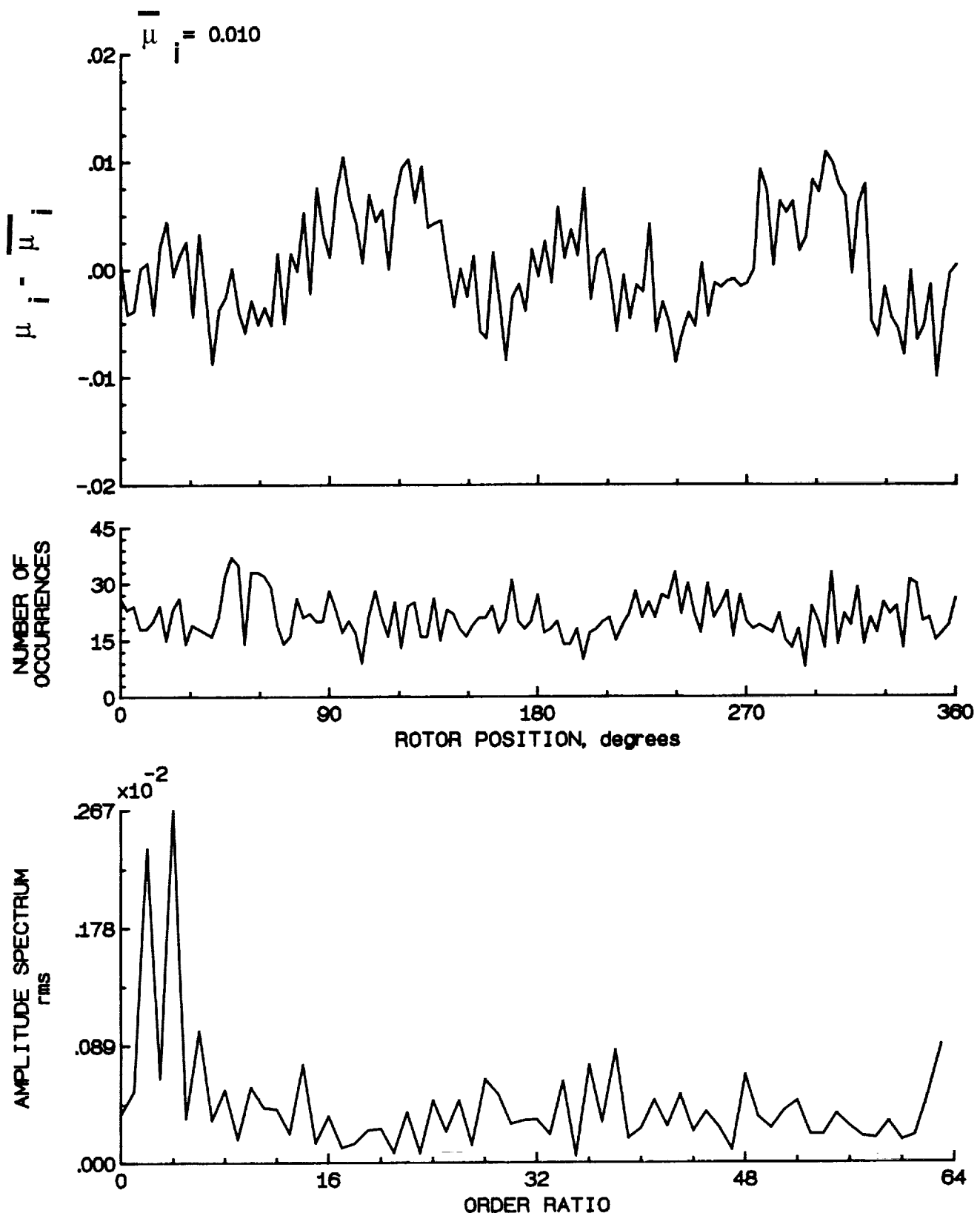


Figure 175.- Induced inflow velocity measured at 330 degrees and r/R of 0.20.

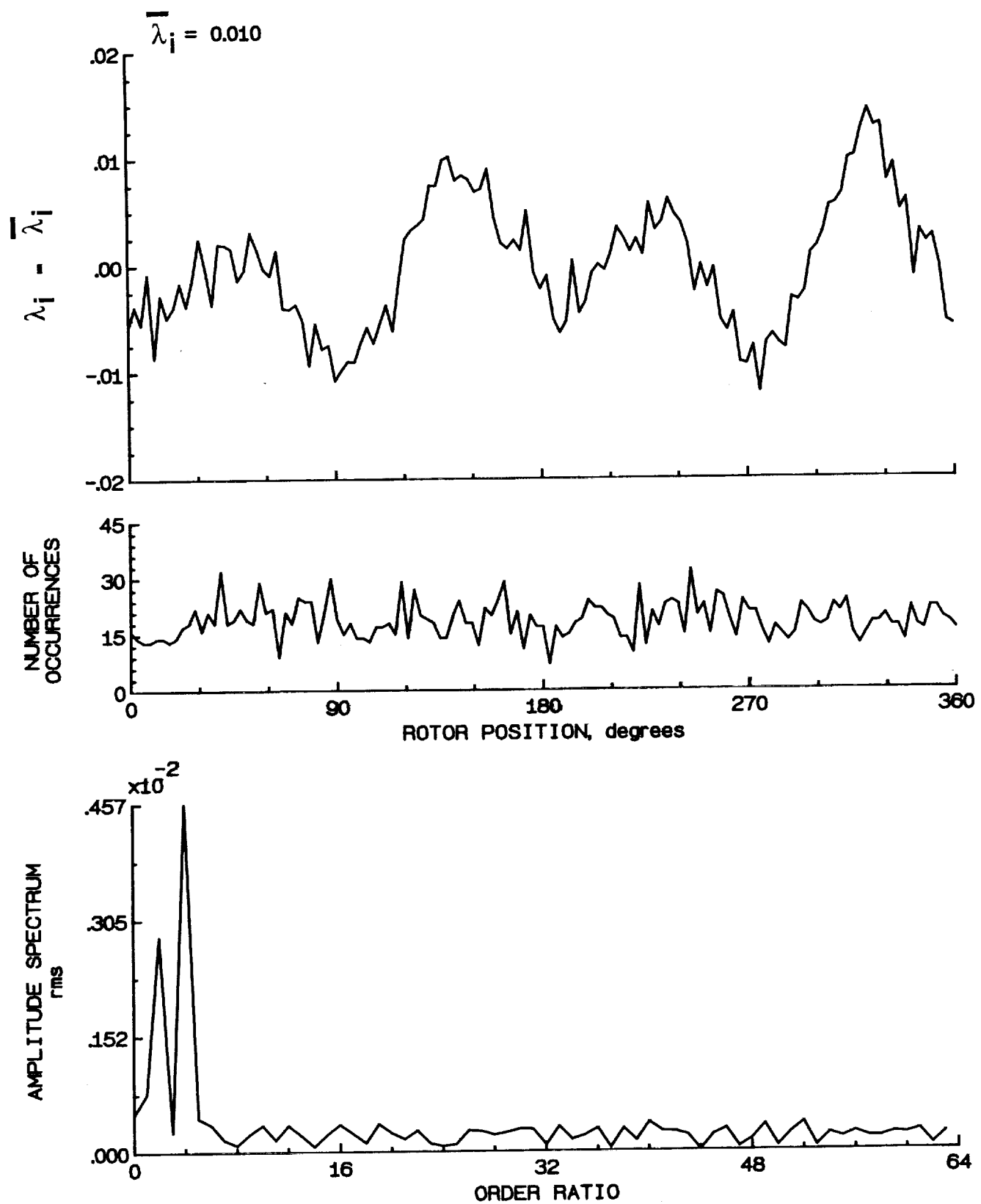


Figure 175.- Concluded.

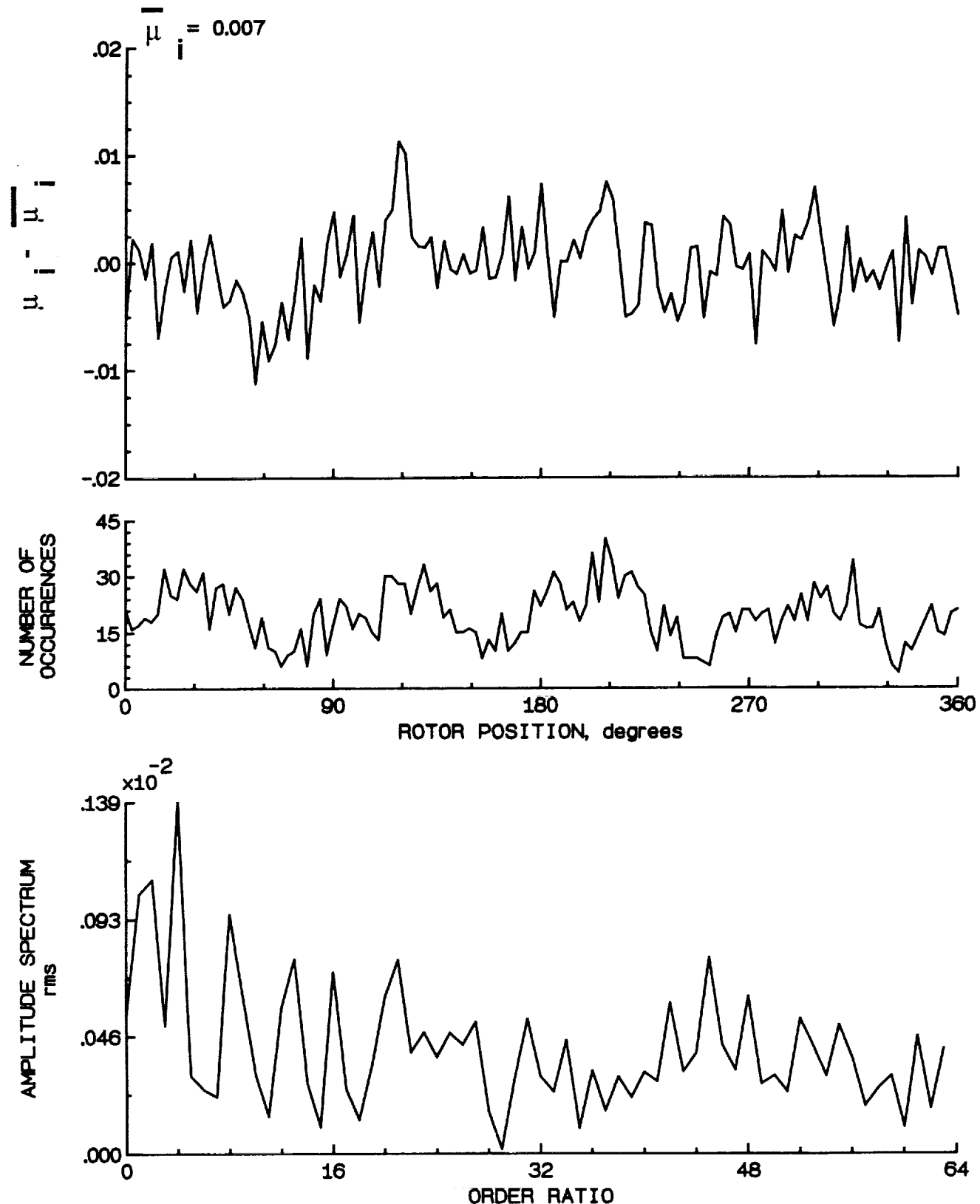


Figure 176.- Induced inflow velocity measured at 330 degrees and r/R of 0.40.

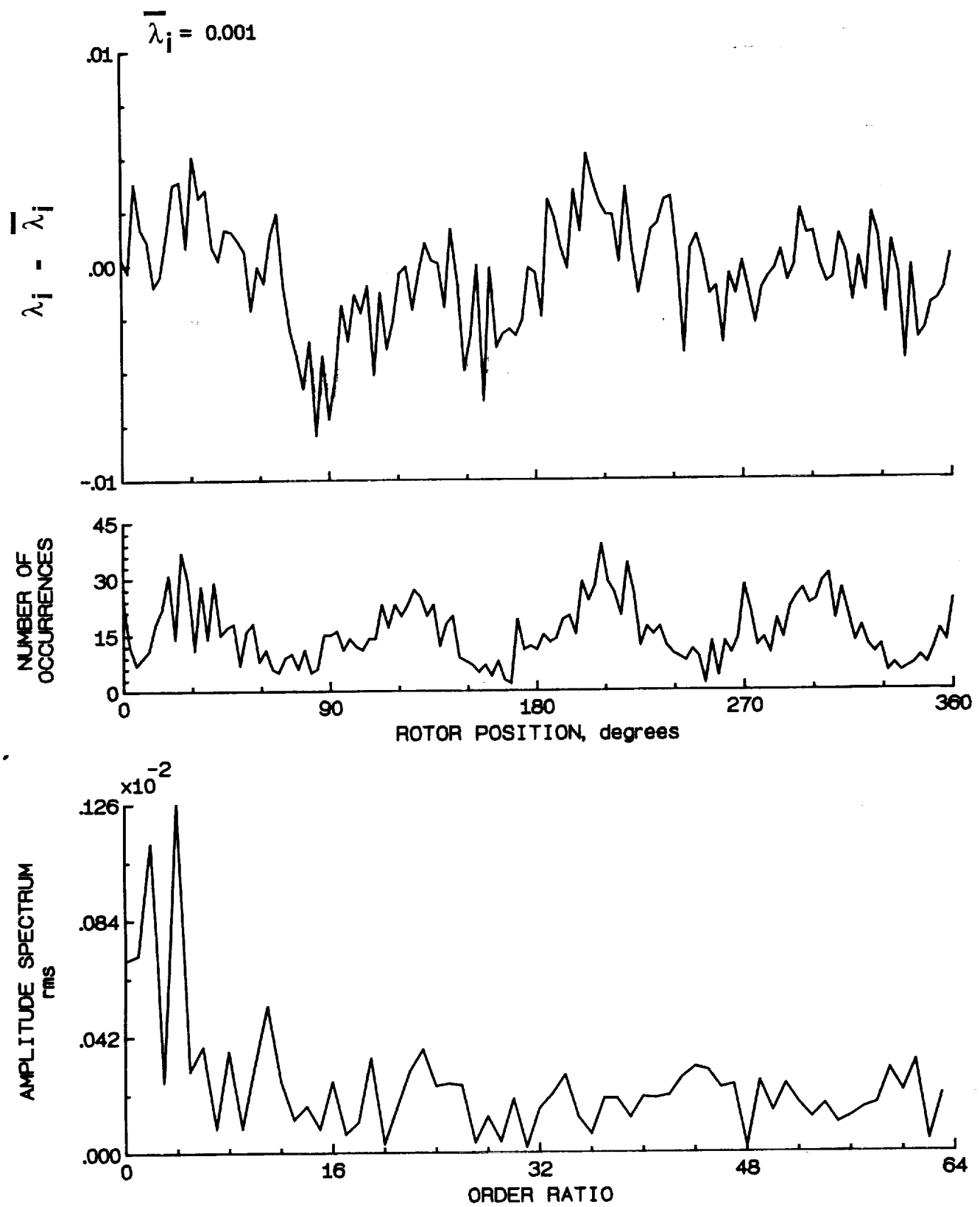


Figure 176.- Concluded.

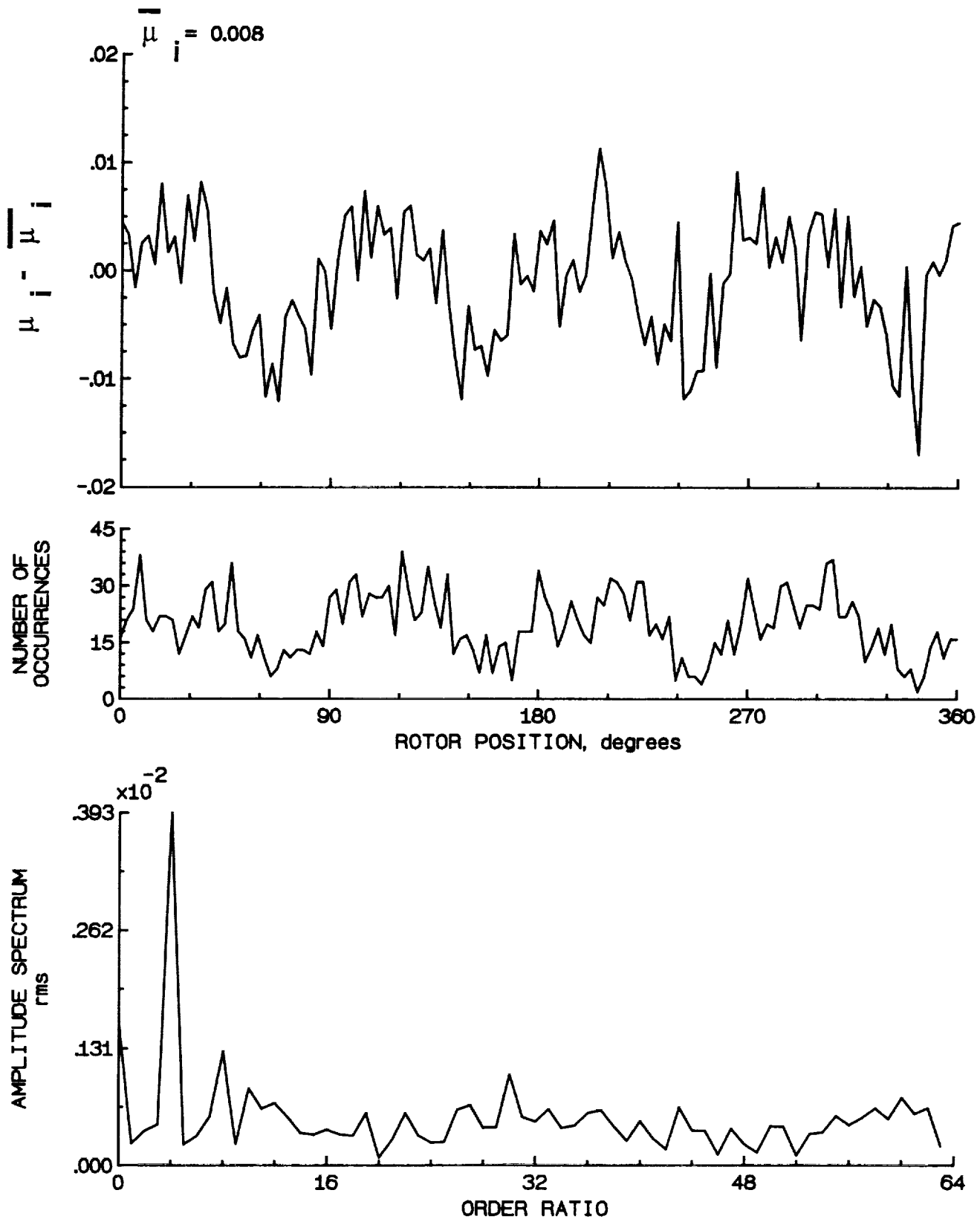


Figure 177.- Induced inflow velocity measured at 330 degrees and r/R of 0.50.

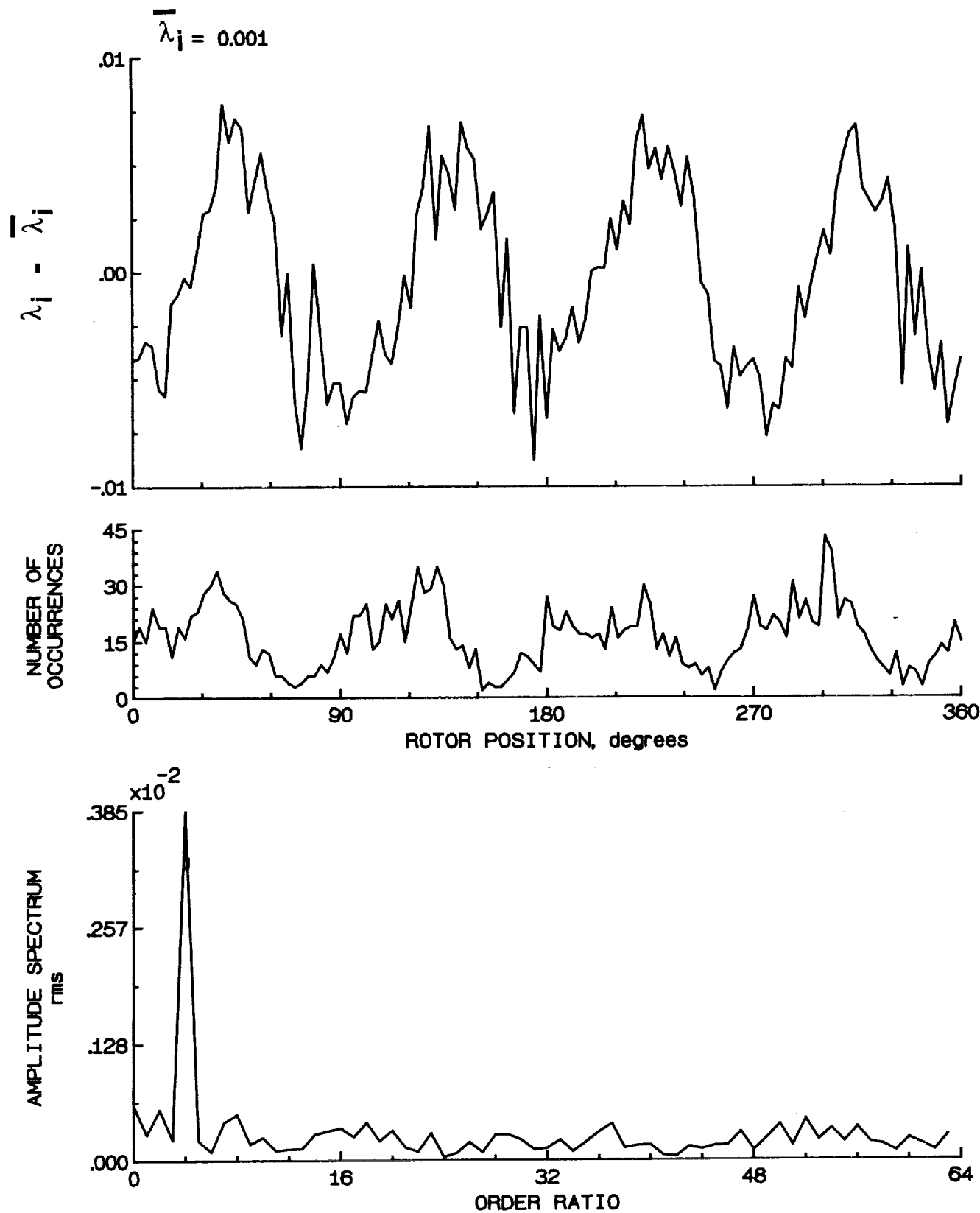


Figure 177.- Concluded.

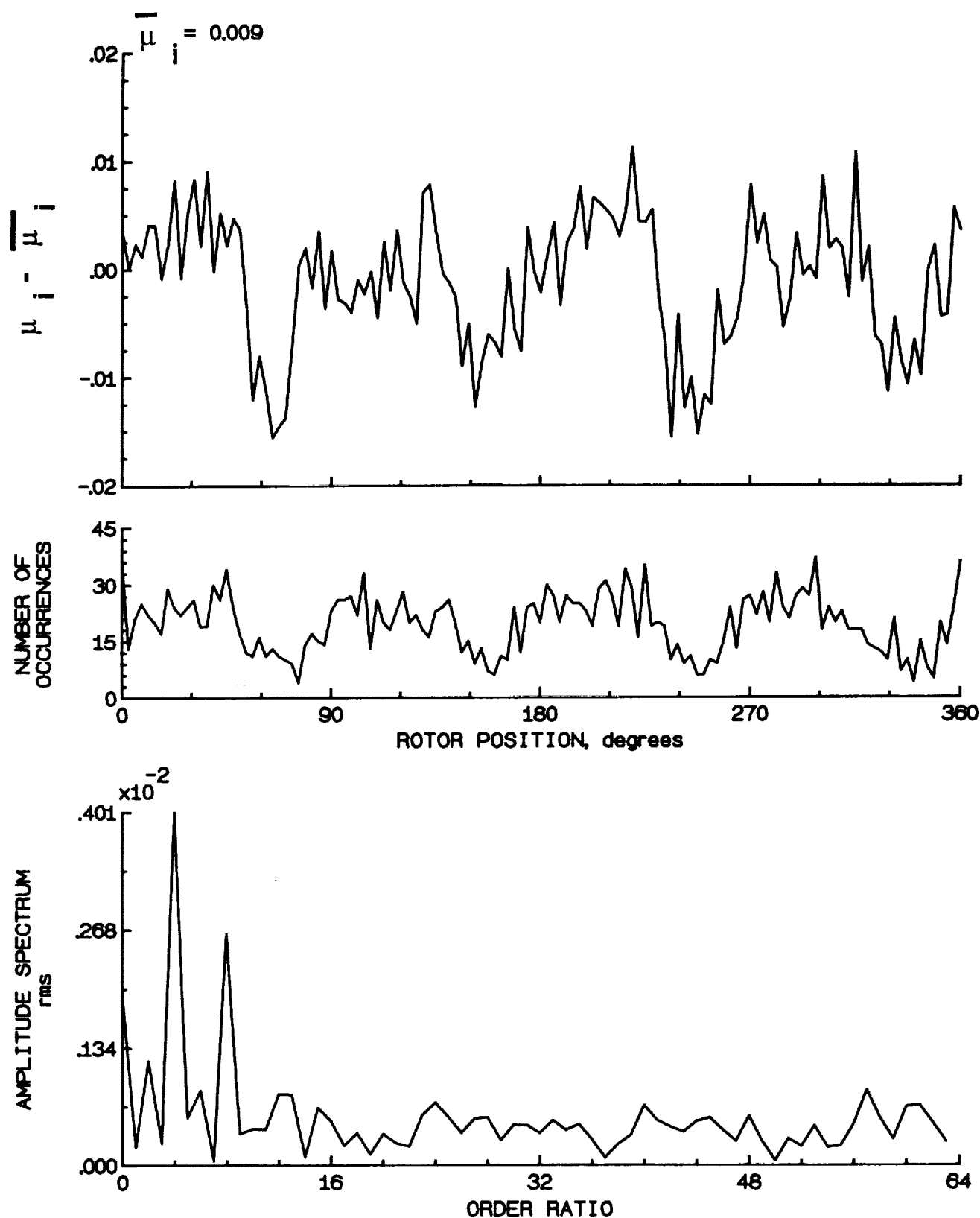


Figure 178.- Induced inflow velocity measured at 330 degrees and r/R of 0.60.

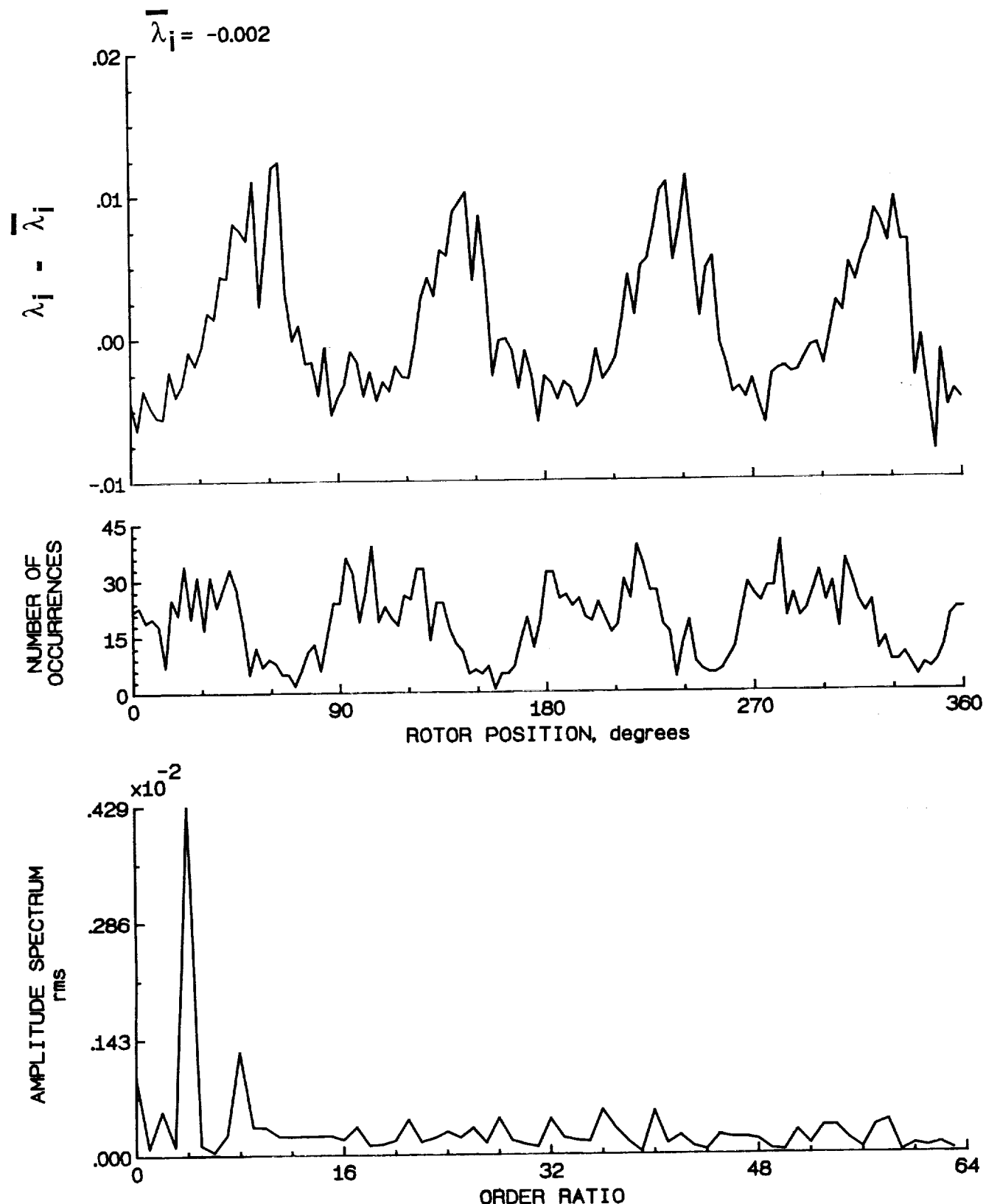


Figure 178.- Concluded.

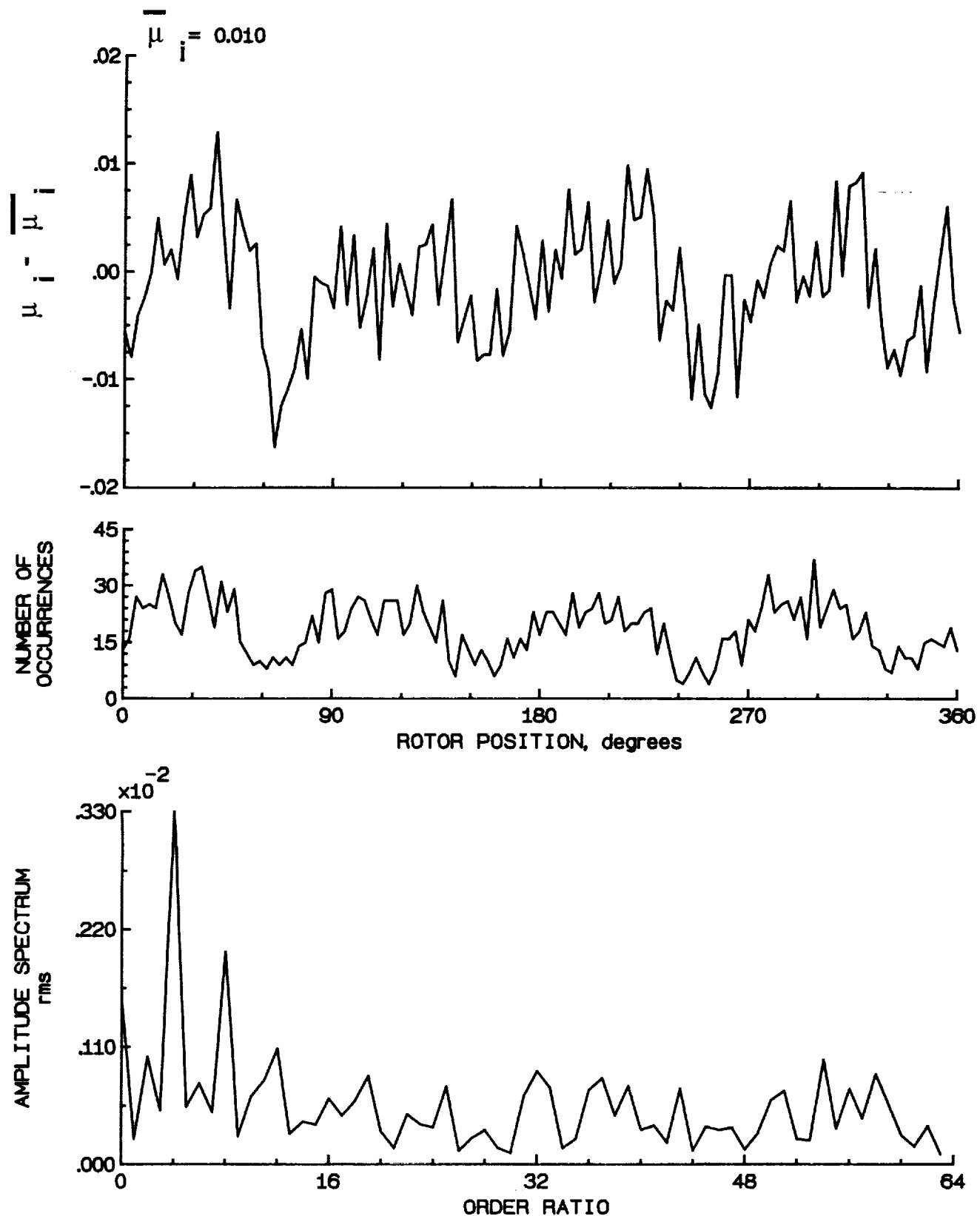


Figure 179.- Induced inflow velocity measured at 330 degrees and r/R of 0.70.

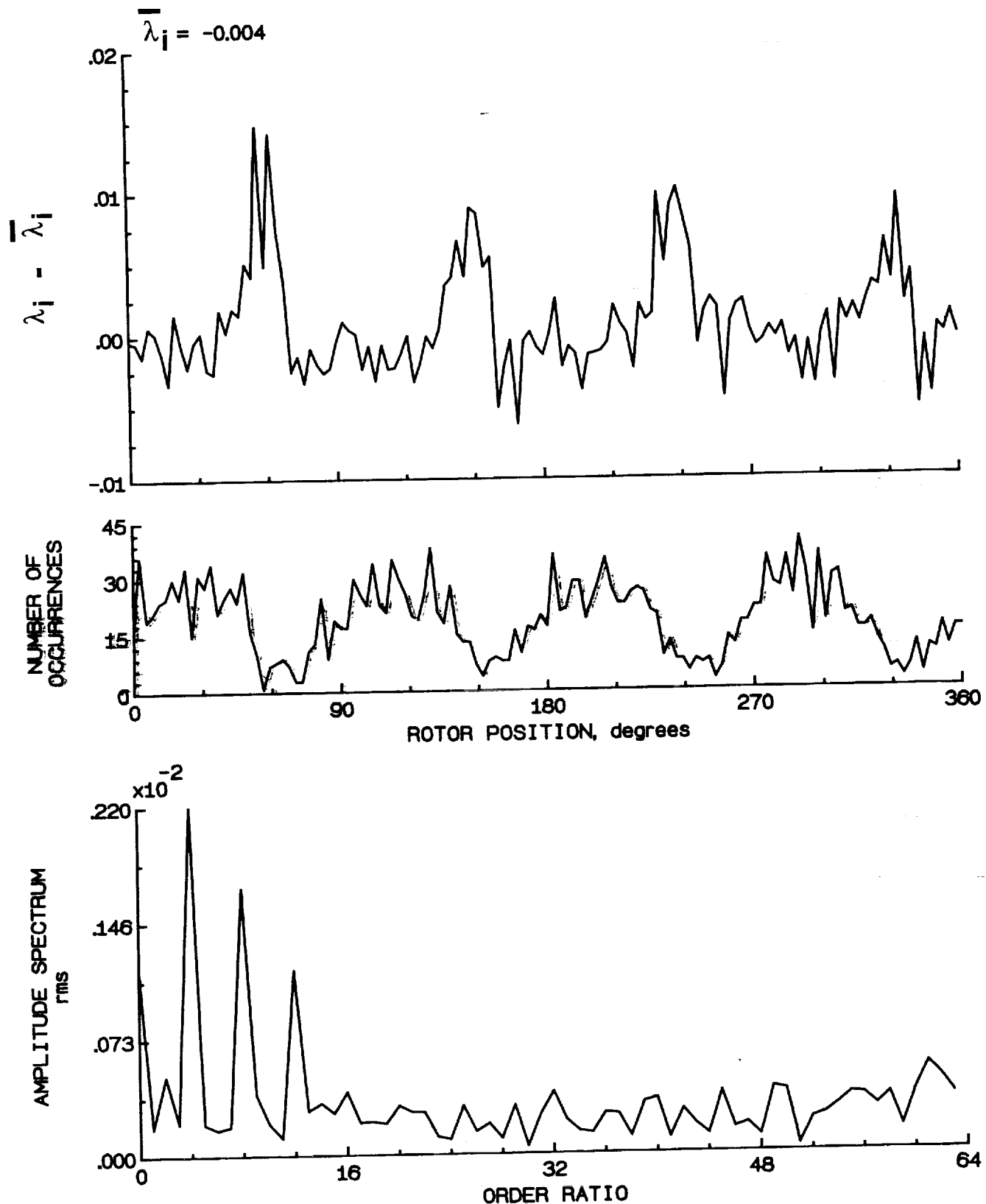


Figure 179.- Concluded.

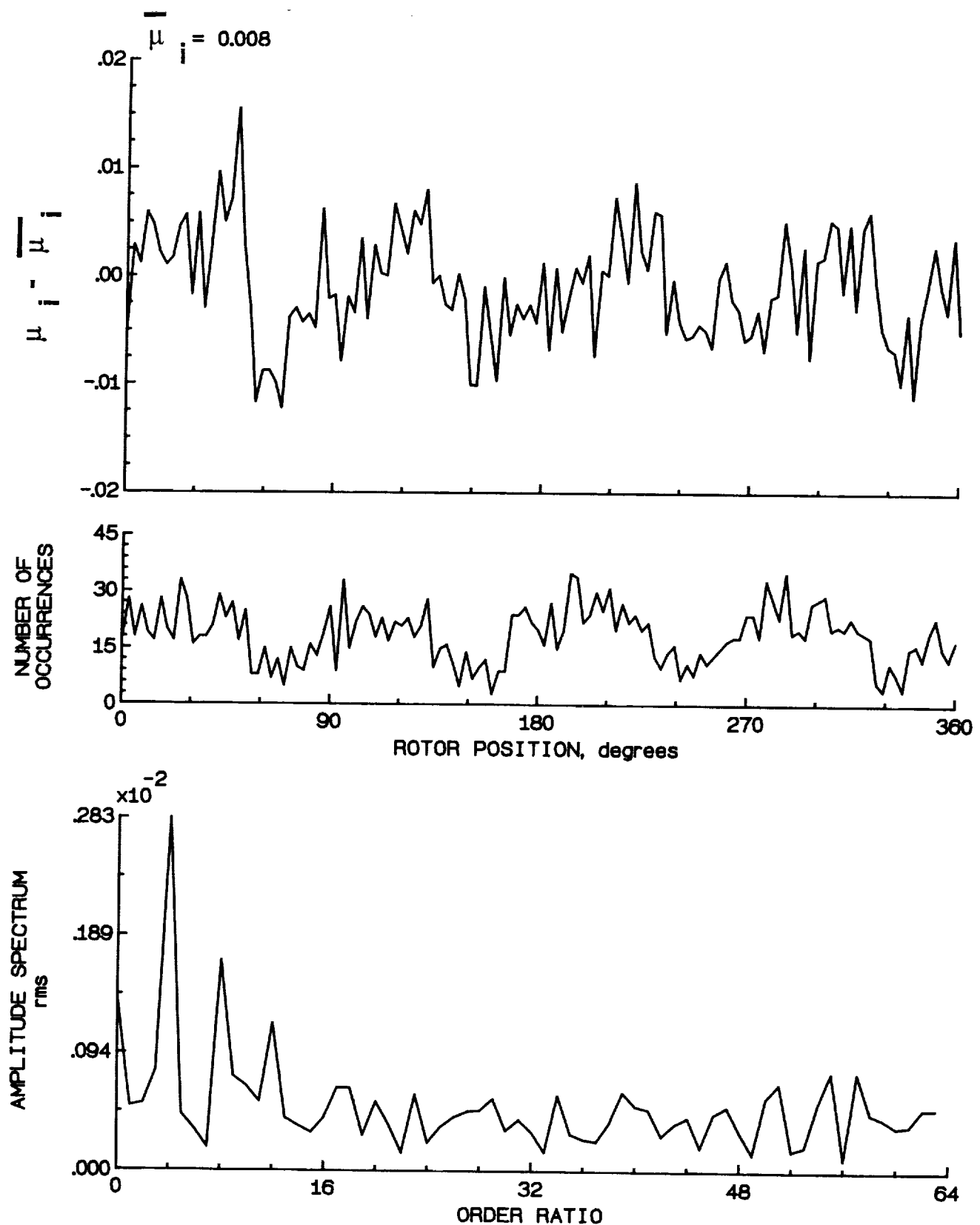


Figure 180.- Induced inflow velocity measured at 330 degrees and r/R of 0.74.

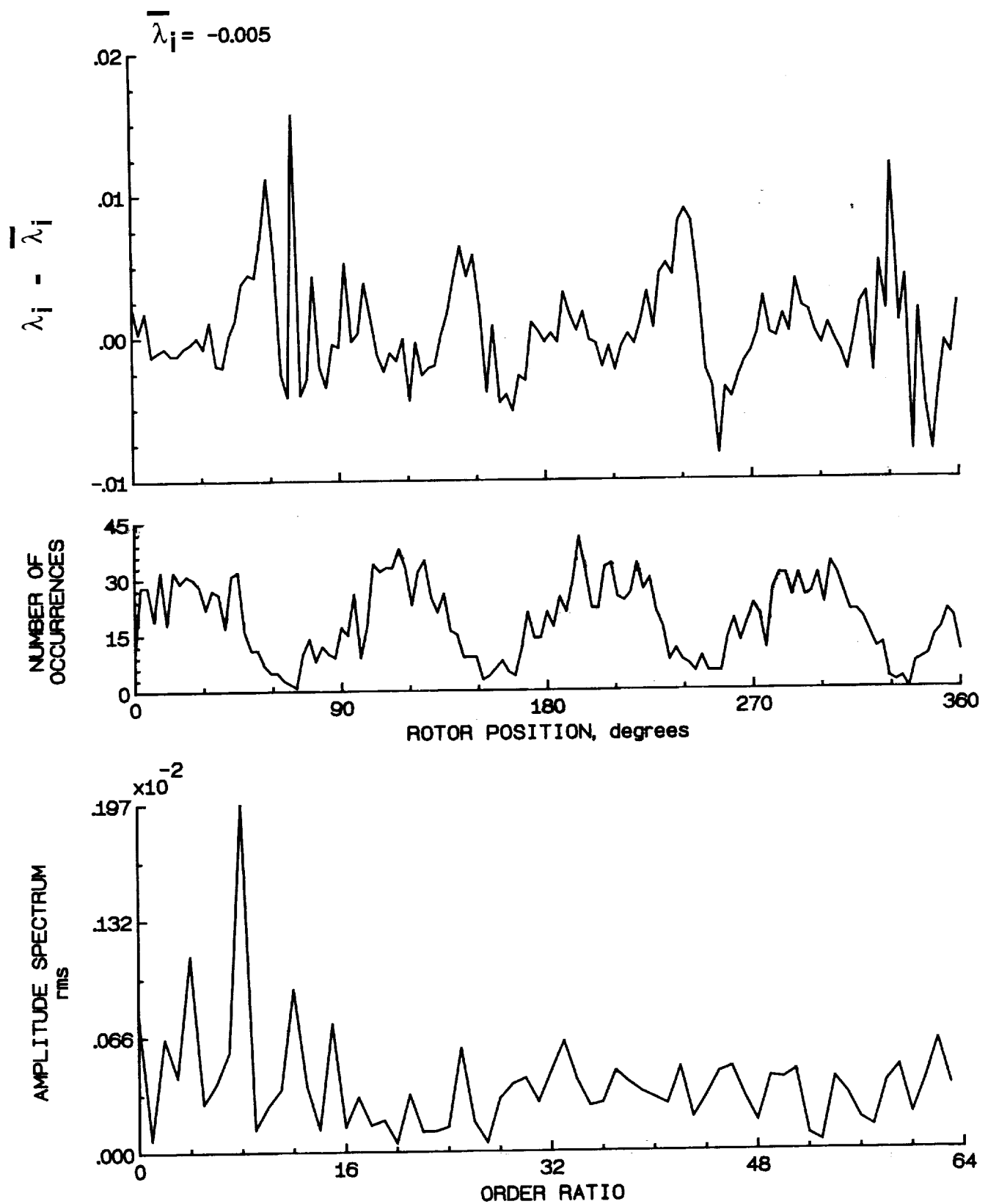


Figure 180.- Concluded.

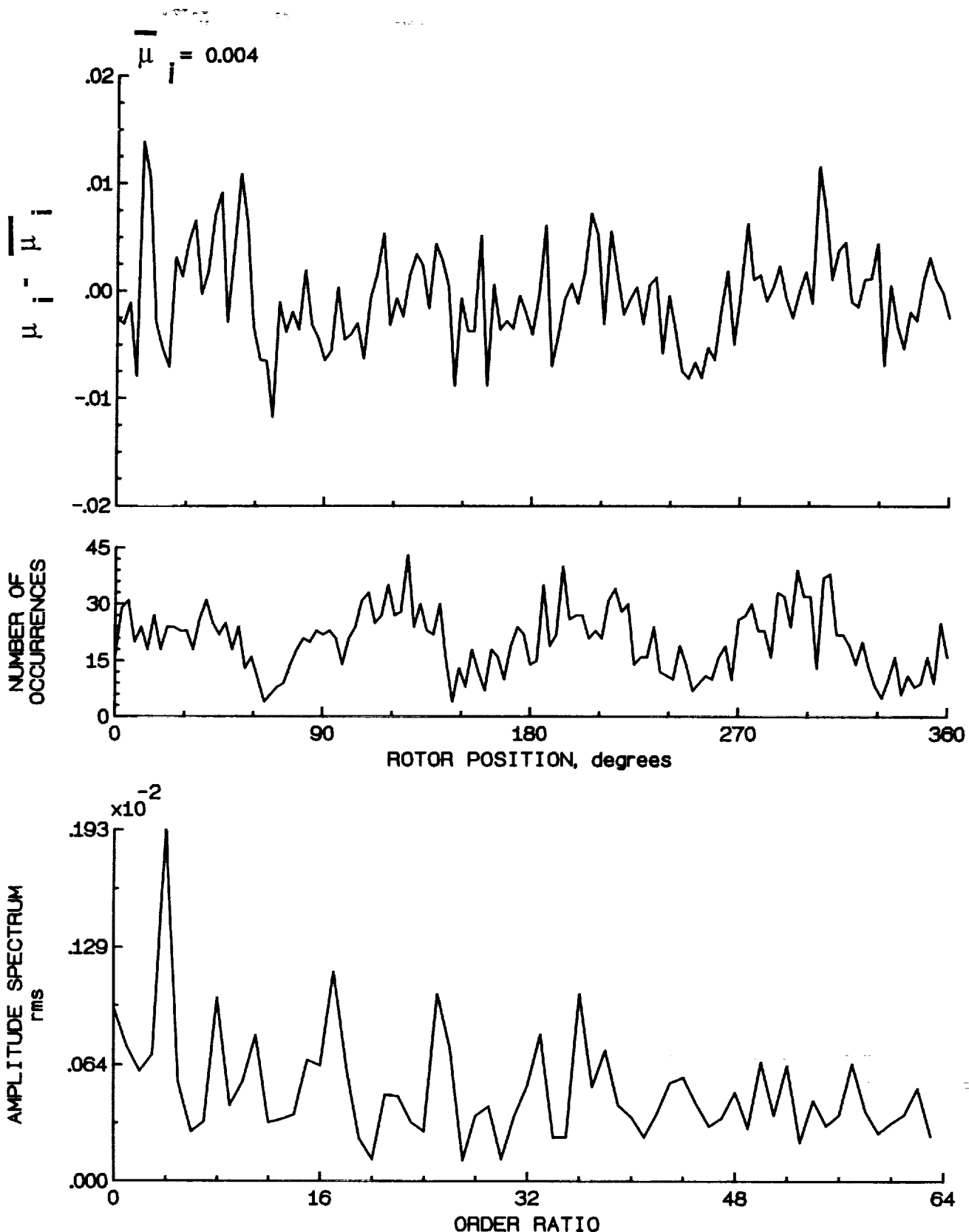


Figure 181.- Induced inflow velocity measured at 330 degrees and r/R of 0.78.

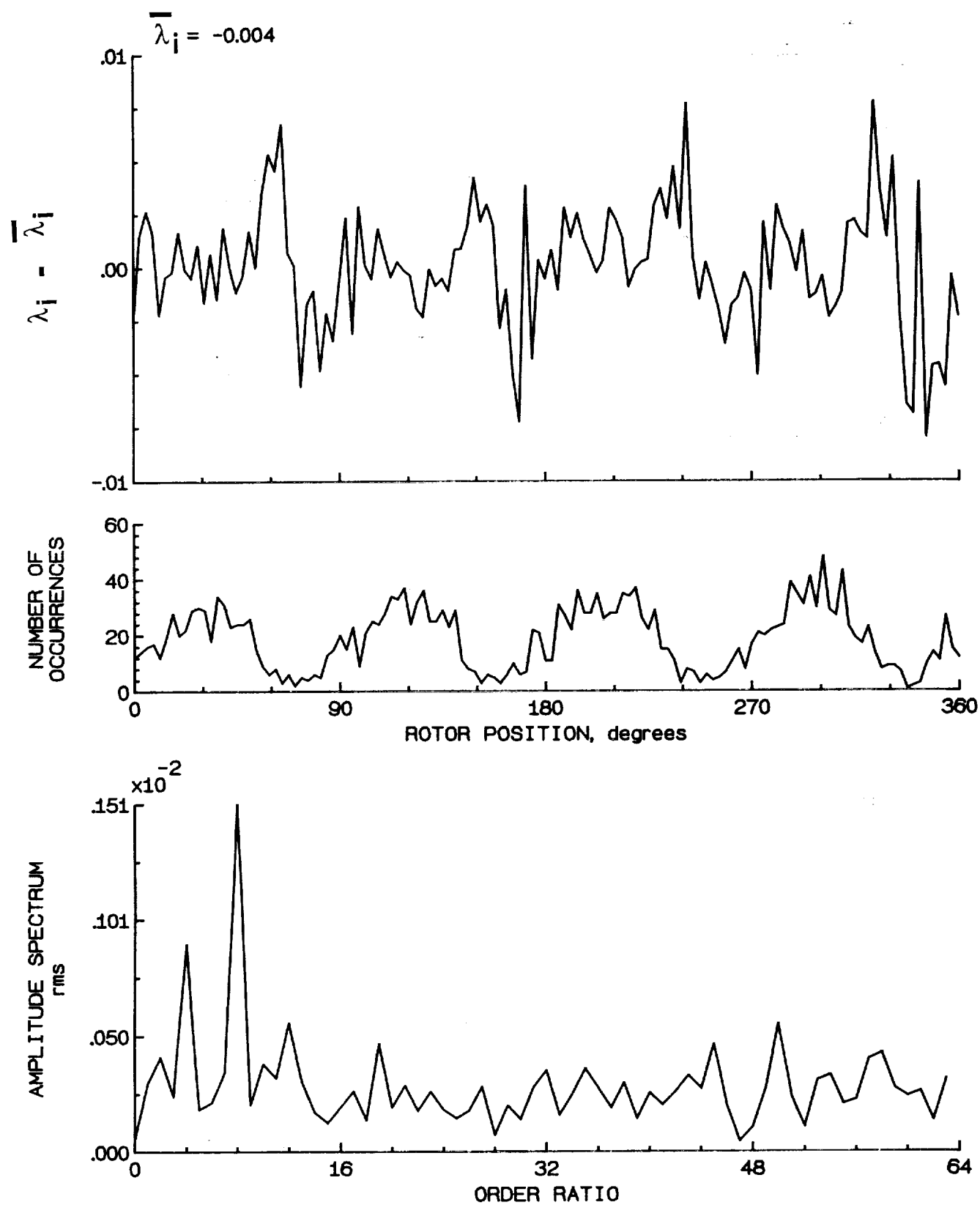


Figure 181.- Concluded.

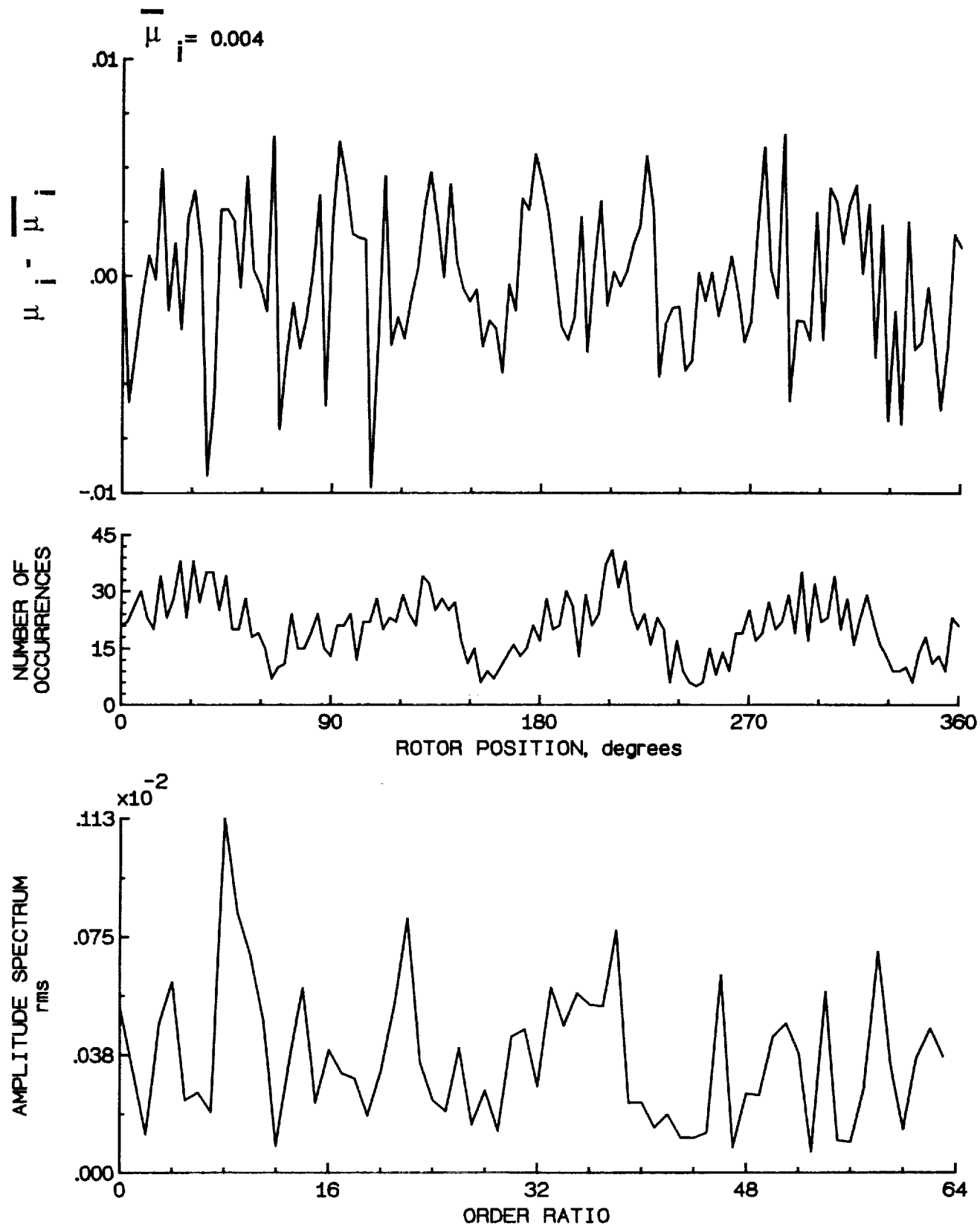


Figure 182.- Induced inflow velocity measured at 330 degrees and r/R of 0.82.

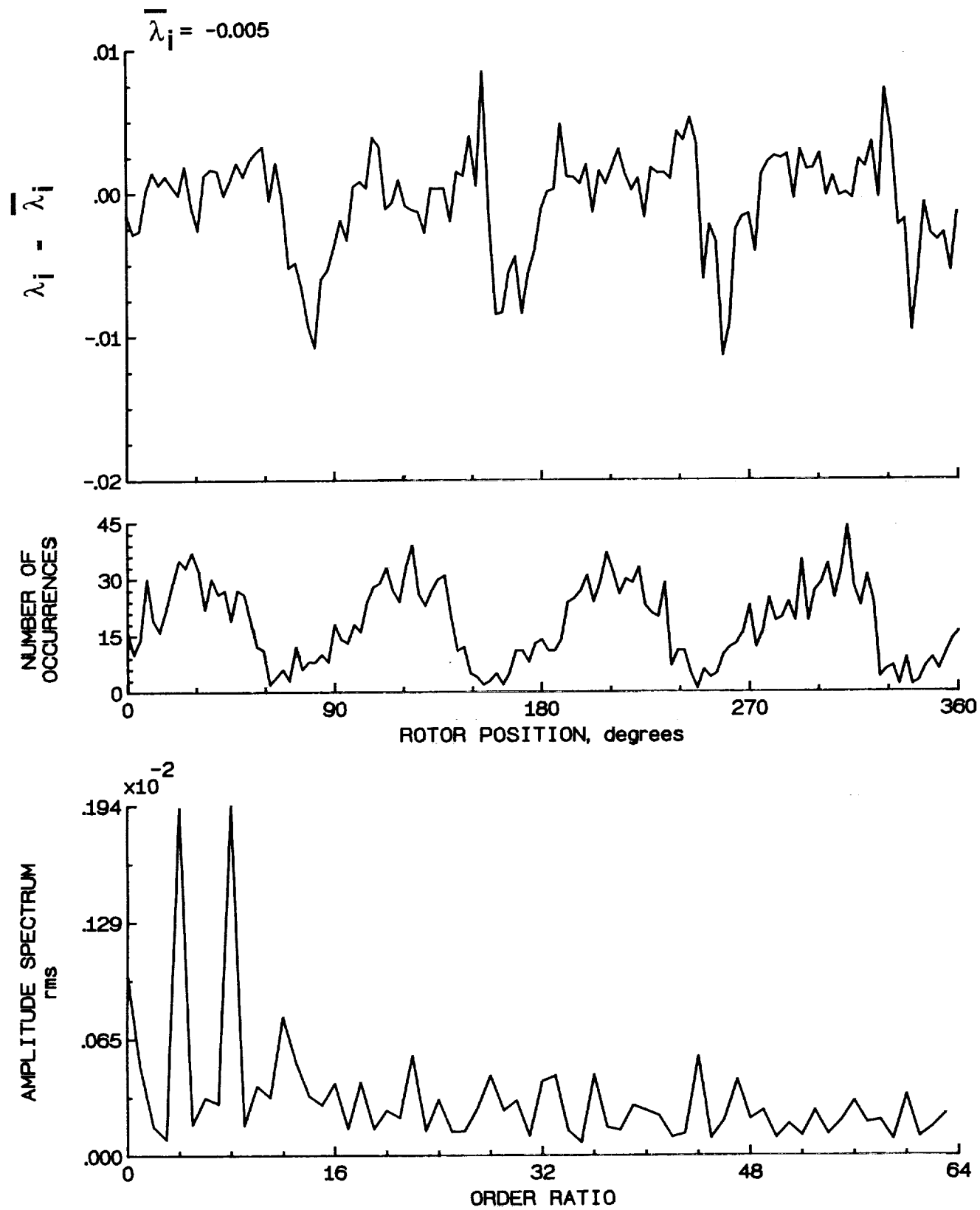


Figure 182.- Concluded.

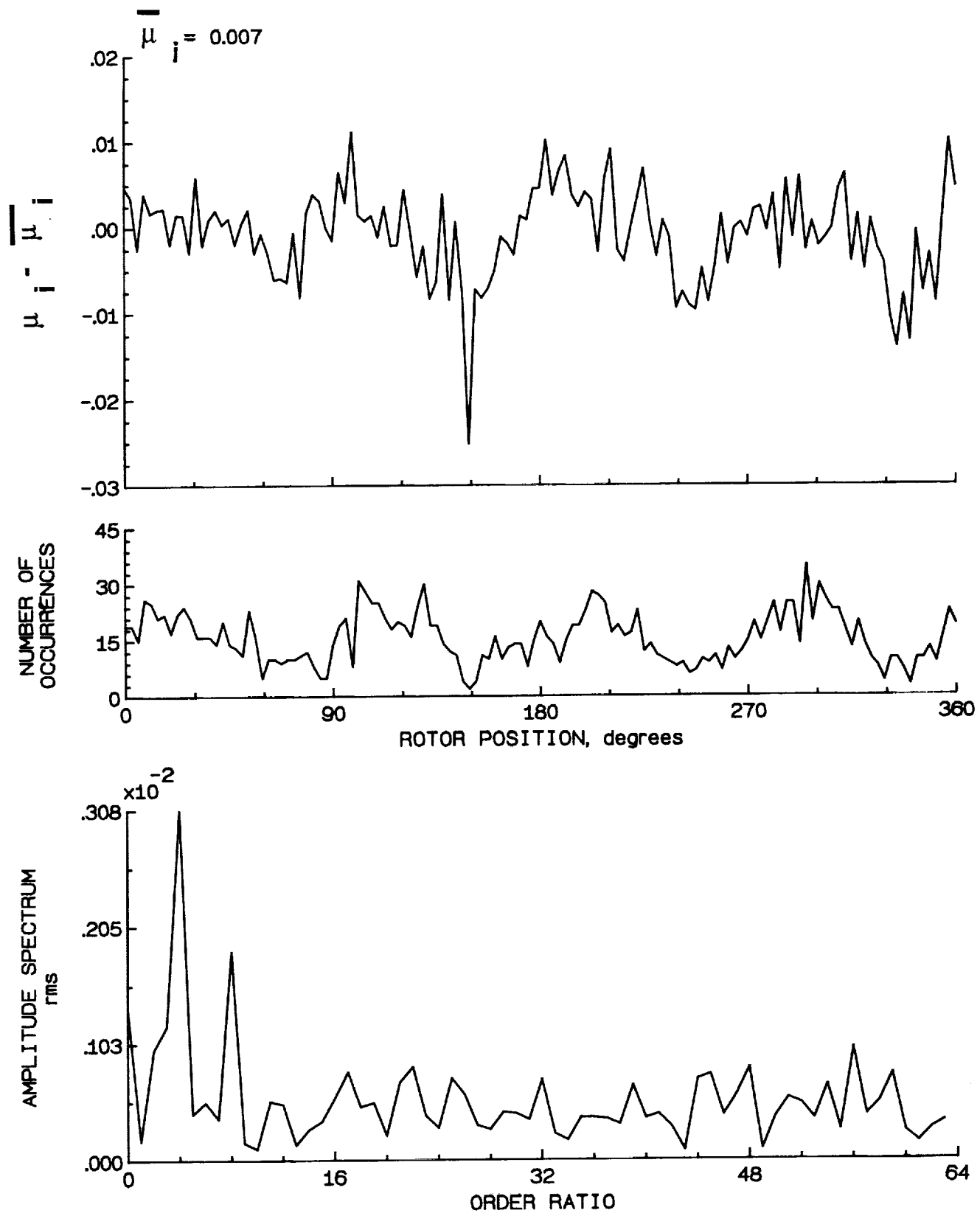


Figure 183.- Induced inflow velocity measured at 330 degrees and r/R of 0.86.

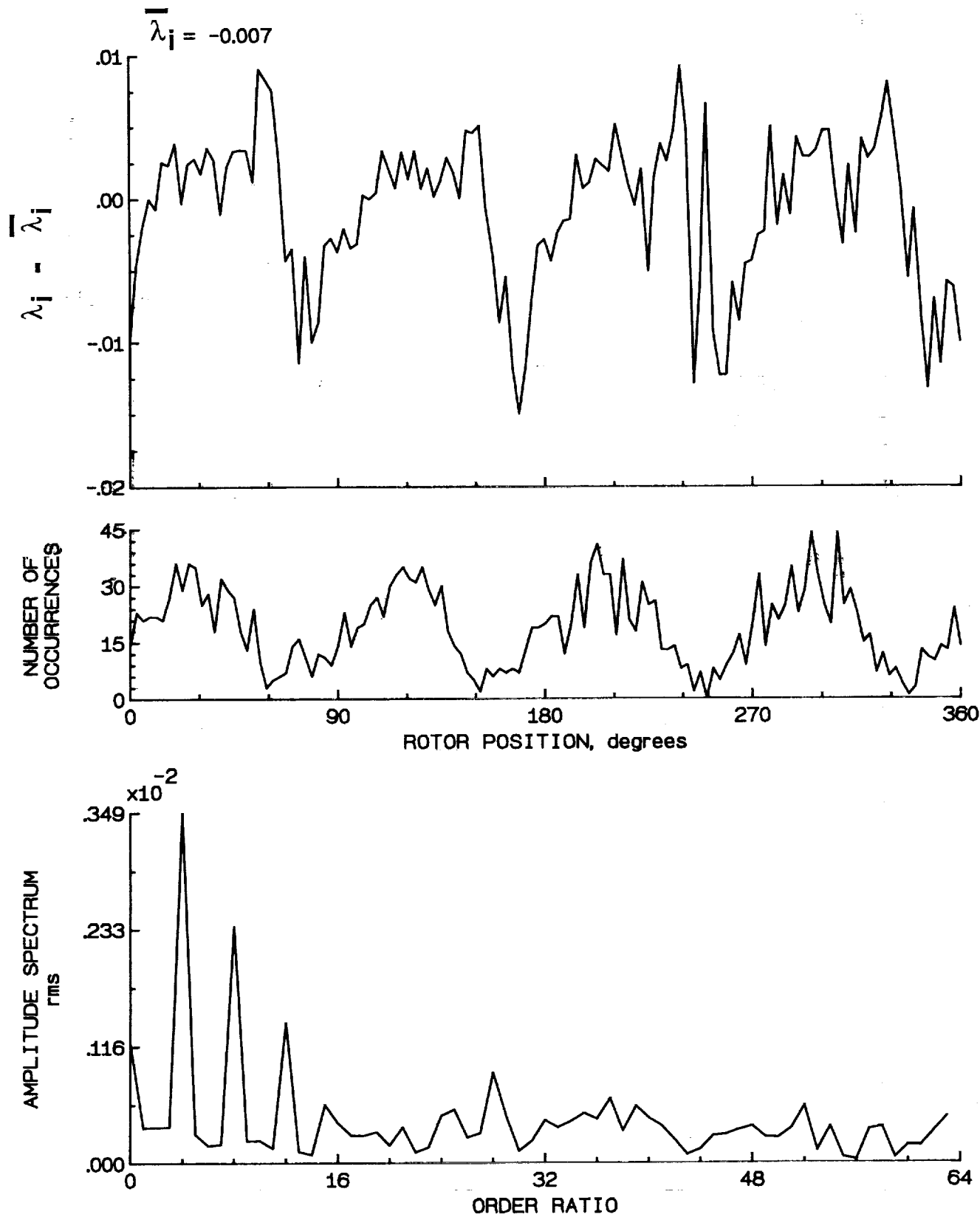


Figure 183.- Concluded.

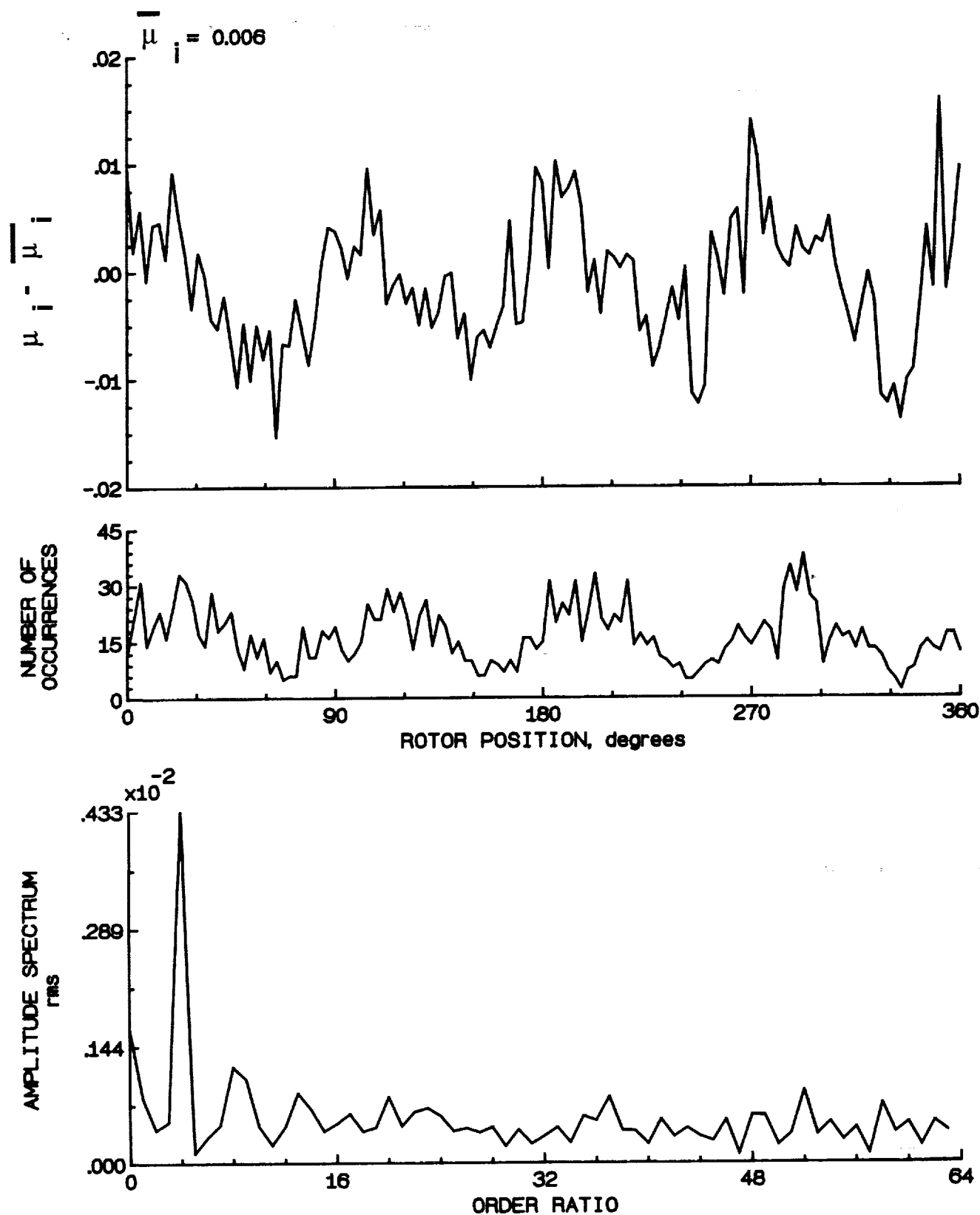


Figure 184.- Induced inflow velocity measured at 330 degrees and r/R of 0.90.

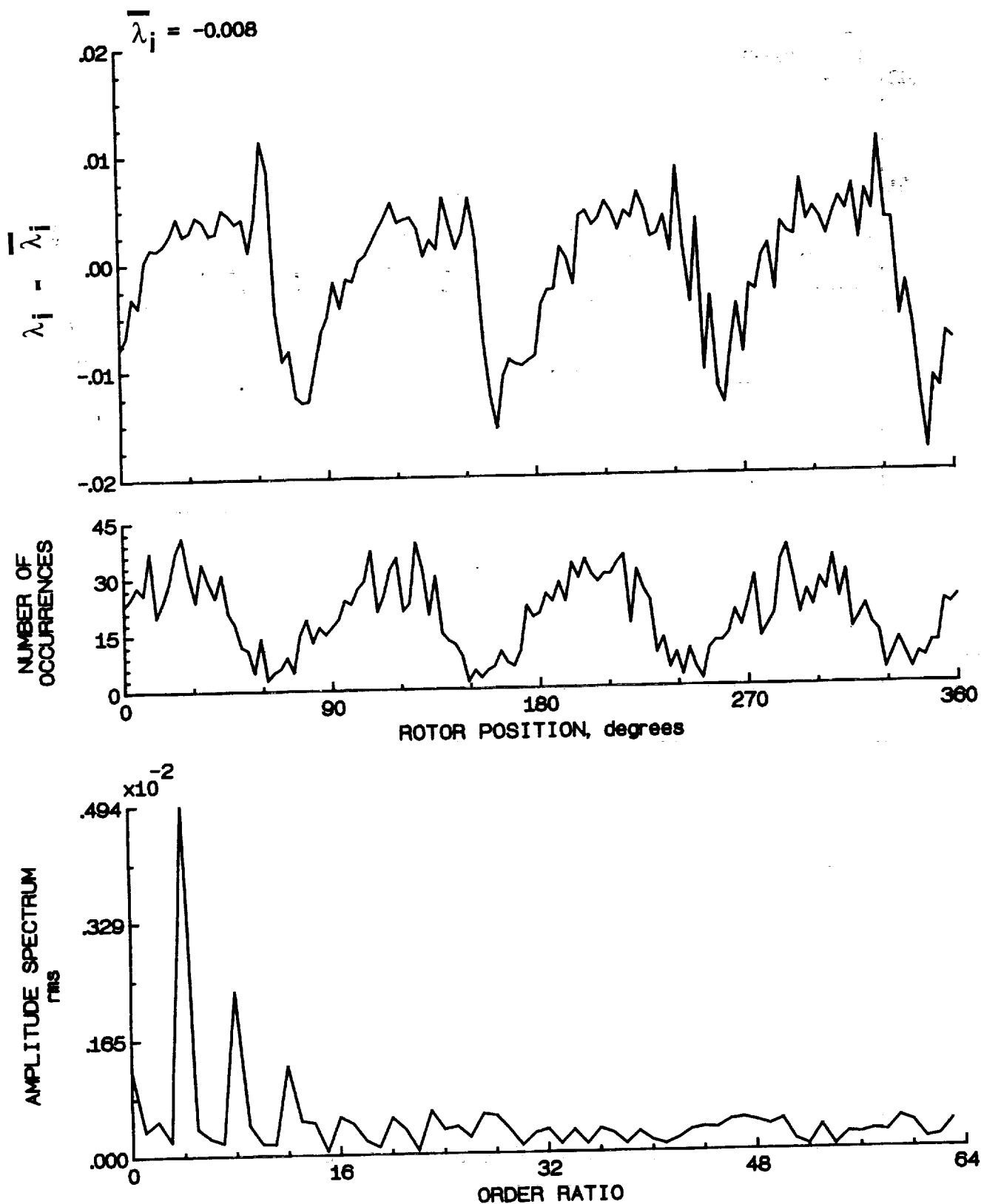


Figure 184.- Concluded.

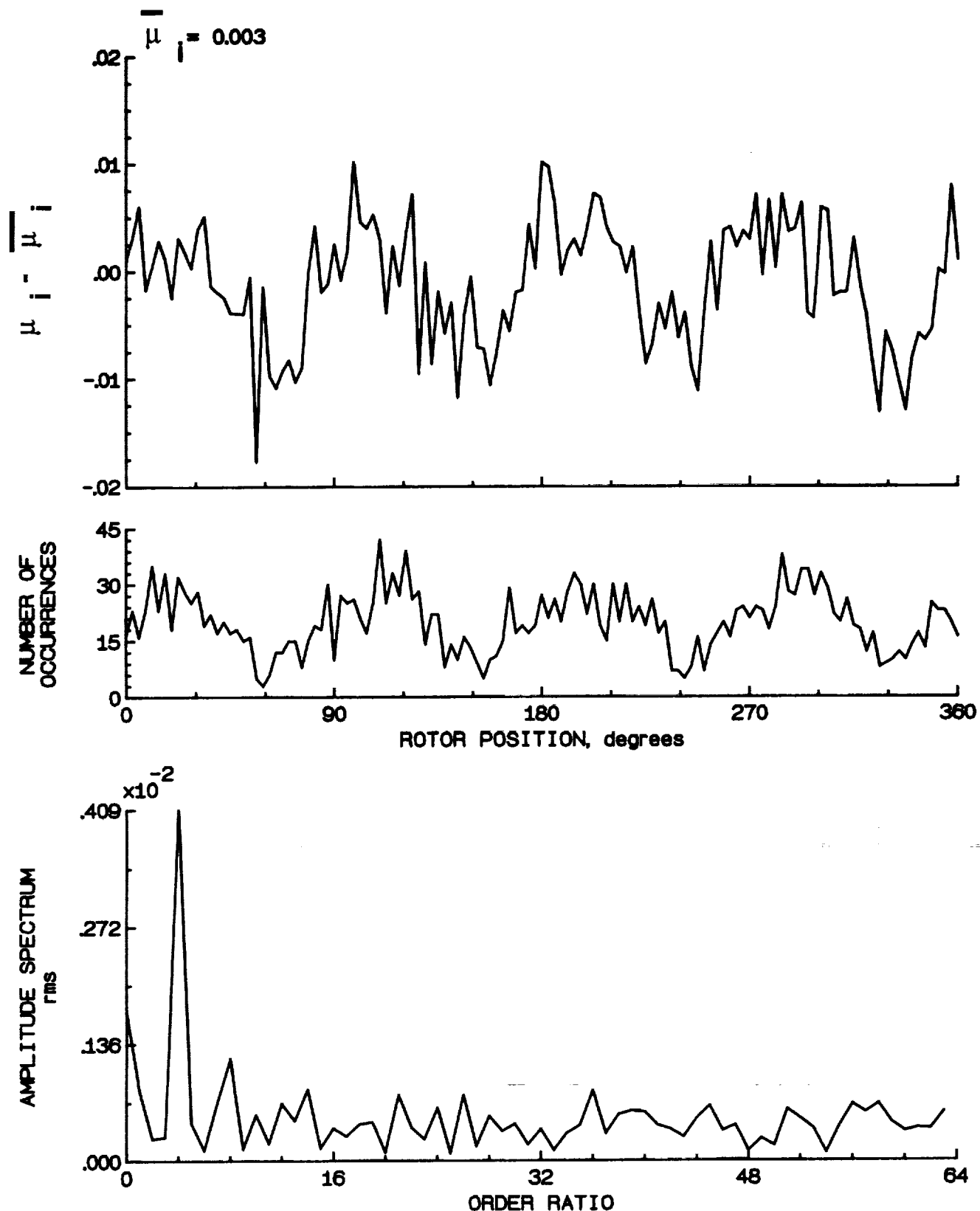


Figure 185.- Induced inflow velocity measured at 330 degrees and r/R of 0.94.

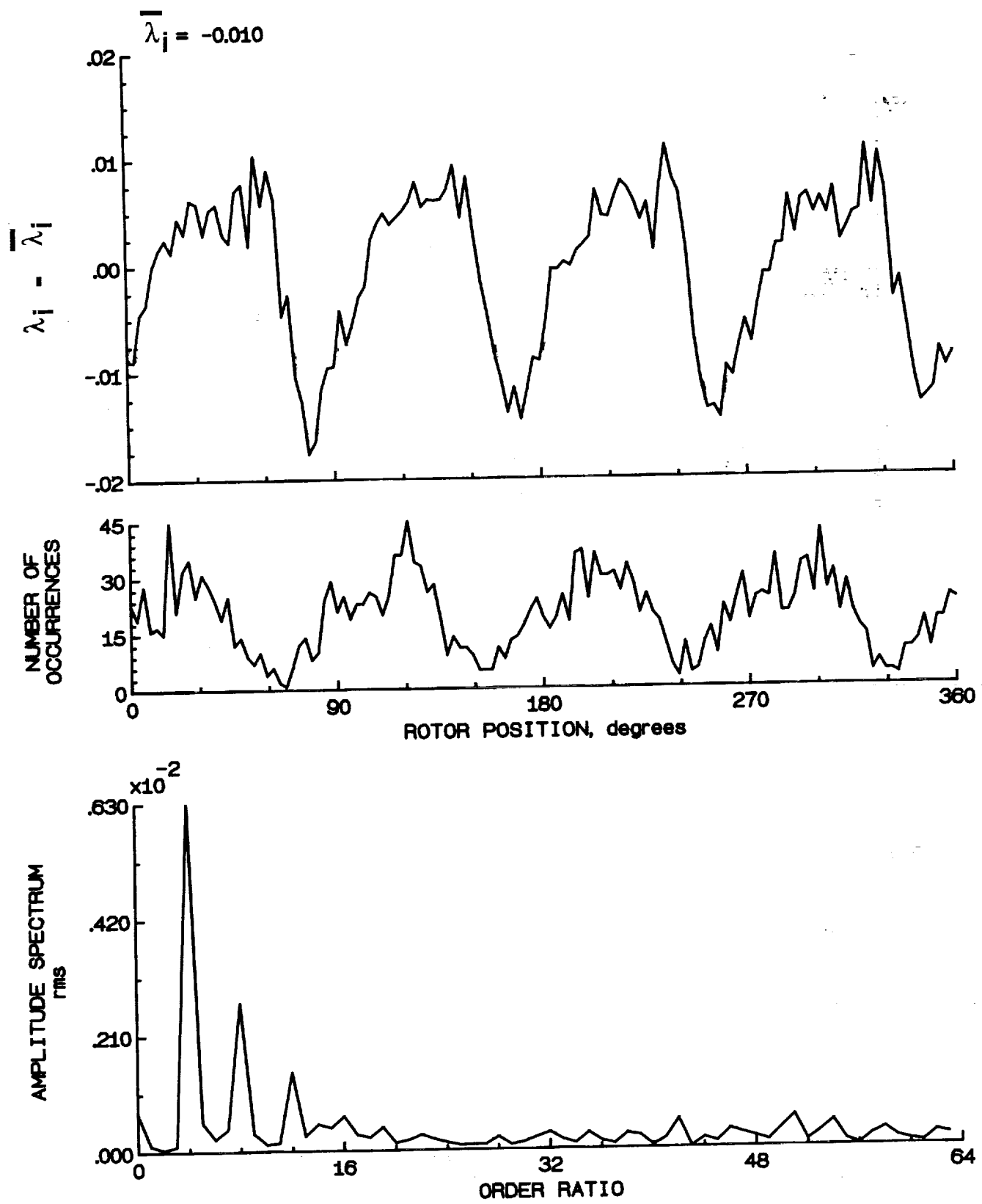


Figure 185.- Concluded.

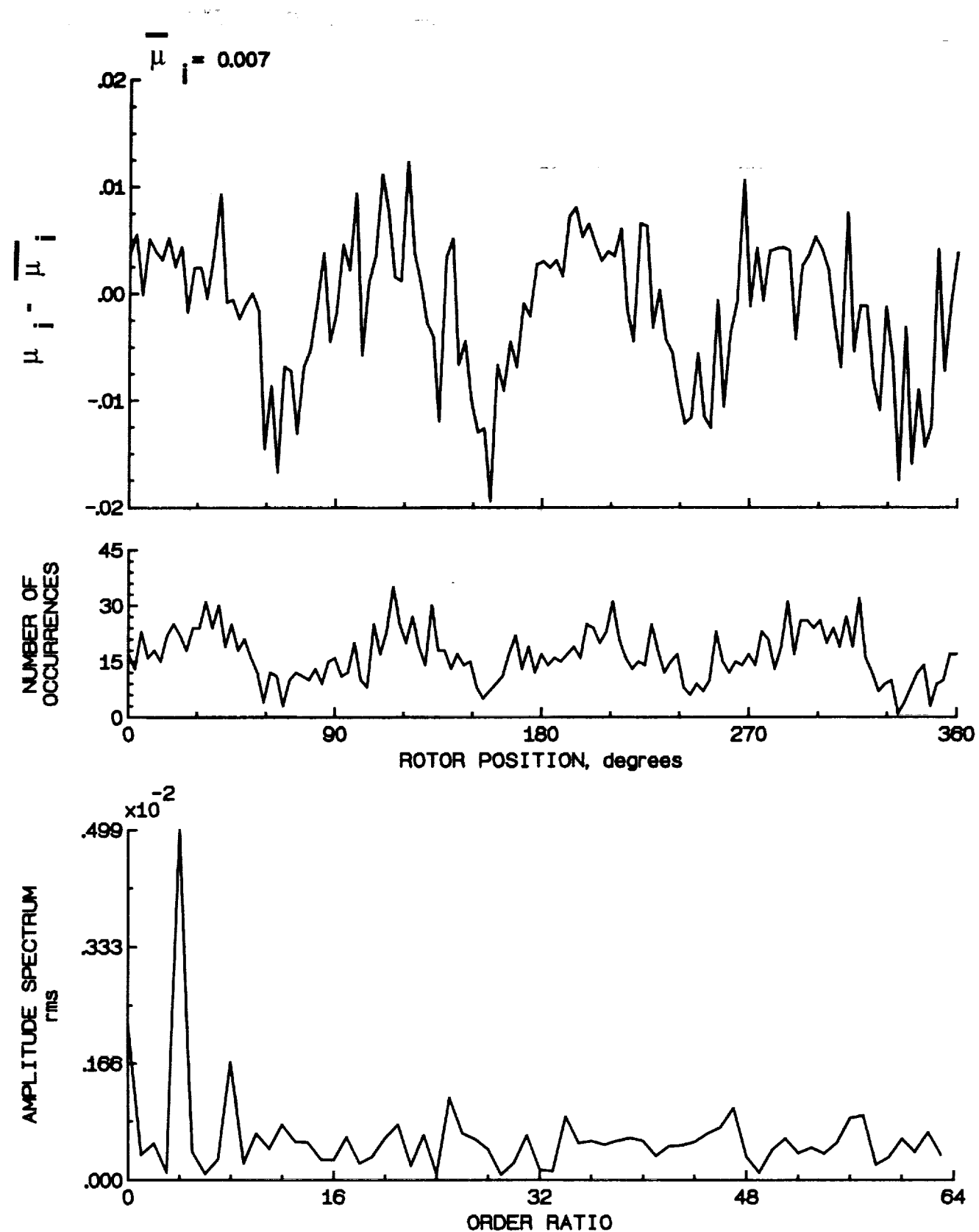


Figure 186.- Induced inflow velocity measured at 330 degrees and r/R of 0.98.

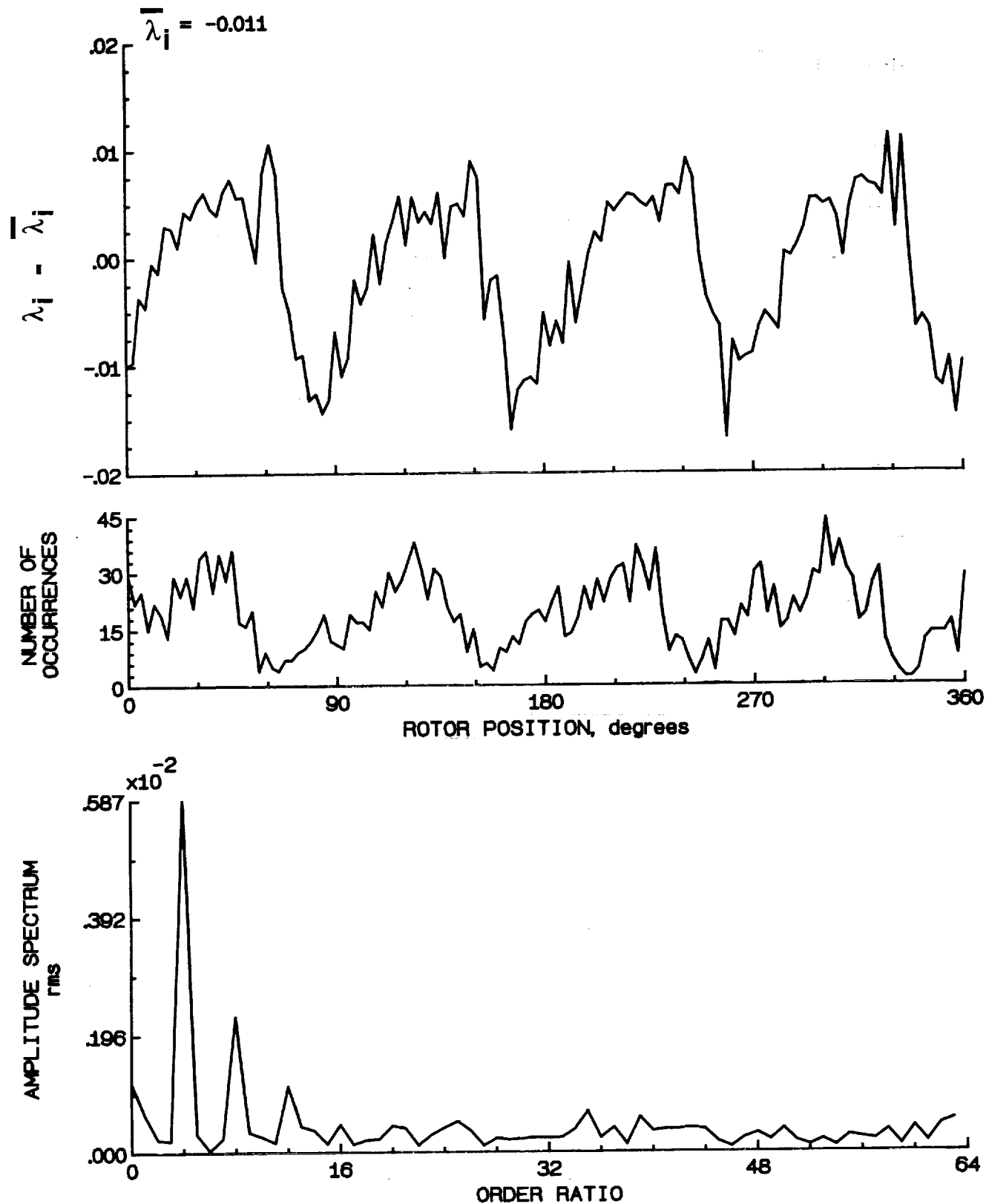


Figure 186.- Concluded.

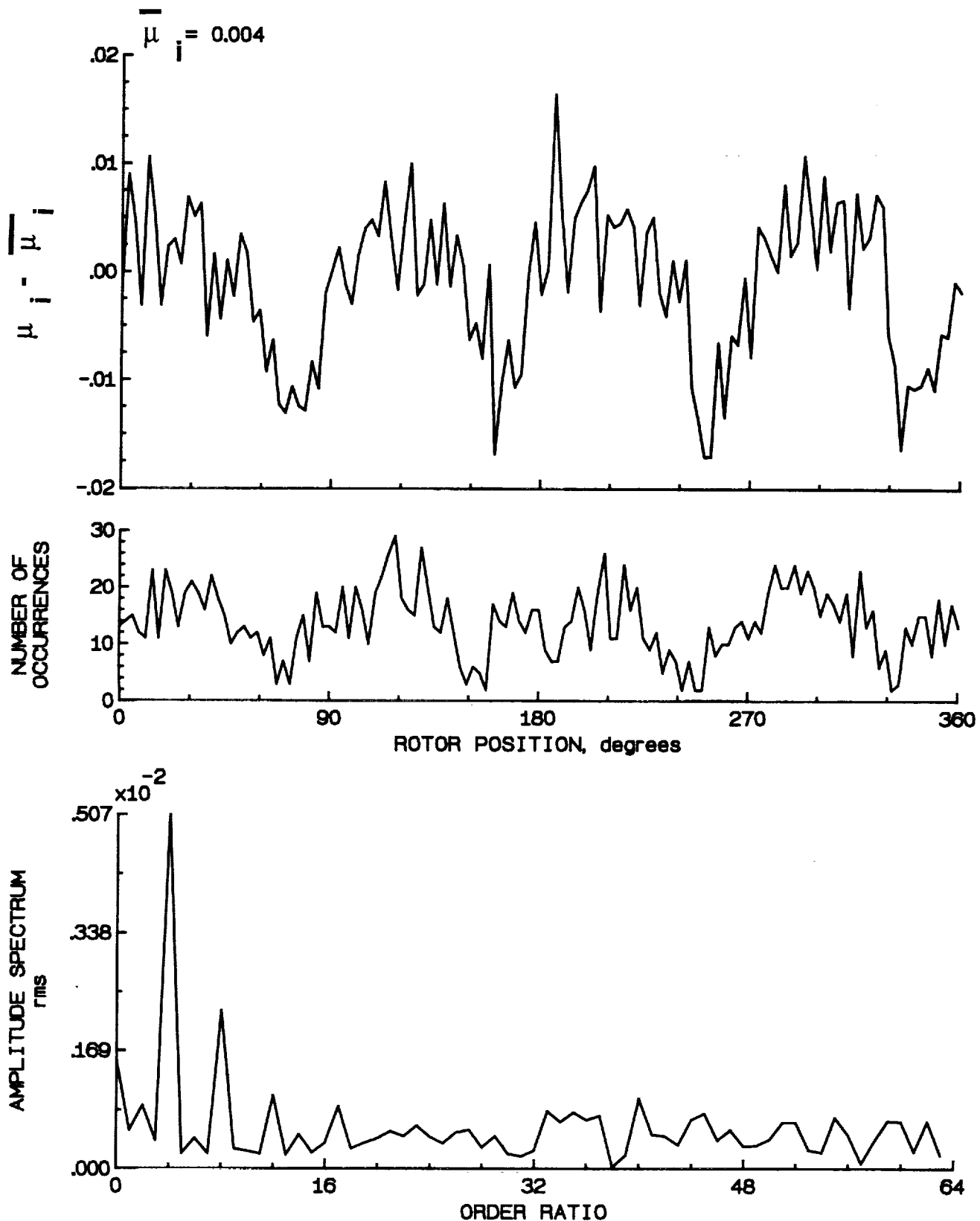


Figure 187.- Induced inflow velocity measured at 330 degrees and r/R of 1.02.

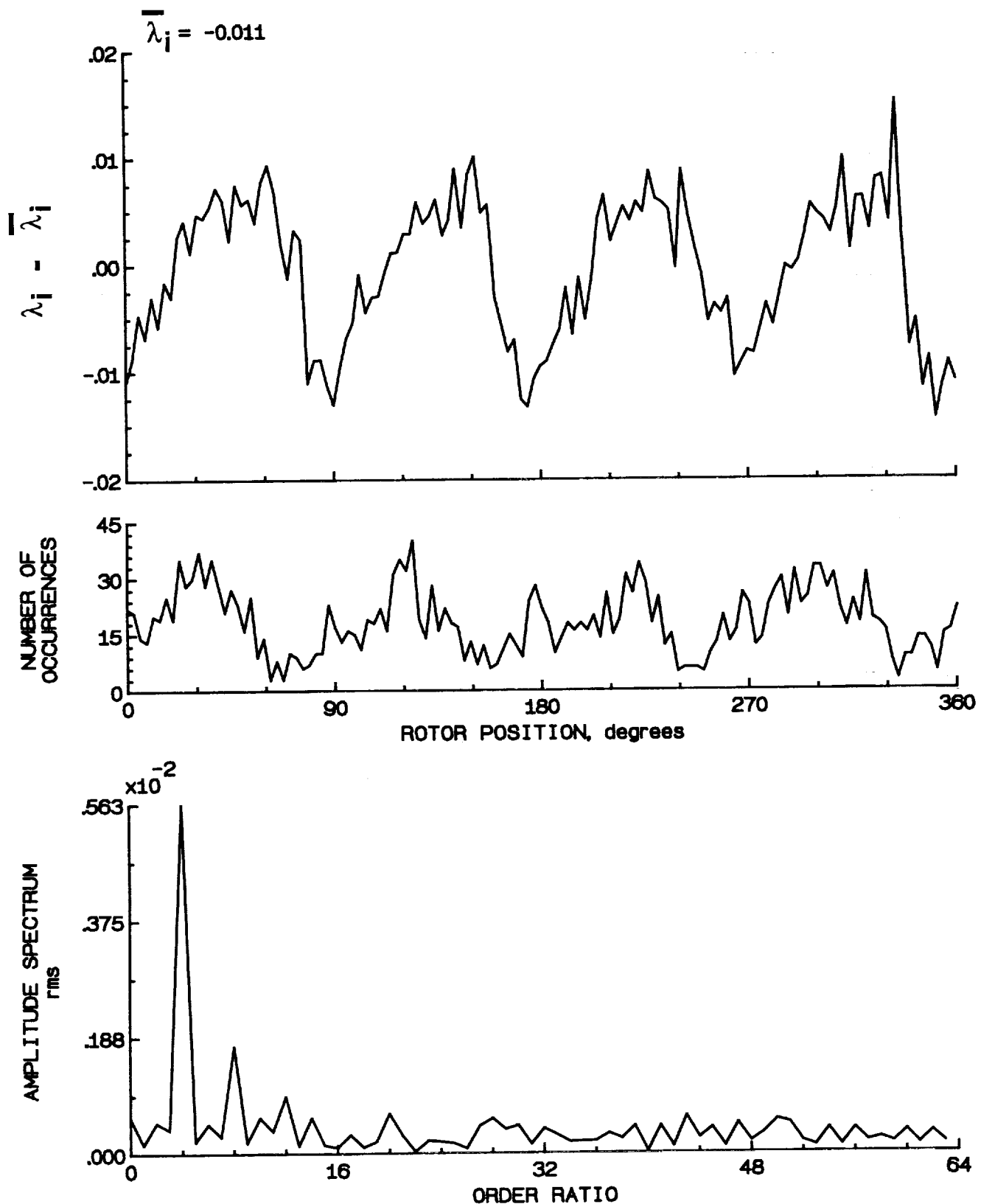


Figure 187.- Concluded.

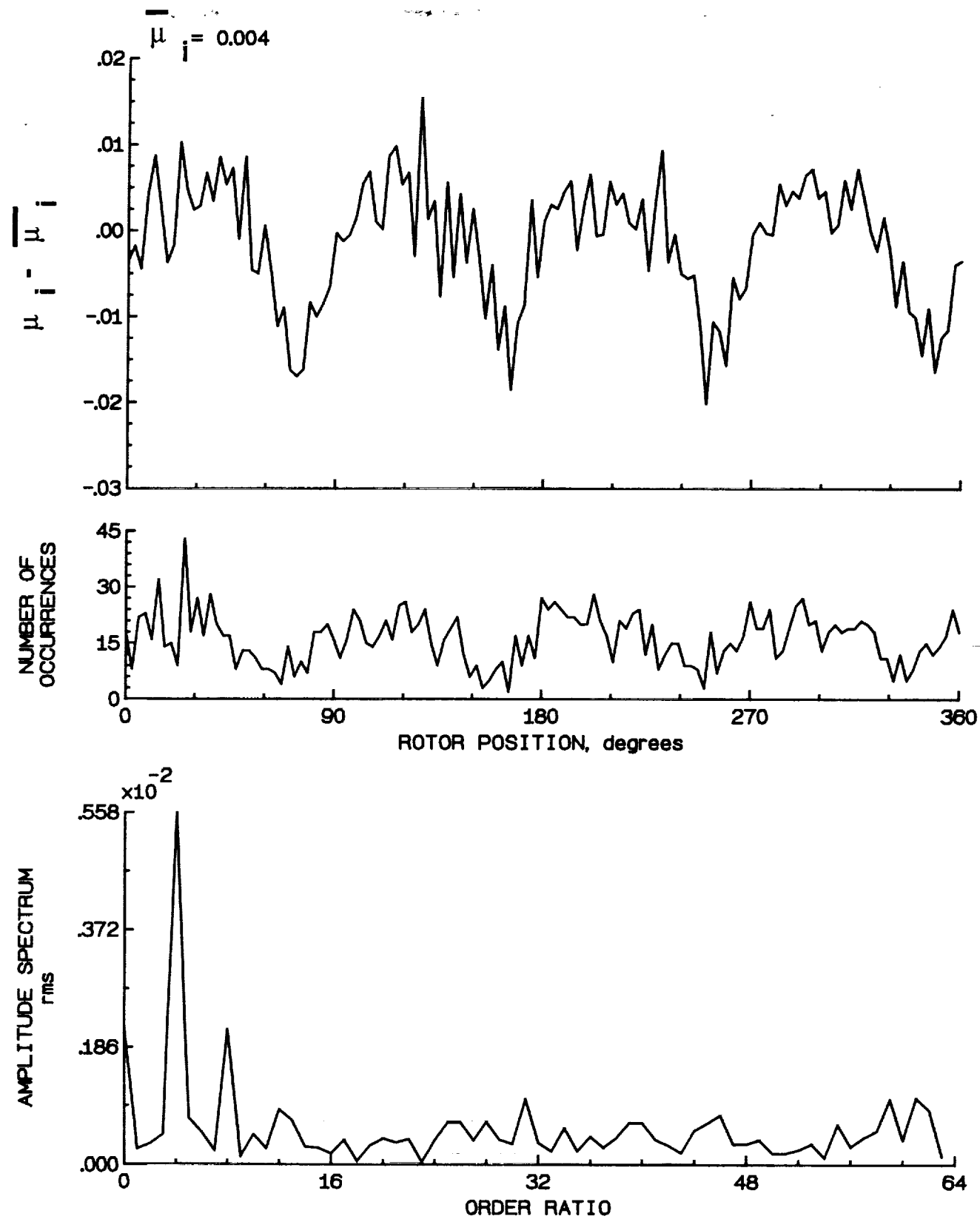


Figure 188.- Induced inflow velocity measured at 330 degrees and r/R of 1.04.

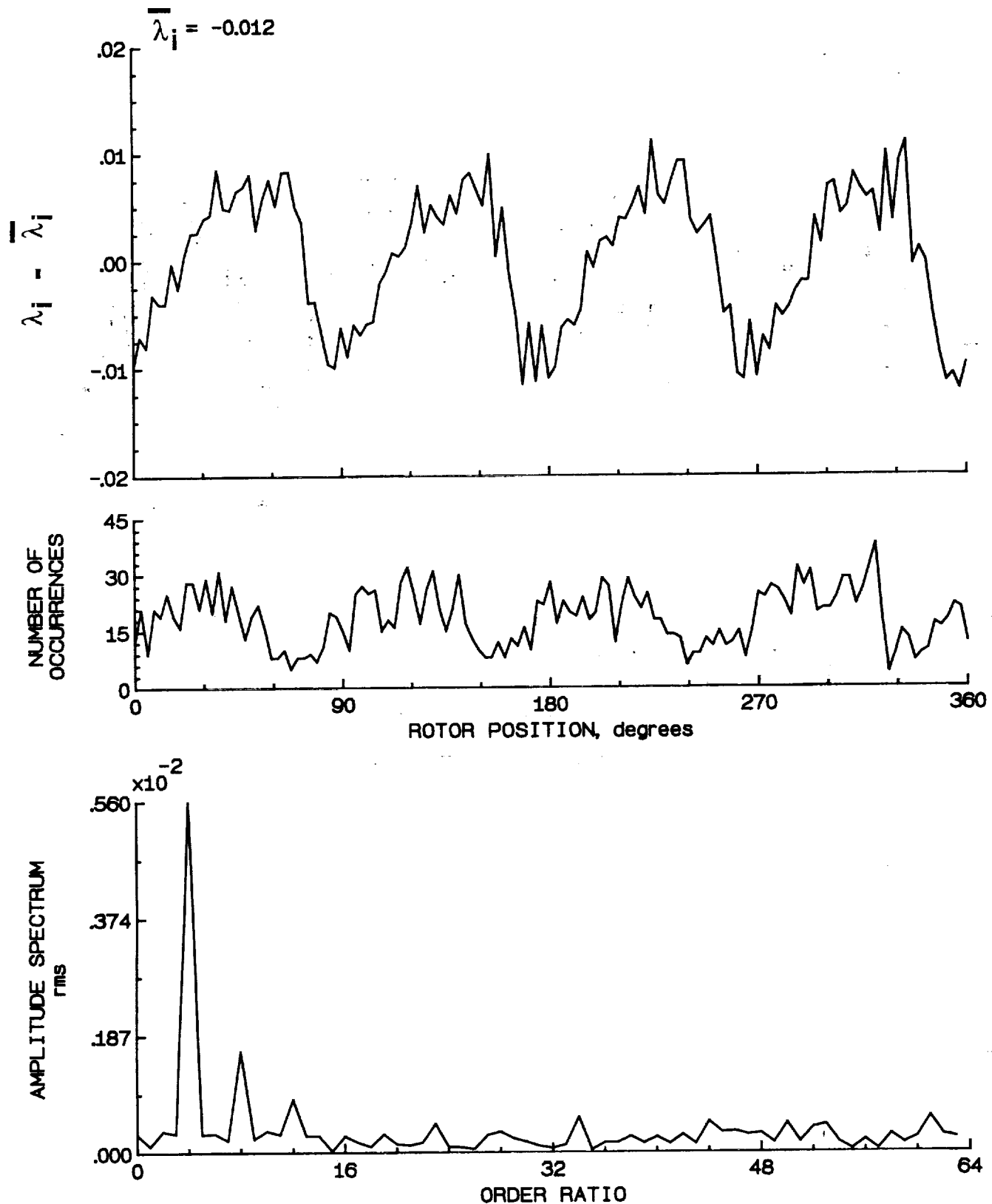


Figure 188.- Concluded.

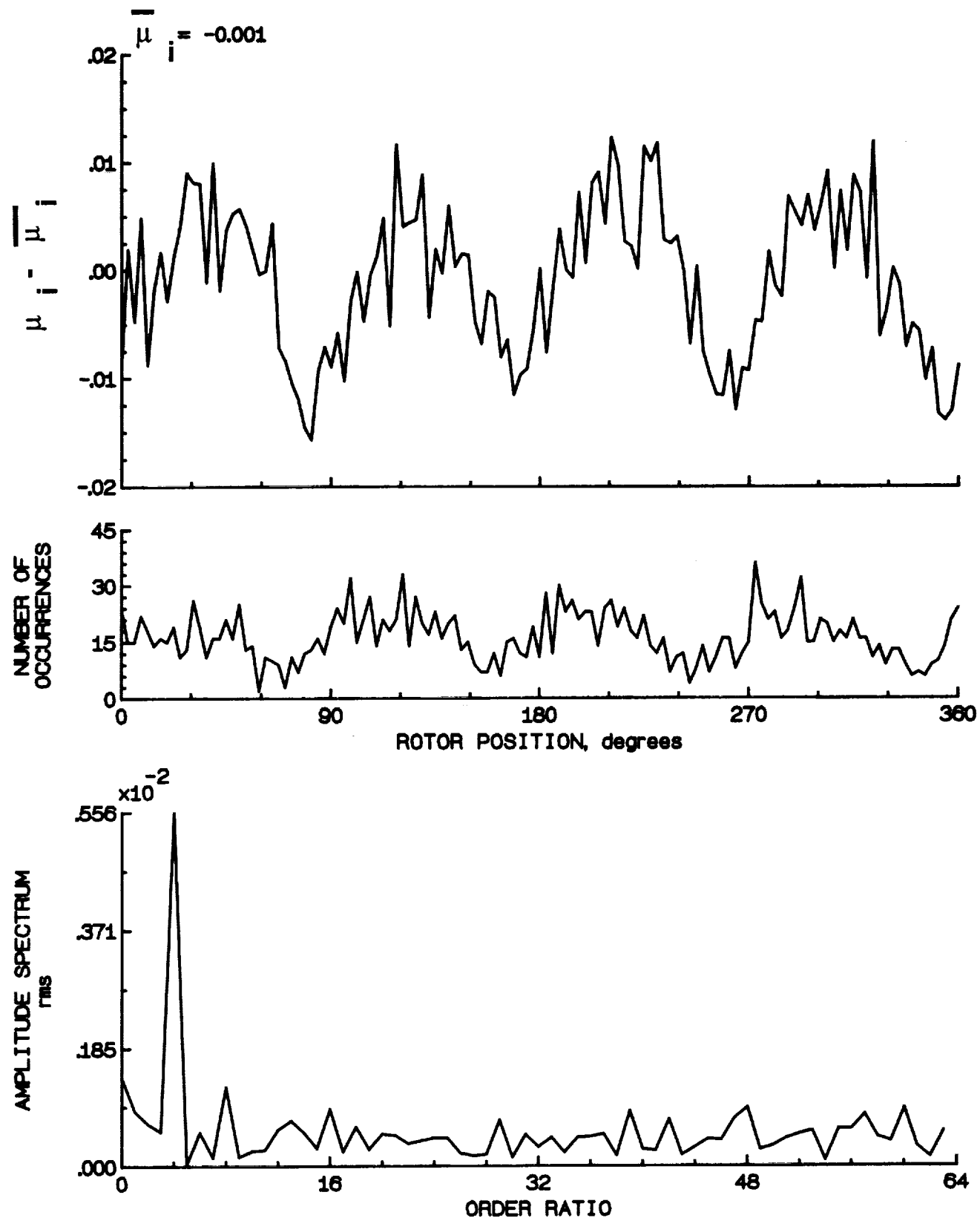


Figure 189.- Induced inflow velocity measured at 330 degrees and r/R of 1.10.

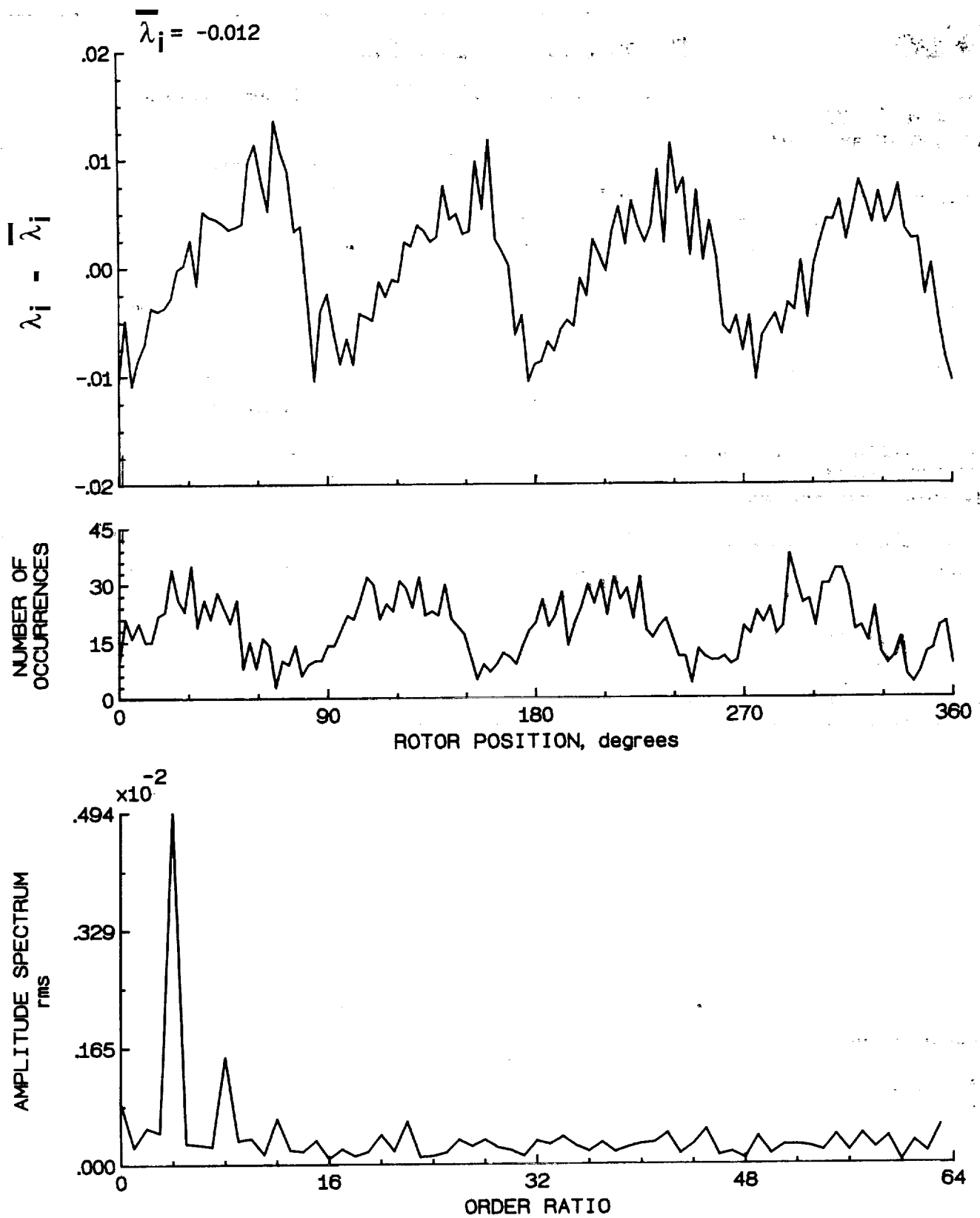


Figure 189.- Concluded.



Report Documentation Page

1. Report No. NASA TM-101599 AVSCOM TM-89-B-002	2. Government Accession No.	3. Recipient's Catalog No.	
4. Title and Subtitle Inflow Measurements Made With a Laser Velocimeter on a Helicopter Model in Forward Flight, Volume VII: Rectangular Planform Blades at an Advance Ratio of 0.40		5. Report Date April 1989	
7. Author(s) Danny R. Hoad, Susan L. Althoff, Joe W. Elliott, and Richard H. Sailey		6. Performing Organization Code	
9. Performing Organization Name and Address Aerostructures Directorate USAARTA-AVSCOM Langley Research Center Hampton, VA 23665-5225		8. Performing Organization Report No.	
12. Sponsoring Agency Name and Address National Aeronautics and Space Administration Washington, DC 20546-0001 and US Army Aviation Systems Command St. Louis, MO 63120-1798		10. Work Unit No. 505-61-51-10	
15. Supplementary Notes Danny R. Hoad, Susan L. Althoff, and Joe W. Elliott: Aerostructures Directorate, USAARTA-AVSCOM, Langley Research Center, Hampton, VA Richard H. Sailey: Planning Research Corporation, Hampton, VA		11. Contract or Grant No.	
16. Abstract <p>An experimental investigation was conducted in the 14- by 22-Foot Subsonic Tunnel at the NASA Langley Research Center to measure the inflow into a scale model helicopter rotor in forward flight ($\mu = 0.40$). The measurements were made with a two-component Laser Velocimeter (LV) one chord above the plane formed by the path of the rotor tips (tip-path-plane). A conditional sampling technique was used to determine the position of the rotor at the time that each velocity measurement was made so that the azimuthal fluctuations in velocity could be determined. Measurements were made at a total of 178 separate locations in order to clearly define the inflow character.</p>			
17. Key Words (Suggested by Author(s)) Rotor model Inflow Laser Velocimetry	18. Distribution Statement Unclassified - Unlimited Subject Category 02		
19. Security Classif. (of this report) Unclassified	20. Security Classif. (of this page) Unclassified	21. No. of pages 388	22. Price A17